JUN 1 3 1990

# The Energetic Gamma-Ray Experiment Telescope (EGRET) Science Symposium



*Proceedings of a science symposium held at*
*NASA Goddard Space Flight Center*
*Greenbelt, Maryland*
*November 15–16, 1989*

**NASA**

# The Energetic Gamma-Ray Experiment Telescope (EGRET) Science Symposium

*Edited by*
Carl Fichtel
Stanley Hunter
Parameswaran Sreekumar
and Floyd Stecker
*Goddard Space Flight Center*
*Greenbelt, Maryland*

**NASA**

EGRET Science Symposium
November 15-16, 1989


Table of Contents

## Bursts and Solar Flares

## Normal Galaxies

## Active Galaxies

## Extragalactic Diffuse Radiation

# INTRODUCTION TO THE SYMPOSIUM

Carl E. Fichtel
NASA/Goddard Space Flight Center
Greenbelt, MD 20771

The principal purpose of this symposium is to provide the EGRET scientists and those with whom we have been working an opportunity to study and improve their understanding of high energy gamma ray astronomy. With this goal in mind, the participation of each of the EGRET scientists has been encouraged and most are presenting talks which will be included in the proceedings. Each of the groups with whom we are collaborating and with whom we have been working over the last several years were invited to present talks and will be doing so, as will each of the groups associated with the other instruments on the Gamma Ray Observatory (GRO). We also have asked several theorists to complete the program by presenting talks related to the subjects under discussion.

Since the principal aim is to learn, active participation is encouraged both by the participants and the other scientists who have joined us. We also encourage you to take advantage of the breaks in the morning and afternoon, as well as the luncheon and dinner periods to pursue subjects of scientific interest with those who are here. If you wish to have your questions and answers included in the proceedings, forms are provided for this purpose.

The Symposium begins with the galactic diffusion radiation both because of the considerable attention that it has received due to its importance in studying galactic cosmic rays, galactic structure and dynamic balance, and because an understanding of its characteristics is important in the study of galactic sources. The galactic objects to be reviewed here include pulsars, bursts, solar flares, and other galactic sources of several types. From these subjects, we shall proceed outward from our galaxy to normal galaxies, active galaxies, and the extragalactic diffuse radiation.

The other members of the organizing committee, Stanley Hunter, Parameswaran Sreekumar, and Floyd Stecker, join me in thanking the many people who have helped us with this symposium and will be continuing to provide assistance during the meeting and afterwards in preparing the proceedings.

We hope that this EGRET Science Symposium will be a stimulating experience for you, kindle your curiosity about some new ideas, perhaps revive your interest in some old ones, and lead to some interesting journal articles.

# Galactic Diffuse Radiation

# MOLECULAR CLOUDS AND THE LARGE-SCALE STRUCTURE OF THE GALAXY

PATRICK THADDEUS AND J. GREGORY STACY
Harvard-Smithsonian Center for Astrophysics, Cambridge, MA 02138 USA

## ABSTRACT

We review the application of molecular radio astronomy to the study of the large-scale structure of the Galaxy and describe the distribution and characteristic properties of the Galactic population of Giant Molecular Clouds (GMCs), derived primarily from analysis of the Columbia CO survey, and its relation to tracers of Population I and major spiral features. The properties of the local molecular interstellar gas are summarized. The CO observing programs currently underway with the Center for Astrophysics 1.2 m radio telescope are described, with an emphasis on projects relevant to future comparison with high-energy $\gamma$-ray observations. Several areas are discussed in which high-energy $\gamma$-ray observations by the EGRET experiment aboard the Gamma Ray Observatory will directly complement radio studies of the Milky Way, with the prospect of significant progress on fundamental issues related to the structure and content of the Galaxy.

## I. HISTORICAL PERSPECTIVE

Since the pioneering work of Shapley and others led to the recognition that the Milky Way is a spiral galaxy, its large-scale structure has been the subject of much investigation. The classical optical studies toward the more distant portions of the Galactic disk made in the early decades of this century were typically confined to a few, well-defined "windows," owing to the severe obscuration in visible light from interstellar gas and dust. With the advent of radio astronomy, following the pioneering efforts of Jansky and Reber, and, in particular, the discovery by Ewen and Purcell in 1951 of the 21 cm hyperfine transition of atomic hydrogen, astronomers could begin to assemble an accurate picture on a Galactic scale of the distribution of matter in the Milky Way. Today, the discipline of Galactic radio astronomy is crucial to the continuing study of our Galaxy and its main constituents.

Within a few years of the discovery of the 21 cm line of atomic hydrogen (H I), the Leiden survey of the northern sky (Muller and Westerhout 1957) and the Sydney survey of the southern sky (Kerr, Hindman, and Gum 1959), done with inexpensive, moderate-size antennas largely dedicated to hydrogen-line work, had completely mapped at ~2° resolution the distant spiral arms around the Galactic equator and followed the local gas to sufficiently high latitudes ($\pm 10°$) to establish a secure foundation for subsequent studies at higher resolutions. Progress has neither been as rapid nor as systematic in the study of the molecular component of the interstellar medium (ISM).

### a) Molecular Radio Astronomy

Until the 1960s, astronomers generally believed that molecules are extremely rare in interstellar space. Nearly all visible matter (99% in terms of number of atoms) in the cosmos is hydrogen and helium. Helium, an inert gas, does not form molecules, and, although hydrogen atoms combine to form $H_2$, the bond is easily broken by the ultraviolet radiation emitted by luminous stars that pervades the interstellar medium. More complicated molecular species were thought even less likely, given the conceptions then current of gas-phase chemistry at the low densities characteristic of the ISM.

During the last three decades observations of molecules in interstellar space have demonstrated dramatically the fallacy of those early assumptions. Rapid advances in microwave spectroscopy following the Second World War enabled accurate laboratory measurement of the frequencies of key molecular transitions and led to the radio detection of interstellar molecules, starting with OH (Weinreb et al. 1963), followed by water vapor and

ammonia (Cheung *et al.* 1968, 1969) and formaldehyde (Palmer *et al.* 1969). An accelerating pace of discovery continues to the present day. To date, nearly 100 interstellar molecules have been detected and identified, ranging from simple diatomics to fairly complex organic structures with molecular weights as large as 147 (see, for example, Winnewisser and Herbst 1987). Molecules exist primarily in the depths of dark nebulae and in dusty circumstellar shells, where concentrations of interstellar gas and dust severely attenuate the ultraviolet radiation that would otherwise break molecular bonds. Star formation takes place within such dense molecular clouds. Multiwavelength studies of numerous molecular transitions provide information on the density and temperature structure of the interstellar molecular clouds that produce stars and on the interaction of both young and evolved stars with their environment through outflows and shocks as they contribute to the continuing dynamic evolution of the interstellar medium.

### b) CO as a Tracer of Molecular Hydrogen

Of all the molecules detected so far, however, interstellar carbon monoxide (CO), discovered by Wilson *et al.* (1970), has probably had the greatest impact on astronomy in general. The second most abundant molecule in interstellar space after $H_2$, CO is a simple, stable diatomic very widely distributed throughout the Galaxy, and it is collisionally excited into detectable emission within clouds where the density exceeds ~100 molecules per $cm^{-3}$. Because the abundance ratio of CO to $H_2$ is relatively high for a trace constituent, about $1:10^5$ and apparently remains fairly constant over a wide range of interstellar conditions, CO has become the standard tracer of molecular hydrogen in the ISM. The $J=1\rightarrow0$ rotational transition of CO at 115 GHz, readily detected at millimeter wavelengths at 2.6 mm, is now the molecular analog of the 21 cm atomic hydrogen line for large-scale studies of interstellar gas in the Galaxy.

The first Galactic CO surveys were confined typically to a strip along the Galactic equator in the northern hemisphere where only a minute fraction of the molecular gas in the Galaxy was actually observed (Scoville and Solomon 1975; Gordon and Burton 1976; Cohen and Thaddeus 1977). Yet some of the most interesting scientific issues raised by the discovery of cosmic molecules, such as the structure and evolution of molecular clouds and their place in the Galactic hierarchy, require unbiased surveys covering large areas of the sky. More than 15 years ago, our group initiated the first large-scale survey of molecular emission intended to encompass the entire Galactic disk. Using an antenna with a modest 1.2 m aperture at Columbia University in New York City, now at the Center for Astrophysics in Cambridge, and a twin instrument located on Cerro Tololo in Chile, we have recently completed at least the first phase of what has turned out to be an extremely ambitious project, since molecular gas in the Galaxy is far more extensive than first supposed. The program has three main objectives: 1) to produce a fairly complete and unbiased inventory at low resolution of both nearby and distant molecular clouds for comparison with other large-scale Galactic surveys, especially the IRAS far-infrared survey at 100 μm and the COS-B survey of diffuse high-energy γ-rays; 2) to survey the distant molecular clouds in the inner Galaxy at full resolution to determine masses and characteristic properties; and 3) to study in detail individual nearby clouds, especially those associated with well-known regions of star formation.

### II. THE COLUMBIA CO SURVEY

The culmination of our low-resolution CO work is a composite map at 0.5 resolution of the molecular clouds in a thick band along the Milky Way, described in detail in Dame *et al.* 1987. Table 1 lists our surveys that contributed to the composite map with other major surveys undertaken with the northern and southern 1.2 m telescopes. All these observing projects have been conducted primarily of the main CO isotope at 115 GHz. The major scientific results of this large compendium of data can be summarized under the following headings (see Dame *et al.* 1987 and references in Table 1 for details).

## TABLE 1
### MAJOR CO SURVEYS UNDERTAKEN WITH THE 1.2 M TELESCOPES IN THE U.S. AND CHILE

| SURVEY | REFERENCES |
|---|---|
| Molecular Clouds in Orion and Monoceros | Kutner *et al.* 1977; Maddalena *et al.* 1986 |
| Cygnus X Region of the Galactic Plane | Cong 1977 |
| Deep Survey of the First Galactic Quadrant | Cohen *et al.* 1980, 1986; Dame *et al.* 1986 |
| Molecular Clouds in the Vicinity of W3, W4, and W5 | Lada *et al.* 1978 |
| GMCs Associated with the Rosette Nebula, NGC 2264, and CMa OB1 | Blitz and Thaddeus 1980 |
| Large Star-Free Cloud in Monoceros | Maddalena and Thaddeus 1985 |
| Wide-Latitude Survey of the First Galactic Quadrant | Dame and Thaddeus 1985, Grenier *et al.* 1989 |
| Supernova Remnants in the Outer Galaxy | Huang and Thaddeus 1985, 1986 |
| The Carina Arm | Cohen *et al.* 1985; Grabelsky *et al.* 1988 |
| Southern High-Latitude Clouds | Keto and Myers 1986 |
| Dark Nebulae in Perseus, Taurus, and Auriga | Ungerechts and Thaddeus 1987 |
| Entire Milky Way (composite survey) | Dame *et al.* 1987 |
| Region of the Galactic Center | Bitran 1987 |
| IR Cirrus in Ursa Major | de Vries, Heithausen, and Thaddeus 1987 |
| Wide-Latitude Survey of the Third and Fourth Galactic Quadrants | May *et al.* 1988; Nyman 1990 |
| Deep Survey of the Fourth Galactic Quadrant | Bronfman *et al.* 1988 |
| Large Magellanic Cloud | Cohen *et al.* 1988 |
| Small Magellanic Cloud | Rubio *et al.* 1989 |
| Southern Coalsack | Nyman, Bronfman, and Thaddeus 1989 |
| Thirty-Four Galactic Clusters | Leisawitz *et al.* 1989 |
| Dark Clouds in Ophiuchus | de Geus *et al.* 1990 |
| The Polaris Flare Near the North Celestial Pole | Heithausen and Thaddeus 1990 |

### a) Giant Molecular Clouds

Approximately half the hydrogen gas in the Galaxy is in molecular form. The $H_2$ gas is more highly concentrated toward the inner Galaxy than the atomic hydrogen and most dense in a "molecular ring" between four and eight kpc in galactocentric radius. Its half-thickness with respect to distance above and below the plane, approximately 87 pc, in contrast to that of atomic H, is close to that of the Population I stars, underscoring the intimate relationship between molecular clouds and regions of star formation. Molecular gas is usually found in extensive complexes, called Giant Molecular Clouds (GMCs), which are clumpy in nature, exhibit power-law relations among size, mass, and velocity dispersion and appear to be in approximate virial equilibrium. The mass spectrum of these giant objects is fairly "flat," with most of the mass residing in the largest concentrations. On the basis of analyses of GMCs extending from the molecular ring at R~4 kpc to the Perseus Arm beyond the solar circle, the mass cutoff for giant molecular clouds at the high end is apparently between $5 \times 10^6$ and $10 \times 10^6$ $M_\odot$, with 50-70% of the total mass in objects more massive than $10^6$ $M_\odot$. Bronfman et al. (1988) derived from a joint analysis of our northern and southern surveys a total molecular mass of $1.2 \times 10^9$ $M_\odot$ between R=2 kpc and the solar circle.

### b) "Local" Molecular Clouds and Dark Nebulae

On the basis of our surveys, the bulk of the molecular gas within about 1 kpc of the Sun has been partitioned into discrete clouds, most of them associated with dark nebulae, opaque "rifts," stellar associations, and other tracers of Population I observed in optical studies of the nearby interstellar medium (Fig. 1). As had been suspected previously from the distribution of dark nebulae, molecular clouds near the Sun are much more common in the northern Milky Way than in the southern: the molecular mass within 1 kpc is 4 times greater in the first and second Galactic quadrants than in the third and fourth. Table 2 summarizes the physical parameters characterizing the local molecular gas. Although conspicuous nearby dark nebulae such as the Taurus and Ophiucus dark clouds and the Great Rift in Cygnus are modest in size and mass relative to the GMCs, owing to their proximity to the solar system they are of considerable interest because star formation, particularly that of late-type stars, can be studied there in great detail.

### TABLE 2

#### MOLECULAR GAS WITHIN 1 KPC

| | |
|---|---|
| rms $z$ dispersion | 74 pc |
| Layer thickness (HWHM) | 87 pc |
| Mass | $4.0 \times 10^6$ $M_\odot$ |
| Surface density | $1.3$ $M_\odot$ $pc^{-2}$ |
| Midplane density | $0.0068$ $M_\odot$ $pc^{-3}$ $0.10$ $H_2$ $cm^{-3}$ |
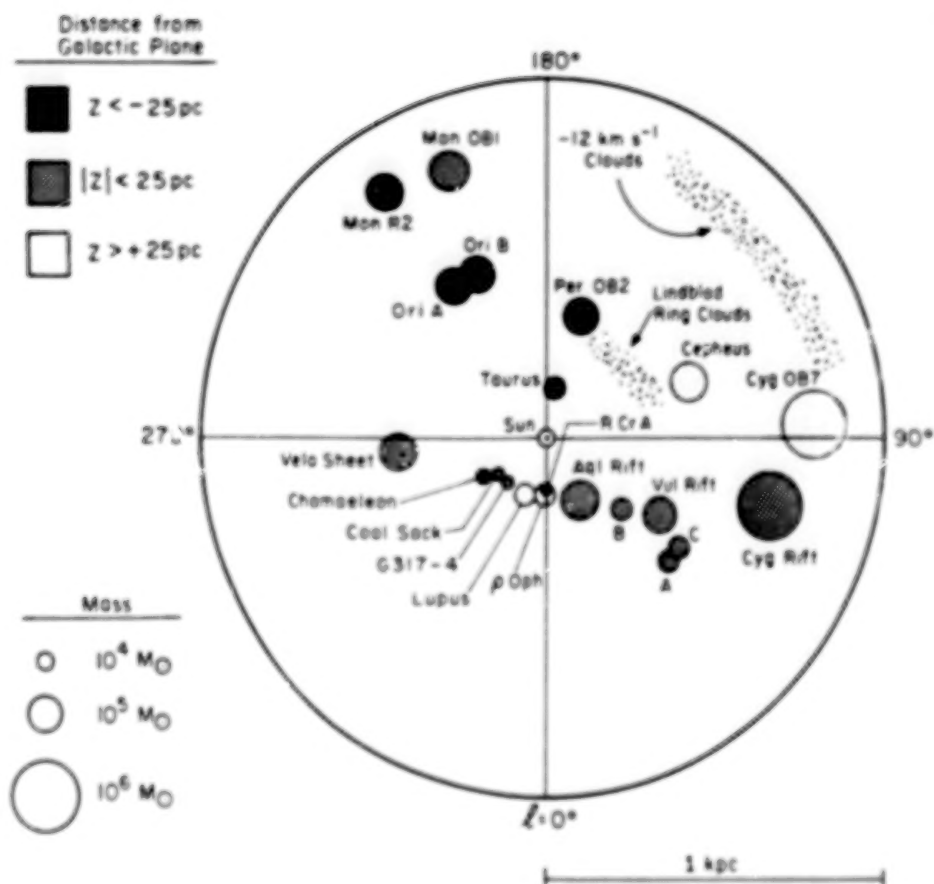
**FIGURE 1.** The distribution in the Galactic plane of molecular clouds within 1 kpc of the Sun (Dame *et al.* 1987). The diameters of the circles are proportional to cloud size; shading indicates distance from the Galactic plane.

### c) Galactic Structure

From an intercomparison of our low-resolution CO survey, 21 cm atomic hydrogen surveys, and the Galactic diffuse high-energy γ-ray emission observed by COS-B, the important CO-to-$H_2$ conversion ratio, X (the ratio of velocity-integrated CO line emission, $W_{CO}$, to $H_2$ column density), required to derive the mass of molecular clouds, has been calibrated over much of the Galaxy. The result of this analysis (Strong *et al.* 1988), $N(H_2)/W_{CO} = 2.3\pm0.3 \times 10^{20}$ molecules cm$^{-2}$ (K km s$^{-1}$)$^{-1}$, is in good agreement with that derived under different, independent assumptions by two other methods, star counts and the virial theorem.

Our northern and southern surveys demonstrated that molecular clouds delineate prominent spiral features in the Galaxy. The Perseus and Carina arms in the outer Galaxy, for example, are particularly well defined in molecular clouds, and, in the local neighborhood,

9

nearly all the clouds within 1 kpc in the first and fourth quadrants apparently lie on a fairly straight ridge more than 1 kpc long which may trace the inner edge of a Local spiral arm.

Although results for the inner Galaxy are much less satisfactory, owing to the well-known problem of the two-fold kinematic distance ambiguity for clouds within the solar circle, we and others have shown that the Sagittarius Arm in the first Galactic quadrant is fairly well defined by large clouds (Dame *et al.* 1986; Clemens *et al.* 1988; Solomon and Rivolo 1989) and that it may join the Carina Arm in the fourth quadrant to constitute a single feature at a pitch angle of about 10° extending nearly three-quarters of the way around the Galaxy (Grabelsky *et al.* 1988). No unambiguous model yet exists, however, for the distribution of the molecular clouds within the molecular ring about halfway to the Galactic center.

## III. PRESENT AND FUTURE WORK

The surveys listed in Table 1 represent a fairly complete inventory of the molecular gas associated with Population I objects in the Galaxy, but nearly all of them could be profitably extended in both resolution and sensitivity. A number of projects, described below, currently underway at the Center for Astrophysics, represent a logical continuation of these early low-resolution surveys.

## TABLE 3

### CURRENT CO OBSERVING PROJECTS — CFA 1.2 M TELESCOPE

| SURVEY | PRINCIPAL OBSERVER(S) |
|---|---|
| Cas A Region | H. Ungerechts, P. Umbanhowar |
| Cygnus X Region | H. O. Leung |
| Gem OB1/IC 443 Complex | J. G. Stacy |
| A First Quadrant Survey of Molecular Clouds in the Outer Arm | S. Digel |
| Diffuse, High-Latitude Molecular Clouds in the Second Quadrant | A. Heithausen |
| M31, Andromeda Galaxy | E. Koper, T. M. Dame |
| Selected Regions at High Latitude (GRO Survey) | J. G. Stacy |

## a) Individual Regions

Our composite low-resolution CO survey is very useful for identifying regions of the Galaxy for high-resolution study. Table 3 lists major observing projects now being undertaken at the CfA with the 1.2 m telescope, nearly all them being carried out at full resolution (1/8°) and high sensitivity; in its present configuration with a superconducting SIS receiver, the CfA instrument is the most sensitive in the world ($T_{SSB}$~60-70 K) at the CO frequency. Giant clouds associated with prominent star-forming regions dominate the list of current observing programs, particularly those, such as the Cas A and Gem OB1 complexes, which, although distant, are also visible optically, allowing detailed comparison of observations taken at many wavelengths. Among many general issues addressed by such studies are some of the most challenging in the fields of star formation, Galactic structure, and interstellar gas chemistry and dynamics: How do these huge concentrations of dense gas form, and how do they evolve? How long do they last? What is the efficiency of star formation? How does star formation depend on density and other parameters, and how destructive is it to the structure and integrity of the parent clouds? If star formation in the giant clouds represents a self-propagating conflagration, as some observations suggest, on what time scale does this process operate and what is the relative contribution to it of the two most likely sources of disruption, supernovae and winds from OB stars?

## b) Isotopic and Multiple Transition Studies

The validity of CO as a mass tracer of molecular clouds is being continually tested. In general, the optical thickness of the CO $1{\rightarrow}0$ line implies that only a fraction of the CO gas in a particular cloud is being observed. For determining masses, CO line saturation appears not to be a serious problem, due to the clumpiness of the gas within a molecular cloud, apparently extending down to the smallest scales observable. Yet observation of more optically thin isotopic species, such as $^{13}CO$ and $C^{18}O$, are highly desirable over a range of scales in order to test existing assumptions fully. Currently, our group is undertaking $^{13}CO$ measurements of several giant molecular clouds in the hope of shedding light on this longstanding issue.

Observations of higher rotational transitions of CO (e.g., $2{\rightarrow}1$ and $3{\rightarrow}2$) are also of interest. Are these largely degenerate with the $1{\rightarrow}0$ transition, or are they a significant new source of information about physical conditions within molecular clouds? We are now collaborating with several observatories (e.g., Bell Labs, University of Cologne) conducting millimeter and submillimeter observations relevant to such an investigation.

## c) High Latitude Studies

Aside from a few surveys that extend to intermediate Galactic latitudes in the direction of previously known star-forming regions, such as the Taurus and Ophiucus dark clouds, only very limited CO observations have been conducted away from the plane of the Galaxy. The IRAS satellite has detected extensive "cirrus" emission at 100 μm (Fig. 2) which suggests the existence of a fairly large amount of molecular gas at high latitudes (Désert *et al.* 1988). Recent work by our group which indicates that the total amount of molecular gas at high latitudes may be seriously underestimated (Heithausen and Thaddeus 1990, see Fig. 3) emphasizes the need for large, unbiased CO surveys comparable in extent to surveys of molecular clouds near the Galactic plane.
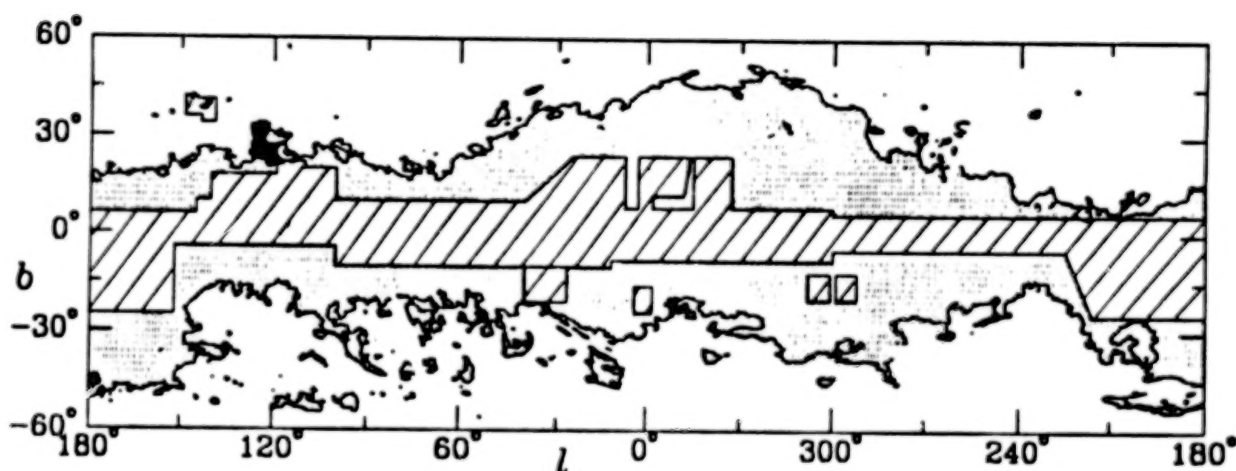
FIGURE 2. Area of most intense IRAS 100 μm emission (above 7 MJy sr$^{-1}$, in gray) compared with the regions surveyed in CO in the Galactic plane by Dame *et al.* 1987 (dashed area), adapted from Heithausen and Thaddeus 1990.

The CfA millimeter-wave group has undertaken several high-latitude surveys, primarily in the second quadrant of the Galaxy in the vicinity of the north celestial pole (Fig. 4), including (see Tables 1 and 3) investigations of the Cepheus and Polaris Flares and the Ursa Major and similar diffuse clouds possibly related to radio continuum Loop III in this direction ($l,b \sim 135°,35°$). Of particular note for this symposium is a project to map selected regions at high latitude for comparison with high-energy γ-ray observations to be conducted by the EGRET experiment aboard the Gamma Ray Observatory (GRO). Five $10° \times 10°$ fields extending from the Galactic plane toward the north Galactic pole, primarily in the direction of local minima in foreground Galactic material, will be mapped in CO at an angular resolution of $0.5$ degrees. This survey represents the largest fully sampled survey of CO emission at high latitude undertaken to date. The data will be used to place stringent quantitative limits on the amount of molecular material in the observed regions that may contribute to the high-energy γ-ray signal detectable by EGRET (Stacy *et al.* 1990; see § IVc below).
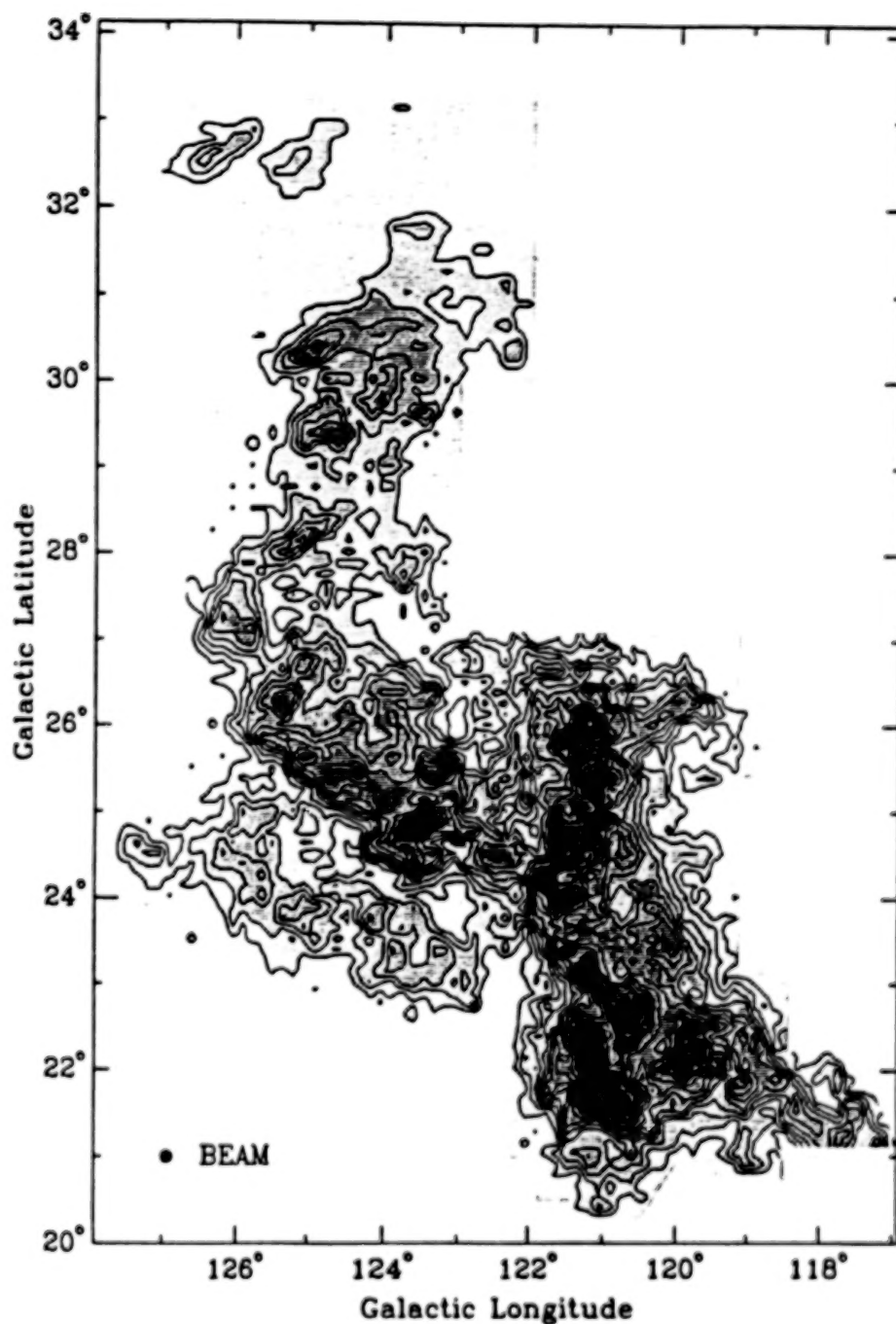
FIGURE 3. Map of velocity-integrated CO emission of the Polaris Flare in the vicinity of the north celestial pole, illustrating the extended and diffuse nature of some high-latitude molecular clouds. Contours range from 0.4 to 13.0 in steps of 0.8 K km s$^{-1}$, adapted from Heithausen and Thaddeus 1990.

# IV. ISSUES RELEVANT TO GRO/EGRET INVESTIGATION

Several areas are outlined below where high-energy γ-ray observations by the EGRET experiment aboard GRO will complement observations at radio wavelengths and may contribute to the resolution of longstanding issues in the study of the structure and content of the Galaxy.

## a) Galactic Structure

The strong correlation within the Galactic disk of diffuse, high-energy γ-ray emission and the large-scale distribution of interstellar matter revealed in radio surveys of the Galaxy is now firmly established, based on analyses of data obtained with both the U.S. SAS-2 and the European COS-B satellites (Hartman et al. 1979; Strong et al. 1988). Because diffuse Galactic γ-rays result from cosmic ray interactions with matter, photons, and magnetic fields in interstellar space, models of the diffuse Galactic γ-ray emission can provide insight into the Galactic cosmic-ray distribution and the overall energy balance of the Galaxy and how this equilibrium is achieved by a partition between cosmic-ray and magnetic-field energy densities and gravitational forces due to Galactic matter (Parker 1969). In anticipation of new, more sensitive γ-ray observations by the EGRET experiment aboard GRO, we are participating in an effort to model the diffuse Galactic γ radiation (Bertsch et al. 1990). A particular incentive for this work is the present availability of well-sampled, large-scale radio surveys of the Galaxy in both H I and CO (Weaver and Williams 1973; Burton 1985; and Kerr et al. 1986; Dame et al. 1987); the continuing analysis of the detailed distribution of molecular clouds in the inner Galaxy, in the first quadrant (Dame et al. 1986; Clemens et al. 1988; Solomon and Rivolo 1989) and the fourth quadrant (Bronfman et al. 1990); and the availability of comprehensive recombination-line (Lockman 1989) and near-infrared (Fazio et al. 1990) surveys which may help in resolving kinematic distance ambiguities for a large fraction of the clouds in the inner Galaxy. Further constraints on the CO-to-$H_2$ conversion factor may be a significant byproduct of such a study, with important consequences for mass estimates of the Galaxy. The greatly enhanced sensitivity and resolution of the EGRET γ-ray telescope, compared with previous experiments of its type, offer the prospect of progress on fundamental questions relating to the distribution, composition, spectrum, and origin of the Galactic cosmic-ray population.

## b) The Galactic Center

A notable anomaly to the fairly tight correlation between the diffuse Galactic γ-ray emission and the distribution of interstellar matter is toward the region of the Galactic center (R≤1.5 kpc), where the γ-ray flux is deficient by nearly an order of magnitude (Blitz et al. 1985). A reexamination of this issue, using a more fully-sampled, wide-latitude CO survey of the Galactic center region (Bitran 1987) and the final COS-B database (Mayer-Hasselwander 1985), attributes the discrepancy between observed and predicted γ-ray emission toward the Galactic center, determined on the basis of mass estimates using the standard $N(H_2)/W_{CO}$ ratio, to a unique population of wide-line molecular clouds. Observations of greatly improved sensitivity and resolution made with the Gamma Ray Observatory should be capable of confirming the wide-line cloud origin of the Galactic center γ-ray deficit and may address important issues related to the origin, evolution, and lifetime of these unique objects and, by extension, of the entire region of the Galactic center (Stacy et al. 1987, 1989).

## c) High Latitude and Extragalactic Studies

The γ-ray analyses in the Galactic plane will be extended to intermediate and high Galactic latitudes to isolate the portion of the high-latitude emission believed of extragalactic origin (Fichtel et al. 1978). One challenging problem facing γ-ray astrophysics is the accurate decomposition of the diffuse, high-energy γ-ray emission ($E_\gamma \geq 30$ MeV) into its two fundamental components: the "local," diffuse emission due primarily to nuclear collisions in interstellar space in our own Galaxy and the cosmic, diffuse γ-ray background radiation. The increased sensitivity and resolution of the high-energy EGRET telescope aboard GRO offer the

exciting prospect of decomposition of the diffuse, γ-ray background into its Galactic and extragalactic components. The high-latitude CO observing program described in § IIIc (see Fig. 4), which is of sufficient sensitivity to account for the presence of all molecular gas likely to contribute to a γ-ray signal detectable by EGRET, will be important to this effort, providing crucial information not now available on the distribution and column density of interstellar molecular hydrogen at high Galactic latitudes.
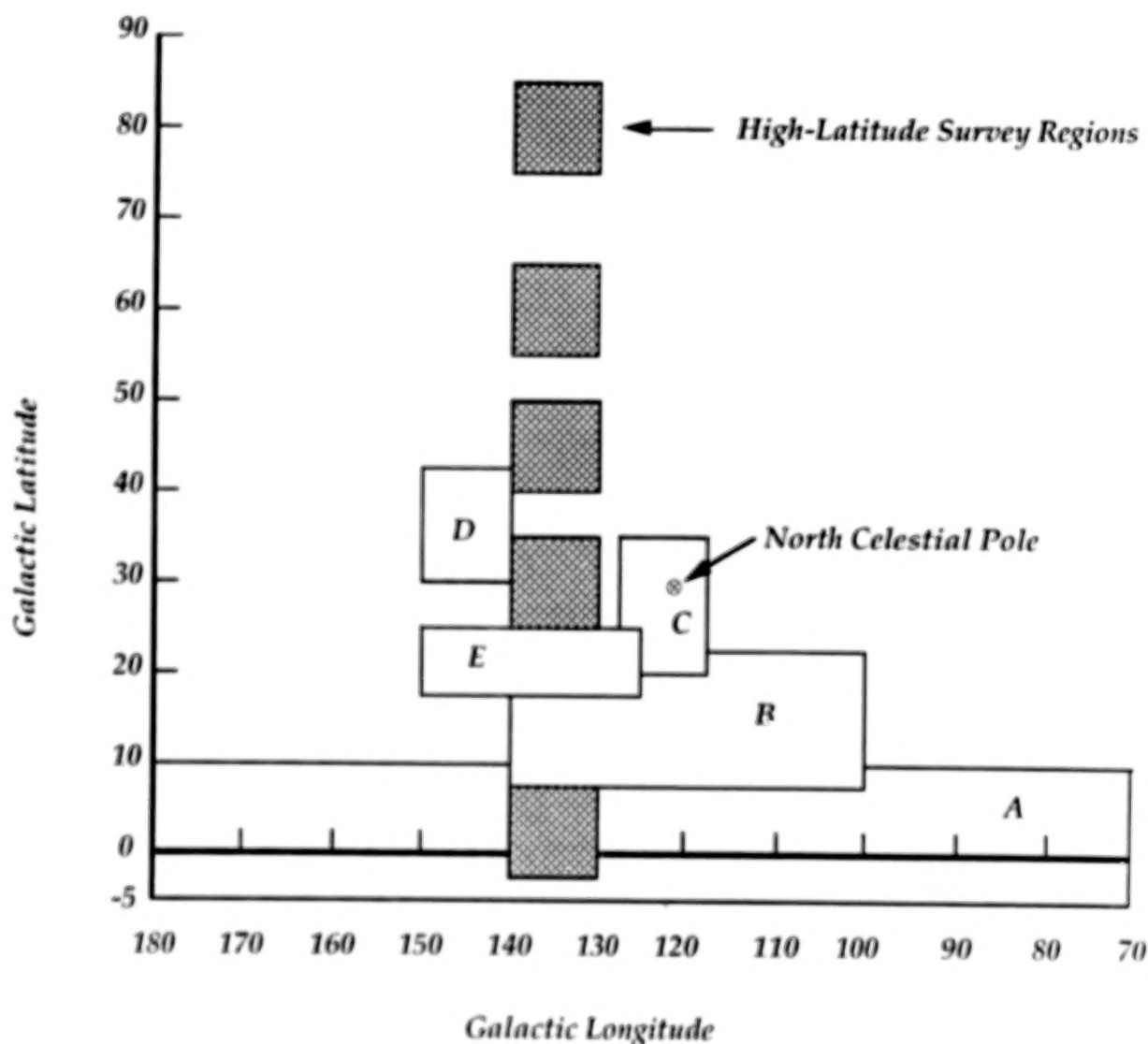


FIGURE 4. Schematic of high-latitude CO survey regions (dark-shaded squares) intended for comparison with GRO observations and their relation to areas previously observed in the second quadrant of the Galaxy with the CfA 1.2 m radio telescope. *Region A*: Part of the CO survey of the Galactic plane by Dame *et al*. 1987. *Region B*: Survey by Grenier *et al*. 1989. *Region C*: Survey by Heithausen and Thaddeus 1990. *Region D*: Survey by de Vries *et al*. 1987. *Region E*: Survey in progress by Heithausen 1990. The position of the north celestial pole is indicated by a ⊗ symbol.

Finally, the possibility of detecting γ-ray emission with the EGRET telescope from galaxies in the Local Group, in particular the Magellanic Clouds and M31 (Özel and Fichtel 1988), is now quite realistic. Comparison of γ-ray observations with atomic and molecular surveys of these objects (e.g., Cram *et al.* 1980; Brinks and Shane 1984; Rohlfs *et al.* 1984; Cohen *et al.* 1988) will afford a direct measure of cosmic-ray densities in galaxies beyond the Milky Way and may provide an important independent determination of the CO-to-$H_2$ conversion factor in galaxies with markedly different distributions of interstellar gas.

## REFERENCES

Bertsch, D. L. *et al.* 1990, *Proc. 21st International Cosmic Ray Conference (Adelaide)*, **1**, 154.

Bitran, M.E. 1987, Ph. D. dissertation, University of Florida.

Blitz, L., and Thaddeus, P. 1980, *Astrophys. J.*, **241**, 676.

Blitz, L., Bloemen, J. B. G. M., Hermsen, W., and Bania, T.M. 1985, *Astron. Astrophys.*, **143**, 267.

Brinks, E., and Shane, W. W. 1984, *Astron. Astrophys. Suppl. Ser.*, **55**, 179.

Bronfman, L. *et al.* 1988, *Astrophys. J.*, **324**, 248.

Bronfman, L. *et al.* 1990, in preparation.

Burton, W. B. 1985, *Astron. Astrophys. Suppl. Ser.*, **62**, 365.

Cheung, A. C., *et al.* 1968, *Phys. Rev. Lett.*, **21**, 1701.

Cheung, A. C., *et al.* 1969, *Nature*, **221**, 917.

Clemens, D. P. *et al.* 1988, *Astrophys. J.*, **327**, 139.

Cohen, R. S., and Thaddeus, P. 1977, *Astrophys. J. (Letters)*, **217**, L155.

Cohen, R. S., Cong, H.-I., Dame, T. M., and Thaddeus, P. 1980, *Astrophys. J. (Letters)*, **239**, L53.

Cohen, R. S. *et al.* 1985, *Astrophys. J. (Letters)*, **290**, L15.

Cohen, R. S., Dame, T. M., and Thaddeus, P. 1986, *Astrophys. J. Suppl. Ser.*, **60**, 695.

Cohen, R. S. *et al.* 1988, *Astrophys. J. (Letters)*, **331**, L95.

Cong, H.-I. 1977, Ph. D. dissertation, Columbia University.

Cram, T. R., Roberts, M. S., and Whitehurst, R. N. 1980, *Astron. Astrophys. Suppl. Ser.*, **40**, 215.

Dame, T. M., and Thaddeus, P. 1985, *Astrophys. J.*, **297**, 751.

Dame, T. M. *et al.* 1986, *Astrophys. J.*, **305**, 892.

Dame, T. M. *et al.* 1987, *Astrophys. J.*, **322**, 706.

Désert, F. X., Bazell, D., and Boulanger, F. 1988, *Astrophys. J.*, **334**, 815.

Ewen, H. I., and Purcell, E. M. 1951, *Nature*, **168**, 356.

Fazio, G. G., Dame, T. M., and Kent, S. 1989, in *IAU Symposium 139, Galactic and Extragalactic Background Radiation – Optical, Ultraviolet, and Infrared Components* (Heidelberg, FRG), in press.

Fichtel, C. E. *et al.* 1978, *Astrophys. J.*, **222**, 833.

de Geus, E. J., Bronfman, L., and Thaddeus, P. 1990, *Astron. Astrophys.*, in press.

Gordon, M. A., and Burton, W. B. 1976, *Astrophys. J.*, **208**, 346.

Grabelsky, D. A. *et al.* 1987, *Astrophys. J.*, **315**, 122.

Grabelsky, D. A. *et al.* 1988, *Astrophys. J.*, **331**, 181.

Grenier, I. A. *et al.* 1989, *Astrophys. J.*, **347**, 231.

Hartman, R.C., Kniffen, D.A., Thompson, D.J., Fichtel, C.E., Ögelman, H.B., Tümer, T., and Özel, M.E. 1979, *Astrophys. J.*, **230**, 597.

Heithausen, A., and Thaddeus, P. 1990, *Astrophys. J. (Letters)*, in press.

Huang, Y.-L., and Thaddeus, P. 1985, *Astrophys. J. (Letters)*, **295**, L13.

Huang, Y.-L., and Thaddeus, P. 1986, *Astrophys. J.*, **309**, 804.

Kerr, F. J., Hindman, J. V., and Gum, C. S. 1959, *Australian J. Phys.*, **12**, 270.

Kerr, F. J. *et al.* 1986, *Astron. Astrophys. Suppl. Ser.*, **66**, 373.

Keto, E. R., and Myers, P. C. 1986, *Astrophys. J.*, **304**, 466.

Kutner, M. L., Tucker, K. D., Chin, G., and Thaddeus, P. 1977, *Astrophys. J.*, **215**, 521.

Lada, C., Elmegreen, B., Cong, H.-I., and Thaddeus, P. 1978, *Astrophys. J. (Letters)*, **226**, L39.

Leisawitz, D., Bash, F. N., and Thaddeus, P. 1989, *Astrophys. J. Suppl. Ser.*, **70**, 731.

Lockman, F. J. 1989, *Astrophys. J. Suppl. Ser.*, **71**, 469.

Maddalena, R. J., and Thaddeus, P. 1985, *Astrophys. J.*, **294**, 231.

Maddalena, R. J., Morris, M., Moscowitz, J., and Thaddeus, P. 1986, *Astrophys. J.*, **303**, 375.

May, J., Murphy, D. C., and Thaddeus, P. 1988, *Astron. Astrophys. Suppl. Ser.*, **73**, 51.

Mayer-Hasselwander, H.A. 1985, *Explanatory Supplement to the COS-B Data Base.*

Muller, C. A., and Westerhout, G. 1957, *Bull. Astr. Inst. Netherlands*, **13**, 151.

Nyman, L. Å., Bronfman, L., and Thaddeus, P. 1989, *Astron. Astrophys.*, **216**, 185.

Nyman, L. Å. 1990, in preparation.

Özel, M. E., and Fichtel, C. E. 1988, *Astrophys. J.*, **335**, 135.

Palmer, P. *et al.* 1969, *Astrophys. J. (Letters)*, **156**, L147.

Parker, E. N. 1969, *Space Science Reviews*, **9**, 651.

Rohlfs, K., Kreitschmann, J., Siegman, B. C., and Feitzinger, J. V. 1984, *Astron. Astrophys.*, **137**, 343.

Rubio, M., and Garay, G. 1989, in *The Physics and Chemistry of Interstellar Molecular Clouds*, eds. G. Winnewisser and J. T. Armstrong (Springer-Verlag: New York), 270.

Scoville, N. Z., and Solomon, P. M. 1975, *Astrophys. J. (Letters)*, **199**, L105.

Solomon, P. M. and Rivolo, A. R. 1989, *Astrophys. J.*, **339**, 919.

Stacy, J. G., Dame, T. M., and Thaddeus, P. 1987, *Proc. 20$^{th}$ International Cosmic Ray Conference (Moscow)*, **1**, 117.

Stacy, J. G., Dame, T. M., Thaddeus, P., and Bitran, M. E. 1989, *Proc. Gamma Ray Observatory Science Workshop*, ed. W. N. Johnson (NASA: Washington, D. C.), 4-67.

Stacy, J. G. *et al.* 1990, *Proc. 21$^{st}$ International Cosmic Ray Conference (Adelaide)*, **1**, 253.

Strong, A.W., Bloemen, J.B.G.M., Dame, T.M., Grenier, I.A., Hermsen, W., Lebrun, F., Nyman, L-Å., Pollock, A.M.T., and Thaddeus, P. 1988, *Astron. Astrophys.*, **207**, 1.

Ungerechts, H., and Thaddeus, P. 1987, *Astrophys. J. Suppl. Ser.*, **63**, 645.

de Vries, H. W., Heithausen, A., and Thaddeus, P. 1987, *Astrophys. J.*, **319**, 723.

Weaver, H. F., and Williams, D. R. W. 1973, *Astron. Astrophys. Suppl. Ser.*, **8**, 1.

Weinreb, S. *et al.* 1963, *Nature*, **200**, 829.

Wilson, R. W., Jefferts, K. B., and Penzias, A. A. 1970, *Astrophys. J. (Letters)*, **161**, L43.

Winnewisser, G., and Herbst, E. 1987, *Topics in Current Chemistry*, **139**, 121.

# DISCUSSION

*Gottfried Kanbach:*

What is your opinion on the problem of optical depth of $^{12}CO$ in clouds and on the ratio of $^{12}CO/^{13}CO$ intensity?

*Pat Thaddeus:*

The optical depth of $^{12}CO$ in the giant clouds is undoubtedly substantial, since the integrated line intensity ratio $W_{12}/W_{13}$ is approximately 5, while the isotopic ratio is probably not greatly different from the terrestrial ratio 89. It is the remarkable empirical constancy of this ratio when averaged over significant parts of molecular clouds which allows $W_{12}$ to serve as a mass tracer. Just why this should be so in terms of radiation transfer is another matter -- it is not well understood. The constancy of $W_{12}/W_{13}$ is plausibly a result of the very complex fractal structure of the clouds -- an indication that they contain many small unresolved elements which do not occult one another greatly along the line of sight or in radial velocity.

*Hermann Rothermal:*

Is there any knowledge about magnetic fields in molecular clouds since this will have implications on the gamma-ray calibration of the $CO/H_2$ empirical factor.

*Pat Thaddeus:*

This is one of the most serious gaps in our knowledge of molecular clouds, and the prospect of filling it is not good. The Zeeman effect of CO and other diamagnetic molecules is far too small to measure, and the molecules with large moments (e.g., radicals like OH, SO, and CN) do not have very strong lines in molecular clouds. Heiler and collaborators have made heroic efforts to make Zeeman measurements with HI in dense regions, with some success, but at only a few locations. The magnitude and direction of the general field in giant clouds is almost entirely unknown. Many clouds though have a pronounced filamentary structure which one suspects is magnetic in origin.

# The Diffuse Galactic Gamma Ray Emission

David L. Bertsch
NASA/Goddard Space Flight Center, Greenbelt, MD 20771

## ABSTRACT

The EGRET detector will provide a much more detailed view of the diffuse galactic gamma ray intensity in terms of higher resolution, greater statistical significance, and broader energy range than earlier missions. These observations will furnish insight into a number of very important questions related to the dynamics and structure of the Galaxy. A diffuse emission model is being developed that incorporates the latest information on matter distribution and source functions. In addition, it is tailored to the EGRET instrument response functions. The analysis code of the model maintains flexibility to accommodate the quality of the data that is anticipated. The discussion here focuses on the issues of the distributions of matter, cosmic rays, and radiation fields, and on the important source functions that enter into the model calculation of diffuse emission. A subsequent paper in this conference reports the details of the analysis and preliminary results.

## INTRODUCTION

When the sky is viewed in the high energy domain of gamma rays, the most prominent feature that is observed is a narrow band of emission that extends along the entire galactic plane. The intensity within the band has a broad maximum in a region of about 100 degrees in longitude, located about the galactic center. This emission feature was first detected by OSO-3 (Kraushaar et al., 1972), and it was been observed extensively in the subsequent SAS-2 (Fichtel et al., 1975; Hartman et al., 1979) and COS-B (Mayer-Hasselwander et al., 1980 and 1982) missions. Figure 1 shows the results from COS-B. The longitude distribution, shows a remarkable amount of structure, and in latitude it falls rapidly with a width of only a few degrees. Bignami and Fichtel (1974) and Bignami et al. (1975) using the SAS-2 data observed that the intensity was enhanced along longitudes associated with tangent directions of spiral arm features. Subsequent analysis of both the SAS-2 (Fichtel et

al., 1975 and Hartman et al., 1979) and COS-B (Mayer-Hassel-wander et al., 1982) data confirmed this correlation.
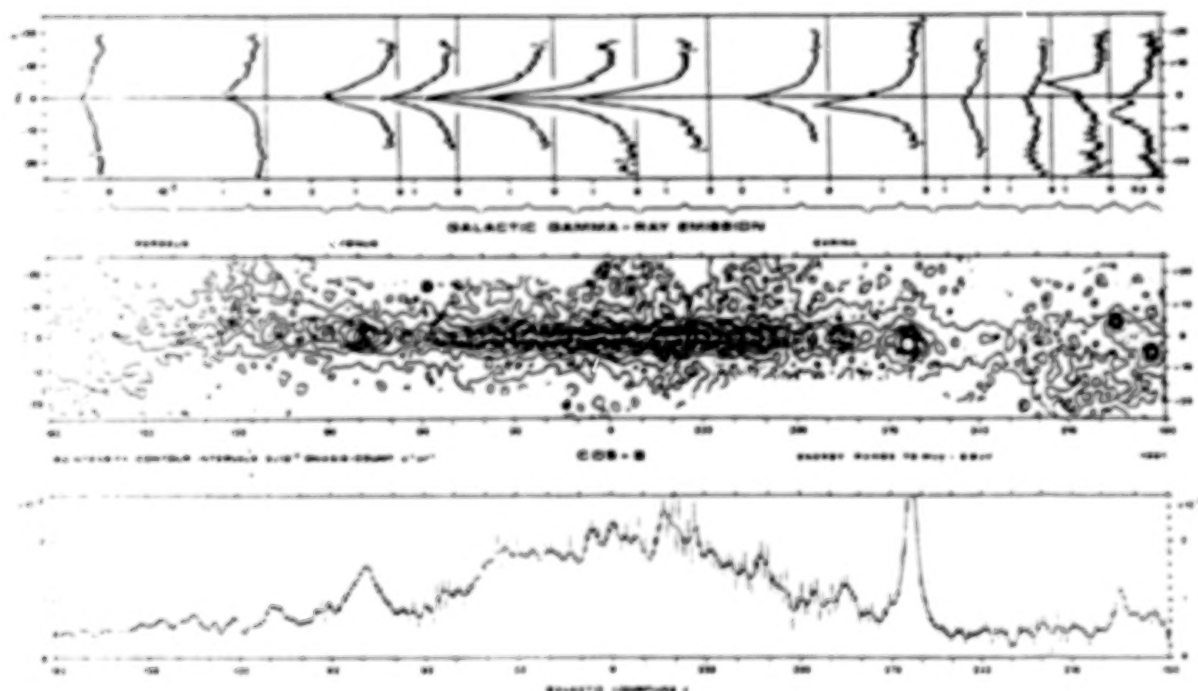


Figure 1. Galactic gamma ray emission observed by COS-B. In the latitude profile, the brackets indicate the interval of longitude used. The contour amp and the longitude profile show on-axis counts per steradian. Contours are in steps of $3 \times 10^{-3}$ per steradian. For the longitude profile, data are averaged over +/-5 degrees. This figure is from Mayer-Hasselwander et al. (1982).

Evidence based on the spatial correlation of intensity with galactic matter distribution, and on the energy spectrum suggests that the emission arises from cosmic ray interactions between interstellar matter and low energy photons. A distribution of point sources that cannot be resolved by the angular response of these two instruments could contribute to the total emission. The uniformity of the energy distribution, and the ability of the diffuse emission processes to explain the gamma ray luminosity and its distribution, however, argues against unresolved sources being a major contributor.

The concert that cosmic ray-matter interactions are the source of the diffuse emission has led to a several modeling efforts wi .m of comparing the observed distribution with the calculated .e. (See, for example, Bignami and Fichtel, 1974; Paul, Casse, and Cesarsky, 1974 and 1976; Schickeiser and Thielheim, 1974; Puget, Stecker, and Bredekamp, 1976; Hartman et al., 1979; Kniffen and Fichtel, 1981; Fichtel and Kniffen, 1984;

Blat et al., 1985; Harding and Stecker, 1985; Bloemen et al., 1986; and Strong et al., 1988 and recent surveys by Fichtel, 1989 and Bloemen, 1989.) The models generally incorporate information on the galactic matter distribution obtained from radio surveys. In addition, the optical and infrared photon fields are assumed, based on stellar populations and infrared surveys. No evidence is available for the cosmic ray distribution, and it is one of the goals of these calculations to identify constraints on the distribution based on the observed gamma ray emission. Three distinct approaches have been followed. The first assumes a distribution of cosmic rays that is coupled in some degree to the matter by magnetic fields. The distribution of gamma rays is then computed and compared to the observations. The process is iterated with different assumptions on the degree and scale size of the coupling until the best fit to the data is obtained. This is the approach taken by the SAS-2 group (e.g., Fichtel and Kniffen, 1984). Another approach employed by Harding and Stecker (1985) uses an unfolding technique to infer the galactic radial dependence of cosmic rays. The third approach used by the COS-B collaboration (e.g., Bloeman et al., 1986) uses a maximum likelihood analysis to determine the cosmic ray intensity in a series of galactocentric bins.

This paper provides a general discussion of the matter, cosmic ray, and radiation field distributions and the source functions for interactions between cosmic rays, matter, and photons. These are the essential ingredients of a model that is under development that will serve in interpreting the EGRET data. More specific details of the calculation and early results from the model are given by Sreekumar (1990) (this conference).

## DIFFUSE EMISSION MODEL FOR EGRET ANALYSIS

During the first 15 months of the GRO mission, EGRET will conduct an all-sky survey. The galactic plane region will be one of the priority observations during this time. The increase in sensitivity of EGRET as compared to SAS-2 and COS-B by over an order of magnitude, together with the improved angular and energy resolution, and the significantly greater energy range will greatly improve knowledge of the gamma ray intensity and distribution in both longitude and latitude.

In anticipation of these results, a new model is being developed as a collaboration between members of the EGRET team and radio astronomers at the Center for Astrophysics. Preliminary results of this work have been reported previously (Bertsch et al., 1990a,b). The new model incorporates the most up-to-date information on the matter distribution from radio survey data. Recent work on interstellar electron energy spectrum is included, as is a refined production spectrum from nucleon interactions. To maintain the greatest flexibility in using trial cosmic ray distributions, the first of the three approaches discussed above is followed, namely, to assume a

21

distribution for cosmic rays, calculate the diffuse emission, convolve the line of sight intensity with the point spread function and energy resolution of EGRET to produce a distribution comparable with the one the instrument produces.

The goals of the study are to provide insight into the cosmic ray distribution, and the degree to which it couples to the matter. Further, since cosmic rays interact equally well with atomic and molecular hydrogen, the model is expected to help to understand the normalization between the atomic and molecular components. At the present time, molecular hydrogen is indirectly inferred from observations of CO. As will be seen in later sections, the source functions of electrons and nuclei have a very different energy dependence, and consequently, the model can be used with observations of the gamma ray energy spectrum as a function of longitude and latitude to study the ratio of cosmic ray electrons and nuclei as a function of location in the galaxy. Also, the observed latitude dependence of the gamma rays might be used to infer differences between the scale height of matter and the low energy photon radiation fields using the model. Finally, the model will provide a means of estimating background in searching for sources and evaluating their statistical significance.

## GALACTIC MATTER DISTRIBUTION

Galactic matter is present in a wide range of forms that include ions, atoms, molecules, and dust grains. The most abundant constituent is atomic and molecular hydrogen, together accounting for 90% of the total, and helium making up nearly all of the rest. The matter is known to be distributed in a thin disk of about 18 Kpc in radius. Atomic hydrogen has a scale height of about 120 pc, while molecular hydrogen is only about 50 pc. Molecular hydrogen appears to dominate in the inner Galaxy, and in the outer Galaxy, atomic hydrogen is more abundant. In addition, the matter distribution is non-uniform with concentrations in spiral arms and molecular clouds. The average density in the plane is about 1 $cm^{-3}$.

Observations from several surveys were joined into a uniform grid to serve as the basis of the current model. For the atomic hydrogen in the latitude interval from +10 to -10 degrees, the surveys of Weaver and Williams (1973), Kerr et al. (1986), and Burton and Liszt (1983) and Burton (1985) are used. The grid resolution is 0.5 degree in longitude and 0.25 degree in latitude, except for the galactic center region (longitude - 10 to 10 degrees) where a one degree spacing in latitude and longitude is used. The molecular hydrogen map is based on several radio surveys of the 2.6 mm line of $^{12}CO$ assembled by Dame et al. (1987). It covers the entire plane in 0.5 degree bins, typically between -10 and 10 degrees of latitude, but with larger excursions in certain locations. The conversion from the CO antenna temperature to molecular hydrogen density is not well established. Because of the differences in the spatial

distribution of atomic and molecular hydrogen, it is possible
that observations together with the model predictions can deter-
mine the normalization. This is another one of the goals of
this calculation. Presently, the analysis is using the value
$2.3 \times 10^{20}$ mol cm$^{-2}$ (K km s$^{-1}$).

The radio maps represent line of sight column densities of
matter as a function of recessional velocity and position. The
galactic rotation curve of Burton and Gordon (1978) is used to
convert from radial velocity to radial distance from the center
of the galaxy. For radii less than that of the sun (taken to be
10 Kpc), the line-of-sight intersects a circle at a given radius
at two points, and at both points, the recessional velocity is
the same. Hence, there is a two-fold ambiguity in the conver-
sion to radius for R < 10 Kpc. This can occur in the first and
fourth quadrants only. When axially symmetric cosmic ray dis-
tributions are used, or when the intensity is proportional to
matter, the ambiguity is of no consequence. Currently, there is
no clear method for resolving the ambiguity. Some guidance can
be obtained from mapping giant molecular clouds whose distance
can be estimated using related HII regions and OB associations.
At present, only about 18% of the molecular hydrogen could be
accounted for in this manner in a study made for the first
galactic quadrant (Dame et al., 1987). Until there is a better
grasp on this problem, it will be necessary to assume in the
model some distribution between the two points of ambiguity. An
equal division is being used at this time.

## COSMIC RAY DISTRIBUTION AND INTENSITY

Protons constitute 90% of the nuclear component of cosmic
rays while helium makes up nearly all of the rest. The electron
component is only about 1% as numerous as nucleons. Evidence
based on the cosmic ray lifetime of somewhat over $10^7$ years de-
duced from the composition of unstable secondaries such as Be$^7$,
together with the average path length of about 4 g cm$^{-2}$ indi-
cated by the abundance of light isotopes, suggest that the
average density traversed by cosmic rays is about 0.1 g cm$^{-2}$
which is only about 10% of the matter density in the plane.
Consequently, they must spend most of their time outside the
plane. In addition, the non-thermal radio continuum, presumably
from electron synchrotron emission in galactic magnetic fields
suggests a scale height of 750 pc from the central plane. The
assumption that the magnetic field and electrons and protons all
have about the same dependence on distance from the plane,
yields a estimate of 1 Kpc for the scale height. This is con-
sistent with the mean matter traversed.

As mentioned above, the distribution of cosmic rays in the
galactic plane is not known from observations. Theoretical
arguments, however, can be made to suggest that the cosmic rays
are coupled at some scale size to the matter through the mag-
netic fields. Cosmic rays are thought to be primarily of galac-
tic origin since their mean lifetime is only about $10^7$ years,

and moreover if they were not, inverse Compton interactions of electrons with the blackbody background would seriously degrade the electron spectrum in the lifetime of the Galaxy. The gravitational attraction of matter in the plane is the only force that constrains the expansive pressure of the cosmic rays and magnetic field. Locally, the energy density of cosmic rays, magnetic field, and the motion of matter are all about 1 eV $cm^{-3}$. This energy density is estimated to be near the maximum expansive pressure that can be contained by the gravitational attraction. In other words, a state of near equilibrium between cosmic rays, magnetic fields, and matter exists. If it is assumed that the conditions in the solar vicinity are typical of the Galaxy as a whole, then the cosmic ray density throughout the Galaxy must be nearly as large as can be contained by the matter, and the cosmic rays are constrained or tied to the matter by closed magnetic field lines.

Based on these arguments, it is expected that the cosmic ray density is correlated with matter density for size scales greater than some threshold value. The size scale, and coupling strength remain to be determined by observations. The coupling scale on the order of spiral arm widths, 0.1 to 1.0 Kpc, have been suggested in earlier models, especially those based on the SAS-2 data (Fichtel and Kniffen,1984).

## GALACTIC PHOTON DISTRIBUTION

Inverse Compton collisions between cosmic ray electrons and low energy photons provides a mechanism for diffuse gamma ray production. Three different radiation fields have been found to be important: blackbody, starlight in the wavelength region near the visible, and the infrared. The spatial distribution of blackbody is of course uniform.

Regarding the interstellar radiation field, Kniffen and Fichtel (1981) assume the emissivity follows the stellar disc population distribution of Bahcall and Soneira (1980), and they normalize the distribution to the local value. Bloemen (1985) used a model developed by Mathis et al. (1983) which gives somewhat lower values. More recently, Chi et al. (1989) develop an interstellar radiation field model also based on Mathis et al. (1983) which is significantly more intense, and has a higher scale height from the plane.

The infrared distribution used by Kniffen and Fichtel (1981) is based on an unfolding of a galactic plane survey by Boisse et al. (1981). The Bloemen (1985) model used results of Mathis et al. (1983) also in the infrared and obtained a significantly lower intensity. Chi et al. (1989) arrive at values similar to Bloemen.

In summary, there is considerable divergence in the intensity and distribution of the interstellar and infrared photon fields. Fortunately, the contribution from inverse Compton scattering is less significant (~10% in the plane) than for the cosmic ray matter interactions. However, since cosmic rays and

perhaps the photon fields have a higher scale height than matter, the Compton process is expected to become more important as distance from the plane increases. At the present stage of development, the model under discussion here does not include the contributions from inverse Compton. After further study of the problem, this source will also be incorporated.

## GALACTIC DIFFUSE EMISSION PROCESS

The previous sections have discussed the basic ingredients for the interactions that produce gamma rays in the interstellar medium. Among the interactions that can occur, the three that are dominant, and will eventually be a part of the model, include nuclear interactions between cosmic rays and matter, bremsstrahlung collisions between electrons and matter, and inverse Compton scattering between electrons and low energy photons. The model does not include synchrotron emission from electrons in the magnetic field as this is estimated to have a negligible contribution. In addition, line emission from dust and grains that are excited by cosmic ray collisions and contributions from unresolved point sources are not intended to be a part of the model.

Gamma rays are produced in collisions of cosmic rays and matter through the production of secondary pions which in turn decay. Neutral pions decay directly usually into two gamma rays, and positive pions decay into positrons that in turn may annihilate near rest to produce a 0.511 Mev line. Stecker (1970,1979) developed a model which was subsequently refined by Dermer (1986) that describes the production of gamma rays by cosmic rays through neutral pion decay. The differential energy spectrum of the production function per atom of interstellar material is shown in figure 2. Notice that the spectrum has a maximum at the half the rest mass of the neutral pion, 68 MeV. This function has been parameterized for incorporation into the model as follows:

For 10 MeV < E < 1.5 GeV,

$$Q_n(E) = alog[-25.58-2.36(logE)-1.04(\log E)^2] \; (cm^3 \; s \; GeV)^{-1}$$

For 1.5 GeV < E < 7 GeV,

$$Q_n(E) = 3.2 \times 10\text{-}27 \; E^{-1.5} \quad (cm^3 \; s \; GeV)^{-1}$$

For 7 GeV < E < 40 GeV

$$Q_n(E) = 4.6 \times 10\text{-}26 \; E^{-2.86} \quad (cm^3 \; s \; GeV)^{-1}.$$

Electrons also interact with matter to produce gamma rays by the bremsstrahlung process. If the electron energy spectrum is a power law, the gamma rays distribution will have the same power law dependence on energy. The interaction is well understood, but considerable uncertainty exists in the electron

spectrum for energies below about 5 GeV due to the influence of solar modulation. Fichtel, Ozel, and Stone (1990) estimated the electron spectrum based on gamma ray observations at energies below the maximum in the nucleon source function (See figure 2.). In this regime, bremsstrahlung dominates. The spectrum they derive was found to tie smoothly to the observed electron spectrum above 10 GeV where modulation is not important. The spectrum from their analysis is shown plotted in figure 3. This spectrum together with the bremsstrahlung cross section results in bremsstrahlung source functions:

For 10 MeV < E < 5 GeV,

$$Q_e(E) = 4.4 \times 10^{-27} \, E^{-2.35} \quad (cm^3 \, s \, GeV)^{-1}$$

For 5 GeV < E < 40 GeV,

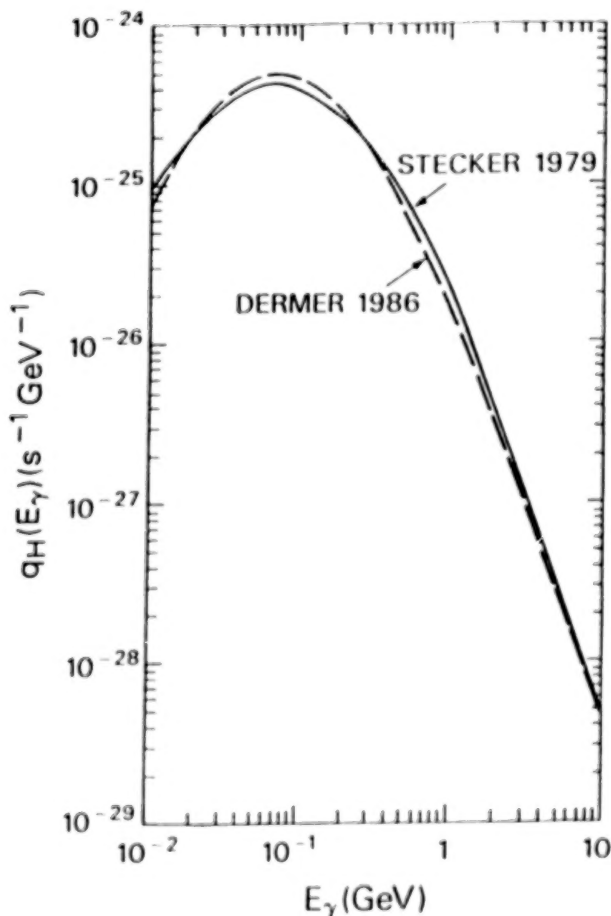$$Q_e(E) = 2.1 \times 10^{-26} \, E^{-3.3} \quad (cm^3 \, s \, GeV)^{-1}$$



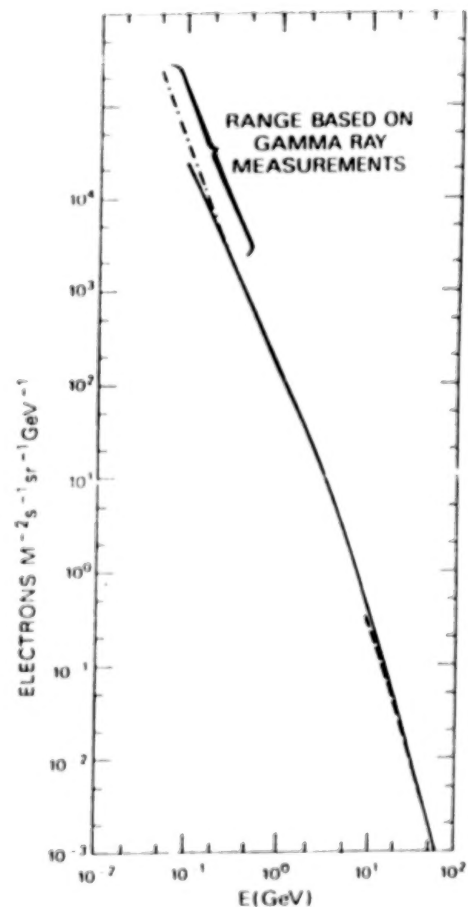Figure 2. Gamma ray production from cosmic ray nucleon interactions. From Stecker (1988).



Figure 3. Interstellar electron differential energy spectrum. From Fichtel, Ozel, and Stone (1990).

Gamma rays produced from the inverse Compton process have an energy that scales from the electron and photon energy according to

$$E_g = (E_e/m_e c^2)^2 \times E_{ph}$$

where $E_g$, $E_e$, and $E_{ph}$ are the gamma ray, electron, and photon energies, and $m_e c^2$ is the electron rest energy. Consequently, very high energy electrons are required to produce gamma rays. For example, a 100 MeV gamma produced by this mechanism requires an electron of energy from 7 to 200 GeV, depending on the target photon energy. If the electron spectrum has a power law dependence with index -a, then the source function for the inverse Compton process has an energy power law with index -(a+1)/2. As mentioned above, the inverse Compton process has not yet been incorporated in the model since the best choice of the photon radiation fields has been made at this stage.

Figure 4, taken from Fichtel and Kniffen (1984) shows the predicted gamma ray spectrum in the galactic plane near the center, together with low energy gamma ray observations. The relative contributions of the three sources just described are identified. Below about 100 MeV, the bremsstrahlung component is dominant, while above 100 MeV, the nuclear contribution is the strongest. Note the relatively minor role of the inverse Compton component. The spectrum shows a clear break in the transition region. Observations such as these, in the detail that will be available from EGRET, will provide
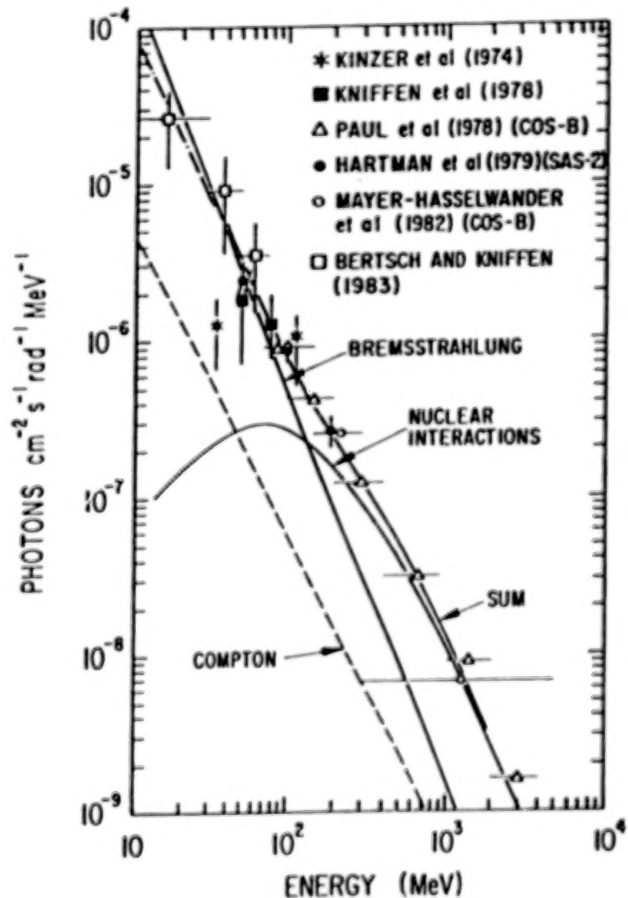


Figure 4. Energy spectrum of galactic radiation in a region near the galactic center. The curves are from a calculation by Fichtel and Kniffen (1984). The contribution from the different sources and the total are labeled. The figure is taken from Fichtel and Kniffen (1984) where references to the data are given.

information on the relative contributions of electrons and cosmic rays as a function of galactic longitude. When observations are made at latitudes off the plane, the Compton contribution may become relatively more significant, and such observations may lead to information on the photon field intensities and scale height.

## REFERENCES

Bahcall, J.N. and Soneira, R.M., 1980, Ap. J. (Letters) 238, L17.

Bertsch, D.L., Dame, T.M., Fichtel, C.E., Sreekumar, P., Stacy, J.G., and Thaddeus, P., 1990a, Proc. 21st Int. Cosmic Ray Conf., OG 3.2-7.

Bertsch, D.L., Dame, T.M., Fichtel, C.E., Sreekumar, P., Stacy, J.G., and Thaddeus, P., 1990b in preparation.

Bignami, G.F. and Fichtel, C.E., 1974, Ap. J. (Letters) 189, L65.

Bignami, G.F., Fichtel, C.E., Kniffen, D.A., and Thompson, D.J., 1975, Ap. J. 199, 54.

Blat, C.L., Issa, M.R., Houston, B.P., Mayer, C.J., Wolfendale, A.W., 1985, Nature 314, 511.

Bloemen, J.B.G.M. 1985, Ph.D. Thesis, University of Leiden.

Bloemen, J.B.G.M. et al., 1986, Astron. Astrophys. 154, 25.

Bloemen, J.B.G.M. 1989, Annual Rev. of Astron. Astrophys. 29.

Boisse, P., Gispert, R., Coron, N., Wijnbergen, J.J, Serra, G., Ryter, C., and Puget, J.L., 1981, Astron. Astrophys. 94, 265.

Burton, W.B., 1985, Astron. Astrophys. Suppl. Ser. 62, 365.

Burton, W.B. and Gordon, M.A., 1978, Astron. Astrophys. 63, 7.

Burton, W.B. and Liszt, H.S., 1983, Astron. Astrophys. Suppl. Ser. 52, 63.

Chi, X., Issa, M.R., Richardson, K.M., Szabelski, J., Wdowczyk, J., and Wolfendale, A.W., 1989, J. Phys. G: Nucl. Part. Phys. 15, 1495.

Dame,T.M., Ungerechts, H., Cohen, R.S., De Geus, E.J., Grenier, I.A., May, J., Murphy, D.C., Nyman, L.A., and Thaddeus, P., 1987 Ap. J. 322, 706.

Dermer, C.D., 1986, Astron. Astrophys. 157, 223.

Fichtel, C.E., 1989, Nucl. Phys. B (Proc. Suppl.) 10B, 3.

Fichtel, C.E., Hartman, R.C., Kniffen, D.A., Thompson, D.J., Bignami, G.F., Ogelman, H.B., Ozel, M.E., and Tumer, T., 1975, Ap. J. 198, 163.

Fichtel, C.E. and Kniffen, D.A., 1984, Astron. Astrophys. 134, 13.

Fichtel, C.E., Ozel, M., and Stone, R.G., 1990, To be published.

Harding, A.K. and Stecker, F.W., 1985, Ap. J. 291, 471.

Hartman, R.C., Kniffen, D.A., Thompson, D.J., Fichtel, C.E., Ogelman, H.B., Tumer, T., and Ozel, M.E., 1979, Ap. J. 230, 597.

Kerr,F.J., Bowers, P.F., Jackson, P.D., and Kerr, M., 1986, Astron. Astrophys. Suppl. Ser. 66, 373.

Kniffen, D.A. and Fichtel, C.E., 1981, Ap. J. 250, 389.

Krausshaar, W.L., Clark, G.W., Garmire, G.P., Borken, R., Higbie, R., Leong, V., and Thorsas, T., 1972, Ap. J. 177, 341.

Mathis, J.S., Mezger, P.G., and Panagia, N., 1983, Astron. Astrophys. 128, 212.

Mayer-Hasselwander, H.A, Bennett, K., Bignami, G.F., Buccheri, R., D'Amico, N., Hermsen, W., Knabach, G., Lebrun, F., Lichi, G.G., Masnou, J.L., Paul, J.A., Pinkau, K., Scarsi, L., Swannenberg., B.N. and Wills, R.D., 1980, Annals of the New York Academy of Sciences 336, 211.

Mayer-Hasselwander, H.A, Bennett, K., Bignami, G.F., Buccheri, R., Caraveo, P.A., Hermsen, W., Knabach, G., Lebrun, F., Lichi, G.G., Masnou, J.L., Paul, J.A., Pinkau, K., Sacco, B., Scarsi, L., Swannenberg., B.N. and Wills, R.D., 1982, Astron. Astophys. 105, 164.

Paul, J., Casse. M., and Cesarsky, C.J., 1974, in The Context and Status of Gamma Ray Astronomy, ed. B. G. Taylor ESRO Sp. 106, 246.

Paul, J., Casse. M., and Cesarsky, C.J., 1976, Ap. J. 207, 62.

Puget, J.L, Stecker, F.W., and Bredekamp, J.H., 1976,Ap. J. 205, 638.

Schickeiser, R. and Thielheim, K.O., 1974, Astron. and Astrophys. 34, 109.

Sreekumar. P., 1990, This conference.

Stecker, F.W., 1970, Ap. and Space Sci. 6, 377.

Stecker, F.W., 1979, Ap. J. 228, 919.

Stecker, F.W., 1988, To be published in the Proc. of the NATO Advance Study Institute on Cosmic Gamma-Rays and Cosmic Neutrinos.

Strong, A.W., Bloemen, J.B.G.M., Dame, T.M., Grenier, I.A., Hermsen, W., Lebrun, F., Nyman, L.A., Pollock, A.M.T.,and Thaddeus, P., 1988, Astron. Astrophys. 207, 1.

Weaver, H.F. and Willaims, D.R.W., 1973, astron. Astrophys. Suppl. Ser. 8, 1.

## DISCUSSION

*Volker Schonfelder:*

The topic of diffuse galactic gamma-ray emission is an ideal example, where the combination of results from more than one GRO telescope will give more information that the result from one instrument by itself. Adding the results on the diffuse emission from COMPTEL to those of EGRET will lead to a clearer seperation of the various diffuse gamma-ray components like $\pi^{\circ}$-decay, bremsstrahlung and the inverse Compton component.

*David Bertsch:*

I am glad you mentioned that point. I had intended to point that out.

# A Model of the Diffuse Galactic Gamma Ray Emission

Parameswaran Sreekumar[1]

NASA/Goddard Space Flight Center, Greenbelt, MD 20771

## ABSTRACT

Our galaxy has been observed to be a source of high energy gamma rays as shown by the two successful satellite experiments, SAS-2 and COS-B. It is generally understood that these diffuse gamma rays result from interactions between energetic cosmic rays and interstellar gas. This work makes use of the most recent data on the distribution of atomic and molecular hydrogen in the galaxy along with new estimates of gamma ray production functions to model the diffuse galactic gamma ray emission. The model allows various spatial distributions for cosmic rays in the galaxy including non-axisymmetric ones. In the light of the expected data from EGRET, an improved model of cosmic ray-matter-gamma ray interaction will provide new insights into the distribution of cosmic rays and the strength of its coupling to matter.

## INTRODUCTION

The surveys carried out by SAS-2 (Hartman et al., 1979) and COS-B (Mayer-Hasselwander et al., 1982) at high energies (>50 MeV) have yielded intensity and distribution of the diffuse gamma-ray emission from the galaxy. The emission, primarily confined to the galactic plane show clear enhancements along tangent directions to the galactic arms as pointed out by Bignami and Fichtel (1974) and Bignami et al.(1975). It is generally accepted that these gamma-rays result primarily from cosmic ray interaction with interstellar gas and photons via pion decay, electron bremsstrahlung and inverse Compton processes (Pollack and Fazio, 1963 and Stecker, 1971). Interstellar gas, primarily consisting of atomic and molecular hydrogen (90% hydrogen and 10% helium), is mapped using 21 cm line emission from the hyperfine transition of neutral hydrogen and 2.6 mm line arising from $J=1 \rightarrow 0$ transition of $^{12}CO$. However, the galactic distribution of cosmic rays has been much harder to carry out. Synchrotron emission from cosmic ray electrons interacting with the interstellar magnetic field does not clearly resolve the issue due to inadequate knowledge of the magnetic field itself. In this context, the recent progress in gamma-ray astronomy has provided what maybe the most valuable tool to study galactic cosmic rays at present. This study reports an attempt to set forth a model based on new gas data and improved gamma-ray source functions to calculate the expected high energy gamma-ray emission from the galaxy.

---

[1]Universities Space Research Association

The galactic containment of cosmic rays is based on the argument that interstellar magnetic fields embedded in the interstellar gas, confine cosmic ray particles to regions within the galaxy. This idea is substantiated by the observation of pressure balance that exists between cosmic rays, interstellar magnetic fields and the kinematic gas pressure (Parker, 1969). As stated by Parker (1976), the cosmic rays, magnetic field and interstellar gas are all coupled to each other so that the propagation and containment of cosmic rays in the galaxy are inseparable from the dynamical theory of the galaxy. The galactic origin of these cosmic rays and their coupling to interstellar gas via the magnetic field is the basis for considering cosmic ray density distribution to be proportional to the local gas density. The strength of the coupling between cosmic rays and matter is unknown at present and is one of the final goals of this investigation. These have been discussed in further detail by others in these proceedings and also in Bertsch et al.( 1990).

Numerous attempts to model the galactic diffuse emission seen by SAS-2 and COS-B in the past (see recent review by Bloemen, 1989) can in general be classified into two approaches. The first approach is to fit the observed gamma-ray data with a axisymmetric multi-parameter function containing measured interstellar gas densities and obtain best fits to the data using techniques such as maximum likelihood (e.g., Strong et al.,1988, Melisse and Bloemen, 1990). In all these cases, an axisymmetric cosmic ray distribution is derived from the best fit parameters. This method does not provide an insight into any possible non-axisymmetric nature of cosmic ray distribution. The second approach which is the basis of this work, directly calculates the expected gamma-ray emission from a calculation using interstellar gas data, known particle interaction cross-sections and photon production source function and an input cosmic ray model (Kniffen and Fichtel, 1981; Fichtel and Kniffen, 1984). Further details on interstellar gas data, cosmic ray models and other details regarding our model are described in the sections below.

## PRESENT MODEL

The calculation presented here attempts to model the high energy diffuse gamma-ray emission from the galaxy arising from cosmic ray interactions with galactic matter. An important final goal of this investigation is to derive a more detailed picture of the cosmic ray distribution in the galaxy. The galactic diffuse emission can be reasonably calculated without an exact picture (full 3-D picture) of the matter distribution provided the distribution is consistent with measured line-of-sight column densities and if the cosmic ray density is uniform throughout the galaxy. There are many indications of a non-uniform cosmic ray density in the galaxy such as synchrotron emission arising from interaction of cosmic ray electrons with interstellar magnetic fields show enhancements along the galactic plane with the intensity increasing towards the inner galaxy. This indicates higher cosmic ray electron density towards the inner galaxy if we assume a fairly uniform galactic magnetic field. At present, more details on the cosmic ray distribution is non-existent and only detailed modelling of the diffuse gamma-ray emission will provide some insights in the near future. The model being presented here, predicts diffuse gamma ray emission from the galactic plane and allows flexibility to incorporate various cosmic ray density distributions as well as a choice of normalization factor which converts integrated antenna temperatures of carbon monoxide into molecular hydrogen column densities. Comparing model predictions to existing data from SAS-2 and COS-B and in the future from EGRET, should enable us to narrow down to a more realistic galactic cosmic ray distribution

### Interstellar gas

Interstellar gas in our galaxy primarily consists of atomic and molecular hydrogen. Most recent estimates indicate the mass of atomic hydrogen in the galaxy to be ~4.8 x $10^9$ $M_0$ and ~3.5 x $10^9$ $M_0$ or more of molecular hydrogen (Kulkarni and Heiles, 1988). The interstellar gas data used in the calculation presented here is a compilation of various galactic surveys by different

groups over many years. The program uses atomic hydrogen data (21 cm emission) surveys of Weaver-Williams (1973) (low latitude galactic H1 survey - l=10°-250°; b=-10°-- +10°), Kerr et al. (1986) (southern H1 survey, l=240°-350°; b=-10°-- +10°) and Burton et al. (1983,1985) (full longitude range and varying latitude range). The latitude range covered by this data set is b=±10°. The molecular hydrogen data (CO) was provided by the Center for Astrophysics in Cambridge from a compilation of fifteen different datasets (Dame et al., 1987). The individual surveys were spread over different latitudes, ranging from b=-25° to +25° with most of them covering ±5° off the galactic plane.

## Cosmic Ray models

The axisymmetric cosmic ray distribution derived by Bloemen et al.(1986) by fitting the COS-B gamma ray data indicated an exponential form. Other non-axisymmetric models such as that of Fichtel and Kniffen (1984) assume correlation between matter density and cosmic ray density distributions. The cosmic ray distributions that have been examined in this work include uniform and radially asymmetric distributions. In the non-axisymmetric case, the cosmic ray density distribution is assumed to be directly proportional to the local interstellar gas density. It is assumed that the spectral shape of the cosmic ray spectrum does not change as a function of location within the galaxy.

## Gamma-ray production from cosmic-ray interaction with matter

The major processes involved in the production of gamma rays are pion decay into electron-positron pairs, electron bremsstrahlung and inverse Compton interaction. Details on the gamma ray production functions for these mechanisms that are used in this calculation, are discussed in an earlier paper in these proceedings and will not be dealt with here. Contribution to the diffuse gamma ray emission from the inverse Compton process is not included in this preliminary calculation and will be included in a later more complete model.

## Description

The model used here directly calculates the gamma ray emission arising from cosmic-ray-gas interactions within the galaxy. The distribution of gas assumed to be mostly in the form of atomic and molecular hydrogen is determined from data taken by various groups as discussed in an earlier section. The galactic plane is divided up from 3.5 kpc to 10.5 kpc into concentric rings 1kpc wide and from 10.5 kpc to 20 kpc into 2 kpc wide rings. The galactic rotation curve of Burton and Gordon (1978) is used to determine the linear velocities corresponding to each concentric ring. Corrections have been made to this rotation curve by Kulkarni (1982) and Fich et al.,(1989), but they are significant only in the outer galaxy (R>10 kpc). Using the local angular velocity which corresponds to the velocity of our frame of reference, one can write down the line of sight component of the linear velocity corresponding to a given galactocentric radius as

$$v(l,R) = R_0 \ (\Omega(R) - \Omega(R_0) \sin (l) \ , \qquad \text{where } \Omega(R_0)=25 \text{ s}^{-1} \qquad (1)$$

The location of the Sun ($R_0$) is taken to be 10kpc. The choice of 8.5 kpc as decided by the 1985 IAU General Assembly, Commission 33 in New Delhi can be easily incorporated into the model when necessary. Kerr and Lynden-Bell (1986) have concluded that kinematic distances within the solar circle derived from a rotation curve and line-of-sight velocities, scale directly with $R_0$. The gas densities will scale inversely with $R_0$ ie., a factor of 1.18 (0.85$^{-1}$) larger while the X-factor used to convert column density of CO into $N(H_2)$ is unaffected (Bronfman et al.,1988). We have decided to use the larger value as the reference value to facilitate comparison with existing results. The integrated intensity of line emission over a velocity range corresponding to a

galactocentric ring and a given line-of-sight is proportional to the column density of matter in the intersecting regions of the ring and is given by

$$W = \int_{v(l,i)}^{v(l,i+1)} T_s \, \tau(v) \, dv \quad \text{where } \tau(v) = -\ln\left(1 - \frac{T_b(v)}{T_s}\right), \quad \text{where } T_s = 125 \text{ K} \quad (2)$$

$T_b$ is the brightness temperature. The normalization factor $X = N(H_2)/W_{CO}$ used to convert integrated CO intensity to molecular hydrogen density has been a constant source of uncertainty in the calculation of the diffuse gamma ray emission. Various authors have used different values of X but it is generally accepted to fall within $1-3 \times 10^{20}$ mol cm$^{-2}$ (K km s$^{-1}$)$^{-1}$ (Strong et al.,1988). We have adopted $X = 2.3 \times 10^{20}$ mol cm$^{-2}$ (K km s$^{-1}$)$^{-1}$ in determining molecular hydrogen densities. Fitting the model to gamma ray data from COS-B, SAS-2 and in the future with EGRET, will clearly allow us to narrow down the present estimates even further.

The total gamma-ray intensity from the interaction of cosmic rays with galactic matter (excluding inverse Compton) can be written as,

$$j(E_\gamma, l, b) = \frac{1}{4\pi} \int dr \left[ q_\gamma^e(E, r=0) \times c_e(r,l,b) + q_\gamma^n(E, r=0) \times c_n(r,l,b) \right] \rho(r,l,b) \frac{ph}{cm^2 \, s \, sr \, GeV} \quad (3)$$

where $\rho(r,l,b)$ is the gas density enhancement factor over local solar value and $c_e(r,l,b)$, $c_n(r,l,b)$ are the corresponding cosmic ray enhancement factors over the average solar system density for electrons and nucleons (Fichtel and Trombka, 1981) We have assumed that the cosmic ray spectral shape does not vary within the galaxy as a whole.

The total hydrogen gas density (atomic + 2 x molecular) in the solar neighborhood was obtained by the Copernicus satellite using UV absorption line measurements. Bohlin et al.( 1978) determined the total density to be 1.15 atoms/cm$^3$. Using the recently determined molecular hydrogen density of 0.10 molecules/cm$^3$ in the 1 kpc region around the sun (Dame et al. ,1987), the local atomic hydrogen density implied is 0.95 atoms/cm$^3$. However the atomic hydrogen radio data used in this calculation, yields the local density to be ~0.5 H atm/cm$^3$ within 500 pc of the sun. The recent calculation carried out by Melisse and Bloemen (1990) also uses n(H1) =0.5 H atm/cm$^3$ and n(H2) = $0.5(X/2.5 \times 10^{20})$. We have replaced n(H2) with our estimates of 0.2 Hatm/cm$^3$ (Dame et al.,1987). This makes the total gas density in the solar neighborhood to be ~0.7 H atm/cm$^3$. In our model, all cosmic ray distributions are normalized to unity in the solar neighborhood.

We have not included contributions from inverse Compton interactions between cosmic ray electrons and ambient photons (infrared, optical and universal blackbody radiation). This is estimated to contribute less than 10% of the total diffuse gamma radiation in the galactic plane. Since cosmic rays are distributed over larger distances (scale height ~700 kpc) than matter, normal to the plane of the galaxy, the inverse Compton component is expected to be more significant at higher latitudes leading to a broader gamma ray distribution in galactic latitudes.

### The Near-Far problem

The galactic rotation curve along with Doppler shifts in emission lines permits us to determine gas density in regions on a galactocentric ring intersected by a given line-of-sight. In the inner galaxy, this leads to two regions, the 'near' and 'far' points where the line-of sight

velocity components are equal. In the outer galaxy the distance is uniquely determined. For a complete model of galactic matter-cosmic ray-gamma-ray interaction which will result in an increased knowledge of the spatial distribution of cosmic rays, it is essential to resolve this distance ambiguity in gas distribution in the inner galaxy. I shall describe below an approach that has been considered though limitations with existing data sets has prevented its successful implementation at present.

It is generally accepted that molecular hydrogen in our galaxy mostly exists in the form of dense molecular clouds and that they lie along galactic spiral arms. Dame et al. (1986) and Bronfman (private communication) have reported cloud listings in the first and fourth quadrants with masses above $10^4$ solar mass. The clouds in the first quadrant clearly mark out some of the galactic arms. These features are less evident in the fourth quadrant. The distances to these clouds have been determined using various techniques and using related observations of HII regions and OB-star associations (ref Dame et al.,1987). An approach to resolve the 'near-far' problem was to use the new survey by the Center for Astrophysics (Dame et al.,1986) of the galactic plane in CO and examine the contribution of the individual molecular clouds to the total emission. If most of the CO emission can be located in clouds whose distances are known, the 'near' and 'far' regions of an inner galaxy ring can be weighted according to the ratio of the cloud masses at the two locations. In the first quadrant, Dame et al.(1986) account for 18% of the molecular mass in the form of unidentified clouds with known distances. Solomon et al.(1989) have published a much larger cloud listing for the first quadrants and claims to be able to account for ~40% of the mass in the form of clouds. Concerns arise regarding mass determination of clouds using the virial theorem since it provides only upper limits and on the completeness of the cloud sample. They have also not provided similar cloud listing for the fourth quadrant. Further studies needs to be carried out on cloud identification particularly with regards to smaller and more distant ones in order to substantiate claims regarding their role in the total observed emission. Thus existing data on molecular clouds in the inner galaxy does not provide a way to resolve the distance ambiguity problem.

## Significance of this model

This model carries out a direct calculation of the diffuse gamma ray emission using the best available data on interstellar gas along with refined gamma-ray source functions for electron bremsstrahlung and pair-production. It permits a choice of possible cosmic ray density distributions of nuclei and electrons independently. The model initially sets out to distribute the interstellar gas over concentric rings, 1 kpc wide. The choice of radial bins allows examination of the galactic morphology such as the 5-kpc 'galactic ring/ spiral arms', within computational and observational limits. The model allows choice of energy ranges from 10 MeV to 30 GeV consistent with EGRET capabilities. The problem of distance ambiguity in the inner galaxy can be examined by allowing different values of near-far distribution ratios that are consistent with existing information on galactic arm structure derived from HII, OB star associations, etc.


## RESULTS

In this preliminary study, the predicted gamma-ray emission agrees reasonably well with the observations of SAS-2 and COS-B on a general level. Highlighting some of the differences between the SAS-2 and COS-B results (Fig.1), the model predicts a greater flux in the fourth quadrant compared with COS-B data while SAS-2 results which show sharper profiles than COS-B, indicate closer agreement. Discrepencies in the model results could arise from various factors such as the choice of an inadequate cosmic ray distribution, inappropriate molecular hydrogen normalization factor and due to the absence of contribution from inverse Compton process. The emission from the inner galaxy ($l=-90°$ to $+90°$) region is dominated by

contribution from molecular gas. This implies that, the model is sensitive in the inner galaxy to the molecular hydrogen normalization. On the other hand, emission from the outer galaxy where there is no distance ambiguity problem or uncertain normalization factors, is mostly determined by the atomic hydrogen component. Thus any new information on the outer galaxy cosmic ray distribution will provide an avenue to tie down the molecular hydrogen normalization factor. It is also possible that the amount of molecular hydrogen that is not seen in CO surveys is not negligible, reducing the intensity predicted by the model. From an observational point of view, existing results have been provided by limited angular resolution instruments giving rise to the possible inclusion of a few unresolved source in the measured emission. With the upcoming launch of EGRET on GRO, this issue may be further resolved.

The small contribution to the measured galactic plane emission from the isotropic diffuse emission is determined from the SAS-2 results (Fichtel et al.,1978; Thompson and Fichtel.,1982) to be ~4 x $10^{-6}$ ph/cm$^2$-s-rad. Contrary to SAS-2, the COS-B experiment spent many years in an eccentric orbit which can introduce significant difficulties in estimating contribution from instrumental background alone. Only the combined instrument + isotropic background contributions have been reported (Mayer Hasselwander et al.,1982). The reported instrumental background is ~5 times the isotropic flux reported by the SAS-2 team. This could partly explain the difference in the flux estimates reported by the two groups. Estimates of the isotropic emission for SAS-2 and COS-B (taken to be ~8x$10^{-6}$ ph/cm$^2$-s-rad) are included in the final figures. I shall now discuss the salient features of the predicted longitudinal gamma-ray distribution resulting from this preliminary model. The results are presented as longitude plots of gamma-ray intensity (ph/cm$^2$-s-rad) where the data has been averaged over the range of +10° to -10° in galactic latitude.

The two cosmic ray distributions being studied here include the simple case of a constant cosmic ray density (equal to the local density) and cosmic ray density proportional to the gas density. The case of a constant cosmic ray density has clearly been shown to be inadequate since it significantly underestimates the gamma ray emission from the inner galaxy inconsistent with observational results from SAS-2 and COS-B (Fig.2). A more realistic model of the cosmic ray distribution would be the case of cosmic rays correlated with interstellar gas. Assuming that cosmic ray density enhancement is equal to gas density enhancements from local value (near solar system), the calculation yields a much better fit to the observed data (Fig.3a,3b). The most interesting aspects of this calculation are seen in the prominent features of the longitude plot of gamma-ray intensity along the galactic plane. The more intense emission arising from large concentrations of gas and cosmic rays in the galactic spiral arms clearly seen in the data, are reproduced by this calculation. These include the tangent point to the 4-kpc arm feature at ~24° and ~342°, the edge of the Scutum and Norma arm at ~36° and ~330° respectively and enhanced emission at ~315° and ~285° from the Crux and Carina arms. The features at ~82° and ~267° maybe due to the local arm. Unfortunately, very strong emission from the point source in Vela, overwhelms contribution from diffuse gamma ray emission around l=267° from the Local arm. The characteristic inter-arm low density region around ~60° is also clearly well reproduced by our model. The tangent to the Sagittarius arm at ~55° is not very dominant. This may not be surprising as seen from CO studies of Dame et al.,(1986) which identified the largest molecular clouds in the first quadrant. The arm itself has been clearly traced by molecular clouds but show only a few large clouds along the line-of-sight tangent to Sagittarius. The region (l~210°-260°) is low in interstellar gas and this is reflected in the lower prediction from the model as compared to SAS-2 results. The model significantly underestimates in this region and may reflect some inadequacies in its preliminary formulation. Modifications to the model in future should make it more complete and it is expected that many of the present inconsistencies will be resolved.
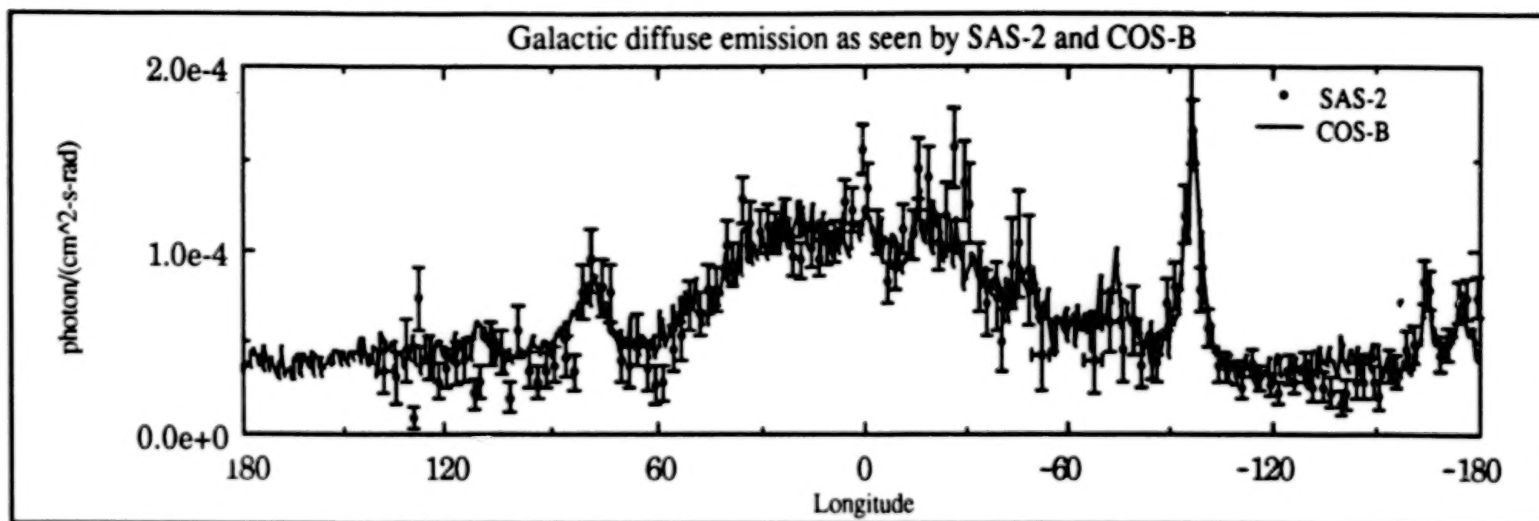
Fig.1: Diffuse gamma-ray emission seen by SAS-2 and COS-B plotted together
(100MeV<E<5GeV). Error bars on COS-B data are left out for plot clarity.
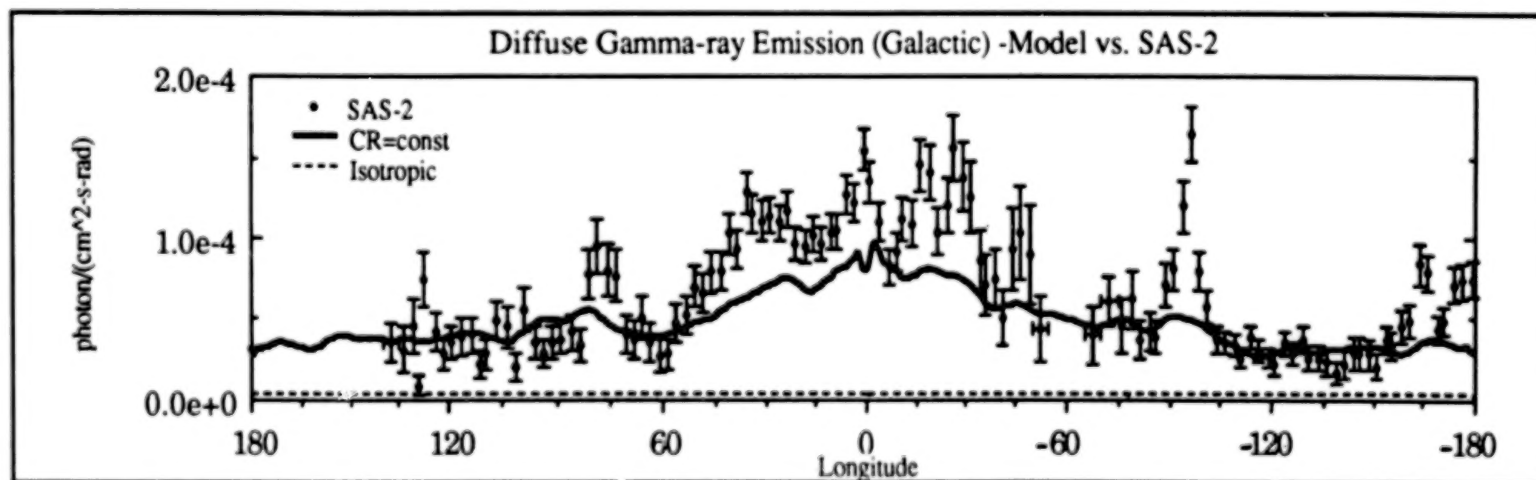
Fig. 2: Results from our model (100MeV<E<5GeV) for the case of a uniform cosmic ray density (local value) along
with SAS-2 data (Hartman et al.,1979). The model significantly underestimates the inner galaxy contribution.
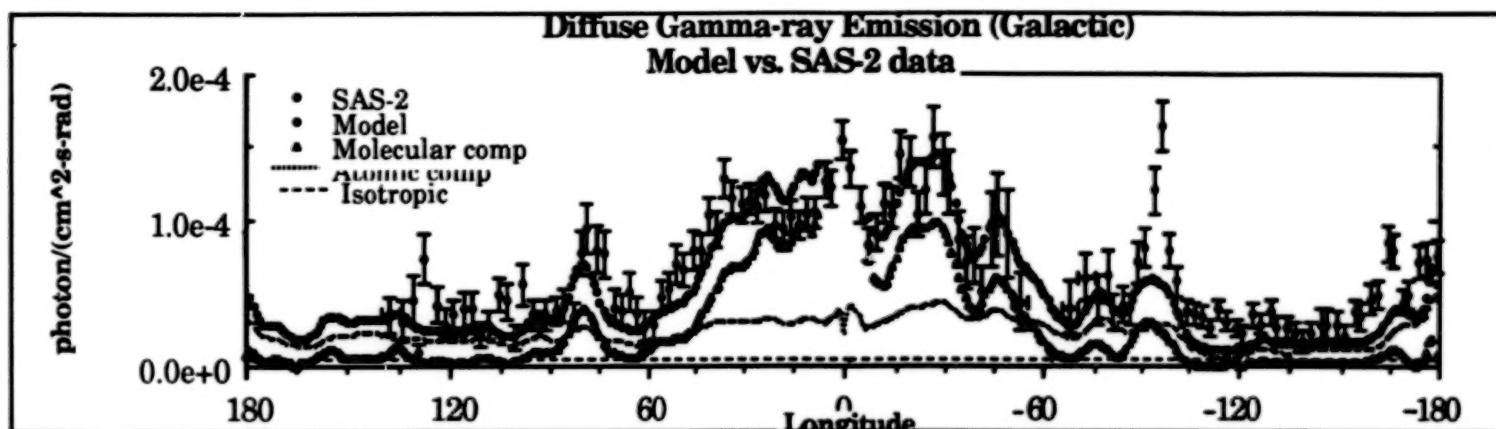
Fig. 3a: SAS-2 data (100MeV<E<5GeV) (Hartman et al.,1979) plotted alongside our model. Cosmic ray density is assumed proportional to local gas density. Contribution from the individual gas components are also shown.
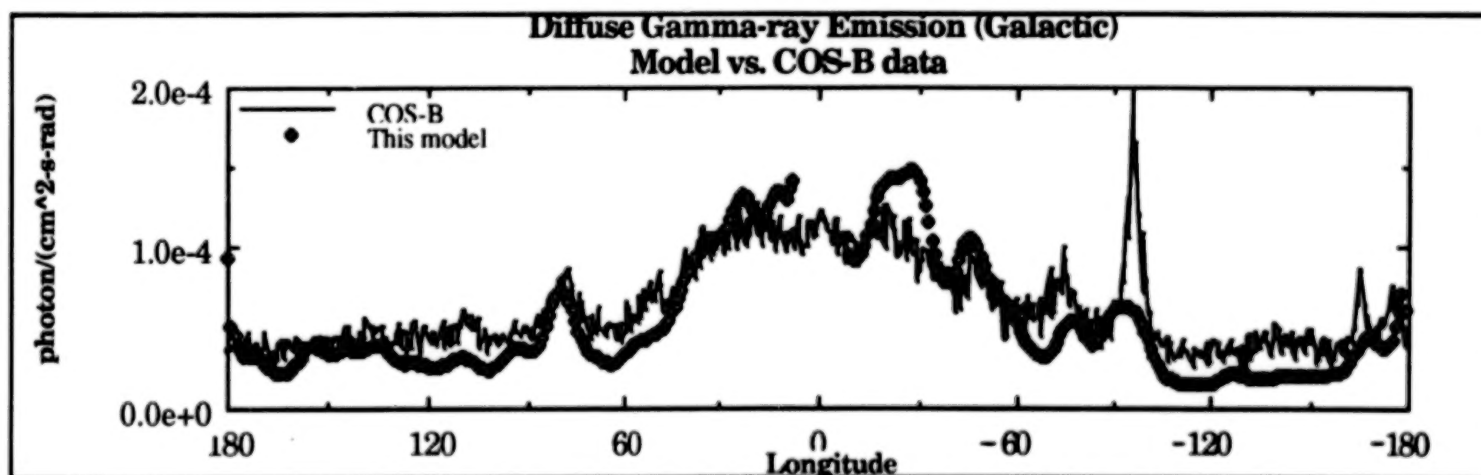


Fig. 3b: COS-B data (Mayer Hasselwander et al., 1982) (100MeV<E<5GeV) plotted alongside our model. Cosmic ray density is assumed to be proportional to local gas density.

38

# FUTURE WORK

The inverse Compton contribution even though small, needs to be included into the present model. The inner galaxy and regions away from the galactic plane are the most sensitive regions with regards to this new component. Various cosmic ray distributions as well as the molecular hydrogen normalization factor X, will be examined to best fit the existing data from SAS-2 and COS-B. New approaches towards resolving the 'near'-'far' problem will be considered. In future, with the launch of GRO, EGRET should provide exciting high quality gamma ray data, leading the way for a significant improvement in our understanding of the galactic cosmic ray distribution and their coupling to interstellar gas.

# REFERENCES

Bertsch, D.L., Dame, T.M., Fichtel, C.E., Sreekumar, P., Stacy, J.G., and Thaddeus, P., 1990, in preparation.

Bignami, G. F., and Fichtel, C. E., 1974, Ap. J. (Letters), 189, L65

Bignami, G. F., Fichtel, C. E., Kniffen, D. A., and Thompson, D. J., 1975, Ap. J. 199, 54.

Bloemen, J. B. G. M., 1989, Annual Review of Astron. Astrophys. 27, 469.

Bloemen, J. B. G. M., et al. 1986, Astr. Ap., 154, 25.

Bronfman, L., Cohen, R.S., Alvarez, H., May, J., and Thaddeus, P., 1988, Astrophys.J., 324, 248.

Burton, W.B., 1985, Astron. Astrophys. Suppl. Ser. 62, 365 and 645.

Burton, W.B. and Liszt, H.S., 1983, Astron. Astrophys. Suppl. Ser. 52, 63.

Burton, W.B. and Gordon, M.A., 1978, Astron. Astrophys. 63, 7.

Dame, T.M., Ungerechts, H., Cohen, R.S., De Geus, E.J., Grenier, I.A., May, J., Murphy, D.C., Nyman, L.A., and Thaddeus, P., 1987, Astrophys.J., 322, 706.

Dame, T.M., Elmegreen, B.G., Cohen, R.S., and Thaddeus, P., 1986, Astrophys.J., 305, 892.

Fichtel, C. E., and Kniffen, D. A., 1984, Astron. Astrophys., 134, 13.

Fichtel, C.E., Trombka, J.I., 1981, Gamma Ray Astrophysics, New Insights into the Universe, NASA SP-453.

Fichtel, C.E., Simpson, G.A., and Thompson, D.J.,1978, Astrophys.J., 222, 833.

Hartman, R., Kniffen, D.A., Thompson, D.J., Fichtel, C.E., Ögelman, H.B., Tümer, T., and Özel, M.E., 1979, Astrophys.J., 230, 597.

Kerr, F.J., and Lynden-Bell, D., 1986, Mon. Not. R. Astr. Soc. 221, 1023

Kerr,F.J., Bowers, P.F., Jackson, P.D. and Kerr, M., 1986, Atron. Astrophys. Suppl. Ser. 66, 373.

Kulkarni, S.R. and Heiles, C., 1988, Galactic and Extragalactic Radio Astronomy, (2nd edition) ed G.L.Verschuur and K.I.Kellermann, Springer-Verlag.

Kulkarni, S.R., Blitz, L., and Heiles, C., 1982, Astrophys.J.(Letters), 259, L63.

Melisse and Bloemen, J.B.G.M., 1990, 21st International Cosmic Ray Conf., (in press).

Parker, E. N., 1969, Space Aci. Rev., 9, 654.

Parker, E. N., 1976, Cosmic Ray Propagation and Containment, in The Structure and Content of the Galaxy and Galactic Gamma Rays, NASA CP-002, 283-300.

Solomon, P.M., and Rivolo, A.R., 1989, Astrophys.J., 339, 919.

Strong, A. W., Bloemen, J. B. G. M., Dame, T. M., Grenier, I. A., Hermsen, W., Lebrun, F., Nyman, L. A., Pollock, A., Thaddeus, P. A., 1988, Astron. and Astrophys, 207, 1.

Thompson, D.J., and Fichtel, C.E., 1982, Astron. and Astrophys., 109, 352.

Weaver, H.F. and Williams, D.R.W., 1973, Astron. Astrophys. Suppl. Ser. 8,1.

## DISCUSSION

*Gottfried Kanbach:*

How do you propose to treat the question of the uncertainty in the distance of the sun to the galactic center, which sets the scale for the model?

*P. Sreekumar:*

The new galactic constants adopted by 1985 IAU meeting at New Delhi gives the distance to be 8.5 kpc instead of the 10 kpc I have used here. Interstellar gas column densities remain unaffected and will not affect a constant cosmic ray density model. However, the volume density in the inner galaxy increases by a factor of 1.18. This will slightly change the cosmic ray proportional to matter model. The results from the model will be examined for the two cases and it is not expected to be very different (ref. Kerr and Lynden-Bell, 1986).

*Floyd Stecker:*

One major reason that your flux prediction is low may be that the value of X you used was 2.3, whereas there are arguments that a value close to 3 may be preferred.

*P. Sreekumar:*

The lower flux predicted was due to a normalization problem associated with the local gas density estimate. Also the choice of X value only affects flux from the inner galaxy where most of the molecular hydrogen is located and does not affect the outer galaxy values. The current best estimate of the X value from gamma-ray astronomy (Strong et al., 1988) is 2.3 or lower. The issue may be further resolved with data from EGRET.

*Wim Hermsen:*

Melisse and Bloemen compared the COS-B gamma ray survey of the Milky Way with a model in which the cosmic-ray density distribution in the Galaxy is correlated with that of the interstellar gas density on scales of typically 100 pc. Such a model was found to fit the gamma-ray data significantly worse than a model in which the cosmic-ray distribution is relatively uniform, being a function of Galactocentric radius only. This is not caused by small-scale discrepancies, but due to the small scale height of the coupling model.

*P. Sreekumar:*

It is generally understood that the scale height of cosmic ray-gas coupling is in the range of a few kpc rather than a ~100 pc. As stated by Melisse and Bloeman (1990), their conclusions may not be valid for a larger scale height.

*Andy Strong:*

The most recent COS-B analysis of the whole galaxy in terms of H1, CO modelling indicated that the molecular component has a steeper spectrum than the atomic. It will be very interesting to see if GRO confirms this. It is therefore important to allow for this possibility in the modelling and not to assume equal spectra.

*P. Sreekumar:*

Your suggestion will be considered seriously as the model is further refined.

# GAMMA RAYS FROM GIANT MOLECULAR CLOUDS

STANLEY D. HUNTER

NASA/Goddard Space Flight Center, Greenbelt, MD 20771

GOTTFRIED KANBACH

Max-Planck-Institut für Extraterrestrische Physik, D-8046 Garching F.R.G.

## ABSTRACT

Giant Molecular Clouds (GMCs) are massive, bounded, cool, dense regions containing mostly $H_2$, but also HI, CO, and other molecules. These clouds occupy < 1% of the galactic volume, but are a substantial part of the interstellar mass. They are irradiated by the high energy cosmic rays which are possibly modulated by the matter and magnetic fields within the clouds. The product of cosmic-ray flux and matter density is traced by the emission of high energy gamma-rays. In this paper, we consider a spherical cloud model and predict the gamma ray flux from several GMCs within 1 kpc of the sun which should be detectable by the EGRET instrument on GRO.

## I. INTRODUCTION

Interaction of cosmic rays with matter in molecular clouds, containing mostly $H_2$, but also HI, CO, and other molecules, produces high energy gamma rays. These gamma rays pass nearly unattenuated through the galaxy and thus, are a good tracer of the product of the cosmic ray flux and the matter density at distant places in our galaxy. The density of HI in these clouds can be observed directly. In cool, dense clouds, the $H_2$ density can be inferred from the intensity of the CO, $J = 1 \rightarrow 0$ transition. If the HI and CO radio observations accurately represent the matter distribution in molecular clouds then the local cosmic ray flux at these clouds can be determined from the gamma ray flux.

The gamma ray production rate as a function of the line of sight matter density, or source function, has been calculated for the Orion clouds by Bloemen, et al. (1984b). They used the CO data from Maddalena, et al. (1986), the HI data derived from Heiles and Habing (1974, $b < -10°$) and Weaver and Williams (1973, $b > -10°$) and the COS-B gamma ray data, Mayer-Hasselwander, et.al. (1982), with a maximum-likelihood technique to derive the parameters in the relationship

$$I_\gamma = A \cdot N(HI) + B \cdot W_{CO} + C$$

where $A$ is the gamma ray production rate per H atom, $B$ is the average $N(H_2)/W_{CO}$ ratio multiplied by the gamma ray production rate per $H_2$ molecule and $C$ is the isotropic galactic diffuse emission and instrumental background level. The CO and HI data were smoothed to match the 1.5° point spread function of COS-B. For $198° < l < 222°$ and $-25° < b < -5°$ their results are:

| Energy Range | 300 - 5000 [MeV] | 100 - 5000 [MeV] |
|---|---|---|
| $A$ [$\gamma$ sr$^{-1}$ s$^{-1}$ atom$^{-1}$] | $(0.52 \pm 0.13) 10^{-26}$ | $(1.70 \pm 0.25) 10^{-26}$ |
| $B$ [$\gamma$ cm$^{-2}$ sr$^{-1}$ K$^{-1}$ (km/s)$^{-1}$] | $(2.7 \pm 1.0) 10^{-6}$ | $(10.1 \pm 1.8) 10^{-6}$ |
| $C$ [$\gamma$ cm$^{-2}$ sr$^{-1}$ s$^{-1}$] | $(2.0 \pm 0.4) 10^{-5}$ | $(5.1 \pm 0.4) 10^{-5}$ |
| $N(H_2)/W_{CO} = B/2A$ [mol cm$^{-2}$ K$^{-1}$ km$^{-1}$ s] | $(2.6 \pm 1.2) 10^{20}$ | $(3.0 \pm 0.7) 10^{20}$ |

The value of $A(300-5000\text{ MeV})$ found is consistent with the average emissivity value determined by Strong, et al. (1982) $(0.59\pm\sim 10\%)\cdot 10^{-26}\,\gamma\,s^{-1}\,sr^{-1}\,atom^{-1}$ using medium latitude galaxy counts and by Bloemen, et al. (1984a) $(0.53\pm 0.14)\cdot 10^{-26}\,\gamma\,s^{-1}\,sr^{-1}\,atom^{-1}$ from the radial distribution of the gamma ray emissivity in the outer galaxy.

The local cosmic ray source strength has most recently been derived by Strong, et al. (1988), by fitting the CO and HI survey data, inverse compton emission, isotropic background and point source contribution to the COS-B diffuse galactic gamma ray emission. They did the fit for six galactocentric rings, 2–4, 4–8, 8–10, 10–12, 12–15 and $> 15$ kpc ($R_\odot = 10$ kpc), and three energy ranges, 70–150, 150–300 and 300–5000 MeV. Their results, for $8 < R < 12$ kpc, are

$$q_0 = \begin{cases} 1.02 \pm 0.10 \times 10^{-26}\,\gamma\,sr^{-1}\,s^{-1}\,atom^{-1} & (70 < E < 150\text{ MeV}) \\ 0.65 \pm 0.06 \times 10^{-26} & (150 < E < 300\text{ MeV}) \\ 0.62 \pm 0.06 \times 10^{-26} & (300 < E < 5000\text{ MeV}) \end{cases}$$

Most source strengths are quoted for the energy range $E > 100$ MeV. Assuming a power law spectra with index $-2.1$, the above results can be expressed in the form

$$q_0 = \begin{cases} 3.7 \times 10^{-5}\,\gamma\,mg^{-1}\,s^{-1}\,sr^{-1} & (20 < E < 100\text{ MeV}) \\ 1.0 \times 10^{-5} & (E > 100\text{ MeV}) \end{cases}$$

We will use the this source function and a spherically symmetric GMC model with radially dependent density to predict the gamma ray emission of GMCs which will be observable by EGRET.

## II. SPHERICAL CLOUD MODEL

Following Solomon et al. (1987), to model the gamma ray emission from GMC's, we consider the simplified case of a spherically symmetric cloud with radial density of the form

$$\rho(r)[g\,cm^{-3}] = \rho_0 \cdot (R_0/r)^\alpha$$

where $R_0$ is the cloud radius. The line of sight column density is given by

$$\sigma(r)[g\,cm^{-2}] = 2\int_0^{\sqrt{R_0^2 - r^2}} \rho(t = \sqrt{r^2 + x^2})\,dx$$

where $r$ is the radial distance between the cloud center and the line of sight, or "impact parameter". Figure 1 shows the line of sight column density for $\alpha = 0$, 1 and 2 normalized for clouds with $M = 10^6\,M_\odot$ and $R = 50$ pc as a function of $r$. A similar model for cloud density was used by MacLaren, et al. (1988) who normalized the density at $r/R_0 = 0.55$.

Analysis of the CO data by MacLaren, et al. (1988), shown in figure 2, suggests that $\alpha$ is close to 1, but it may be almost 2 for some clouds. This can also be seen by comparing the $\alpha = 1$ column density with the $W_{CO}$ contours of the Orion A and B cloud peaks in figures 6 and 7 of Maddalena, et al. (1986). The peak at $(\alpha = 5^h 44^m, \delta = 0°)$, for example, has a fairly linear density fall-off with radial distance from the peak and a long tail. We include $\alpha = 0$ and 2 as limiting cases.

## III. PREDICTED EMISSION OBSERVED BY EGRET

The diffuse galactic gamma ray spectrum above about 10 MeV is composed of an $E^{-2.3}$ Brehmstrahlung component and the $\pi^0$ decay spectrum centered at about 70 MeV. We will consider here gamma rays with energies above about 100 MeV, where the $\pi^0$ spectrum begins to dominate. The effective area of EGRET in this energy region is about $1460\,cm^2$.
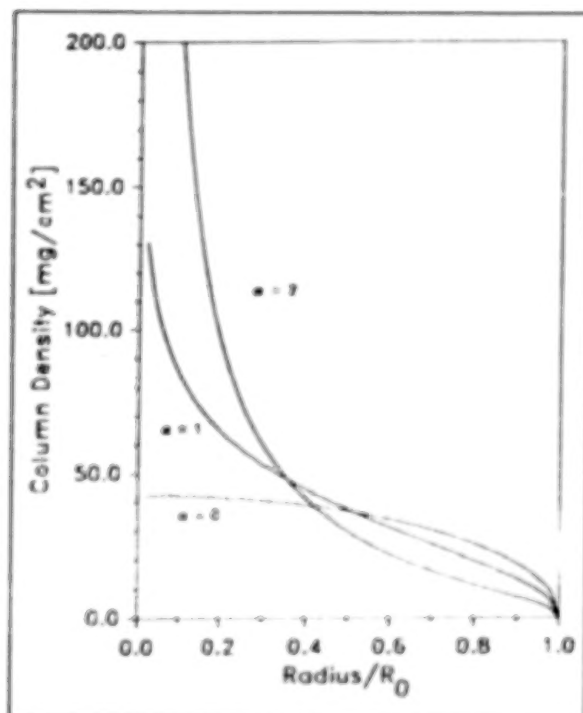
Figure 1. Column density as a function of impact parameter for a cloud with density given by $\rho = \rho_0 \cdot (R_0/r)^\alpha$, for $\alpha = 0$, 1 and 2, normalized to the same total mass, $M = 10^6 \, M_\odot$, and radius, $R = 50 \, pc$.



Figure 2. Column density of hydrogen (arbitrary units) derived from CO data vs. normalized cloud radius for several local molecular clouds. The solid curves a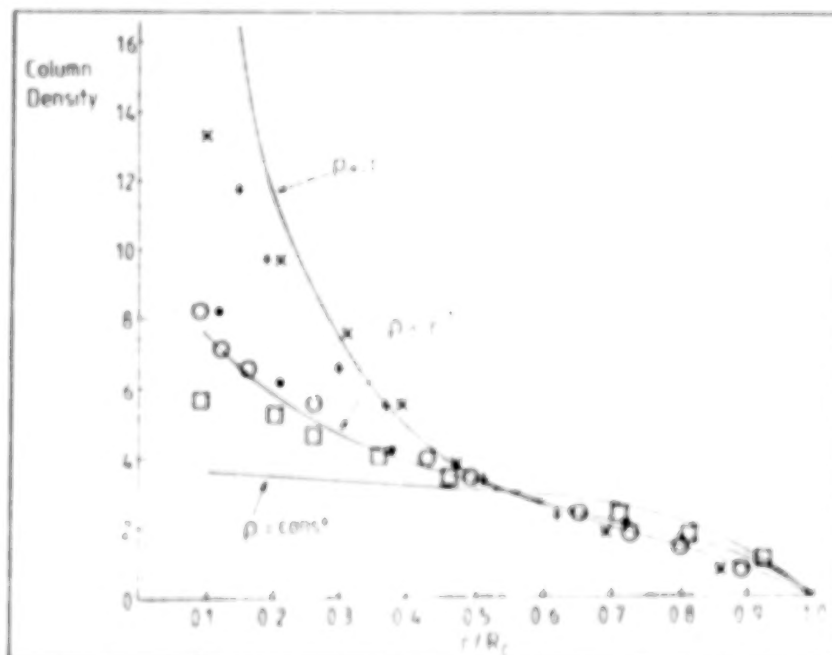re column densities for spherical clouds with density given by $\rho = \rho_0 \cdot (R_0/r)^\alpha$, for $\alpha = 0$, 1 and 2, normalized at $r/R_0 = 0.55$. Orion($A+B$), ($+$); Taurus, ($\circ$); Perseus, ($\times$ and $\square$). From MacLaren et al. (1988).
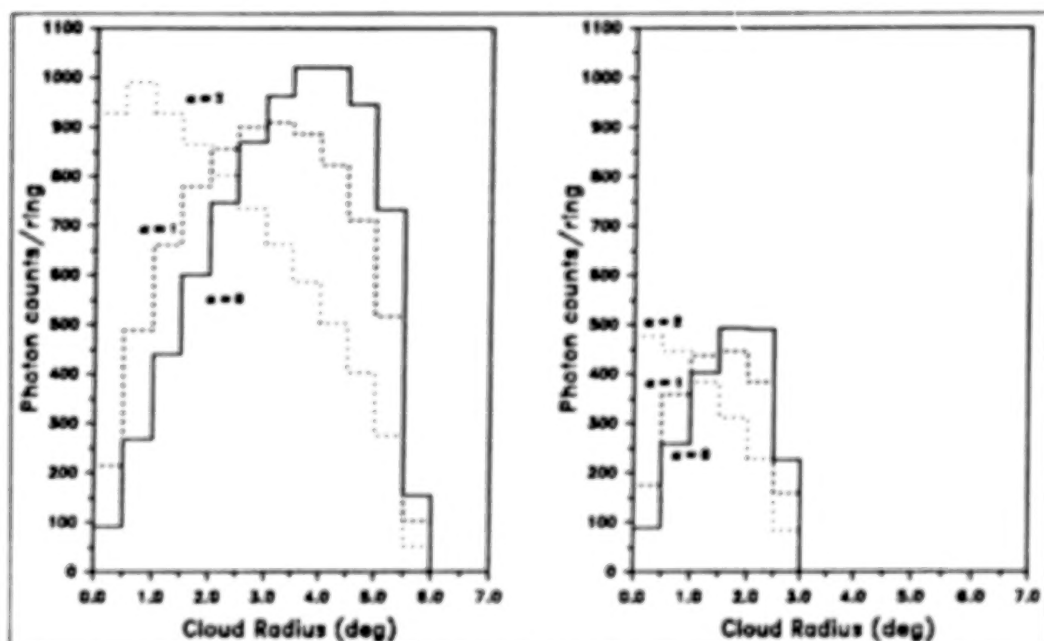
Figure 3. Number of gamma rays observed from a hypothetical GMC with cloud density given by $\rho = \rho_0 \cdot (R_0/r)^\alpha$, for $\alpha = 0$, 1, and 2, $M = 10^6\,M_\odot$, $R_0 = 20$ pc at $D = 500$ pc (left) and 1000 pc (right). The total counts for $T_{obs} = 6 \times 10^5$ s are given per 0.5° ring.

To match the EGRET instrument angular resolution of about 0.5° for gamma ray energies above 100 MeV, it is appropriate to sum the total number of gamma-rays observed from a cloud into rings of width 0.5°. Thus, the total line of sight mass of a ring with inner radius $r_1$ and outer radius $r_2$ is given by

$$\Sigma(r_1, r_2)[g] = 2\pi \int_{r_1}^{r_2} r \cdot \sigma(r)\,dr$$

If all the sources of gamma ray production in the cloud can be expressed in terms of a single source function, such as that derived by Strong, et al. (1988), then the approximate gamma ray flux from the ring is

$$\text{Counts/ring}[\gamma\,\text{sr}^{-1}\,\text{s}^{-1}] = f \cdot q_0 \cdot \Sigma(r_1, r_2)$$

where $q_0\,[\gamma\,\text{g}^{-1}\,\text{sr}^{-1}\,\text{s}^{-1}]$ is the local cosmic ray source function and $f$ is the relative cosmic ray intensity at the cloud. The calculation of the number of observed gamma ray from a GMC requires knowledge of the total mass of the cloud and the distance to the cloud in addition to the sensitivity or effective area of the detector.

$$\text{Counts}_{obs}/\text{ring} = A_{eff} \cdot T_{obs} \cdot 4\pi/4\pi D^2 \cdot \text{Counts/ring}$$

where $A_{eff}\,[\text{cm}^2]$ is the energy dependent effective area, $T_{obs}\,[s]$ is the observation time and $D\,[\text{cm}]$ is the distance to the cloud.

In figure 3 the number of counts, $E > 100$ MeV, per 0.5° ring are shown for a hypothetical $10^6\,M_\odot$ cloud with 50 pc radius immersed in cosmic rays of the local density ($f = 1$) for an observation time of $6 \times 10^5$ s (effective time for a two week observation) at a distance of 500 and 1000 pc respectively. The diffuse galactic and extra-galactic gamma ray emission has not been included. Significant differences in the count profile can be seen for the different values of $\alpha$. For $\alpha = 0$ the cloud appears very much as a ring with a sharp edge. For $\alpha = 1$ the ring structure is still visible, but the edge is softer. For $\alpha = 2$ the cloud appears as a bright spot with a soft edge.

We have calculated the number of gamma rays which EGRET can expect to observe in a typical two week observation for the clouds listed in table 1. These clouds, selected from the work by Dame et al. (1987), are more than 25 pc above or below the galactic plane, within 1 kpc of the sun and have masses greater than $1 \times 10^4$ $M_\odot$, see figure 4 .

## TABLE 1

| | $l^o_{min}$ | $l^o_{max}$ | $b^o_{min}$ | $b^o_{max}$ | D[pc] | $M[10^5 M_\odot]$ |
|---|---|---|---|---|---|---|
| Cygnus OB7 | 87.0 | 99.0 | -3.0 | 8.0 | 800 | 7.5 |
| Cepheus | 100.0 | 120.0 | 11.0 | 22.0 | 450 | 1.9 |
| Taurus | 163.0 | 178.0 | -22.0 | -9.5 | 140 | 0.3 |
| Orion B | 202.5 | 208.0 | -21.0 | -6.0 | 500 | 1.7 |
| Orion A | 208.5 | 218.0 | -21.0 | -14.5 | 500 | 1.6 |
| Chamaeleon | 295.0 | 305.0 | -20.0 | -12.0 | 215 | 0.1 |

From Dame et al. (1987)
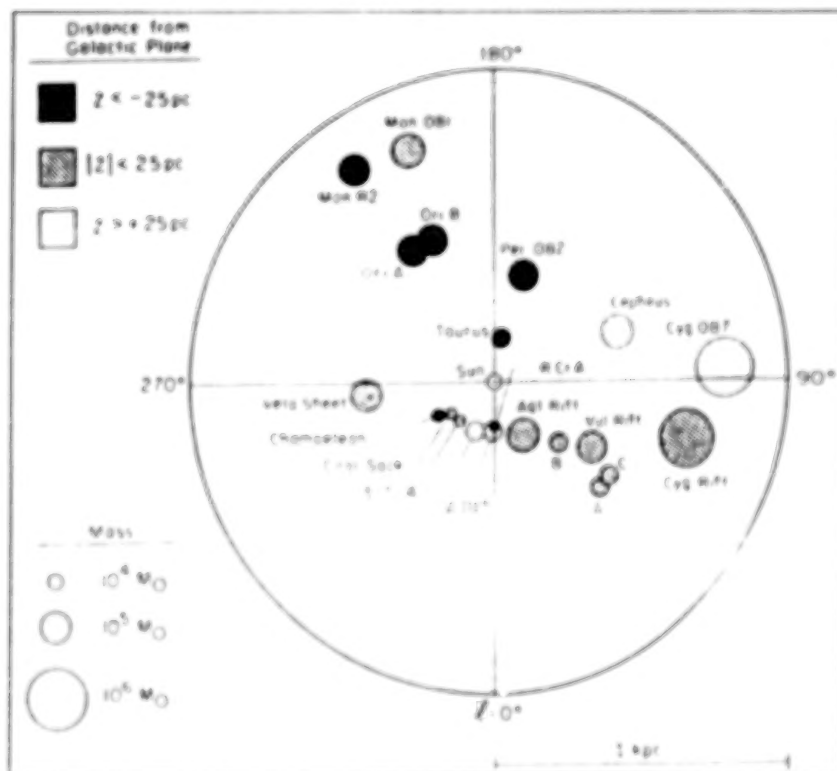


Figure 4. The distribution of GMCs with mass greater than $1 \times 10^4$ $M_\odot$ within 1 kpc of the sun. Adapted from Dame et al. (1987).

Combining the emission data of Strong et al. (1988) with the mass, radius and distance data in Table 1, we can calculate the high energy (E > 100 MeV) gamma ray emission from these clouds. Figure 5 , a, b and c, shows the estimated number of gamma rays (E > 100 MeV which will be observed from each of these clouds during a two week observation ($6 \times 10^5$ s) summed into $0.5^\circ$ circular bins. In each figure, the diagonal dotted line is the estimated number of counts from

the diffuse emission for the same observation. The diffuse gamma ray emission (E > 100 MeV
was estimated using the data given by Fichtel et al. (1978). The appropriate longitude data was
averaged over the width of the cloud in latitude.

We now consider the statistical significance of these observations in two ways. The significance
of the gamma ray observed in a ring over the background reaches a broad maximum at about 30%
of the cloud radius and falls to zero at the cloud edge, as defined by the model. The significance of
'he total number of gamma rays observed from a cloud over the background reaches a maximum
at about 82% of the cloud radius and then starts to fall as the background begins to dominate the
signal. These values are model dependent, however, it is clear that knowledge of the cloud radii will
be important in the analysis of a wide field of view gamma ray observation to determine the gamma
rays which are produced in molecular clouds. Table 2 gives the modeled detection significance (in
standard deviations) of the ring of maximum significance and of the total cloud for the six clouds
listed in table 1.

### TABLE 2

| | Significance of | |
| | Maximum Ring | Total Cloud |
| --- | --- | --- |
| Cygnus OB7 | 2.2 | 5.5 |
| Cepheus | 14.0 | 39.6 |
| Taurus | 23.5 | 64.0 |
| Orion B | 21.4 | 47.1 |
| Orion A | 24.4 | 50.7 |
| Chamaeleon | 6.9 | 15.1 |

(in standard deviations)

## IV. CONCLUSION

Clouds with masses greater than about $10^5$ $M_\odot$ and closer than about 1 kpc should be detectible
with the EGRET instrument in a two week observation. In addition, local and cloud-to-cloud
variations in the product of the column density and the cosmic ray density should be resolvable
for many of these clouds. We expect to also be able to detect some clouds to distances of a several
kpc, and should be able to use these clouds as tracers of the cosmic ray density in more distant
parts of the galaxy.

## V. REFERENCES

Bloemen, J.B.G.M., Bennett, K., Bignami, G.F., Blitz, L., Caraveo, P.A., Gottwald, M., Hermsen,
    W., Lebrun, F., Mayer-hasselwander, H.A., Strong, A.W.: 1984a, *Astron. Astrophys.* **135**, 12

Bloemen, J.B.G.M., Caraveo, P.A., Hermsen, W., Lebrun, F., Strong, A.W., Thaddeus, P.: 1984b,
    *Ap. J.* **139**, 37

Dame, T.M., Ungerechts, H., Cohen, R.S., de Geus, E.J., Grenier, I.A., May, J., Murphy, D.C.,
    Nyman, L.-Å., Thaddeus, P.: 1987, *Ap. J.* **322**, 706

Fichtel, C.E., Simpson, G.A., Thompson, D.J.: 1978, *Ap. J.* **222**, 833

Heiles, C. Habing, H.J.: 1974, *Astron. Astrophys. Suppl.* **14**, 1

MacLaren, I., Richardson, K.M., Wolfendale, A.W.: 1988, *Ap. J.* **333**, 821

Maddalena, R.J., Morris, M., Moscowitz, J., Thaddeus, P.: 1986, *Ap. J.* **303**, 375
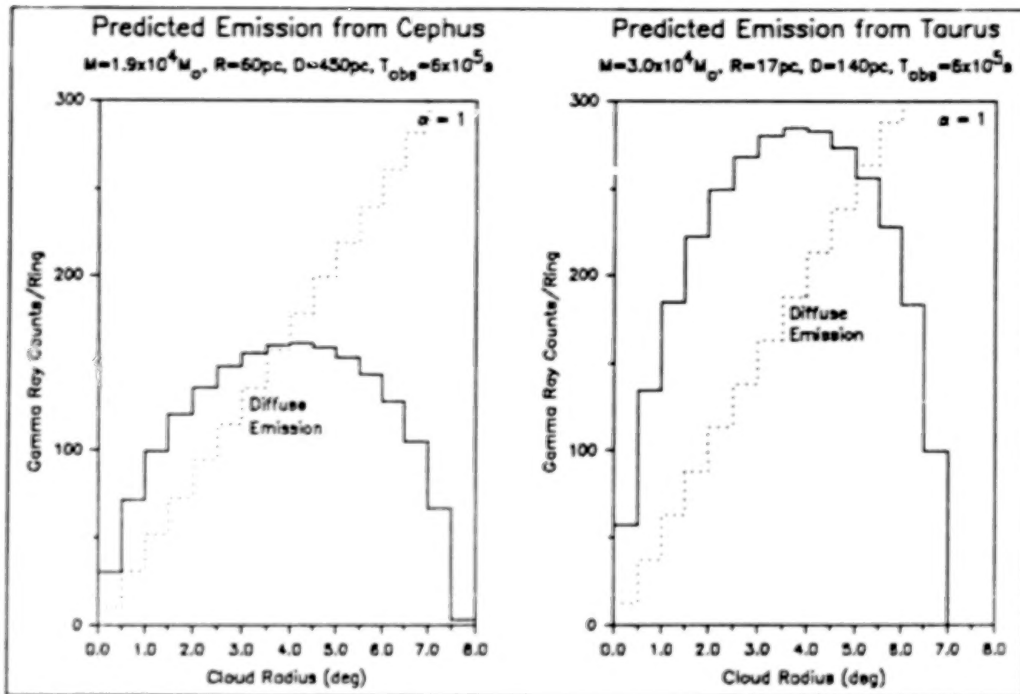
Figure 5.a Estimated gamma ray counts (E > 100MeV) from GMCs in Cephus (left) and Taurus (right) summed into 0.5° circles for a two week observation. The dotted line is the estimated diffuse emission for the same observations.
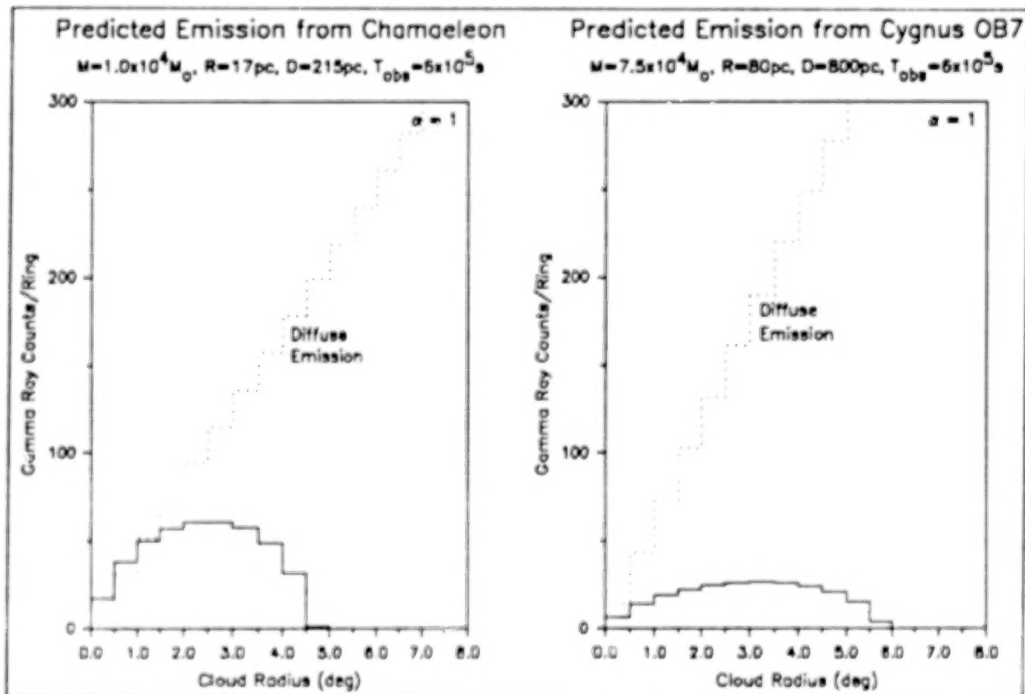


Figure 5.b Estimated gamma ray counts (E > 100MeV) from GMCs in Chamaeleon (left) and Cygnus (right) summed into 0.5° circles for a two week observation. The dotted line is the estimated diffuse emission for the same observations.
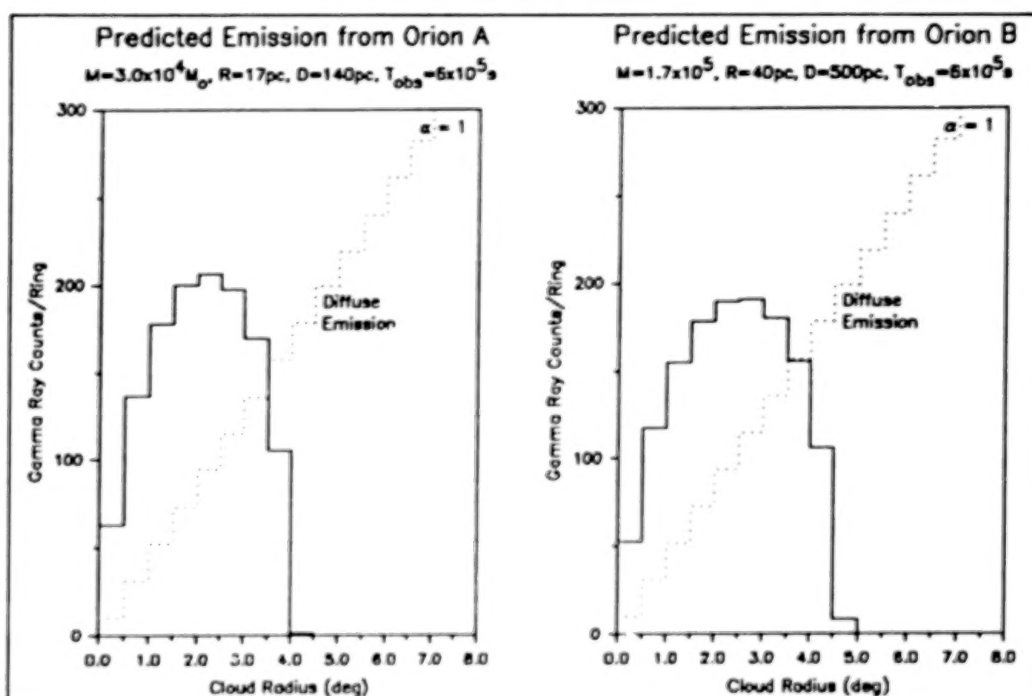
Figure 5.c Estimated gamma ray counts (E > 100MeV) from Orion_A (left)
and Orion_B (right) summed into 0.5° circles for a two week observation.
The dotted line is the estimated diffuse emission for the same observations.

Mayer-Hasselwander, H.A., Bennett, K., Bignami, G.F., Buccheri, R., Caraveo, P.A., Hermsen,
    W., Kanbach, G., Lebrun, F., Lichti, G.G., Masnou, J.L., Paul, J.A., Pinkau, K., Sacco, B.,
    Scarsi, L., Swanenburg, B.N., Wills, R.D.: 1982, *Astron. Astrophys.* **105**, 164

Solomon, P.M., Rivolo, A.R., Barrett, J., Yahil, A.: 1987, *Ap. J.* **319**, 730

Strong, A.W., Bloemen, J.B.G.M., Dame, T.M., Grenier, I.A., Hermsen, W., Lebrun, F., Nyman,
    L.-Å., Pollock, A.M.T., Thaddeus, P.: 1988, *Astron. Astrophys.* **207**, 1

Strong, A.W., Bignami, G.F., Bloemen, J.B.G.M., Buccheri, R., Caraveo, P.A., Hermsen, W.,
    Kanbach, G., Lebrun, F., Mayer-Hasselwander, H.A., Paul, J.A., Wills, R.D.: 1982, *Astron.
    Astrophys.* **115**, 404

Weaver, H., Williams, D.R.W.: 1973, *Astron. Astrophys. Suppl.* **8**, 1

# COMPLEMENTARY INFORMATION FROM mm-WAVE-, INFRARED- AND GAMMA RAY ASTRONOMY

## H. ROTHERMEL, M. CAMERON, A. ECKART
## MAX-PLANCK-INSTITUT FUR EXTRATERRESTRISCHE PHYSIK
## 8046 GARCHING, FRG

## I. INTRODUCTION

Infrared- and gamma-ray astronomy are similar in both their technical challenge and their unique scientific promise. The technical challenge arises from the need for complicated space-borne instrumentation like sizeable sparkchamber telescopes on one side, kryogenic telescopes and detectors on the other, and complex techniques of background rejection, necessary in both regimes. The enormous promise of IR and gamma-ray observations is the absence of extinction and unique information not available in any other wavelength range such as the Visible, UV, X-Ray or conventional Radio window.

Infrared astronomy is particularly well suited to study the physical condition (temperature and density) of the interstellar matter in our galaxy and in external galaxies, and the investigation of the cosmological 3K background radiation which, of course, has its maximum spectral density in the Far-Infrared. This leads to a first albeit less important connection because the 3K background is partner in the gamma-ray production through the inverse Compton process.

Table 1 gives an overview of the subdivision of wavelength ranges, importance of extinction, observing techniques and scientific objectives in both IR broadband measurement and spectroscopy. It is interesting to see how the extinction by interstellar dust, which adds up to 40 magnitudes in the Visible, decreases with increasing wavelength. In the Far-Infrared there is virtually no extinction throughout the galaxy a fact that also holds for gamma ray astronomy.

## II. INFRARED AND mm-WAVE SPECTROSCOPY IN THE GALAXY

The importance of MIR and FIR dust emission, as measured by IRAS (Neugebauer et al., 1984) will be addressed by Stecker in the next paper. Therefore, I shall skip this topic for the sake of shortness. A review is given e.g. by Cox and Mezger, 1989.

Infrared spectroscopy may be less common knowledge and seems to be of considerable importance for gamma-ray astronomy because it provides specific information on temperature, density, molecular abundances and chemistry of interstellar gas. NIR lines, as listed in table 1, are emitted by ionisation regions and, as far as molecular lines are concerned, from shock-exited hot gas. A spectrum of the Orion KL source (fig. 1, taken from Watson, 1982) illustrates the wealth of information available at infrared and millimeter wavelengths. We recognize that emission lines are most numerous and intense in the FIR. FIR fine structure lines are excited by the photo electric effect (Tielens and Hollenbach, 1985) whereas molecular line emission is excited by collision with hydrogene and intensity ratios of lines from different species or different transitions from one species allow to determine density and temperature. For example the 63 $\mu$m OI/158 $\mu$m CI ratio is not much dependent on temperature and probes density whereas the 63 $\mu$m OI/145 $\mu$ OI ratio probes temperature because of different exitation energy. For standard line ratios not even a compilation is necessary because density and temperature can be taken from diagrams (Watson, 1982) where care must be taken, of course, that line emission is not received from two or more sources in the beam. Fig. 1 indicates also that the rotational ladder of CO starting with the lowest transition at 2.6 mm wavelength extends up into the FIR. These higher transitions are intersting because they are emitted by dense warm clumps in star formation regions. For a given telescope higher

TABLE 1
OVERVIEW ABOUT INFRARED ASTRONOMY

| Wavelength ranges | near infrared (NIR) | mid infrared (MIR) | far infrared (FIR) |
|---|---|---|---|
| wavelength | 1 to 5 $\mu$m | 5 to 30 $\mu$m | 30 - 300 $\mu$m |
| extinction towards gal. center ($A_{vis}=40^m$) | $20^m$ to $4^m$ | $4^m$ to $0.7^m$ | negligible |
| typical objects | stars | imbedd. stars, warm dust, ice and silicon features, radiation from PAHs | cold dust, protostars?, galaxies, cosmological background |
| observations | ground based in atmosph. windows | ground based in very few atmosph. windows, spaceborne telescopes | no atmosph.   windows, airplane-, balloon, satellite-measurements, cooled telescopes |
| spectroscopy | HI Spectrum (Paschen, Bracket, Pfund Series) Br $\alpha$ 4.06 $\mu$m Br $\gamma$ 2.17 $\mu$m<br><br>V-r transitions of $H_2$, CO | Fine Structure Lines SIV 10.6 $\mu$m NeII 12.6 $\mu$m<br><br>V-r transitions of $CO_2$, $NH_3$, $SiH_4$, etc. | Fine Structure Lines CI, CII, OIII, etc.<br><br>rotational transitions CO, $^{13}CO$, $C^{18}O$ $NH_3$, HCN, $HCO^+$, OH, etc. |

transitions at shorter wavelengths also allow for better angular resolution. Molecular hydrogene, present in dense and massive clouds in the galactic plane, is probably the most important component of interstellar matter. Gamma radiation is produced in these clouds by cosmic radiation through the $\pi_0$ decay. This radiation, addressed in a separate paper by Hunter in this symposium, is a major part of the resolved gamma radiation from the galactic disc as observed by SAS-2 and COS-B. Cosmic radiation not only produces gamma rays, it also is partly responsible for the synthesis of complex molecules in the clouds by the introduced ionisation because in the gas phase molecules form almost exclusively through ion reactions.
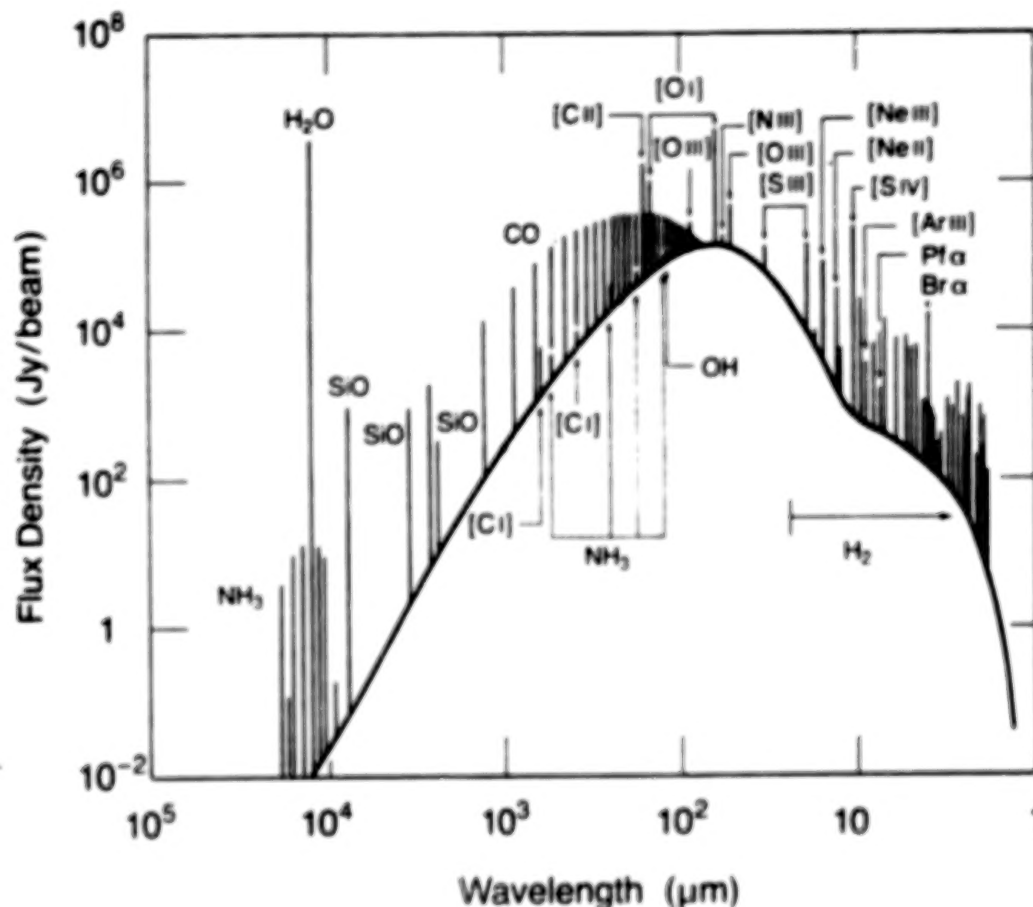


Fig. 1 Spectrum of the Orion KL source from 1 $\mu$m to 10 mm wavelength taken from Watson, 1982.

The line emission of the lowest rotational transition of CO at 2.6 mm wavelength is considered to be the workhorse to trace molecular hydrogene. However, $H_2$ column density does not follow directly from the observed $^{12}CO$ (1-0) line flux because the line is saturated and its exitation depends on density and temperature in the emitting region. Furthermore, the molecular abundances are not certain. If there are no additional observations of isotopic CO lines and other rare molecules probing for optical depth and density and of higher rotational transitions of CO at submillimeter or FIR wavelengths, probing for gas temperature, the $H_2$ column density cannot be computed reliably from 2.6 mm data. Without this additional information an empirical calibration factor has to be used to convert the 2.6 mm line flux into $H_2$ column densities. As addressed already by Thaddeus in the first talk, a number of methods are used to find this calibration factor at specific sources where the $H_2$ column density or mass can be determined by an independent measurement such as visual extinction or virial theorem. (For references see e.g. Van Dishoeck and Black, 1987). Where $H_2$ column density is evaluated from extinction, IR measurements are attrac-

tive because extinction, derived in the Visible by star counts or other methods, can be measured directly by multiple wavelength IR photometry on the basis of a well established wavelength dependence of extinction (table 1). A self consistent model for HI, CO and resolved gamma ray emission has been presented which results in the above calibration factor under certain assumptions on the distribution of cosmic rays (Black and Fazio, 1973; Lebrun et al., 1983; Bloemen et al., 1984, 1986; Blitz et al., 1985; Li, Riley, and Wolfendale, 1983; Riley et al., 1984; Bhat et al., 1985; Bhat, Mayer, and Wolfendale, 1986). If the hydrogene density could be determined reliably through independent methods such as submillimeter- and IR spectroscopy the above model could produce detailed information about the distribution of cosmic radiation in the galaxy.

An interesting question for gamma ray astronomers is whether FIR- and mm-spectroscopy could determine ionisation rates produced by cosmic radiation and UV radiation of young stars. A number of emission lines of ionized molecules (e.g. $HCO^+$) can be measured, however, so far no line could be identified as a specific tracer for ionisation because apart from $H_2$ all molecules known are formed through the ionisation channel since ions have a larger reaction rate.

## III. IR- AND mm WAVE-OBSERVATIONS OF CENTAURUS A

The rest of this paper is dedicated to an extragalactic source. Nearby external galaxies, even if they are not of a merging or starburst type, are very attractive because they give us a global picture with kpc resolution from an outside point which is essentially impossible to derive from our own galaxy. Centaurus A is a giant elliptical galaxy which has been studied at almost any accessible wavelength range because it is the nearest radio galaxy and has a prominent dust lane. Using the recently established 15 m SEST telescope in La Silla (Chile) the galaxy was mapped in its 2.6 mm CO emission. In addition spectra of the J = 1-0 and J = 2-1 transition of $^{12}CO$ and $^{13}CO$ and an upper limit for J = 1-0 of $C^{18}O$ were obtained at selected positions. The $^{12}CO$ (1-0) contour radio map is shown as an overlay on the optical plate (fig. 2) with the continuum radio source removed from the data.

Maps of Cen A taken at 50 and 100 $\mu$m with the IRAS CPC are shown in fig. 3. Both radio and infrared emission are well aligned with the dust band. If the infrared emission is due to dust heated by UV radiation of young stars and if CO emission traces molecular gas, available for star formations, the ratio of IR luminosity over molecular mass is a measure for star formation efficiency (SFE). For Cen A a SFE of 18 Solar luminosities per Solar mass are found, a value which agrees with the canonical number for isolated galaxies (Young and Sanders, 1986). Starburst galaxies would have a 10 times higher star formation efficiency and probably a accordingly higher Supernova rate and diffuse gamma ray flux. If the diffuse gamma radiation of Cen A would be comparable to the flux measured towards the galactic center by SAS-2 and COS-B the 30" by 180" source is diluted by a factor of 10 000 considering the angular resolution of the EGRET spark-chamber telescope. This flux is clearly not detectable.

Nevertheless, besides upper limits from SAS-2 and COS-B (Bignami et al., 1979 and Pollock et al., 1981) detection of a gamma-ray continuum from Cen A is claimed on a 4 $\sigma$ level by Ballmoos, 1985 and Grindlay et al., 1975 as well as detection of gamma ray line emission on a 3 $\sigma$ level by Hall et al., 1976. To examine these marginal detections Cen A probably should be revisited by the EGRET instrument. A significant upper limit or a reliable detection of gamma radiation might contribute important information on the nature of the source.
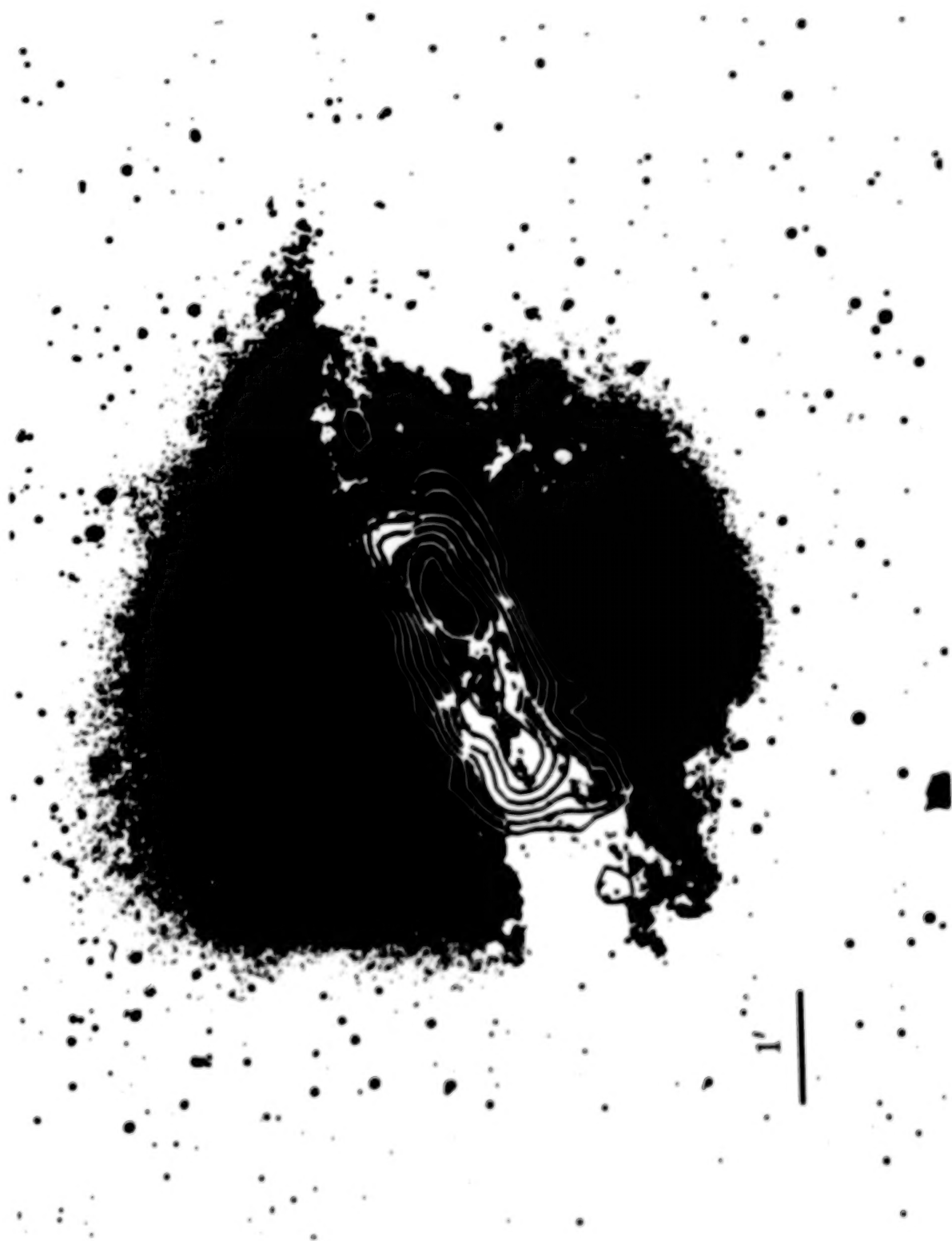
Fig. 2  Cen A optical plate with the 2.6. mm CO emission contours overlaid (Eckart et al., 1989 and 19990a).
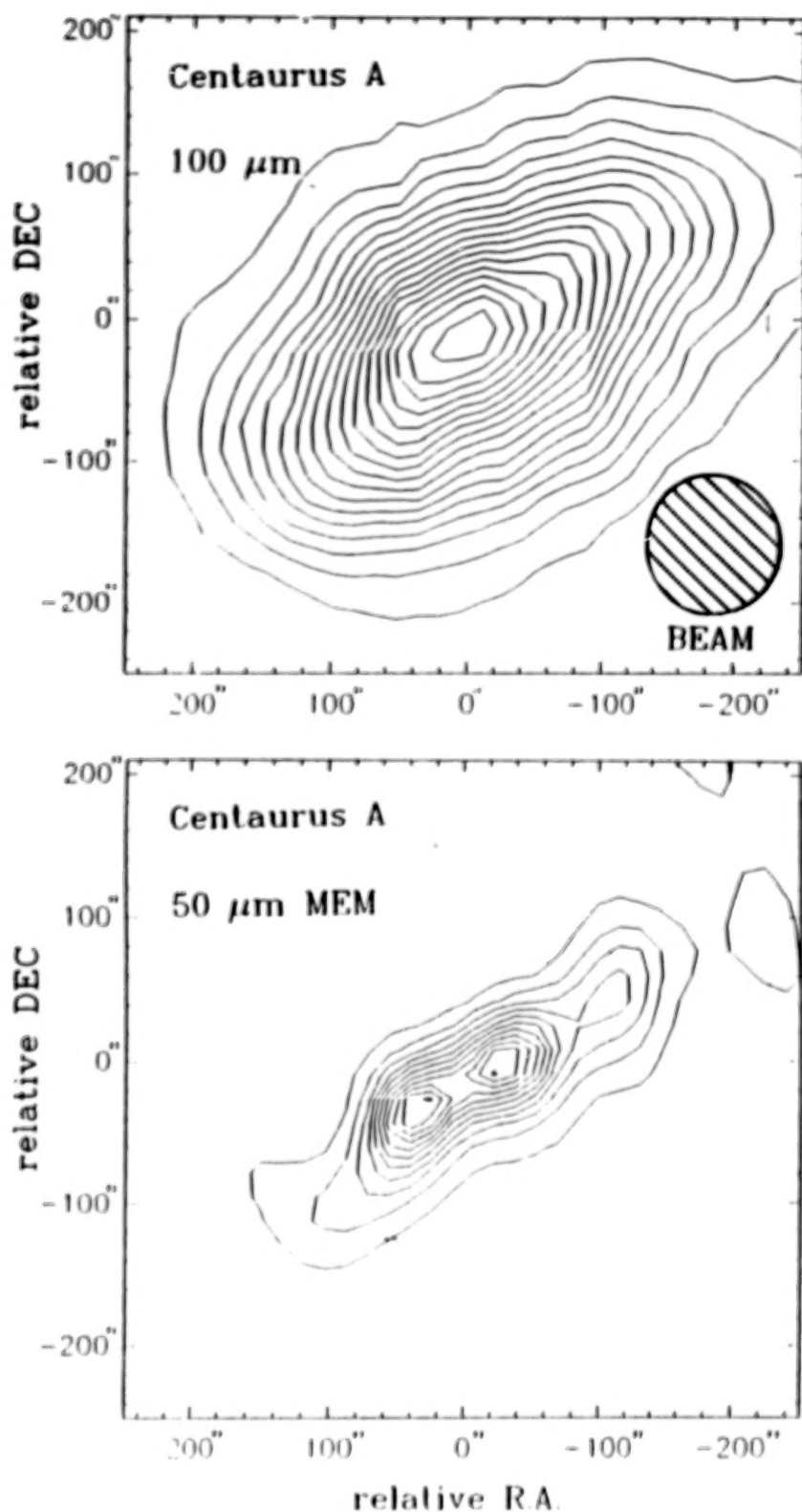
Fig. 3. Above: 100 μm map of Cen A taken by the IRAS CPC instrument. The lowest contour line is 6 % of the peak brightness of 581 MJy/sr. Below: 50 μm map taken by the same instrument and because of better signal to noise deconvolved by a maximum entropy method. The lowest contour line is 9 % of the peak brightness of 399 MJy/sr (Eckart et al., 1990a).

The nucleus of Cen A is both a strong radio-continuum (fig. 4) and X-ray source. Little is known about the nature of this source and there is a reasonable chance that it emits also gamma radiation providing the source is not too compact. Gamma radiation cannot coexist with high X-ray luminosity in a compact source (e.g. a neutron star) because of $e^+$, $e^-$ pair production by interaction of gamma ray and X-ray photons (Herterich, 1974). The X-ray luminosity of Cen A is 4 orders of magnitude higher than Crab, but the question remains whether the source is compact enough that gamma radiation is shielded. From the observed variability of the X-ray source in the order of 3 years the upper limit of its size is 1 pc. The radio point source remains unresolved in the milliarcsecond range (Kellermann, 1974; Shaffer and Schilizzi, 1975) corresponding to less than $4 \cdot 10^{16}$ cm.
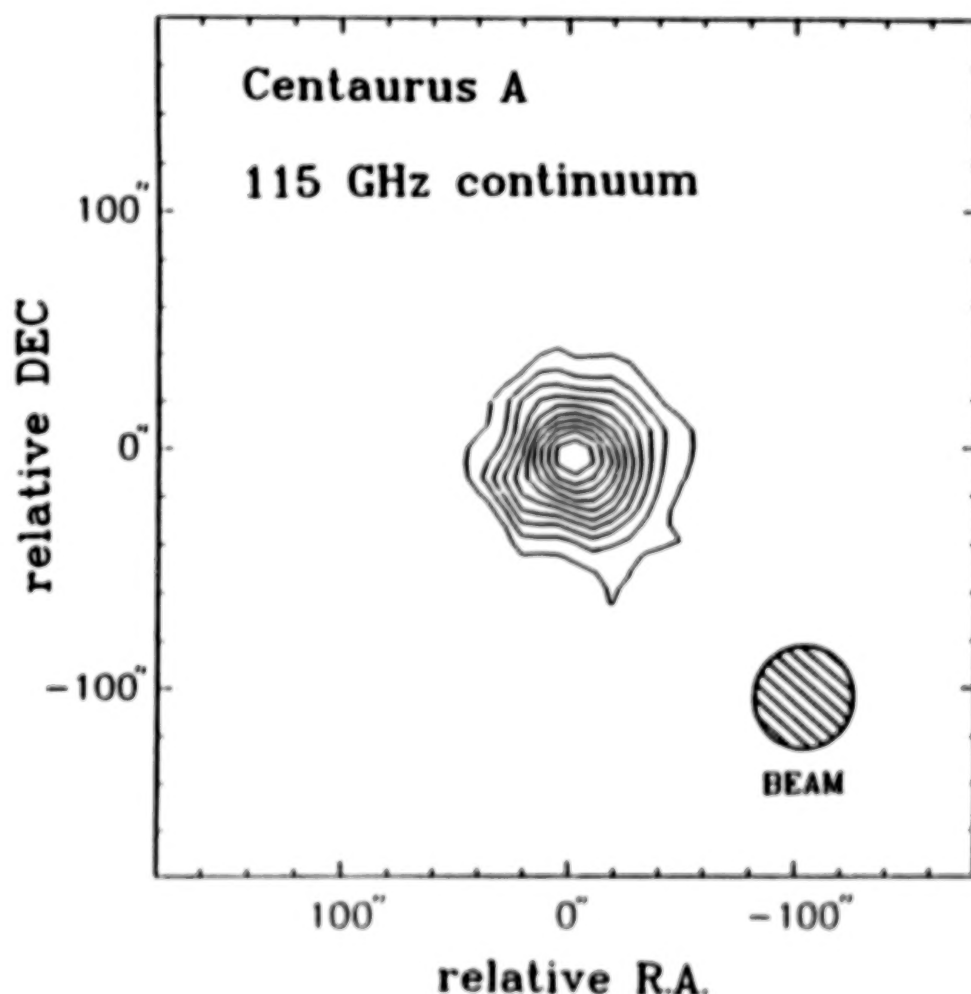


Fig. 4. Contour map of the 2.6 mm continuum emission of Cen A. This unresolved point source coincides with the nucleus of the galaxy (Eckart et al., 1990a).

Extinction of the low energy X-rays is not important as far as the measured luminosity of the source is concerned because 10 - 100 MeV photons would interact with the X-ray spectrum above 2 keV, but from the X-ray extinction below 2 keV a column density in the line of sight of 1.3
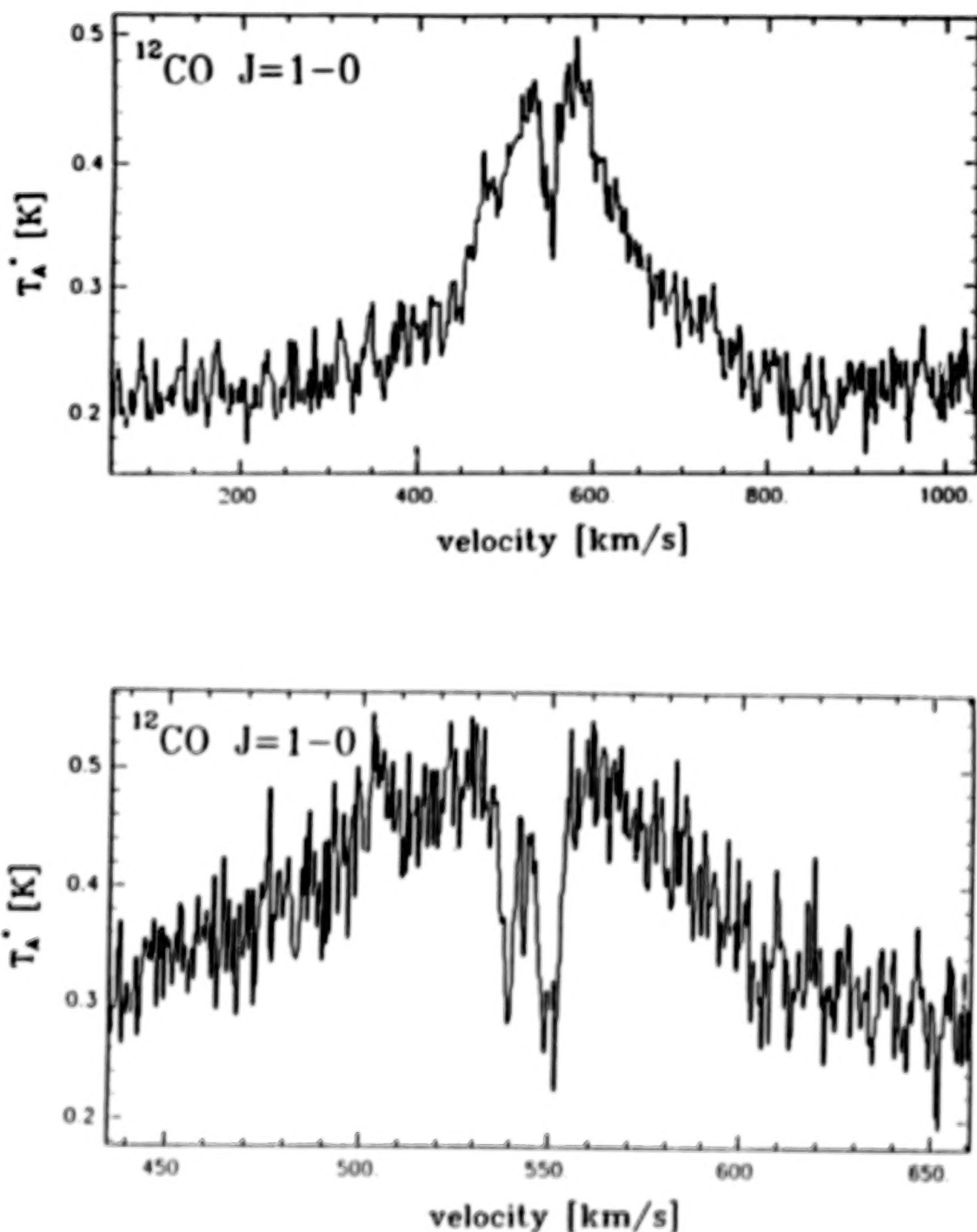
Fig. 5. 2.6 mm CO emission spectrum of Cen A towards the central continuum source. The spectrum appears on a flux density pedestal provided by the nuclear continuum source (5a) and the CO emission shows prominent absorption lines (better resolved at 5b) which are due to individual emitting molecular clouds, seen in absorption in front of a continuum point source of very high surface brightness (Eckart et al., 1990a).

$\cdot\ 10^{23}$ atoms/cm$^2$ (Stark et al., 1976) is derived. The column density towards the radio point source can be estimated independently in 2 ways:

a)  The integrated CO emission towards the center of Cen A (fig. 2) is used to compile a density of $7\cdot 10^{17}$ CO molecules/cm$^2$. Dividing by the relative abundance for dense galactic clouds of $8\cdot 10^{-5}$ we get $9\cdot 10^{21}$ H$_2$ molecules/cm$^2$ or $1.8\cdot 10^{22}$ H atoms/cm$^2$ (Eckart et al., 1989 and 1990a). Adding $0.8\cdot 10^{22}$ H atoms/cm$^2$ from the 21 cm HI observations (van Gorkom, 1987) and dividing by 2 because the source is in the middle of the emitting region, the total column density in the line of sight is $1.3\cdot 10^{22}$ H atoms/cm$^2$.

b)  Alternatively the H$_2$ column density can be evaluated from the CO line absorption of individual clouds in the line of sight towards the radio point source (fig. 5). (The lines of emitting clouds are seen in absorption because the point source has very high surface brightness). The strongest absorbing cloud has a density of $1\cdot 10^{17}$ Co molecules/cm$^2$ (Eckart et al., 1990b) corresponding to $0.25\cdot 10^{22}$ H atoms/cm$^2$. Fig. 5b reveals at least 3 clouds at different Doppler-shifts which implies a density of almost $10^{22}$ H atoms/cm$^2$. The amount of atomic hydrogene, measured in absorption (Van der Hulst et al., 1983) is only $10^{21}$ H atoms/cm$^2$ for a cloud and can be neglected.

Although both methods give roughly the same result, Method b seems to be more appropriate because it probes directly for matter in front of the radio point source. The fact that the column density observed in front of the radio source is 10-times smaller than the observed density in front of the X-ray source suggests that the X-ray source is smaller and deeper imbedded in absorbing material.

If the $r = 10^7$cm is a radius for a stellar X-ray source where photon-photon interaction is important (Heterich 1974), this must be scaled up for the nucleus of Cen A by the square root of the luminosity ratio ($= 100$) to a radius of $10^9$ cm. This is comfortably below the upper limit for the diameter of the radio point source ($< 4\cdot 10^{16}$ cm) and there is also no immediate conflict with a smaller size for the X-ray source, hence gamma radiation cannot be excluded by X-ray Gamma-ray absorption on grounds of so far available information.


## IV. ACKNOWLEDGEMENT

## REFERENCES

Bhat, C.L., Issa, M.R., Houston, B.P., Mayer, C.J., and Wolfendale, A.W. 1985, Nature 314, 511.
Bhat, C.L., Mayer, C.J. and Wolfendale, A.W. 1986, Phil Trans. R. Soc. Lond., A 319, 249.
Black, J.H. and Fazio, G.G. 1973, Ap.J. (Letters), 185, L7.
Black, J.H. and Willner, S.P. 1984, Ap.J., 279, 673.
Blitz, L., Bloemen, J.B.G.M., Hermsen, W., and Bania, T.M. 1985, Astr. Ap., 143, 267.
Bloemen, J.B.G.M., Caraveo, P.A., Hermsen, W., Lebrun, F., Maddalena, R.J., Strong, A.W., and Thaddeus, P. 1984, Astr. Ap., 139, 37.
Bloemen, J.B.G.M., Strong, A.W., Blitz, L., Cohen, R.S., Dame, T.M., Grabelsky, D.A., Hermsen, W., Lebrun, F., Mayer-Hasselwander, H.A., and Thaddeus, P. 1986, Astr. Ap., 154, 25.
Cox, P., Mezger, P.G., Astron. & Astrophys. Rev. 1989, p. 49.
Eckart, A., Cameron, M., Rothermel, H., Wild, W., Zinnecker, H., Rydbeck, G., Olberg, M., Wicklind, T., ESO Workshop on Extranuclear Activity, Garching, FRG, May 1989.
Eckart, A., Cameron, M., Rothermel, H., Wild, W., Zinnecker, H., Rydbeck, G., Olberg, M., Wicklind, T. 1990a, Ap. J. (submitted).
Eckart, A. et al. 1990b (in preparation).

Grindlay, J.E. et al. 1975, Ap. J. (Letters), 197, L 9.

Herterich, K. 1974, Nature, 250, p. 311.

Hall, R.D. et al. 1976, Ap. J., 210, p. 631.

Kellermann, K.I. 1974, Ap. J. (Letters) 194, L 135.

Lebrun, F. et al. 1983, Ap. J., 274, 231.

Neugebauer, G., Habing, H.J., van Duinen, R., Aumann, H.H., Baud, B., Beichman, C.A., Beintema, D.A., Boggess, N., Clegg, P.E., de Jong, T., Emerson, J.P., Gautier, T.N., Gillett, F.C., Harris, S., Hauser, M.G., Houck, J.R., Jennings, R.E., Low, F.J., Marsden, P.L, Miley, G., Olnon, F.M., Pottasch, S.R., Raimond, E., Rowan-Robinson, M., Soifer, b.T., Walker, R.G., Wesselius, P.R., and Young, E., March 1984, Ap. J., 278, L1-L6.

Van der Hulst, J.M., Golish, W.F., Hashick, A.D. 1983, Ap. J. (Letters), 204, L37.

Van Dishoeck, E.F., Black, J.H. in G.E. Morfill and M. Scholer 1987 (eds.), Physical Processes in Interstellar Clouds, 241-274, D. Reidel Publishing Company.

Van Gorkom, J.H. 1987, IAU Symposium on Structure and Dynamics of Elliptical Galaxies, de Zeeuw, T. (ed.), 421.

Shaffer, D.B. and Schilizzi, R.T. 1975, Astron. J., 80, p. 753.

Stark, J.P., Davison, P.J.N., Culhane, J.L. 1976, Mon. Not. Astr. Soc. 194, Short Communication 35 P.

Tielens, A.G.G.M., Hollenbach, D. 1985, Ap. J. 291, 722.

Watson, D.M. 1982, XV. ESLAB Symposium on Galactic and Extragalactic Infrared Spectroscopy, Toledo, Spanien.

Young, J.S., Sanders, D.B. 1986, Ap. J. 302, 680

# IMPLICATIONS OF THE IRAS DATA FOR GALACTIC GAMMA-RAY ASTRONOMY AND EGRET

F. W. STECKER
Lab. for High Energy Astrophysics, NASA Goddard Space Flight Center
Greenbelt, Maryland 20771, U.S.A.

## ABSTRACT

Using the results of $\gamma$-ray, millimeter wave and far infrared surveys of the galaxy, one can derive a logically consistent picture of the large scale distribution of galactic gas and cosmic rays, one tied to the overall processes of stellar birth and destruction on a galactic scale. Using the results of the IRAS far-infrared survey of the galaxy, we have obtained the large scale radial distributions of galactic far-infrared emission independently for both the northern and southern hemisphere sides of the Galaxy. We find the dominant feature in these distributions to be a broad peak coincident with the "5 kpc" molecular gas cloud ring. We also find evidence of spiral arm features. Strong correlations are evident between the large scale galactic distributions of far infrared emission, $\gamma$-ray emission and total CO emission. There is a particularly tight correlation between the distribution of warm molecular clouds and far-infrared emission on a galactic scale. The 5 kpc ring has been evident in existing galactic $\gamma$-ray data. The extent to which the more detailed spiral arm features are evident in the more resolved EGRET data will help to determine more precisely the propagation characteristics of galactic cosmic rays.

## I. INTRODUCTION

Using observational and theoretical arguments from other branches of astronomy, Stecker (1969) pointed out that the most likely explanation for the $\gamma$-ray flux from the inner plane of the Galaxy observed by the pioneering OSO-3 satellite experiment (Clark, et al. 1968) was the existence of a significant component of interstellar molecular hydrogen gas in cool dense clouds. More recent satellite observations imply that $\gamma$-ray emission is highly non-uniform in the Galaxy, and that its emissivity distribution peaks about halfway between the sun and the galactic center. The $\gamma$-ray emissivity distribution bears a strong resemblance to the distribution of molecular clouds in the Galaxy. This similarity, coupled with the lack of enough gas in atomic form (HI) to explain the $\gamma$-ray measurements, led to the supposition that $H_2$ is far more abundant in the inner Galaxy than HI, and that $H_2$ plays the major role in producing galactic $\gamma$-rays (Stecker, et al. 1975). The $H_2$ hypothesis was proven by observation five years later with the discovery of a large, roughly ring-shaped distribution of molecular clouds in the inner galaxy (Scoville and Solomon 1975). A detailed survey of most of the galactic plane was made from the SAS-2 satellite detector (Fichtel, et al. 1975). The proof of the correlation of galactic $\gamma$-ray emissivity (deduced from the SAS-2 data) with the molecular cloud component in the inner galaxy followed quickly (Solomon and Stecker 1974; Stecker, et al. 1975). Further analysis indicated that the cosmic-ray distribution in the inner galaxy is similar to that of supernova remnants and pulsars, supporting the hypothsis that most cosmic-rays are galactic in origin (Stecker 1975; Stecker 1976; Stecker and Jones 1977). Harding and Stecker (1985) (hereafter designated HS) performed a joint analysis of the SAS-2 and COS-B data, supporting the earlier conclusion of a galactic radial cosmic-ray gradient and the galactic origin hypothesis. By

taking a "synoptic" approach to galactic astronomy (Stecker 1981), using mm-wave and far-infrared galactic surveys and studies of other galaxies in conjunction with the galactic $\gamma$-ray surveys, one can relate galactic $\gamma$-ray production to the birth and death of young Population I stars in the Galaxy (Stecker 1976). As a new consideration here, we will present a detailed unfolding of the 100 $\mu$m IRAS survey of the Galaxy and show how it sheds light on the meaning of past and future $\gamma$-ray surveys.

## .II. GALACTIC GAMMA-RAY PRODUCTION

Gamma-rays are produced in the Galaxy primarily by the electromagnetic processes of bremsstrahlung and Compton interactions of cosmic-ray electrons with interstellar gas and radiation fields respectively and by the strong interactions of cosmic-ray nuclei with interstellar gas, resulting in the production and almost immediate decay of neutral pions (Stecker 1971).

The pion decay $\gamma$-ray component can be calculated from the expression

$$q_\pi(E_\gamma) = 8\pi n_H \mu \int_{E_{th}}^{\infty} dE_p \, I(E_p) \int_{\lambda(E_\gamma)}^{\infty} dE_\pi (E_\pi^2 - m_\pi^2)^{-1/2} \zeta_\pi(E_p) \sigma_\pi(E_\pi; E_p) \quad (1)$$

where $\lambda(E_\gamma) = E_\gamma + (m_\pi^2/4E_\gamma)$ , $\zeta_\pi$ is the neutral pion multiplicity, and $\mu$ is a multiplicative enhancement factor which takes account of $\alpha$p, p-He and $\alpha$-He interactions as well as pp interactions. This formula is derived in detail by Stecker (1971).

The calculation of this component hinges on the development of a model for the pion production function $\sigma(E_\pi; E_p)$ which adequately describes the cross section and energy distribution of neutral pions produced in pp interactions at a given energy $E_p$ as determined by accelerator data. The first such model, the "isobar-plus-fireball model", was developed by Stecker (1970) who noted the importance of nucleon isobar channels at the primary energies where most of the pions are produced. An update utilizing Feynman scaling for $E_p > 5$ GeV, the "isobar-plus-scaling" model, was introduced by Stecker (1979) to calculate both the $\gamma$-ray and neutrino production spectra from pion decay. with emphasis on a discussion of the high energy neutrinos. Dermer (1986) has shown that such models which include isobar production provide an excellent fit to the accelerator data on pion production.

The differential $\gamma$-ray spectra from the various interactions discussed above are shown in Fig. 1 and the production rates for energies above 100 MeV are shown in Table 1 (Stecker 1989). The exact numbers given in Fig. 1 and Table 1 are not as significant as their relative rank of importance. It is clear that pion decay and bremsstrahlung are by far the most important production mechanisms, with their relative importance being energy dependent. As shown in Fig. 1, in the $\gamma$-ray energy range above 100 MeV, it is expected that $\pi^\circ$ decay $\gamma$-rays dominate over bremsstrahlung $\gamma$-rays in the Galaxy. The reverse is true for lower-energy $\gamma$-rays since the $\pi^\circ$ decay spectrum turns over at ~70 MeV.

**TABLE I**
**LOCAL GALACTIC γ-RAY PRODUCTION RATES (STECKER 1989)**

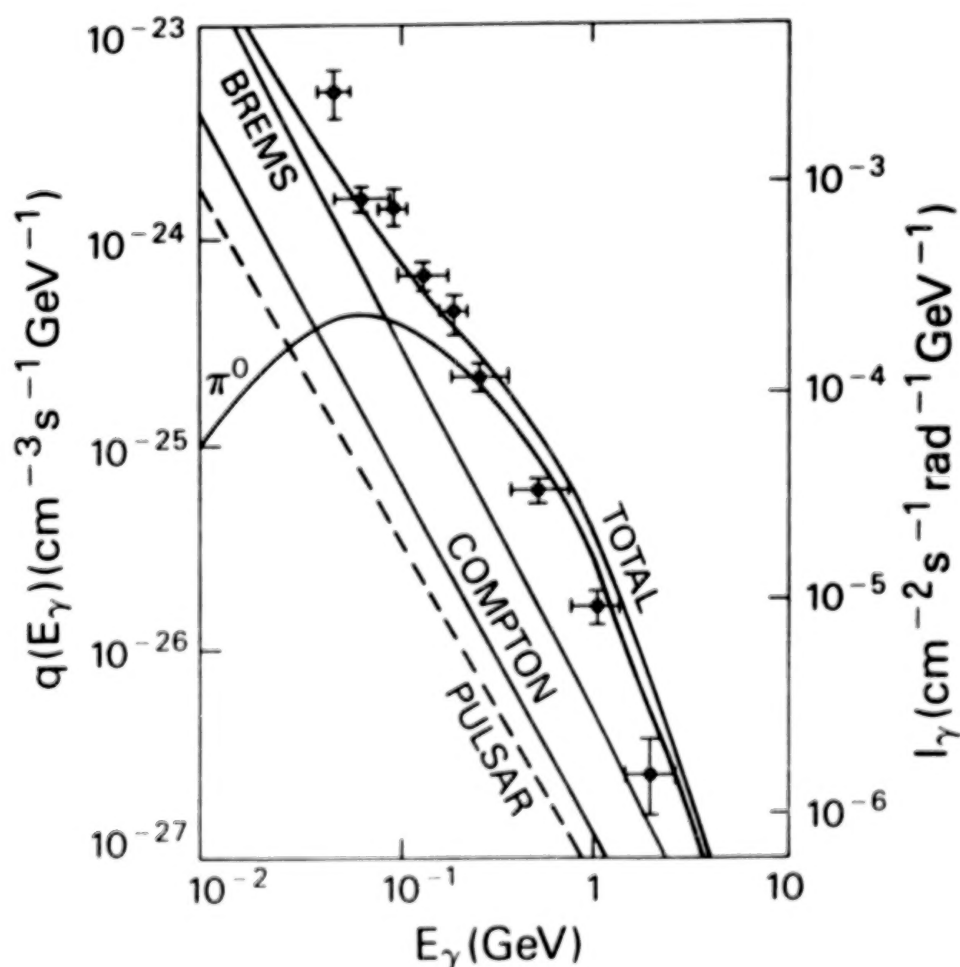| Process | $q(>0.1\ \mathrm{GeV})\ (\mathrm{cm}^{-3}\mathrm{s}^{-1})$ | Fraction of Total |
|---|---|---|
| Pion Decay | $1.51 \times 10^{-25}$ | 66% |
| Bremsstrahlung | $6 \times 10^{-26}$ | 26% |
| Compton: | | |
|   Blackbody | $6 \times 10^{-27}$ | |
|   Far Infrared | $3 \times 10^{-27}$ | 5% |
|   Starlight | $2 \times 10^{-27}$ | |
|   Total | $1.1 \times 10^{-26}$ | |
| Pulsar Contribution | $6 \times 10^{-27}$ | 3% |
| Total Rate | $2.3 \times 10^{-25}$ | |



Fig 1.  Local differential production spectra for major diffuse production processes and the pulsar component (left hand scale).  The right hand flux scale and data points are from COS-B and SAS-2 inner Galaxy data.

## III.  MM-WAVE CO SURVEYS

The vast bulk of the interstellar gas is in the form of hydrogen. Hydrogen in atomic form can be mapped by radio telescopes because of its spectral line at 21cm wavelength. However, hydrogen in molecular form does not emit such radio waves; the strongest spectral features from the $H_2$ molecule are at ultraviolet wavelengths, not useful for large scale galactic structure studies. This radiation can only travel a mere kpc or so, before being absorbed by the interstellar dust.

Since the $H_2$ molecule is the most stable form of hydrogen at low temperature, and since it is expected to be the predominant form of hydrogen in cool dense clouds, it is important to determine the abundance and distribution of $H_2$ on a galactic scale. Radio emission from other molecules coexisting with $H_2$ in cool interstellar molecular gas clouds can be used to trace $H_2$ in the Galaxy. Because of its relative abundance as compared with other interstellar molecules (excluding $H_2$), the CO molecule has become a useful $H_2$ cloud tracer. This molecule has a radio spectral line at 2.64mm. The results of extensive galactic CO surveys have been published (Sanders, et al. 1986, Clemens, et al. 1986, Dame, et al. 1987, Bronfman, et al. 1988). These surveys, together with previous CO surveys have firmly established that the galactic distribution of $H_2$ clouds is dramatically different from that of the more uniformly distributed atomic hydrogen. The atomic hydrogen gas density is relatively constant on a large scale in regions of the Galaxy between 4 and 15 kpc galactocentric radius, falling off inside of 4 kpc and outside of 15 kpc. In contrast, the $H_2$ clouds have an entirely different distribution. They also fall off inside of 4 kpc (with the exception of a small nuclear region within 200 pc of the galactic center). However, the $H_2$ clouds are strongly concentrated in an annular region or ring, reaching a peak density at a radial distance of ~5 kpc (Scoville and Solomon 1975), the same place where the $\gamma$-ray emission peaks (Solomon and Stecker 1974) and become almost non-existent outside of 10 kpc from the galactic center. Observations of the molecular cloud distribution in other spiral galaxies have revealed that some of these galaxies also have a ring-shaped distribution of molecular clouds (Young and Scoville 1982; Myers and Scoville 1987).

## IV.  COSMIC RAYS IN THE INNER GALAXY

As discussed above, radio 2.6 mm-wave surveys of the Galaxy indicate that the average density of $H_2$ is ~2 mol $cm^{-3}$ in the molecular cloud ring at a galactocentric distance of of ~5 kpc, the "Great Galactic Ring", and drops off dramatically at <4 kpc and in the outer Galaxy. In the solar galactic neighborhood, most of the interstellar gas is probably HI. The increase in interstellar gas in the inner galaxy alone is not sufficient to explain the increased $\gamma$-ray emission there as deduced from the galactic $\gamma$-ray surveys. An accompanying increase in the cosmic ray intensity in the Great Galactic Ring is also called for. A deduction of the implied cosmic-ray distribution from the $\gamma$-ray observations shows that the cosmic rays increase (relative to the local intensity) by a factor of ~ 2-3 at a maximum coincident with the maximum in the gas density, in the 5 kpc region (Stecker 1976; Harding and Stecker 1985). This phenomenon is usually referred to as the galactic cosmic-ray gradient. The cosmic-ray distribution deduced using the $\gamma$-ray observations in conjunction with the deduced variation of total gas (HI+$H_2$) in the Galaxy is, within experimental error, identical to the distribution of supernova

remnants and pulsars (Stecker 1975; Stecker and Jones 1977). This result is prima facie evidence that the bulk of the cosmic radiation originates either in galactic supernova explosions or the resulting pulsars. The striking resemblance between the distribution of cosmic rays implied by the existing $\gamma$-ray data and the distribution of supernova remnants and pulsars found by galactic radio surveys thus supports the hypothesis that most observed cosmic rays are born in our own Galaxy.

HS derived the radial distribution of $\gamma$-ray emission in the Galaxy from flux longitude profiles by geometrical unfolding techniques (e.g., Puget and Stecker 1974). Using both the final SAS-2 results and the COS-B results, they analyzed the northern and southern galactic regions separately. HS then made use of CO surveys of the southern hemisphere (Sanders, et al. 1984; Robinson, et al. 1984) in conjunction with the northern hemisphere CO data, to derive the radial distribution of cosmic rays on both sides of the galactic plane. They found that, in addition to the "5 kpc ring" of enhanced emission, there is evidence from the asymmetry in the radial distributions for spiral features which are consistent with those derived from the distribution of bright HII regions. They also found positive evidence for an increase in the cosmic ray flux in the inner Galaxy, particularly in the 4-5 kpc region, in both halves of the plane.

HS found general agreement in the shapes of the COS-B and SAS-2 emissivity distributions, the dominant features being a peak between 4 and 5 kpc in the North and a peak near 4 kpc in the South (taking the distance between the Sun and the Galactic Center to be 8.5 kpc). This seems to describe an asymmetric ring of emission. This emission region, which is a more large scale feature than an individual spiral arm, I will refer to as the "Great Galactic Ring". There is also a secondary peak of emission at ~6 kpc galactocentric radius in the South, which is more pronounced in the COS-B data. This feature, first pointed out by Stecker (1977), can be associated with the tangential direction to a spiral arm at ~310°, referred to either as the Crux arm or an extension of the Sagittarius arm. HS presented a crude map of the Galaxy at $\gamma$-ray wavelengths. Their map resembles the more precise CO cloud map obtained from the Massachusetts-Stony Brook survey by Clemens, et al. (1988), also showing the "Great Galactic Ring".

Information on the distribution of gas in the Galaxy can be used in conjunction with the observed $\gamma$-ray emissivity to yield information on the galactic cosmic-ray distribution. The cosmic-ray density is proportional to $q_\gamma$, the $\gamma$-ray emissivity per H-atom, as derived from the observed $\gamma$-ray volume emissivity, total gas density, $n_{TOT}$, and gas scale height. The total gas density is the sum of molecular, $n_{H_2}$, and atomic, $n_{HI}$, densities, $n_{TOT} = 2\ n_{H_2} + n_{HI}$. $H_2$ densities were derived from galactic CO surveys. Longitude-velocity data from these surveys can be analysed using a galactic rotation curve to give CO radial emissivity distributions, which can then be converted to $H_2$ densities.

Figure 2 shows the radial distribution of $q_\gamma$(> 100 MeV) derived by HS. If all of the $\gamma$-ray emission were from diffuse processes, then $q_\gamma$ would be proportional to the density of cosmic rays. The emissivity per H-atom derived from both the SAS-2 and COS-B data show evidence for an increase in the inner Galaxy in both the north and the south. The difference in the results may be partly due to uncertain subtractions for intrinsic background in the COS-B

detector (see discussion in HS and Stecker 1989).

Stecker and Jones (1977) investigated the effect of diffusion halo models on the galactocentric radial distribution of cosmic rays and made γ-ray emissivity fits to the SAS-2 data using a SN-pulsar source distribution for thin and thick (10 kpc) halos respectively. They showed that a large (10 kpc or more) diffusion halo can flatten the cosmic-ray gradient in the outer galaxy (see Fig. 3). However, the determination of a cosmic-ray gradient in the outer galaxy is quite difficult because of the uncertainty in separating distances along the line of sight without the type of rotational velocity information available to radio astronomers. Strong, et al. (1987) and Mayer, et al. (1987) find some hint of a cosmic-ray gradient in the outer Galaxy.
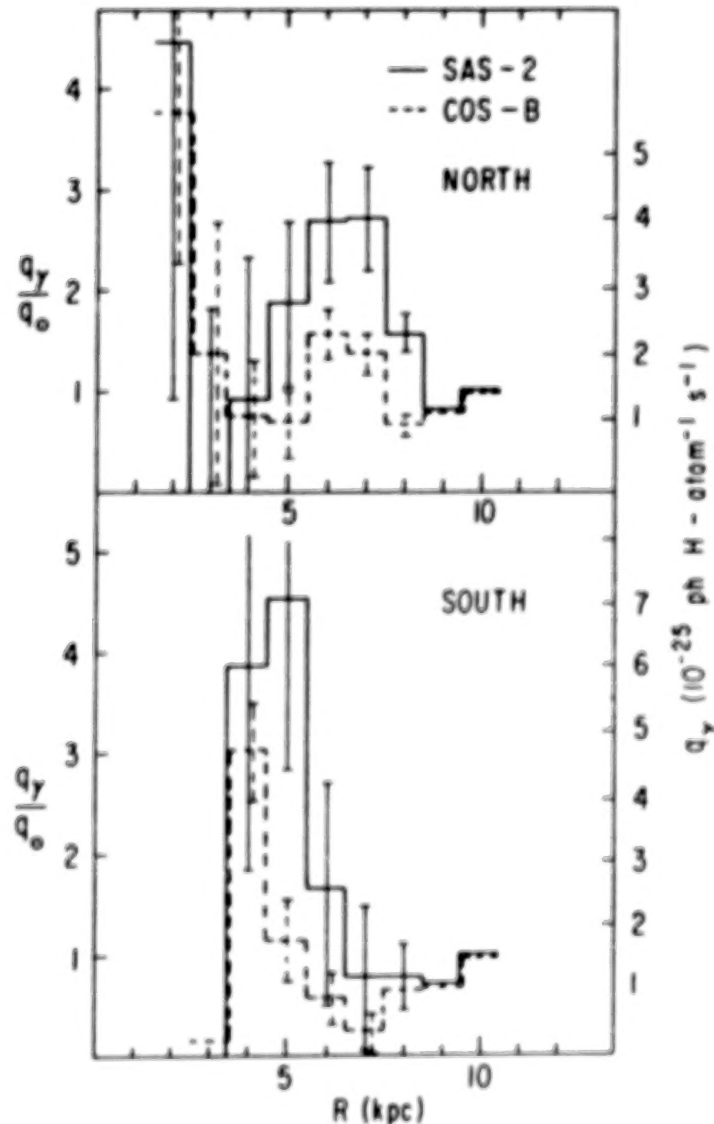


Fig. 2. Cosmic-ray distribution in the galactic plane obtained by Harding and Stecker (1985) from unfoldings of the SAS-2 and COS-B data.

3.00

2.40

SOURCE

1.00

L•5kpc

L•10kpc

1.20

0.60

0.00

0.0    5.0    10.0    15.0    20.0

R(kpc)

FLUX(ARBITARY UNITS)
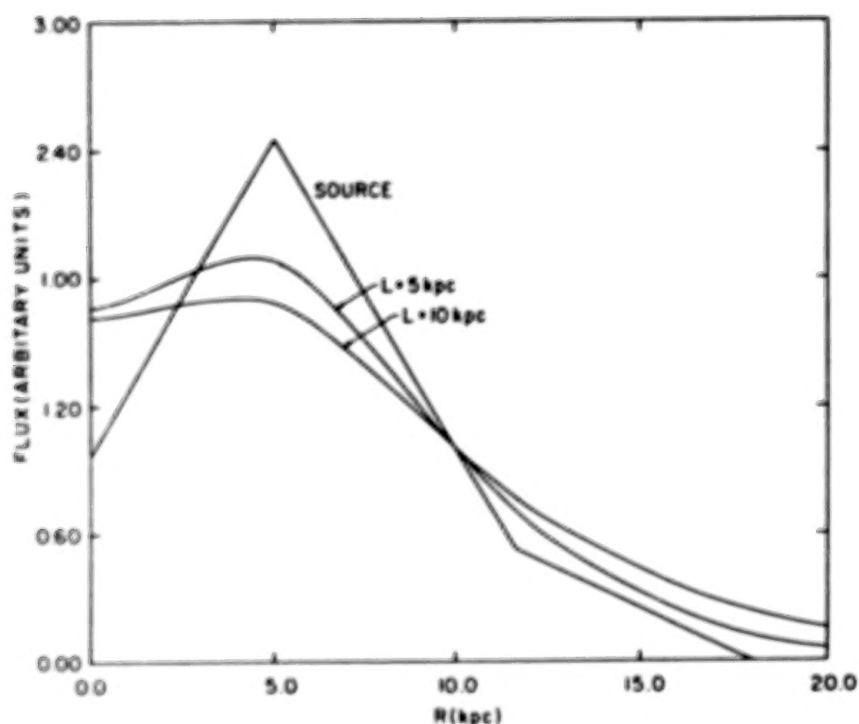
Fig. 3. Galactic radial distributions of cosmic-ray intensity using a weighted pulsar source model with a negligible diffusion halo and using diffusion halo models of thickness 5 and 10 kpc (Stecker and Jones 1977)

## VII. OTHER SURVEYS OF THE GALAXY AND THEIR IMPLICATIONS

Other Population I phenomena track with the radial distribution of CO, exhibiting the 5-kpc maximum. The pulsar and $\gamma$-ray distributions are remarkably similar (Harding and Stecker 1981). The distribution of HII regions and ionized gas (Lockman 1976) also falls into this category as does the distribution of far infrared emissivity (see below). All of these data lend support to the idea that the $H_2$ cloud component of the interstellar medium plays the active dynamical role in Population I star formation processes which result in the observable structural characteristics of spiral galaxies (Burton 1976, Stecker 1976). The far infrared emission is from reradiation by dust of energy released primarily in the UV range by O, B and A stars.

Fazio and Stecker (1976) predicted that the galactic far infrared (FIR) distribution should also exhibit a strong correlation with the CO distribution and should have a pronounced peak at ~ 5 kpc. This has indeed proved to be the case. Their basic hypothesis was that the bulk of the FIR radiation was the emission of dust heated by radiation from young Population I stars located

near molecular cloud complexes. In a detailed study of local complexes of giant molecular clouds, OB associations and HII regions using IRAS data, Leisawitz (1987) has shown that about 50-80% of the total luminosity is associated with molecular clouds seen in CO emission, 10-25% is associated with the HII regions, and the remainder surrounding the complex.

## VIII. ANALYSIS OF THE IRAS SURVEY OF THE GALAXY

The IRAS survey provides the first unobscured view of the IR distribution over the entire galactic disk. However, in determining the galactic distribution of IR emissivity, we do not have the additional information provided by velocity data, as one has in the case of radio line surveys. In the use of the essentially one dimensional galactic longitude flux distribution to obtain a galactocentric radial distribution of emission, one finds a commonality with the analysis of galactic $\gamma$-ray data, for which geometrical unfolding techniques have been developed (Puget and Stecker 1974; HS). A group of us (Stecker, et al., 1989) has been using these techniques on the IRAS data. We present here our first results. We will restrict ourselves to a presentation and discussion only of the 100 $\mu$m infrared emission outside of 0.3 of the Sun-Galactic Center distance from the Galactic Center, excluding the strong source of emission in the very central region of the Galaxy. An extensive and quantitative report of all of our results, including other IRAS wavelength channels as well as a treatment of the inner 3 kpc of the Galaxy will be presented elsewhere.

We assumed cylindrical symmetry in each half of the galactic plane separately, so that the infrared emissivity derived in each half-plane would be a function of galactocentric radius R, independent of the height above the galactic plane up to a characteristic height h. Denoting $r \equiv R/R_\theta$, where the solar galactic radius $R_\theta$ is presently defined to be 8.5 kpc, the flux as a function of longitude is given by

$$I(\ell) = R_\theta/2\pi \int_0^{b_m} db \int_0^{(h/R_\theta)\cot b} \epsilon(r) \, d\rho \qquad (2)$$

where b is galactic latitude, $\epsilon$ is emissivity per unit volume and $\rho$ is line-of-sight distance in solar galactic radial units. If we divide the flux into inner and outer Galaxy contributions, assuming the outer Galaxy emissivity to be a constant out to some maximum radius $R_m$, the inner Galaxy emissivity can be unfolded using Laplace transforms (Puget and Stecker 1974) into the form

$$\epsilon_i(r) = \frac{2(1-r^2)}{h} \int_{r^2}^{r_m^2} d\eta \, (\eta-r^2)^{-1/2} \frac{d}{d\eta}(-\, I_i(\ell)\sec \ell) \qquad (3)$$

where $\eta \equiv \sin^2\ell$. This method has been shown to work well if confined to the longitude range within 60° of the galactic center, thus unfolding the inner Galaxy flux within the range $0 \leq r \leq 0.86$.

The IRAS 100$\mu$m fluxes were integrated over a range of ±1° in galactic latitude around the midplane. The resultant distribution is shown in Fig. 5. To eliminate pointlike and small extended sources, thus separating out the underlying diffuse emission, an infinum filter was employed. This filter
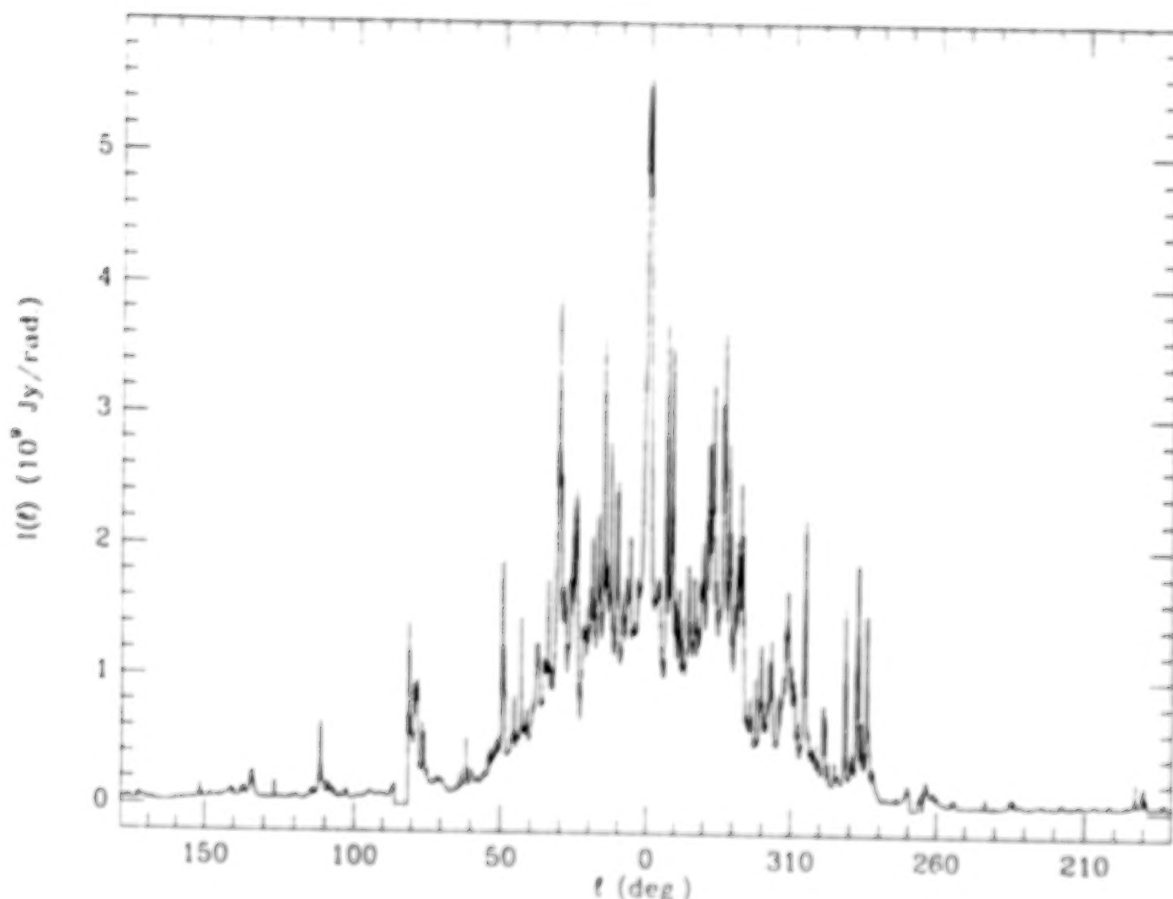
Figure 5.   The observed 100 μm IRAS flux longitude distribution from the galactic plane integrated over ± 1° in latitude.

chooses the greatest lower bound to the latitude integrated intensity in longitude intervals of 1°, cutting out features of less than 1° angular extent. We were then left with a few strong nearby far-infrared source which happen to be located at low galactic longitude such as M16, M17, W22, W33 and FIR 352.3. Because these sources are relatively close and strong, they were not removed with the automatic infinum filter method and had to be removed by subtraction and interpolation. Since they are at low longitudes and nearby, the effect of leaving them in would be to produce an artificial overestimate of the far-infrared emissivity inside of 4 kpc from the galactic center when the geometric unfolding algorithm was applied. After these sources were also removed, the longitude profile of the emission was regenerated by spline fitting the remaining diffuse flux values. The resulting distribution obtained is shown in Fig. 6. In order to give a more intelligible picture of the galactic large scale structure, a further averaging over 4° intervals in longitude was used before unfolding in order to obtain the radial distribution of the diffuse emissivity. We have checked our calculations by using the unfolded emissivity distributions and integrating them over the line-of-sight for various galactic longitudes as in eq. (2) to regenerate the FIR longitude distribution. The derived longitude profile faithfully reproduces the IRAS data profile, thereby demonstrating the accuracy of the unfolding technique.
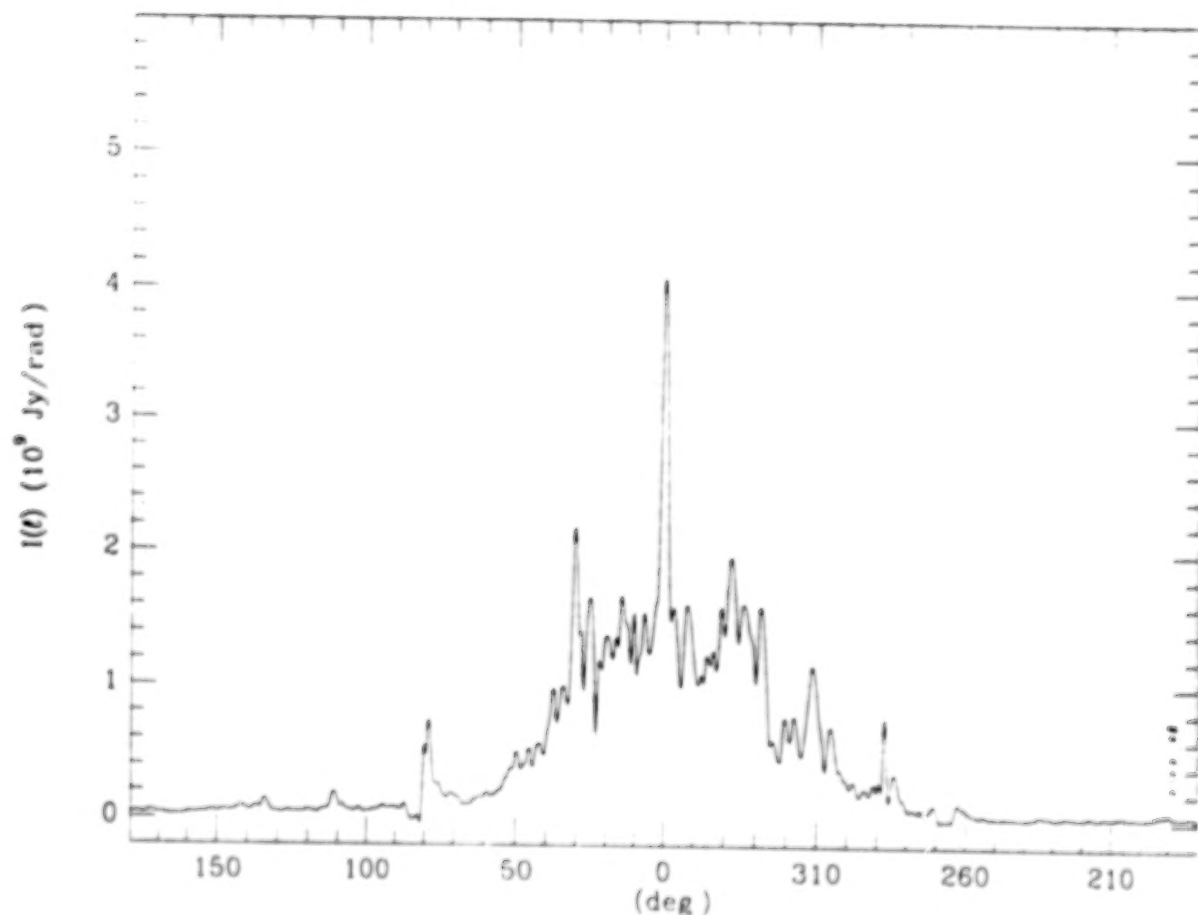
**Figure 6.** The IRAS flux distribution derived from Fig. 5 but with point sources removed.

A *prima facie* case for the close relationship between galactic γ-ray emission can be demonstrated by a direct comparison of their galactic longitude distributions. The has been done by the author (Stecker 1990) using the SAS-2 data, which are free of intrinsic detector background problems. A comparison of the diffuse IRAS emission profile (Fig. 6) with the 0.3-5 GeV COS-B longitude profile, obtained directly from the data tape, is shown in Fig. 7. We used the higher energy data because, although the photon count is lower, the angular resolution is better. We have offset the COS-B profile in Fig. 7, by subtracting a constant average background flux of $3 \times 10^{-5}$ (cm$^2$ s sr)$^{-1}$ in order to get a reasonable fit, something which was unnecessary in the case of the SAS-2 data. The author feels that owing to the uncertainty in the COS-B in-flight detector background, this additional "renormalization" may be allowable (Some may wish to consider our offset as merely suggestive or pedagogical.) At any rate, the future EGRET data should unambiguously determine the γ-ray flux in the anticenter direction.

The only obvious strong differences in the two profiles arise from the

Fig. 7. A comparison of the point source subtracted IRAS longitude distribution shown in Fig 6 (light curve) with the COS-B 0.3-5 GeV galactic γ-ray flux profile averaged over ± 10° in latitude obtained from the final COS_B data tapes (heavy zig-zag line) with an additional offset subtraction of $3 \times 10^{-5}$ $(cm^2 \ s \ sr)^{-1}$ (see text).
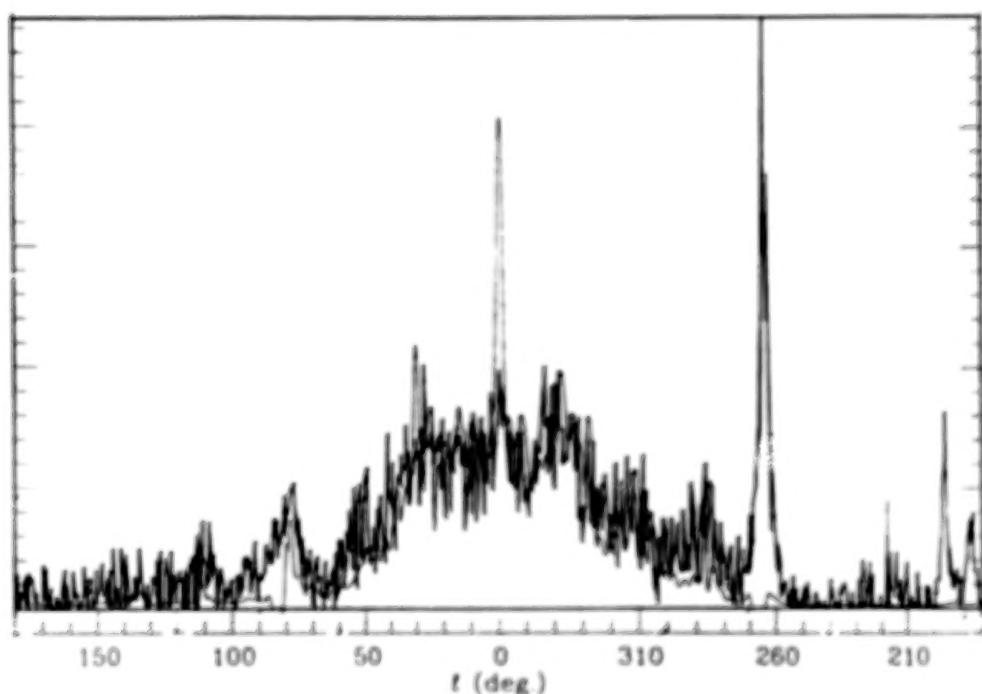
known sources which are left in, viz., the strong FIR source at the galactic center and the three intense γ-ray sources being the Crab and Geminga in the anticenter direction and the Vela pulsar at ι ~ 270°.

The galactic far-infrared radial emissivity distributions which we obtained from our unfolding using eq. (3) are shown in Figures 7 through 9 and compared with the radial distributions of other galactic components. Error bars are shown in the case of the γ-ray data which are a result of the statistics of the relatively few photons involved. Of course, in the case of the IRAS data, such statistical errors are negligibly small. As can be seen from Figure 8, the distribution of γ-ray emission, obtained by unfolding the SAS-2 and COS-B longitude data (HS), correlates well with the FIR emission on a galactic scale, supporting the thesis that the galactic γ-ray emission is associated with the most active regions of young star formation in the Galaxy (Stecker 1976). A further test of this hypothesis lies in a comparison of the distributions of FIR and CO emission. Figure 9 shows a comparison with the total CO cloud emission, whereas Figure 10 shows a comparison for the northern hemisphere with the distribution of warm clouds.

The correlation between our unfolded FIR distribution and the warm CO cloud distribution is remarkably striking, indicating that IRAS is most sensitive to the warmer molecular clouds. This is not surprising, since the 100μm IRAS emission drops sharply for grain temperatures below 25 K. An important implicit result here is that the pure geometrical unfolding used here to treat the IRAS data does not give significant distortions from the distribution obtained from CO data which makes use of velocity information.
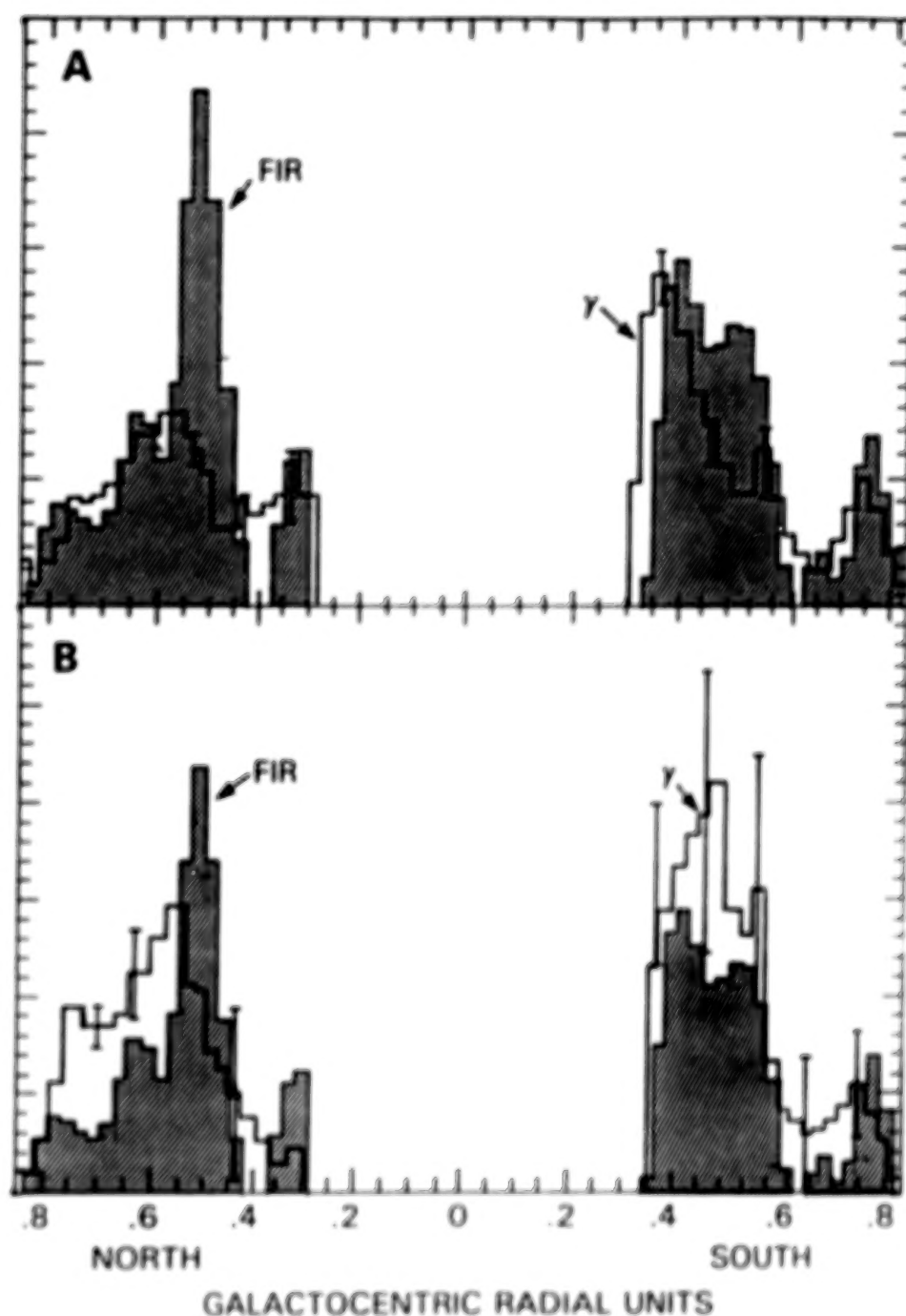
Fig. 8. (A) Relative γ-ray emissivity as a function of galactocentric distance derived from the COS-B data at energies greater than 100 MeV (Harding and Stecker 1985) as compared to the FIR emissivity distribution obtained here by a similar unfolding of the IRAS 100 μm longitude map integrated over ±1° in latitude. (B) A similar plot comparing the FIR distribution with the > 100 MeV γ-ray distribution obtained from the SAS-2 data by Harding and Stecker (1985).
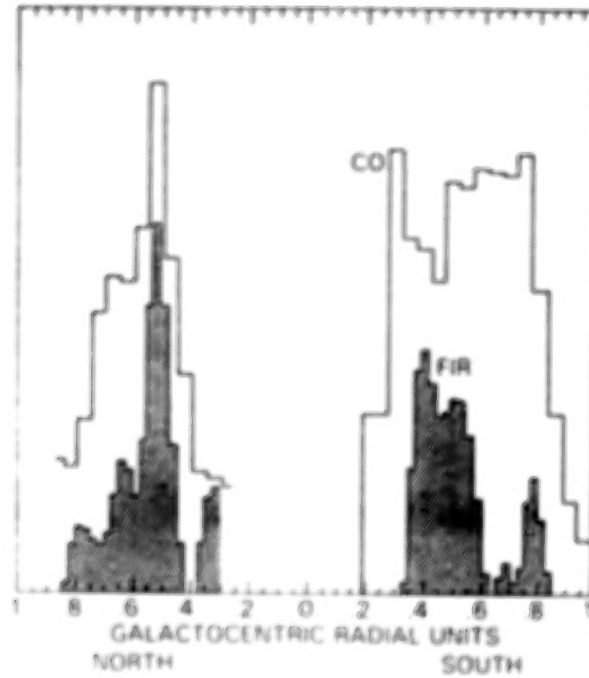
Fig. 9.   A comparison of the total CO distribution in the southern galactic hemisphere at latitude 0° (Robinson, et al. 1984) and in the northern galactic hemisphere integrated over 1° (Scoville and Sanders 1986) with the FIR emissivity distribution (as in Fig. 8).
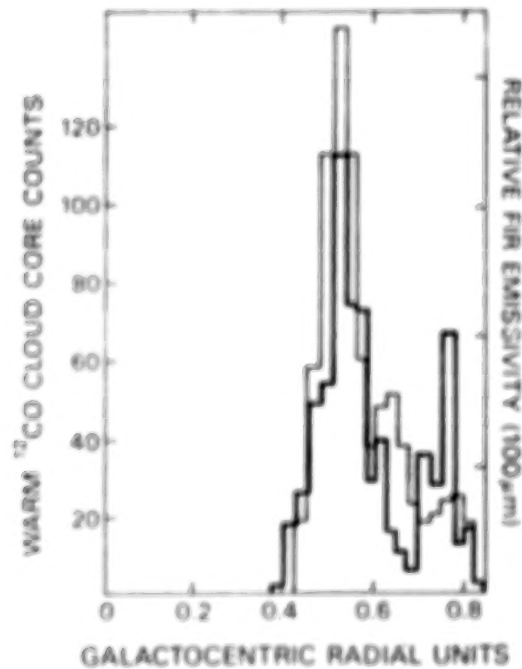


Fig. 10.   A comparison of the warm CO cloud distribution in the northern hemisphere (Solomon, Sanders, and Rivolo 1985) (heavy histogram) with the FIR emissivity distribution from the northern hemisphere as in Figs. 8 and 9 (light histogram).

73

The overall FIR and warm CO emissivity distributions appear to be consistent with the concentration of these components to spiral arms as delineated by HII regions. However, the total CO distribution appears to be more diffused than the far-infrared emission. The overall picture which emerges appears to support the view that the total molecular cloud population is not confined only to spiral arms, but that the warm clouds, strongly heated by O and B stars, are associated with spiral arm structure.

Both the warm CO and FIR distributions show characteristic peaks in the north at radial units of -0.5 and -0.75 corresponding to the 5 kpc ring and Sagittarius arm respectively. There is a hint of a possible secondary peak in both distributions at -0.6. One could speculate that this is an indication that two spiral arms may lie within the 5 kpc ring. Figure 10 also suggests that the FIR emissivity per cloud is higher in the 5 kpc ring than in the Sagittarius arm. The total CO and $\gamma$-ray distributions also correlate well in the northern region, but do not show detailed structure. In the case of the $\gamma$-rays, this may be due in part to the poorer angular resolution; there is some hint of a shoulder in the $\gamma$-ray distribution corresponding to the Sagittarius arm. In the south, one sees both the 5 kpc ring and peaks at -0.8 corresponding to the Crux arm in both the $\gamma$-ray and FIR distributions.

Our results, clearly showing the 5 kpc ring, are in general agreement with earlier balloon flight results of Caux, et al. (1984) and with the coarser unfolding of the IRAS data by Burton, et al. (1986) and Sodroski (1988), who also find evidence for strongly peaked emission originating in the 5 kpc ring. Of the 14 nearby Sa and Sb type spiral galaxies surveyed in CO emission, 5 have been found to have molecular cloud rings (Young 1987). Young and Scoville (1982) have noted a distict correlation between the spatial distributions of blue-light emission and molecular clouds in Sc galaxies. For our Galaxy, Scoville and Good (1987) find that molecular clouds associated with HII regions are almost an order of magnitude brighter per unit cloud mass than clouds not associated with HII regions, the difference owing to the presence of O and B stars in the former. One must conclude that the large amount of far-infrared emission coming from the GGR strongly implies a large increase in the gas density and star formation rate there.

The fundamental result presented here is that a direct deconvolution of the far infrared luminosity distribution, independent of both the atomic and molecular gas observations, yields a radial distribution which clearly shows the molecular cloud ring at 4-8 kpc. This feature is clearly seen in all population I tracers e.g., CO, radio HII regions, pulsars and SN remnants, as well as $\gamma$-rays (Stecker 1976), but not in 21 cm HI surveys.

This result clearly links the molecular cloud distribution (rather than atomic) to the cycle of star formation and hence luminosity generation in the Galaxy. The picture of galactic activity borne out by $\gamma$-ray, CO and far-infrared surveys of the Galaxy delineates the cycle of activity in regions of active star formation. The OB associations condense out of cool dusty molecular clouds through gravitational collapse. The O and B stars ionize the gas around them to create HII regions and heat the dust in the surrounding clouds, causing them to reradiate in the far infrared band. At the end of their short life they explode into supernovae. Cosmic rays are produced

either in the shock waves generated by the supernova explosions or in the pulsars which they leave behind. Colliding with atomic nuclei primarily in molecular clouds, they produce γ-rays. The compound effect of cosmic rays and molecular clouds being enhanced in the 5 kpc ring leads to strong γ-ray emission there. In an analogous way, the compound effect of enhanced dust density and radiation from the massive young stars leads to strong far-infrared emission in the 5 kpc ring. Since the gas-to-dust ratio in the Galaxy appears to be relatively constant, and since the supernovae are from the massive stars, it is logical to expect a strong large scale correlation between FIR and γ-ray emission. It follows from all of this evidence that the region of the 5 kpc molecular ring is a place where the young objects in the Galaxy are most prolific (Stecker 1976).

It remains to be seen what EGRET, with its higher angluar resolution and sensitivity and expectedly low intrinsic background. will show us about the morphology of the galactic plane in γ-rays. However, because of the close relationship between the FIR emission, given by the very high resolution IRAS survey, and the galactic γ-ray emission, a detailed comparison of morphologies will shed light on the distribution of galactic cosmic rays and their diffusion characteristics.

## ACKNOWLEDGMENTS

## REFERENCES

Bronfman, L., Cohen, R. S., Alvarez, H., May, J., and Thaddeus, P., 1988, Ap. J. **324**, 248.

Burton, W. B., 1976, Ann. Rev. Astron. Ap. **14**, 275.

Burton, W. B., Duel, E. R., Walker, H. J., and Jongeneelen, A. A. W., 1986, in Light on Dark Matter (ed. F. P. Israel) Reidel, Dordrecht, p357.

Caux, E., et al., 1984, Astron. Ap. **137**, 1.

Clark, G. W., Kraushaar, W. L. and Garmire, G. P., 1968, Ap. J., **153**, L203.

Clemens, D. P., Sanders, D. B., and Scoville, N. Z., 1988, Ap. J. **327**, 139.

Dame, T. M., et al., 1987, Ap. J. **322**, 706.

Dermer, C. D., 1986, Astron. Ap. **157**, 223.

Fichtel, C. E., et al., 1975, Ap. J. **198**, 163.

Fazio, G. G. and Stecker, F. W., 1976, Ap. J. **207**, L49.

Harding, A. K. and Stecker, F. W., 1985, Ap. J. **291**, 471.

Lockman, F. J., 1979, Astrophys. J. **232**, 761.

Mayer, C. J., et al., 1987, Astron. Ap. **180**, 73.

Mayer-Hasselwander, H. A., et al., 1982, Astron. Ap. **105**, 164.

Myers, S. T. and Scoville, N. Z., 1987, Ap. J. **312**, L39.

Puget, J. L. and Stecker, F. W. 1974, Ap. J., **191**, 323.

Roberts, W. W., Jr., et al., 1975, Astrophys. J. **196**, 381.

Robinson, B. J., et al., 1984, Ap. J. **283**, L31.

Sanders, D. B., Solomon, P. M., and Scoville, N. Z., 1984, Ap. J., **276**, 182.

Sanders, D. B., Clemens, D. P., Scoville, N. Z., and Solomon, P. M., 1986, Ap. J. Suppl. **60**, 1.

Scoville, N. Z. and Good, J. C., 1987, in Star Formation in Galaxies NASA-CP **2466**, (ed. C. J. Lonsdale Persson), p.3.

Scoville, N. Z. and Sanders, D. B., 1986, in Interstellar Processes, ed. H. Thronson and D. Hollenbach (Dordrecht: Reidel), p. 21.

Scoville, N. Z. and Solomon, P. M., 1975, Astrophys. J. **199**, L105.

Solomon, P. M. and Mooney, T. J., 1988, in Galactic and Extragalactic Star Formation (eds. M. Fich and R. Pudritz) Reidel, Dordrecht, in press.

Solomon, P. M. and Rivolo, A. R. 1987, in The Galaxy (ed. G. Gilmore and B. Carswell) Reidel, Dordrecht, p.105.

Solomon, P. M. and Sage, L. J., 1988, preprint.

Solomon, P. M., Sanders, D. B. and Rivolo, A. R., 1985, Ap.J. **292**, L19.

Solomon, P. M. and Stecker, F. W., 1974, Proc. ESLAB Gamma-Ray Symposium, Frascati (ESRO SP-106), p. 253.

Sodroski, T. J., 1988, unpublished.

Stecker, F. W., 1969, Nature **222**, 865.

Stecker, F. W., 1970, Astrophys. and Space Sci. **6**, 377.

Stecker, F. W., 1971, Cosmic Gamma Rays (Baltimore: Mono Book Corp.).

Stecker, F. W., 1975, Phys. Rev. Letters, **35**, 188.

Stecker, F. W., 1976, Nature **260**, 412.

Stecker, F. W., 1977, Ap. J., **212**, 60.

Stecker, F. W., 1979, Astrophys J. **228**, 919.

Stecker, F. W., 1981, Proc. Greenbank Workshop on The Phases of the Interstellar Medium (Greenbank, N.R.A.O.) ed. J. Dickey, p. 151.

Stecker, F. W., 1989, in Cosmic Gamma Rays, Cosmic Neutrinos and Related Astrophysics ed. M. M. Shapiro and J. P. Wefel (Dordrecht: Kluwer Acad. Press), p. 85

Stecker, F. W., 1990, to be published in a Festschrift for Maurice Shapiro, Univ. Chicago Press, in prep.

Stecker, F. W., Harding, A. K., Skibo, J., Scoville, N. Z., and Good, J. C.,
  1989, submitted for publication.
Stecker, F. W., and Jones, F. C. 1977, Ap. J., 217, 843.
Stecker, F. W., Solomon, P. M., Scoville, N. Z., and Ryter, C E., 1975, Ap.
  J., 201, 90.
Strong, A. W., et al., 1987, in Proc. 20th Intl. Cosmic Ray Conf. (Moscow) 1,
  125.
Young, J. S., 1987, in Star Formation in Galaxies NASA CP-2466 (ed. C. J.
  Lonsdale Persson) p. 197.
Young, J. S. and Scoville, N. Z. 1982, Astrophys. J., 260, L41.

## DISCUSSION

*Joe Taylor:*

Was your elimination of point sources from the IRAS map done before or after the integration over latitude? It seems to me it would be more effective if done before.

*Floyd Stecker:*

The elimination of point sources was performed after the integration over $\pm 1°$ in latitude. We estimate that performing the cut before integration (2 dimensionally) will not make a significant difference in our large-scale results, however, we can look at this more closely.

*Volker Schonfelder:*

I would like the COS-B team members to discuss the discrepancies in galactic longitude distributions from SAS-2 and COS-B.

*Hans Mayer - Hasselwander:*

The longitude distributions derived from both experiments are found to be in good agreement on a large scale (inner galaxy -outer galaxy). On a scale of several degrees in some places significant differences are found. These most likely are attributable to long term changes in the instruments sensitivities which probably in all cases could not be corrected in a perfect manner.

*Wim Hermsen:*

A comparison of the skymaps derived from the data in the final COS-B data base with SAS-2 skymaps showed that the distributions are fully consistent on a large scale (e.g. outer galaxy, inner galaxy intensity ratios). There remain small scale differences which in part might be real. Furthermore, there is no remaining background problem in the COS-B data.

*Pulsars*

# RADIO PULSAR TIMING OBSERVATIONS FOR GRO

J. H. Taylor

Joseph Henry Laboratories and Physics Department
Princeton University
Princeton, New Jersey 08544

### Abstract

Gamma rays probably provide the best diagnostic tool for probing the enigmatic physics of pulsar magnetospheres. At present, however, only two pulsars—the young, nearby ones in the Crab and Vela X supernova remnants—have been reliably detected at gamma-ray energies. With adequate radio observations to provide independent timing information, Gamma Ray Observatory should be able to detect a number of additional pulsars, and the results will be of great benefit in testing magnetospheric theories and models. Timing observations for this purpose have been started at a number of radio observatories around the world. In this paper I describe the general procedures being used, and I give a status report on the work by the Princeton group.

## I. INTRODUCTION

The Crab and Vela pulsars have shown that gamma rays emitted by pulsars, and the associated electrodynamical processes, together account for a substantial fraction of a spinning neutron star's rotational energy losses. However, despite some early reports that proved premature, additional confirmed examples of gamma-ray/radio pulsars have not yet been found. For this reason we have very little statistical information on the range of parameters and distinguishing characteristics of gamma-emitting pulsars. The greatly increased sensitivity of instruments aboard Gamma Ray Observatory now gives us new reason for hope, and I believe we can be reasonably confident that GRO will succeed in detecting at least a few more examples of periodically pulsed gamma rays from radio pulsars.

With the planned schedule for pointing the GRO spacecraft, a number of radio pulsars will simultaneously lie in the field of view for periods of about two weeks. Even for the very bright Crab and Vela pulsars, the number of gamma photons detected in this time will be orders of magnitude less than the number of elapsed pulsar periods. This sparseness of data, together with the substantial background levels, will make it extremely difficult to search for unknown (or poorly known) periodicities in the gamma-ray data treated by itself. On the other hand, if accurate radio timing data are available it will be possible to phase-resolve the gamma-rays, in turn, for each of the pulsars in the field of view. Histograms of the calculated phases will then represent the pulsar's integrated waveform at gamma-ray energies, and it will be possible to average these coherently for the duration of the pointing session or even over several sessions. For this technique to be effective, the gamma photons must time-tagged at the time of observation with an accuracy of $\lesssim 1$ ms. This will be accomplished easily by the instrumentation aboard GRO.

Although a definitive model for the emission mechanism of radio pulsars does not yet exist, enough is known that one can make educated guesses about which ones might be good gamma-ray candidates. However, the incremental cost of making timing observations of a sizable list of radio pulsars is small enough to encourage making the observing lists rather long, thereby hedging all theoretical bets and minimizing the chances that interesting gamma-ray pulsars will be overlooked for want of the necessary radio data. In planning the appropriate observing strategies it is important to note that the young, fast pulsars thought most likely to show detectable gamma-ray emission have much poorer rotational stabilities than older pulsars. For this reason, it is desirable that the radio timing observations be contemporaneous with the collection of gamma-ray data, or nearly so.

Efforts toward providing concurrent radio support observations have been started by groups using the Arecibo, Green Bank, Jodrell Bank, and Parkes radio telescopes. An attempt has been made to coordinate the observing lists, taking advantage of the differing sensitivities and sky coverage of the telescopes to maximize the size of the total list, while keeping redundancies to a minimum. Approximately 125 pulsars are being observed at Arecibo, 140 at Green Bank, 130 at Jodrell Bank, and 100 at Parkes. The details of the observing lists may change as observing experience is accumulated over the next few months, but I do not expect any significant reduction in the total number of pulsars being timed. (In fact, the observing lists are probably more likely to grow than to shrink.) In Figure 1, I present a map in galactic coordinates of the pulsars currently on the observing lists at the four Observatories.

## II. PULSAR TIMING METHODOLOGY

My group at Princeton is concentrating its GRO-related efforts at two of the NRAO[1] telescopes at Green Bank: a 26 m antenna operated for the United States Naval Observatory, and the 42 m telescope. The majority of pulsars on our list require the sensitivity of the 42 m telescope, and data-taking for them is scheduled in sessions of several days duration every two to three months. Most of the observations are made at frequencies near 400 MHz, with a few others near 1420 MHz. A total of 115 pulsars are being observed in this program. The data acquisition system is based on a digital, FFT-based "spectral processor" recently completed by the NRAO electronics division. In our mode of operation, this specialized hardware records, every 2 minutes and for each sense of circular polarization, a two-dimensional array of measured intensities as a function of observing frequency and pulse phase. An example of such a data array is presented as a gray-scale plot in Figure 2.

Analysis of the data begins with the removal of obvious interference such as the several vertical and horizontal streaks in Figure 2 (which came from a distant thunderstorm and aircraft communications, respectively). The data are then "de-dispersed" by summing along sloping lines corresponding to the dispersion measure of the particular pulsar, and the resulting profile, similar to the one at the bottom of Figure 2, is matched with a standard profile to determine its phase at the accurately recorded time of observation. This procedure yields an equivalent pulse time of arrival, or TOA, with an accuracy that depends on the signal-to-noise ratio. Typical accuracies are around $10^{-3}$ to $10^{-4}$ periods.

---

[1]The National Radio Astronomy Observatory is operated by Associated Universities, Inc., under an operating agreement with the National Science Foundation.
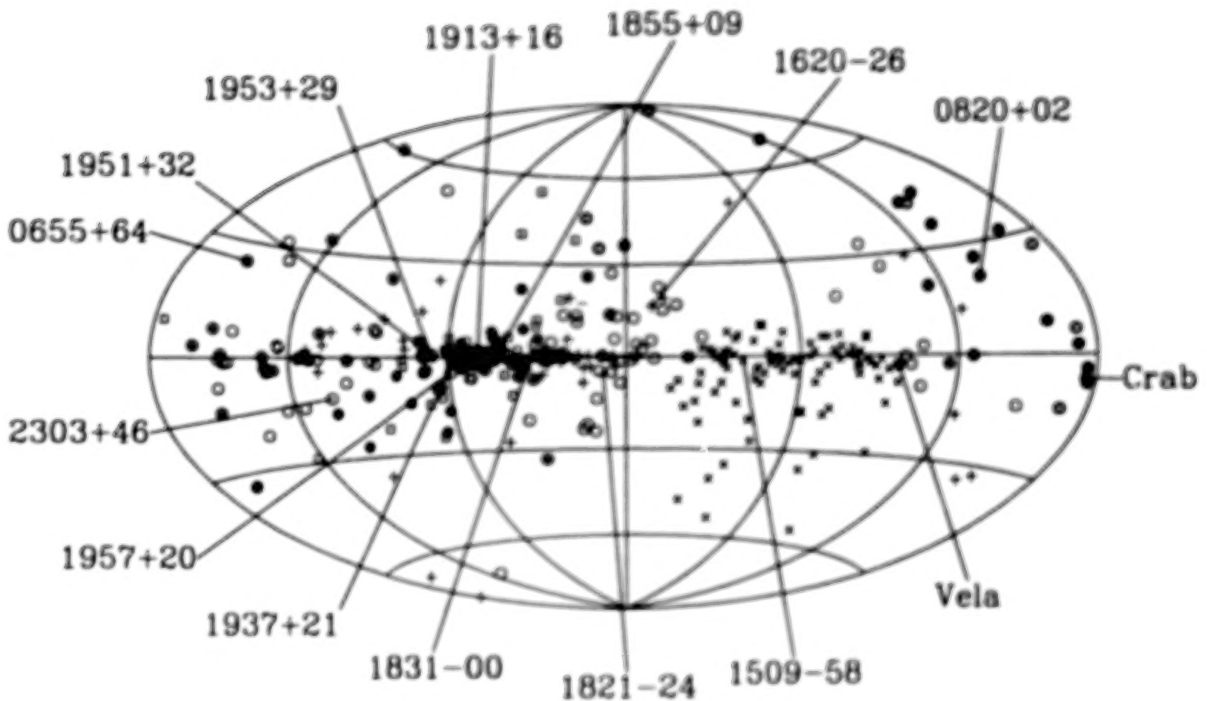
Figure 1: A map in galactic coordinates showing the radio pulsars being timed for GRO at four radio observatories: Arecibo (□), Green Bank (○), Jodrell Bank (+), and Parkes (×).

The strongest 35 pulsars being timed at Green Bank are observed much more often, using an automated system at the 26 m telescope. This antenna is used for VLBI observations (in connection with the timekeeping mission of the USNO) for 24 hours about every 5 days. For the remainder of the time it is dedicated to pulsar timing, using receivers built at NRAO for this purpose and a data acquisition and analysis system built at Princeton. The observations are made at a center frequency of 610 MHz, and profiles are recorded in 16 channels of 1 MHz bandwidth for each sense of circular polarization.

Telescope pointing and data acquisition chores are carried out by two 80286-class personal computers, loosely connected by a serial link carrying time and status messages every 10 seconds. The computers follow the same schedule, proceeding in sequence through a list of 35 pulsars and carrying out a 20- to 60-minute observation of each one. When an observation has been finished, the recorded data are sent over an Ethernet link to a minicomputer running UNIX, and stored there on disk. At 0200 local time every morning—when the minicomputer is generally not very busy—a background task awakens, processes any new pulsar timing data that it finds on its disk, and E-mails the new TOAs to Princeton. This system has been working reliably through most of 1989, and is now producing good TOAs for at least 29 pulsars, including several of the top prospects for detection by GRO.

### III. STATUS REPORT

Some examples of standard profiles for pulsars observed with the 26 m telescope are
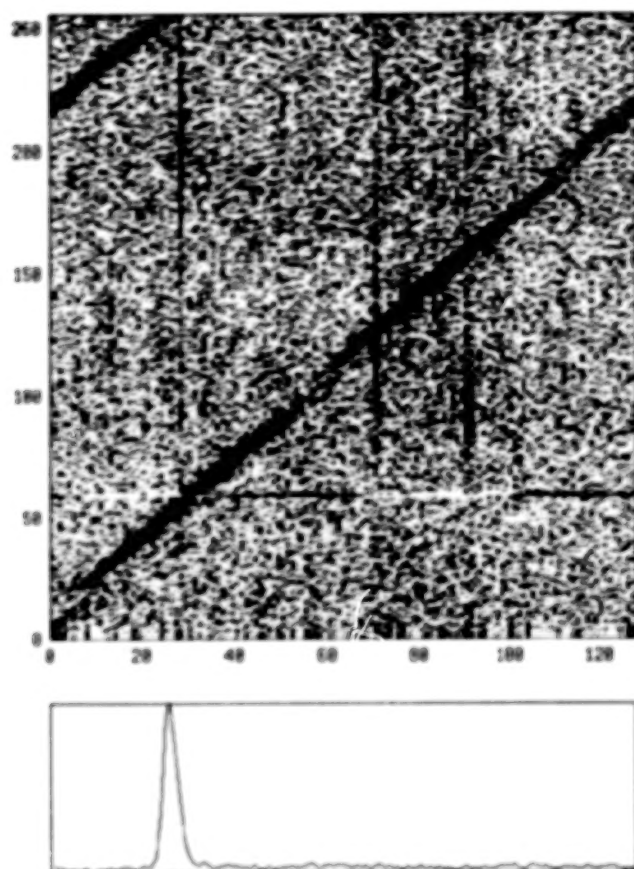
Figure 2: An example of data recorded using the NRAO Spectral Processor. The ordinate represents frequency channel number, in this case running from 400 MHz (bottom) to 380 MHz (top); the abscissa is pulsar phase over a full period. The de-dispersed average waveform of the pulsar is shown at the bottom.

shown in Figure 3. Similar profiles are now being produced from data recorded in the first three observing sessions with the 42 m telescope, in June, August, and October 1989, so that analysis of these data can proceed as well. After the standard profiles have been matched with observed profiles by a least-squares procedure, the resulting TOAs for each pulsar are accumulated in files from which they can be recalled and subjected to a multi-parameter solution for the relevant timing and astrometric parameters.

Post-fit residuals from the timing solutions are one of the best indicators of data quality, and they also yield interesting information on the amount of "timing noise" exhibited by a particular pulsar. Some representative plots of the residuals for PSRs 0329+54, 0740-28, and 1237+25 are presented in Figure 4. Parameters determined from these solutions are listed in Table 1, as an example of the information that the program will produce.

**Table 1: Examples of Astrometric and Spin Parameters for Three Pulsars, from 1989 Data.**

| Parameter | PSR 0329+54 | PSR 0740−28 | PSR 1237+25 |
|---|---|---|---|
| Right ascension (J2000) ... | 03 32 59.44(4) | 07 42 49.040(10) | 12 39 40.43(9) |
| Declination (J2000) ....... | +54 34 43.7(2) | −28 22 45.0(4) | +24 53 49.3(9) |
| Period (s) ................. | 0.714519923020(14) | 0.166759979250(5) | 1.38244920284(8) |
| Period derivative $(10^{-15})$... | 2.079(15) | 16.793(3) | 0.96(8) |
| Epoch (JD−2440000) ..... | 7735.0 | 7735.0 | 7735.0 |

Figures in parentheses represent uncertainties in the last digits quoted.
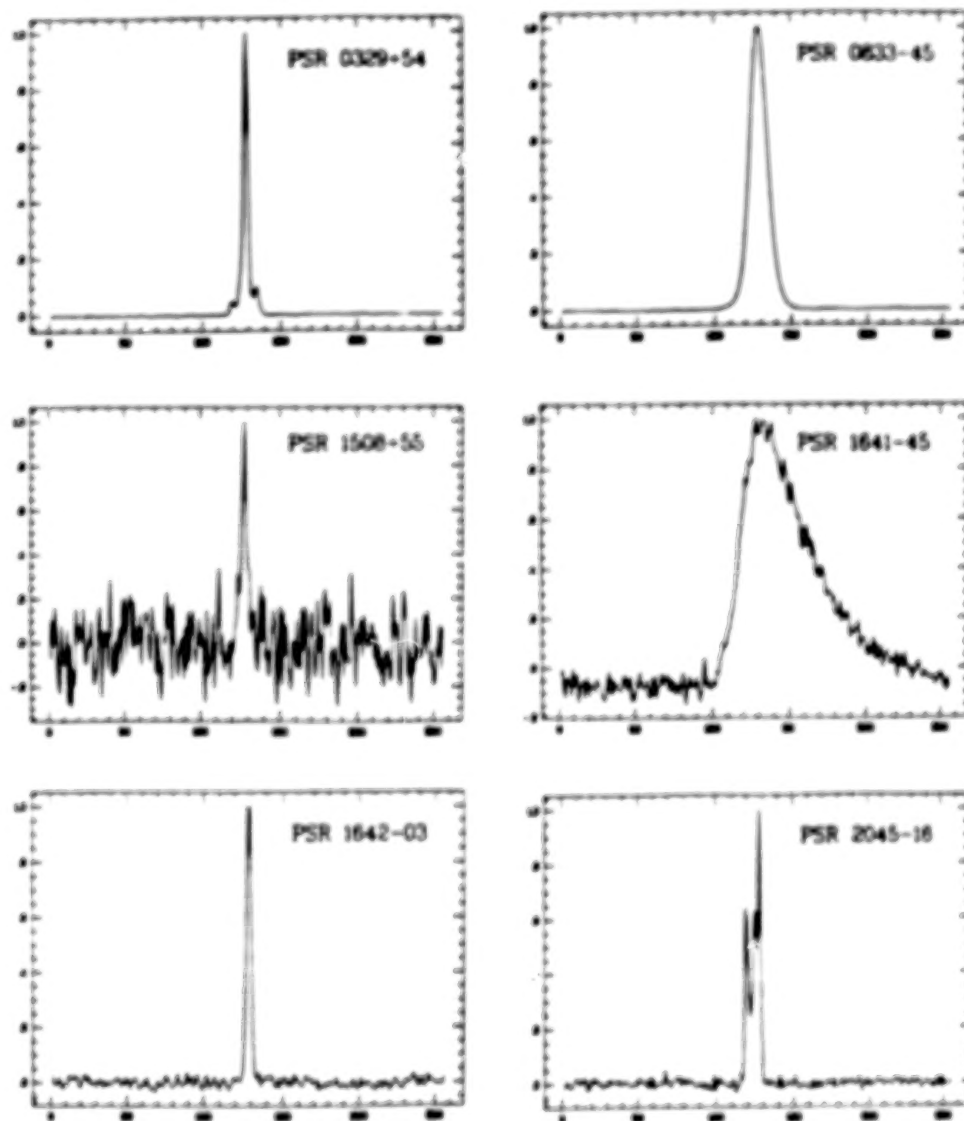


Figure 3: Standard profiles for nine pulsars being observed with the NRAO 26 m telescope at 610 MHz.
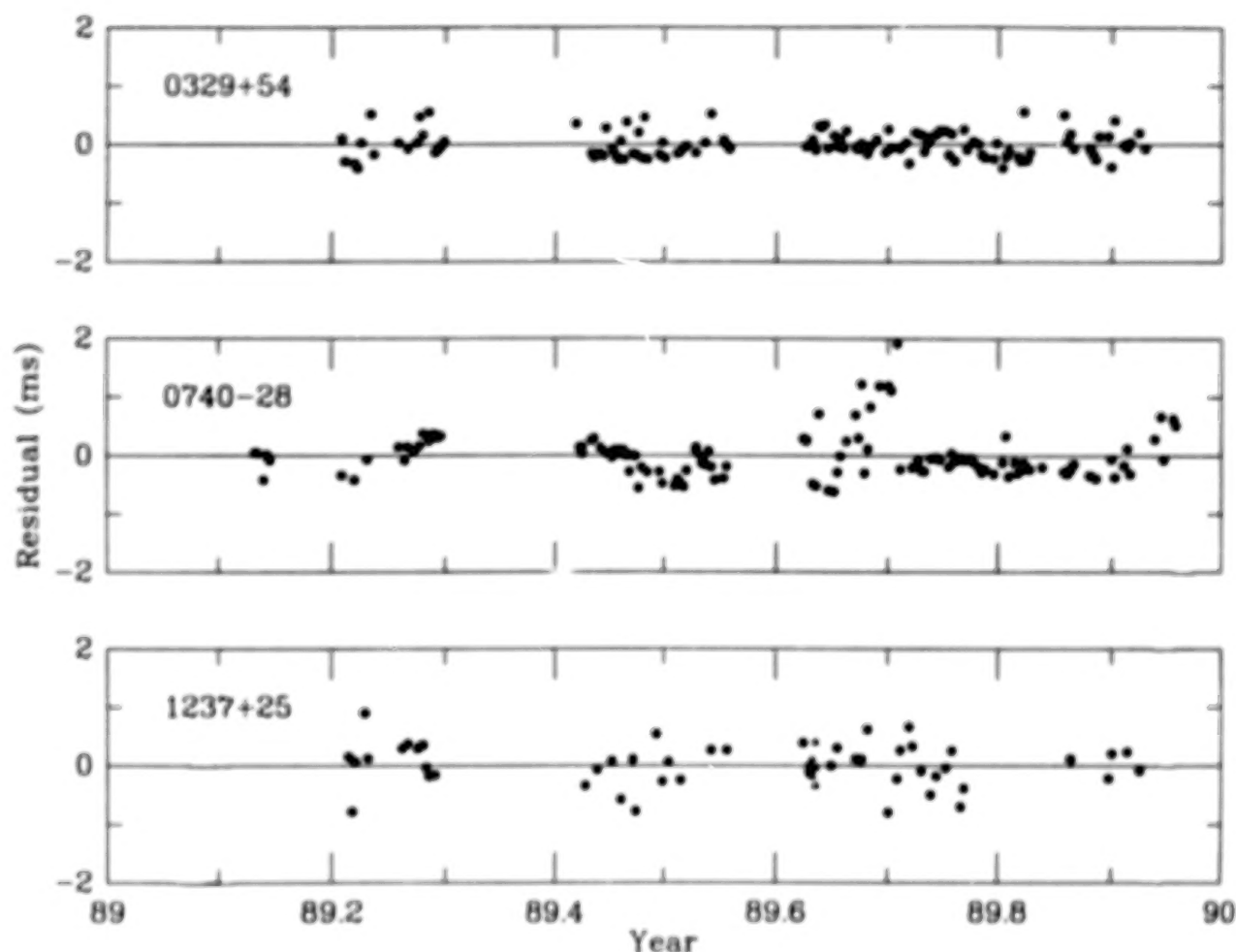
Figure 4: Post-fit residuals for timing observations of PSRs 0329+54, 0740-28, and 1237+25. The data have been averaged to a single equivalent arrival time per day. Filled triangles in the plot for PSR 1237+25 represent data taken with the 42 m telescope and the NRAO Spectral Processor; all other measurements were made with the 26 m telescope and the automated observing system described in the text.

# DISCUSSION

*R. Buccheri:*

You have shown that for some pulsar the residuals are not randomly distributed around zero but show trends whose time scale may be of the order of the GRO observing time (2 weeks). A fit of radio pulses limited to the time interval where the trend is observed, could result in a value for period significantly different from that derived by radio measurements done once every three months?

*Joe Taylor:*

Although in a few extreme cases it is true that pulsar "timing noise" can be seen over time scales as short as a few weeks, the total phase variation over such an interval is a very small fraction of a period. Barring an actual "glitch" during a GRO pointing session, there should be no problem in assigning accurate pulsar phases to GRO gamma rays.

*Jane MacGibbon:*

Can you update us on the status of the limits on $G\mu$ in cosmic string theory from changes in the pulsar periods?

*Joe Taylor:*

High precision timing of millisecond pulsars at Arecibo shows phase fluctuations of no more than a microsecond or so over as much as seven years. This result implies an upper limit of $\Omega_g < 10^{-7}$ for the fractional energy density (relative to closure density) in a stochastic background of gravitational waves with periods around several years.

# GAMMA RADIATION FROM RADIO PULSARS

Malvin Ruderman[†]

*Department of Physics*
*Columbia University*
*New York, NY 10027*

## ABSTRACT

The probable magnetospheric location and source of the $\gamma$-ray emission from some young radiopulsars is discussed. The suggested evolution of this emission as a function of pulsar period gives a diminished $\gamma$-ray luminosity for a more rapidly spinning pre-Crab pulsar. A greatly enhanced one, similar to that of unidentified Cos B sources, is predicted for a sligthly slower post-Vela pulsar, followed by a relatively rapid quenching of the $\gamma$-ray luminosity at still longer periods. Possible anomalous exo-magnetospheric pulsed MeV and TeV-PeV radiation from the Crab pulsar is considered briefly.

## I. GEOGRAPHY OF THE MAIN GAMMA-RAY EMISSION SOURCE

Among the almost 500 known radiopulsars only the relatively young rapidly spinning Crab and Vela neutron stars are confirmed $\gamma$-ray sources. The ultimate sources of this pulsed radiation are particle accelerators powered by neutron star spin-down. There are significant clues in the observed data from these two pulsars which suggest properties and locations of these accelerators.

The pulsed radiation from optical to GeV and perhaps even to $10^{12}$eV is coincident to within subpulse peak location measurement accuracy. If the emission source lies within the pulsars' magnetospheres or in the neighborhood of their light cylinder radii ($1.5 \times 10^8$cm for the Crab pulsar and $4 \times 10^8$cm for Vela) the emission source position for all of this radiation is probably coincident to within less than $10^4$cm, very much lessthan magnetosphere radii. Three arguments then suggest that this position, the same for all energetic emission and the non-precursor part of the radio emission, must be very much more than 10 neutron star radii above the stellar surface. Most likely is a source near the light cylinder.

i) There is evidence (e.g., Dowthwaite *et al.* 1984) that the Crab Pulsar's pulsed $\gamma$-ray spectrum extends to at least $10^{12}$eV. Such energetic $\gamma$-rays could not cross a magnetic filed larger than several $\times 10^6$G without conversion to $e^{\pm}$ pairs. A magnetic field satisfying the constraint for $10^{12}$eV $\gamma$-ray to escape is not found within the Crab pulsar's magnetosphere at a radius less than about half the distance to its light cylinder.

ii) The location of the Crab's optical emission, and, by inference, the X-ray and $\gamma$-ray emission coincident with it is constrained by limits on the efficiency of those emission processes which can give optical light. The observed optical intensity (assuming a

beam shape almost fully extended in latitude as argued below) implies that the optical luminosity efficiency $(\hat{f})$ satisfies

$$\hat{f} \equiv \frac{L_{\text{opt}}}{L_{\text{KE}}} > \frac{L_{\text{opt}}}{I\Omega\dot{\Omega}} \sim 10^{-5} \tag{1}$$

with $L_{\text{opt}}$ the optical luminosity, $L_{\text{KE}}$ the rate at which energy is pumped by the spinning star into the kinetic energy of particles which emit the light, and $I\Omega\dot{\Omega}$ the total Crab pulsar spindown power inferred from its measured angular spin frequency $(\Omega)$, decay rate $(\dot{\Omega})$ and calculated moment of inertia $(I)$. Acceleration of $e^-$ (or $e^+$) along $B$ gives optical radiation with

$$\hat{f}_{\parallel} \ll 10^{-6}. \tag{2}$$

For curvature radiation of photons with energy $\hbar\omega$ from centripetal acceleration

$$\hat{f}_{\text{curv}} \sim \frac{\hbar\omega}{m_e c^2} \frac{e^2}{\hbar c} \sim 10^{-8}. \tag{3}$$

For synchrotron radiation by electrons with Lorentz factor $\gamma$ and pitch angle $\theta$ in a magnetic field $B$,

$$\hbar\omega \sim \frac{\gamma^2 eB}{\sin\theta m_e c} > 10^5 \left(\frac{R_*}{r}\right)^3 \text{eV}. \tag{4}$$

Here the local Crab pulsar magnetic field is approximated as dipolar and expressed in terms of the ratio of stellar radius $(R_*)$ to radial coordinate $r$. To achieve the needed strong luminosity at optical frequencies the distance $r \gg 10r_* \sim 10^7$cm. Finally, inverse Compton scattering into the optical regime is hugely suppressed in the presence of the large neutron star magnetic field. Any $e^-(e^+)$ near the star moves along $B$ (because of very rapid synchrotron loss). In the electron's rest frame the soft photon to be up-scattered to optical energies moves almost parallel to $B$. The Thomson cross section for photon scattering $(\sigma_T)$ to angular frequency $\omega$ is then reduced to

$$\sigma \sim \sigma_T \left(\frac{\omega m_e c}{eB\gamma}\right)^2 \sim 10^{-15}\sigma_T \tag{5}$$

nea. the star. This cross section is much too small for up-scattering of microwave photons to be an important contributor to the Crab pulsar's optical luminosity. Thus only sychrotron radiation from electrons at distances $r$ approaching the light cylinder radius survives among the canonical incoherent processes for optical photon emission from a pulsar magnetosphere.

iii) The absolute magnitude of the Crab pulsar's energetic radiation luminosity also constrains the emission source location. The maximum net magnetospheric current along (open) magnetic field lines through any pulsar accelerator should not itself give a magnetic field which significantly exceeds the neutron star's own magnetic field anywhere along current flow lines (along $B$) between the polar cap $(B \equiv B_*)$ and the light

cylinder. This limits the net particle flow through any accelerator which accelerates $e^-$ and $e^+$ in opposite directions to

$$\dot{N} \lesssim \frac{\Omega^2 B_* R_*^3}{ec} < 10^{34} \text{ s}^{-1}. \tag{6}$$

If the accelerator is near the stellar surface pair production in the $10^{12}$G magnetic field (Sturrock 1971) limits the potential drop ($\Delta V$) along $\boldsymbol{B}$ to

$$\Delta V \lesssim 10^{12} \text{ Volts}. \tag{7}$$

This is much smaller than the $5 \cdot 10^{35}$erg s$^{-1}$ from the Crab pulsar in the X-ray – GeV spectral interval (for a beam shape that gives a similar observed luminosity from almost all directions). Only for $r > 10^7$cm could local $B$ be low enough to allow $\Delta V$ to exceed $10^{14}$ Volts.

## II. EMISSION BEAM STRUCTURE AND EFFICIENCY

We assume (and it is a consequence or assumption of most models) that the electrons and/or positrons injected in the the Crab's dominant magnetospheric particle accelerators are locally produced. For an accelerator close to the stellar surface these pairs could originate in the conversion of $10^2$MeV curvature $\gamma$-rays to $e^\pm$ pairs in the huge stellar magnetic field. Hwever, for accelerators as far from the star as indicated above $\gamma + \gamma \to e^+ + e^-$ is a much more important pair production mechanism. If there is strong $e^\pm$ production and acceleration of $e^-/e^+$ in the Crab magnetosphere where $r \gg R_*$, the associated radiation from these electrons (or their progeny) has several properties which are not dependent upon the detailed way in which the acceleration and radiation are achieved.

1) Because intitially accelerated $e^-/e^+$ move relativistically along local $\boldsymbol{B}$ most of the primary energetic radiation is emitted parallel to the $\boldsymbol{B}$ at the accelerator. The flow of $e^-(e^+)$ accelerated toward the star will be approximately matched by $e^+(e^-)$ flowing away from it. The same is true for any $e^\pm$ pairs created by $\gamma$-rays from the accelerator in locations where $e^\pm$ are not separated by local electric fields along $\boldsymbol{B}$. It follows from this that the emission from around these $e^- - e^+$ symmetric accelerators must consist of four beams of similar strengths (cf. Figure 1). First, a beam from outward (i.e., moving along $\boldsymbol{B}$ away from the neutron star) moving $e^-(e^+)$ or $e^\pm$ paris. Second, an almost equivalent beam from inward (i.e., moving along $\boldsymbol{B}$ toward the star) moving $e^+(e^-)$ or $e^\pm$ pairs. Finally phenomena on open $\boldsymbol{B}$-field lines connected to the star at a polar cap should be matched by very similar ones on $\boldsymbol{B}$-field lines from the opposite polar cap. Because the radiation source is so far from the stellar surface all of the radiation ultimately escapes through the light cylinder. (For near surface accelerators inward directed beams could be blocked.)

2) These four beams (only two of which would be visible to any observer) should have a very large longitudinal spread. This follows because the needed accelerator potential
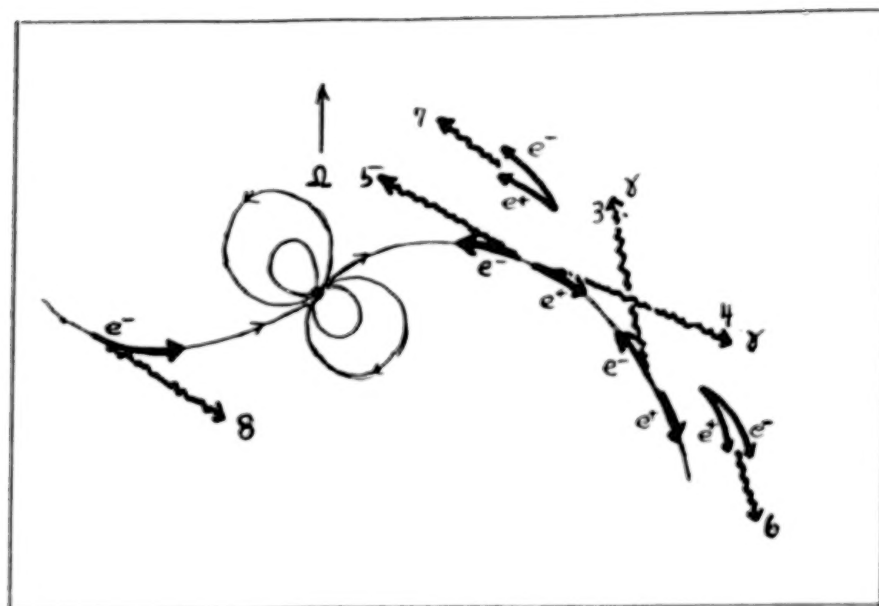
**Figure 1.** The geometry for photon emission from outer-magnetosphere accelerators which accelerate $e^-/e^+$ along local $\boldsymbol{B}$ with an electric field component $\boldsymbol{E} \cdot \hat{\boldsymbol{B}}$ within the accelerator. The resulting radiation from curvature radiation, synchrotron radiation, or inverse Compton scattering is a fan covering almost all latitudes. Similar beams go outward (4, 6) and inward (3, 7). Because of dipolar symmetry the observer who sees outward moving photons (4) in one subpusle will also see inward moving photons (8) from the other side of the star in a later arriving second subpulse as the star rotates. Gamma-ray beam crossing such as shown for 3 and 4 will sustain $e^{\pm}$ production around the accelerator.

drop in the Crab magnetosphere ($\Delta V > 10^{14}$ Volts) and the associated electric field along $\boldsymbol{B}$ ($\boldsymbol{E} \cdot \hat{\boldsymbol{B}} > 10^6$ Volts cm$^{-1}$) are so large that accelerated $e^-/e^+$ quickly achieve energies that are radiation reaction limited (by curvature radiation if inverse Compton scattering on abundant soft photons does not limit accelerated $e^-/e^+$ energies first). As a result the primary radiation, and that from secondary pairs, is determined by the accelerator $\boldsymbol{E} \cdot \hat{\boldsymbol{B}}$ which tends to be flat through the accelerator (rather than the potential drop which grows monotonically from one end to the other). The very large $\Delta V$ needed in the outer magnetosphere can be achieved only in a very long accelerator. Therefore similar $\gamma$-ray emission is expected for great distances along a downward (upward) curving $\boldsymbol{B}$-field line through the relevant accelerators. One consequence is a large probability that any observer would see two beams of energetic radiation from the accelerator no matter what the angle between the pulsar's spin ($\boldsymbol{\Omega}$) and its dipole moment or the direction to the observer. This suggested geometry (Figure 1) receives some support from two features of the observed optical, X-ray and $\gamma$-ray radiation from several young pulsars. First, searches of the Crab and Vela supernova remnants and also that containing PSR 0540-693 for such young pulsars did indeed discover them. If the rotating beams were cone-like with longitudinal widths comparable to their observed widths in latitude such a success rate would be highly improbable. The

*a priori* probability for intercepting both the Crab and Vela energetic radiation beams would not have exceeded about 1/25. Longitudinally extended fan-like beams (or very wide angle hollow cones) are more plausible alternatives. Second, all three pulsars have a double beam structure. While the large 140° subpulse separation of the Crab and Vela pulsars might suggest successive observation of North and South magnetic poles, the very much smaller 80° separation observed in PSR 0540 (Middleditch and Pennypacker 1985) argues against such an interpretation. However these separations are quite compatible with the geometry of Figure 1 where aberration and time of flight differences would give observed subpulse phase separations which can vary greatly for different viewing or tilt angles (e.g., photons 4 and 8 of Figure 1 would arrive at any observer with a time separation comparable to the time of flight difference across the light cylinder, i.e., $\Omega^{-1}$).

3) Because radiation reaction limits the $e^-/e^+$ energy achieved in the accelerator essentially the full potential drop energy $e\Delta V$ is radiated away from the accelerator. Thus the magnetosphere accelerator is almost 100 percent efficient as a radiation source.

4) Finally, the expected accelerator geometry has crossing $\gamma$-ray beams in the outer-magnetosphere (e.g., beams 3 and 4 of Figure 1) which gives copious $e^\pm$ production from $\gamma + \gamma \to e^- + e^+$ (or $\gamma + X \to e^- + e^+$ with $10^2 - 10^3$ MeV $\gamma$-rays).

## III. AN EMISSION MODEL

It has been argued elsewhere (Ruderman 1987a, Cheng, Ho, and Ruderman 1986 a,b, hereafter CHR I and II) that expected current flow in many young pulsar megnetospheres can lead to charge deficient regions ("gaps") in which $\mathbf{E} \cdot \dot{\mathbf{B}}$ grows until limited by pair production processes. For Crab pulsar or PSR 0950 outer-magnetosphere parameters a series of processes can give self-sustained $e^\pm$ production and associated energetic radiation:

a) Any $e^\pm$ produced in an accelerator gap is instantly separated by large $\mathbf{E} \cdot \dot{\mathbf{B}}$. Because of magnetic field line curvature each oppositely accelerated lepton radiates multi-GeV curvature $\gamma$-rays.

b) These $\gamma$-rays collide with KeV X-rays, from d) below, to make $e^\pm$ pairs. Pairs created in the accelerator gap itself repeat process a) above.

c) In the Crab magnetosphere pairs created beyond the gap boundary lose their energy to optical-MeV synchrotron radiation and also to higher energy $\gamma$-ray creation when they inverse Compton scatter on the same X-ray flux which was responsible for their creation.

d) The X-ray flux from snychrotron radiation is also that which originally caused materialization of the curvature $\gamma$-rays of b) and the inverse Compton scattering of c). Because of the beam crossing of Figure 1, $e^\pm$ and $\gamma$-rays interact mainly with the crossing X-ray flux radiated by the oppositely directed pairs.

e) A further generation of $e^\pm$ paris from crossed $\gamma$-ray fluxes of c) radiates soft photons extending down to far IR for Vela (CHRII). Some of this passes through the accelerator gap where it can be inverse Compton scattered by primary gap accelerated $e^-/e^+$.

This cyclic chain a) – c) of processes, bootstraps a self-sustained emission of radiation with calculated self-consistent spectra shown in Figures 2 and 3 for Crab and Vela parameters (CHR I and II). Calculated intensity spectra for PSR 0540 are compared with optical and X-ray observations and GRO thresholds in Figure 4 (Ho 1989).
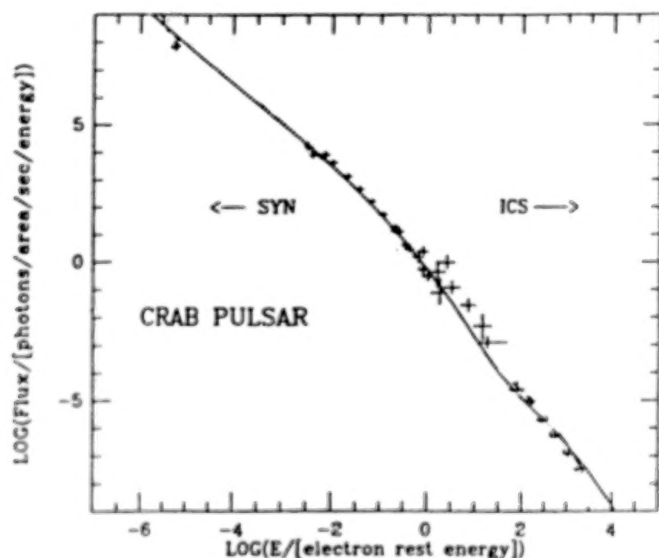


**Figure 2.** Comparison of Crab pulsar observations and a model prediction for an outer-magentosphere gap. (The normalization is adjusted arbitrarily.) SYN refers to synchrotron radiation and ICS to inverse Compton (from CHR II ).
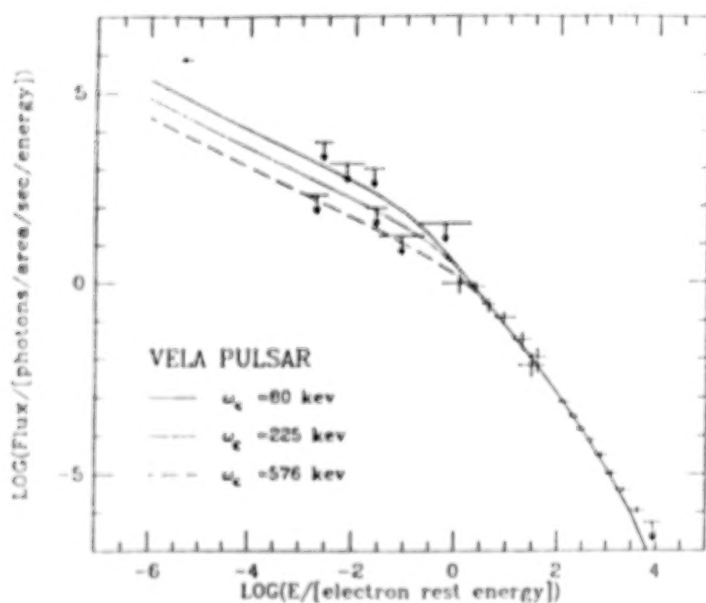


Figure 3. Comparison of Vela pulsar observations and model predictions from CHR II. The $\omega_c$ refer to Eq. (8).
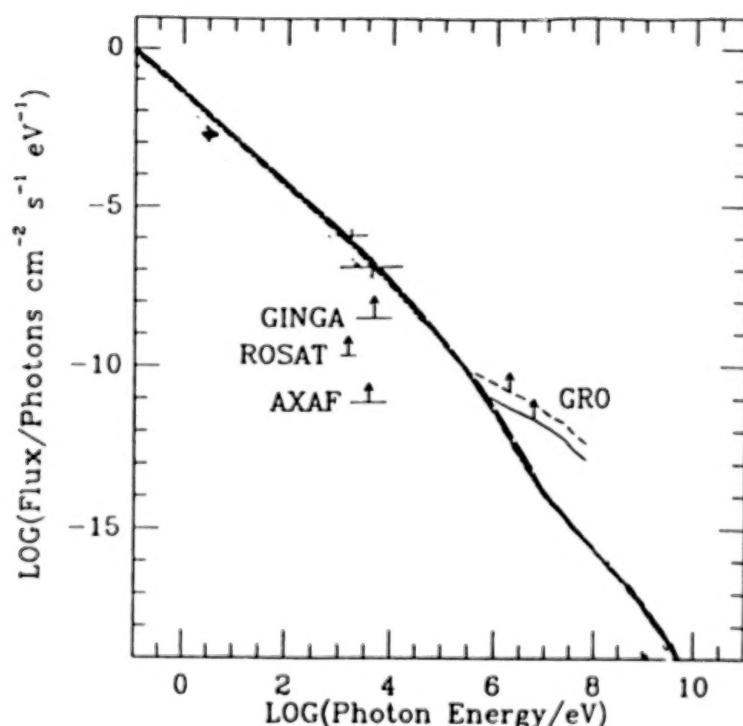
**Figure 4.** Observations and model predictions for PSR 0950 (Ho, 1989). GRO thresholds are also indicated.

The calculated break in the Vela spectrum which greatly suppresses the X-ray part of the spectrum is a direct consequence of the limited time ($\tau$) spent by synchrotron radiating $e^{\pm}$ pairs in the outer-magnetosphere. Those pairs moving inward are reflected in the converging **B**-field and join with outward moving pairs in passing out through the light cylinder. The critical sychrotron radiation frequency ($\omega_c$) achieved by the $e^{\pm}$ pairs before this happens has a $\tau$ and local B dependence (CHR II)

$$\omega_c \propto \tau^{-2} B^{-3} \propto \tau^2 \Omega^{-9} \propto \Omega^{-7} \tag{8}$$

A spectral break calculated to occur at around 40 eV in the Crab spectrum would be at $10^2$ keV in Vela's if additional corrections relating to initial pitch angle are neglected.

The rough agreement of calculated spectra and subpulse features from such outer-magnetosphere accelerator models with those observed (Figures 2, 3, and 4) may support using such models to predict the dependence of $\gamma$-ray luminostiy on pulsar period ($P$).

## IV. GAMMA-RAY PULSAR EVOLUTION

Calculated $\gamma$-ray luminosities of Crab-Vela type $\gamma$-ray pulsars ($B_* \sim 3 \cdot 10^{12}$G) as a function of a pulsar period is given in Figure 5 (Ruderman and Cheng 1988, Ruderman 1987b). For $P < P_{crab}$, $B$ in the outer-magnetosphere is greater than that of the Crab pulsar at the same fractional distance ot its light cylinder. One consequence is that it is much easier to limit the growth of outer-magnetosphere accelerator gaps by pair production. The $\gamma$-ray luminosity, which equals the accelerator power needed to achieve this limit, is roughly proportional to $P$ in this regime. The Vela pulsar has a much different mix of the processes a) – e) of Section II than that in the larger (local) $B$ of the Crab outer-magnetosphere. A much larger fraction ($f$) of its total spin-down power appears in $L_\gamma(f \sim 10^{-2})$ than was the case for the Crab ($f \sim 10^{-3}$). As the pulsar period grows beyond Vela's, local $B$ decreases and $\omega_c$ increases well above an MeV so that the efficiency for $\gamma + \gamma \to e^- + e^-$ is diminished: an increasing $f$ and $L_\gamma$ are then required to sustain needed outer-magnetosphere $e^\pm$ production. $L_\gamma$ grows until it somewhat exceeds $10^{36}$erg s$^{-1}$ and $f \to 1$. No further growth is then possible and self-sustained outer-magnetosphere accelerator pair production ceases for still longer $P$. The estimated number ($\sim 40$) and luminosity of such intense $\gamma$-ray sources are of the same order as those of the still unidentified strong Cos B sources. It is tempting to propose that these Cos B sources are indeed dying Vela type $\gamma$-ray pulsars. Even if various outer-magnetosphere accelerator details do not survive, the general argument that lengthening $P$ beyond Vela's will increase $f$ (a growth already apparent in the transition from the Crab to Vela pulsars) may be expected to be quite robust so that the predicted growth in $L_\gamma$ and subsequent $\gamma$-ray turn-off should remain valid.

Strong $\gamma$-ray sources may also be achieved for much smaller $P$ when $B_*$ is small enough. The magnetospheres of many members of the millisecond pulsar family resemble the outer-magnetosphere of the Vela family so that many of them may be detectable as strong $\gamma$-ray pulsars.

The crucial question of how canonical radio pulsars may continue to be radio emitters even if strong outer-magnetsophere $e^\pm$ production is quenched has been discussed elsewhere (Ruderman and Cheng 1988, Ruderman 1987b).

## V. OTHER ORIGINS FOR CRAB PULSAR MeV AND TeV RADIATION

Because the Crab model calculations and observations cover a spectral interval of 10 orders of magnitude and a photon flux spanning 20 the log-log plot of Figures 2, 3 and 4 show a rather promising fit. The data theory comparison in Figure 6 (Ho 1989) more clearly emphasizes the differences between theory and observations. We note first that the calculated synchrotron light is almost an order of magnitude larger than that observed. However, the Crab model calculation does not exploit the spectral break of Equation 8 which is predicted to be near optical frequencies for the Crab outer-magnetosphere. Its inclusion can very significantly reduce model predictions. The failure of the model to reach observed intensities around an MeV raises more serious questions. The data themselves have been acquired in a variety of different programs and show considerable scatter and lack of consistency. The largest observed excesses over model calculations are generally
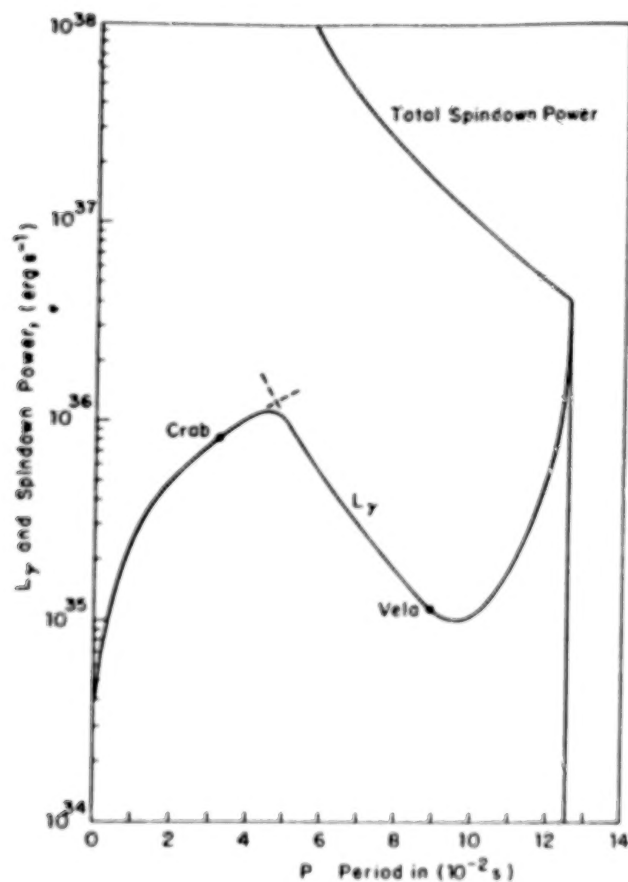
**Figure 5.** Model calculations for the evolution of the $\gamma$-ray luminosity ($L_\gamma$) of a strongly magnetized ($B_* \sim 3 \cdot 10^{12}$G) pulsar as a function of pulsar period ($P$) (Ruderman and Cheng 1988).
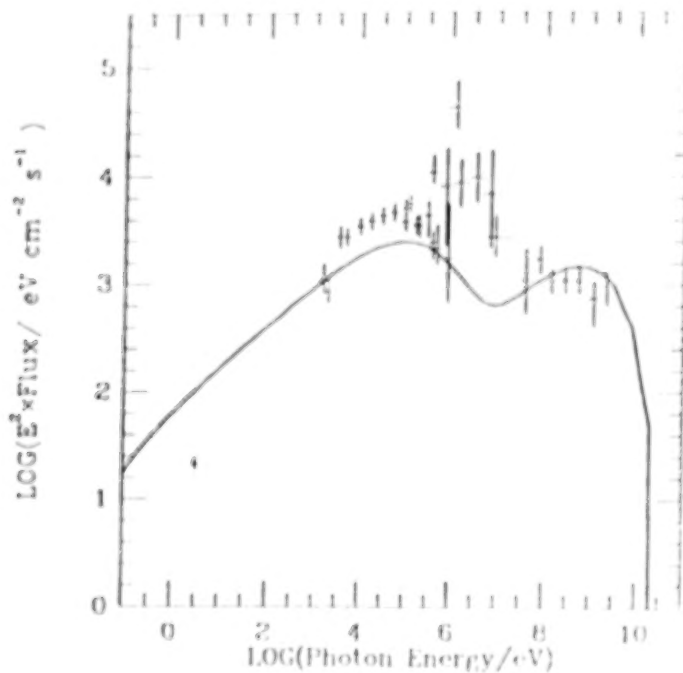


Figure 6. Emitted energy per decade of photon frequency for the crab pulsar (Ho, 1989)

those from long term observations from satellites; rocket, and balloon flight data have been closer to theoretical predictions (cf. Scönfelder 1983, White *et al.* 1985, Graser and Schönfelder 1982). It is, perhaps, possible that much of the excess is in transient activity usually missed in shorter time observations. A spectrally broad (transient) excess around an MeV may possibly have a very different kind of origin from the rest of the Crab pulsar emission. Most of the Crab spin-down power is probably carried beyond the magnetosphere light cylinder as a 30 Hz (electro-)magnetic field spun off by the rotating dipole of the neutron star and a TeV – PeV $e^\pm$ wind. The pairs are created within the magnetosphere (Section IIIe) but receive most of their ultimate energy beyond it from acceleration by the magnetic dipole radiation. This ultra-relativistic $e^\pm$ wind (whose power may approach $5 \cdot 10^{38}$ erg s$^{-1}$) can inverse Compton scatter on the pulsar's radio and optical emission. Near the magnetosphere where there is still a significant angle between the wind direction and that of the radiation photons (both approach exact radial flow only far from the magnetosphere). Inverse Compton scattering of the very abundant photons at the low end of the pulsar's radio emission spectrum may convert enough of these into MeV $\gamma$-rays to give a dominant contribution to the observed pulsed $\gamma$-ray photons in that spectral region. A large additional pulsed inverse Compton contribution by the Crab pulsar's exo-magnetospheric outgoing $e^\pm$ wind would then also be expected from inverse Compton scattering on the abundant pulsed soft X-ray emission coming from within the magnetosphere. These up-scattered $\gamma$-rays should acquire up to the full TeV–PeV energy of the wind electrons. Transient pulsed $10^{14}$eV $\gamma$-rays from the Crab have indeed been reported recently (Rao 1989) in simultaneous observations by the Kolar Gold Field air-shower group in India and the Baksan group in the USSR. Both the high luminosity $(3 \times 10^{36}$ erg s$^{-1}$ if isotropic) and $\gamma$-ray energy would make a magnetospheric origin for this radiaiton implausible ($10^{14}$eV $\gamma$-rays cannot traverse $B \gtrsim 10^4$G).

I am happy to thank Drs. V. Schönfelder and C. Ho for very helpful remarks.

# References

Cheng, K., Ho, C. and Ruderman, M. 1986a, *Ap.J.*, **300**, 500 (CHR I) and *Ap.J.*, **300**, 522 (CHR II).

Dowthwaite *et al.* 1984, *Ap.J. (Letters)*, **286**, L35.

Graser, U. and Schönfelder, V. 1982, *Ap.J.*, **263**, 677.

Ho, C. 1989, *Ap.J.*, **342**, 396.

Middleditch, J., and Pennypacker, C. 1985, *Nature*, **313**, 659.

Rao, M. 1989, *IAU Circular No. 4883* (Oct. 23, 1989).

Ruderman, M. 1987a, *High Energy Phenomena around Collapsed Stars*, ed. F. Pacini (Dordrecht: Reidel), p. 145.

Ruderman, M. 1987b, *Proc. 13$^{th}$ Texas Symposium on Relativistic Astrophysics*, ed. M. Ulmer (Singapore: World Scientific), p. 448.

Ruderman, M., and Cheng, K.S.1988, *Ap.J.*, **335**, 306.

Schönfelder, V. 1983, *Advances in Space Res.*, **3**, No. 4, 59.

Sturrock, P. 1971, *Ap.J.*, **164**, 529.

White, R. *et al.* 1955, *Ap.J. (Letters)*, **299**, L93.

# DISCUSSION

*Chuck Dermer:*

1) In your model for the Crab pulsar, what is the magnetic field strength where the X-rays are comptonized by high energy electrons? Could resonant magnetic compton scattering be important? 2) Are the high energy gamma-rays produced by photopion production from accelerated high-energy protons susceptible to attenuation from gamma-gamma or gamma-B pair production before escaping?

*Mal Ruderman:*

1) The relevant magnetic field is somewhat dependent upon the geometry of the neutron star dipole moment, spin axis, and observer direction. It is in the $10^6$ - $10^7$ G range. The compton scattering electrons still have relativistic momentum components perpendicular to the local B. In such a case I don't think there are any longer large resonant effects. 2) TeV gamma-rays would be strongly absorbed if they pass through the Crab pulsar's optical photon beam unless the passage occurs well beyond the light cylinder (or if the optical beam has holes). PeV gamma-rays must also avoid passage through a magnetic field stronger than $10^4$ G which would again put their origin well beyond the light cylinder.

# GAMMA RADIATION FROM THE CRAB AND VELA PULSARS

Gottfried Kanbach

*Max-Planck-Institut für Physik u. Astrophysik*
*Institut für Extraterrestrische Physik*
*D-8046 Garching, F.R.G.*

## ABSTRACT

The young pulsars in Crab and Vela have been observed as very efficient emitters of high energy gamma radiation. While their radiation in the radio-, optical- and X-ray range was always known to differ considerably, the gamma-ray emission on a superficial level appears quite similar:

- lightcurves with two narrow peaks, separated by 141° (Crab) and 153° (Vela)
- photon energies in excess of 1 GeV with spectra that can be described by a power-law for Crab and a broken power-law for Vela.

The detailed observations of these sources with the COS-B instrument, extending over nearly seven years, have revealed significant differences in the characteristics of the pulsars in the gamma-ray domain. Secular changes in the temporal (Crab) and spectral (Vela) properties above 50 MeV have been found. These tantalizing signatures of the pulsar emission processes must now be explored in more detail and over a larger spectral range with the GRO instruments in order to gain a deeper understanding of the physics of young neutron stars.

## I. INTRODUCTION

The conventional model for a pulsar holds that all radiative emissions of such an object are powered by the loss of rotational energy of a neutron star:

$$\dot{E}_{rot} = 4\pi^2 I \dot{P} P^{-3}$$

If a part $\eta$ (=efficiency) of this energy loss is transformed into high energy photons of an average energy $< E_\gamma >$ which are beamed into a solid angle $\Omega$ the observer at a distance $d$ can register a photon flux of:

$$\phi = \frac{\dot{E}_{rot}\eta}{<E_\gamma>} \times \frac{1}{\Omega d^2}$$

while being illuminated by the beam. The time duty cycle $\beta$ reduces the beam flux to the time average flux $< \phi >= \phi \times \beta$, which can be written in suitable units as:

$$< \phi >= 7 \times 10^{-9} I_{45} \dot{P}_{-15} P^{-3} \eta \beta \Omega^{-1} d_{kpc}^{-2} \quad (\gamma > 100 \, MeV) \, cm^{-2} \, s^{-1}$$

where $I_{45}$ is the moment of inertia in units of $10^{45} \, g \, cm^2$

$\dot{P}_{-15}$ is the period change in $10^{-15} \, s/s$

$P$ is the period in seconds.

The assumed gamma spectrum is proportional to $E^{-2}$. A pencil beam emission geometry and reasonable assumptions on $I_{45}$ and distance lead to the following requirements for the efficiency $\eta$ for the Crab and Vela pulsars:

Crab: $<\phi> = 2.6 \times 10^{-6} \ (\gamma > 100 \ MeV) \ cm^{-2} \ s^{-1} \quad \rightarrow \quad \eta \approx 10^{-3}$

Vela: $<\phi> = 1.2 \times 10^{-5} \ (\gamma > 100 \ MeV) \ cm^{-2} \ s^{-1} \quad \rightarrow \quad \eta \approx 10^{-2}$

Even allowing for some uncertainty in the assumed parameters, these efficiencies indicate a major energy loss process and show that gamma-ray observations probe the central high-energy engine of young pulsars.

## II. THE CRAB PULSAR AND NEBULA

Gamma-ray observations of the galactic anticenter region with the instruments on SAS-2 (1972/73) and COS-B (1975-1982) have confirmed the Crab pulsar (PSR0531+21) as a strong source of high energy photons and have provided a detailed picture of the temporal and spectral characteristics of its emission. The recent analysis of the COS-B data by Clear et al., 1987 is summarized in the following section. COS-B accumulated a total exposure of $1.5 \times 10^8 \ cm^2 s$ above 50 MeV in 6 observation periods spanning the time from September 1975 to March of 1982. The instrument registered about 860 photons from the pulsar and $\sim$ 900 from the unpulsed source. A pulsar lightcurve constructed from photons in the range 50-3000 MeV is shown in figure 1 with a bin size of $\sim$ 0.66 ms. The extremely narrow pulses ( FWHM between 1 and 2 ms) are separated in phase by $0.39 \pm 0.02$, equivalent to $140° \pm 7°$. If the magnetic field in the emission region shapes the beam pattern, e.g. as would be expected in models invoking curvature radiation, the angular divergence of the field lines should be between $10°$ and $20°$ in this region.

Between the two peaks of emission, the Crab pulsar, most pronounced at X-ray energies around 100 keV, shows a so-called interpulse component. The COS-B observations revealed this interpulse component for the first time at energies above 50 MeV. One recent interpretation of the interpulse (Hasinger, 1985) in a one-pole hollow cone model puts the origin of this component into an outflow of particles over the polar cap, which radiate curvature radiation, while the main pulses are generated in a synchrotron process close to the light cylinder. This interpretation will have to be investigated in the context of apparent secular time variations of the pulsar light curve as will be presented below.

The spectrum of the pulsed radiation can be derived from the analysis of phase histograms pertaining to selected energy intervals, as shown in figure 2. The two emission peaks are clearly visible into the 800-1500 MeV range (the 'pulse-phase interval' from $\varphi = 0.1$ to 0.6 has 39 counts while the equally long 'background' interval has only 13 counts). In the highest energy band from 1.5 to 3 GeV one finds 14 'pulsed' counts vs. 5 in the 'background'. With a poisssonian probability of $5 \times 10^{-4}$ this accumulation of counts is due to a chance fluctuation. It is therefore
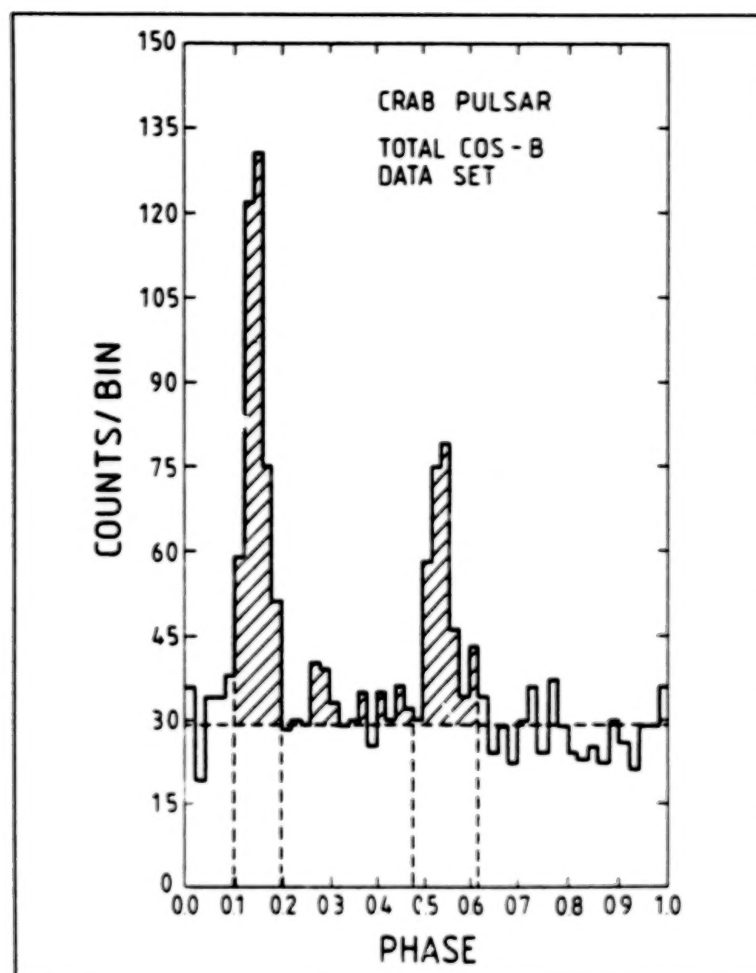
Figure 1: The Crab Pulsar lightcurve for 50 - 3000 MeV
from the total COS-B data set

likely that Crab produces pulsed photons with energies in excess of 1 GeV!

Clear et al. derived the spectra for the components of the lightcurve, first-, second-, and inter-pulse, independently. Within statistics they found that the spectra could all be described with a power law of index $-(2.00 \pm 0.10)$ between 50 and 3000 MeV. The total spectrum is

$$\Phi(E) = (2.86 \pm 0.5) \times 10^{-4} \, E^{-2.00 \pm 0.10} \text{ photons (cm}^2 \text{ s MeV)}^{-1}$$

The average share of the first pulse is 50%, of the second 34% and of the interpulse 16%. Although we think that a significant secular variation in the ratio of the first to the second pulse is present in the SAS-2 and COS-B data, the absolute fluxes of the components during the six COS-B observations show no significant variations which exceed the large statistical and systematic uncertainties.

The unpulsed, steady emission of the Crab is derived from a comparison of 'pulsed' and 'unpulsed' skymaps of the region. A strong, steady source, contributing nearly 50% to the signal below about 500 Mev, was detected and its spectrum can be described as a power law of index -2.7. Although intensity and spectral slope of this unpulsed emission from the Crab
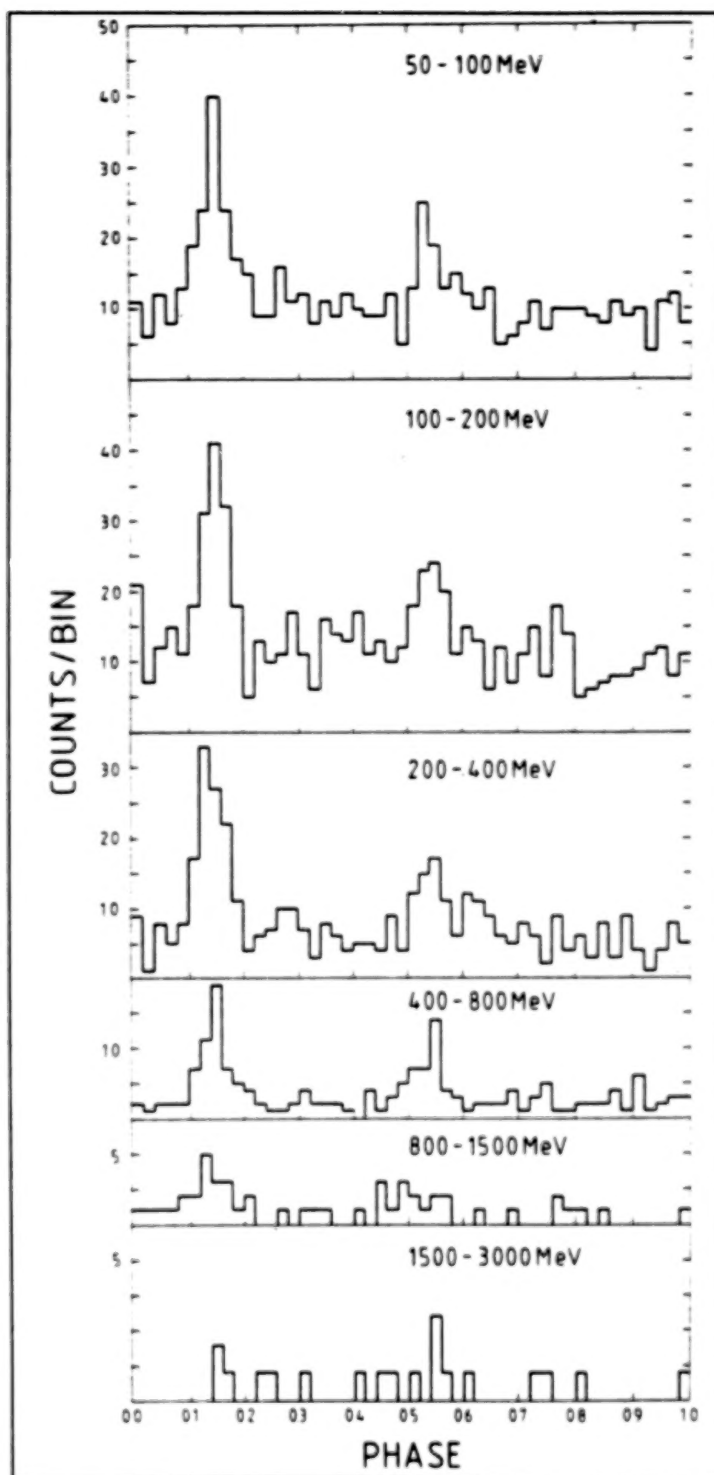
Figure 2: Crab Pulsar phase histograms for six energy
bands from the total COS-B data set

is consistent with the extrapolation of the spectrum at hard X-rays, an identification of this
emission with the nebula would be premature: neither at X-rays nor in the gamma energy range
is the angular resolution sufficient for the separation of a possible steady flux from the neutron
star and from the extended nebula.

Wills et al., 1982 observed in the COS-B Crab data a possible temporal variation in the relative count rates from the first and second pulses. Figure 3 shows the pulse ratio $P_2/P_1$ observed during the COS-B mission augmented by a data point from the SAS-2 observations above 35 MeV. The probability that these secular variations are due to chance fluctuations was estimated by Clear et al. to be about 1%. It should be noted that simultaneous observations of the Crab lightcurve between 2 and 6 keV from a small X-ray detector on COS-B showed no variations of this type.

Notwithstanding the scant observational evidence, it is interesting to speculate on the possibility of a periodic process that manifests itself in such a variation at gamma-ray energies: a tentative fit of the data with a sine function

$$P_2/P_1 = 0.9 - 0.5 \, sin(2\pi(t - 1975.5)/14a)$$

leads to a period of about 14 years. The fit is shown in figure 3. A possible explanation could be found in a free nutation of the neutron star: Goldreich, 1970 stated:..'if circumstances exist in which the free nutation is excited, the narrow beaming of pulsar signals would make it easy to detect'. So we assume that the radiation pattern at gamma-ray energies cycles periodically with an amplitude of typically $10°$ (i.e. the size of a beam) and we observe changes in the relative pulse strengths due to their particular alignment.

The frequency of a free nutation $\Omega$ is proportional to differences in the principal angular momenta of a tri-axial rigid body $(I_3 - I_1)/I_1$ and to $\omega \cos \alpha$, the product of the spin frequency and the cosine of the nutation amplitude. Goldreich describes two possible momenta imbalances for rotating neutron stars:

- dipole induced moment differences: $\sim 10^{-11} R_6^4 B_{12}^2 M^{-2}$

- crust rigidity induced moment differences: $\sim 10^{-11} R_6^7 \mu_{30} M^{-3} P^{-2}$

with radius $R_6$ (in $10^6$ cm), surface magnetic field $B_{12}$ (in $10^{12}$ Gauss), mass $M$ in $M_\odot$, period $P$ in seconds and $\mu_{30}$ is the shear modulus in units of $10^{30}$ dynes cm$^{-2}$.

For the hypothetical Crab nutation we have $\Omega/\omega \cos \alpha \approx 8 \times 10^{-10}$. This is to be compared with values based on the dipole induced (magnetic stress) and rigidity induced moment differences for Crab: reasonable values of $B_{12} \approx 4$, $M \approx 1.4$ lead to $\Omega/\omega \cos \alpha \approx 7 \times 10^{-11} R_6^4$ for the magnetic stress case and to $\Omega/\omega \cos \alpha \approx 3 \times 10^{-9} R_6^7 \mu_{30}$ for the effect of the star's rigidity. The shear modulus for a neutron star mantle is not known, but has been estimated to $\mu_{30} \ll 1$. A most important parameter is of course the stellar radius (really the mass - radius relation, i.e. the equation of state). In spite of the unknowns, the explanation of the hypothetical nutation as a magnetic stress effect would require $R_6 \approx 1.8$, which is entirely in agreement with estimates of $R_6 = 1.6$ by Pandharipande et al., 1976. If the mechanical explanation with a rigid crust is accepted with a similar radius value, then $\mu_{30}$ should be around $10^{-2}$.

The observation of nutation could clearly help in these fundamental questions of neutron star physics. With the hope that GRO might shed some light on this speculation I finish this excursion.
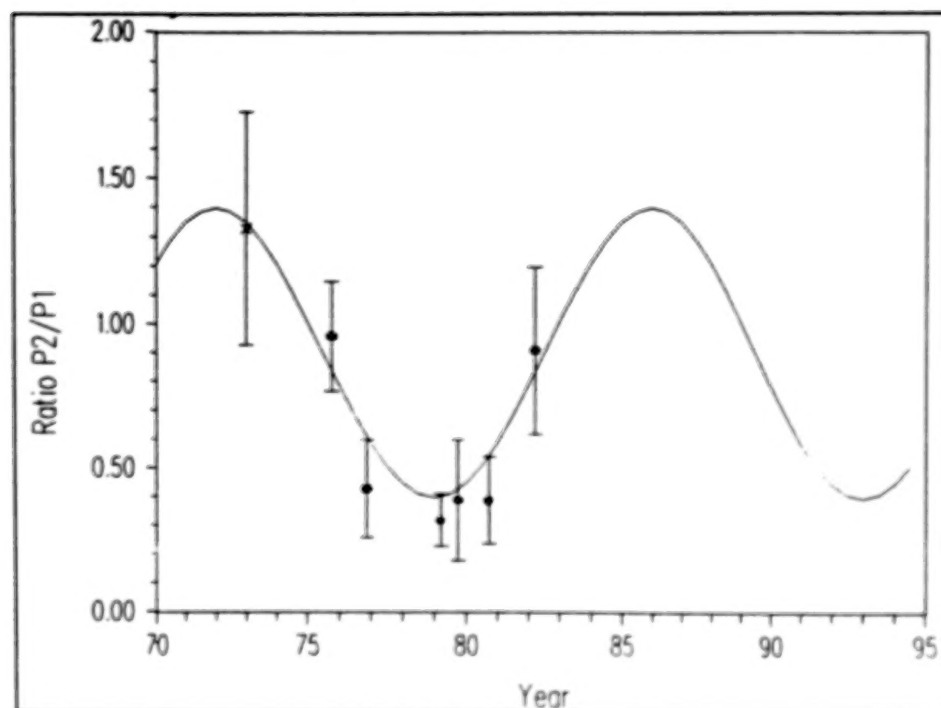
Figure 3: Secular variation of the ratio of counts in the second pulse and in the first pulse of the Crab lightcurve. The COS-B data (•) are for 50-3000 Mev, the SAS-2 point (×) (1973) for > 35 MeV. The sine function fit is discussed in the text.

## III. THE VELA PULSAR

The best information presently available on the high-energy emission of PSR0833-45 is again provided by the extensive COS-B database, which contains ten relevant observations between October, 1975 and May, 1981 with a total exposure of $1.5 \times 10^8$ $cm^2 s$ between 50 MeV and 5 GeV on the source. About 3000 photons above 50 MeV and 1700 above 100 MeV were detected by COS-B from Vela and were used in a detailed analysis by Grenier, Hermsen and Clear, 1988. The EGRET instrument should be able to accumulate about three times as many photons in the course of a single 2-week observation period. Considering the richness of information on the pulsar emission processes already apparent in the COS-B data, it is quite reasonable to expect further refinements and exciting new results based on the EGRET observations; it would however also be necessary to provide for regular, repeated observations to cover the long-term variations.

Confirmed detections of the Vela pulsar have been reported at radio, optical and gamma-ray energies. A compilation of the pulse characteristics at these frequencies is shown in figure 4. At X-ray energies Vela has only been detected as a steady source but no pulsed signal has yet been found. In the analysis of the COS-B data Grenier et al. defined several phase regions of the pulsar lightcurve and named the components in sequence: Pulse 1, Interpulse-1, Interpulse-2, Pulse 2, Trailer and background as indicated in figure 4. It will be seen that these phase components show sufficiently different radiation characteristics (temporal and spectral)

to justify the assumption that we observe different physical phenomena at different phases of the pulsar period.
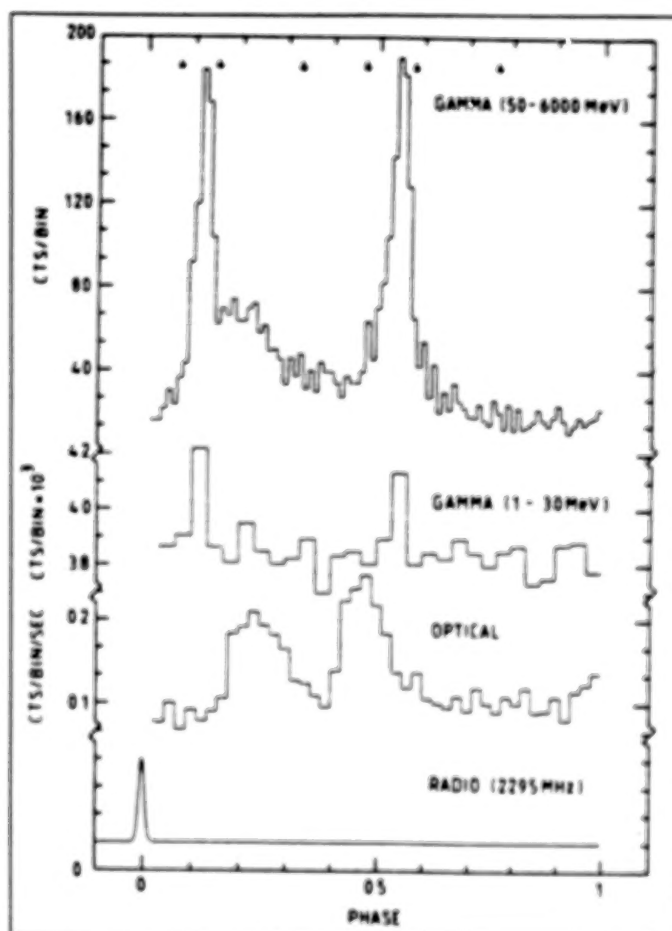


Figure 4: The Vela Pulsar lightcurves at gamma ray (50-6000 MeV, total COS-B data set, 1-20 MeV, Tümer et al., 1984) optical and radio frequencies. Phase intervals as described in the text are indicated in the high-energy histogram.

The phase separation of the pulse maxima in Vela is $0.426 \pm 0.006$ corresponding to an angle of $153° \pm 2°$, which is marginally larger than for the Crab pulsar. The sharpness of the pulses, in particular of the first pulse, is even more visible in a lightcurve with 0.5 ms binsize (Kanbach et al., 1980): a spike at the first pulse ($3 - 4\sigma$ excess) is contained in one phase bin. The beaming mechanism of Vela must be able to collimate parts of the emission to within a few degrees!

The gamma-ray flux from Vela turned out to be quite variable on time scales between weeks (lower limit due to counting statistics) and years. Flux differences of up to a factor of three have been detected by Grenier et al., most pronounced at lower energies. Figure 5a depicts the flux at 50 MeV - 5 GeV over the epochs of COS-B observations, while a 'zoom' with higher

time resolution is shown in figure 5b for the years 1975-78. It is tempting to associate the flux increase during the first observations with a large glitch in pulsar period and -derivative, which occured sometime between Sept. 25 and Oct. 15, 1975: with a rise-time scale of about 11 days and a decay scale of 137 days (shown as curves in figure 5b) this gamma ray flare peaked about a month after the glitch. The pulsar's energy source, the rotational braking, increases by about 1% after a glitch. Since the gamma-ray luminosity nearly doubled after the glitch and the normal gamma-ray efficiency is also about 1% we would have to conclude that nearly all of the glitch related power increase would have to be converted into high energy emission.
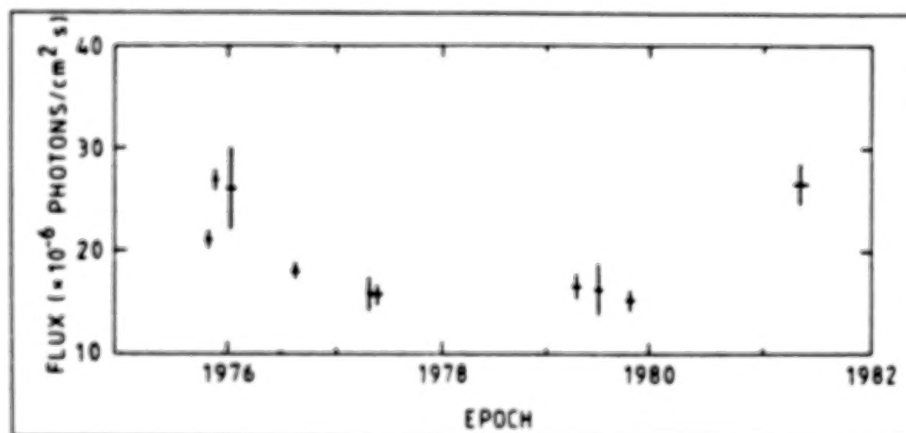


Figure 5a: Vela pulsar integrated gamma ray flux for 50-6000 MeV at epochs of COS-B observations
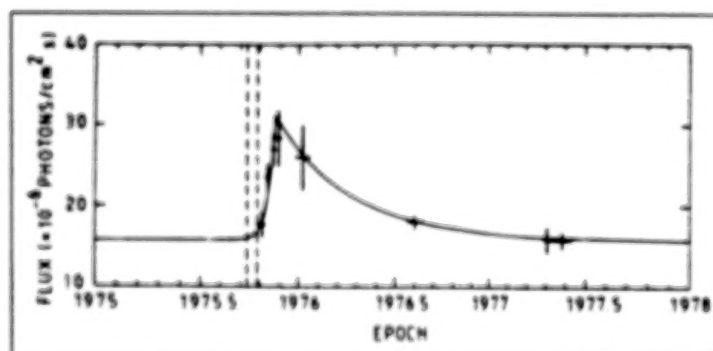


Figure 5b: Higher time resolution gamma ray flux for 50-6000 MeV

Unfortunately we have little further evidence to associate such episodes of enhanced gamma-ray luminosity with glitches in the pulsar's rotation: the next period discontinuity after the October 1975 glitch occured between June 20 and July 13, 1978. The COS-B observation nine months later during April, 1979 showed no exceptional luminosity, which is not surprising in view of the possible time-scale of a few months for a glitch related gamma flare. During the last Vela exposure of COS-B during April and May, 1981 however we find an enhanced flux without

a report of a period glitch in the preceding months. Five months later (October 1981) the next glitch occured!

This puzzle of irregular intensity variations is further complicated if one looks to other wavelengths. At radio energies, a long term variability ( factor of 2 to 3 in intensity) has been observed with a rather regular time scale of a few (2.5 to 3) years. These radio intensity changes however don't seem to be related to the gamma-ray fluctuations; as a possible explanation for the radio changes McAdam, 1981 has proposed precessional effects on the beaming geometry. The relevant ratio of $\Omega/\omega \cos\alpha$ for the Vela pulsar would be about $1 \times 10^{-9}$ and is therefore comparable to the value quoted above for the Crab pulsar.

The total pulsed gamma-ray spectrum, averaged over all COS-B observations of PSR0833-45, is shown in figure 6. It is evident that a single power law is insufficient to describe the spectrum from 50 to 5000 MeV. Grenier et al. derived the following fits for the radiation above and below 300 MeV:

$$F(50 \leq E \leq 300 MeV) = (2.74 \pm 0.21) \times 10^{-4} E_{MeV}^{-1.72 \pm 0.07} \text{ photons / cm}^2 \text{ s MeV}$$
$$F(300 \leq E \leq 5000 MeV) = (2.71 \pm 0.04) \times 10^{-3} E_{MeV}^{-2.12 \pm 0.07} \text{ photons / cm}^2 \text{ s MeV}$$

The intensity of the Vela pulsar allows a much more detailed analysis of the spectrum as a function of phase and epoch. As indicated in figure 4 five components have been defined in the lightcurve and the analysis of Grenier et al. showed that each component has individual characteristics as well as common features with respect to the average spectrum. A common feature of all components is the spectral index of the high energy emission above 300 MeV. Within errors the slopes of all distinct spectra agree with the average value given above. At low energies (50-300 MeV) however the pulsar varies significantly over phase and epoch.

Figure 7 (a reproduction of figure 9 in Grenier et al., 1988) shows the fits to the Vela spectra, differentiated by phase intervals, for five COS-B observation epochs with the best exposures. The maximum likelihood fits are based on two power laws between 50 - 300 MeV and 300-5000 MeV. The whole pulsed emission, in panel 7f, shows the relative stability of the pulsar above 300 MeV. At lower energies the spectral slope and intensity vary significantly. The flux variations shown in figure 5 are almost entirely due to the low energy range. The average spectrum of the first pulse is significantly softer than the spectra of interpulse-1 and pulse 2. These spectral differences and the individual variations seem to indicate that the emission in the respective phase intervals is generated by different processes and perhaps at different locations in the pulsar's magnetosphere.

The strength of a continuous, steady source coincident with the Vela pulsar was determined in a comparison of skymaps constructed for the pulsed phase intervals and for the background interval. In contrast to the Crab result no localized steady source could be found at Vela over the total energy range. The upper limit of the ratio of unpulsed to pulsed flux ranges from 6% at high energies to 9% at energies around 100 MeV. The upper limit to the integral flux above 100 MeV is thus about $9 \times 10^{-7}$ $cm^{-2}s^{-1}$. Following the suggestion of Pinkau, 1970 and the estimates of Higdon and Lingenfelter, 1975 a limit to the gamma-ray emission from the Vela
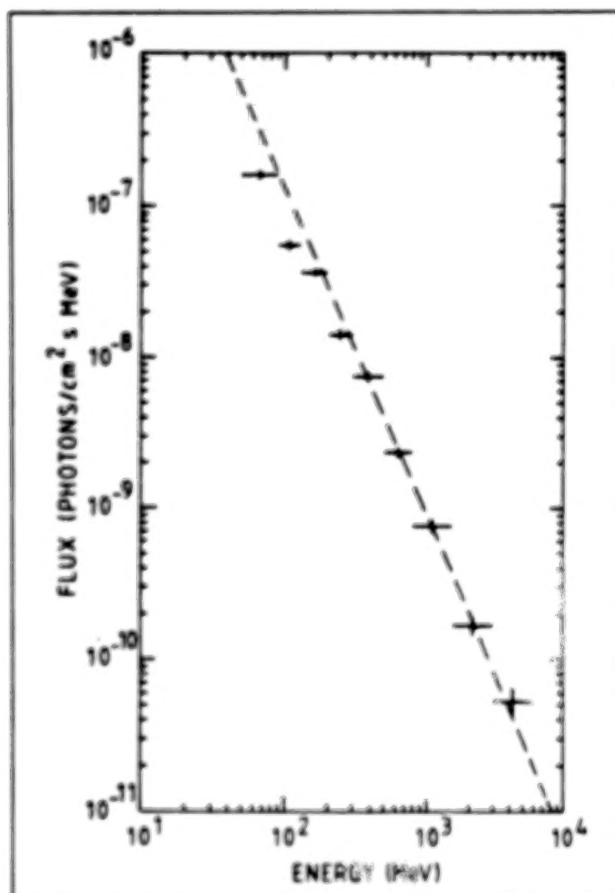
Figure 6: Differential pulsed gamma-ray spec-
trum of PSR0833-45 averaged over all
COS-B observations. The dashed line
is a fit to the data above 300 MeV

supernova remnant, and thus to the product of matter and cosmic ray density, can be derived from the quoted flux limit. We assume a matter density of 0.6 cm$^{-3}$, a distance of 460 pc to the remnant and a yield function of $1.4 \times 10^{-13}$ $\gamma(> 100 MeV)$ per second per target atom/cm$^3$ and per erg of cosmic ray protons an ions. The upper limit of the cosmic ray energy in the remnant is then about $2.5 \times 10^{50}$ erg. Higdon and Lingenfelter estimate the requirement on the cosmic ray production in one supernova under the hypothesis that the galactic cosmic ray density is produced and maintained by supernova events which occur with a rate of one in 50 years. They find that a supernova needs to produce $3 \times 10^{49}$ to $10^{50}$ ergs in cosmic rays. The derived limit for the Vela SNR is therefore not yet constraining this model of cosmic ray origin. Data of better statistics and definition, as expected from EGRET, might however be the basis for a new consideration of the validity of this model.


IV. CONCLUSIONS

Two of the brightest high-energy gamma-ray sources known, the Crab and Vela pulsars, have
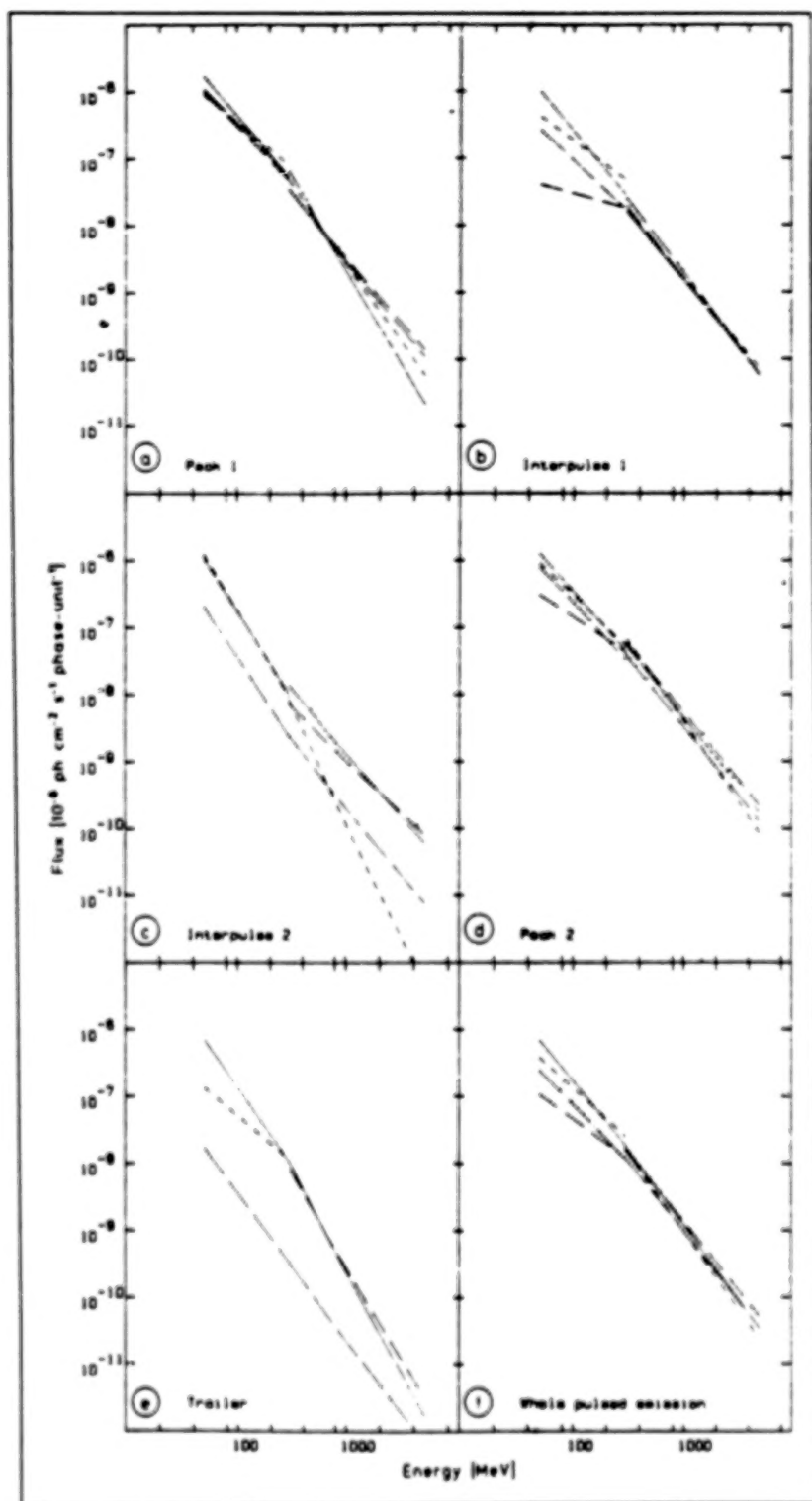
Figure 7: Differential pulsed gamma-ray spectra from PSR0833-45 for individual phase intervals and observation epochs. Maximum likelihood fits for the ranges 50-300 MeV and 300-5000 MeV are shown. For the sequence of COS-B observations refer to Grenier et al., 1988.

111

shown already a great wealth of temporal and spectral detail in their emission above about 50 MeV in the data from the SAS-2 and COS-B missions. Lightcurve variations over time as observed in Crab and phase dependent spectra as well as time variability in flux and spectra for Vela are indications of emission processes that are far from being understood theoretically. Progress in our understanding of these sources can certainly be obtained if we provide for GRO observations that monitor the behaviour of Crab and Vela over the total duration of the mission at regular intervals. We should further be prepared to react with GRO if unusual events are detected at other wavelengths from the young pulsars (e.g. glitches, strong variations in radio flux).

## REFERENCES

Clear, J., Bennett, K., Buccheri, R., Grenier, I.A., Hermsen, W., Mayer-Hasselwander, H.A., and Sacco, B., 1987, *Astron.Astrophys.* **174**, 85.

Goldreich, P., 1970, *Astrophys.J.* **160**, L11

Grenier, I.A., Hermsen, W., and Clear, J., 1988, *Astron.Astrophys.* **204**, 117.

Hasinger, G., 1984, in M. Kafatos and R. Henry (eds.),
    *The Crab Nebula and Related SNRs*, Cambridge University Press, p. 47

Higdon, J.C., and Lingenfelter, R.E., 1975, *Astrophys.J.* **198**, L17.

Kanbach, G., Bennett, K., Bignami, G.F., Buccheri, R., Caraveo, P.A., D'Amico, N., Hermsen, W., Lichti, G.G., Masnou, J.L., Mayer-Hasselwander, H.A., Paul, J.A., Sacco, B., Swanenburg, B.N., and Wills, R.D., 1980, *Astron.Astrophys.* **90**, 163

McAdam, W.B., 1981, *Proc.Astr.Soc.Austr.* **4**, 219

Pandharipande,V.R., Pines, D., and Smith, R.A., 1976, *Astrophys.J.* **208**, 550.

Pinkau, K., 1970, *Phys. Rev. Letters*, **25**, 603.

Tümer, O.T., Dayton, B., Long, J., O'Neill,T., Zych, A., and White, R.S., 1984, *Nature* **310**, 214.

Wills, R.D., Bennett, K., Bignami, G.F., Buccheri, R., Caraveo, P.A., Hermsen, W., Kanbach, G., Masnou, J.L., Mayer-Hasselwander, H.A., Paul, J.A., and Sacco, B., 1982, *Nature* **296**, 723.

# DISSCUSSION:

*Matthew Bailes:*

The efficiency of the gamma-ray production from the Vela Pulsar is often quoted as 0.01. This is dependent on the assumed distance, which is uncertain by a factor of ~2, leading to an uncertainty of ~4 in the gamma-ray efficiency.

*Gottfried Kanbach:*

The distance estimate is not the only uncertainty that enters the calculation of the gamma-ray efficiency of a pulsar. The moment of inertia of the rotating neutron star and the beaming geometry, i.e. the solid angle of emission are also uncertain to a similar amount. It appears however, that the 1% efficiency for Vela can be regarded as a lower limit to the conversion of rotational energy into gamma radiation.

# GAMMA RAY PULSARS: MODELS AND OBSERVATIONS

DAVID J. THOMPSON
NASA/Goddard Space Flight Center
Greenbelt, MD 20771

## ABSTRACT

Data from the EGRET instrument on the Gamma Ray Observatory will be useful in examining predictions made by models of gamma-ray pulsars. The high-energy spectra of pulsars and the luminosities of pulsars other than the Crab and Vela can be used to study and possibly differentiate such models.

## I. INTRODUCTION

The two known gamma-ray pulsars, the Crab and Vela, have been used as guides for the development of models of high-energy radiation from spinning neutron stars. Two general classes of models have been developed: those with the gamma radiation originating in the pulsar magnetosphere far from the neutron star surface (outer gap models) and those with the gamma radiation coming from above the polar cap (polar cap models). The goal of this paper is to indicate how EGRET can contribute to understanding gamma ray pulsars, and especially how it can help distinguish between models for emission.

In the outer gap model (Cheng, Ho, and Ruderman, 1986a, 1986b; Ruderman, 1990), electron acceleration in a pulsar magnetosphere takes place in a charge-depleted region well away from the neutron star surface. Model calculations show that the Crab and Vela pulsars are different from one another. For a Crab-type gap, the primary photons are produced by curvature radiation of the electrons. The primary photons annihilate with X-rays to produce secondary electrons. These secondary electrons produce X-rays by synchrotron radiation and also inverse Compton scatter these X-rays up to gamma ray energies. The radiation in the EGRET energy range will originate from inverse Compton scattering.

The Vela pulsar for the outer gap model is different in that the primary photons are inverse Compton scattered infrared photons with much higher energy than those of the Crab. These photons also produce electron secondaries, and the gamma rays which are seen are synchrotron radiation from the secondary electrons.

In a polar cap model (e.g. Daugherty and Harding, 1982), the particle acceleration takes place just above the polar cap of the neutron star. Here the magnetic field is much stronger than in the outer gap. The accelerated particles form a cascade. Electrons produce curvature radiation photons, which annihilate. The secondary electrons produce photons by both curvature and synchrotron radiation. These photons may also annihilate, until the cascade reaches the point where the photons (gamma rays) can escape. The Crab and Vela in this model are similar.

With a reasonable choice of assumptions, either of these models can reproduce the observations of the Crab and Vela. They are fundamentally different models, however. The polar cap model sees gamma ray emission as a general property of young radio pulsars, with the Crab and Vela working by similar mechanisms (Harding, 1981). The outer gap model, on the other hand, not only views the Crab and Vela as different from each other, but suggests that gamma-ray emission is limited to a subset of all pulsars, and that gamma-ray pulsars do not evolve into older radio pulsars (Ruderman and Cheng, 1988).

## II. ENERGY SPECTRA OF GAMMA RAY PULSARS

One characteristic of EGRET compared to previous high energy gamma-ray telescopes like SAS-2 and COS-B is its broader energy range (about 20 MeV to 30,000 MeV) and better energy resolution (Hughes, et al., 1986). Features not seen previously in the Crab and Vela energy spectra might be visible to EGRET.

For the outer gap model, the feature in the gamma-ray range is a break in the spectrum above a few GeV. In the case of Vela, this results from the maximum energy that the secondary electrons can have in the outer gap ($10^{13}$ eV), assuming that the synchrotron radiation occurs in a field of about 5000 gauss (Cheng, Ho, and Ruderman, 1986b). The Crab spectrum in the outer gap model shows a similar fall-off in the few GeV range, in this case resulting from the combination of the upper limit on the secondary electron energies and the energies of the X-rays which are being inverse Compton scattered to the gamma-ray range (Ho, 1989).

The polar cap model also shows a fall-off in the few GeV range for both the Crab and Vela pulsars (Harding, 1981, Daugherty and Harding, 1982). This turnover in the cascade model results from two factors: 1. the curvature radiation gamma-ray spectrum has a maximum for a given set of conditions; and 2. the higher energy gamma rays are more likely to convert to pairs in the magnetic field, because they can convert farther out where the field is lower. Both these effects serve to suppress the high energy gamma rays.

These two models predict such similar high-energy spectral shapes that EGRET cannot expect to distinguish them. Nevertheless, EGRET can address the question of whether there is such a turnover in the spectrum. Figure 1 shows the COS-B data for the Crab spectrum (Lichti, et al., 1980), along with a model calculation (Harding, 1981) and a power law fit to the COS-B data. Although the final analysis of the EGRET response above a few GeV is not complete, the estimated sensitivity (Hughes, et al., 1980; Thompson, 1986) can be used to calculated the relative response to the different spectra. For a two week exposure, a continuing power law spectrum would yield about 30 photons above 5 GeV detected by EGRET. Under similar conditions, a spectrum with a break near 2 GeV would produce fewer than 10 photons above 5 GeV. Although the numbers are small, the difference is significant, because at these energies the angular resolution of EGRET allows the source to be separated clearly from any galactic or extragalactic diffuse gamma radiation. A similar change of spectral shape would be even more significant for Vela, because it is a factor of 3 more intense than the Crab. If the spectrum extends in a near power law beyond 10 GeV, however, a higher energy cutoff would probably not be visible to EGRET.
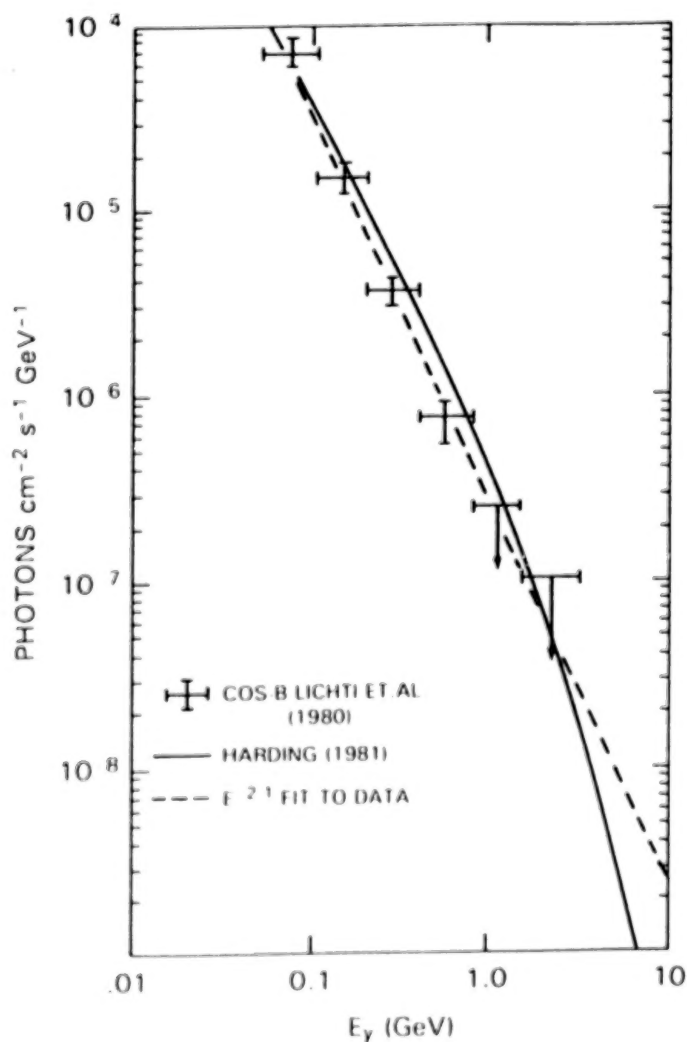


Figure 1 -- High-energy spectrum of the Crab pulsar. Data points from COS-B: Lichti, et al. (1980). Solid curve: model of Harding (1981). Dashed curve: $E^{-2.1}$ fit to data.

## III. MODEL PREDICTIONS FOR OTHER PULSARS

Another approach to distinguishing models is to look at the
model predictions for other pulsars.  It is, of course, possible
that the Crab and Vela are so different from other pulsars that they
are the only gamma-ray pulsars, but there are enough other
candidates around that that seems unlikely.  Ruderman and Cheng
(1988) suggested, for example, that some of the other COS-B sources
might be undiscovered pulsars.  The concept used in the present work
is to start from the radio pulsar direction, looking for
characteristics which might indicate gamma ray emission from some
sources which are already known to be pulsars.

The solid line in Figure 2 (based on the work of Ruderman and
Cheng 1988) shows the estimated gamma ray luminosity for short-
period pulsars with characteristics like those of the Crab and Vela.
This figure has been normalized to the Crab and Vela observations,
assuming radiation into approximately one steradian.  Pulsars with
periods shorter than about 50 msec are Crab-like, while those with
longer periods are similar to Vela.  In the outer gap model, the
luminosity function cuts off at about 125 msec for Vela-like
pulsars.  This occurs when the outer gap essentially fills the
magnetosphere and is quenched.  Pulsars with longer periods are
expected to have no gamma-ray emission.
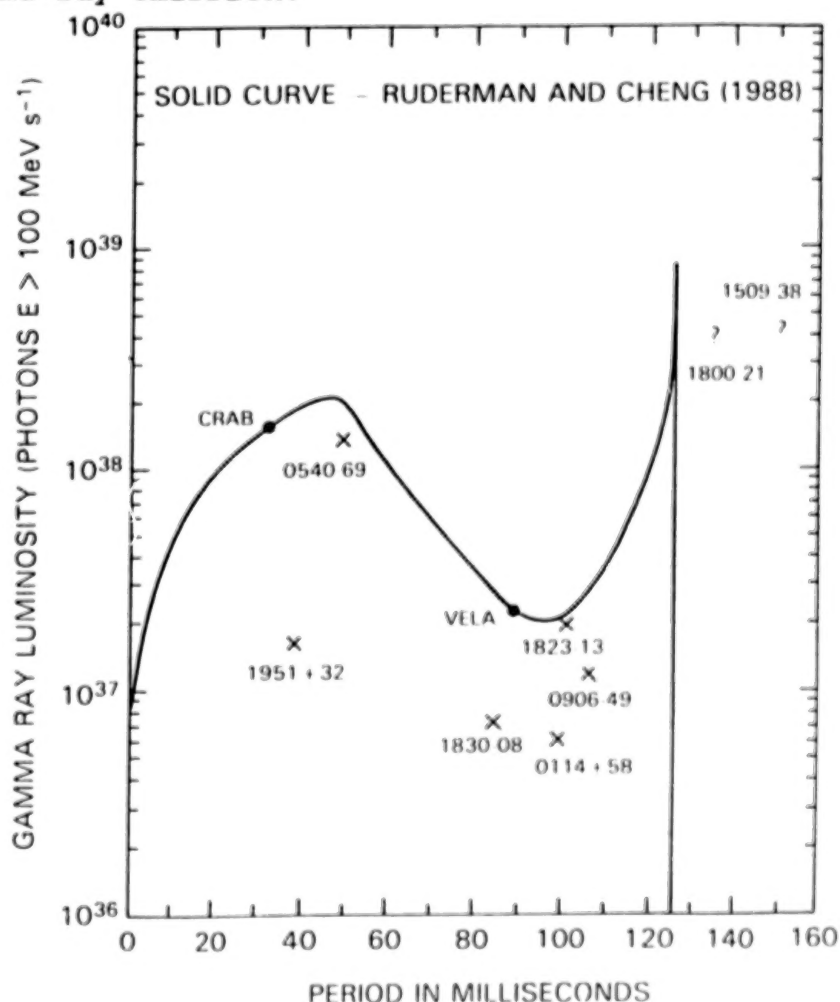


Fig. 2 Gamma-ray pulsar
luminosities in the
outer gap model.
Solid line: calculation
of Ruderman and Cheng
(1988)
Data points: present
calculation.  The ?
for 1800-21 and 1509-38
indicate the large
uncertainty.

Following Cheng, Ho, and Ruderman (1986b), the luminosity for other pulsars should be proportional, at least in first approximation, to $B/P^2$ , where P is the pulsar period and B is the calculated magnetic field at the surface. This comes from the fact that the potential drop in the outer gap and the particle flow are both proportional to this quantity. For pulsars with a given period, this implies that the luminosity should be proportional to the surface magnetic field, calculated from the standard formula

$$B = ( 10^{30} I P \dot{P} / a^6 )^{1/2} \text{ gauss} \tag{1}$$

where P is the pulsar period, $\dot{P}$ the period derivative, and a the pulsar radius, generally assumed to be $1 * 10^6$ cm. Parameters for the other pulsars shown on this figure are drawn from a recent update (Taylor, 1988) of the Manchester and Taylor (1981) compilation.

Two pulsars in this figure are shown with periods just beyond the 125 msec cutoff. These are pulsars with calculated fields greater than those of the Crab and Vela. Such pulsars should be able to sustain an outer gap out to longer periods, and should fall somewhere on the rising part of the curve. Clearly, estimates for these two pulsars are very uncertain, but they are potentially luminous gamma-ray pulsars.

The polar cap model is in some sense easier, because it is based on the idea that pulsars follow a common evolutionary path. This means that the Crab and Vela parameters can be used to extrapolate to other pulsars in the context of the model. Harding's (1981) fit to the observations gave

$$L (>100) = 1.2 * 10^{35} B12^{0.95} P^{-1.7} \text{ photons s}^{-1}. \tag{2}$$

where B12 is the pulsar field in units of $10^{12}$ gauss. This fit is also based on an assumption of radiation into about one steradian.

In the polar cap model, there is no explicit mechanism which limits the gamma-ray emission (as the quenching of the outer gap does), but the ultimate limiting factor is still the same: the power source for the pulsar is its rotational energy loss, and no process can expect to extract all that energy in the form of gamma rays. In applying this formula, it is important to look at what fraction of the total energy loss it represents, and realize that too large a fraction is not physically meaningful.

Table 1 shows the results of both model calculations for some of the most interesting pulsars, including the Crab and Vela for reference. Luminosities have been converted to flux values, using the estimated pulsar distances and the same 1 steradian emission solid angle assumed in the model calculations.

## Table 1
## PULSAR PARAMETERS

| NAME | P(s) | P($*10^{-15}$ s/s) | d(kpc) | B(gauss) | $F(>100)$ ph $s^{-1}$ $cm^{-2}$ Polar cap | Outer gap |
|------|------|------|------|------|------|------|
| 0531+21 (Crab) | .033 | 422.4 | 2 | $3.7*10^{12}$ | $3.*10^{-6}$ | $3.*10^{-6}$ |
| 0833-45 (Vela) | .089 | 124.7 | .5 | $3.3*10^{12}$ | $1.0*10^{-5}$ | $1.0*10^{-5}$ |
| 0114+58 | .101 | 5.8 | 1.5 | $7.8*10^{11}$ | $2.1*10^{-7}$ | $4.0*10^{-7}$ |
| 0540-69.3 | .050 | 509.2 | 55 | $5.0*10^{12}$ | $3.0*10^{-9}$ | $4.0*10^{-9}$ |
| 0906-49 | .107 | 13.9 | 3.2 | $1.2*10^{12}$ | $6.6*10^{-8}$ | $1.8*10^{-7}$ |
| 1823-13 | .101 | 76.0 | 5.5 | $2.8*10^{12}$ | $5.4*10^{-8}$ | $1.1*10^{-7}$ |
| 1830-08 | .085 | 9.0 | 8.5 | $8.9*10^{11}$ | $1.0*10^{-8}$ | $1.4*10^{-8}$ |
| 1951+32 | .039 | 5.9 | 2.5 | $4.8*10^{11}$ | $2.5*10^{-7}$ | $4.2*10^{-7}$ |
| 1509-58 | .150 | 1520.0 | 6.7 | $1.5*10^{13}$ | $9.3*10^{-8}$ | $9.3*10^{-7}$? |
| 1800-21 | .134 | 125.0 | 5.2 | $4.1*10^{12}$ | $5.4*10^{-8}$ | $1.5*10^{-6}$? |
| 0355+54 | .156 | 4.4 | 1.6 | $8.4*10^{11}$ | $9.6*10^{-8}$ | ---- |
| 0740-28 | .167 | 16.8 | 1.5 | $1.7*10^{12}$ | $1.9*10^{-7}$ | ---- |
| 1055-52 | .197 | 5.8 | 0.9 | $1.1*10^{12}$ | $2.5*10^{-7}$ | ---- |

120

The pulsars in addition to the Crab and Vela fall into three groups:

The first six are ones for which both models predict gamma-ray emission at about the same level, within a factor of three. These are the ones most like the Crab and Vela and should tell if the Crab and Vela are really different from other radio pulsars in some feature relevant to gamma-ray emission.

The second two are those near the limit of the outer gap model. If this model is correct, then they may be on the upward part of the curve and be strong sources, or they may be over the edge and non-sources. The question marks indicate the high degree of uncertainty in these estimates.

The third group contains pulsars with periods and fields which should not be able to sustain an outer gap, but which might be gamma ray sources in the polar cap model. This group in particular could be much larger if equation (2) extrapolates to pulsars with longer periods. The pulsars shown are some which are relatively fast (periods shorter than 200 msec), relatively nearby (distances less than 2 kiloparsecs), and energetically reasonable (less than 10% of their rotational energy loss appears in the form of gamma rays).

## IV. OBSERVATIONAL CONSIDERATIONS

The next question is: Which of these might EGRET see? Based on simple counting statistics, the estimated EGRET sensitivity, and the known diffuse galactic and extragalactic radiation, here are some guidelines:

1. EGRET should be able to see any pulsar with a flux above 100 MeV of a few $* 10^{-7}$ photons $cm^{-2}$ $s^{-1}$ in a single good two week exposure. This is an intensity about 0.1 of the Crab pulsar. Figure 3 is a simulation of a phase plot of a pulsar with this flux (and a Crab-like double peak structure) seen in the galactic center region.

2. In a two week exposure, EGRET will have trouble detecting pulsars at the $1 * 10^{-7}$ photons $cm^{-2}$ $s^{-1}$ level in the galactic center region, due to the high intensity galactic radiation, but should be able to see pulsars with this intensity in regions away from the center. Away from the high intensity portion of the galactic ridge, the galactic radiation is a factor of five or more less intense.

3. Even under the best of circumstances, EGRET will be unlikely to detect pulsars with a flux less than $10^{-8}$ photons $cm^{-2}$ $s^{-1}$.
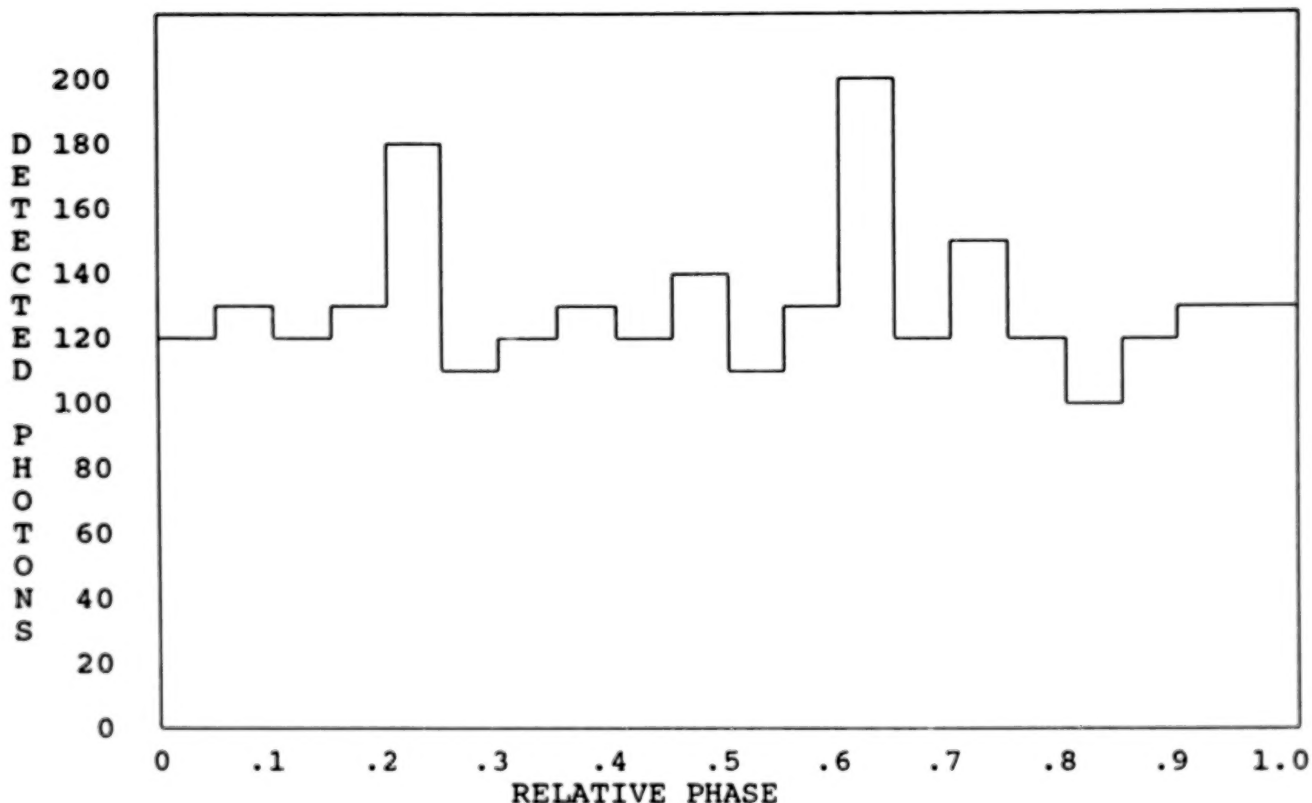
Figure 3 - Simulated phase plot of a pulsar with 0.1 the Crab
    flux and a double-peak emission, in the high-intensity region
    near the galactic center.  Two week exposure with EGRET, with
    the pulsar on-axis.

From these guidelines and Table 1, it is clear that these model
predictions span this range -- pulsars 0114+58 and 1951+32 should be
detectable if either model is a good description of the gamma-ray
emission process; 0540-69 (which is in the Large Magellanic Cloud)
and 1830-08 are not likely candidates due primarily to their
distance; and all the rest are in between.  If the outer gap model
is an accurate representation of the gamma-ray emission process,
then pulsars 0906-49, 1509-38, and 1800-21 could all be detectable.
In light of the large uncertainty at the limit of the outer gap
model, however, the best discriminator between the models will
probably be the longer period pulsars 0355+54, 0740-28, and 1055-52.
Detection of any of these (which should not be able to support an
outer gap) would suggest particle acceleration and gamma-ray
production in some other region of the magnetosphere, such as the
polar cap model predicts.

In summary, EGRET should be able to contribute to an improved
understanding of gamma ray pulsars.  It should be able to look for
the predicted turnover in the high energy spectrum of the more
intense pulsars.  More significant is the prospect of being able to
detect additional pulsars which may distinguish models of gamma ray
emission.

## REFERENCES

Cheng, K.S., Ho, C., and Ruderman, M. 1986a, Ap. J. 300, 500.

Cheng, K.S., Ho, C., and Ruderman, M. 1986b, Ap. J. 300, 522.

Daugherty, J.K., and Harding, A. 1982, Ap. J. 252, 337.

Harding, A.K. 1981, Ap. J. 245, 267.

Ho, C. 1989, Proc. Gamma Ray Observatory Science Workshop, ed. W. N. Johnson, p. 4-174.

Hughes, E.B., et al. 1986, IEEE Trans. Nucl. Sci. NS-33, 728.

Hughes, E.B., et al. 1980, IEEE Trans. Nucl. Sci. NS-27, 364.

Lichti, G.G., et al. 1980, Non-Solar Gamma Rays (COSPAR), ed. R. Cowsik and R.D. Wills (New York, Pergamon), p. 49.

Manchester, R.N., and Taylor, J.H. 1981, Astron. J. 86, 1953.

Ruderman, M. 1990, these proceedings.

Ruderman, M. and Cheng, K.S. 1988, Ap. J. 335, 306.

Taylor, J.H. 1988, private communication.

Thompson, D.J. 1986, Nuc. Inst. and Meth. A251, 390.

## DISCUSSION

*Alice Harding:*

The polar cap model predicts a sharp cutoff in the gamma-ray spectrum above a few GeV, which is due to pair production in the strong magnetic field. Thus, the break in the spectrum would have a different shape from that predicted by the outer gap model.

*R.J. Slobodrian:*

I am glad that ions have been mentioned. A recent review article on double layers has suggested that they are relevant as astrophysical accelerators to $10^{14}$ - $10^{15}$ eV -- for example, in pulsars (young), where both ions and electrons are available. I would like to know the opinion of experts on the possible relevance of such double layers in young pulsars (only thus far proven gamma-ray emitters).

*Mal Ruderman:*

Wherever the magnetic field is very strong, e.g. near the surface of a magnetized neutron star, there is copious pair production if the potential drop (along B) exceeds $10^{12}$ volts. This would be expected to keep such accelerator potentials there well below the $10^{14}$ - $10^{15}$ volt range. Far away, e.g. in the outer magnetosphere, an accelerator "gap" is a kind of double layer in this range.

*Chip Meegan:*

In the gap model, what distinguishes the gamma ray pulsars, which turn off, from pulsars that evolve into longer-period radio pulsars?

*Mal Ruderman:*

A growing charge depletion region in the outer magnetosphere may be limited by $e^{\pm}$ production there as proposed for the Crab and Vela pulsars, but also by transport into that region of $e^{\pm}$ made elsewhere. These may be separated far from the star by electric fields much weaker than those needed to make them in the outer magnetosphere. It is very much easier to make pairs in the very large B above a part of the polarcap than in an accelerator near the light cylinder. Possible transport of such pairs to where they are needed in the outer magnetosphere depends upon the magnetic field structure around the neutron star; it would not generally occur for a pure dipole but may for somewhat more complicated fields. Another possibility is a switching to real pair production from quasi-pair production from ion stripping above the polarcap as a neutron star cools with age.

# THE SENSITIVITY OF EGRET TO GAMMA-RAY POLARIZATION

JOHN R. MATTOX*

Code 662, NASA/Goddard Space Flight Center, Green Belt, MD 20771

## ABSTRACT

A Monte Carlo simulation shows that EGRET does not even have sufficient sensitivity to detect 100% polarized gamma rays. This is confirmed by analysis of calibration data.

## I. INTRODUCTION

Yang (1950) first pointed out that the azimuthal orientation of the plane of the pair-produced electron and positron could be used to determine linear polarization of gamma rays. Maximon and Olsen (1962) have calculated the azimuthal dependence of the pair production cross section which may be expressed as

$$\sigma(\phi) = \frac{\sigma_o}{2\pi}[1 + PR\cos(2\phi)], \qquad (1)$$

where $\phi$ is the angle between the electron-positron plane and the gamma ray polarization. $P$ is the fractional linear polarization, and $R \approx 0.1$ is the strength of the quadrupole asymmetry of the pair production process.

Kelner et al. (1975) first pointed out the possibility of polarimetry in gamma ray astronomy using spark chamber instruments. However, multiple Coulomb scattering of the electron and positron after pair production reduces the asymmetry. A crude estimate (Mattox, Mayer-Hasselwander, and Strong 1990) indicates that R is reduced to

$$R' = R \times e^{-2\Phi^2}. \qquad (2)$$

Where

$$\Phi = 14L^{1/2}$$

is the rms change in $\phi$ (assuming a Gaussian distribution) due to multiple Coulomb scattering. The EGRET pair production foils are $L = 0.022$ radiation lengths thick. Thus $\Phi = 2.1$ radians, and $R' = R \times 2 \times 10^{-4}$ — making polarimetry impossible. However, this approximation is based upon a simple geometric approximation and neglects the distribution of momenta in pair production and the fact that multiple Coulomb scattering occurs in spaced tantalum foils. Therefore, the Monte Carlo simulation described in section II has been done to obtain a better knowledge of the effect of multiple Coulomb scattering.

The EGRET telescope aboard the Gamma Ray Observatory will have the greatest sensitivity to polarization of any gamma ray telescope to date because of thinner pair production plates and larger sensitive area. EGRET was calibrated at the Stanford Linear Accelerator Center (SLAC) with an inverse compton scattered gamma ray beam (Mattox et al. 1987). Because the frequency

---

* National Research Council/National Academy of Sciences Research Associate

doubled YAG laser photons where linearly polarized before scattering, the gamma rays were 99.8% polarized at 100 MeV (Murray and Fieguth, 1978; Abe et al. 1984). The analysis of the EGRET calibration data for polarization is described in section V.

## II. Monte Carlo Simulation

The sensitivity of EGRET to polarization has been studied with three coupled computer programs. Program I uses the differential cross section of Maximon and Olsen (1962) in the limit of complete screening for pair production (their equations (4), (7), and (8)). For a specific gamma ray energy and 100% polarization, the momenta of the positron and electron are chosen randomly according to this cross section. The selection is cut off at an electron or positron energy less than 10% of the gamma ray energy ($E_{e\pm} > 0.1E_\gamma$). Particles with energy less than $\approx 5$ MeV will not often propagate far enough to create the second track needed for event acceptance.

Program II uses the EGS4 Monte Carlo program (Nelson et al. 1985) to study the propagation of the electron and positron through the EGRET spark chamber. The depth within the first tantalum foil of pair production is chosen randomly from a uniform distribution. A list of the locations of energy deposition in the spark chamber modules (tracks) is generated. Figure 1a shows program II tracks graphically for one event. The effect of multiple Coulomb scattering is immediately seen by comparing this to figure 1b which shows the same event without Coulomb scattering.
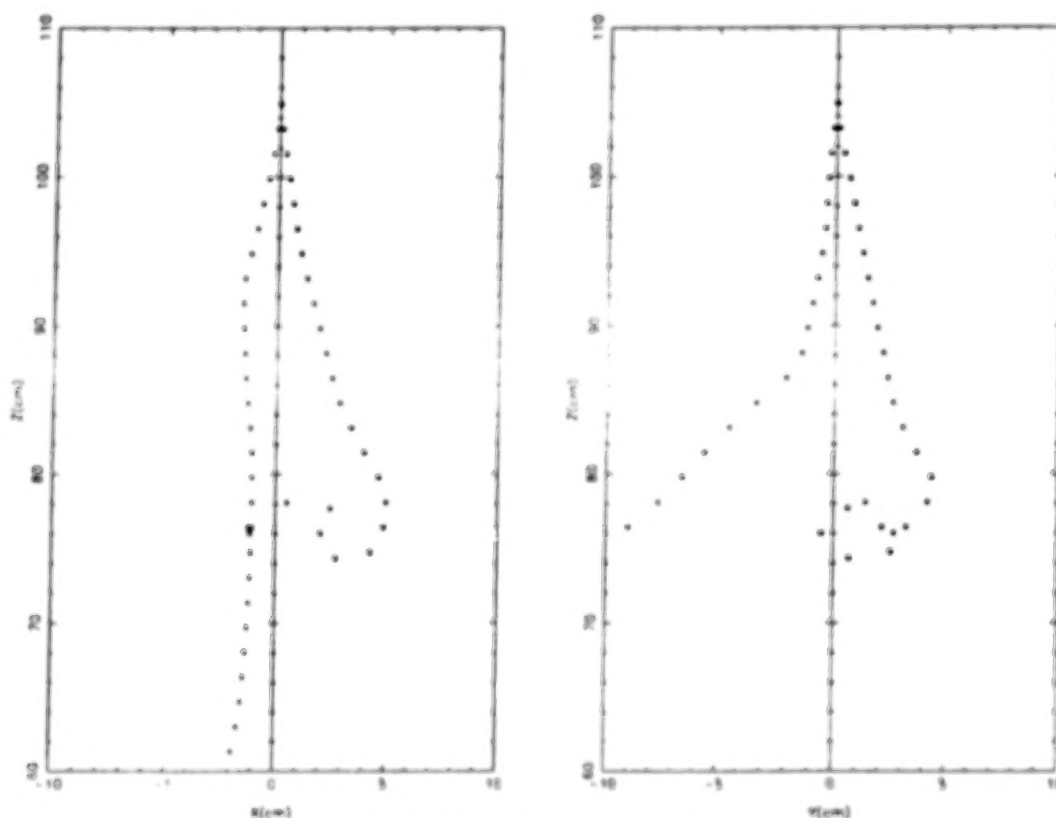


Figure 1a. A graphical representation of the tracks generated by program II. The energy depositions due to the electrons are shown with dots, depositions due to the positrons with stars. The gamma ray energy was 100 MeV, the opening angle was 0.042 radians, the electon-positron plane was located at azimuth $\phi = 45°$, and incidence was downward along the Z axis.
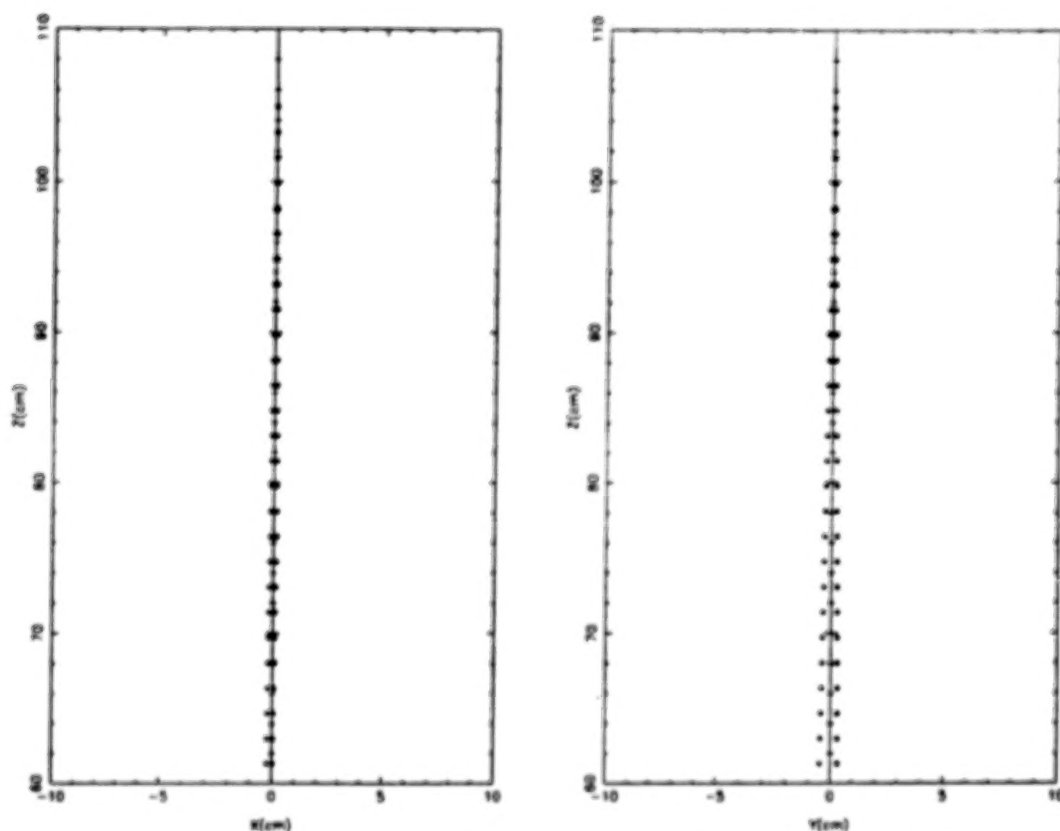
Figure 1b. The same initial positron and electron directions as figure 1a, however the tantalum pair production foils have been replaced by vacuum. The lateral position uncertainty of EGRET has not yet been introduced.

The tracks are then analyzed by program III to determine the distribution of the azimuthal orientations of the pair planes. This program begins by introducing the lateral $(X, Y)$ uncertainty of EGRET. The EGRET spark chamber wires are separated by 0.8 mm. Tracks have been found to be $\approx 3$ wires wide. However, the mean of the spark locations has been found to be within $\approx 1$ wire spacing of the actual track location. In the simulation, the coordinates are changed to that of the next wire at a smaller coordinate. Then, the routine DIRCTN from the EGRET data analysis system (Bertsch 1989) is used to find the track directions. The cross product of the track directions is found. Because of multiple Coulomb scattering, lateral position uncertainty, and transfer of momentum to the nucleus, the cross product can deviate several degrees from being perpendicular to the gamma ray direction. Therefore, the the azimuthal orientation (with respect to the $X$ axis) of the component of the cross product perpendicular to the gamma ray direction is noted. Because polarization creates a quadrupole asymmetry, the angle is reduced to the range 0° to 180° by subtracting 180° if the angle is greater than 180°.

The result is illustrated in figure 2 which shows the azimuthal distribution for 100 MeV gamma rays. The solid line shows the distribution of equation (1). This was obtained as a system check by changing one byte in program II to replace tantalum with vacuum for the pair production foils, and another byte in program III so that the lateral uncertainty is not introduced. It is important to add that an instrument without pair production material would actually have no efficiency. In this simulation, pair production continues to occur by fiat outside of the EGS4 routine. The ratio of the bins centered at 135° and 45° (the the asymmetry ratio) is $z = 1.27$.
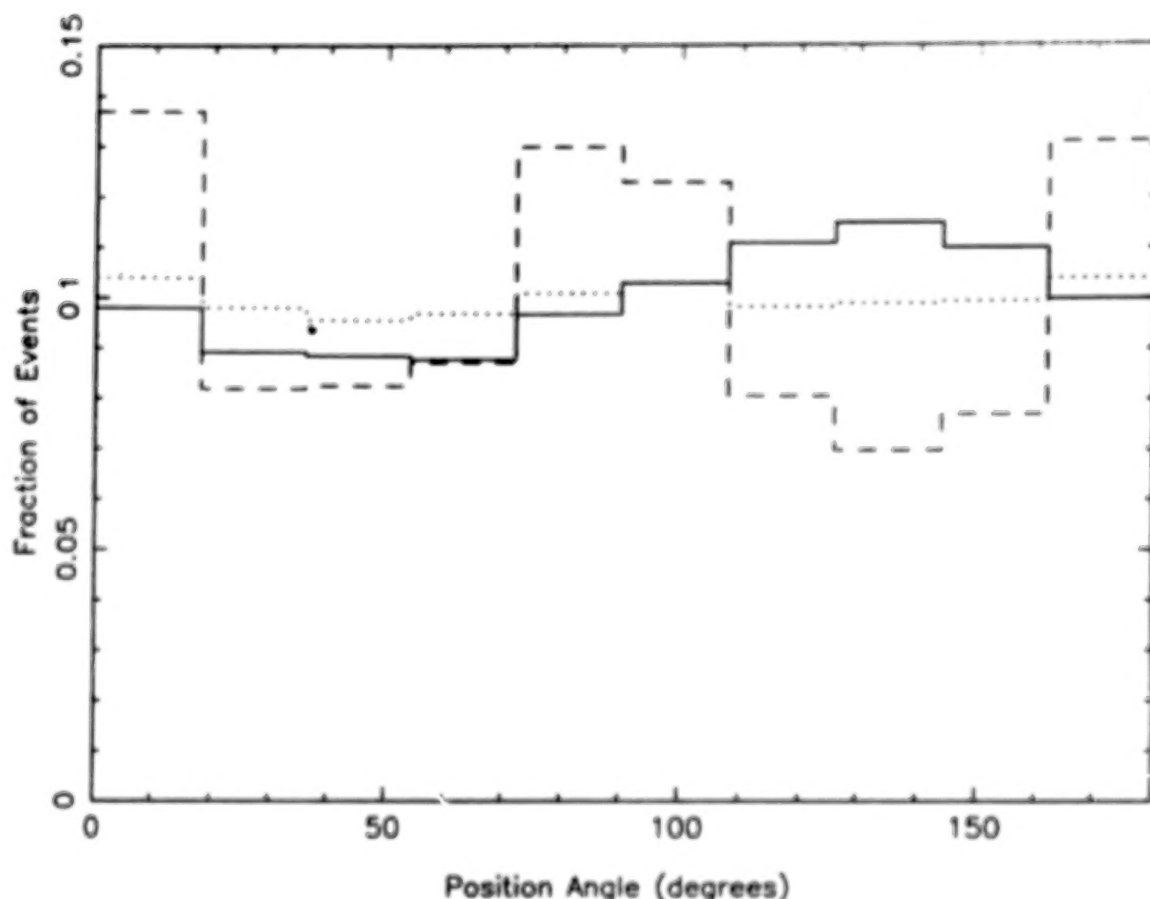
Figure 2. Azimuthal distribution of electron-positron planes for polarized 100 MeV gamma rays in EGRET. The solid line is the distribution of equation (1). The dotted line is the Monte Carlo result for 350 kiloevents. The dashed line is the distribution of 3065 on-axis SLAC calibration events.

The dotted line in figure 2 shows the distribution which results when the multiple Coulomb scattering in the tantalum foils is included, and the lateral uncertainty is included. The excess along the $X$ and $Y$ axes ($0°$, $90°$, $180°$) is due to the lateral position uncertainty. If the plane of the pair is close to being along an axis, it is possible that the lateral uncertainty will cause it to be found exactly along the axis. The polarization dependence is preserved to a small degree. The asymmetry ratio is $z = 1.037 \pm 0.008$. This is a $5\sigma$ significance detection for 100% polarization of $3.5 \times 10^5$ events knowing the direction of polarization. The polarization asymmetry after multiple Coulomb scattering can be related to the the asymmetry ratio:

$$R' = \frac{z-1}{z+1} = 0.018 \pm 0.004$$

From equation (2), the corresponding standard deviation due to multiple Coulomb scattering and lateral position uncertainty is $\Phi = 0.96 \pm 0.05$. This is a factor of two better than the crude estimate.

Without knowing the polarization position angle, the second harmonic test (Mattox, Mayer-Hasselwander, and Strong 1990) is the most sensitive test for polarization. The required number of events for a $3\sigma$ detection, assuming 100% polarization, is $N = 27.6R'^{-2} = 85^{+56}_{-28}$ kiloevents. The one sigma statistical error limits are due to the limited number of events simulated. However, only 49,000 good calibration events were obtained at 100 MeV at SLAC. Also, 4 months of observation of the most intense gamma ray source, the Vela Pulsar, is expected to yield $\approx 55$ kiloevents ($80 < E_\gamma < 150$MeV).

At 200 MeV, the asymmetry ratio with no multiple Coulomb scattering and no lateral position uncertainty is $z = 1.27$. With multiple Coulomb scattering and lateral position uncertainty, the Monte Carlo study of 100 kiloevents with 100% polarization yields $z = 0.994 \pm 0.14$. A 98% confidence lower limit on the number of events needed for a $3\sigma$ significance detection is 220 kiloevents. With multiple Coulomb scattering, but with no lateral position uncertainty, polarization is apparent for 100 kiloevents, $z = 1.032 \pm .014$.

At 50 MeV, the asymmetry ratio with no multiple Coulomb scattering and no lateral position uncertainty is $z = 1.26$. With multiple Coulomb scattering and lateral position uncertainty, the Monte Carlo study of 350 kiloevents yields $z = 1.020 \pm 0.008$. The number of events needed for a $3\,\sigma$ significance detection using the second harmonic test is thus $282^{+510}_{-137}$ kiloevents.

### III. Further Study of Multiple Coulomb Scattering

The effect of multiple Coulomb scattering and lateral position uncertainty was observed directly by creating a list of events all having an identical azimuthal alignment of the pair production plane, positron energy equal to electron energy, and equal transverse momenta. This list was then analyzed by programs II and III. For 50 MeV gamma rays, the result is shown in figure 3 for the most probable opening angle ($\Omega$ =0.042 radians).
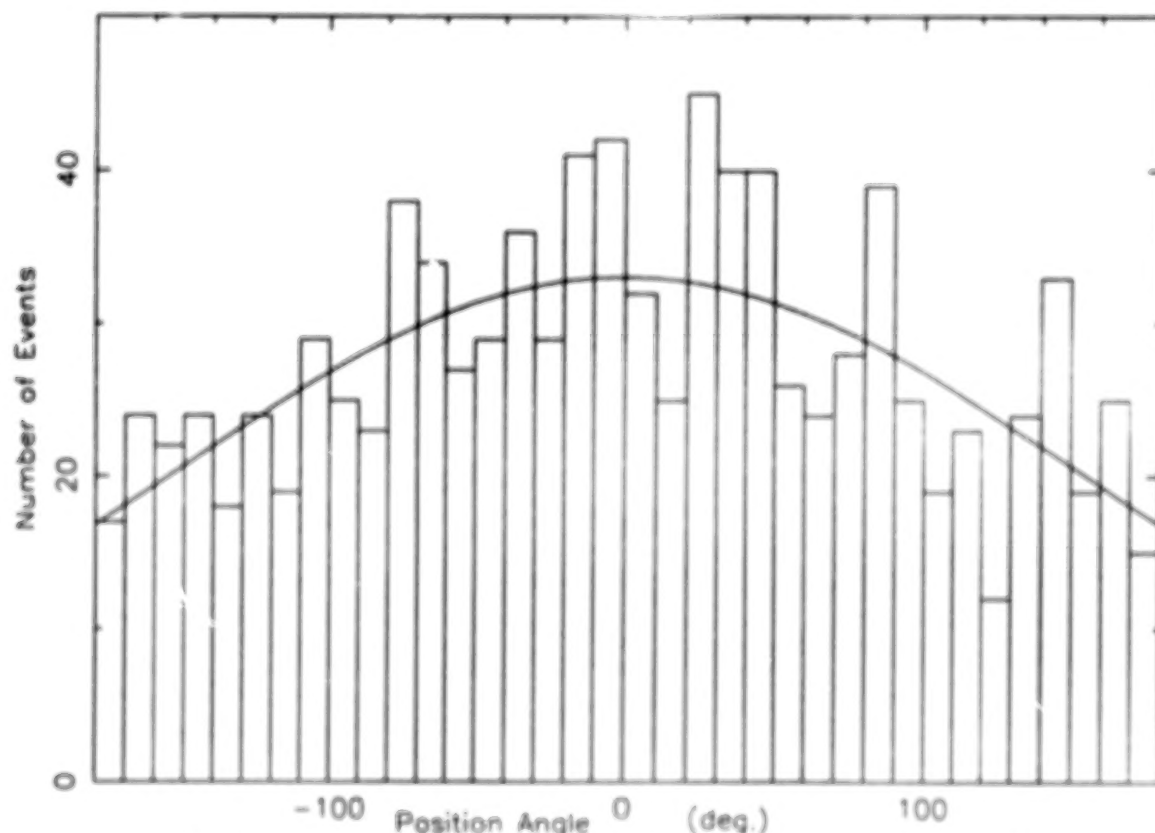


Figure 3. The azimuthal distribution due to multiple Coulomb scattering and lateral position uncertainty for events pair producing with identical azimuthal alignment of the pair production plane. The positron and electron have equal transverse momenta and their energies are both equal to half of the gamma ray energy (50 MeV). The opening angle is 0.042 radians.

The solid line is the gaussian approximation of Mattox, Mayer-Hasselwander, and Strong (1990) for the distribution of scattering angles with rms value $\Phi = 2.71$ radians giving the best fit. For 100 MeV, and the most probable opening angle ($\Omega = 0.021$), $\Phi = 2.84$. It was noted that $\Phi$ decreased with larger opening angle: $\Omega = 0.042$, $\Phi = 1.82$; $\Omega = 0.084$, $\Phi = 1.47$; $\Omega = 0.168$, $\Phi = 0.61$. The simulation over the entire cross section in section II yielded a value of $\Phi = 0.96$. Therefore, it is apparent that pair production events with wide opening angles are important in polarization sensitivity. Because there is substantial cross section at large opening angles, it is understandable that the integral of the effect of multiple Coulomb scattering and lateral position uncertainty over the cross section yields a smaller $\Phi$ than the crude estimate of equation (2) which assumes the most probable opening angle.

## IV. A Study of the Effect on Sensitivity of Selection Criteria

Kotov (1988) suggested that the sensitivity to polarization may be enhanced by selecting events for which both the electron and positron energies exceed 20% of the gamma ray energy. A minor change to program I produced this selection criterion. In practice, the selection criterion could not be so well implemented because of limited energy resolution of the electron and positron through scattering. With $E_{e\pm} > 0.2E_\gamma$, the asymmetry ratio with no multiple Coulomb scattering and no lateral position uncertainty is $z = 1.33$, an improvement of 19% in $R$. With multiple Coulomb scattering and lateral position uncertainty, the Monte Carlo study of 250 kiloevents with 100% polarization yields $z = 1.049 \pm 0.010$, an improvement of 33% in $R'$. The fact that $R'$ increases more than $R$ is probably due to a mitigation of the effect of multiple Coulomb scattering, although the lack of statistical significance prevents a definitive conclusion.

From Rossi's (1952, eq. 2.19.15) approximation for the total pair production cross section in the limit of complete screening, the number of events would decrease 28% by changing from $E_{e\pm} > 0.1E_\gamma$ to $E_{e\pm} > 0.2E_\gamma$. Thus, to get the 48 kiloevents needed for $3\sigma$ significance with the second harmonic test, 67 kiloevents events would be required. This is an improvement (although the statistical significance is not great) over 85 kiloevents, but still EGRET would not have useful polarization sensitivity.

Kozlenkov and Mitrofanov (1985) suggested that sensitivity to polarization could be improved by selecting events only if the observed pair-opening angle exceeded a minimum value. Program III was modified to compare the actual opening angle of program I to the opening angle determined by analysis of EGRET Monte Carlo tracks. A scatter plot is show in figure 4. A weak correlation is noted. Often events with a small actual opening angle are observed to have a large measured opening angle due to multiple Coulomb scattering. The grouping of events at quantized actual opening angle is due to the scheme used in program I to select from the cross section at 20 discrete values for each of 4 variables.

A Monte Carlo study with 220 kiloevents was done with $E_{e\pm} > 0.2E_\gamma$, and $E_\gamma = 100$ MeV. With the criterion $\Omega > 0.3$ radians, 11 kiloevents were accepted. The resultant asymmetry ratio is $z = 1.038 \pm 0.044$. With the criterion $\Omega > 0.15$ radians, 72 kiloevents were accepted. The resultant asymmetry ratio is $z = 1.052 \pm 0.018$. The lack of statistical significance (due to finite computing resources) prevents a quantative assessment. However, it is apparent that this scheme does not offer an improvement in sensitivity sufficient to make polarimetry viable with EGRET.
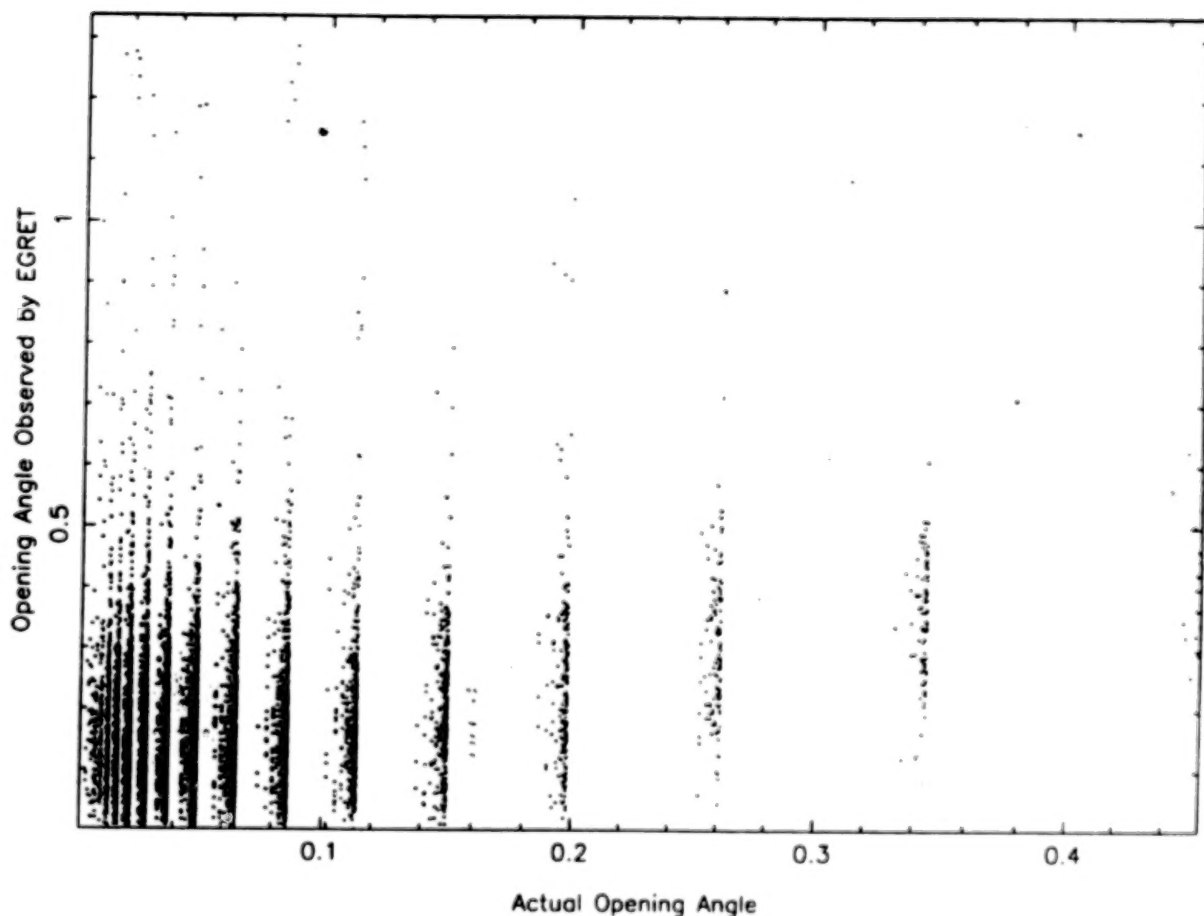
Figure 4. A scatter plot of the opening angle observed by EGRET versus the actual opening angle for 10 kiloevents at 100 MeV with $E_{e\pm} > 0.2E_{\gamma}$.

## V. Calibration Data Analysis

The azimuthal distribution of 3065 of the 4088 good, on-axis, 100 MeV SLAC events is shown in figure 2 with the dashed line. The other 1023 events were found to have the track slopes equal in at least one projection, or had only one track fitted. The azimuth is in spark chamber coordinates; but the instrument did not rotate during on-axis calibration so that the gamma ray polarization was at a fixed azimuthal position. The direction of gamma ray polarization during calibration could have been determined at the time of calibration by measuring the direction of polarization of the laser. Unfortunately, this was not done.

Except for the excesses along the axes (0°, 90°, 180°), no significant features are seen. These excesses are due to the limited lateral resolution of EGRET. It is apparent that this effect is larger than for the Monte Carlo simulation. This may be explained by the inability of EGRET to resolve

dual tracks when they are close together near the pair production vertex because of the ≈3 wire width of the tracks — an effect not included in the Monte Carlo simulation. This effect makes the polarization sensitivity of EGRET even worse than indicated in section II.

A similar result was found for the 4543 good events in the on-axis SLAC calibration at 200 MeV. Larger excesses along the axes than at 100 MeV (due to smaller opening angles) are seen. As for 100 MeV, no indication of azimuthal asymmetry due to polarization is seen.

## VI. CONCLUSION

A Monte Carlo study shows that the sensitivity of EGRET to polarization peaks around 100 MeV. However, more than $10^5$ gamma-ray events with 100% polarization would be required for a $3\sigma$ significance detection — more than available from calibration, and probably more than will result from a single source during flight.

A drift chamber gamma ray telescope under development (Hunter and Cuddapah 1989) will offer better sensitivity to polarization. The lateral position uncertainty will be improved by an order of magnitude. Also, if pair production occurs in the drift chamber gas (xenon at 2 bar) instead of tantalum foils, the effects of multiple Coulomb scattering will be reduced.

## References

Abe, et al. 1984, *Phys. Rev. Lett.* , **53**, 751.

Bertsch, D. et al., *Proceedings of the Gamma Ray Observatory Science Workshop*, Goddard Space Flight Center, April 10-12, 1989.

Kelner, S.R., Kotov,Yu.D., and Logunov, V.M. 1975, *Sov. J. Nucl. Phys.* , **21** , 313.

Hunter, S.D., Cuddapah, R. *Proceedings of the Workshop on High Energy Astrophysics in the 21st Centuary*, Taos, 11-14 December 1989.

Kotov, Y.D. 1988, *Space Sci. Reviews* , **49**, 185.

Kozlenkov, A.A., and Mitrofanov, I.G. 1985, *Sov. Astron.* , **29** , 591.

Mattox, J.R., Mayer-Hasselwander, H.A., Strong, A.W. Submitted to *Astroph. J.*, 1990.

Mattox, J.R., Hofstadter, B., Hughes, E.B., Lin, Y.C., Nolan, P.L., Walker, A.H. 1987, *Nucl. Instrum. Meth.* , **B24**, 888.

Maximon, L.C., Olsen, H. 1962, *Phys. Rev.* , **126**, 310.

Murray, J.J., Fieguth, T. *Report on SHF for the SLAC Hybrid Facility Workshop*, March 10-11, 1978.

Nelson, W.R., Hirayama, H., Rogers, D.W.O. SLAC-Report-265, December 1985.

Rossi, B. *High-Energy Particles*, Prentice-Hall, Englewood Cliffs, NJ, 1952.

Yang, C.N. 1950, *Phys. Rev.* , **77**, 722.

# Other Galactic Gamma Ray Sources

# TeV RADIATION FROM THE CRAB NEBULA AND OTHER MATTERS

R. C. LAMB, Iowa State University, Ames, Ia 50011

## ABSTRACT

The detection of the Crab Nebula via the Cherenkov imaging technique places TeV astronomy on a secure observational footing. This paper presents the motivation for TeV observations, a discussion of the atmospheric Cherenkov technique, the experimental details of the Crab Nebula detection, and its scientific implications. The present dilemma of VHE/UHE astronomy is that the Crab appears to be the only source whose showers match theoretical expectations. The situation will be clarified as improved ground-based detectors come on-line with sensitivities matching those of the GRO instruments.

## I. SCIENTIFIC MOTIVATION

Gamma rays provide direct information about the highest energy processes which occur in nature. The various bands of the gamma ray portion of the electromagnetic spectrum are shown in figure 1. The instruments of the Gamma Ray Observatory will cover the five decades from 0.1 MeV to 10 GeV with a factor of 10 to 20 improvement over previous satellite instruments; however, the 2000 cm$^2$ detection area of the highest energy instrument, EGRET, means that only a few photons greater than 10 GeV will be detected. Thus gamma rays of higher energy must be detected via shower techniques, either by means of the Cherenkov light from the cascade particles or by means of the particles themselves. In figure 1 I have indicated the approximate range of the Cherenkov technique, 0.1 to 10 TeV, and the band covered by extensive air shower arrays. Gaps exist between each of these bands. Developing instruments which fill these gaps is a major challenge for gamma ray astronomy above 10 GeV.
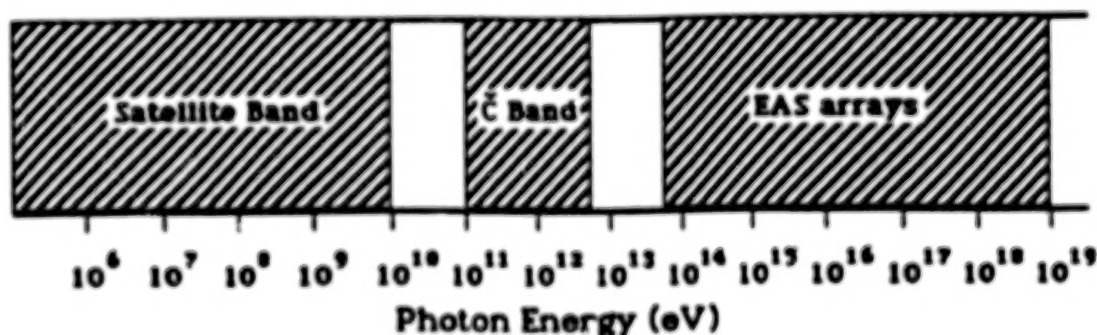


Figure 1. The gamma-ray portion of the electromagnetic spectrum. The cross-hatched portions indicate bands which are covered by present instruments. Gaps exist for ~ 10 to ~ 100 GeV and for ~ 5 to ~ 50 TeV.

Two major motivations for ground-based gamma ray astronomy are the identification of sources of VHE and UHE cosmic rays and understanding relativistic objects.

For energies up to a few times $10^{13}$ eV, acceleration of protons in supernova shock waves is a favored explanation for the origin of cosmic rays, however this mechanism fails for higher energies (Hillas 1984). An accurate enumeration of the total power output by the TeV and PeV sources will be a step toward direct verification of the shock wave hypothesis and may lead to identification of other sources of VHE/UHE cosmic rays.

It is now clear that some of the VHE/UHE sources contain rapidly spinning, highly magnetized neutron stars, in which a substantial fraction of the energy output is in the form of relativistic beams. A well developed TeV astronomy should help determine the particle identify of the beams (electronic or hadronic) and illuminate the nature of the various acceleration mechanisms which produce the beams.

Progress in understanding relativistic objects will be maximized through a multi-wavelength approach in which observations at satellite energies are complemented by coordinated ground-based observations.

## II. THE ATMOSPHERIC CHERENKOV TECHNIQUE

A photon with an energy above a few tens of GeV may be detected on the ground by means of the air shower Cherenkov light. This light is emitted by those charged particles in the shower which have velocities, $v/c$, greater than $1/n$ where n is the index of refraction of the atmosphere. For a $10^{12}$ eV shower approximately $10^6$ Cherenkov photons are emitted spread over a region on the ground of a few x $10^8$ cm$^2$.

The information content of the Cherenkov photons is high quality both from the point-of-view of the Cherenkov photon statistics and because these photons are dominantly from the region of the shower's maximum development and therefore less subject to shower-to-shower fluctuations.

This information in principle allows air showers from gamma-rays and cosmic rays to be distinguished from one another, as illustrated by the Whipple Observatory Collaboration's detection of the Crab Nebula discussed below. Because of this feature the technique has the ability to prove that the shower primary is in fact a gamma-ray, and we can look forward to future improvements in the Cherenkov technique is which the unwanted cosmic ray background is reduced substantially beyond what has already been achieved.

Because of the large collection area per independent Cherenkov collection mirror, TeV detectors are intrinsically high-rate devices, with detection rates for the brightest sources of a few photons/minute and burst rates even higher. This feature can be used to search for pulsars that would be hidden at x-ray and radio-wave energies. The mean free path of gamma-rays is 5 x $10^{25}$ H-atoms/cm$^2$ vs $< 10^{22}$ for x-rays. Radio pulses from x-ray binaries may not escape due to plasma absorption. Thus there may be pulsars that are only detectable in gamma-rays. Recognition of this fact has motivated several groups to search for a possible pulsar associated with Cygnus X-3 (Chadwick et al. 1985 and Zyskin et al. 1987)

The high-rate capability can also be used to explore short time scale phenomena indicative of time varying acceleration and/or changes in beam-target geometry.

The ultimate capabilities of the atmospheric Cherenkov technique have not been fully explored. Most recently Hillas (1989) has shown that angular resolutions of 2 - 3 arc minutes are possible with the technique with an ideal imaging detector.

## III. DETECTION OF THE CRAB NEBULA

The Whipple Observatory's gamma ray telescope consists of a 10 meter reflector in which an array of fast photomultipliers, located in the focal plane, is used to image individual air showers. Showers are detected at a rate of approximately 3 Hz, more than 99% of which are due to cosmic rays. The shower images are recorded and gamma ray candidates are selected in off-line analysis, using a procedure determined by Hillas (1985) from Monte Carlo simulations tailored to the Whipple instrument.

A simple moment analysis of the pattern of light is used in which second moments of the light around its centroid are used to derive size and orientation parameters for each shower image. Simulations and observations agree that in the original 37 element ($0.5^{\circ}$ pixel spacing) camera cosmic-ray background showers have a mean size of $1.0^{\circ}$ (full-width half height) whereas gamma-ray showers have a mean size of $0.5^{\circ}$. Furthermore, gamma-ray showers are more elongated (except for showers whose axis falls within 50 meters of the reflector). The elongation is such than the major axis of the light is oriented preferentially radially from the center of the field-of-view. These differences can be summarized by saying that the Cherenkov light images from a gamma-ray source are more compact and point to the source.

Although six parameters were originally introduced by Hillas, one parameter, the "azwidth", appears to be more effective than any other single parameter and as effective as any combination of parameters. Azwidth is defined to be the rms width of the shower images in the azimuthal direction of the image plane.

With this parameter and with the cut values of azwidth as set in advance by the Hillas' simulations the Whipple group has published a 9 $\sigma$ detection of the Crab Nebula (Weekes et al. 1989) using a relatively coarse resolution camera ($0.5^{\circ}$ pixel separation) and, more recently, an independent 15 $\sigma$ detection (Lang et al. 1990) with a higher resolution camera ($0.25^{\circ}$ pixel).

The distribution of azwidth values for the 9 $\sigma$ detection (Weekes et al. 1989) is shown in figure 2b, with a comparison of the expected behavior of azwidth values for simulated gamma-ray and proton-initiated showers in figure 2a. The peak of the observed azwidth distribution, near $0.4^{\circ}$, is in agreement with the simulations for proton showers. The only significant difference in the on-source and off-source distributions is in the region of small azwidth as expected if the on-source region is a source of TeV gamma rays. The difference of the two distributions in this region is shown in the inset to figure 2b.
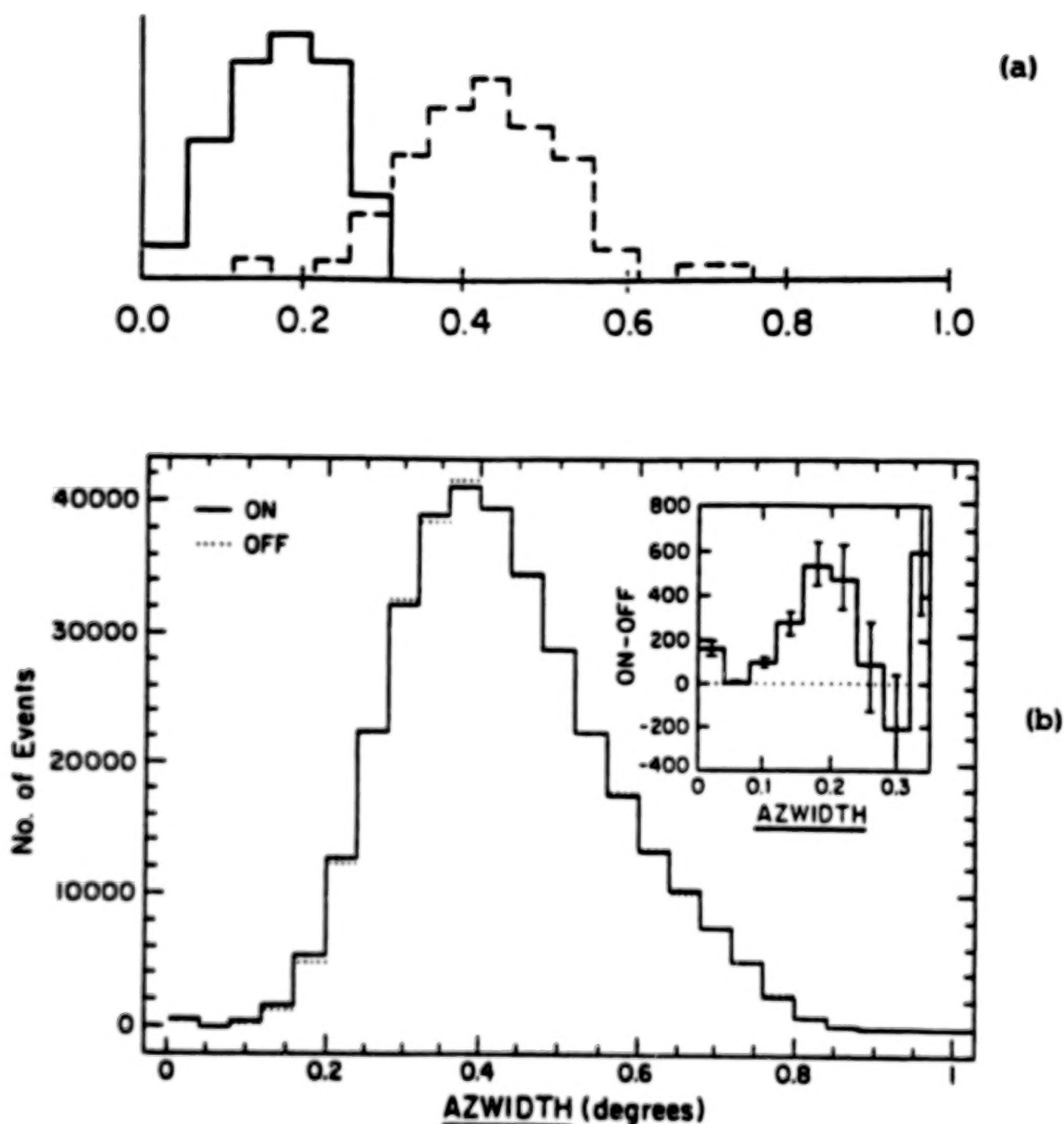
**Figure 2.** (a) Distribution of AZWIDTH for simulated shower events (Hillas 1985): gamma-ray initiated showers, solid line (-); proton-initiated showers, dashed line (--); (b) Distribution of AZWIDTH for observed showers (Weekes et al. 1989). On source, solid line (-); off source, dotted (...). The difference in the two distributions is shown in the inset.

The Whipple's observations of the Crab Nebula have been subjected to a number of tests for possible systematic errors. For example, the signal does not depend on the order of the comparison between on-source and off-source regions. If the signal were noise related then it should be most apparent for showers with total light near threshold; it is not. There is a third magnitude star, Zeta Tauris, in the field of view of

the camera. In order to test for the effect of such a star on the Cherenkov images, a
control region of the sky was chosen in which a third magnitude star was present as a
false "on-Crab" region whereas no such star was present in the false "off-Crab" region.
Comparison of the two false regions showed no excess either before or after the
azwidth selection was made. Many other tests were made, as described in Weekes et
al. (1989), with similar results. The Whipple's detection of the Crab Nebula appears to
be a solid result of TeV astronomy.

Independent support for this result comes from the University of Michigan's
observations. With twin 11 meter diameter mirrors, each with 7 element cameras,
Akerlof et al. (1989) have a 5.8 σ detection of the Crab Nebula produced by the
application of imaging type cuts on a raw 2.3 σ excess.

There is no evidence for time variability on a month-a-month basis in the
Whipple's Crab signals. If we assume little or no variation over two decades it is
meaningful to compare the earliest Whipple Crab detection (Fazio et al. 1972) without
imaging with the more recent imaging results. Table I gives the comparison. As the
reader can see, an overall gain in sensitivity of a factor of 10 has been achieved, i.e. the
signal/background has improved by a factor of 100.

## TABLE I
### SENSITIVITIES OF DIFFERENT DETECTORS
### FOR OBSERVATIONS OF CRAB NEBULA

| Date | Imaging | Time on Source (h) | σ | Gain Factor vs. non-imaging system | References |
|------|---------|--------------------|---|-----------------------------------|-----------|
| 1968-72 | no | 150 | 3 | 1 | Fazio et al. 1972 |
| 1986-88 | yes(0.5° pixel) | 80 | 9 | 4 | Weekes et al. 1989 |
| 1988-89 | yes(0.25° pixel) | 30 | 15 | 10 | Lang et al. 1990 |

## IV. SIGNIFICANCE

The bulk of the radiation reported by both the Whipple group (Weekes et al.
1989) and by the University of Michigan group (Akerlof et al. 1989) is not pulsed at the
Crab pulsar frequency. The integral photon flux values from these measurements is
shown in figure 3, along with the extrapolations from lower energies of the COS-B
results (Clear, et al. 1987) for both the pulsed and unpulsed components. The TeV
points falls approximately midway between the extrapolations of the lower energy
observations.

The TeV observations and a synchrotron-self Compton model for TeV emission
(Rieke and Weekes 1969) constrain the magnetic field of the Nebula to be
approximately what is expected on the basis of energy equipartition arguments, namely
$\sim 6 \times 10^{-4}$ G, Measurements of the differential energy spectrum of the source in this
spectral region should be forthcoming, and, in the context of the synchrotron-self
Compton model, determine the spectral behavior of the parent population of relativistic
electrons.
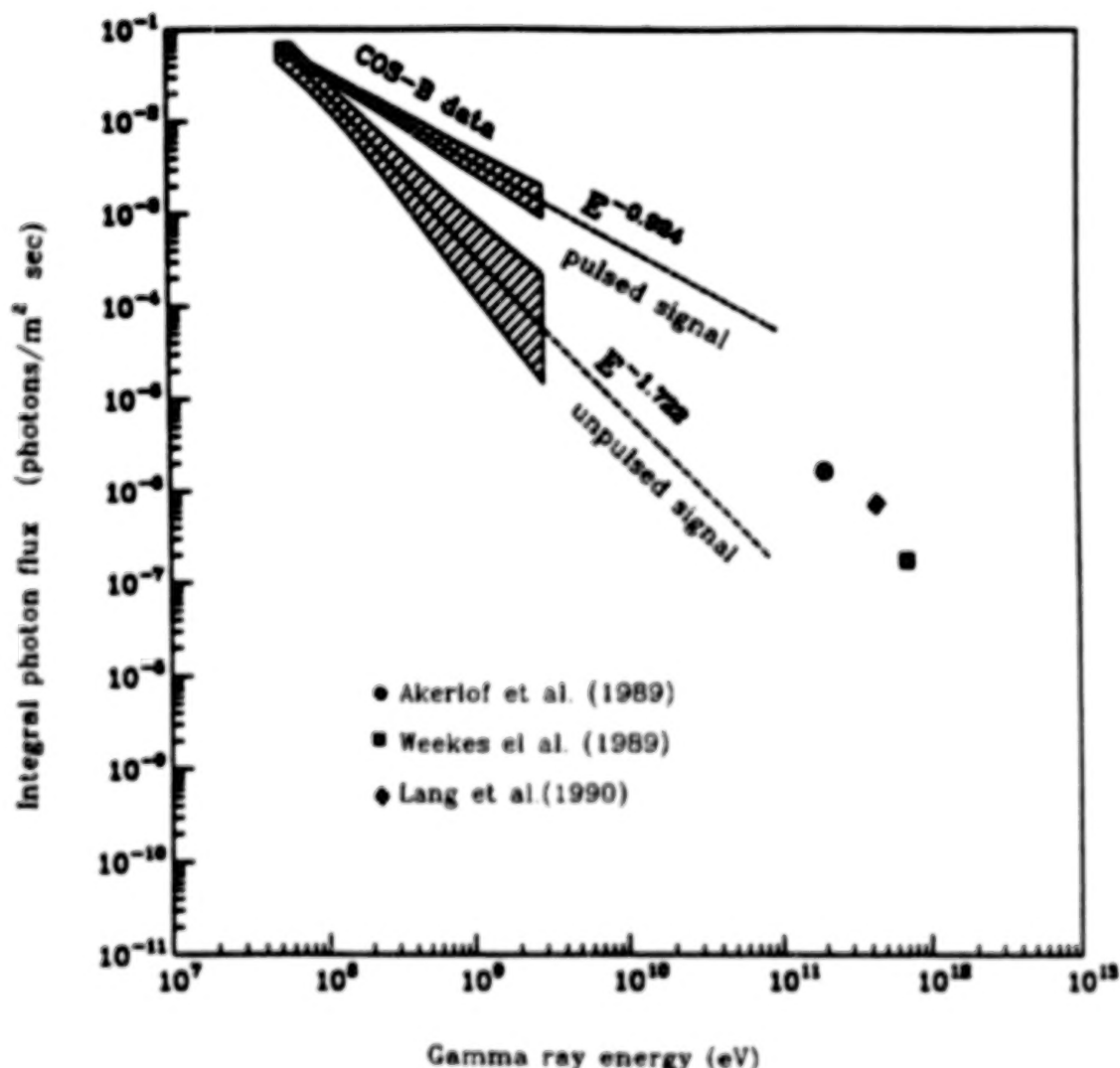
**Figure 3.** The gamma-ray energy spectrum of the Crab nebula and pulsar above 70 MeV.

## V. OTHER SOURCES

More than a dozen other sources have been reported at both TeV and PeV energies. See Weekes (1988) for a recent compilation. A potential major embarrassment of the field of VHE/UHE gamma ray astronomy is that so far the Crab Nebula is the only source for which the signals behave as expected of photons. The optimist would say that this strong evidence that "new physics" is afoot. The pessimist/realist would say that this is strong evidence that no source (other than the Crab) has been seen. Bonnet-Bidaud and Chardin (1988) have expressed this latter view in their review of Cygnus X-3. My own view is that the number of independent sightings of such binary sources as Cygnus X-3, Hercules X-1, and Vela X-1 are too

numerous and too strong to ignore. The question of "new physics", however, is a much bigger question and one that is a long way from being proved. As someone said recently, "extraordinary claims require extraordinary evidence." The extraordinary evidence is not at hand (yet).

The failure of other source signals to behave as expected of photons has been emphasized by Hillas (1987) at the Moscow ICRC. At air shower energies two traditional methods of reducing the background exist, one of which (muon content) is on a secure calculational footing; however, the other method, which uses age cuts, is not.

Calculations (Protheroe and Turver 1979; Stanev, Vankov, and Halzen 1985) show that gamma-ray showers are relatively poor in muons (10% or less of the content of proton showers of the same size); thus a cut on muon poor showers should improve sensitivity. In fact the original Cygnus X-3 PeV detection (Samorski and Stamm 1983) showed signals with a muon content roughly equal to that of background cosmic ray showers.

The other selection technique used at air shower energies is an age parameter cut. The use of this parameter has been called into question by simulation of PeV gamma-ray and proton air showers by Hillas (1987). These simulations make two points: 1) age is a relatively poor discriminant between gamma-ray and cosmic-ray showers, and 2) what discrimination exists is such that gamma-ray showers are younger on average rather than older than the cosmic-ray background showers of the same energy. The selection of Samorski and Stamm picked showers with age values greater than 1.3, relatively old and inconsistent with Monte Carlo expectations for gamma-rays.

The CYGNUS group, operating an air shower array at Los Alamos National Laboratory, has reported evidence for burst signals from Hercules X-1 (Dingus et al. 1988) on a time scale of 30 minutes. The apparatus is sensitive to air showers of energies greater than 50 TeV. Their signals are anomalous in that they are not poor in muons.

Signals reported by the Whipple Collaboration at TeV energies from the direction of Hercules X-1 (Reynolds et al 1990) are also anomalous in that they disappear when the azwidth imaging cut is applied to them.

## VI. TeV ASTRONOMY IN THE GRO ERA

The sensitivities of detectors operating in the VHE/UHE energy range are improving. In addition to the Whipple instrument Cherenkov imaging detectors exist at the Crimean Astrophysical Observatory (operational 1989) and the Yerevan Physical Institute (construction begun 1988), and plans for a high angular resolution instrument have been proposed by the JANZOS collaboration to be located in Australia. At higher energies the CYGNUS collaboration is extending their array to a ground coverage area of $0.8 \times 10^5$ m$^2$ and the Chicago, Michigan, Utah installation will have a coverage of $2.5 \times 10^5$ m$^2$ within two years.

The Whipple instrument will be upgraded with the addition of a second reflector 11 meters in diameter (GRANITE project). It should be complete and ready to take data in early 1991. Figure 4 shows the sensitivities of the new ground-based instruments in comparison with the sensitivities expected of the GRO instruments. Note that the vertical scale of the differential sensitivity has been multiplied by the 2.5 power of the gamma-ray energy. As one can see there is a good match by the ground-based instruments to the sensitivities of GRO instruments.
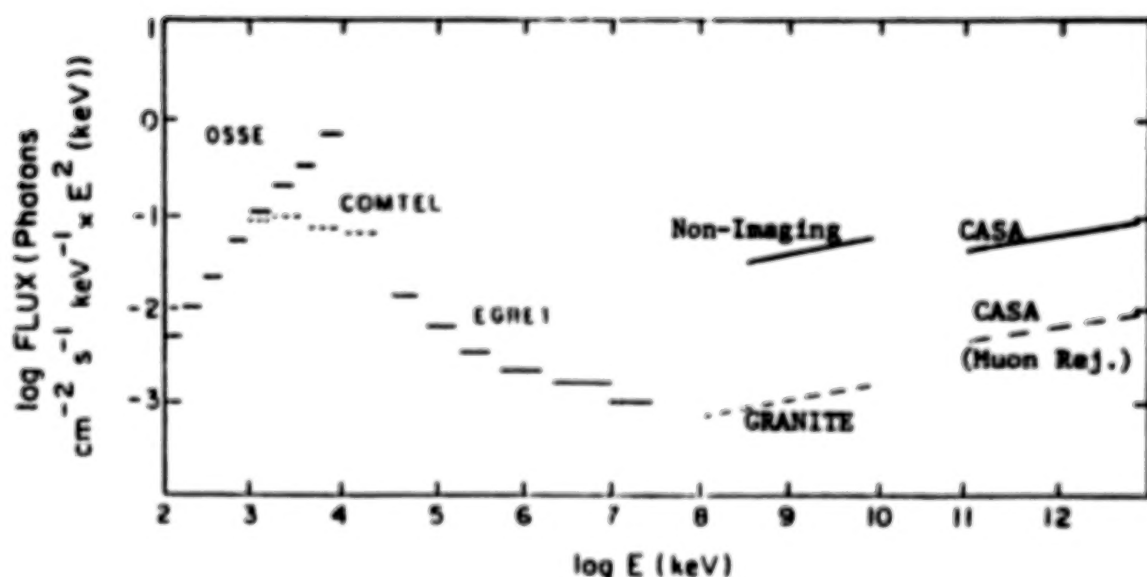
**Figure 4.  Minimum flux sensitivity in different bands of the gamma-ray spectrum.**

A vigorous program of coordinated observations between GRO and the ground-based Cherenkov receivers is anticipated.  If GRO is pointed at a target of mutual interest during a dark moon period and the source transits near midnight, then the on-time of Cherenkov receivers can approach 25% under the assumption of good weather. Thus a good overlap in simultaneous observations can be anticipated.  Of course, for a reasonably steady source like the Crab Nebula, simultaneity is not necessary.  For the Crab, many interesting questions regarding spectral changes for the pulsed and unpulsed components can be addressed by combining data from EGRET and the most sensitive of the Cherenkov receivers.

## REFERENCES

Akerlof, C. et al. 1989, Proc. of the Gamma Ray Observatory Science Workshop, NASA/Goddard Space Flight Center, 4-49.
Bonnet-Bidaud, J.M. and Chardin, G. 1988, Physics Reports, 170, 325.
Chadwick, P.M. et al. 1985, Nature, 318, 642.
Clear, J. et al. 1987, Astro. Ap., 174, 85.
Dingus, B.L. et al. 1988, Phys. Rev. Letters 61, 1906.
Fazio, G.G. et al. 1972, Ap.J. Letters, 175, L117
Hillas, A.M. 1984, Am. Rev. Astron. Ap., 22, 425.
Hillas, A.M. 1985, 19th Int. Cosmic Ray Conf., La Jolla, 3, 445.

Hillas, A.M. 1987, 20th Int. Cosmic Ray Conf., Moscow, 2, 262.

Hillas, A.M. 1989, Proc. of the Crimean Workshop on VHE Gamma Ray Astronomy, 134.

Lang, M.J. et al. 1990, 21st Int. Cosmic Ray Conf., Adelaide, paper OG4.3-2.

Protheroe, R.J. and Turver, K.E. 1979, J. Phys. G., 5, 1613.

Reynolds, P.T. et al. 1990, 21st Inst. Cosmic Ray Conf., Adelaide, paper OG4.2-2.

Rieke, G. H. and Weekes, T.C. 1969, Ap.J., 155, 429.

Samorski, M. and Stamm, W. 1983, Ap.J. Letters, 268, 47.

Stanev, T., Vankov, Ch.P. and Halzen, F. 1985, 19th Int. Cosmic Ray Conf., La Jolla, 7, 219.

Weekes, T.C. 1988, Physics Report, 160, 1.

Weekes, T.C. et al. 1989, Ap.J., 342, 379.

Zyskin, Yu. L. et al. 1987, Astron. Circ. Bur. Astron. Info., USSR Acad. Sci. No. 1508.

## DISCUSSION

*Carl Fichtel:*

Will any of the other Cerenkov observatories have either a fine grid of photomultipliers comparable to the Whipple one or two telescope system?

*Dick Lamb:*

The Crimean Astrophysical Observatory has a Cherenkov imaging system with a 37-element camera which is essentially ready to begin observations. An imaging system is under construction at the Yereban Physical Institute, and the JANZOS collaboration plans a high resolution camera (pixel size 0.15°) for operation in Australia.

*R. Buccheri:*

Does Whipple Observatory confirm the 12.6 ms pulsar detected by the Durham group in the Cyg X-3 source?

*Dick Lamb:*

The Whipple Observatory collaboration does not confirm either the 12.6 ms pulsation reported by Durham nor a 9.22 ms pulsation reported by the Crimean Astrophysical Observatory.

# THE ILLUSIVE GEMINGA: WHAT IS IT?

## DONALD A. KNIFFEN
NASA/Goddard Space Flight Center, Greenbelt, MD 20771

## ABSTRACT

The first unassociated gamma-ray source was discovered by SAS-2 in 1973 (Kniffen, et al., 1975) and later confirmed by COS-B (Bennett, et al., 1977). Following the announcement, there were numerous attempts to find a counterpart, and many models were developed to explain the source. Now over fifteen years later this illusive source still remains as one of the major riddles of astrophysics. Why is an object, which is able to emit such energetic photons, so well concealed at other wavelengths? The association with the *Einstein* source 1E 0630+178 is the most favored (Bignami, Caraveo, and Lamb, 1983), but this cannot be considered proven. The pulsar emission model of Ruderman and Cheng (1988) is appealing in its broad applicability, but awaits observational confirmation. The EGRET instrument on the Gamma-Ray Observatory will provide a major improvement in observational capability to better define the location and spectrum of this source, and hopefully will lead to a confident identification.

## I. INTRODUCTION

Among the first gamma-ray sources detected by SAS-2, superseded only by the Crab Nebula and Vela radio pulsars was an unidentified source in the Galactic anti-center region at l=195, b=+5. Later confirmed by the COS-B collaboration, this source is listed in their second catalog as 2CG195+04. It is the second most intense source above 100 MeV, next to the Vela pulsar, and has the hardest spectrum of any source for which one is obtained. Although the lack of unique signatures such as contemporary time fluctuations has not allowed a definitive identification of Geminga (See Bignami, Caraveo, and Lamb, 1983, for the origin of this alias.), the latter reference claims identification with an Einstein source 1E 0630+178 and Moffat et al. (1983) possibly with a Z=1.2 Quasar. The outer gap model of Ruderman and Cheng (1988) seems to fit the observations well and would favor a galactic pulsar model. The wide beam predicted by this model might account for many hard spectra gamma-ray sources, not identified as radio pulsars, where a narrower beam is expected.

## II. OBSERVATIONAL HISTORY

The first discovery of a gamma-ray discrete source not associated with a known object was reported by the SAS-2 group (Kniffen et al., 1975). A contour plot of the galactic anti-center region for gamma-rays above 35 MeV (Figure 1) showed a clear excess at l=195, b=+5. This result was confirmed by the COS-B Collaboration (Bennett, et al., 1977) who reported a position of l=196, b=+4. In the second COS-B catalog (Swanenburg, et al.,
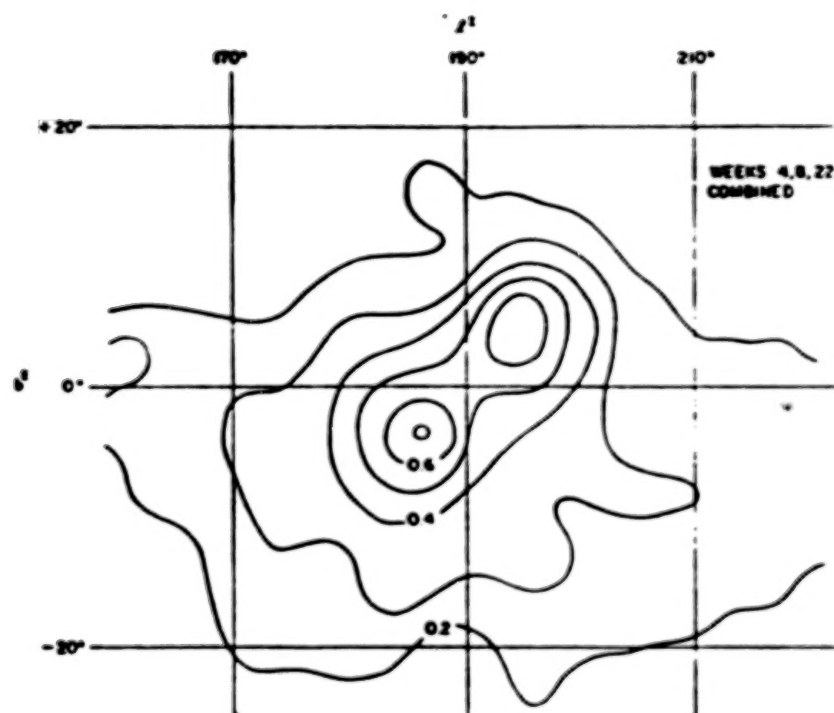
Fig. 1. Contour plot from the original discovery
of γ195+5 Kniffen, et al., 1975). This plot
refers to gamma-rays above 35 MeV.

1981), the location of 2CG195+04 is given as l=195.1, b=+4.5. An
error radius of 0.4 degrees, although statistically precise, may
still contain systematic errors resulting from the very compli-
cated structure of the diffuse or unresolved discrete source
emission in this region. Geminga is the second most significant
source listed in the 2CG catalog, the Vela pulsar being the most
significant. The flux above 100 MeV given in the 2CG catalog is
$4.8 \times 10^{-6}$ ph cm$^{-2}$s$^{-1}$ in agreement with the SAS-2 flux (>100 MeV)
of $(4.3 \pm 0.9) \times 10^{-6}$ cm$^{-2}$s$^{-1}$ (Thompson, et al., 1977).

Although both SAS-2 (Thompson, et al.,1977) and COS-B
(Swanenburg, et al.,1981) indicate a hard spectrum for Geminga,
the only published spectrum is given by Hermsen (1980) and is re-
produced in Figure 2. Not only is the spectrum the hardest of any
source for which a spectrum was obtained, it appears to bend over
below 100 MeV. Despite many observational attempts, no gamma-ray
detections below 100 MeV have been reported (Haymes, Meegan and
Fishman, 1979; Graser and Schönfelder, 1982).

Reports of a weak indication of a 59 second periodicity in
the flux seen by SAS-2 (Thompson, et al. 1977) were confirmed by
COS-B (Masnou, et al., 1977) and also evidence for x-ray period-
icity in the *Einstein* and EXOSAT data was reported by Bignami,
Caraveo and Paul (1984). A later analysis (Buccheri, et al.,
1985) questioned the significance of these claims. Confirmation
with the high sensitivity of EGRET should be awaited before these

results are taken seriously in modeling the gamma-ray emission from 2CG195+04.
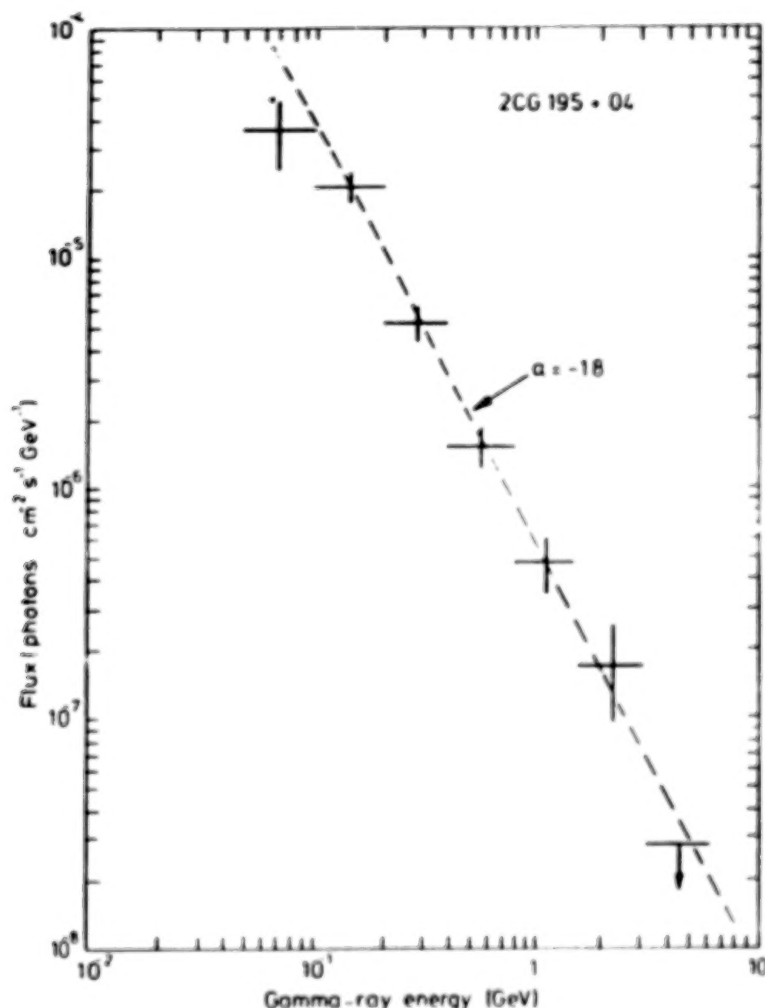


Fig. 2. Differential energy spectrum of the Source 2CG195+04 observed by COS-B (Hermsen, 1980). The dashed line is a power law fit to the data points.

## III. THE SEARCH FOR COUNTERPARTS

Following the discovery of Geminga, extensive searches of existing catalogs (Cesarsky, Cassè, and Paul, 1976; Bignami, Macccacaro, and Paizas, 1976; Thompson, et al., 1977) showed no candidates at other wavelengths based on the lack of positional coincidences.

The first claim of an association resulted from a HEAO-A2 observation of a weak x-ray source for which the HEAO-1 and COS-B error boxes overlapped (Lamb and Worral, 1979). However, the significance of the positional coincidence was not strong and no

other compelling characteristic of the x-ray source supports the identification.

*Einstein* IPC observations of the region provided four candidate x-ray sources (Bignami, Caraveo and Lamb, 1983). The Einstein source, 1E 0630+178 the strongest of these four weak sources, was found to have a soft spectrum, display no absorption feature, and to have a spatial extent consistent with the instrument point spread function. Lack of a VLA detection at 6 cm or optical sources in the error box implies an unusually high x-ray to optical luminosity ratio. These unique features led Bignami, Caraveo and Lamb to claim an association. Subsequently Caraveo, et al. (1984) proposed a 21st magnitude blue star as the optical counterpart, but Halpern, Grindlay and Tyler (1985) argued against this association.

A deeper optical search by Bignami, et al. (1987) revealed two sources having r magnitudes ~24.5 and ~25.5, and suggested the fainter as a candidate for association based on its bluer spectrum. Using the Hale 5m telescope with three color CCD photometry, Halpern and Tytler (1988) find this object to be the bluest, by far, in the field, and argue it could be a very compact synchrotron source.

An alternative association has been suggested by Moffat, et al. (1983). These authors identify the best candidate radio source from a survey of the COS-B error box by Sieber and Schlickeiser (1982) with a 19th magnitude z=1.2 quasar, QSO 0630+180. The radio source has the flattest radio spectrum in the region and is the only one with a clear optical counterpart. The quasar association implies a gamma-ray luminosity of about $10^{48}$ ergs s$^{-1}$.

A search of the Geminga error box at 21 cm by Spoelstra and Hermsen(1984) revealed over 15 sources between ~4 and 50 mJy. None were deemed by the authors to have sufficiently anomalous properties to be considered viable candidates for association with the gamma-ray object.

## IV. INTERPRETATION

The current situation with regard to the identification of the source, originally given the name $\gamma$195+5 (Kniffen, et al., 1975), is still far from resolved. The possibility that it is a quasar cannot be ruled out since 3C273 appears to be well established as a gamma-ray source (Bignami, et al., 1981), and the quasar 0241+622 is a candidate for 2CG135+01 (Apparao, et al., 1978). The gamma-ray luminosity of ~$10^{48}$ ergs s$^{-1}$ deduced if the association with QSO 0630 +180 is correct is ~$10^2$ times that deduced for 3C273!

Assuming the association with 1E 0630+178 and the apparently association with a faint blue counterpart is correct, the characteristics which must be explained include luminosity ratios

$L_\gamma/L_x \tilde{} 1000$, $L_x/L_{opt} \tilde{} 1800$, the lack of an extended x-ray syn-
chrotron nebula, and a soft x-ray spectrum. As discussed by
Halpern (1989), the only known objects with such a high $L_x/L_{opt}$
ratio are neutron star binaries with low-mass companions, and
some radio pulsars or other compact objects related to supernova
remnants. The large $L_C/L_x$ ratio is consistent with a pulsar,
where the gamma-rays are produced far from the surface to avoid
degradation of the spectrum by self absorption and reprocessing.
Since the emission cone would be larger near the speed of light
cylinder than at the polar cap (Cheng and Ruderman, 1980), it is
reasonable that the pulsed emission would be seen at gamma-ray
energies, but not in the radio. Unfortunately, statistical limi-
tations prevent a period search in the gamma-ray observations.

The most comprehensive model for explaining Geminga as a
pulsar is given by Ruderman and Cheng (1988). They note the simi-
larities with Vela in the luminosity ratios, and that Vela, un-
like Geminga has an extended x-ray nebula. They argue this is
consistent with their model of pulsar spectral evolution in which
the x-ray luminosity of a Vela like pulsar becomes increasingly
small compared to the gamma-ray luminosity. The source mechanism
for the gamma-rays from such objects is synchrotron emission by
$e^{\pm}$ pairs created in the neutron star's outer magnetosphere.
Geminga would be a further evolution of a Vela like pulsar in
this scenario in which the magnetic pole has become nearly
aligned with the spin axis. One consequence of the near alignment
is a smaller x-ray synchrotron nebula. Another is that the modu-
lation of any gamma-ray emission at the pulsar rotation period
would be small, and difficult to detect. Ruderman and Cheng
(1988) present plausible arguments that the 20 unidentified
sources in the COS-B 2CG catalog could be a manifestation of pul-
sars in this stage. The final stage of the evolution of such ob-
jects is reflected as hard spectra gamma-ray burst sources.

Other models have been proposed to explain the observed
properties of Geminga (Maraschi and Treves, 1977; Langer and Rap-
paport, 1982; Nulsen and Fabian, 1984; Bisnovatyi-Kogan, 1985)
but recent work has left them in less favor and they will not be
discussed here.

## V. PROSPECTS FOR IDENTIFYING GEMINGA

None of the associations with Geminga which have been de-
scribed above are definitive. The probability of finding an *Ein-
stein* HRI source in the COS-B error box is about 5 percent
(Halpern, Grindlay, and Tytler, 1985). The optical association
with a faint blue object adds to the case, but cannot be
considered entirely decisive. The case for the radio-bright
quasar is even less convincing with about a 20 percent chance
probability (Moffat, et al., 1983). A more confident association
will await the improved observations with HST, ROSAT, AXAF and
GRO. In all cases there will be remarkable improvements in
sensitivity and resolution. With GRO/EGRET, the observations will
not only be vastly more sensitive and with better precision in

both position and energy, but the spectrum will be measured up to 20 GeV or more, where the position can be determined even more accurately. Thus the prospects for understanding the "Illusive Geminga" appear very good. Furthermore, the expanded catalog of sources which the great leap in sensitivity will provide, will shed new light on the interesting possibility that "radio quiet" pulsars are a major explanation for the unidentified gamma-ray sources.

## VI. REFERENCES

Apparao, K.M.V., Bignami, G.F., Maraschi, L., Helmken, H., Margon, B., Hjellming, R., Bradt, H.V., and Dower, R.G., 1987, Nature, 274, 450.

Bennett, K., Bignami, G.F., Bonnardeau, M., Buccheri, R., Hermsen, W., Kanbach, G., Lichti, G.G., Mayer-Hasselwander, H.A., Paul, J.A., Scarsi, L., Stiglitz, R., Swanenburg, and Wills, R.D., 1977, Astr. Ap., 56, 469.

Bignami, G.F., Maccacaro, T., and Paizis, 1976, Astr. Ap., 51, 319.

Bignami, G.F., Caraveo, P.A., and Lamb, R.C., 1983, Ap. J., 272, L9.

Bignami, G.F., and Hermsen, W., 1983, Ann. Rev. Astr. Ap., 21, 67.

Bisnovatyi, G.S., 1985, Nature, 315, 555.

Buccheri, R., D'Amico, N., Hermsen, W., and Sacco, B., 1985, Nature, 316, 131.

Caraveo, P.A., Bignami, G. F., Vigroux, L., and Paul, J.A., 1984, Ap. J., 276, L45.

Graser, U., and Schönfelder, V., 1981, Ap. J., 263, 677.

Halpern, J.P., and Tytler, D., 1988, Ap. J., 330, 201.

Halpern, J.P., Grindlay, J.E., and Tytler, D., 1985, Ap. J., 296, 190.

Haymes, R.C., Meegan, C.A., and Fishman, G.J., 1979, Astr. Ap., 79, 88.

Hermsen, W., **Gamma-Ray Sources**, Ph. D. Thesis, University of Leiden, 1980.

Kniffen, D.A., Bignami, G.F., Fichtel, C.E., Hartman, R.C., Ögelman, H., Thompson, D.J., Özel, M.E., and Tümer, T., 1975, Proc. 14th Internat. Cosmic Ray Conf., 1, 100.

Langer, S.H., and Rappaport, S., 1982, Ap. J., 257, 733.

Maraschi, L., and Treves, A., 1977, Astr. Ap., 61, L11.

Masnou, J.L., Bennett, K., Bignami, G.F., Buccheri, R., Caraveo, P., D'Amico, N., Hermsen, W., Kanbach, G., Lichti, G.G., Mayer-Hasselwander, H.A., Paul, J.A., Swanenburg, B.N., and Wills, R.D., 1977, 12th ESLAB Symposium, ESA-SP124, 33.

Lamb, R. C. and Worral, D. M., 1979, Ap. J., 231, L121.

Moffat, A.F.J., Schlickeiser, R., Shara, M.M., Sieber, W., Tuffs, R., and Kühr, H.,1983, Ap. J., 271, L45.

Nulsen, P.E.J., and Fabian, A.C., 1984, Nature, 312, 48.

Ruderman, M., and Cheng, K.S., 1988, Ap. J., 335, 306.

Sieber, W.,and Schlickeiser, R., 1982, Astr. Ap., 113, 314.

Spoelstra, T.A.Th., and Hermsen, W., 1984, Astr. Ap., 135, 135.

Swanenburg, B.N., Bennett, K., Bignami, G.F., Buccheri, R., Caraveo, P., Hermsen, W., Kanbach, G., Lichti, G.G., Masnou, J.L., Mayer-Hasselwander, H.A., Paul, J.A., Sacco, B., Scarsi, L., and Wills, R.D., 1981, Ap. J., 243, L69.

Thompson, D.J., Fichtel, C.E., Hartman, R.C., Kniffen, D.A., and Lamb, R.C., 1977, Ap. J., 213, 252.

# COS-B GAMMA-RAY SOURCES BEYOND THE PREDICTED DIFFUSE EMISSION

## H. A. MAYER-HASSELWANDER[*] AND G. SIMPSON[**]

## ABSTRACT

COS-B data have been reanalysed using for background subtraction the modelled galactic diffuse gamma-ray emission based on HI- and CO-line surveys and the gamma-ray data itself. A methodology has been developed for this purpose with the following three features: automatic generation of source catalogs using correlation analysis, simulation of trials to derive significance thresholds for source detection, and bootstrap sampling to derive error boxes and confidence intervals for source parameters. The analysis shows that about half of the 2CG sources are explained by concentrations in the distribution of molecular hydrogen. Indication for a few weak new sources is also obtained.

## I. INTRODUCTION

The question of the nature of those galactic gamma-ray "point-sources" (Swanenburg et al. 1981) which are not identified with objects visible in other wavelength regimes has been outstanding for some years. While two well-known sources, the Crab- and Vela-pulsars, demonstrate the existence of compact objects emitting gamma rays in the > 70 MeV regime, the emission of gamma rays by interaction of galactic cosmic rays with the interstellar gas and with galactic photon fields also is a well-known fact. Concentrations in the galactic molecular-hydrogen distribution are seen in CO-emission-line surveys (e.g. Dame and Thaddeus 1985). Such concentrations in the gas distribution, irradiated by the ambient galactic cosmic-ray flux, are good candidates for some of the 2CG sources. The search for point sources, which cannot be explained by emission from gas, is motivated by the interest in narrowing down as far as possible this class to galactic objects which are really compact. The better the diffuse background emission is known, the better the population of really compact gamma-ray objects can be defined.

## II. METHOD

The inputs are the distribution of diffuse gamma-ray emission predicted using tracers of HI and H2 (Bloemen et al. 1986, Strong et al. 1989), a model of the inverse Compton emission, and the COS-B gamma-ray data. Within a few degrees of longitude from the galactic center the model breaks down, there the data are interpolated from the values in neighbouring longitude bins. The gamma-ray data used is the final COS-B database (Mayer-Hasselwander et al. 1985, Mayer-Hasselwander 1985). The data are analyzed in three energy ranges: 70-150, 150-300, and > 300 MeV. The analysis consists of three phases: 1) accidentals rate definition, 2) catalog generation, 3) and source parameter study. For a description of the method see Mayer-Hasselwander and Simpson (1988). In addition to the crosscorrelation estimator, also the likelihood estimator used by Pollock et al. (1985) has been applied leading to very similar results. Results for 1) and examples for 3) have been published by Simpson and Mayer-Hasselwander (1986) and Simpson and Mayer-Hasselwander (1987). The significance thresholds were chosen such, that 0.33 accidental sources can be expected in each of the three energy ranges, or 1 source in all three. This criterion gave the following threshold values (sigma): 70-150 MeV: 4.1, 150-300 MeV: 3.9 and > 300 MeV: 3.7.

[*] Max-Planck-Institut für extraterrestrische Physik,
8046 Garching, FRG,

[**] Space Science Center, University of New Hampshire,
Durham, NH 0Z824, USA
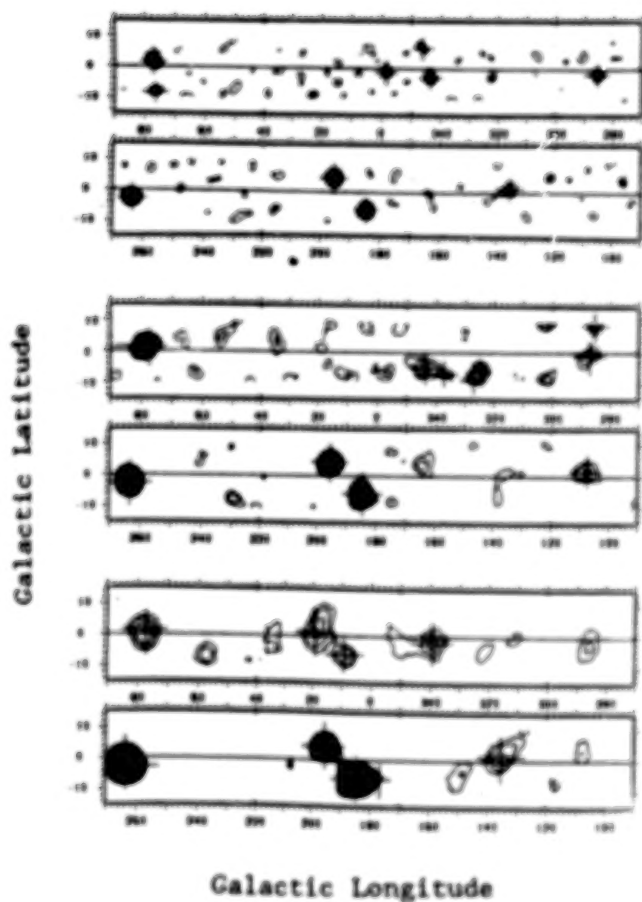
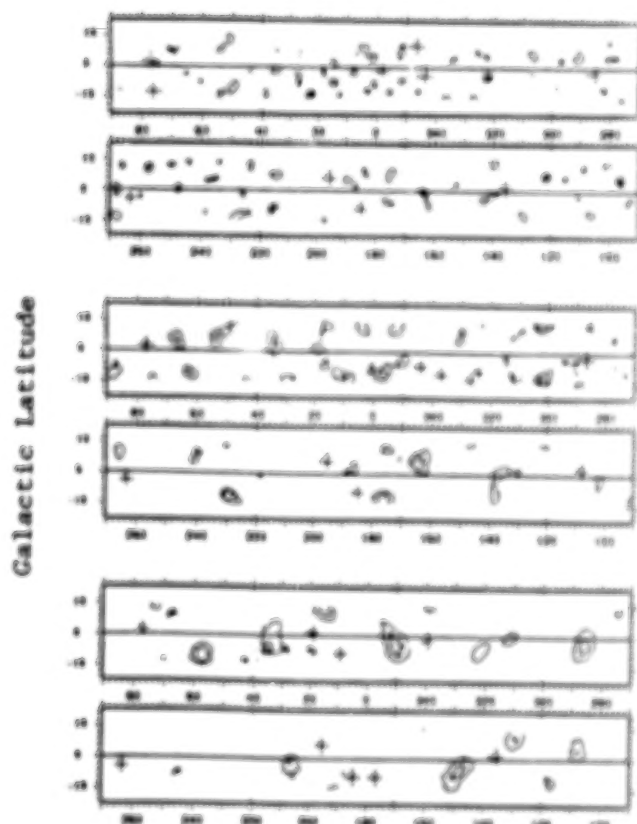> 300 MeV

150 - 300 MeV

70 - 150 MeV

Fig. 1a.--Significance maps of crosscorrelated signal. Lowest contour is at 2 sigma, contour intervals are 1 sigma. Crosses indicate source locations.

**Galactic Longitude**

> 300 MeV

150 - 300 MeV

70 - 150 MeV

Fig. 1b.--Significance maps after removal of all signals detected above threshold. Contour lines as in figure 1a.

**Galactic Latitude**

154

## III. RESULTS

The revised catalog is presented. The original significance maps are shown in Figure 1a and the residual significance maps after subtraction of all sources above threshold are given in Figure 1b. The results refer to the latitude range b < 10° and in the tables are grouped in three classes: confirmed 2CG-sources, 2CG-sources explained by gas concentrations, and new sources.

Confirmed 2CG-sources:
From the 22 2CG-sources within the field analyzed here, only 8 are detected above the significance threshold after subtraction of the predicted diffuse emission. Slightly different parameters are found for these sources as listed in Table 1. Differences are to be expected, since the subtraction of the structured diffuse-emission background may cause the source peaks to shift and to alter in amplitude. The source locations refer to the highest energy range within which the source is detected.

### TABLE 1

### CONFIRMED "2CG" SOURCES

| 2CG name | position+ | | > 300 MeV | | 150-300 MeV | | 70-150 MeV | |
|---|---|---|---|---|---|---|---|---|
| | L | B | flux $cm^{-2}s^{-1}$ $*10^7$ | sigma | flux $cm^{-2}s^{-1}$ $*10^7$ | sigma | flux $cm^{-2}s^{-1}$ $*10^7$ | sigma |
| 2CG078+01 | 77.2 | +1.8 | 4.6 | 6.5 | 7.9 | 7.4 | 11.3 | 5.3 |
| 2CG135+01 | 135.8 | +1.0 | 2.8 | 4.5 | 10.0 | 2.2 | 10.2 | 5.0 |
| 2CG184-05 | 184.5 | -5.9 | 7.0 | 8.9 | 10.8 | 10.3 | 34.5 | 13.7 |
| 2CG195+04 | 195.2 | +4.2 | 13.3 | 12.4 | 12.8 | 11.8 | 21.8 | 10.2 |
| 2CG263-02 | 263.6 | -2.6 | 37.6 | 19.1 | 35.6 | 17.8 | 59.5 | 17.2 |
| 2CG284-00 | 285.2 | -1.8 | 5.8 | 4.2 | 6.6 | 3.9 | 12.3 | 3.5 |
| 2CG342-02 | 343.5 | -2.9 | 4.7 | 4.6 | 6.5 | 4.6 | 16.3 | 4.7 |
| 2CG359-00 | 358.0 | -1.4 | 3.5 | 3.7 | - | - | - | - |

+ position as derived in > 300 MeV energy range

2CG sources explained by gas concentrations:
Within the area analyzed, 14 of 22 2CG-sources are not detected above the statistical significance threshold. In the majority of the cases actually no positive signal is detected, indicating that the excesses are fully attributable to gas enhancements. In the case of 2CG036+01, 2 and 3 sigma excesses still are seen in two neighbouring energy ranges giving some support for the existence of this source. These 2CG-entries are listed in Table 2 for completeness.

New sources:
It is clear that all the stronger sources must have been found in earlier analyses. So all the 9 new sources listed in Table 3 are rather weak and are detected above threshold in one energy range only. In some cases excesses are seen in more than one energy-range; this makes the source at 176.4-5.6 especially interesting. It is difficult to assess the "point-source" quality for these sources: most are seen in the lower energy ranges where the point-spread-distribution is wide. If they are not point-like, the excesses would indicate local inadequacies of the background model. It is noteworthy that in directions to the inner Galaxy the latitude distribution of the new sources is wider than the latitude distribution of the diffuse emission. This can be understood as a twofold selection effect: only nearby sources are intense enough to be detectable individually and, in

## TABLE 2

### "2CG" SOURCES EXPLAINED BY GAS CONCENTRATIONS OR WITH SIGNIFICANCE BELOW THRESHOLD

```
..........................................................................
2CG name        Remarks
..........................................................................
2CG006-00       no excess
2CG013+00       no excess
2CG036+01       2 and 3 sigma excesses in low and medium range
2CG054+01       no excess
2CG065+00       no excess
2CG075+00       2 sigma excess in high range only;
                confusion by source at l - 77.2 not excluded
2CG095+04       3 sigma excess in high range only
2CG121+04       3 sigma excess in high range only
2CG218-00       2 sigma excess in medium range only
2CG235-01       no excess
2CG288-00       no excess
2CG311-01       2 sigma excess in low range only
2CG333+01       no excess
2CG356+00       no excess
..........................................................................
```

## TABLE 3

### NEW SOURCES INDICATED BY THIS ANALYSIS

| Position* L B deg | | > 300 MeV flux $cm^{-2}s^{-1}$ | sigma | 150-300 MeV flux $cm^{-2}s^{-1}$ | sigma | 70-150 MeV flux $cm^{-2}s^{-1}$ | sigma | Remarks |
|---|---|---|---|---|---|---|---|---|
| 9.6 | -5.7 | · | · | · | · | 12.0 | 4.7 | |
| 18.6 | +1.4 | · | · | 4.1 | 2.2 | 17.5 | 4.7 | extended? |
| 76.4 | -8.1 | 1.4 | 4.1 | · | · | · | · | |
| 107.4 | +1.9 | · | · | 5.9 | 4.3 | 7.0 | 3.2 | |
| 176.4 | -5.6 | 1.0 | 2.0 | 1.5 | 3.2 | 5.7 | 4.2 | extended? |
| 285.1 | +8.7 | · | · | 5.2 | 4.2 | · | · | |
| 324.7 | -6.1 | · | · | 5.3 | 4.5 | · | · | |
| 327.2 | -8.7 | · | · | 1.7 | 5.0 | · | · | |
| 336.8 | -6.9 | · | · | 4.2 | 4.0 | · | · | |

addition, even nearby sources, if at low latitudes in the 1st or 4th quadrant, are buried in the high statistical fluctuations caused by the intense diffuse emission seen towards the inner Galaxy.

Of specific interest is the source seen in the low and medium energy range with a maximum at l = 18.6, l = +1.4, which well may correspond to possible pulsed gamma-ray emission from the new binary PSR 1820-11, for which Li and Wu (report December 1988) claim to have found evidence in the COS-B data.

<u>Confidence Intervals:</u>

Using the Bootstrap method, error boxes and the intensity uncertainty is derived directly from the data. These results are presented for the sources seen in the energy range >300 MeV in the figures 2 a to 2i. The uncertainty of the source location is given by the probability density distribution which is indicated by contour levels. The maximum value is normalized to equal 10. The crosses indicated for the Vela- and Crab- PSRs are well within the derived error boxes and give confidence that the systematic attitude measurement error of the COS-B satellite is not significantly deterioriating the instruments source-locating capabilities. For the source 2CG195+04 the identification with the source E 0630+178, respectively the optical source G*, as suggested by Bignami et al. (1983, 1988) has gained likelihood through the reduced errorbox derived in this analysis.

Fig. 2.--Errorboxes and intensity distributions for sources observed in the energy range >300 MeV. The crosses in figures a) and b) indicate the actual pulsar positions. The cross in figure c) indicates the position of the tentative counterpart E 0630+178. The contour levels indicate relative probabilties to find the source at a given postion, if the experiment is repeated. The integral intensity distribution indicates the error of the intensity determination; the dashed lines indicate the 80% confidence interval.
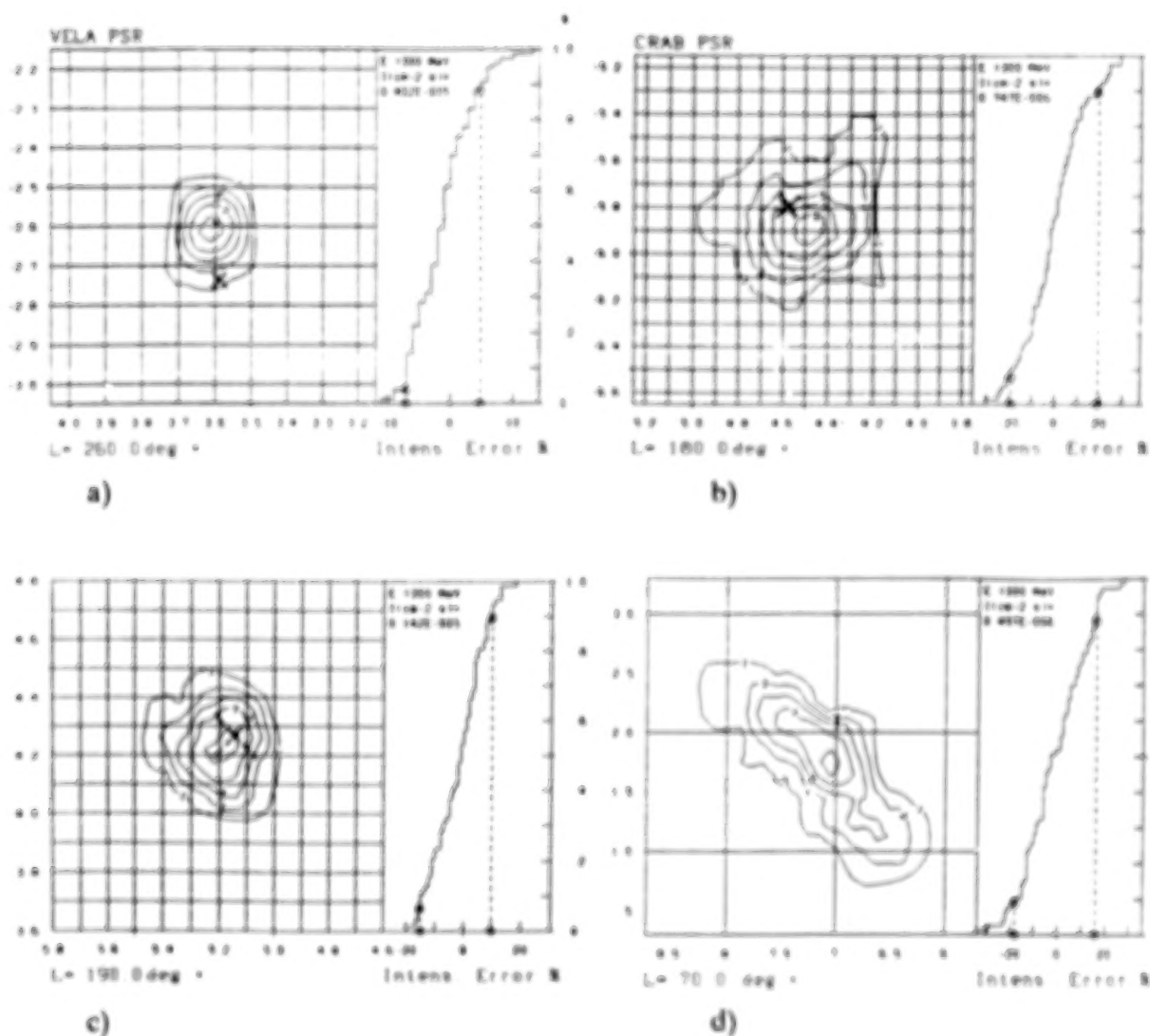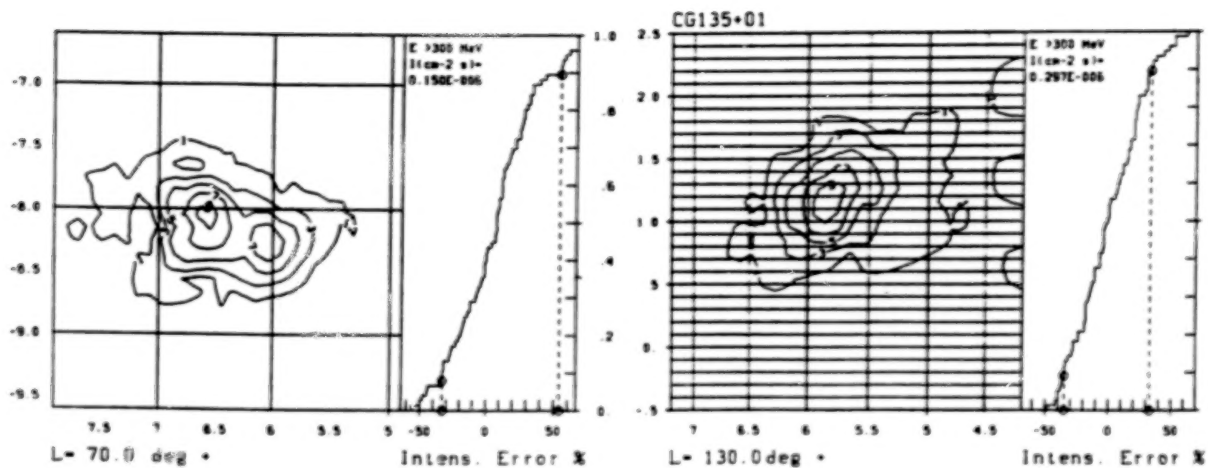
e)

f)
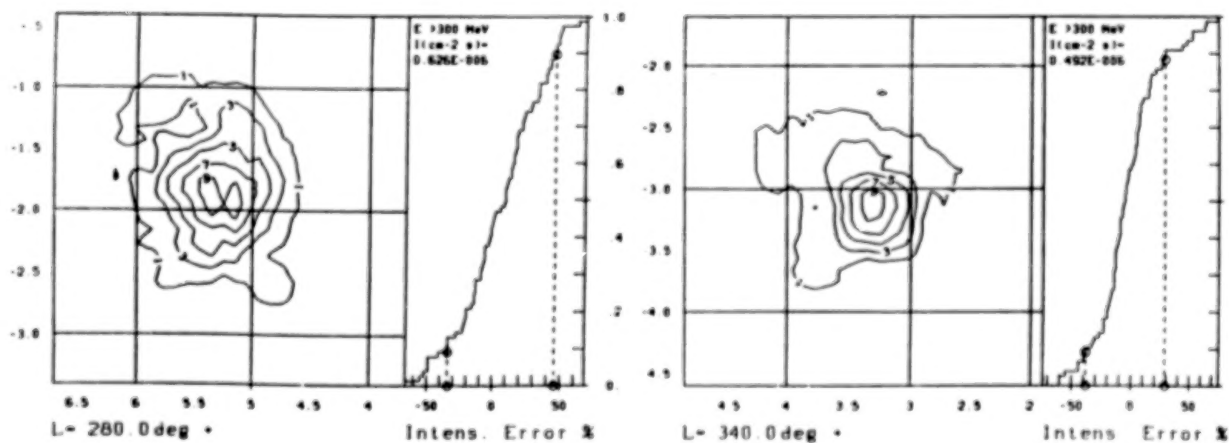
g)

h)
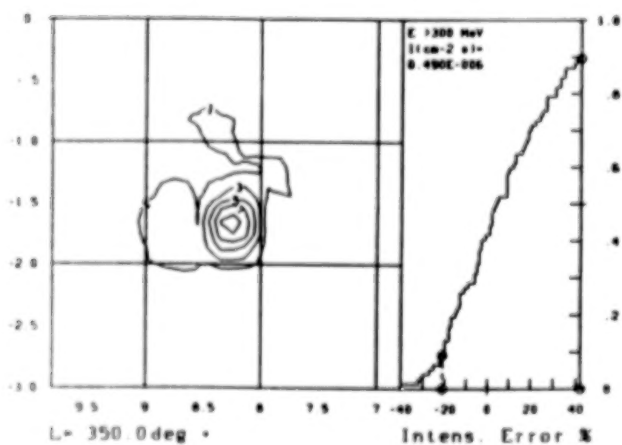
i)

## IV. CONCLUSION

The analysis shows that the "diffuse" gamma emission from gas - cosmic-ray interaction is the likely explanation for about half of the 2CG sources. Several sources remain as interesting counterparts for compact objects or active regions. A number of new source candidates were detected. As most are seen in the lower energy ranges, where the angular resolution is rather limited and systematic uncertainties in the analysis are larger, and as their intensity is relatively low, these enhancements should be taken as indications only. They clearly need confirmation by the new gamma-ray telescopes soon to be launched.

## ACKNOWLEDGEMENTS

## REFERENCES

Bignami, G.F., and Caraveo, P.A., 1983, Astrophys. J., 272, L9-L13.
Bignami, G.F., Caraveo, P.A., and Paul, J.A., 1988, Astron. & Astrophys., 202, L1-L4.
Bloemen, J.B.G.M., et al., 1986, Astron. & Astrophys., 154, 25-41.
Dame, T.M., and Thaddeus, P.A., 1985, Astrophys. J., 297, 751-765.
Hermsen, W., 1980, Thesis Univ. of Leiden.
Mayer-Hasselwander, H.A., 1985, Proc. 19th ICRC, OG2.1-13, La Jolla.
Mayer-Hasselwander, H.A., 1985, Explanatory Supplement to the COS-B Database, Report Space Science Department, ESTEC, Noordwijk.
Pollock, A.M.T., et al., 1985, Astron. & Astrophys., 146, 352-362.
Simpson, G., and Mayer-Hasselwander, H.A., 1986, Astron. & Astroph., 162, 340-348.
Simpson, G., and Mayer-Hasselwander, H.A., 1987, Proc. 20th ICRC, OG2.1-14, Moscow.
Strong, A.W., et al., 1988, The Radial Distribution of Gamma Rays IV:   The   Whole   Galaxy, Accepted for publication by Astron. Astrophys..
Swanenburg, B.N., et al., 1981, Ap. J., 242, L69-L73.

## DISCUSSION

*Floyd Stecker:*

After subtracting out a diffuse background based on gas density, can you say if the remaining source in Cygnus must be point-like, or could it still be diffuse?

*Hans Mayer-Hasselwonder:*

The remaining excess appears to be elongated over about 1.5 degrees. This can be taken as an indication for having two neighboring sources. These sources as well could be really compact objects or unresolved hot spots in the cosmic-ray distribution or gas concentrations not seen in CO-line observations.

# MORE DATA ON (POSSIBLE) GAMMA-RAY (POINT) SOURCES

W. HERMSEN
Laboratory for Space Research Leiden, P.O. Box 9504,
2300 RA  Leiden, The Netherlands

## ABSTRACT

The "2CG" catalogue of gamma-ray sources was compiled before detailed knowledge was available on the fine-scale structure of the diffuse Galactic gamma-ray emission. Two independent analyses to discriminate sources which are either compact objects or due to very local and strong enhancements in the Galactic cosmic-ray distribution from those which are artifacts due to the clumpy gas distribution are about to be completed: a maximum likelihood analysis and a cross correlation analysis. Arguments are given why differences, and therefore confusion, in the resulting source lists can be expected.

Detailed analysis of all COS-B gamma-ray data on Geminga (2CG195+04), reveals the existence of a drastic spectral break below 200 MeV. A power-law spectrum with index -1.88 fits the data above about 100 MeV to 3.2 GeV, however, there are also indications for a spectral break above these energies. For energies above about 100 MeV no evidence for long-term time variability has been found.

The error region of Geminga has been searched for a radio counterpart at wavelengths of 90, 49, 21, 6 and 2 cm using the Westerbork Synthesis Radio Telescope and the Very Large Array. So far 16 sources have been detected in this error region. In the direction of 1E0630+178, the Einstein X-ray source proposed to be a Vela-like pulsar and the counterpart of Geminga, no radio source has been found at 21, 49 and 90 cm with $3\sigma$ upperlimits on the flux densities ranging from 0.5 mJy at 21 cm to 4.5 mJy at 90 cm

Detailed structures in local molecular cloud complexes are sofar only resolved in gamma rays for the closest and most massive complexes, namely those in the Orion-Monoceros and the Ophiuchus regions. For both region, there is circumstantial evidence for gamma-ray emission from molecular gas that was photodissociated after the passage of a SN shell.

## I. INTRODUCTION

The increase in average exposure of the galactic plane region by more than an order of magnitude comparing the SAS-II mission with the COS-B mission didnot result in a proportional increase in the number of identified compact objects. The structured diffuse gamma-ray background makes the search for sources difficult, and the relatively large error regions on the source positions render in many cases several candidate-counterpart objects. The improvement in statistics and angular resolution foreseen for the

EGRET data in the same energy range, and the practically new measurements at the adjacent soft gamma-ray energies by COMPTEL, with angular resolution similar to COS-B, but with improved statistics, should achieve a break-through in the study of compact objects and small-scale active regions.

In this paper some results from ongoing detailed analyses of COS-B data will be reported, supplementing results reported in other papers presented during this symposium, and providing some guidance in the early GRO data analysis. Chapter II, with a discussion on the search for Galactic point sources, complements the presentation by Mayer-Hasselwander; chapters III and IV complement the review paper on Geminga (2GC195r04) by Kniffen; chapter V supplements the paper on gamma-ray emission from clouds by Hunter.

## II. GALACTIC POINT SOURCES BEYOND THE DIFFUSE EMISSION

*Introduction.* The correlation between diffuse galactic gamma rays and gas tracers has been studied in great detail by Strong et al. (1988), using the final COS-B database and HI and CO (tracer of the molecular hydrogen distribution) surveys covering the entire Galactic plane. A good quantitative fit to the gamma-ray distribution is obtained using a model in which the detailed structure of the total gas distribution has been folded with a circularly symmetric Galactic cosmic-ray density distribution to predict the gamma-ray distribution. Those features in the gamma-ray data, which are not explained by this model, are due to active regions in which the cosmic-ray density is locally enhanced, or are due to compact objects. A search for these features, would result in an update of the "2CG" gamma-ray source catalogue (Swanenburg et al. 1981), which was esthablished before Galactic surveys of the CO-line emission were available.

*Methods.* The first attempt to search systematically for such features was undertaken by Pollock et al. (1985a,b) using a maximum likelihood method. However, at that time only a small fraction of the Galactic plane region was mapped in CO, and the analysis was limited to energies above 300 MeV.

Mayer-Hasselwander and Simpson (1988, see also Simpson and Mayer-Hasselwander, 1987, and Mayer-Hasselwander in this volume) presented results from a search for sources in excess to the same model predictions for the diffuse gamma-ray background. They applied the cross correlation analysis of Hermsen (1980) to all gamma-ray data of the Galactic plane region (in three energy intervals: 70-150 MeV, 150-300 MeV, 300-5000 MeV) and to the model predictions to find the excess structures, calibrating confidence intervals with bootstrap sampling. The derived source list is a first attempt to arrive at a final COS-B list.

In Pollock and Hermsen (1990; final paper in preparation) the results from the maximum likelihood analysis of all COS-B data will be presented, applying the analysis to the same three

differential energy ranges, as well as to the total energy range. Furthermore, the analysis has been applied to the data from each single observation period, and to the combined total COS-B sky distribution. The advantages of this approach (in comparison to the correlation analysis) are the following:

(i) the maximum likelihood analysis is performed on the parameters of single events; the events are not sorted in sky bins.

(ii) the analysis of single observations allows the detection of sources which vary over time scales of months to years.

(iii) in the large-scale correlation study of the diffuse Galactic gamma-ray emission only four strong sources have been taken into account (Strong et al. 1988); therefore, it was decided to treat the absolute level of the structured diffuse gamma-ray background as a free parameter for each observation period.

(iv) the likelihood analysis can naturally test the structure of a significant excess above the diffuse gas emission using the single event distribution, to decide whether the data support the presence of one source, or whether more sources are located closely together.

It is evident that the differences in the two appraoches will result in differences between the derived source lists; particularly the conclusions on variable sources and multiple-source structures will differ. Therefore it will be mandatory to perform a detailed comparison between the two sets of results in order to guarantee a usefull input to the GRO analysis.

*Example output.* In Figure 1 an example of a Log-likelihood ratio map is shown, indicating the weight of evidence (see discussion in Pollock et al., 1985) for a point source in each position in the 20° field-of-view of COS-B during one observation of the Anti-Centre region centered on Geminga, for three energy intervals. Evidently, there remain only two sources above the predicted diffuse emission: Crab and Geminga. The differences in spectral shape are remarkable: The Geminga profiles saturate for the higher energies, while the source barely shows up at low energies; the Crab is clearly most significant at low energies.

*A new variable source?* As a preliminary result, an interesting example of the degree of "confirmation" and "contradiction" (and therefore confusion) between the results from the two approaches is given: Mayer-Hasselwander and Simpson (1988) published the detection of two new gamma-ray sources at $(l,b)=(324.7°,-6.1°)$ and $(l,b)=(327.2°,-8.7°)$ at significance levels of $4.5\sigma$ and $5.0\sigma$, respectively, and both were only seen in the 150-300 MeV energy range. In fact, in their correlation output using all COS-B data, they found one extended excess centered at about $(l,b)=(325.5°,-7.0°)$, which they interpreted as being due to two sources. However, the sources were not resolved in the correlation output, nor was a statistical test applied to the event distribution using a two-sources model. Therefore, the claim that two sources were discouvered, is questionable.

COS-B period 14 70<MeV<150
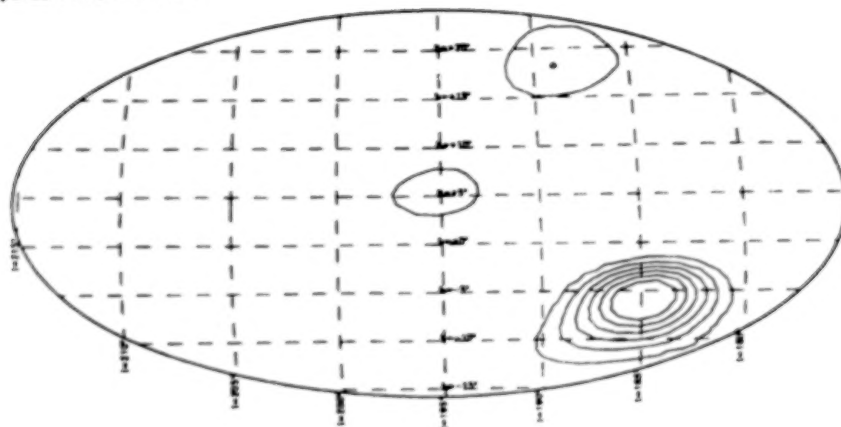
COS-B period 14 150<MeV<300
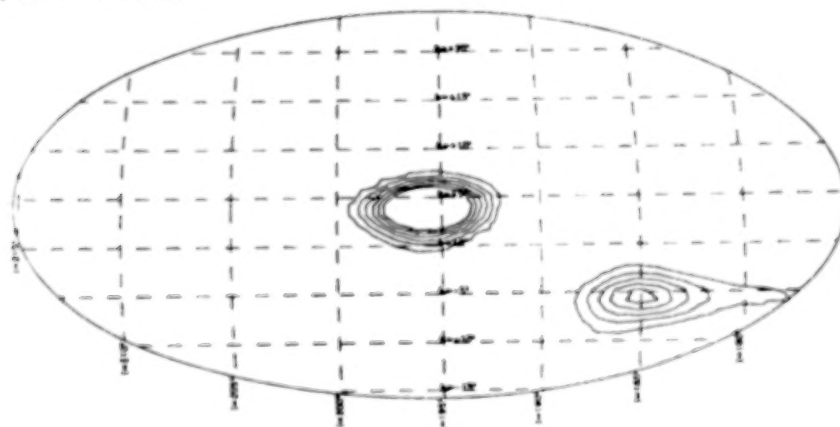
COS-B period 14 300<MeV<5000
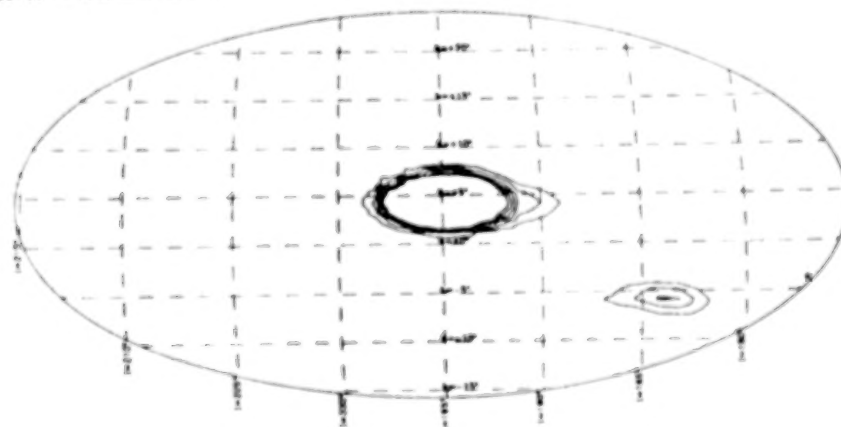
Fig. 1. Log-likelihood-ratio ($\lambda$) maps for observation period 14 for three energy intervals. Contour levels: $\lambda$ = 2, 4, 6, 8, 10, 12.

The general source region around (325.5°,-7.0°) was in the field of view of COS-B during three observations, numbers 7, 33 and 61, at inclination angles 8°, 17° and 9°, respectively. The likelihood analysis for the single observations rendered no detection for periods 7 and 33, but **confirmed** the excess using data from period 61 (see Figure 2). Indeed, for the intermediate

energy range a significant detection can be claimed. Since the latter period was not available when the "2CG" catalogue was generated, this explains the absence of this entry in the catalogue. Preliminary inspection of the likelihood contours in Figure 2, suggests that only one source causes the effect, instead of the claimed two. In conclusion, the likelihood analysis confirms the presence of a significant excess centered at about (l,b)=(325.5°,-7.0°), which, however, seems to be due to a **single time variable source**. More detailed analysis is in progress (Pollock and Hermsen, 1990; full paper in preparation).
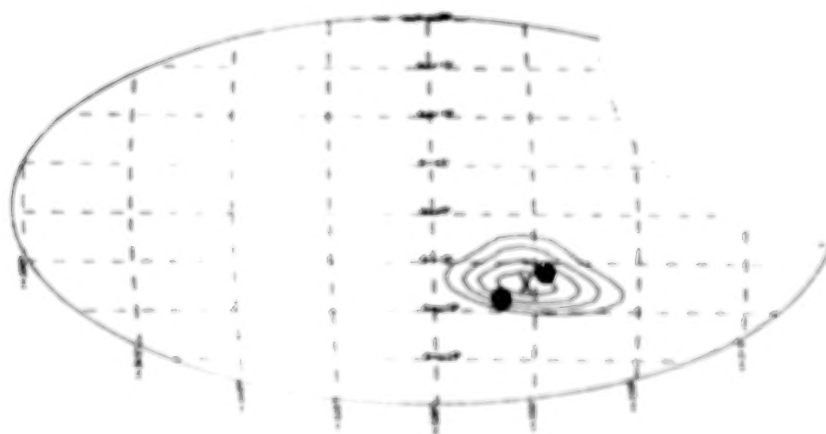


Fig. 2. Log-likelihood-ratio ($\lambda$) map for observation period 61 (150-300 MeV). Contour levels: $\lambda$= 2,4,6,8. The single evidence for a point source is found at about (l,b)=(325.5°,-7.0°) (indicated by the cross). The two dots indicate the source positions reported by Mayer-Hasselwander and Simpson. The area deleted from the field of view around l=315° at positive latitudes was contaminated by gamma rays coming from the earth.

## III. VARIABILITY AND SPECTRAL PROPERTIES OF THE HIGH-ENERGY GAMMA-RAY EMISSION FROM GEMINGA

*Introduction.* The strong gamma-ray source 2CG195+04 (Geminga) located in the general anti-centre direction, remains an enigma since its discovery in 1975 by the SAS-2 team. Although the relatively small source region (a conservative error radius $\leq$ 0.4°) has been studied in great detail over the entire electromagnetic spectrum, a definite identification of the source has not been achieved so far.

Most attempts to identify the source concentrated on the X-ray source 1E0630+178, located close to the centre of the error circle. After some earlier claims for identification had to be withdrawn, the proposal by Halpern and Tytler (1988), that 1E0630+178=Geminga is a Vela-like pulsar seems to make a good chance, although they and Bignami et al. (1988) also list some problems with this interpretation (see also the review by Kniffen in these proceedings). If the above identification is correct, Geminga may be characterized by high $L_g/L_x$ and $L_x/L_v$ ratios of the order of $10^3$, and the source distance can be as much as 750-1000 pc, based on the X-ray spectrum. Recently, Ruderman and

Cheng (1988) developed for Geminga a model including an evolved, aligned, Vela-like pulsar. A detailed study of the gamma-ray emission from Geminga, its spectral properties and long-term evolution, is essential to provide source parameters which can be tested against this and other models.

*Data and analysis.* Geminga was in the field-of-view of COS-B five times between 1975 and 1982, out of which initially four periods (14,39,54,64) were selected by Grenier, Hermsen and Hote (1990; full paper in preparation) because of the small source aspect angle (<10°). The energy distribution of the emission between 50 MeV and 5 GeV was analysed for each period independently using the maximum-likelihood analysis developed to describe the Vela pulsar emission (Grenier et al. 1988). An important aspect of this analysis is that the photons are not binned (spatially nor in energy) but treated individually. To describe the bulk of the gamma rays detected in the large field-of-view of COS-B, four different components were considered: 1. an isotropic background emission; 2. the diffuse galactic emission; 3. the point-sources from the Crab pulsar and its nebula; 4. the point-source Geminga supposed to be in the direction l=195.1° and b=4.2° (Masnou et al. 1981). While power-law spectra for the instrumental and galactic background were fitted together with the Geminga spectrum, the stable spectra of the emission from the Crab pulsar and its nubula were taken from the study by Clear et al. (1987). The gamma-ray photons and characteristics of the telescope have been selected from the Final COS-B Database. Details on the maximum likelihood analysis can be found in Grenier et al. (1988). This procedure has the advantage of taking full account of the modest energy and spatial resolutions of the COS-B detector, and that of being sufficiently sensitive to derive spectra for separate observations.

*Results.* Masnou et al. (1981) combined the data from four observations (0,14,39,54) to determine an average spectrum, applying a conventional method in which the data were binned (Figure 3). The derived spectral shape was consistent with a power-law with index -1.8 between 100 MeV and 3.2 GeV, and it flattened and steepened slightly (<2σ) at lower and higher energies, respectively. Therefore, as a first approximation, the likelihood analysis was performed to derive the single-power-law spectra that best fit the emission from Geminga in the 50 MeV to 5 GeV interval, for each of the selected observations (14,39,54,64). The results for each period and for the combination of all four observations are listed in Table 1, together with their 1σ statistical errors.

The fit values for the individual observations and for the total spectrum are within their uncertainties consistent with the result by Masnou et al.: Between about 100 MeV and 3200 MeV no long-term variability can be claimed in the spectral indices and in the fluxes inferred from the single-power-law spectra.

**TABLE I**

Single-power-law fit to the Geminga spectra (50-5000 MeV) for
each observation and for all periods together.

Period 14    $(4.66^{+3.01}_{-1.96})10^{-4}E^{-(2.02\pm0.10)}$ ph $cm^{-2}s^{-1}$ $MeV^{-1}$

Period 39    $(1.19^{+0.84}_{-0.50})10^{-4}E^{-(1.77\pm0.10)}$ ph $cm^{-2}s^{-1}$ $MeV^{-1}$

Period 54    $(1.41^{+1.32}_{-0.69})10^{-4}E^{-(1.80\pm0.12)}$ ph $cm^{-2}s^{-1}$ $MeV^{-1}$

Period 64    $(2.06^{+1.42}_{-0.87})10^{-4}E^{-(1.87\pm0.10)}$ ph $cm^{-2}s^{-1}$ $MeV^{-1}$

All periods    $(2.16^{+0.70}_{-0.52})10^{-4}E^{-(1.88\pm0.05)}$ ph $cm^{-2}s^{-1}$ $MeV^{-1}$

Closer inspection of the data reveals that below 100 MeV and
above 3.2 GeV for all observations the data points are
systematically below the one-power-law fit. Thus, there are
indications for spectral breaks around 100 MeV and around 3 GeV.
The first might explain the failure of soft gamma-ray instruments
to detect Geminga, sofar. In Figure 1 we could note that Geminga
is already unexpectedly week over the interval 70-150 MeV,
possibly due to a strong suppression of the lowest-energy events.
It is noted, that flux values assigned to energy bins in a
conventional method (data points), depend on the used effective
sensitive area for each bin, which is a function of the assumed
input spectrum. If a very strong change in spectral shape occurs
around 100 MeV (e.g. from index +1.0 to index -2.0), this change
can easily be overlooked using the wide energy bins and the
assigned flux value for the 50-100 MeV bin will inadvertently be
wrong (too high). Therefore, the likelihood analysis has been
applied to the single photon spectra, to test a two-power-law
spectrum with two independent indices below and above a break
energy. Different break energies between 100 and 400 MeV have
been tested. The introduction of a second break at higher
energies was not attempted since too few photons have been
detected from Geminga above 3 GeV (typically less than 10 per
observation) to constrain such a fit. Preliminary results
indicate a pronounced break and a significant improvement in the
quality of the fit (compared to the one-power-law fit) for each
observation. The analysis is still in progress, and will also be
performed for observation 0 (Grenier, Hermsen and Hote, 1990, in
preparation). The first results are shown in Figure 3: The best
power-law fits for the data of periods 39 and 54 for some
selected break energies. The data support the presence of a break
in the Geminga spectrum. The fact that in both cases the change
in index becomes more (extremely) drastic selecting a lower break
energy, indicates that the real break energy is most likely below
200 MeV.

*Discussion.* Maximum likelihood analysis of the COS-B Geminga
data confirms that the Geminga spectrum from about 100 MeV up to
a few GeV is consistent with a power-law spectrum with index of
about -1.88. Furthermore, there is no evidence for significant

long-term time variability in flux and spectral shape of the gamma-ray emission in this energy interval. Preliminary results at lower energies provide evidence for a spectral break below 200 MeV. This break might in fact be very drastic (e.g. from index +1 to -1.9), and offers an explanation for the failure to detect Geminga so far at soft gamma-ray and hard X-ray energies. There are hints for a second break (steepening at GeV energies). The odd spectrum, sketched above, differs substantially from the spectrum of the Vela pulsar emission. The latter is particularly interesting, given the proposed identification with a Vela-like pulsar (e.g. Halpern and Tytler, 1988; Bignami et al., 1988; Ruderman and Cheng, 1988).
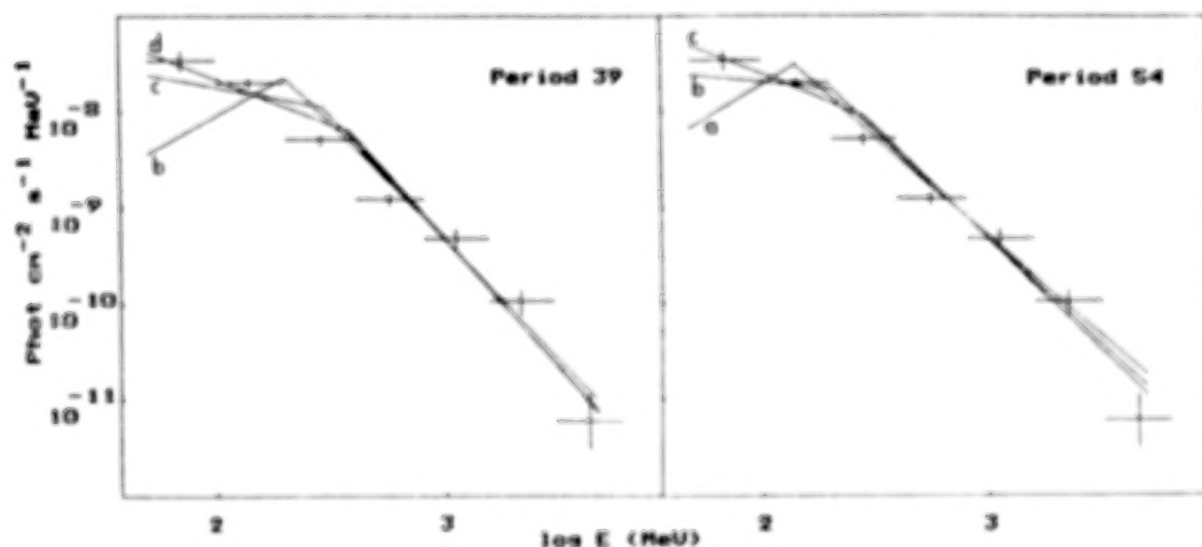


Fig. 3. Two-power-law spectral fits to the Geminga data of observations 39 and 54. Break energies: a) 140 MeV; b) 200 MeV; c) 290 MeV; d) 380 MeV. The data points show the average Geminga spectrum from Masnou et al. (1981) for periods 0,14,39 and 54 (the 50-100 MeV flux value appears now to be wrong since a spectral break was not taken into account for the sensitive area calculation).

## IV. ON THE IDENTIFICATION OF THE ENIGMATIC GAMMA-RAY SOURCE GEMINGA: AN EXTENSIVE SURVEY IN THE RADIO BAND.

*Introduction.* In Chapter III the proposed identification of Geminga with the X-ray source 1E0630+178 was discussed. However, there is no final proof yet of that identification, therefore it is still appropriate to discuss other attempts for identification.

Sieber and Schlickeiser (1982) and Spoelstra and Hermsen (1984) started the search for the Geminga counterpart from the radio band. The latter search ( at a wavelength of 21 cm, 1412.0 MHz, using the Westerbork Synthesis Radio Telescope) was the most sensitive one, and a total of 15 sources were detected in the error region with fluxes between about 4 and 50 mJy. Three sources, one of them a quasar, were found to be significantly variable. However, none of these sources appeared to have highly
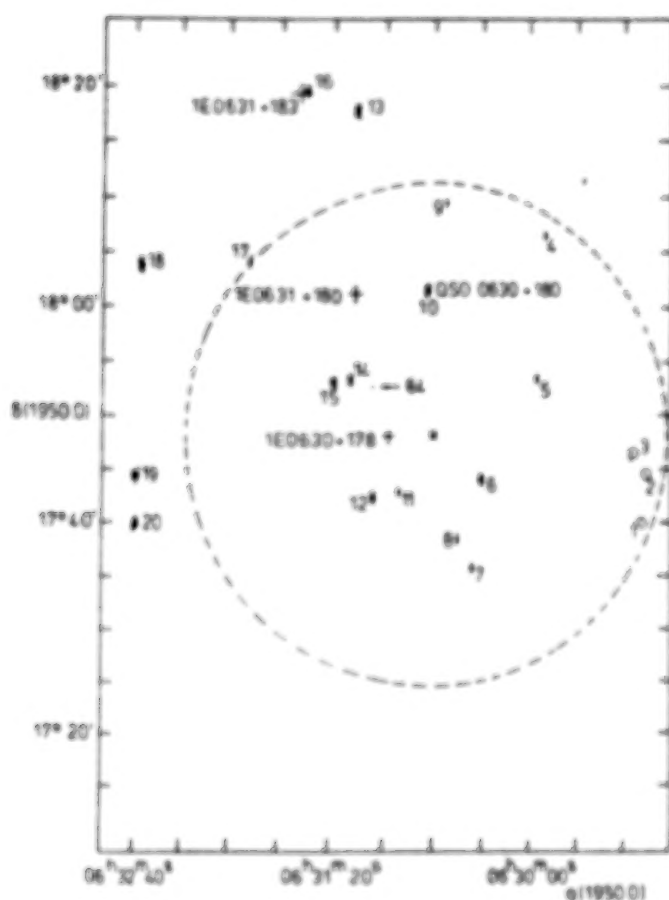
Fig. 4. Contour plot of the field searched at 21 cm wavelength
for a possible counterpart of Geminga using data from a 12-h
observation in 1982. All detected radio sources are indicated
(63W1=1, 63W2=2, etc), including three sources not seen in this
observation (o). Also indicated are the best estimate of the
Geminga position (x), its error circle (broken line), three
Einstein sources (+), and a QSO (63W10). Lowest contour level: 1
mJy. The arrow points at the tiny feature, which is the new
source 63W64, discovered at 6 cm wavelength.

anomalous properties at radio wavelengths. Furthermore, Spoelstra
and Hermsen reported that no counterpart could be detected in
their search for 1E0630+178 with a 3σ upper limit of 0.5 mJy.

*New data.* Hermsen and Spoelstra (1990) continued this work to
obtain an extended and deep survey of this source region in
radio. Using the Westerbork and VLA telescopes, data have been
collected at 2, 6, 21, 49 and 90 cm, in order to obtain accurate
radio spectra and data on time variability of the sources, in the
hope to find an anomalous radio source leading to an
identification of Geminga. Another point of interest was to
search for a radio counterpart of 1E0630+178 at larger
wavelengths. Finally, the 1.5m Danish telescope in La Silla, was
used to search for optical counterparts of the most interesting
sources. In this paper some results are presented from the radio

survey; the analysis of the 2 cm data is still in progress, and a full paper is in preparation (Hermsen et al., 1990).

*Results.* Spoelstra and Hermsen detected in total 20 sources (source numbers 63W1,...,63W20) at 21 cm, making 12 observations over the years 1980, 1981 and 1982. Figure 4 shows the Geminga error region with the position of all radio sources with flux densities larger than a few mJy. This total sky area was also viewed at 327 MHz and 608.5 MHz (about 90 and 49 cm), and part of the central region inside the error circle also at 4874 MHz (6cm) (centered at the sources 63W6 and 63W15, which showed time variability at 21 cm). Details on these Westerbork measurements and on the VLA observations at 2 cm will be given in the full paper.

It is interesting to report that all sources detected inside the Geminga error circle at 21 cm, have also been seen at 49 and 90 cm, and that no additional detection could be claimed at these longer wavelengths. The weakest source at 49 cm was 63W9 (9.4 ± 1.8 mJy) and the weakest at 90 cm 63W2 (11.2 ± 1.2 mJy). The noise in these radio maps was about 1.5 mJy . Therefore, $3\sigma$ upper limits for sources not detected in the Geminga error circle are at about 4.5 mJy at 49 cm and 90 cm. These upper limits apply also to the Einstein X-ray source 1E0630+180, again not seen in our surveys.

Sky regions covering the sources 63W6, 63W14 and 63W15 have been viewed at 6 cm, and the radio spectra of these sources are shown in Figure 5. One should keep in mind that 63W6 and 63W15 showed variability in their flux densities of about 20% at 21cm, therefore average values have been given in Figure 5.

Surprisingly, one new source has been detected at 6 cm, dubbed 63W64 (a high source number, since the new list contains many new sources at longer wavelengths outside the Geminga error region). The flux density at 4874 MHz is (3.2 ± 1.0) mJy, and its position $\alpha(1950.0)$ = $(06^h31^m05.52^s ± 0.07^s)$ and $\delta(1950.0)$ = (+17°53'06.8"±2.9"). In fact, inspection of the radio maps at 21, 49 and 90 cm revealed source features at 21 and 50 cm at the position of 63W64, which, however, were below a $3\sigma$ detection threshold. In Figure 5 the spectrum of this source is presented as well, and the source position has been indicated in Figure 2.

*Discussion.* Our extensive survey in the radio band of the Geminga error region reveals a new weak source (63W64), exhibiting a very hard, flat spectrum. An optical counterpart has been found in our measurements from Chile (in collaboration with H. Pedersen) for this source, as well as for some of the other sources. This source, as well as the variable sources reported by Spoelstra and Hermsen (1984) seem to be sufficiently interesting to study them further for a possible identification with Geminga.

If the identification with a Vela-like pulsar (Halpern and Tytler; Bignami et al.) is correct , then of our results only the
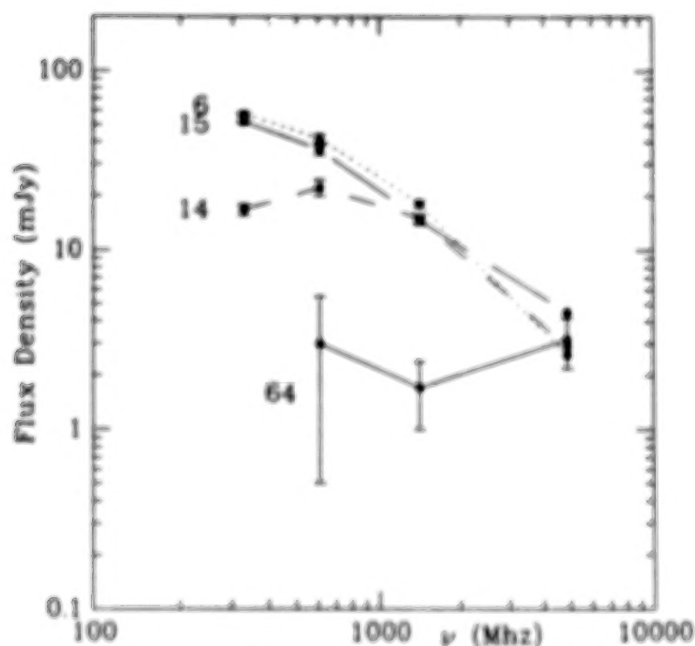
**Fig. 5.** The measured radio spectra from 90cm to 6cm for the variable sources 63W6 and 63W15, as well as for 63W14 and the new source 63W64. All error bars (1σ) are indicated, except for those at 6cm: the 1 mJy error bar given for 63W64 at 6 cm is typical for the other sources.

radio upper limits (0.5mJy at 21 cm up to about 4.5 mJy at 90 cm) are relevant for the Geminga problem. In this respect it is of interest to note that pulsar models predict a broader radio beam at longer wavelengths. Therefore, the chance to detect the Geminga radio pulsar at longer wavelengths increases for geometrical reasons. A deeper survey in radio is also valuable in order to attempt to detect the predicted weak synchrotron nebula which should surround the Vela-like source, or to improve on our upper limits.

## V. CIRCUMSTANTIAL EVIDENCE IN THE OPHIUCHUS AND ORION REGIONS FOR SUPERNOVA SHELLS INTERACTING WITH CLOUDS

*Introduction.* The Galactic diffuse gamma-ray distribution in the COS-B energy range traces predominantly the product of the interstellar matter (mainly HI and $H_2$) density and CR density: $\pi^\circ$-decay gamma rays resulting from nucleus (GeV protons)-nucleus interactions, and electron-Bremsstrahlung gamma rays from electron ($\leq$1 GeV)-ISM nucleus interactions. The mapping of nearby cloud complexes provides the GRO teams the unique opportunity to study dense active regions in detail to verify these expectations from CR-matter interactions and to search for possible local enhancements in CR density. The complexes in the Orion/Monoceros region were the first for which already with COS-B a detailed correlation study between the gamma-ray data and CO (tracer of $H_2$) and HI maps could be performed. A good two-dimensional correlation was found between the gamma-ray structures and the total gas distribution, explaining the former in terms of

interactions of the gas with cosmic rays of local density, distributed uniformly in this region (Bloemen et al. 1984).

Early analysis of COS-B data revealed also a significant excess in the direction of the Ophiuchus dark cloud complex (distance about 130 pc) (Swanenburg et al. 1981). Morfill and colleagues (1981) compared the reported flux with mass estimates for the Rho Oph dark cloud and concluded that an enhancement in cosmic-ray density by a factor of about 3 was required, or that the mass and/or distance estimates were wrong. They suggested that the gamma-ray source may be the result of the acceleration of Galactic cosmic rays by an old supernova remnant (the North Polar Spur, Loop I, radius ±115 pc) and its interaction with the Rho Oph cloud. However, after more COS-B data on the region became available, Hermsen and Bloemen (1983) showed that the general structure of the Ophiuchus cloud complex, as delineated in extinction maps and OH data, was in fact resolved in gamma rays. A comparison between the total mass estimated from OH data (Wouterloot 1981) and the gamma-ray flux from the total complex indicated that the measured gamma-ray flux is at most a factor 2 higher than expected, assuming cosmic rays of local density throughout the complex. Given the large experimental uncertainties, this was considered to be insufficient evidence for a local CR enhancement.

*Data and results.*
*Ophiuchus/Upper-Scorpius Region.* Recently, a complete CO survey of the Ophiuchus region also became available (de Geus 1988). Figure 6 shows the measured gamma-ray distribution using all available COS-B data on this area for energies between 100 MeV and 6 GeV, as well as the integrated HI column density map and the velocity integrated CO antenna temperature ,W(CO), distribution. The gamma-ray 'beam' is significantly broader than those at radio - and mm wavelengths. Nevertheless, significant structure is visible in the gamma-ray data, showing particularly the molecular cloud complex. Using the $N(H_2)/W(CO)$ conversion factor and the gamma-ray emissivities determined for the solar neighbourhood in the large-scale correlation study by Strong et al. (1988), it can be shown that the gamma-ray intensities predicted for the molecular clouds as traced by CO data are fully consistent with the measurements: There is no indication for an enhancement of cosmic rays inside these clouds. However, the gamma-ray structure appears to be more extended towards somewhat lower longitudes and higher latitudes, already visible in the early map of Hermsen and Bloemen (1983). Therefore, a map of the differences between the predicted structures (using Figures 6b, 6c) and the measurements (Figure 6a) has been determined (Figure 6d). Care has been taken that no significant negative fluctuations are present with respect to the predictions, by adjusting the scaling parameters locally within their uncertainties. Figure 6d shows that at the positions of intense CO emissions the distribution is consistent with zero intensity, but that adjacent to the cloud structures, e.g. at about $(l,b)=(351°,18°)$ and at somewhat higher latitudes, excesses
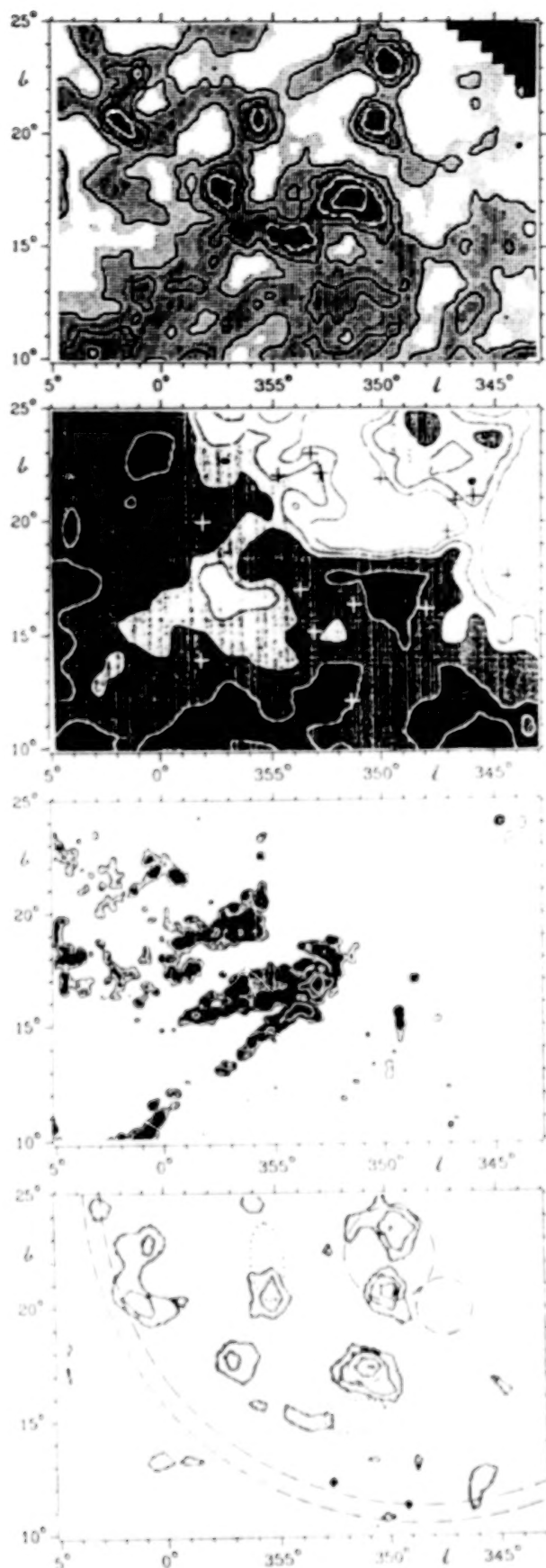
**Figure 6 :** The Ophiuchus region:

a) Gamma-ray intensities; energies between 100 MeV and 6 GeV. Contour lines at multiples of: $5.\times 10^{-5}$ ph cm$^{-2}$s$^{-1}$sr$^{-1}$; dark area in corner has low exposure.

b) Integrated HI column densities, contour values 12.5, 13.5, 14.5, 17.5, and $20 \times 10^{20}$ cm$^{-2}$. Positions of the brightest stars (earlier than B2) are plotted as plusses (de Geus 1988).

c) Velocity-integrated CO antenna temperature W(CO) for $-8<v<20$ km s$^{-1}$. Contour values: 5.0, 20.0, 55.0, 112.5 K km s$^{-1}$ (de Geus).

d) Differences between the observed (a) and predicted diffuse emission based on the HI and CO surveys and the model parameters deduced by Strong et al. (1988). Energies 100-5000 MeV. Contour levels: 8, 13, 18,...x10$^{-5}$ ph cm$^{-2}$s$^{-1}$sr$^{-1}$. Dash-dotted circles outline HII regions in Sharpless's catalogue (1959); dotted lines show bright nebula from Lynds's catalogue (1965). Dashed circle segments sketch the expanding shell of radius 40 pc, which overtook the Ophiuchus complex.

173

remain visible. **The first excess coincides with a HII region and with a considerable amount of dust, visible in IR maps (de Geus 1988). Also the excesses at about (l,b)=(350°,22°) are spatially consistent with HII regions and regions with a considerable amount of dust emission with practically no CO present. Again, the reflection nebula at about (l,b)=(355°,22°) is spatially correlated with a dust cloud.**

*Orion/Monoceros Region.* In the Introduction I mentionend that Bloemen et al. (1984) concluded that for the Orion/Monoceros region a good two-dimentional correlation was found between the gamma-ray structures and the total gas distribution. Figure 7 (from Bloemen et al. 1984) shows the similar distributions for Orion/Monoceros as is shown for Ophiuchus in Figure 6. All positive excesses in Figure 7d donot coincide with cloud structures and are located in sky regions in which the CO coverage was poor or missing. However, meanwhile the CO coverage has been completed and particularly one excess structure located at about $(l,b)=(209°,-21°)$ remained. This can be seen in the new map in Figure 8, which is produced similarly as Figure 6d (see also the "finding chart" of Bloemen (1989).

The IRAS data show also in this case enhanced IR emissivity extending over the area of the gamma-ray excess. As will be discussed below, this is another example of a gamma-ray excess adjacent to a molecular cloud, in a region with a considerable amount of dust and HII.

*Discussion.* Evidently, there appear to be some features in the gamma-ray data of the Ophiuchus/Upper-Scorpius and Orion/ Monoceros regions which are not explained by CO and HI structures. Both regions have been studied in great detail earlier, based on measurements at other wavelengths.

*Ophiuchus/Upper-Scorpius Region.* From a detailed study of the stars and the interstellar medium of the Scorpio-Centaurus OB association, de Geus (1988) recently pointed out that a HI shell (radius about 40 pc) around the stars in Upper Scorpius appears to be created by stellar winds of the early type stars present in Upper Scorpius (indicated in Figure 6b) and by a supernova explosion of a massive star of about 40 $M_\odot$ and about 1 Myr ago. The detailed structure of the interstellar medium, including the elongated CO structures can be explained as being due to the passage of the SN shock (the approximate position has been sketched in Figures 6c,d, although in this region the spherical bubble representing the HI shell has been disturbed due to the interaction with the cloud complex).

Discussing the HII and IR structures at $(l,b)=(351°,18°)$ and taking into account the presence of a strong UV field, de Geus concluded that part of the Rho Oph molecular cloud that was originally located in this region has been photodissociated after the passage of the shock front. A similar conclusion can be drawn on the structures around $(l,b)=(350°,22°)$ : a photodissociated
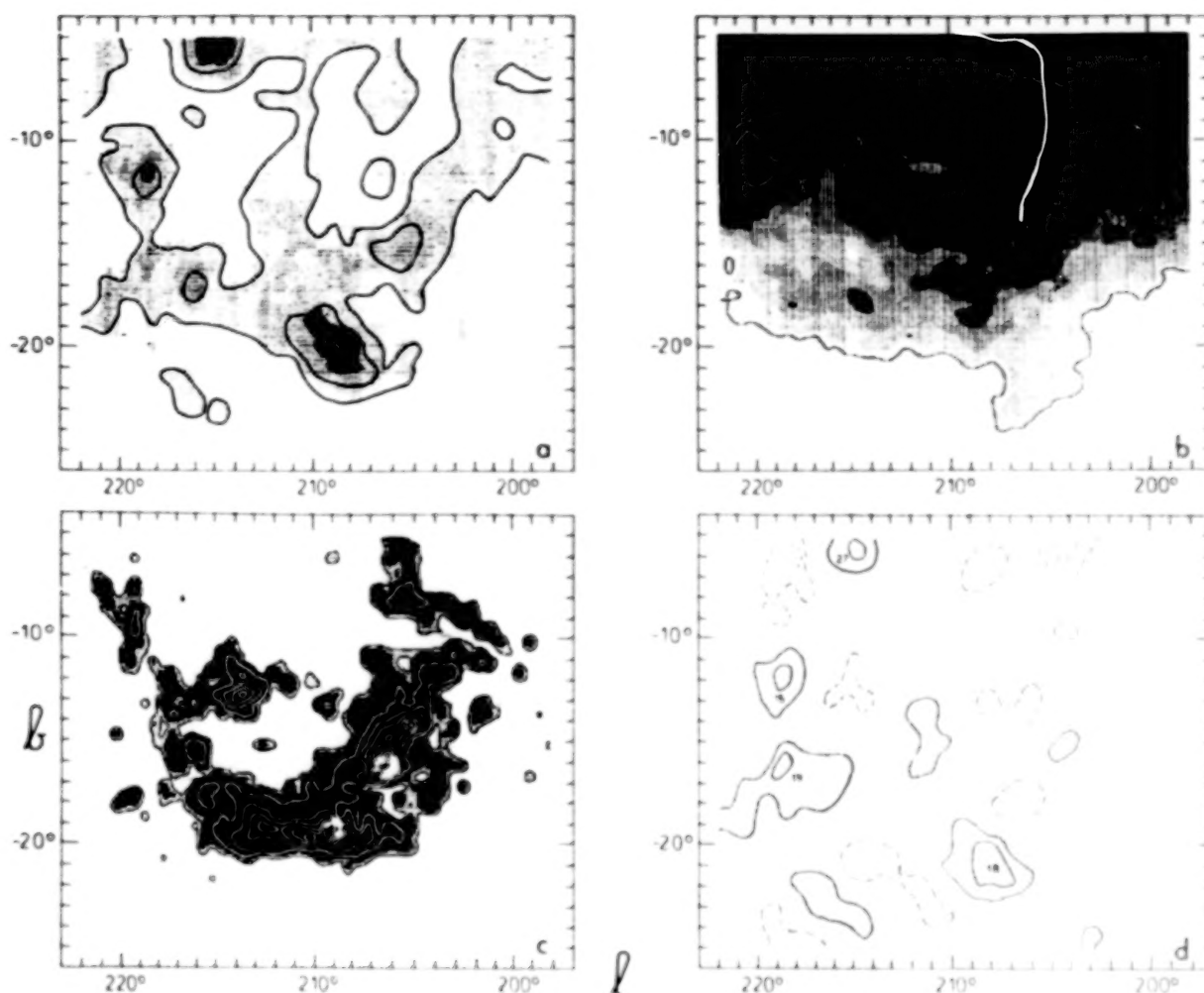
Fig. 7. The Orion-Monoceros region (from Bloemen et al. 1984; see there for additional explanation): a) Gamma-ray intensities in the 100-5000 MeV energy range. b) Total HI column densities. c) Velocity-integrated CO antenna temperatures W(CO). d) Map of the differences between the observed and the expected intensities. The gray areas and the full contours indicate positive excesses; the white regions and the dashed contours indicate deficiencies.

remnant of a molecular cloud. Blandford and Cowie (1982) discussed the scenario of a dense cloud overtaken by a strong supernova blast wave, in which dissociated molecules behind the shock, in a medium of enhanced gas and magnetic field density, are predicted to show up in gamma rays. However, this case seems to be different in that the SN-cloud interaction triggered star formation, and that the young stars apparently dissociated the gas clouds.

The important question arises: Do we need an enhancement in CR density inside this shell structure to explain the excess gamma-ray flux? Taking the preliminary mass estimates by de Geus, an enhancement in CR density of about an order of magnitude would be required to explain each of the excesses. It is unlikely that a CR enhancement in these dissociated molecular clouds originates

from the interaction described by Blandford and Cowie (1982), because, the CO complex is also overtaken by the shock, while no CR enhancement is found in the molecular clouds, but would then be expected.



Fig. 8. Map of differences between the observed and predicted diffuse emission similar to Fig. 6d (see there for energy range and contour levels). Dashed line gives limit of exposure. The CO coverage is complete over this area. Not all excesses are significant; the excess at $l=209°$ might be the only significant one.

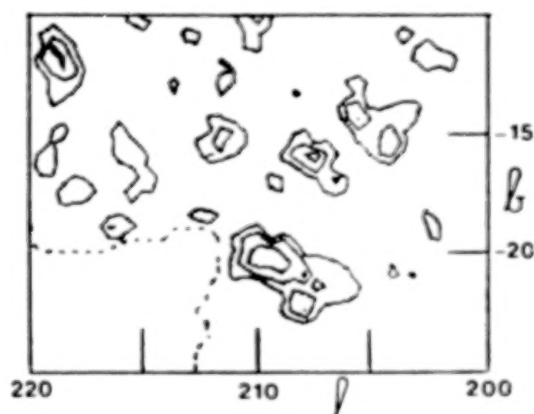*Orion-complex region.* Cowie, Songaila and York (1979) analysed UV absorption-line measurements for stars in or near the Orion OB1 and the ᴧ Orionis associations, and interpreted their results together with those from previous 21-cm and visual absorption-line measurements. Very much similar to the findings of the Geus for the Ophiuchus region, they found highly ionized cloud material, which must be photo ionized by radiation from the young neighbouring Ori OB1 stars. Furthermore, they suggested that the observed gas features are caused by the effects of a recent supernova and of multiple supernovae, stellar winds and rocket-accelerated clouds, in combination with ionization by the association stars.

More recently, Bally et al. (1987) presented a large-scale $^{13}CO$ map of the Orion molecular cloud and concluded also that the morphology may be the consequence of the formation and evolution of the Ori OB1 association centered north of the molecular cloud. Similarly to the situation for Ophiuchus, the adjacent gamma-ray excess at about $(l,b)=(209°,-21°)$ is located in a dense HII region on the side of the cloud facing the Ori OB1 association, so that part of the cloud that first experienced the interaction with the shock front ( or superbubble) that overtook and shaped the cloud complex.

An alternative explanation for the gamma-ray excesses adjacent to the Ophiuchus and Orion cloud complexes is the production of Inverse Compton gamma rays due to electron-photon interactions in enhanced photon fields around the early type stars. However, these stars ionized the ISM locally, and it seems difficult to maintain the required enhancements in photon density together with some enhancement in electron density in the ionized medium around the stars, to explain the gamma-ray excesses. More accurate experimental data is required, such as more detailed mass estimates, and better spectral information in the gamma-ray domain. The Soviet-French Gamma-1 mission, and the NASA GRO

mission will provide more accurate spatial and energy distributions which might help discriminating the different possible production mechanisms.

## References
Bally, J. et al., 1987, Ap. J. Letters, **312**, L45.
Bignami, G.F. et al., 1988, Astr. Ap., **202**, L1.
Blandford, R.D., Cowie, L.L., 1982, Ap. J. **260**, 625.
Bloemen, J.B.G.M. et al., 1984, Astr. Ap., **139**, 37.
Bloemen, J.B.G.M., 1989, Ann. Rev. of Astr. Ap., **27**.
Clear J. et al., 1988, Astr. Ap., **174**,85.
Cowie, L.L.,Songaila, A., York, D.G., 1979, Ap. J., **230**, 469.
De Geus, E.J., 1988, Ph.D. Thesis, Leiden University.
Grenier I.A. et al., 1988, Astr. Ap., **204**, 117.
Grenier, I.A., Hermsen, W., Hote, C., 1990, in Proc. XXI ICRC, Adelaide.
Halpern J.H. and Tytler D., 1988, Ap. J., **330**, 201.
Hermsen, W., 1980, Ph.D. Thesis, Leiden University.
Hermsen, W., Bloemen, J.B.G.M., 1983, "Surveys of the Southern Galaxy", eds. W.B. Burton, F.P. Israel, p. 65, Reidel Publ. Comp.
Hermsen, W., Spoelstra, T.A.Th., 1990, Proc. XXI ICRC, Adelaide.
Masnou et al., 1981, Proc. XVIIth ICRC, Paris, 1, 177.
Mayer-Hasselwander, H.A. and Simpson, G., 1983, "Advances and perspectives in X-ray and gamma-ray astronomy" eds. J.A.M. Bleeker, W. Hermsen, Advances in Space Research, Vol. 10, Nr. 2, 89, Pergamon Press.
Morfill, G.E. et al., 1981, Ap. J. **246**, 810.
Pollock et al.,1985a, Astr. Ap., **146**, 352-362.
Pollock et al.,1985b, 19th ICRC, La Jolla, **1**, 338-341.
Pollock, A.M.T., Hermsen, W., 1990, in Proc. XXI ICRC, Adelaide.
Simpson, G., Mayer-Hasselwander, H.A., 1987, XX ICRC, Moscow, **1**, 89.
Ruderman M. and Cheng K.S., 1988, Ap. J., **335**, 306.
Spoelstra, T.A.Th. and Hermsen, W., 1984, Astr. Ap. **135**, 135.
Sieber, W. and Schlickeiser, R., 1982, Astr. Ap. **113**, 314.
Strong et al., 1987, Astr. Ap. Suppl., **67**,283.
Strong et al., 1988, Astr. Ap., **207**, 1-15.
Swanenburg et al., 1981, Ap. J. Letters, **243**, L69.
Thompson et al., 1977, Ap. J. Letters, **214**, L17.
Wouterloot, J.G.A., 1981, Ph.D. Thesis, Leiden University.

## DISCUSSION

*John Mattox:*

Is it possible to include the spectral break point in the maximum likelihood analysis of Geminga?

*Wim Hermsen:*

It is possible, but CPU-time consuming. What we can do now is to compare the maximum likelihood values for the different selected break energies. This will give already a clear indicator which break energy is favored by the data.

# What Can Gamma Rays Tell Us about Binary X-Ray Sources and SNR's?

M. P. Ulmer

Department of Physics and Astronomy, Northwestern University

## I. INTRODUCTION

This is a short, informal summary of the paper I presented at the EGRET Workshop. I divided this paper into 3 main areas: black holes, neutron stars in binary X-ray source systems, and SNR's.

## II. BLACK HOLES

A good overall resource is Nolan's Ph.D. thesis (1982). Besides basic references, the thesis provides an analytic form of a spectrum from a comptonized plasma plus a broadened 0.5 MeV line that fit the spectrum of Cyg X-1. This may not be the correct model, but it is analytic and can be used to fit our data. The work of Liang and Dermer (1988) and references therein give a *theoretical* interpretation to the data which suggests that the gamma rays and X rays are coming from entirely different regions (Ling 1988; Dermer and Liang 1988; Liang and Dermer). The spectrum allegedly has a (transient?) bump at about 1 MeV. The predicted 50 to 300 keV count rate for OSSE is about 300 cts/sec. In the 300 keV to 1 MeV range, it is about 30 cts/sec. This leads to the exciting possibility of doing auto/cross-correlation analyses on the data. Also, the very hard spectrum plus the bump at about 1 MeV can be hypothesized to be a signature for black holes. Therefore, it will be interesting to observe others and see if they have this signature: 0620-00 (a transient, unfortunately), and GX339-4 (about 10 times weaker than Cyg X-1). Also, we can ask if the spectra of the Galactic Center and AGN's have the same distinctive shape as Cyg X-1 (Ling). Of course, the physics around a $10^6$ to $10^8 M_\odot$ black hole is very different from that around 5 to $10 M_\odot$ black holes, so if the 1 MeV signature is not seen, we cannot/should not take this as evidence against the existence of massive black holes in AGN's. I also note that Ling and Wheaton (1989) claim a narrow feature in Cyg X-1, but it does *not* look real to me.

Bottom Line. Favorite sources: Cyg X-1, 0620-00, and GX339-4. Science: spectral signature of black hole accretion disks; physics of emission regions with spectral fitting and time variability studies.

## III. NEUTRON STARS IN BINARY X-RAY SOURCE SYSTEMS

A major resource for a list of targets is Joss and Rappaport (1984). I found three observational areas related to these objects. First, there are cyclotron line features. So far these have only been observed at around 60 keV. We can hope to observe either higher harmonics of these features or other systems with higher energy features. (The energy of the feature that goes linearly with the magnetic field is about 12 keV for a $10^{12}$ G field.)

Second, there are lines that can come from the accretion of material onto the polar cap region. The main parameter that the gamma ray line flux depends on is the accretion rate. In terms of apparent brightness, this translates into the observed X-ray brightness. Brecher and Burrows (1980) predict a marginally observable flux from Sco X-1 at 2.2 MeV. The other strong lines are down by a factor of 10. These lines are 0.5 MeV, 4.4 MeV (C) and 6.1-6.3 MeV (O). Bildsten, Salpeter, and Wasserman (1989) have modified this theory slightly and have concentrated on binaries that they think are accreting nearly pure $^4$He. These binaries are ones with low masses and short periods. They (Bildsten *et al.*) do not predict intensities, however. The best bet is to hope that Brecher and Burrows got the lines right, but the intensities wrong. If we can see these lines they should tell us the value of M/R for the accreting neutron star. In the case of a few of these (especially Her X-1) M is known quite well so that a detection should tell us the equation of state of a neutron star. Third, as rotating neutron stars are thought to be accelerators of cosmic rays, it is possible that cosmic ray winds from a pulsar will produce observable quantities of gamma ray lines *not redshifted* from the surface of the companion "normal star." Vestrand (1989) has an article on this; Cyg X-3 is his favorite target. One could easily imagine that other objects could fall into this class, from "normal systems" such as Her X-1 to "oddball systems" such as SS 433. Cyg X-3 should just be observable (naturally) at 2.2 MeV and 0.5 MeV (could this be the real source of the alleged 1 MeV bump from Cyg X-1, and the fact that all MeV detectors have had such a broad field of view that people have mistaken Cyg X-3 for Cyg X-1?)

Bottom Line. Favorite sources: Her X-1, Vela XR-1, Cen X-3, Sco X-1, Cyg X-3, SS 433. Also one can consider a cast of about 12 other (Joss and Rappaport 1984) pulsing X-ray sources plus the strongest galactic bulge sources. Further, based on the suggestion of Bildsten, Salpeter, and Wasserman (1989), I also include 1820-30, 1626-67, and 1916-05. Science: cyclotron lines; accretion induced gamma ray lines which will allow a M/R measurement; pulsar winds interacting with companion stars which will produce evidence that cosmic rays are accelerated in copious quantities by pulsars in binary systems.

## IV. SNR'S, OLD AND NEW

A good resource is Weiler and Sramek (1988). Also, see Seward (1989). For SN1987A, I refer you to the GRO Workshop and the Nuclear Spectroscopy workshop. From Leising (1989), the only line we can really expect to barely detect is 122 keV from $^{57}$Co. If the SIGMA experiment is successfully launched in December 1989 and works well, we (OSSE) could be scooped on this. Our best hope for an exciting result is that the theory is wrong (enough) so that there are some detectable lines above approximately 1 MeV.

As far as the other remnants are concerned, the first thing that comes to mind is to look for a "Crab-like" non-thermal radiation effect, although one object, W28, may also be interacting with a molecular cloud and producing lines. Taking a *very* simplistic approach, we can normalize to the Crab Nebula radio flux and predict which should be the strongest SNR's for us to see in the gamma ray region (besides the Crab): W28 (molecular cloud interaction as well?), Vela, W50 (SS 433), and MSH 15-52 (contains PSR1509-58, radio and X-ray pulsars). Others that may be centrally influenced and hence interesting are CTB 80 (contains a milli-second pulsar with an optical bow shock), CTB 109 (contains a central binary X-ray source which is a "slow" pulsar, also close to a molecular cloud), G27.4+00

(Kes 73, contains an X-ray source in the center). Other objects that seem to be the most likely to be detectable based on radio and X-ray information from Seward (1989) are: CTA 1, G21.5-0.9, and G29.9-0.3 (Kes 75).

Two other points that were brought to my attention by Matz and Purcell (1989) are: (1) the hope of seeing $^{44}$Ti at 1.157 MeV from fairly young SNR's. By fairly young SNR's we mean those less than about 100 years old which were missed by optical or radio surveys. Cas A at about 300 years old would produce about $10^{-5}$ photons cm$^{-2}$ s$^{-1}$ at the Earth (Woosley and Pinto 1988—from which we have taken the value of produced $^{44}$Ca as $10^{-4} M_\odot$). Given the uncertainties in the theory, distance estimates, age estimates, and even type of supernova that produced Cas A, the overall uncertainty in our flux estimate from Cas A is nearly a factor of 10. If we are lucky, then, the flux from Cas A could be as high as $10^{-4}$ photons cm$^{-2}$ s$^{-1}$ at the Earth. (2) The existence of an $e^+e^-$ pair wind could also produce detectable quantities of 0.5 MeV gamma rays. Taking the flux predicted from the Crab by Sturrock (1971), the Crab Nebula should be detectable at about $2 \times 10^{-4}$ photons cm$^{-2}$ s$^{-1}$ at the Earth (assuming a 2 kpc distance to the Crab). Other particularly attractive pulsar/SNR systems are PSR 1951+32 (Hester and Kulkarni 1988) and 1957+20 (Kulkarni and Hester 1988) both of which have been shown to have bow shocks. Sturrock's paper predicts that the $e^+e^-$ winds will be negligible for old ($\sim 10^8$ G magnetic field) milli-second pulsars such as 1951+32 and 1957+20. We have reason to hope, however, that the $e^+e^-$ pair production is higher than predicted by Sturrock's model. For example, Kulkarni and Hester, referring to a preprint by Phinney and Evans, claim that radio studies may give "diagnostic information about the energy spectrum of $e^+e^-$ pairs in the pulsar wind" of 1957+20. Certainly, gamma ray studies have the potential of providing invaluable information about the very existence of $e^+e^-$ pairs in the pulsar wind. For further arguments for large $e^+e^-$ pair winds, see Arons (1981, 1983) who argues for the existence of substantial $e^+e^-$ winds from milli-second pulsars. Arons' wind model depends on the magnetic field to the 2/5 power and inversely on the pulsar period to the 9/5 power, so that milli-second pulsars can be more copious producers of $e^+e^-$ pairs in Arons' models than in Sturrock's theory.

Bottom Line. Favorite sources: Crab, W28, Vela, W50, MSH 15-52, CTB 80, CTB 109, G27.4+00, PSR 1957+20, Cas A, plus a galactic plane scan searching for $^{44}$Ti. Also, one can consider CTB 109, CTA 1, G21.5-09, and G29.9-0.3 (Kes 75). Science: acceleration of cosmic rays and their interaction with the surrounding magnetic field and interstellar medium, nucleosynthesis of $^{57}$Co and $^{44}$Ti, and $e^+e^-$ winds.

## V. ACKNOWLEDGEMENTS

## REFERENCES

Arons, J. 1981, *Ap. J.*, **248**, 1099.
Arons, J. 1983, *Nature*, **302**, 301.
Bildsten, L., Salpeter, E., and Wasserman, I. 1989, in *Proceedings of the Gamma Ray Observatory Science Workshop*, ed. W. Johnson, p. 4-343.

Bildsten, L., Salpeter, E., and Wasserman, I. 1989, private communication.

Brecher, K., and Burrows, A. 1980, *Ap. J.*, **240**, 642.

Dermer, C. D., and Liang, E. P. 1988, in *AIP Conference Proceedings*. Vol. **170**, *Nuclear Spectroscopy of Astrophysical Sources*, ed. N. Gehrels, and G. Share (New York: American Institute of Physics), p. 326.

Hester, J. J., and Kulkarni, S. R. 1988, *Ap. J. (Letters)*, **331**, L121.

Joss, P. C., and Rappaport, S. A. 1984, *Ann. Rev. Astr. Ap.*, **22**, 537.

Kulkarni, S. R., and Hester, J. J. 1988, *Nature*, **335**, 801.

Leising 1989, private communication.

Liang, E. P., and Dermer, C. D. 1988, *Ap. J. (Letters)*, **325**, L39.

Ling, J. C. 1988, in *AIP Conference Proceedings*. Vol. **170**, *Nuclear Spectroscopy of Astrophysical Sources*, ed. N. Gehrels, and G. Share (New York: American Institute of Physics), p. 315.

Ling, J. C., and Wheaton, W. A. 1989, *Ap. J. (Letters)*, **343**, L57.

Matz, S. M., and Purcell, W. R. 1989, private communication.

Nolan, P. L. 1982, Ph.D. thesis, University of California, San Diego.

Seward, F. D. 1989, *Space Sci. Rev.*, **49**, 385.

Sturrock, P. A. 1971, *Ap. J.*, **164**, 529.

Vestrand, W. T. 1989, in *Proceedings of the Gamma Ray Observatory Science Workshop*, ed. W. Johnson, p. 4-274.

Weiler, K. W., and Sramek, R. A. 1988, *Ann. Rev. Astr. Ap.*, **26**, 295.

Woosley, S. E., and Pinto, P. A. 1988, in *AIP Conference Proceedings*. Vol. **170**, *Nuclear Spectroscopy of Astrophysical Sources*, ed. N. Gehrels, and G. Share (New York: American Institute of Physics), p. 98.

M. P. ULMER: Northwestern University, Department of Physics and Astronomy, 2145 Sheridan Road, Evanston, IL 60208

# GAMMA RAYS FROM PULSAR WIND SHOCK ACCELERATION

ALICE K. HARDING

NASA/Goddard Space Flight Center, Greenbelt, MD 20771

## ABSTRACT

A shock forming in the wind of relativistic electron-positron pairs from a pulsar, as a result of confinement by surrounding material, could convert part of the pulsar spin-down luminosity to high energy particles through first order Fermi acceleration. High energy protons could be produced by this mechanism both in supernova remnants and in binary systems containing pulsars. The pion-decay gamma rays resulting from interaction of accelerated protons with surrounding target material in such sources might be observable above 70 MeV with EGRET and above 100 GeV with ground-based detectors. Acceleration of protons and expected gamma-ray fluxes from SN1987A, Cyg X-3 type sources and binary pulsars will be discussed.

## I. INTRODUCTION

Although the Crab and Vela pulsars are among the strongest known gamma-ray point sources, their pulsed radiation represents only a minor fraction of their total spin-down energy loss. The radio pulses contain on average $\approx 10^{-5}$ of the power released and even the pulsed gamma rays from the Vela pulsar represent only .05% of the spin-down luminosity. At least in these cases, acceleration of particles within the magnetosphere is not an efficient means of tapping the spin-down power of a pulsar, the bulk of which is released at or outside the light cylinder as electromagnetic dipole radiation at the pulsar spin frequency. Because the expected plasma frequency just outside the pulsar magnetosphere is above the frequency of the vacuum dipole wave (Arons 1981), the spin-down power will be transported as an MHD wind of relativistic electron-positron pairs (Rees and Gunn 1974, Kennel and Coroniti 1984). If a pulsar wind interacts in some way with a surrounding medium, then a large fraction of the pulsar spin-down power might be channeled into observable radiation through the acceleration of particles.

One possibility is the confinement of a pulsar wind by an expanding supernova remnant. This evidently occurs in the Crab nebula, where 20 - 30% of the $5 \times 10^{38}$ erg s$^{-1}$ released by the pulsar appears as synchrotron radiation from relativistic electrons. Rees and Gunn (1974) pointed out that a standing reverse shock must form in the confined pulsar wind, as it decelerates to the subsonic velocity of the shell. Gaisser, Harding and Stanev (1987, 1989) proposed that acceleration of charged particles could take place at the pulsar wind shock through the first order Fermi mechanism. Charged particles travelling back and forth across the shock by scattering from magnetic irregularities, gain energy in each crossing-recrossing cycle. This mechanism is capable of accelerating protons as well as electrons to high energies. Evidence of proton acceleration could appear as high energy $\gamma$-rays from decay of neutral pions, produced when the protons undergo nuclear interactions with material of the supernova envelope. Although the density of the Crab supernova shell is now too low to produce observable $\gamma$-rays from proton interactions, very young supernova remnants like SN1987A might be good sources to look for signatures of proton acceleration (Berezinsky

and Ginzburg 1987, Nakamura *et al.* 1987).

Acceleration of particles in pulsar wind shocks and production of high energy $\gamma$-rays may also take place in binary systems (Harding and Gaisser 1990), where the atmosphere, wind or magnetosphere of the companion can confine the pulsar wind. There may in fact be evidence that such an interaction of a pulsar wind with a companion star is occurring in PSR1957+20, the recently discovered eclipsing millisecond pulsar (Fruchter *et al.* 1988). A stationary shock would in this case form between the pulsar and companion near the pressure balance point. Pulsars buried inside molecular clouds may also have confined winds, producing shock-accelerated cosmic rays inside the clouds and such sources may contribute to an enhancement of the diffuse galactic gamma-ray emission.

This paper discusses the acceleration of protons and production of gamma-rays by pulsar wind shocks and the prospects for detection by EGRET of > 70 MeV $\gamma$-rays from young supernova remnants and binary pulsars. It appears that EGRET may be more sensitive to detection of these signals than the ground-based air shower arrays currently in operation.

## II. PULSAR WIND SHOCK FORMATION

The power in magnetic dipole radiation from a pulsar with rotation frequency $\Omega$ and magnetic dipole moment $m$ is

$$L_d = \frac{2m^2\Omega^4 \sin^2\theta}{3c} \approx 4 \times 10^{43}\,\mathrm{erg/s}\,B_{12}^2 P_{ms}^{-4} \tag{1}$$

where $P_{ms}$ is the period in ms, $B_{12} = (B_o/10^{12}\mathrm{Gauss})$ is the surface magnetic field, and $\theta$ is the angle between the dipole and rotation axes. Virtually all of this power may appear as a relativistic wind which carries both particles (predominantly electron-positron pairs) and wound-up magnetic field away from the pulsar. Since the magnetic field is dipolar ($\approx r^{-3}$) inside the pulsar light cylinder, $r_{LC} = c/\Omega = 5 \times 10^6\,\mathrm{cm}\,P_{ms}$, and toroidal ($\approx r^{-1}$) in the wind, the field strength at a distance r is

$$B = B_o\left(\frac{r_o}{r_{LC}}\right)^3\left(\frac{r_{LC}}{r}\right) = 8 \times 10^9\mathrm{Gauss}\,B_{12}P_{ms}^{-3}\left(\frac{r_{LC}}{r}\right), \tag{2}$$

where $r_o = 10^6$ cm is the neutron star radius. Winds from pulsars with short periods have higher magnetic fields because the light cylinder, inside which the field falls off most rapidly, is closer to the neutron star.

Confinement of pulsar winds can occur if surrounding material provides enough pressure to balance the wind ram pressure. The confining material then creates a standing reverse shock in the wind. If the pulsar is surrounded by a supernova remnant, then the pulsar wind sweeps out the inner part of the expanding envelope to form a roughly spherical cavity around the pulsar, filled with relativistic particles and magnetic field. A binary companion may also provide pressure in the form of a stellar wind, atmosphere or magnetosphere to shock the pulsar wind.

### a) Supernova Remnants

The situation where a pulsar wind is confined by the inner part of an expanding supernova shell is shown schematically in Figure 1. The pulsar wind model of a supernova remnant was

first proposed by Rees and Gunn (1974) and by Pacini and Salvati (1973) to explain how the power generated by spin-down of the Crab pulsar is converted to relativistic particles which radiate the observed synchrotron emission. The model assumes that the spin-down power from a young pulsar inside the remnant drives a relativistic MHD wind with luminosity $L_d$ approximated by Eqn (1). The radius of the shock $r_s$ is calculated (Rees and Gunn 1974) by balancing ram pressure in the wind with the accumulated energy density in the shocked wind cavity:

$$r_s = \sqrt{\frac{u_{min}}{3c}}\, u_{min}\, t \approx 3.5 \times 10^{13}\,\text{cm}\; t_{yr}\, u_{500}^{3/2}.\tag{3}$$

where $t_{yr}$ is the age of the supernova in years and $u_{500} = u_{min}/500\,\text{km s}^{-1}$ is the velocity of the inner envelope.

From Eqn (2), the magnetic field in the pulsar wind can be estimated at $r = r_s$ as

$$B_s \approx 10\,\text{G}\; B_{12}\, P_{10}^{-2}\, t_{yr}^{-1}\, u_{500}^{-3/2}\tag{4}$$

The above expression gives $B \approx 10^{-4}$ G for the Crab pulsar, which is in good agreement with the field inferred from the observed synchrotron emission from the nebula.
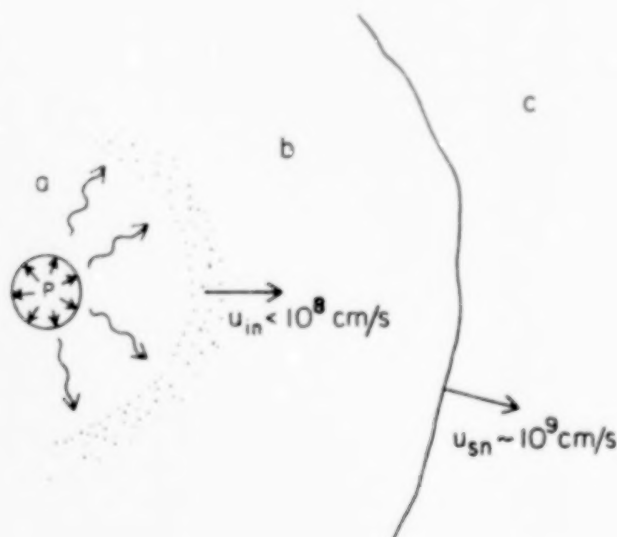


FIG. 1 - Schematic view of a pulsar wind in a supernova remnant. The inner circle of radius $r_s$ is the reverse shock in the wind generated by the pulsar (P), whose rotation axis is normal to the plane of the figure. Region (a) is the shocked pulsar wind cavity, which is confined by the supernova envelope (b), expanding into the interstellar medium (c).

b) Binary Pulsars

Pulsar wind shocks can also form in binary systems containing rapidly spinning, non-accreting pulsars. Accretion will not take place if the light cylinder of the rotating neutron star, $r_{LC}$, is inside the Alfven radius, $r_A = 1.5 \times 10^8\, B_{12}^{4/7}\, \dot{M}_{18}^{-2/7}$ cm, where $\dot{M}_{18} = \dot{M}/10^{18}\,\text{g s}^{-1}$ is the accretion rate. In this case, the ram pressure from the pulsar wind outside the light cylinder everywhere exceeds the ram pressure of the accretion flow and cannot

maintain a stable force balance condition analogous to the Alfven radius. Any accreting material will be blown away by the pulsar wind. Therefore, systems having short period pulsars with

$$P < 31\,\mathrm{ms}\,B_{12}^{4/7}\,\dot{M}_{18}^{-2/7} \tag{5}$$

will be powered by rotation (Ruderman et al. 1989, Harding and Gaisser 1990).

There are several possibilities for confining a pulsar wind in a binary system, at least over a limited solid angle. If the companion star generates a wind, possibly induced by the incident pulsar luminosity, a shock forms where ram pressure of the two winds balance (cf. Fig. 2). In the absence of a stellar wind, the pulsar wind can be confined by the static atmosphere or magnetosphere of the companion where the gas or magnetic pressure balances the ram pressure of the pulsar wind.
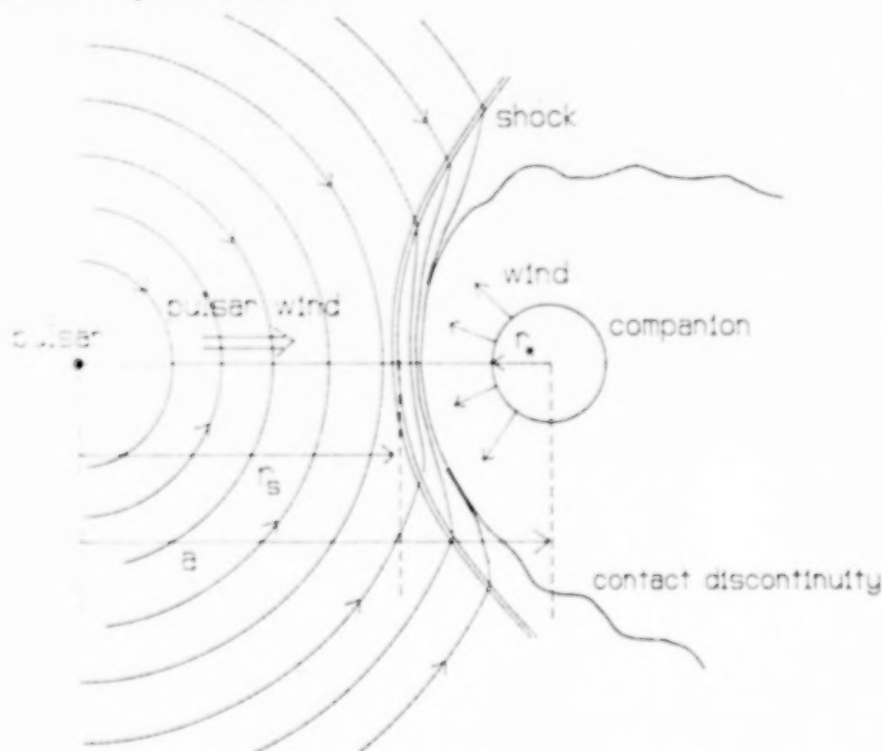


FIG. 2 - Schematic view of pulsar wind shock formation in a binary system for the case of confinement by the companion star wind.

In the case where the pulsar wind is confined by a stellar wind from the companion, the shock location is determined by balancing $L_d/(4\pi r^2 c)$ with $(\rho v^2)_w = \dot{M}_w v_w/(4\pi r^2)$ or

$$\frac{L_d}{4\pi r_s^2 c} = \frac{\dot{M}_w v_\infty}{4\pi (a - r_s)^2}\left[1 - \frac{r_*}{a - r_s}\right]^{1/2} \tag{6}$$

where $\dot{M}_w$ and $v_\infty$ are the mass loss rate and terminal velocity of the wind, $r_s$ is the distance of the shock from the neutron star and $r_*$ is the companion star radius. An approximate solution for the shock location $r_s$ in the limit $r_s \ll a - r_*$, is

$$\frac{r_s}{a} \approx \frac{\sqrt{A_w}}{1 + \sqrt{A_w}} \tag{7}$$

$$A_w = -\frac{L_d}{\dot{M}_w v_w c} = \frac{2 \times 10^7 B_{12}^2 P_{ms}^{-4} (\frac{r_*}{R_\odot})^{1/2}}{\dot{M}_{18} (\frac{v_\infty}{v_{esc}}) (\frac{M}{M_\odot})^{1/2}} \tag{8}$$

where $M$ is the companion star mass and $v_{esc} = (2GM/r_*)^{1/2}$ is the escape velocity from the companion. The quantity $A_w$ is essentially the ratio of pulsar wind ram pressure to stellar wind ram pressure and is the critical parameter determining solutions for $r_s$. In order to calculate the location of the shock, one needs a model for the companion star wind which gives values for $\dot{M}$ and $v_\infty$. Harding and Gaisser (1990) discuss two possible models in which the wind from the companion is induced by the pulsar wind luminosity: 1. If the pulsar wind luminosity incident on the companion star exceeds its Eddington luminosity, a wind will be driven by radiation pressure, 2. If the incident luminosity is sub-Eddington, then a thermally-driven wind may result (Cheng 1989). In the latter case, the shock radius turns out to be independent of the pulsar luminosity, with the quantity $A_w = 11.5(v_\infty/v_{esc})^3(a/r_*)^2$ from Eqn (8) dependent only on the system geometry and the wind terminal velocity.

If the companion star has a surface magnetic field, $B_*$, then magnetic pressure may be sufficient to stand off the pulsar wind. In this case, the shock location can be found by balancing $[B_*(r_s)]^2/8\pi$ with $L_d/(4\pi r_s^2 c)$. Assuming a dipole field, solutions for the shock location are determined by the quantity

$$A_m = \frac{2L_d}{B_*^2 a^2 c}, \tag{9}$$

which scales with the ratio of pulsar wind ram pressure to magnetic pressure. The condition that the shock form above the companion star surface, or $(a - r_s) \geq r_*$, requires that $A_m \leq (1 - r_*/a)^2 \leq 1$, which from Eqn (9) gives a limit on the companion star field capable of standing off the pulsar wind,

$$B_* \geq \left(\frac{2L_d}{c}\right)^{1/2} \frac{1}{(a - r_*)}. \tag{10}$$

If neither a wind or a magnetosphere of the companion provides enough pressure to stand off the pulsar wind above its surface, then the static gas pressure of the atmosphere, $\rho kT/m_H$, will balance the pulsar wind ram pressure. In this case, pressure balance will occur close to the companion star surface, so that the shock distance from the pulsar is $r_s \approx a - r_*$.

## III. PARTICLE ACCELERATION

Following the pioneering work of the late seventies (Axford $et$ $al.$ 1977, Blandford and Ostriker 1978), shock acceleration has gained considerable attention as a mechanism for generating highly energetic particles in a variety of astrophysical sources ranging from supernovae to the Earth's bow shock. If the shock is formed by collisionless processes, particles can travel back and forth across the shock front by scattering from magnetic irregularities, gaining some energy on each crossing. The theory of diffusive shock acceleration (cf. Drury 1983 for review) has concentrated primarily on strong parallel shocks (where the magnetic field is parallel to the shock normal). The standard treatment also is for non-relativistic shocks for which $u_1, u_2 \ll c$. Such a shock produces a power law spectrum of accelerated particles

escaping downstream with index of the differential energy spectrum $\alpha = (\xi + 2)/(\xi - 1)$, where $\xi$ is the shock compression ratio.

The shock in the pulsar wind differs from the canonical case in two ways. First, because of the toroidal field of the wind, the shock is quasi-perpendicular rather than parallel. Second, the shock is relativistic in that the velocity of the unshocked wind relative to the shock front is $u_1 \approx c$. Treatments of acceleration by relativistic shocks (Peacock 1981; Kirk and Schneider 1987) indicate that they are more efficient at accelerating particles than non-relativistic shocks (the energy gain per crossing is larger). Calculations show that the accelerated particle spectrum is flatter than for a non-relativistic shock with the same compression ratio. However, the resulting spectral index is somewhat uncertain, since the two approximations usually made to treat scatterings in the non-relativistic case, pitch angle scattering or hard-sphere scattering, give different results in the relativistic case (Ellison 1989, private comm.). Thus, the description of particle acceleration by relativistic shocks is still incomplete.

The maximum energy to which (charged) particles can be accelerated in the shock is determined by the balance of the energy gain rate with losses. The energy gains of the particles crossing the shock compete with energy losses through radiation and inelastic collisions and with diffusion away from the shock. In almost all situations, the pulsar wind shock will form well outside the pulsar light cylinder, where the magnetic field in the wind is low and consequently synchrotron radiation from protons will not be important. The maximum energy, $E_p^{\max}$, to which protons can be accelerated by a spherical shock of radius $r_s$ is therefore found by equating the acceleration time to the time, $t_d \approx r^2/D$, for protons to diffuse away from the shock, where $D$ is the diffusion coefficient and $r$ is usually taken to be the shock radius. The minimum value of the diffusion coefficient, $D_{\min} = r_L v/3$, where $r_L = 3.3 \times 10^9 \mathrm{cm}\, E_{\mathrm{TeV}}/B$ is the Larmor radius, $v$ is the particle velocity, and $E$ is the particle energy, gives an upper limit on the acceleration rate and hence an upper limit on the maximum energy that can be achieved. For the pulsar wind, which is highly relativistic (Kennel and Coroniti 1984), $u_1 \approx c$, and the resulting estimate for the maximum proton acceleration energy, using the non-relativistic treatment (Lagage and Cesarsky 1983), is

$$E_p^{\max} \approx \sqrt{\frac{3(\xi - 1)}{\xi(\xi + 1)}} \, \epsilon B_s r. \tag{11}$$

Because of the inverse dependence on field strength, which from Eq (2) is large, and the relativistic velocity of the wind, the pulsar wind shock is extremely efficient at accelerating particles to high energy.

In cases where the shock radius is the same as the distance of the shock from the pulsar, the magnetic field strength at the shock from Eqn (2) with $B_s = B(r = r_s)$ gives a maximum proton energy of

$$E_p^{\max} \approx 7 \times 10^{18} \,\mathrm{eV}\, B_{12} P_{\mathrm{ms}}^{-2} = 10^{16} \,\mathrm{eV}\, L_{38}^{1/2} \tag{12}$$

for a strong shock with $\xi = 4$. It is interesting that the maximum energy in Eqn (12) depends only on pulsar parameters and is independent of the structure and dynamics of the confining material. This is because $E_p^{\max} \propto r_s B_s$ and the magnetic field at the shock, $B_s$, is inversely proportional to $r_s$. This scale invariance of the maximum proton acceleration energy makes this mechanism applicable to models of binary sources of VHE and UHE $\gamma$-rays as well as to pulsars in supernova remnants. Furthermore, there is a simple relation between the pulsar

spin-down luminosity, $L_{38} = L_d/10^{38} \mathrm{erg\,s^{-1}}$, and the predicted maximum proton energy. Eqn (12) will hold for pulsar wind shocks in supernova remnants, because the confining shell will form a spherical shock around the pulsar at a distance $r = r_s$.

For pulsar wind shocks in binary systems, the geometry is somewhat more complicated and Eqn (12) then represents an upper limit to the maximum proton energy. In the case of confinement by a stellar wind or magnetosphere, the diffusion length scale which determines the maximum proton energy depends on how close the shock is to the companion star. If $r_s \ll a - r_*$, then the radius of the shock will be approximately $r_s$ and the diffusion timescale, $t_d = r_s^2/D$, but if $r_s \approx a - r_*$ with the shock near the companion star, then the shock radius will be approximately $r_*$ and $t_d = r_*^2/D$. The maximum proton energy in these two cases is (Harding and Gaisser 1990)

$$ E_p^{\mathrm{max}} = 7 \times 10^{18} \, \mathrm{eV} \, B_{12} P_{\mathrm{ms}}^{-2} \begin{cases} 1, & r_s \ll a - r_* \\ \dfrac{r_*}{(a-r_*)}, & r_s \approx a - r_* \end{cases} \tag{13} $$

Note that in the case $r_s \ll a - r_*$, the $r_s$ dependence drops out of $E_p^{\mathrm{max}}$ as in Eqn (12), so that the maximum proton acceleration energy depends only on pulsar parameters. In the case of wide binaries, where $r_s \approx a - r_*$, the maximum proton energy may be substantially reduced.

## IV. GAMMA-RAY PRODUCTION

Protons accelerated at the pulsar wind shock could produce high energy gamma rays and neutrinos through the decay of neutral pions, which would result when the protons interact with surrounding material (or conceivably ambient photons if their density is high enough). The bremsstrahlung emission from electrons produced as secondaries in the nuclear interactions may also make a contribution at low energies, although the magnetic fields in these sources are high enough to make the bremsstrahlung negligible at higher energies. In the case of young supernovae, the target material is the expanding envelope. In binary systems, the target material could be the companion star wind or atmosphere. Since the geometry and proton transport in these situations are so different, we discuss gamma-ray production in these two types of sources separately.

### a) Supernova Remnants

Supernovae are considered to be likely sites of cosmic-ray acceleration and it was noted some time ago that evidence for such acceleration might be observed in young supernova remnants in the form of gamma-rays from nuclear interactions of accelerated protons (Berezinsky and Prilutsky 1978; Sato 1977; Shapiro and Silberberg 1979). Following the explosion of SN1987A in the Large Magellanic Cloud, a number of experiments have attempted to detect these $\gamma$-rays over a wide range of energies (see Harding 1989 for review) and models of the pion-decay $\gamma$-ray production from nuclear interactions have been developed and refined (e.g. Gaisser et al. 1987, 1989 [GHS]; Berezinsky and Ginzburg 1987; Yamada et al. 1987). These models assume that acceleration of protons results from the presence of a pulsar deep inside

the remnant. Their results indicate that details of the confinement of accelerated protons and the mixing of protons with gas in the envelope make a crucial difference in the predicted gamma-ray fluxes and light curves.

Thus far, the models have made highly simplified assumptions about the transport and distribution of protons in the envelope in order to calculate gamma-ray fluxes and light curves. For example, Yamada *et al.* (1987) assume that the accelerated protons are not confined at all and freely propagate through the envelope. The resulting light curve peaks and decays within a year after the explosion. On the other hand, GHS have assumed that the protons are confined by the high magnetic field surrounding the pulsar. The production of $\gamma$-rays through nuclear interactions then requires that the cosmic rays mix with the gas in the envelope by diffusion or bulk motion. The mixing of the shocked wind with the gas in the envelope could result, for example, from Rayleigh-Taylor instabilities at the wind-envelope interface. The exact amount of energy going into $\gamma$-rays then depends on the degree of mixing of shell material with the shocked wind containing the accelerated protons and magnetic field. In this case the light curves can peak as late as 6 years after the explosion. They also showed that the light curves were very sensitive to the assumed distribution of protons in the envelope and to the degree of mixing of protons with gas.
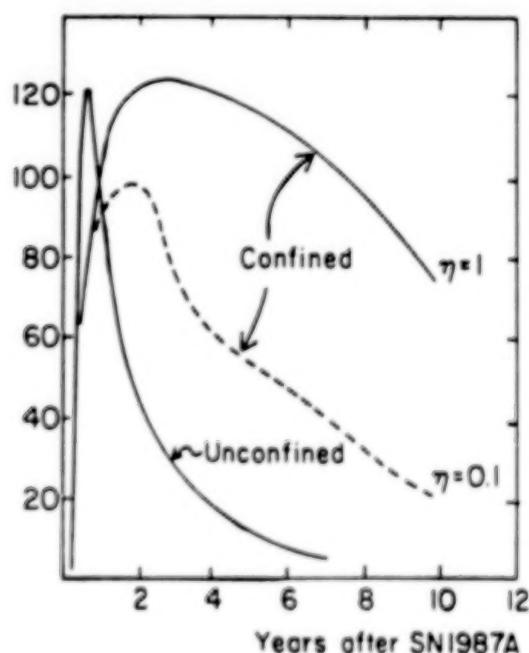


FIG. 3 - Comparison of light curves for models with confinement (from GHS) and free propagation (from Nakamura *et al.* 1987).

Figure 3 shows the calculated gamma-ray light curves in these two cases for SN1987A, showing that if the protons are unconfined the source has already peaked, whereas if the confinement picture is correct the source may last long enough to be detectable with future satellite experiments. In the case of proton confinement, the high energy photon signal will be observable between time $t_1$ when the shell becomes optically thin to $> 100$ MeV $\gamma$-rays and time $t_2$ when the shell becomes so diffuse that protons lose their energy from adiabatic expansion before interacting. For a total ejected mass $M \approx 15\,M_\odot$, $t_1 \approx 1$ year. The time $t_2$

occurs when the interaction rate of accelerated ions with the gas falls below the expansion rate. After this time the dominant energy loss will be by adiabatic expansion (Berezinsky and Prilutsky, 1978). If the accelerated particles are not completely mixed with the gas in the expanding envelope, $t_2$ depends on the amount of the gas mixed into the cosmic ray bubbles and could even be such that $t_2 < t_1$ (i.e. photon production never occurs) if there is not enough mixing.

Cosmic ray mixing and transport in a supernova shell has been considered in greater detail by Harding *et al.* (1990a,b). Assuming that protons are accelerated at a constant rate by the shock deep inside the pulsar wind cavity, they must diffuse to the wind-envelope boundary, suffering adiabatic losses from the expansion. This boundary is Rayleigh-Taylor unstable because the low-density pulsar wind is exerting a pressure on the denser overlying envelope. At the boundary, bubbles containing pulsar wind, tangled magnetic field and cosmic rays will grow and penetrate the inner edge of the envelope through Rayleigh-Taylor instability. Transport of the bubbles outward through the envelope together with leakage of material into the bubbles provides the mixing of cosmic rays and target material necessary for gamma-ray production. From the maximum growth timescale and scale size of the instability, they find that Rayleigh-Taylor perturbations will reach the non-linear phase in less than a year. The estimated rate at which the bubbles move out into the envelope indicate that the cosmic rays will stay confined in the inner part of the shell while interacting. Protons confined to the slowest moving, densest part of the envelope will have a lower energy loss rate from adiabatic expansion and a higher nuclear interaction rate than protons distributed uniformly throughout the envelope (GHS). These factors contribute to a higher gamma-ray productivity. This must be balanced, however, with the larger attenuation of gamma-rays coming from deep inside the envelope.
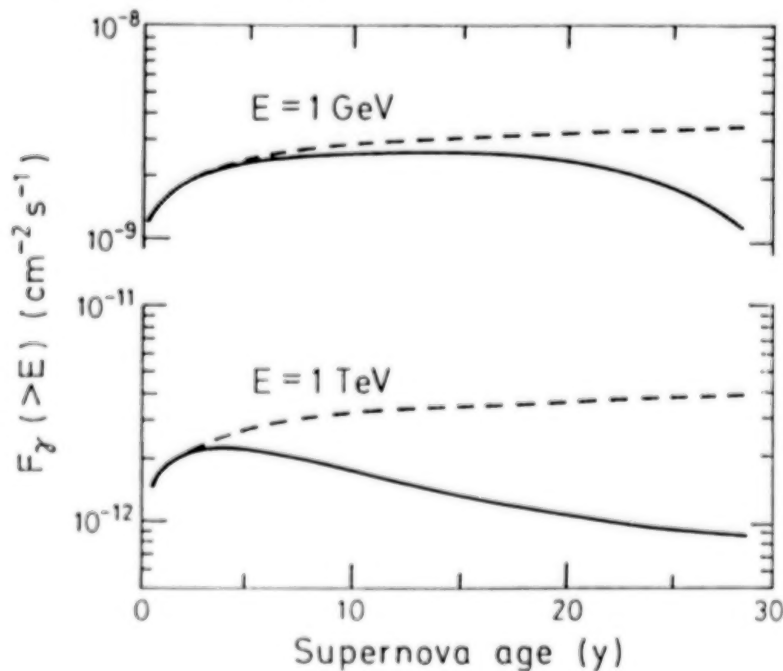


FIG. 4 - GeV and TeV gamma-ray light curves for SN1987A showing result of a full treatment (solid curve) and assuming that all protons entering envelope interact immediately (dashed curve). Fluxes are normalized to a proton luminosity of $10^{39}\,erg\,s^{-1}$.

The spectrum of cosmic rays convected into the envelope will differ from that produced by shock acceleration due to adiabatic deceleration in the expanding cavity and the finite rate of convection out of the cavity. Harding *et al.* (1990a,b) find that these factors can make a significant difference in the predicted gamma-ray fluxes over previous models, which assumed that the spectrum of interacting protons is the same as the acceleration spectrum. In fact the full diffusion treatment results in a peak gamma-ray flux nearly a factor of ten lower than that predicted by GHS, who did not consider the details of injection into the shell. Also, because the rate of diffusion of the protons in the envelope depends on their energy, the light curves should be energy dependent. Figure 4 shows light curves for SN1987A from a Monte Carlo calculation which models the injection, diffusion and nuclear interactions of protons in the expanding envelope using model 10HMM of Pinto and Woosley (1988). The difference between the TeV and GeV light curves, evident after only a few years, illustrates the necessity of taking account of diffusion and adiabatic deceleration.

Several experiments sensitive in both the TeV (air Cherenkov arrays) and the 100 TeV (air shower arrays) region are operating in the Southern hemisphere and have searched for high energy signals from SN1987A since its discovery. The experiments cover a range of time periods and energies, but none of these experiments has at present reported a continuous signal from the supernova. However, many of the reported flux upper limits (see Harding 1989, for review) are based on measurements taken before the time when the shell is expected to become optically thin. The only signal reported so far is from the JANZOS air shower experiment, which observed a transient flux of photons above 3 TeV on January 14-15, 1988 of $F_\gamma(> 3\text{TeV}) \sim 2 \times 10^{-11}\,\text{cm}^{-2}\,\text{s}^{-1}$ at the $4\sigma$ level (Bond *et al.* 1988b).



FIG. 5 - Minimum proton luminosity vs. proton spectral index required for a detectable signal by air shower experiments and by EGRET, using sensitivity limits from Gaisser *et al.* (1989), Ciampa *et al.* (1988), Bond *et al.* (1988a) and Kanbach *et al.* (1988).
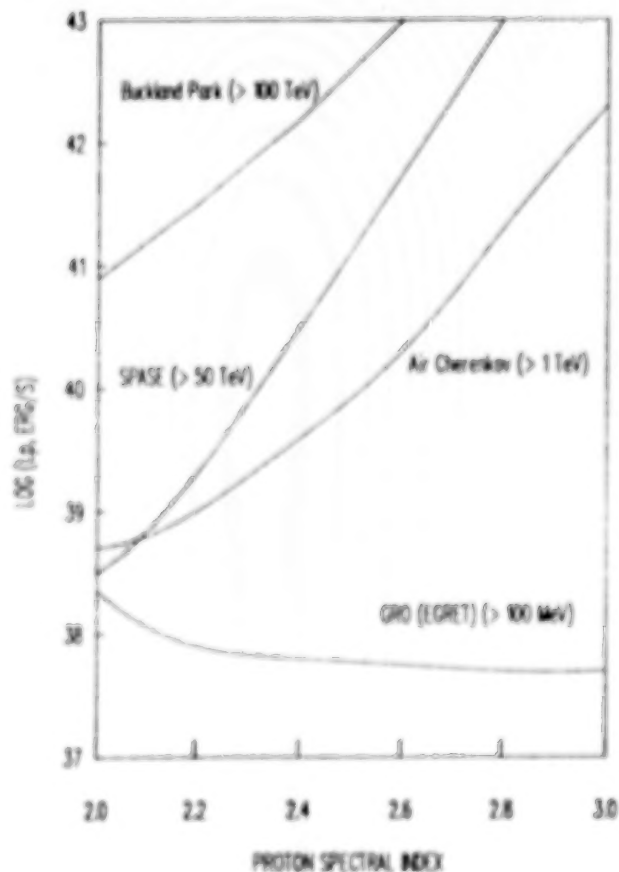
Figure 5 shows the dependence on proton spectral index of the minimum proton luminosity required for detection of a signal by various instruments, using the model of GHS. Because of its high altitude and favorable location (the supernova is always at the same zenith angle of $21^\circ$), the South Pole Air Shower Array (SPASE) has a relatively low threshold, less than 50 TeV. From Figure 5, it is evident that detectors with higher energy thresholds are more sensitive to the proton spectral index. Given the pulsar power limit of $10^{38}$ erg/s from the bolometric light curve, which may now be levelling off (Bouchet et al. 1990), the ground-based air shower detectors will only be able to see a signal from SN1987A if the proton spectral index is near 2. As the proton spectral index increases, more of the power appears at lower $\gamma$-ray energies. The EGRET detector is most sensitive around the $\pi^0$-decay peak and would detect a $\gamma$-ray signal more easily for higher proton spectral indices, but is in fact the most sensitive even for spectral index 2.

If a TeV signal is seen, the accompanying $\gamma$-ray flux around 100 MeV should be well above threshold for detection by EGRET, which has a sensitivity level of $5 \times 10^{-8}$ cm$^{-2}$s$^{-1}$. Comparison of the curves in Fig. 5 shows that even if there is no visible TeV signal there could still be a detectable signal around 0.1-1 GeV. This could happen if the proton spectrum cuts off below 10 TeV or if it is too steep to produce an observable signal above 1 TeV. An interesting possibility remains for observing a high luminosity $\gamma$-ray signal from SN1987A. Woosley and Chevalier (1989) have suggested that the 0.5 ms observed optical periodicity (Kristian et al. 1989) is the rotation period of a central pulsar which has been spun up by accretion of $\approx 0.1 M_\odot$ of the inner envelope that did not reach escape velocity in the explosion. A strong surface magnetic field, temporarily buried by the accreted material, may eventually emerge and the pulsar could turn on with a very high spin-down luminosity.

b) Binary Pulsars

Acceleration of protons at pulsar wind shocks in binary systems may also produce observable VHE and UHE $\gamma$-rays through nuclear interactions. If the target material in these systems is provided by the companion star wind or atmosphere, the $\gamma$-ray signal would be periodic with the binary orbital period. If the shock is near the companion then the target subtends a relatively large solid angle at the proton source (i.e. the shock). This model therefore can convert accelerated proton luminosity into $\gamma$-rays more efficiently than models in which the protons are accelerated at the pulsar. There are a number of known binary sources where acceleration in a pulsar wind shock could be occurring. The binary X-ray source Cygnus X-3 has been reported to be a source of TeV and possibly PeV $\gamma$-rays at the 4.8 hr X-ray period. Both accretion and pulsar rotation have been suggested as the power source in this system, but the energy implied by the TeV and PeV $\gamma$-rays may favor (and perhaps require) a pulsar. There are also a number of binary systems known to contain spinning-down pulsars. The recent discovery of an eclipsing radio pulsar (Fruchter et al. 1988) has generated considerable interest in the interaction of a pulsar wind with a companion star.

The observed parameters of these systems may be used to compute the flux of pion-decay $\gamma$-rays expected in the pulsar wind model. The integral photon flux at Earth, averaged over

the orbital period of the binary, may be written as

$$\Phi_\gamma(> E_\gamma) = \frac{\Delta\phi_\gamma}{\Delta\Omega\, d^2} \frac{\Delta X}{\lambda}\, \epsilon_\gamma\, \epsilon_p\, L_d, \tag{14}$$

where $\Delta\Omega$ is the solid angle into which the accelerated protons are emitted, $d$ is the distance to Earth, $\Delta\phi_\gamma$ is the duty cycle which represents the fraction of the orbital period during which photons are emitted toward the observer, $\epsilon_\gamma$ is the gamma-ray production efficiency, $\epsilon_p$ is the efficiency for proton acceleration, $\Delta X$ is the target thickness and $\lambda \approx 60\,\mathrm{g\,cm^{-2}}$ is the proton interaction length. The factors in this equation have been grouped in this way for comparison with earlier estimates of the relation between the observed signal and luminosity at the source, especially the estimate of Hillas (1984) for Cygnus X-3. In addition, for $E_\gamma > 10^{14}$ eV, absorption of photons in the microwave background due to $\gamma\gamma \to e^+e^-$ must be accounted for.

## TABLE 1
## GAMMA-RAY FLUX FROM BINARY PULSARS

| PSR | P (ms) | Log($\dot{P}$) | $P_b$ (days) | d (kpc) | $L_d$ (erg/s) | $E_p^{max}$ (TeV) | $\Phi_\gamma(> 1\mathrm{TeV})$ (ph cm$^{-2}$s$^{-1}$) | $\Phi_\gamma(> 100\mathrm{MeV})$ (ph cm$^{-2}$s$^{-1}$) |
|---|---|---|---|---|---|---|---|---|
| 1913+16 | 59 | -17.1 | 0.32 | 4.33 | 1.6 (33) | 50.3 | 4.5 (-14) | 7.3 (-10) |
| 0655+64 | 195.6 | -18.2 | 1.03 | 0.27 | 3.4 (30) | 2.35 | — | 5.9 (-10) |
| 1831-00 | 520.9 | -17 | 1.81 | 3.13 | 2.9 (30) | 2.15 | — | 3.6 (-12) |
| 1855+09 | 5.4 | -19.8 | 12.33 | 0.44 | 4.1 (33) | 81.2 | 1.2 (-11) | 1.6 (-7) |
| 2303+46 | 1066.4 | -15.4 | 12.34 | 2.0 | 1.3 (31) | 4.64 | — | 3.7 (-11) |
| 1953+29 | 6.1 | -19.5 | 117.35 | 2.92 | 5.7 (33) | 95.6 | 4.2 (-13) | 5.5 (-9) |
| 0820+02 | 864.9 | -16 | 1232.4 | 0.79 | 6.3 (30) | 3.18 | — | 1.2 (-10) |
| 1957+20 | 1.61 | -19.9 | 0.381 | 1.0 | 1.2 (35) | 445 | 8.9 (-11) | 8.9 (-7) |
| 1620-26 | 11.1 | -18.1 | 191.44 | 2.1 | 2.4 (34) | 195 | 3.6 (-12) | 4.2 (-8) |
| CYG X-3 | 12.6 | -13.5 | 0.2 | 10 | 6.2 (38) | 3 (4) | 3.4 (-9) | 3.4 (-5) |

Table 1 lists the known binary pulsars with some of their observed parameters: pulsar period $P$, period derivative $\dot{P}$, orbital period $P_b$ and distance $d$ (cf. Dewey $et\ al.$ 1986). Source distances (except for Cyg X-3) were determined from radio pulse dispersion measure, assuming a mean interstellar electron density $(n_e) = .03\,\mathrm{cm^{-3}}$. The table also shows the pulsar dipole luminosity from Eqn (1), the maximum energy of protons which could be accelerated at the pulsar wind shock from Eqn (13) and the predicted $\gamma$-ray fluxes, $\Phi_\gamma$, above 1 TeV and 100 MeV. According to Eqn (13), the maximum proton acceleration energy may depend on shock radius in those systems where $r_s/a \ll 1$. Determination of the shock radius, however, requires knowing what confines the pulsar wind, $i.e.$, companion star wind, atmosphere or magnetosphere. The maximum proton energies listed in the table do not include any geometrical reduction factor, so for some of the sources the actual shock acceleration energy could be much lower. The predicted $\gamma$-ray fluxes are calculated from Eqn (14), assuming a thick target $(\Delta X = \lambda)$, a proton solid angle $\Delta\Omega = 1$ sr, proton

acceleration efficiency $\epsilon_p = 0.5$ and gamma-ray duty cycle $\Delta\phi_\gamma = 1$ (which effectively gives a peak flux). The gamma-ray production efficiency, $\epsilon_\gamma$, is computed from a convolution of the differential spectrum of accelerated protons, assumed to be a power law with index $\alpha = 2$, with the target density, the production cross section for $\pi^0$'s and the $\pi^0$ decay spectrum (Gaisser 1988, Harding and Gaisser 1990). The bremsstrahlung emission from secondary leptons has been ignored.

The low mass X-ray binary Cygnus X-3 has been observed as a source of TeV and possibly PeV $\gamma$-rays at the 4.8 hr X-ray period (see Goodman 1989, for review). The luminosity required in accelerated protons to produce the observed $\gamma$-ray flux could be as high as $10^{39}$ erg/s (Hillas 1984; Nagle, Gaisser and Protheroe 1988), depending on assumptions about the beaming factor and spectrum. Since this power exceeds the Eddington limit for accretion onto a neutron star, it has been suggested that the power source is rotational energy release by a fast pulsar (Bignami et al. 1973, Vestrand and Eichler 1982). A period of 12.6 ms in TeV $\gamma$-rays has been reported by the Durham group (Chadwick et al. 1985). The periodicity, not yet confirmed by other groups (Ramana-Murthy 1989), appears sporadically in the signal and measurements of changes in this period over $\approx 7$ years give a period derivative $\dot{P} \approx 3 \times 10^{-14}$ s s$^{-1}$ (Turver 1989, priv. comm.). If interpreted as electromagnetic dipole spin-down of a pulsar, these values of $P$ and $\dot{P}$ give a magnetic field strength of $6 \times 10^{11}$ G and dipole luminosity $6 \times 10^{38}$ erg s$^{-1}$.

Since the shock location and maximum proton acceleration energy depend on the pulsar dipole luminosity, the pulsar period and magnetic field need not be known separately in applying the pulsar wind shock model to the Cyg X-3 system. The maximum proton acceleration energy, $E_p^{max}$, scales with $L_d^{1/2}$. Assuming the dipole luminosity $L_d = 6 \times 10^{38}$ erg s$^{-1}$ implied by the values of $P$ and $\dot{P}$ observed by Chadwick et al. (1985) gives $E_p^{max} = 3 \times 10^4$ TeV. Because Cygnus X-3 is a close binary, the geometrical factor in Eqn (13) is close to unity. Using the formula in Eqn (14) for two values of proton spectral index $\alpha$, the predicted flux of $>$ TeV $\gamma$-rays from the source is $3.4 \times 10^{-9}$ ph cm$^{-2}$ s$^{-1}$ for $\alpha = 2$ and $3.0 \times 10^{-11}$ ph cm$^{-2}$ s$^{-1}$ for $\alpha = 2.7$. The predicted flux of $> 100$ MeV $\gamma$-rays is $3.4 \times 10^{-5}$ ph cm$^{-2}$ s$^{-1}$ for $\alpha = 2$ and $1.9 \times 10^{-4}$ ph cm$^{-2}$ s$^{-1}$ for $\alpha = 2.7$. In order to compare with phase-averaged observed fluxes, the peak flux predictions should be multiplied by the observed 4.8 hr duty cycle, $\Delta\phi_\gamma \approx 0.1$. With the assumptions made, the $\alpha = 2$ TeV flux predicted for Cygnus X-3 is greater than has been observed (Dowthwaite et al. 1984). The $> 100$ MeV fluxes tabulated are consistent with the SAS 2 measurement (SAS 2 is $1.1 \times 10^{-5}$ above 35 MeV, Lamb et al. 1977, Fichtel et al. 1987 and earlier references therein), but are somewhat above the upper limit from the COS B observations (Hermsen et al., 1987), which is about $10^{-6}$ for $> 70$ MeV photons. The primary reason that the predicted fluxes are high in the pulsar wind acceleration model is because of the much higher efficiency for generating a gamma-ray signal from Cyg X-3 than the Vestrand-Eichler model. Since the accelerator is closer to the target material, a greater fraction of the accelerated protons can interact to produce gamma-rays. Consequently, the fraction of the pulsar spin-down power which is converted to accelerated protons need not be as large. Alternatively, emission from the source may be sporadic at the highest energies.

A number of radio pulsars have been discovered in binary systems and some of these could possibly be observable sources of high energy $\gamma$-rays. Since the parameters of the companion star winds are not determined in these systems (in several systems, the companion is probably a neutron star and a wind would not be expected) it was assumed that $r_s \ll a - r_*$ to

calculate $E_p^{max}$. There are several sources (aside from Cyg X-3) for which the predicted fluxes of $> 100$ MeV $\gamma$-rays are above or near EGRET sensitivity threshold of $5 \times 10^{-8}$ ph cm$^{-2}$s$^{-1}$. Because of the dependence of maximum proton energy on pulsar luminosity, these are also the systems capable of producing $\gamma$-rays above 1 TeV. One of these, PSR1957+20, is the eclipsing millisecond pulsar believed to be evaporating its companion by means of an induced wind (Phinney *et al.* 1988, Kluzniak *et al.* 1988, Cheng 1989). If the mass loss from the companion is sufficient to evaporate it in the pulsar's lifetime ($\dot{M} \approx 10^{16}$ g/s), then Eqn (7) gives a shock distance of $r_s/a \approx 0.6$, or a stand-off distance from the companion of $0.4a$, corresponding roughly to the required eclipse radius. Another system, PSR1855+09, contains a 5 ms pulsar and is at a distance of less than 500 pc, giving a predicted flux $> 100$ MeV which is well above EGRET sensitivity.

Recently, emission at TeV energies has been reported by von Ballmoos *et al.* (1989) and de Jager *et al.* (1989) from these two binary pulsars. Data from PSR1957+20, folded with the 9 hr orbital period, shows a peak in the phase plot at the position of the $L4$ Lagrange point. The reported peak flux above 2 TeV is $1.1 \times 10^{-9}$ photons cm$^{-2}$s$^{-1}$, much higher than the predicted flux in Table 1. This difference is due to the small $\gamma$-ray solid angle of $\Delta\Omega \approx .009$ derived by von Ballmoos *et al.* (1989) from the width of the phase peak ($\Delta\phi_\gamma = .018$), whereas $\Delta\Omega = 1$ sr was taken to compute the fluxes in Table 1. A peak at the $L4$ position in the orbital phase plot of PSR1957+20 may also have been seen at $> 100$ MeV in COS-B data (von Ballmoos *et al.* 1989). A TeV signal was also reported by de Jager *et al.* (1989) at the 5.4 ms pulsar period of PSR1855+09 at a marginal significance level. Signals which are observed to be pulsed at the pulsar period, however, must originate from acceleration near or within the pulsar magnetosphere and would not be expected from particles accelerated at the pulsar wind shock.

The currently favored model for the origin of binary systems containing short period pulsars is spin up by an accretion disk (Alpar *et al.* 1982). The accretion spin-up period depends on the neutron star magnetic field, with a spin-up period in the 10 ms range requiring a field around $10^9$ Gauss. This evolution model accounts quite well for the observed binary pulsars, which all have low magnetic fields. The high luminosity implied by the observed Cyg X-3 gamma-ray flux requires not only a short period but also a high magnetic field, incompatible with an accretion spin-up evolution. A fast pulsar as the power source in Cyg X-3 would therefore have originated in a relatively recent supernova explosion that occurred within the pulsar spin-down time of 7000 yr. Confined pulsar wind sources of this type would be more rare than the accretion spun-up binary pulsars, which have ages of around $10^8$ yr.

## V. CONCLUSION

Pulsars are one of the most important sources planned for study by EGRET. Although the primary focus will be the detection of pulsed gamma-ray signals, the possibility of shock acceleration in sources containing pulsars makes the search for steady gamma-rays from young supernovae and gamma-rays pulsed at the orbital period of binary pulsars also worthwhile. Observation of evidence for proton acceleration in supernovae would be very exciting. Although a steady high energy gamma-ray signal has yet to be detected from SN1987A with current ground-based detectors, EGRET may offer the best sensitivity and therefore the best chance for observing a signal from this source. Evidence for proton acceleration

in binary systems may already have been observed in the form of > TeV gamma-rays from Cyg X-3 and several other binary X-ray sources.. The current controversy surrounding the existence of a periodic 4.8 hr signal in 100 MeV gamma-rays from Cyg X-3 will hopefully be resolved by EGRET. In addition, several radio pulsars in binary systems appear to be good gamma-ray source candidates. Those with the shortest orbital periods would be the easiest to identify in a limited observing time.

The pulsar wind shock model described here is only one possibility for particle acceleration near pulsars. However, it provides a means for channelling a large fraction of the full rotational energy loss of the pulsar into relativistic particles. If EGRET is able to detect gamma-rays from some of these systems, it may also be possible to identify the peak at 70 MeV which is the signature of pion-decay, indirect evidence for proton acceleration. Furthermore, any indication that efficient particle accelerators exist in binary systems known to contain spinning-down pulsars will help in understanding systems like Cyg X-3, where the source of power is still a mystery.

## REFERENCES

Alpar, M. A., Cheng, A. F., Ruderman, M. A. and Shaham, J. 1982, *Nature*, **300**, 728.

Arons, J. 1981, in *IAU Symposium 94: Origin of Cosmic Rays*, eds. G. Setti, G. Spada and A. W. Wolfendale (Reidel, Dordrecht), p. 175.

Axford, W. I., Leer, E. and Skadron, G. 1977, *Proc. 15th Intl Cosmic Ray Conf.*, **11**, 132.

Berezinsky, V.S. and Ginzburg, V.I. 87, *Nature*, **329**, 807.

Berezinsky, V.S., and Prilutsky, O. 78, *Astr. Astrophys*, **66**, 325.

Bignami, G. F., Maraschi, L. and Treves, A. 1973, *Astron. Astrophys.*, **55**, 155.

Blandford, R. D. and Ostriker, J. P. 1978, *Ap. J. Letters*, **221**, L29.

Bond, I.A. *et al.*, 1988a, *Phys. Rev. Letters*, **61**, 1110.

Bond, I. A. *et al.*, 1988b, *Phys. Rev. Letters*, **61**, 2292.

Bouchet, P., Danziger, I. J. and Lucy, L. B. 1990, IAU Circular No. 4933.

Chadwick, P. M. *et al.* 1985, *Nature*, **318**, 642.

Cheng, A. F. 1989, *Ap. J.*, **339**, 291.

Ciampa, D. *et al.*, 1988, *Ap. J. Letters*, **326**, L9.

de Jager, O. C. *et al.* 1989, *Nuclear Phys. B (Proc. Supp.)*, in press.

Dewey, R. J. *et al.* 1986, *Nature*, **322**, 712.

Dowthwaite *et al.* 1984, *Nature*, **309**, 691.

Drury, L. O'C. 1983, *Rep. Prog. Phys.*, **46**, 973.

Fichtel, C. E., Thompson, D. J. and Lamb, R. C. 1987, *Ap. J.*, **319**, 362

Fruchter, A. S., Stinebring, D. R. and Taylor, J. H. 1988, *Nature*, **333**, 237.

Gaisser, T. K. 1988, in *Proc. Snowmass Summer Workshop*, in press.

Gaisser, T. K. *et al.*, 1989, *Phys. Rev. Letters*, **62**, 1425.

Gaisser, T. K., Harding, A. K. and Stanev, T. 1987, *Nature*, **329**, 314.

Gaisser, T. K., Harding, A. K. and Stanev, T. 1989, *Ap. J.*, **345**, 423.

Goodman, J. 1989, *Nuclear Physics B (Proc. Supp.)*, in press.

Harding, A. K. 1989, *Proc. 14th Texas Symposium on Relativistic Astrophysics*, ed. E. Fenyves, in press.

Harding, A. K. and Gaisser, T. K. 1990, *Ap. J.*, submitted.

Harding, A. K., Mastichiadis, A. and Protheroe, R. J. 1990a, in *Proc. of 21st Intl. Cosmic Ray Conf.*, in press.

Harding, A. K., Mastichiadis, A. and Protheroe, R. J. 1990b, *Ap. J.*, in preparation.

Hermsen, W. *et al.* 1987, *Astron. Astrophys.*, **175**, 141.

Hillas, A. M. 1984, *Nature*, **312**, 50.

Kanbach, G. *et al.*, 1988, *Space Sci. Rev.*, **49**, 69.

Kennel, C. F. and Coroniti, F. V. 1984, *Ap. J.*, **283**, 694.

Kirk, J. G. and Schneider, P. 1987, *Ap. J.*, **315**, 425.

Kluzniak, W., Ruderman, M. A., Shaham, J. and Tavani, M. 1988, *Nature*, **334**, 225.

Kristian, J. *et al.*, 1989, *Nature*, **338**, 234.

Lagage, P. O. and Cesarsky, C. J. 1983, *Astr. Ap.*, **125**, 249.

Lamb. R. C., Fichtel, C. E., Hartman, R. C., Kniffen, D. A. and Thompson, D. J. 1977, *Ap. J. Letters*, **212**, L63.

Nagle, D. E., Gaisser, T. K. and Protheroe, R. J. 1988, *Ann. Rev. Nucl. Part. Sci.*, **38**, 609.

Nakamura, T., Yamada, Y., and Sato, H. 1987, *Progr. theor. Phys.*, **79**, 1065.

Pacini, F. and Salvati, M. 1973 *Ap. J.*, **186**, 249.

Peacock, J. A. 1981, *M.N.R.A.S.*, **196**, 135.

Phinney, E. S., Evans, C. R., Blandford, R. D. and Kulkarni, S. R. 1988, *Nature*, **333**, 832.

Pinto, P.A. and Woosley, S.E. 1988 *Nature*, **333**, 534.

Ramana-Murthy, P. V. 1989, *Nuc. Phys. B (Proc. Supp.)*, in press.

Rees, M. J. and Gunn, J. E. 1974, *M.N.R.A.S.*, **167**, 1.

Ruderman, M. A., Shaham, J., Tavani, M. and Eichler, D. 1989, *Ap. J.*, **343**, 292.

Sato, H. 1977, *Prog. Theor. Phys.* **58**, 549.

Shapiro, M.M. and Silberberg, R. 1979, in *Relativity, Quanta and Cosmology* (ed. DeFinis, F.) (Johnson Reprint Corporation, New York), **2**, 745.

Vestrand, W. T. and Eichler, D. 1982, *Ap. J.*, **261**, 251.

Von Ballmoos, P. *et al.* 1989, *Proc. of GRO Science Workshop*, p. 4-182.

Woosley, S. E. and Chevalier, R. A., 1989, *Nature*, **338**, 321.

Yamada, Y., Nakamura, T., Kasahara K., and Sato, H. 1987, *Progr. Theor. Phys.*, **79**, 426.

# DISCUSSION

*Volker Schonfelaer:*

In the gamma-ray spectrum from SN1987, which you showed, there was a gap between the $\pi^\circ$ - decay component and the electron synchrotron component. Would this gap not be filled by bremsstrahlung of secondary electrons from $\pi^\pm$ production?

*Alice Harding:*

Bremsstrahlung from secondary electrons and positions would be present depending on the strength of the magnetic field and the density in the envelope. In the pulsar wind model, the magnetic field is high enough where the protons interact to make synchrotron radiation dominate the secondary lepton's energy loss.

*Mal Ruderman:*

Characteristic estimates for $e^-/e^+$ energies in a pulsar wind suggest TeV (and perhaps more in many cases). Even before reaching a shock boundary these electrons can produce TeV gamma-rays by compton scattering on optical light (or IR) from a nearby companion in close binaries or other sources in SNR's. Has this contribution to TeV gamma-ray emission from pulsar winds been considered?

*Alice Harding:*

To my knowledge, no one has made a calculation of this contribution.

# Spectral Determinations for Discrete Sources with EGRET

E. B. Hughes and P. L. Nolan
W. W. Hansen Laboratories
Stanford University
Stanford, CA 94305

## Abstract

The ability of the EGRET telescope to determine the spectral parameters of point sources in 14-day exposures, as planned for the initial survey phase of the GRO mission, is explored by numerical simulation. Results are given for both galactic and extragalactic objects as a function of source strength and for representative levels of diffuse background emission.

## I. Introduction

Four of the discrete sources in the second COS-B catalog (Swanenburg *et al.* 1981) have intensities strong enough for spectral measurements to be made in the range 50 MeV to 3 GeV. These are the Crab and Vela pulsars, the source 2CG 195+04 (Geminga), and the quasar 3C273. The pulsed emission from the Crab can be represented by a power law with an index $-2.00 \pm 0.10$ from 50 MeV to 3 GeV (Clear *et al.* 1987), while the pulsed output from Vela is best fitted with an index $-1.72 \pm 0.07$ from 50–300 MeV and a steeper index $-2.12 \pm 0.07$ from 300–3,000 MeV (Grenier, Hermsen, and Clear 1988). The source 2CG 195+04 exhibits a spectral index of $-1.8$ in the range 100 MeV to 3.2 GeV (Masnou *et al.* 1981), while 3C273 displays a spectral shape that can be characterized by a power law index of $-2.5^{+0.6}_{-0.5}$ in the range 50 MeV to 800 MeV (Bignami *et al.* 1981). The remaining 21 sources identified by COS-B are too weak, relative to the COS-B sensitivity, to permit spectral measurements, but all are broadly consistent with an index of $-2.0$ when the flux ratio of $\gamma$ rays above 100 MeV and 300 MeV respectively is examined. In general, the shape of the observed spectrum of high-energy $\gamma$ rays is expected to be a good indicator of the physical mechanism responsible for their production.

Just as the EGRET telescope, due to its larger effective area, improved directional sensitivity and better energy resolution, is expected to be able to detect discrete $\gamma$ ray sources with a threshold sensitivity approximately a factor of 20 below that of COS-B, so should EGRET also, for the same reasons, be able to provide spectral determinations for sources weaker than the four already characterized. In this note, for the source strengths accessible to EGRET, we examine the precision of the spectral determinations that should be forthcoming.
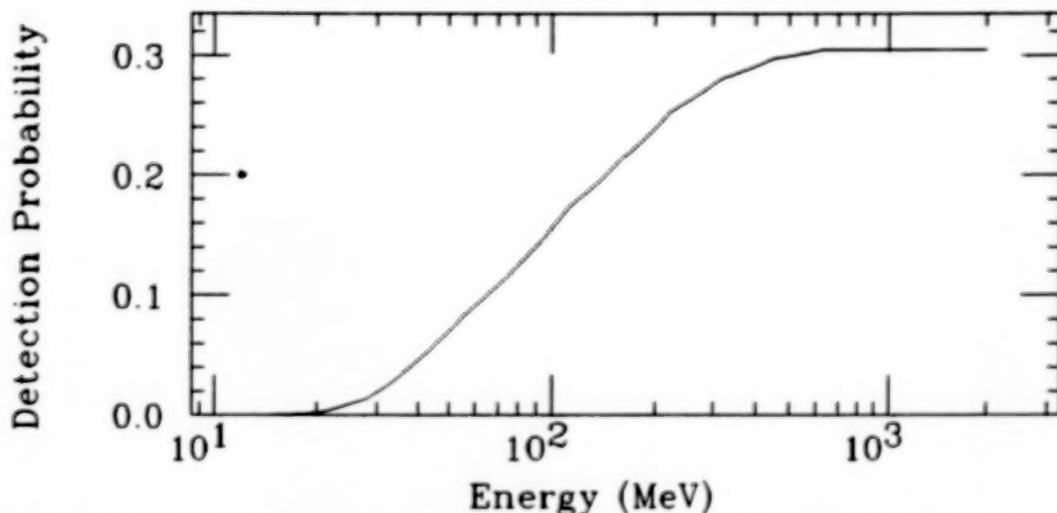
Figure 1: Approximate EGRET detection efficiency used in the simulations. The maximum efficiency of 0.3 corresponds to an effective area of 2000 cm$^2$.

## II. Method

Our method of analysis is to simulate an EGRET observation, typically for a 14-day period, under the assumption that both the point source and the local diffuse background are characterized by a power law emission spectrum $I(E) = AE^{-\alpha}$. This observation is then analyzed to determine the source parameters $A$ and $\alpha$. By repetition of the EGRET simulation and parameter determination, usually for 100 trials, the measured uncertainties on the parameters $A$ and $\alpha$ are established.

The EGRET efficiency for $\gamma$-ray detection is assumed to vary with energy as shown in Figure 1, and the lineshape for $\gamma$-ray energy measurement to be as shown in Figure 2. The EGRET angular resolution for $\gamma$ rays, projected onto one transverse dimension, is assumed to follow the power law $\sigma_{rms}(E) = k(E/1\,\text{MeV})^{-0.6}$ with $k = 56°$. This is accommodated in the spectral simulations by defining an acceptance cone, of half angle $\theta(E)$, relative to the source direction. The width of this cone is taken as proportional to $\sigma_{rms}(E)$ with a proportionality constant $C$. The fraction of source counts $f$ accepted at any energy by the cone is then $f = 1 - e^{-C^2/2}$, which for $C = 1.5$ is 0.68. The EGRET characteristics just defined are not those that will eventually emerge from a detailed analysis of the EGRET calibration data. They are simply approximations made for the purpose of the present calculations. For example, they do not reflect the probable exclusion of edge events with degraded energy resolution or a possible reduction in detection efficiency at the highest energies due to self-veto from backscattered soft photons.
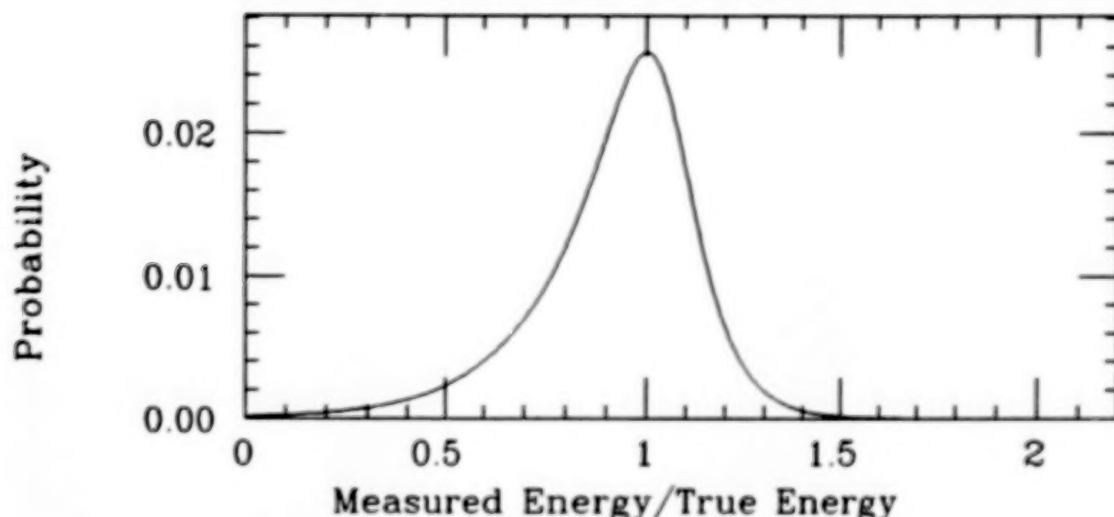
202

Figure 2: Approximate EGRET energy response function used in the simulation.

Consider the simulation of a point source equal in intensity to the pulsed emission from the Crab; viz. $I(E) = 4.8 \times 10^{-4} E^{-2.10}$ γ rays cm$^{-2}$s$^{-1}$MeV$^{-1}$. The observing time is 14 days, the duty factor (due to earth occultation and SAA transits) is 50%, the maximum EGRET effective area is 2000 cm$^2$ and the acceptance cone efficiency is 68%. The mean number of incident γ rays during this observation, N, is first obtained by analytical integration. Thereafter, for each simulation, the actual number of incident γ rays is randomized with a variance of N. The simulation is carried out by randomly selecting γ rays from the assumed spectrum and, for each such γ ray, consulting Figure 1 to decide, in a random way, if the γ ray is detected. For detected γ rays the measured energy is assigned by random selection from the resolution function specified in Figure 2 and the event is assigned to an appropriate energy bin.

In addition to the source, an overlapping diffuse background is also in general detected. Simulation of this background flux proceeds as for the source itself with the assumption that its strength, at all energies, is constant over the relevant acceptance cone of the instrument. The number of background γ rays at any energy, unlike the source, is proportional to the solid angle of the acceptance cone. This means that if the source and background have similar spectral shapes, the ratio of source to background counts increases rapidly with increasing γ ray energy.

Table I shows the average number of source and background counts obtained for the simulation of a source with Crab-like intensity in the presence of a background typical of the Crab environment. The counts are distributed in 20 bins of logarithmically increasing
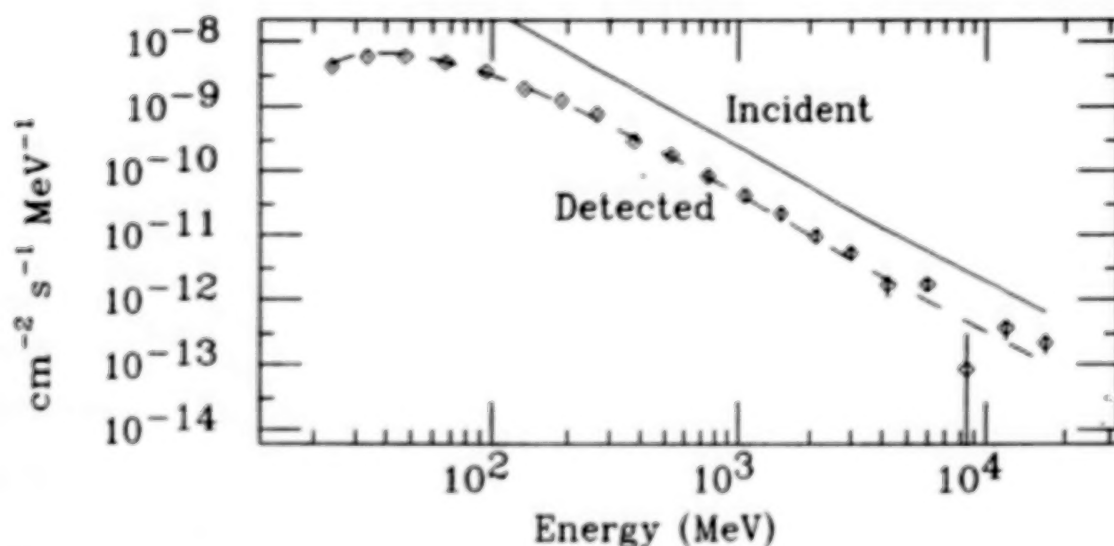
Figure 3: A typical simulation of the measured spectrum of a source with Crab-like intensity and background.

---

width over the nominal EGRET range of 20–20,000 MeV. The simulation actually extends to energies above and below this range, to reproduce properly the population of the extreme bins due to the EGRET energy lineshape.

In the analysis of a simulated EGRET observation, the first step is to subtract from the observed spectrum (source plus background) an estimate of the measured background. The latter is obtained by simulating the background spectrum many times, usually for 1,000 trials, and taking the mean. The resultant statistical errors in the mean spectrum are thus very small. This is justified because, in principle, for any EGRET observation the overlapping background can be deduced from a statistical analysis or modelling of the relatively large background field surrounding the source that will also be observed. The result of a simulation for a source with Crab-like intensity in the presence of a background typical of the galactic anticenter region is shown in Figure 3.

The source parameters are determined by minimizing the function

$$\chi^2 = \sum_j w_j (n_j - b_j - C_j(A, \alpha))^2, \tag{1}$$

where the summation extends over the energy bins defined by the observation, $n_j$ is the number of photons observed in energy bin $j$, $b_j$ is the expected number of background counts, $C_j(A, \alpha)$ is the expected number of counts due to the trial source spectrum, and $w_j = n_j^{-1}$ is a weighting factor. The use of this weighting factor actually introduces a

| Bin | Energy (MeV) | Source counts | Bkgd. counts |
|---|---|---|---|
| 1 | 20–28 | 143.5 | 584.1 |
| 2 | –40 | 293.6 | 892.4 |
| 3 | –56 | 404.8 | 883.8 |
| 4 | –80 | 437.0 | 666.9 |
| 5 | –112 | 422.2 | 430.9 |
| 6 | –159 | 370.4 | 257.5 |
| 7 | –224 | 305.7 | 142.1 |
| 8 | –317 | 237.7 | 74.6 |
| 9 | –448 | 174.3 | 35.7 |
| 10 | –632 | 123.7 | 17.1 |
| 11 | –893 | 86.7 | 8.2 |
| 12 | –1262 | 58.3 | 4.0 |
| 13 | –1783 | 39.8 | 1.7 |
| 14 | –2518 | 27.1 | 0.9 |
| 15 | –3557 | 18.5 | 0.4 |
| 16 | –5024 | 12.9 | 0.2 |
| 17 | –7096 | 8.5 | 0.1 |
| 18 | –10024 | 5.8 | 0.0 |
| 19 | –14159 | 4.2 | 0.0 |
| 20 | –20000 | 2.9 | 0.0 |
|  | 20–20000 | 3177.3 | 4000.6 |

Table I: Average source and background counts for a Crab-like observation.

small bias in $\alpha$ when bin populations $n_j < 10$ are involved. The effect is to produce a best-fit model spectrum slightly steeper than the known input spectrum. Our simulations show that this bias in $\alpha$ is comparable in size to the statistical error, or smaller. It may be reduced by repeating the analysis with $w_j = (C_j + b_j)^{-1}$, with $C_j$ taken from the first iteration. This was not done for the simulations reported here because the problem has very little effect on the size of the uncertainties in $\alpha$, which are the main objective of this study.

In principle, $C_j(A, \alpha)$ is given by

$$C_j(A, \alpha) = \int_0^\infty G\varepsilon(E)R_j(E)AE^{-\alpha}dE, \tag{2}$$

where $R_j(E)$ is the probability of assigning a detected $\gamma$ ray of energy $E$ to the $j$th bin, $\varepsilon(E)$ is the detector efficiency shown in Figure 1, and $G$ is the EGRET geometric area of $\sim 6500\text{cm}^2$. In particular, for an arbitrary energy resolution function, it is simpler to
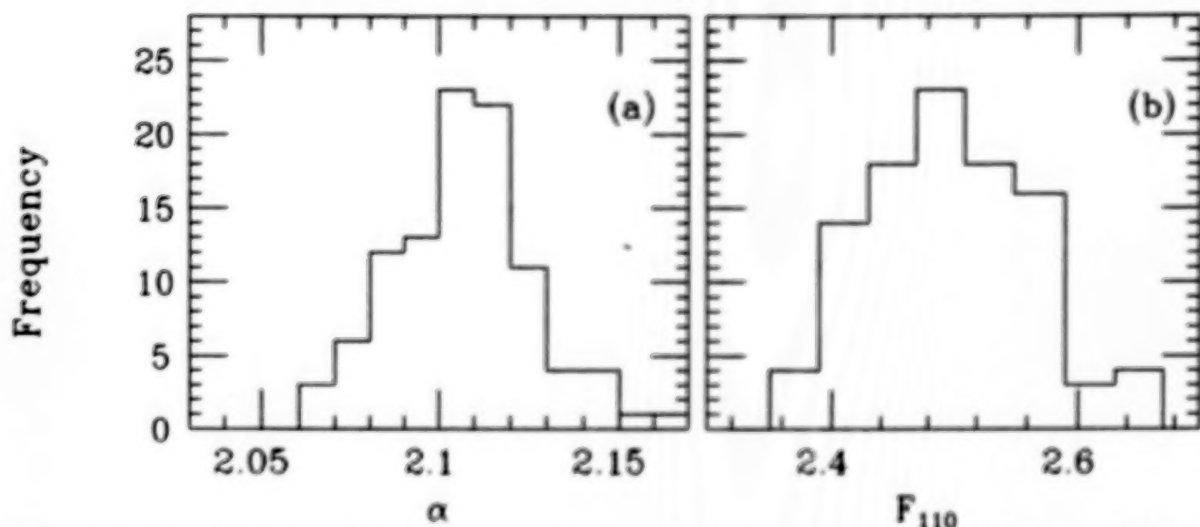
Figure 4: Distributions of fitted parameters in simulations of the Crab: (a) Spectral index $\alpha$ (mean 2.107, standard deviation 0.020). (b) Flux at 110 MeV ($= A \times 110^{-\alpha}$) in units of $10^{-8}\text{cm}^{-2}\text{s}^{-1}\text{MeV}^{-1}$.

obtain $C_j$ by numerical integration, whereby

$$C_j(A, \alpha) = \sum GR_{ij}t_i AE_i^{-\alpha} \Delta E_i. \tag{3}$$

$R_{ij}$ is an EGRET response matrix that specifies the probability that a detected $\gamma$ ray of energy $E_i$ will be found in the bin $E_j$. $R_{ij}$ is obtained in a separate calculation in which the energy response function is integrated over a set of 270 bins for true energy and typically 20 bins or fewer for observed energy. The true energy bins are chosen to be narrower than the instrument energy response function, so that $R_{ij}$ is independent of the incident spectrum.

Repetition of the above procedure provides a distribution function for the parameters $A$ and $\alpha$ from which both the mean and uncertainty of their determinations can be obtained. These distributions, for the simulation of the source with Crab-like strength and Crab-like background, are reproduced in Figure 4. The correlation between the parameters is reduced by normalizing the spectrum at the intermediate energy of 110 MeV.

### III. Results

A summary of the estimated precision with which the spectral index $\alpha$ can be determined in a 14-day EGRET observation is shown in Figure 5 for representative galactic
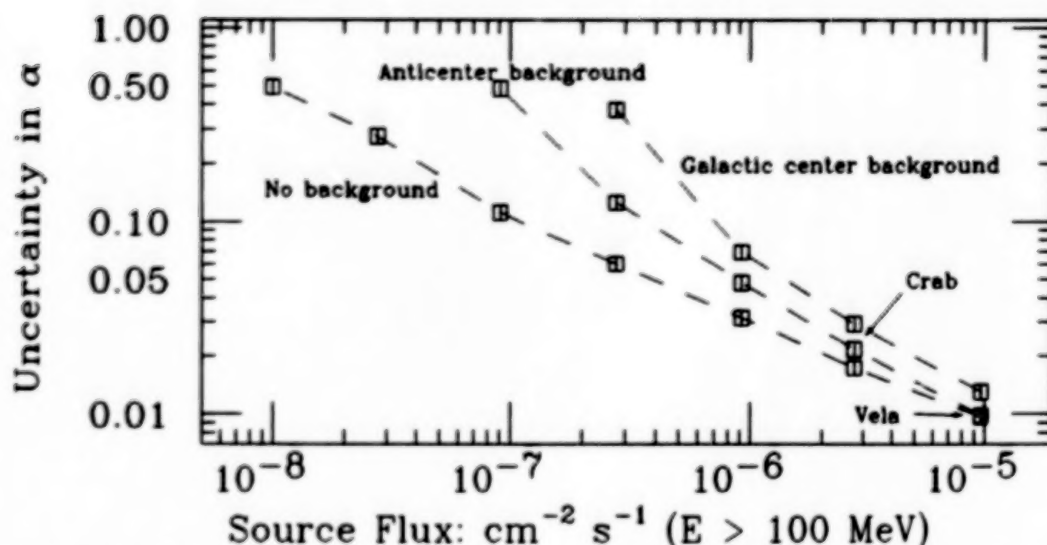
206

Figure 5: Statistical uncertainty in spectral index for galactic sources as a function of source strength for different diffuse backgrounds.

point sources. The simulated observations are generated for sources and backgrounds with a spectral index of 2.1 and results are given both as a function of the source intensity and the level of diffuse background. The influence of the latter is exhibited through the use of background intensities characteristic of the galactic center and anticenter regions, and also, for reference, in the absence of a background. For example, Figure 5 shows that the spectral index for a source of Vela-like intensity ($10^{-5}$cm$^{-2}$s$^{-1}$ ($E > 100$ MeV)) observed against a galactic anticenter background should be measureable, from a statistical standpoint, with an uncertainty close to about 0.01. This result corresponds to the detection of 11,112 source and 3,997 background counts in the range 20–20,000 MeV. For comparison, in a total elapsed observing time of 300 days COS-B was able to detect 2,412 source and 828 background counts in the range 50–5,000 MeV and thereby determine the Vela spectral index to an uncertainty of 0.07. Similarly, a single 14-day EGRET observation of a source with Crab-like intensity ($2.8 \times 10^{-6}$cm$^{-2}$s$^{-1}$($E > 100$ MeV)) with 2,177 source counts and 3,997 background counts should yield $\alpha$ with an uncertainty of 0.02, whereas it required 175 days of exposure, resulting in the detection of 800 source and 900 background counts, for COS-B to determine $\alpha$ to within 0.1. These results suggest that, with EGRET, it should be possible to search for variations in the Crab and Vela spectra, and also weaker sources, as a function of binary phase and epoch with good sensitivity.

For sources of intensity $10^{-6}$cm$^{-2}$s$^{-1}$ ($E > 100$ MeV) the spectral index is measureable by EGRET to a precision of 0.05–0.07, depending upon the background level. Such

sources are at the COS-B threshold of detectability and are too weak for COS-B to provide index measurements. For sources of strength $10^{-7}$cm$^{-2}$s$^{-1}$ (E > 100 MeV), close to the EGRET threshold of detectability, the index for those in the anticenter region is measureable to within 0.5 in 14 days. At this source strength, the measurement error becomes very sensitive to the background level and, as indicated in Figure 5, the precision of the index determination is significantly reduced as the background approaches that typical of the galactic center. The mean number of source counts that will be detected for this source strength is 397, whereas the background counts will range from 3,997 in the anticenter region to 21,320 in the galactic center region. The distribution of the detected source counts with energy may be obtained by scaling from Table I, but are reproduced, for convenience, in Table II for sources of strength $10^{-6}$ and $10^{-7}$cm$^{-2}$s$^{-1}$ (E > 100 MeV).

| Bin | Energy (MeV) | Crab counts | $10^{-6}$ counts | $10^{-7}$ counts |
|---|---|---|---|---|
| 1 | 20–28 | 143.5 | 51.2 | 5.1 |
| 2 | –40 | 293.6 | 104.9 | 10.5 |
| 3 | –56 | 404.8 | 144.6 | 14.5 |
| 4 | –80 | 437.0 | 156.1 | 15.6 |
| 5 | –112 | 422.2 | 150.8 | 15.1 |
| 6 | –159 | 370.4 | 132.2 | 13.2 |
| 7 | –224 | 305.7 | 109.2 | 10.9 |
| 8 | –317 | 237.7 | 84.9 | 8.5 |
| 9 | –448 | 174.3 | 62.2 | 6.2 |
| 10 | –632 | 123.7 | 44.2 | 4.4 |
| 11 | –893 | 86.7 | 31.0 | 3.1 |
| 12 | –1262 | 58.3 | 20.8 | 2.1 |
| 13 | –1783 | 39.8 | 14.2 | 1.4 |
| 14 | –2518 | 27.1 | 9.7 | 1.0 |
| 15 | –3557 | 18.5 | 6.6 | 0.7 |
| 16 | –5024 | 12.9 | 4.6 | 0.5 |
| 17 | –7096 | 8.5 | 3.0 | 0.3 |
| 18 | –10024 | 5.8 | 2.1 | 0.2 |
| 19 | –14159 | 4.2 | 1.5 | 0.2 |
| 20 | –20000 | 2.9 | 1.0 | 0.1 |
|  | 20–20000 | 3177.3 | 1134.8 | 113.5 |

Table II: Average source counts for Crab-like and weaker sources of $10^{-6}$ and $10^{-7}$cm$^{-2}$s$^{-1}$ (E > 100 MeV). The associated background counts are identical to those given in Table I for each source.

If the duration of an EGRET observation is extended from 2 weeks to 10 weeks, then the limitations imposed by the diffuse background, especially in the galactic center region,
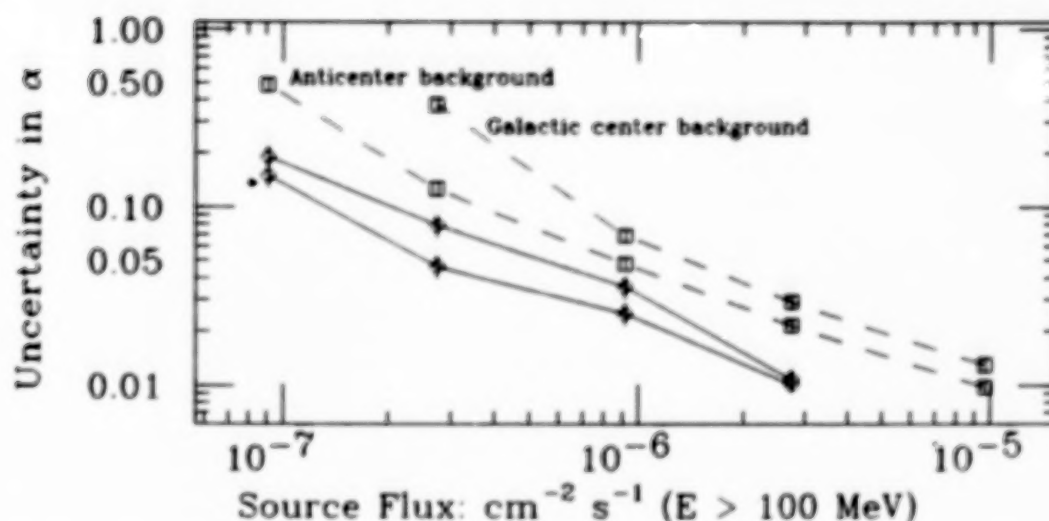
Figure 6: Uncertainty in measurement of spectral index for galactic sources as a function of observing time. Dashed lines: 2-week observations. Solid lines: 10-week observations.

are much reduced. A comparison of the results obtained for these two observing times at the two representative levels of diffuse background is shown in Figure 6. For sources of intensity close to $10^{-7}$cm$^{-2}$s$^{-1}$ (E > 100 MeV), the spectral index is measureable with an uncertainty of about 0.2.

The spectrum of the extragalactic source 3C273 was found by COS-B to be consistent with a power law index of $2.5^{+0.6}_{-0.5}$. The total observing time was 71 days. The EGRET capability, in 14-day observing periods, for representative extragalactic objects with a spectral index of 2.5 is indicated in Figure 7. In a single observation, for a source of 3C273-like intensity $(7 \times 10^{-7}$ cm$^{-2}$s$^{-1}$ $(E > 100 \text{MeV}))$, the spectral index is measureable to a precision of close to 0.05. The variation of this measurement error with source intensity and background level is given in Figure 7. This figure indicates that EGRET should be able to obtain useful spectrum measurements for extragalactic sources one tenth as strong as 3C273.

Another measure of the EGRET capability is the degree to which departures from the simple power law shape can be detected. Evidence for such a departure has been provided by the COS-B observations (Grenier, Hermsen and Clear 1988) which suggest, for the Vela pulsar, a spectral break at about 300 MeV. The preferred spectral index in the range 50–300 MeV is $1.72 \pm 0.07$, whereas in the range 300–5,000 MeV it is $2.12 \pm 0.07$. An indication of the detectability of such spectral breaks by EGRET is provided by the results summarized in Figure 8(a). These results are obtained by simulating a source of
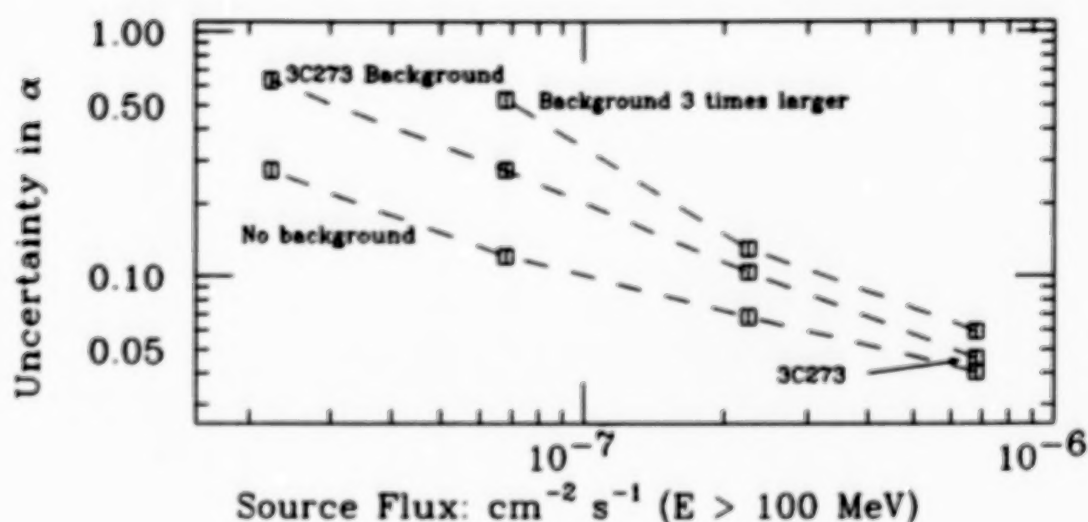
**Figure 7:** Statistical uncertainty in spectral index for representative extragalactic sources as a function of source strength for different diffuse backgrounds.

---

Crab-like intensity with a spectral break at a specified energy in the range 100–1,000 MeV. The goodness of fit to a single power law index (averaged over 30 trials) is displayed as a function of the spectral index encountered above each of the assumed break energies. Also indicated, by the dashed horizontal lines, is the confidence level with which a spectral break can be established. For example, a spectral break at 300 MeV for a source of Crab-like strength should be detectable with 95% confidence if it exceeds 0.1 in magnitude. Similar results for a source with the characteristics of 3C273 are given in Figure 8(b). The variations of the sensitivity to a spectral break with break energy revealed in Figure 8 reflect the hardness of the spectrum of each source. EGRET is least sensitive to a break at 100 MeV in the hard Crab spectrum, but it is least sensitive at 1000 MeV in the softer 3C273 spectrum.

The results in Figures 8 are summarized in a more compact fashion in Figure 9. Here the index change that can be detected with 95% confidence is shown for both the Crab and 3C273 sources as a function of the energy at which the index change occurs. These results refer to standard 14-day EGRET observations. If the observing period is longer, then improved sensitivity is achieved. Figure 10 shows the sensitivity expected for 3C273 and for galactic sources of strength 10% of the Crab if the observing period is increased to 10 weeks.
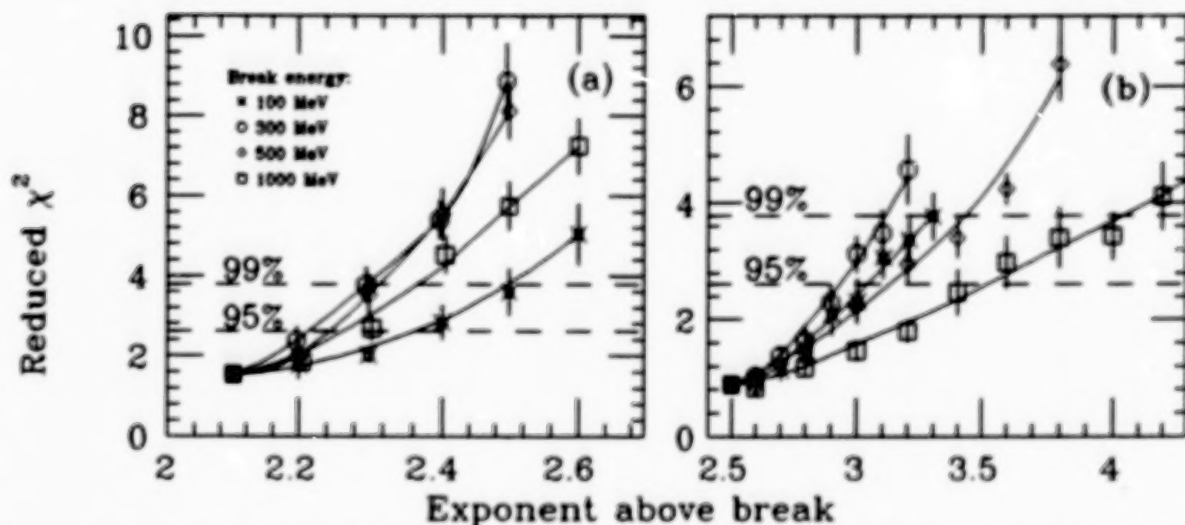
Figure 8: Goodness of fit for broken power law spectra when the fitting model is a single power law. The various curves correspond to different break energies. These simulations were done with 5 energy bins, so $\chi^2$ has 3 degrees of freedom. (a) Crab. (b) 3C273.

## IV. Summary

A quantitative exploration has been made of the capability of the EGRET telescope to measure the spectral shapes of high-energy $\gamma$-ray sources in the range 20–20,000 MeV. Using a simple power law as a reference spectrum, it is shown that for galactic objects equal in strength to 10% of the pulsed Crab emission the power law index should be measureable to better than 0.2 in the anticenter region and to a precision of about 0.4 in the galactic center region in a typical observing time of 14 days. If this observing time is extended to 10 weeks then the level of precision should be in the range 0.04 to 0.08 depending upon the local background intensity. As the source strength $S$ increases, the precision should improve, from a statistical standpoint, approximately as $S^{-1/2}$. For extragalactic objects equal in intensity to 10% of 3C273 and in background fields typical of the 3C273 environment, the spectral index should be measurable to about 0.3 in 14-day exposures. The level of precision for such objects is also examined as a function of source and background intensity. Finally, in anticipation of emission spectra more complex than the simple power law, the detectability of index changes at specific energies in power law spectra is quantified.

All of the uncertainties reported above are purely statistical. In practice, it will be necessary to be alert to systematic errors that could affect the determination of spectral parameters. These include changes over time in the detector efficiency with energy.
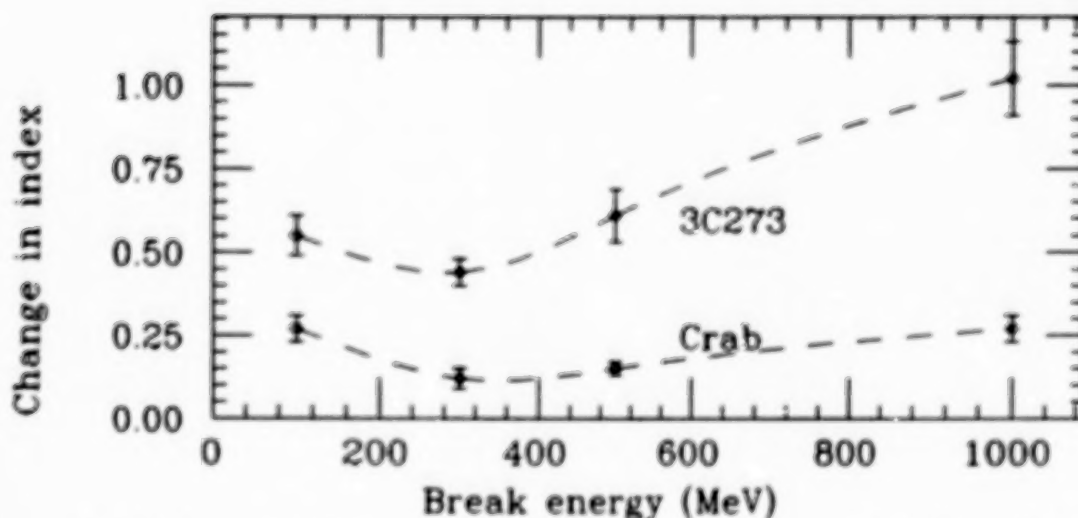
Figure 9: Minimum spectrum break detectable in 2 weeks with 95% confidence for Crab-like and 3C273-like spectra below the break.

---

To a lesser degree, the statistical fluctuations in the calibration of the efficiency and energy response function will also affect the results in a systematic way. The results also depend on the assumed parametrization of the EGRET efficiency, energy resolution, and angular resolution. The latter, in particular, determines the number of background counts detected and becomes increasingly important as the source strength decreases.

## References

Bignami, G. F., Bennett, K., Buccheri, R., Caraveo, P. A., Hermsen, W., Kanbach, G., Lichti, G. G., Masnou, J. L., Mayer-Hasselwander, H. A., Paul, J. A., Sacco, B., Scarsi, L., Swanenburg, B. N., and Wills, R. D. 1981, *Astron. Astrophys.*, **93**, 71.

Clear, J., Bennett, K., Buccheri, R., Grenier, I. A., Hermsen, W., Mayer-Hasselwander, H. A., and Sacco, B. 1987, *Astron. Astrophys.*, **174**, 85.

Grenier, I. A., Hermsen, W., and Clear, J. 1988, *Astron. Astrophys.*, **204**, 117.
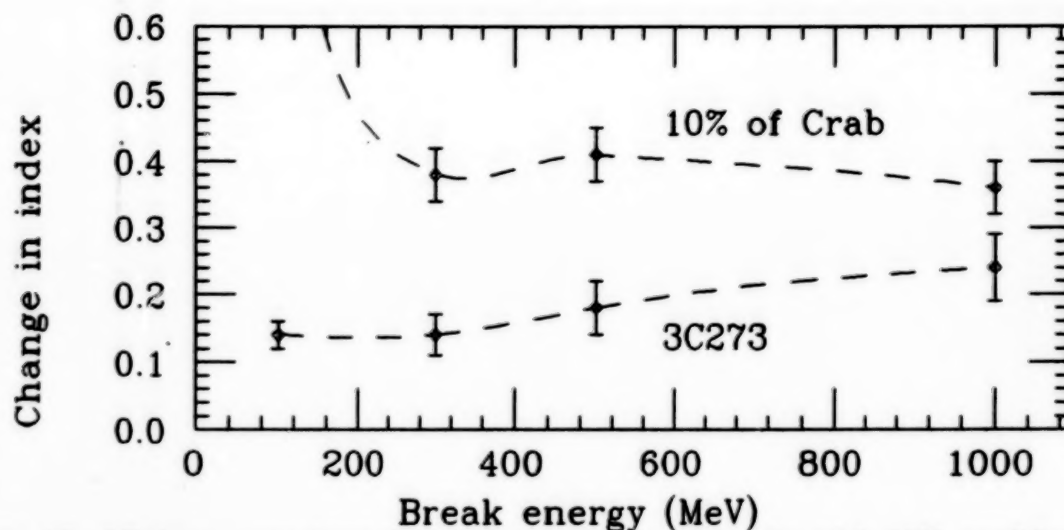
Figure 10: Minimum spectrum break detectable in 10 weeks with 95% confidence for sources with 3C273-like and 10% Crab-like spectra below the break. A break at 100 MeV or below is not detectable in the Crab-like source.

Masnou, J. L., Bennett, K., Bignami, G. F., Bloemen, J. B. G. M., Buccheri, R., Caraveo, P. A., Hermsen, W., Kanbach, G., Mayer-Hasselwander, H., Paul, J. A., and Wills, R. D. 1981, *17th International Cosmic Ray Conference*, paper XG4.3-12, **1**, 177.

Swanenburg, B. N., Bennett, K., Bignami, G. F., Buccheri, R., Caraveo, P., Hermsen, W., Kanbach, G., Lichti, G. G., Masnou, J. L., Mayer-Hasselwander, H. A., Paul, J. A., Sacco, B., Scarsi, L., and Wills, R. D. 1981, *Ap. J.*, **243**, L69.

# Bursts and Solar Flares

# GAMMA RAY BURSTS:
## CURRENT STATUS OF OBSERVATIONS AND THEORY

CHARLES A. MEEGAN
NASA/Marshall Space Flight Center
Marshall Space Flight Center, AL 35812

## ABSTRACT

Gamma-ray bursts display a wide range of temporal and spectral characteristics, but typically last several seconds and emit most of their energy in the low-energy gamma-ray region. The burst sources appear to be isotropically distributed on the sky. Several lines of evidence suggest magnetic neutron stars as sources for bursts. A variety of energy sources and emission mechanisms have been proposed.

## I. INTRODUCTION

Gamma-ray bursts (GRBs) may be summarized as brief, intense emissions of hard X-rays and gamma rays, lasting from milliseconds to tens of seconds, from sources isotropic in the sky, not generally repeating, and not detected at other wavelengths.

Since their discovery in 1973 (Klebesadel, Strong, and Olsen 1973) by the Vela satellites, hundreds of gamma-ray bursts have been observed. Magnetic neutron stars are usually invoked as the sites of gamma-ray bursts, but there is still no consensus in the nature of the sources or the emission mechanisms. The remarkable difficulty in understanding GRBs is primarily due to the dearth of observations of the burst sources at other wavelengths. Another problem is that GRBs encompass a wide range of temporal and spectral characteristics, so it is not yet clear how many separate phenomena we are dealing with. Recent reviews of GRBs include Liang and Petrosian (1986), Hurley (1988), and Higdon and Lingenfelter (1990).

This review follows the standard practice of identifying bursts by their date of occurrence. For example the burst of 1979 March 5 is GB 790305. Lower case letters are appended to distinguish bursts occurring on the same day.

## II. TEMPORAL CHARACTERISTICS

Gamma-ray bursts exhibit a wide range of temporal characteristics, with durations that range from less than 0.1 s to over 100 s. Figure 1 (from Hurley 1988) shows the time histories of three very different events. The uppermost burst in Figure 1 consists of a single spike lasting less than 0.1 s; the middle burst consists of a single peak lasting a few seconds; the lowermost burst lasts at least 60 s and exhibits complex structure. Such complex temporal structure is quite common in GRBs and has been detected down to the limiting time resolution of instruments
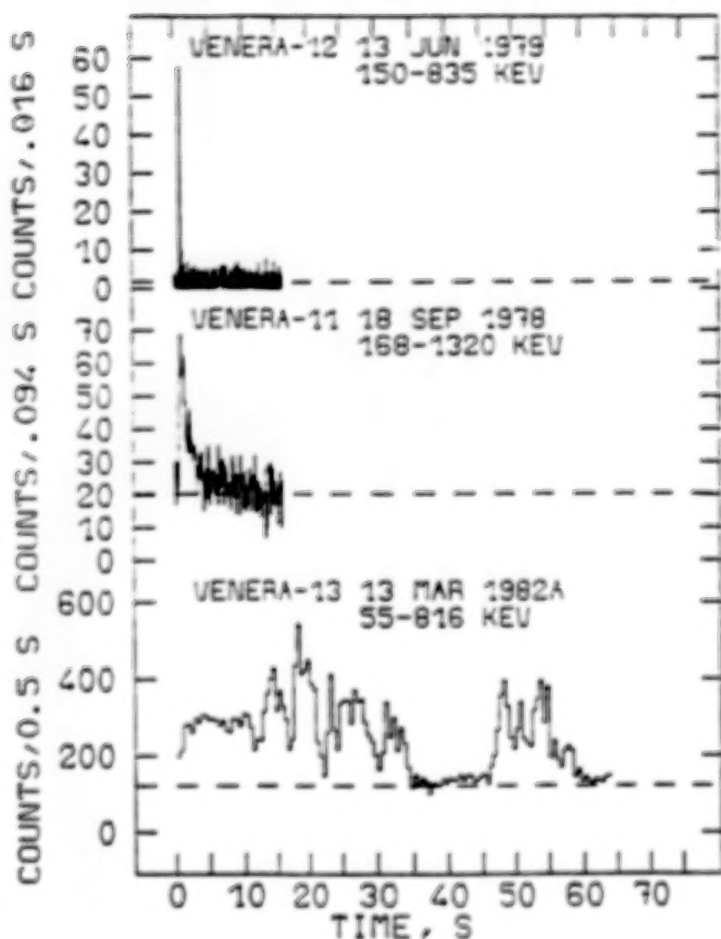
Figure 1. Three bursts (from Hurley 1988) showing a wide range of temporal structure. The dashed lines indicate background rates.

flown to date. In contrast, however, is the time history of GB 830801b, shown in Figure 2, which is smoothly varying (Kuznetsov et al. 1986). Classifications of bursts based on time histories have been proposed (Norris et al. 1984; Barat et al. 1984a), but none have found wide acceptance.

Periodicities are notably absent from GRBs. The only burst with an obvious periodicity is GB 790305, with an 8-s period (see Section IV). Kouveliotou et al. (1988) have presented evidence for a 2.2 periodicity in PVO and SMM data for GB 840805b. Schaefer and Desai (1988) have shown that no other claims of periodicities are statistically convincing. The paucity of measurements of periodicities has hampered understanding of the sources gamma-ray bursts. If
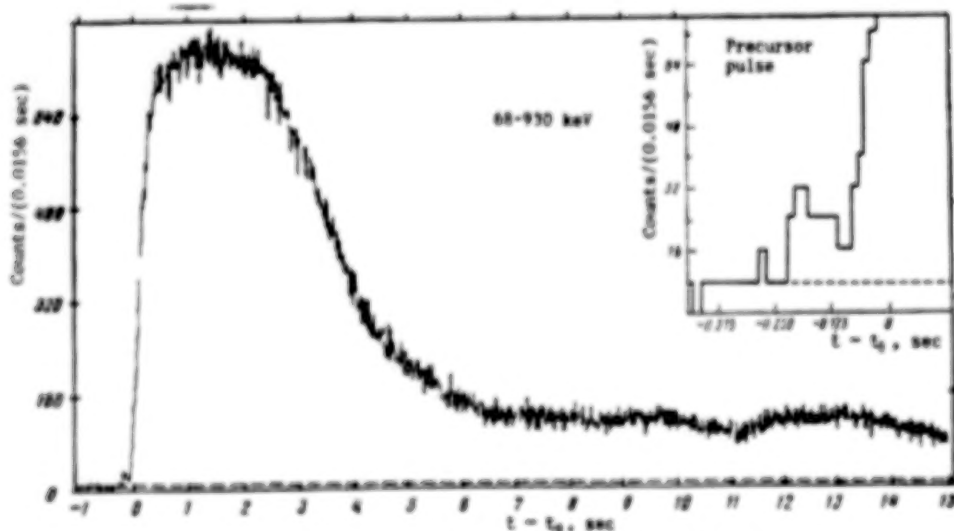


Figure 2. The time profile of GB 830801b shows no evidence of rapid variability.

bursts are indeed produced by neutron stars, periodicities might be expected and would help to constrain the models. It may be that periodicities are often present but are obscured by the short duration and variability of the bursts.

### III.  SPECTRA AND SPECTRAL EVOLUTION

Some typical features of gamma-ray bursts are illustrated in Figure 3. These features may be summarized as follows: (1) Most of the energy is emitted in the hard X-ray and gamma-ray region. (2) Below a few hundred keV, the photon number spectra are reasonably well characterized by the function $E^{-1} \exp(-E/kT)$. (3) Absorption features have been seen in the spectra of many bursts in the 10 to 100 keV region (Mazets et al. 1981). These have been interpreted as cyclotron lines (see below). (4)
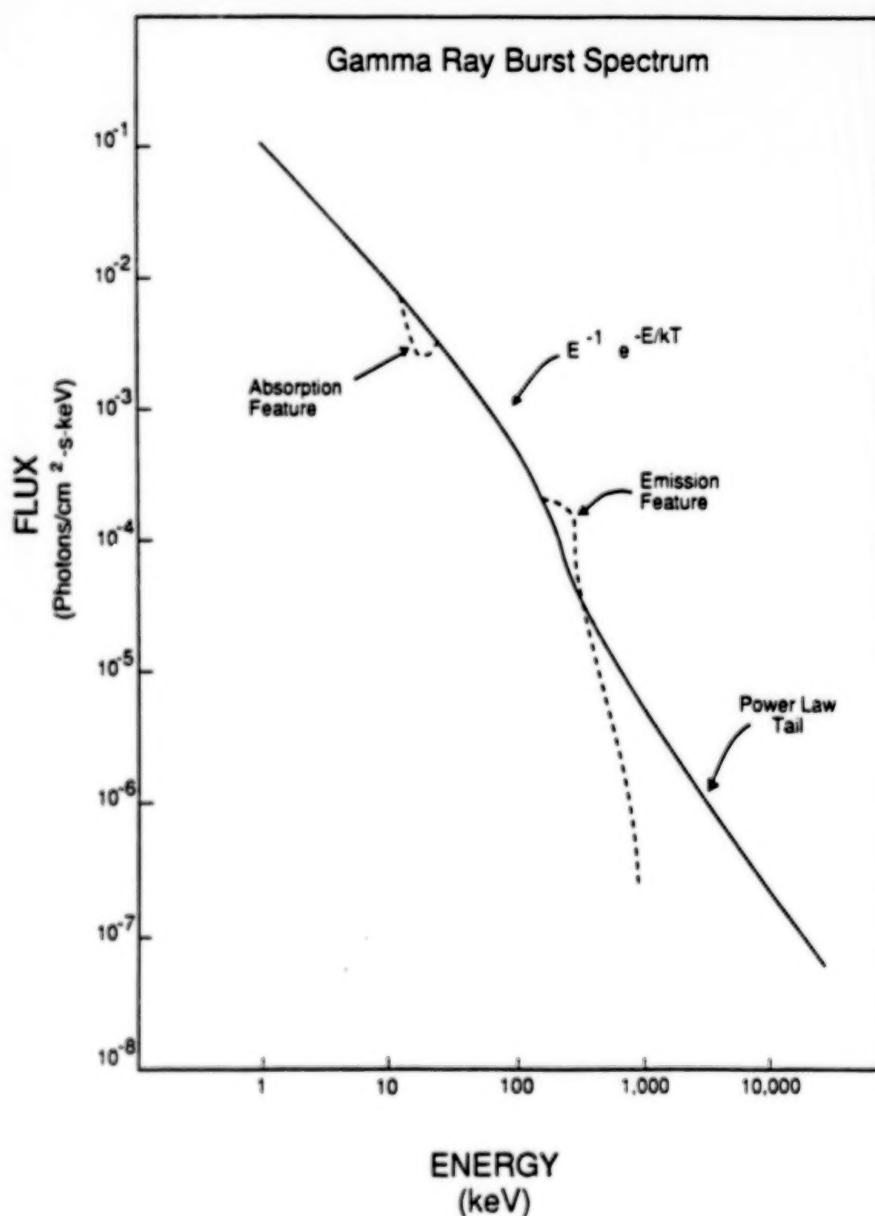


Figure 3.  Typical features of gamma-ray burst spectra.

Emission features at around 400 keV have been reported. These have been interpreted as red-shifted annihilation lines. (5) Hard power law tails extending above 1 MeV have been observed in a majority of the bursts detected by SMM (Matz et al. 1985).

It should be kept in mind that most published spectra are integrations over times that may be long compared to time scales for spectral evolution. Rapid spectral variations are commonly observed by instruments capable of detecting them. Barat et al. (1984b) reported that the annihilation peaks in GB 781104 occurred in short time intervals. Norris et al. (1984) reported that the spectra of individual pulses in ten strong bursts showed a hard to soft evolution.

Soft X-rays have been detected from GRBs and they typically last longer than the gamma-ray emission. The intensity of the X-rays, however, is lower than would be expected if the gamma rays were emitted isotropically near the surface of a neutron star.

The best example of cyclotron absorption lines comes from GB 880205, observed by GINGA (Murakami et al. 1988). Figure 4 shows several different fits to the data, showing that the data require a spectral feature, and that a good fit is obtained using two approximately equal, narrow absorption lines at 19 and 39 keV. Fenimore et al. (1988) have explained these features as cyclotron absorption lines in a magnetic field of $1.7 \times 10^{12}$ G. The narrowness
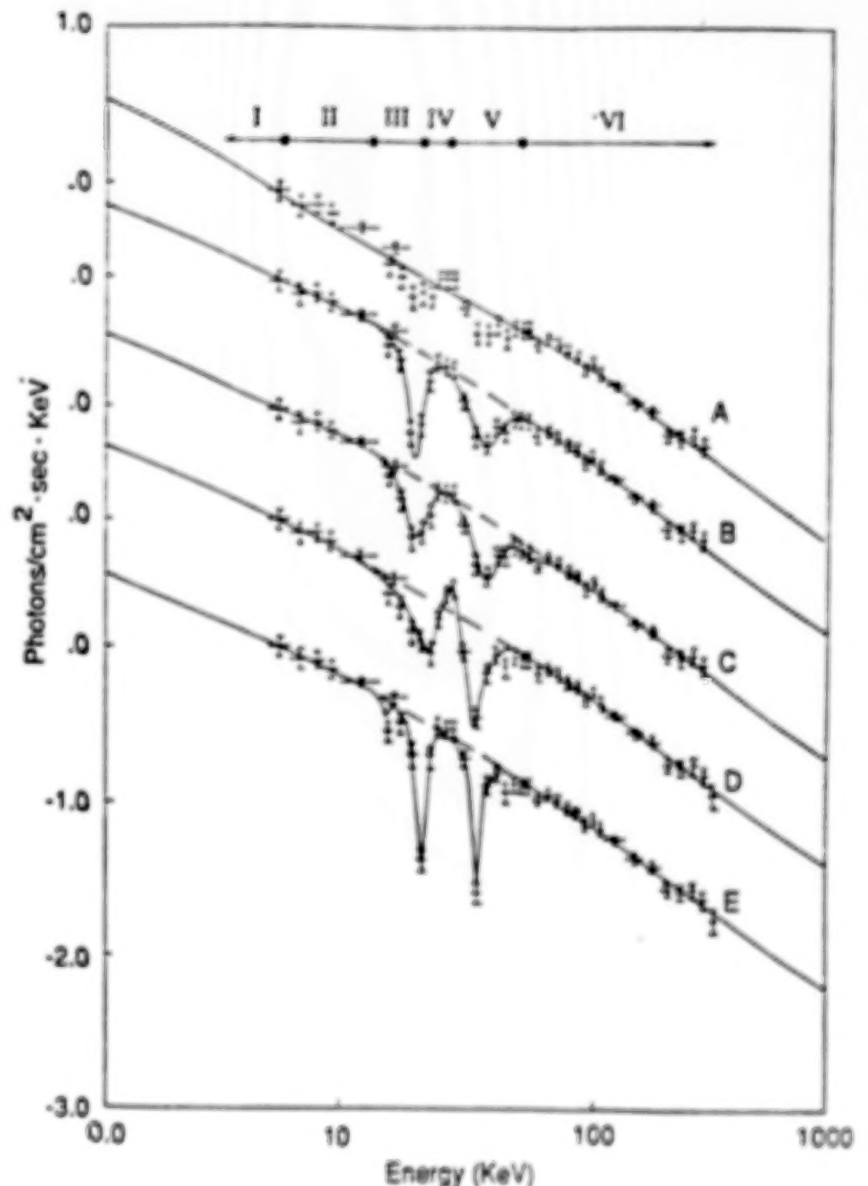


Figure 4. Spectral fits for GB 880205, showing evidence for cyclotron absorption lines (from Murakami et al. 1988).

of the lines implies a cool plasma in the region of line formation, while the continuum is produced in a much hotter region.

## IV.   SOFT GAMMA REPEATERS

Although no scheme for classifying bursts has met with universal approval, there is a consensus that certain burst sources, the Soft Gamma Repeaters (SGRs), form a distinct class. The characteristics of these bursts are short time scales, soft spectra, and repetitive behavior on a wide range of time scales. Three SGRs have been identified: SGR 0520-66, SGR 1900+14, and SGR 1806-20.  The naming convention specifies the celestial coordinates.

The source SGR 0520-66 is the source of the most intense burst ever observed, the 1979 March 5 event.  Figure 5 shows the time history of this unique event.  This burst consisted of an intense initial spike, lasting only a fraction of a second, followed by a slowly decaying tail with a clear 8-s period.  The initial risetime is unresolved and appears to be less than 0.2 ms.  The location of the source is coincident with N49, a supernova remnant in the Large Magellanic Cloud (LMC).  We are thus faced with the uncomfortable observation that the most intense GRB appears to be extragalactic.  The most widely accepted model for this burst involves vibrations of a neutron star following a phase transition in the core (Ramaty et al. 1980).  Cline (1980) has produced a review of the March 5 event.  This source is included in the class of SGRs because recurrent, but much less
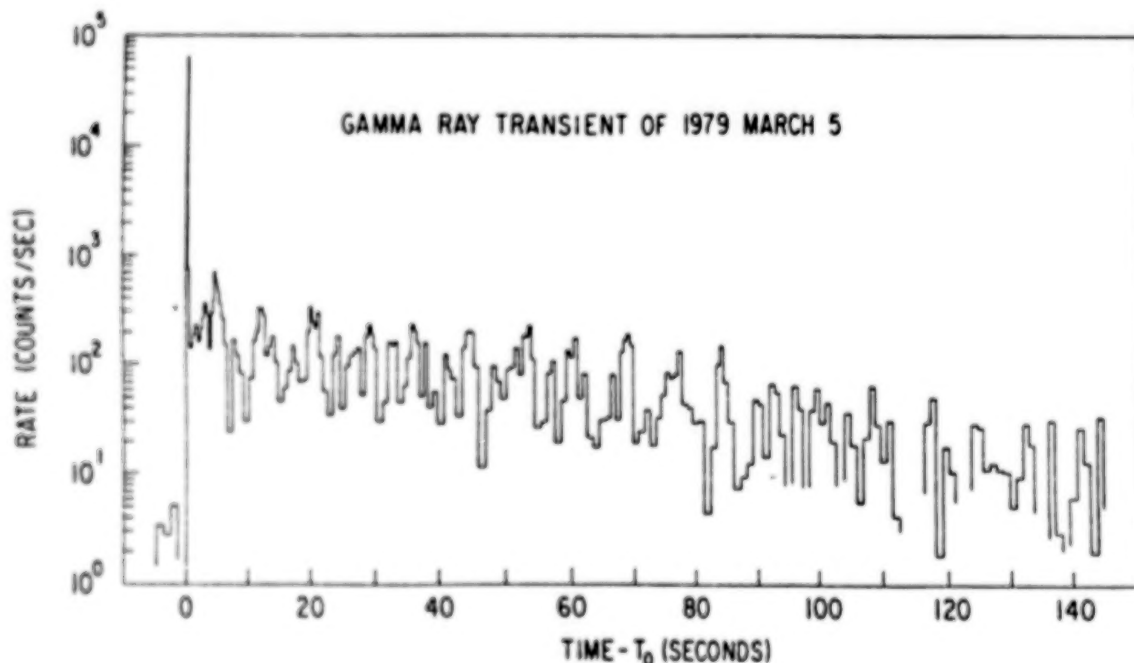


Figure 5.  Time history of the unique event GB 790305 (from Cline et al. 1980).

intense, bursts were subsequently observed by the KONUS experiment (Golenetskii, Ilyinskii, and Mazets 1984).

The source SGR 1806-20 has produced at least 110 bursts (Laros et al. 1987; Atteia et al. 1987a; Kouveliotou et al. 1987). Figure 6 shows the rate of bursts from this source observed on the ICE spacecraft. The bursts appear to be clustered on a wide range of time scales. Models for this source include accretion of comets onto neutron stars (Livio and Taam 1987), accretion of comets onto magnetic white dwarfs (Boer, Hameury, and Lasota 1989), and starquakes (Norris et al. 1989).

## V. SEARCHES AT OTHER WAVELENGTHS

Clearly, the detection of burst sources at other wavelengths would further theoretical understanding of gamma-ray bursts. A number of attempts have been made to observe both quiescent and burst emission in several wavebands. In general, these attempts have not been successful. For a summary of searches for burster counterparts see Pederson et al. (1986) and references therein.

The only burst with good evidence for an optical counterpart is the 1979 March 5 event. This burst is probably associated with N49, a supernova remnant in the LMC. Only six other bursts have positions determined accurately enough to make optical searches worthwhile. While some candidates have been identified, no probable associations have emerged. As a result of these studies, it is concluded that most gamma-ray bursts are probably not associated with main sequence stars.

A number of studies of archival plates have been undertaken in an attempt to find optical transients at the locations of burst sources (Schaefer 1981; Schaefer et al. 1984; Atteia et al. 1985; Hudec
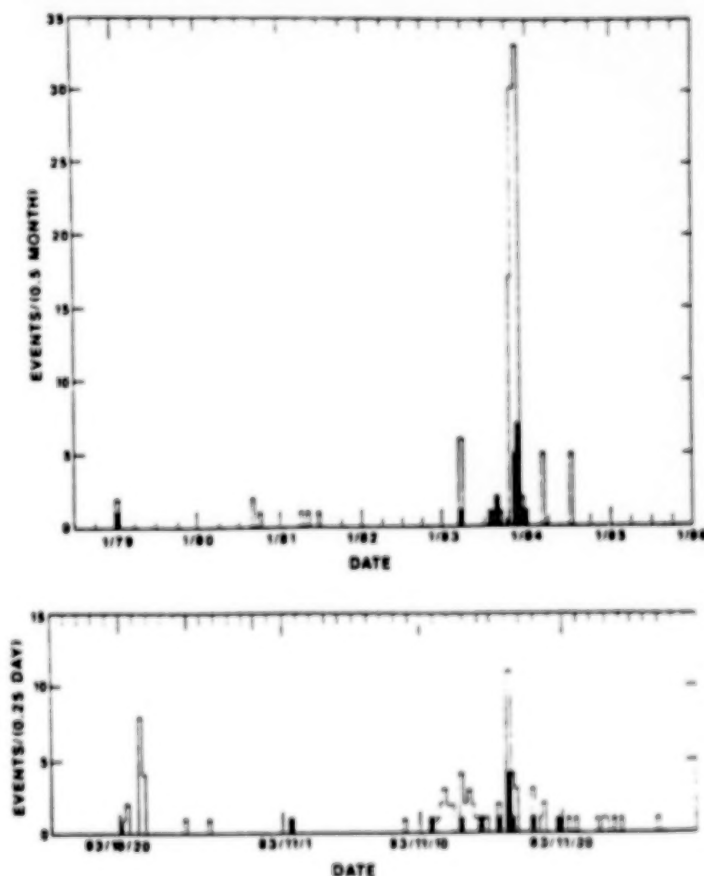


Figure 6. Rate of occurrence of 110 bursts from the Soft Gamma Repeater SGR 1806-20 observed by ICE (from Laros et al. 1987). The filled-in segments of the histograms indicate the number of bursts also observed by other spacecraft.

222

et al. 1987). Claims of identification of three burst sources have been re-analyzed by Zytkow (1989), who finds that the evidence is not conclusive.

Searches for X-ray counterparts of well-localized bursters have been made using data from the Einstein Observatory (Pizzichini et al. 1986) and EXOSAT (Boer et al. 1988). A weak source was detected by Einstein at the location of GB 781119, but not seen by EXOSAT. The low intensity of quiescent X-ray emission from gamma-ray bursters places distance-dependent constraints on the temperatures and accretion rates in neutron star models. For example, the thermonuclear model predicts accretion rates close to the upper limits derived from X-ray observations.

Searches for radio counterparts (Schaefer et al. 1989) and infrared counterparts (Schaefer et al. 1987) have produced no probable associations, further constraining the models.

## VI. SPATIAL DISTRIBUTION

Hartmann and Epstein (1989) have made the most detailed study of the spatial distribution of bursts using the Atteia catalog (Atteia et al. 1987b). They have computed the dipole and quadrupole moments of the distribution of 84 localized bursts. The distribution of these sources is shown in Figure 7. The burst distribution is consistent with isotropy. Hartmann, Epstein, and Woosley (1989) have examined the implications of the isotropic distribution for neutron star models of bursts. They attempted to calculate the distribution of old neutron stars and
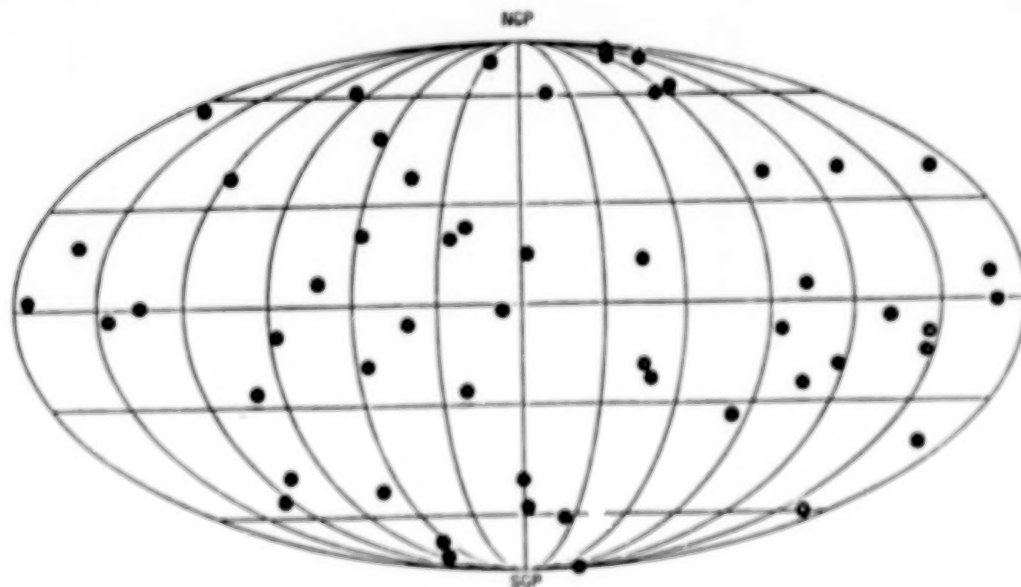


Figure 7. Distribution in galactic coordinates of 84 localized bursts from the Atteia catalog (Atteia et al. 1987b).

concluded that the burst sources must be within about 2 kpc for isotropy. Paczynski (1989) also attempted to calculate the neutron star distribution and got a·very different answer. It must be concluded that we do not really know the distribution of old neutron stars. If gamma-ray bursts are finally determined to arise from old neutron stars, then the spatial distribution of bursts may provide new information on the distribution of neutron stars.

The size distribution of bursts also presents information on the distribution of the burst sources. However, this technique has been fraught with difficulties. The size distribution typically has been produced as a number of bursts above a fluence S (ergs/ $cm^2$) versus S (log N-log S). It has been repeatedly pointed out that instruments trigger on flux, not fluence, and the sensitivity as a function of fluence is typically not well determined. Figure 8 shows a log N-log S curve from the Los Alamos workshop (Epstein 1988). At high S, the -3/2 law seems to be obeyed, indicating a uniform distribution in three dimensions, consistent with the angular isotropy. At medium S, the curve seems to be flattening, possibly indicating the beginning of the
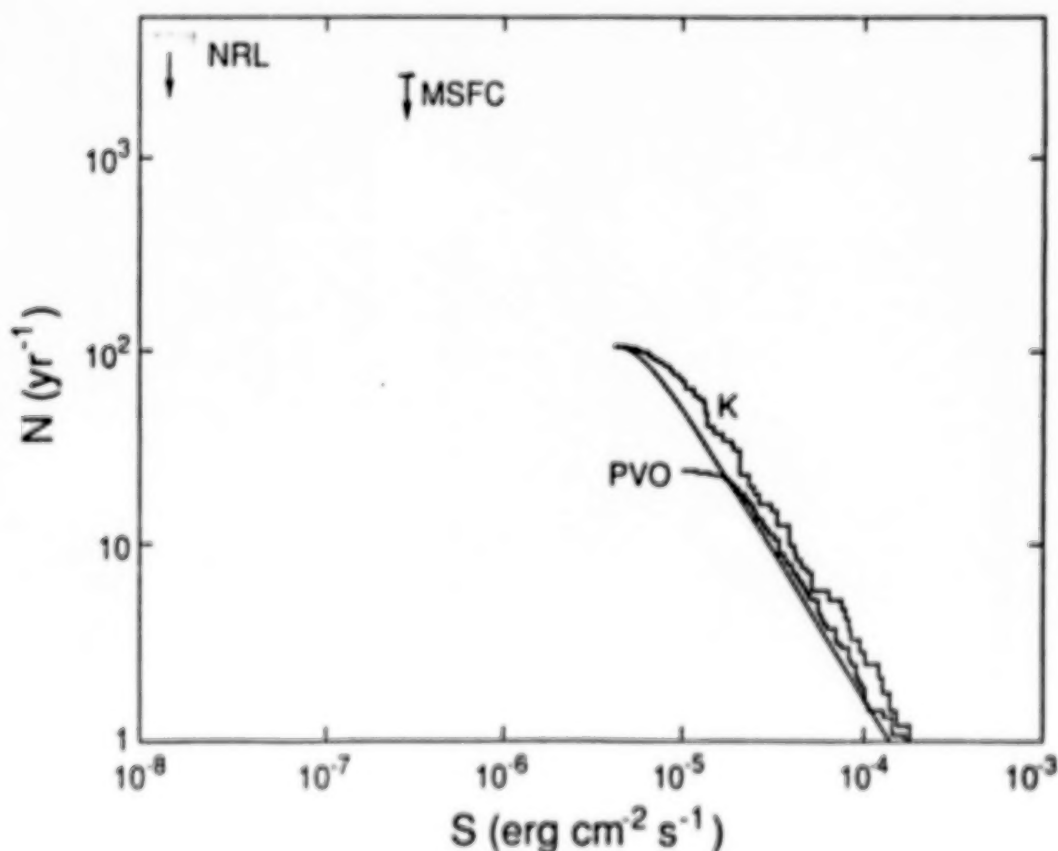


Figure 8. Size distribution of gamma-ray bursts. The distribution at high S is consistent with isotropy. Upper limits at low S indicate a flattening of the curve.

galactic plane distribution. However, this region contains great uncertainty in the sensitivity correction. The upper limits at the low end indicate that the curve is flattening.

An important statistical test, the $V/V_{max}$ test, has been used by Higdon and Schmidt (1989) to examine the KONUS catalog for evidence of spatial non-uniformity. In this test, the intensity of each burst is compared to the minimum intensity required for detection of that burst. This test effectively removes the problems inherent in computing detector sensitivities. The $V/V_{max}$ test cannot be considered a replacement for the size distribution because it does not relate the observations to physically important parameters, such as source distance and energy output, and it cannot be used by experiments that obtain only upper limits to burst rates. The $V/V_{max}$ test is, however, an important internal test for data sets that can employ it. When applied to the KONUS observations, the $V/V_{max}$ test indicates that the observed burst intensities are consistent with an isotropic distribution in space.

## VII. THEORETICAL ISSUES

Theoretical papers on gamma-ray bursts are almost as difficult to categorize as the bursts themselves. Part of the problem is that most contributions are not complete models, but focus primarily on one aspect of the problem, such as the source of the energy or some detail of the emission mechanism. In the remainder of this paper, theoretical work is divided into three categories: the sites of the bursts, the energy sources, and the emission mechanisms. A complete "model" of gamma-ray bursts would require all three elements. For example, a thermonuclear model of the energy source and a synchrotron emission model are not really competing models, but separate, essential pieces of the puzzle.

It is important to note that the wide range of burst phenomena indicate that more than one model may be required. For this reason, it is useful to attempt to categorize bursts in a meaningful way. On the other hand, it must be kept in mind that very different observational characteristics may result from minor changes in the parameters of a model. For example, the angle between the viewing direction and the magnetic field can have a large effect on the energy spectrum. Also, the accretion rate and neutron star temperature greatly influence the nature of bursts in the thermonuclear model.

## VIII. SITES

The sites of gamma-ray bursts must satisfy a variety of observational constraints, including the isotropy, lack of obvious recurrence, time profiles, energy spectra, and lack of counterparts. The site most often mentioned for GRBs is a nearby magnetic neutron star. Evidence for neutron stars as a site is summarized in Table 1. The cyclotron lines are perhaps the best

TABLE 1.  Nearby Magnetic Neutron Stars as Sources
          of Gamma-Ray Bursts

---

EVIDENCE FOR:

RAPID VARIABILITY
CYCLOTRON LINES
ANNIHILATION LINES (?)
LACK OF OPTICAL COUNTERPARTS


DIFFICULTIES:

DISTRIBUTION OF NEUTRON STARS UNKNOWN
HIGH ENERGY EMISSION
LACK OF X-RAY EMISSION
LACK OF PERIODICITY


OTHER SITES PROPOSED:

MAGNETICALLY ACTIVE STELLAR SYSTEMS
SUPERCONDUCTING STRINGS
GRAVITATIONAL LENSING OF DISTANT SOURCES

---

evidence for neutron stars.  However, the high energy tails
indicate a low magnetic field (or beaming of the radiation along
the field lines).  The rapid variability indicates a small
spatial region for the source, while photon-photon interactions
at small volumes should cut off the spectrum at low MeV energies.
The distribution of old neutron stars is not known, but there
ought to be enough to satisfy the requirements of isotropy and
repetition rate.  The lack of optical counterparts is acceptable
if the neutron star temperature is less than around a million
degrees.  Features at around 400 keV have been interpreted as
red-shifted annihilation lines, but may be explained in other
ways.  Some of these difficulties are common to just about any
model of GRBs.  If neutron stars are the sites of most GRBs, then
a comparison of the burst rate with estimates of the number of
neutron stars in the galaxy indicates that the repetition time
must be less than about 500,000 years.  This time is shortened
further if not all neutron stars make bursts. A lower limit to
the repetition rate is determined from the statistics of the
bursts and is usually quoted at around 10 years.

Other sites for gamma-ray bursts have been suggested.  Vahia
and Rao (1988) have revived the idea of large flares in magnet-
ically active stellar systems, such as cataclysmic variables and
RS Can Ven systems.  This model requires the assumption that
burst locations determined via interplanetary timing are inac-
curate.  Extragalactic models have not disappeared.  Babul,
Paczynski, and Spergel (1987) suggest superconducting cosmic

strings, a disadvantage of which is that they are not known to exist. McBreen and Metcalf (1988) propose gravitational lensing of distant sources. This model implies that locations determined by interplanetary timing are not correct. Although these non-neutron star models are decidedly a minority opinion, the fact that they continue to be published is testimony to the difficulties in accounting for the observed properties of bursts.

## IX. ENERGY SOURCES

Within the framework of the neutron star as the source of GRBs, a number of possibilities have been suggested for the source of the energy. Table 2 lists several of the most frequently discussed. In the thermonuclear model, explosion of accreted matter is posited. This model enjoys the most attention, and calculations are extensive, as will be discussed below. A difficulty is that the accretion must be low enough to avoid violating the constraints of the X-ray observations, which appears to be possible. Accretion of comets and asteroids and episodic accretion from a disc have also been suggested. These models run into difficulty maintaining the accretion in the face of super-eddington luminosities (in the latter case) and in retaining asteroids and comets in the evolution of a neutron star. Starquake models use the rotational energy of the neutron star. These models have been analyzed as a class by Blaes et al. (1989) who concluded that the energy and time scale requirements could be met but that recurrence of bursts presented a problem. They still concluded that starquakes represented the "most viable model." The phase transition model is a corequake model, in which a phase transition in nuclear matter occurs in the core of the neutron star. This model was used by Ramaty et al. (1980) to explain the March 5 event quite successfully. However, it is of limited applicability since this represents a single event in the life of a neutron star and cannot explain most bursts.

TABLE 2.  Energy Sources for Neutron Star Models

| |
| --- |
| THERMONUCLEAR EXPLOSION OF ACCRETED MATTER |
| ACCRETION OF COMETS, ASTEROIDS, OR FROM A DISK |
| STARQUAKE (CRUST) |
| PHASE TRANSITION (CORE) |
| REJUVENATED PULSAR |

Ruderman and Cheng (1988) proposed the rejuvenated pulsar as a GRB source as part of study to put GRB sources in an evolutionary framework. They propose that the sources are aligned rotators with periods in the 0.1- to 0.2-s range. These neutron stars have evolved from gamma-ray pulsars and require a "match" to reignite the pulsar mechanism.

# X. EMISSION MECHANISMS

A complete theoretical description of gamma-ray bursters must include a quantitative account of the production of the observed spectra. This requires understanding how the released energy is converted into high energy particles, and then how the particles generate the photon spectrum. A number of important considerations arise. The first problem encountered is the requirement for getting the energy out primarily in the gamma-ray region. The computed spectra must not exhibit higher X-ray flux than is observed. In the neutron star models, this means the gamma rays must be generated far enough from the surface to prevent reprocessing a significant fraction of the energy into X-rays. Another difficulty is the generation of narrow cyclotron absorption lines, which implies high magnetic fields and cool plasma, along with high energy power law tails, which implies hot plasma and low fields or beaming of the gamma rays along the field lines. An important consideration in models incorporating high fields is the very short time ($\sim 10^{-16}$ s) for particles to lose energy due to synchrotron radiation. Thus, particle acceleration must occur parallel to the magnetic field, and burst time scales must be governed by energy input, not cooling times. Another complication in comparing observed and computed spectra is that the observed spectra are usually integrations over times longer than typical temporal variations within the burst.

A summary of the status of burst emission mechanisms as of 1984 is provided in Chapter 2 of Liang and Petrosian (1986). A number of more recent publications have addressed the problem of computing spectra from assumed particle distributions in neutron star models of gamma-ray bursts. Brainard and Lamb (1987) have proposed a two-component (thermal plus non-thermal) electron distribution. Canfield, Howard, and Liang (1987) considered Compton upscattering of soft photons by a one-dimensional electron distribution. Baring (1988) included quantum effects in strong magnetic fields. Melia (1988) considered reprocessing of gamma radiation at the neutron star surface. Sturrock, Harding, and Daugherty (1989) proposed the "cascade" mechanism, whereby electron-photon cascades are produced via curvature radiation. Other work (Brainard 1989; Ho and Epstein 1989; Dermer 1989) specifically addressed the issue of suppressing the X-radiation.

The model of gamma-ray bursts that has received the most attention recently is the thermonuclear model, wherein matter is accreted onto a neutron star until it reaches temperatures and densities high enough for ignition. The implications of this model have been developed extensively (Hameury et al. 1982, 1983; Hameury, Bonazzola, and Heyvaerts 1983; Bonazzola et al. 1984; Hameury et al. 1985). A diagram of the main features of the thermonuclear model is presented in Figure 9. Here, matter is accreted at a rate of about $E^{-15}$ solar masses per year on a strongly magnetized ($10^{12}$ G) neutron star. A hydrogen flash ignites a fast helium flash when a critical temperature and density are reached. The energy is transported to the neutron star

Neutron Star
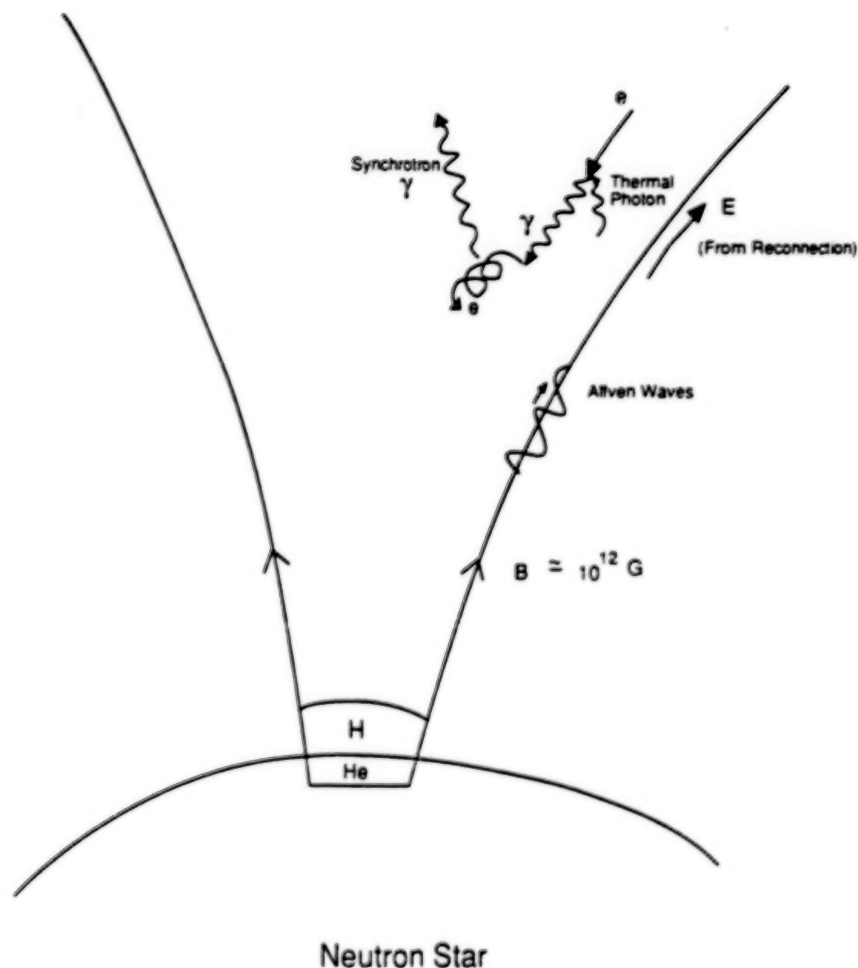
Figure 9.  General features of the thermonuclear model.
Accreted matter ignites, generating Alfven waves that
propagate into the magnetosphere.  Magnetic reconnection
generates electric fields that accelerate electrons.


magnetosphere via Alfvén waves.  Magnetic reconnection generates
an electric field parallel to the magnetic field, which acceler-
ates electrons and positrons to many MeV.  The specific emission
mechanism considered by Hameury et al. (1985) is one in which the
particles scatter soft thermal and synchrotron photons to high
energies, but beamed along the magnetic field.  These gamma rays
then excite electrons to high Landau levels, thus generating the
observed gamma-ray spectrum via synchrotron radiation.

I would like to thank William Paciesas and Robert B. Wilson for comments on this manuscript.

## REFERENCES

Atteia, J. L., et al. 1985, Astr. Ap., 152, 174.
Atteia, J. L., et al. 1987a, Ap. J. (Letters.), 320, L105.
Atteia, J. L., et al. 1987b, Ap. J. Suppl., 64, 305.
Babul, A., Paczynski, B., and Spergel, D. 1987, Ap. J. (Letters), 316, L49.
Barat, C., et al. 1984a, Ap. J., 285, 791.
Barat, C., et al. 1984b, Ap. J. (Letters), 286, L11.
Baring, M. 1988, M.N.R.A.S., 235, 79.
Blaes, O., Blandford, R., Goldreich, P., and Madau, P. 1989, Ap. J., 343, 839.
Boer, M., et al. 1988, Astr. Ap.. 202, 117.
Boer, M., Hameury, J. M., and Lasota, J. P. 1989, Nature, 337, 716.
Bonazzola, S., et al. 1984, Astr. Ap., 136, 89.
Brainard, J. J. 1989, Ap. J. (Letters), 341, L67.
Brainard, J. J., and Lamb, D. Q. 1987, Ap. J., 313, 231.
Canfield, E., Howard, W. M., and Liang, E. P. 1987, Ap. J., 323, 565.
Cline, T. L. 1980, Comm. Ap., 9, 13.
Cline, T. L., et al. 1980, Ap. J. (Letters), 237, L1.
Dermer, C. D. 1989, Ap. J. (Letters), 347, L13.
Epstein, R. I. 1988, Astro. Lett. Communications, 27, 229.
Fenimore, E. E., et al. 1988, Ap. J. (Letters), 335, L71.
Golenetskii, S. V., Ilyinskii, V. N., and Mazets, E. P. 1984, Nature, 307, 41.
Hameury, J. M., Bonazzola, S., and Heyvaerts, J. 1983, Astr. Ap., 121, 259.
Hameury, J. M., et al. 1982, Astr. Ap., 111, 242.
Hameury, J. M., et al. 1983, Astr. Ap., 128, 369.
Hameury, J. M., et al. 1985, Ap. J., 293, 56.
Hartmann, D., and Epstein, R. I. 1989, Ap. J., in press.
Hartmann, D., Epstein, R. I., and Woosley, S. E. 1989, Ap. J., in press.
Higdon, J. C., and Lingenfelter, R. E. 1990, Annual Reviews of Astronomy and Astrophysics, in preparation.
Higdon, J. C., and Schmidt, M. 1989, Ap. J., in press.
Ho, C., and Epstein, R. I. 1989, Ap. J., 343, 277.
Hudec, R., et al. 1987, Astr. Ap., 175, 71.
Hurley, K. 1988, in Proc. Erice School on Cosmic Gamma Rays and Cosmic Neutrinos, eds. M. Shapiro and E. Wefel (Boston: Kluwer), in press.
Klebesadel, R. W., I. B. Strong, and R. A. Olsen 1973, Ap. J. (Letters) 182, L85.
Kouveliotou, C., et al. 1987, Ap. J. (Letters), 322, L21.
Kouveliotou, C., et al. 1988 Ap. J. (Letters), 330, L101.
Kuznetsov, A. V., et al. 1986, Soviet Astr. (letters), 12(5), 315.

Liang, E. P., and Petrosian, V. (eds.) 1986, Gamma Ray Bursts (New York: AIP).
Laros, J. G., et al. 1987, Ap. J. (Letters), 320, L111.
Livio, M., and Taam, R. E. 1987, Nature, 327, 398.
Matz, S. M., et al. 1985, Ap. J. (Letters), 288, L37.
Mazets, E. P., et al. 1981, Nature, 290, 378.
McBreen, B., and Metcalf, L. 1988, Nature, 332, 234.
Melia, F. 1988, Ap. J. (Letters), 334, L9.
Murakami, et al. 1988, Nature, 335, 234.
Norris, J. P., et al. 1984, Nature, 308, 434.
Norris, J. P., et al. 1989, in Proceedings of the Gamma Ray Observatory Workshop, ed. W. Neil Johnson, pp. 4-479.
Paczynski, B. 1989, Ap. J., in press.
Pederson, H., Pizzichini, G., Schaefer, B., and Hurley, K. 1986, in Gamma-Ray Bursts, eds. E. P. Liang and V. Petrosian (New York: AIP), p. 39..
Pizzichini, G., et al. 1986, Ap. J., 301, 641.
Ramaty, R., et al. 1980, Nature, 287, 122.
Ruderman, M., and Cheng, K. S. 1988, Ap. J., 335, 306.
Schaefer, B. 1981, Nature, 294, 722.
Schaefer, B., et al. 1984, Ap. J. (Letters), 286, L1.
Schaefer, B., et al. 1987, Ap. J., 313, 226.
Schaefer, B., et al. 1989, Ap. J., 340, 455.
Schaefer, B., and Desai, U. D. 1988, Astr. Ap., 195, 123.
Sturrock, P. A., Harding, A. K., and Daugherty, J. K. 1989, Ap. J., 346, 950.
Vahia, M. N., and Rao, A. R. 1988, Astr. Ap., 207, 55.
Zytkow, A., 1989, Ap. J., in press.

## DISCUSSION

*Don Kniffen:*

What is the lower limit to the period in the search for burst source periodicities? Specifically, does the search cover the periods expected if the burst sources are spent pulsars?

*Thomas Cline:*

Generally, periodicities or their limits, are set in the fractional - to several second region, and may be valid only in the case for the 79 March 5 event. Internal neutron star periods are acoustic, or several KHZ, and cannot be monitored; spin periods in the fractional second region may be undetectable in the event time variations.

*Demos Kazanas:*

We should really look for models that can reproduce a large number of bursts with variation of one (or maybe two) parameters. To my knowledge such an approach has not been taken yet.

231

# WHAT IS LEARNED FROM HIGH ENERGY BURSTS AND FLARES

EDWARD J. SCHNEID

Grumman Corporation, Bethpage, N.Y. 11714

## ABSTRACT

The Energetic Gamma Ray Experiment Telescope (EGRET) with its large NaI Total Absorption Shower Counter (TASC) has the scientific capability of performing spectroscopy of high energy cosmic gamma ray bursts and solar flares. EGRET, with a spectroscopy energy range from 0.6 to 140 MeV, provides a unique opportunity to increase our understanding of the high energy mechanisms of gamma ray bursts and solar flares. A likely interpretation of gamma ray burst sources is that they are rotating, magnetized neutron stars. High magnetic fields can influence the emission of high energy gamma rays, so observational spectroscopic data at high energies can provide information on the upper limits of the magnetic fields in the GRB regions of magnetized neutron stars. Likewise spectroscopy of high energy gamma rays can provide information useful for deriving the flare proton spectrum which in turn can lead to an understanding of high energy solar flare particle acceleration mechanisms.

## I. INTRODUCTION

Many gamma ray bursts (GRB) and gamma ray solar flares have been observed with satellite borne instruments. These observations have provided valuable information about these objects but our understanding is not complete at this time. The NASA Gamma Ray Observatory (GRO) with four separate detector systems will provide a coordinated spectroscopic observation covering the gamma ray energy range extending beyond 140 MeV. The Energetic Gamma Ray Experiment Telescope (EGRET) will provide data for the energy range greater than 10 MeV that has not been measured in any detail before. These new data can be compared to the predictions from the models used for interpreting high energy bursts and flares.

## II. EGRET BURST AND FLARE MEASUREMENT CAPABILITIES

One component of the EGRET instrument is a large NaI Total Absorption Shower Counter (TASC) to determine the energy of the secondary electron-positron pair produced by high energy gamma rays. The TASC dimensions are 77. cm. square by 20. cm. thick. The TASC has a further scientific goal of providing spectroscopy of high energy cosmic GRB's and solar flares. For this purpose, a separate low energy processor performs a pulse height analysis of the omnidirectional radiation signals. These data are stored in a 256 channel spectrum that spans the range of 0.6 to 140 MeV. The details of these spectra are presented in Table 1. The energy spectrum is divided into seven energy bands having different energy resolution. Two modes of accumulation are possible for these TASC spectra. First, a background / solar mode in which a continuous energy analysis occurs and a spectrum is taken every 32.8 seconds. In the burst mode, a set of four consecutive spectra are accumulated in response to a signal from GRO Burst and Transient Source Experiment

(BATSE). In this mode, accumulation times of each spectra are preset by command in steps of 0.125 seconds up to 15.87 seconds.

### Table 1. TASC LOW ENERGY PROCESSOR
### LOW ENERGY SPECTRA

| Accumulation Channels | Compression Factor | Telemetered Channels | Energy Range(MeV) |
|---|---|---|---|
| 0-127 | 2 | 0-63 | 0.6-2.18 |
| 128-255 | 4 | 64-95 | 2.18-4.81 |
| 256-511 | 8 | 96-127 | 4.81-10.1 |
| 512-1023 | 16 | 128-159 | 10.1-20.6 |
| 1024-2047 | 32 | 160-191 | 20.6-41.6 |
| 2048-4095 | 64 | 192-223 | 41.6-83.6 |
| 4096-8191 | 128 | 224-256 | 83.6-167(140) |

### ACCUMULATION TIMES

| | |
|---|---|
| Bgd / Solar | 32.768 seconds fixed |
| Burst (BATSE Triggered) | Four Sequential Spectra. Accumulation of each commandable in steps of 0.125 secs. from 0.125 to 15.875 seconds |

Background corrected TASC spectra will be generated for all detected burst and flare events. If the direction to the event is known, a correction for attenuation and spectral modification of the gamma rays due to the material of the spacecraft can be made. Utilizing the known response functions for the TASC, the source gamma ray emission spectra can be derived.

## III. THEORY OF GAMMA RAY BURSTS

The consensus on the likely origin of gamma ray bursts is that they are associated with magnetized neutron stars. This is based largely on the rapid oscillations seen in some events, low energy features in others that may be absorption or emission at cyclotron fundamentals, and a high energy 430 keV emission feature in a few events that may be red shifted annihilation radiation. Other explanations have been proposed such as neutron starquakes (Blaes, et. al., 1989) and Be/X-Ray binaries (Melia, 1988b) but are insufficient to account for the energy radiated in a single burst.

The energy spectrum of GRB's is roughly a broken power law consisting of a low energy spectrum that rises with a spectral index, 0.8 to1, and a high energy spectrum that falls with a spectral index, 1 to 2.5. The transition between the high and low energy regions occurs between 100 keV and 1 MeV suggesting a link to the rest mass energy of the electron. The hard spectral form for gamma rays > 1 MeV implies that most of the GRB luminosity is emitted in these high energy gamma rays.

Observation of absorption features in the 30-70 keV region have provided some estimate of the magnetic fields near the neutron stars. Figure 1 taken from Fenimore, et. al., 1988, shows fitted data acquired during a 5.0 second time period for gamma ray burst GB 880205. The curves represent various functions used to fit the spectral data and shows that the fits are complient with the assumed fitting functions. Fenimore was able to conclude from these analyses that the lines are associated with electron cyclotron harmonics in a magnetic field of $1.7 \times 10^{12}$ G or from a combination of absorption by H-like and He-like ion in a $4 \times 10^{13}$ G. These field estimates are consisted with the analyses of Konus events requiring fields of $> 10^{12}$ G.
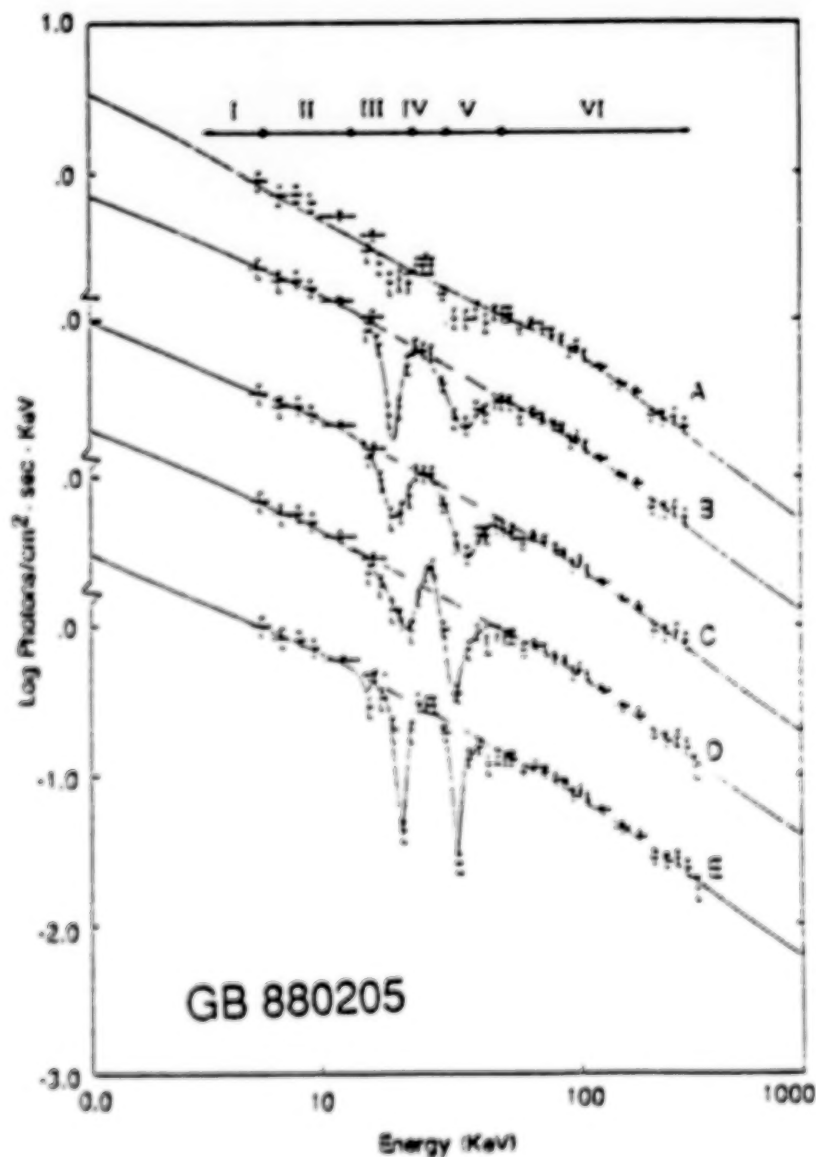


Fig. 1. Various functions fitted to the spectral acquired during the 5.0s time period of the gamma ray burst G B 880205. Curve A using three power law function shows line structure is still required. Curves B-E are fits with several spectral shape and line features.

The presence of gamma rays greater than 10 MeV in a large number of GRB's places a constraint on the GRB models having on magnetized neutron stars with strong fields. High energy gamma rays can interact with the magnetic field and create electron- positron pairs. These interactions can lead to a cut-off in the spectrum. The attenuation length for these high energy gamma rays is strongly dependent on the field strength and the direction of the gamma ray relative to the magnetic field.

Analysis of the Solar Maximun Mission (SMM) data by Matz, et. al., 1985, concluded that the magnetic fields for the high energy region must be less than the $10^{12}$ G required by the low energy absorption features. Matz analyzed 72 statistically significant events identified as having cosmic origin based on spectral and temporal characteristics as well as coincident observation by other experiments. The magnetic fields required for the low energy absorption features can produce spectral cut-offs within the < 9 MeV region of the SMM data. The cut-off depends on the energy of the photon, the field strength, and the sine of the angle between the photon direction and the direction of the magnetic field. For a fixed field, there is a maximum angle for which a photon can escape the region of the field. At higher energies the angle decreases, therefore a burst is observable at smaller solid angles, i.e., the emissions are beamed. At any given field strength, the fraction of all bursts which are observable above any energy should be the solid angle of escape divided by the two pi (the solid angle for isotropic emission at the surface of the star). The 72 SMM events are assumed to represent a random set of observation angles. Figure 2 shows a comparison between the experimental data and the fraction of predicted events for two magnetic field strengths. The results for a field strength of 2 x $10^{12}$ G, would predict far fewer events than seen by the SMM experimentat the higher energies. Agreement with the SMM data would require a field of less than $10^{12}$ G in the high energy burst region. In a later article by Meszarios, et. al., 1989, an analysis was performed that showed that the SMM detection
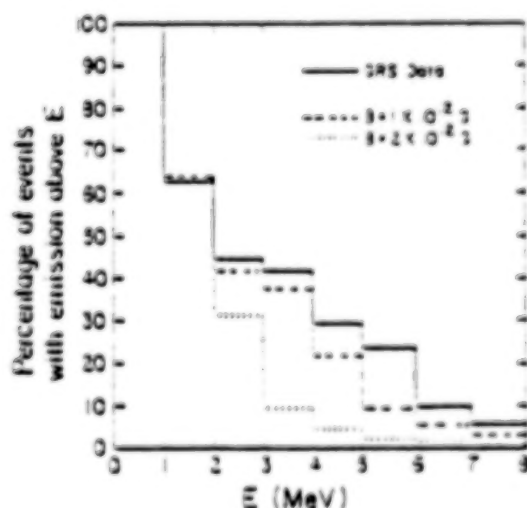


Fig. 2. The solid line is the burst event data in terms of percentages of all observed events. The dashed line indicates the power-low spectra and percentage of burst spectra with observable photon emission >E assuming a field of 1 x $10^{12}$ gauss at the source. The dotted line shows the result for a field of 2 x $10^{12}$ gauss.

rates at high photon energies could still be compatible with some of the neutron stars having magnetic fields strength extending to $4 \times 10^{12}$ G.

The previous analyses are based on the statistical analysis of a set of the number of GRB events detected. EGRET measurements of GRB spectra at high energies that either show no cut-off or a clear energy cut-off can establish the limits of the strength of the magnetic field in the region of the GRB's.

It is possible to conceive of models that have the high energy emissions coming from a different region of the star and away from the strong field regions where the absorption features are produced. Figure 3 taken from Hartmann, et. al., 1988, graphically illustrates such a model. The power law GRB occurs in the low field region and heats the plasma near the neutron star to the generate the other spectral features of the GRB's. Melia, 1988a, studied GRB's with a similiar model that reprocesses the GRB high energy emission and was able to fit the observed data from GB 811016. Figure 4, taken from the paper of Melia, shows the composite spectrum from the irradiation of a neutron star and a cold accretion disk by an incident power law spectrum. Clearly for this case, multi region models can describe the data but provides no additional information on initiating causes of the GRB event or the strength of the magnetic field in the GRB region.
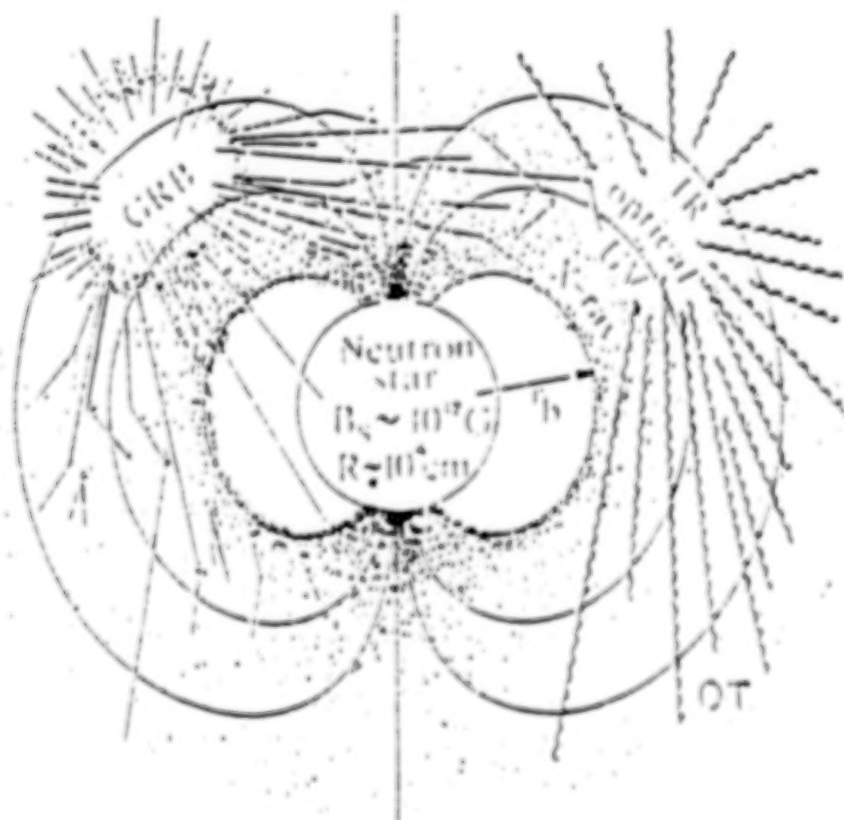


Fig. 3. Schematic view of the reprocessing model. The burst of hard photons energizes the plasma electrons resulting in the observed low energy emission features.
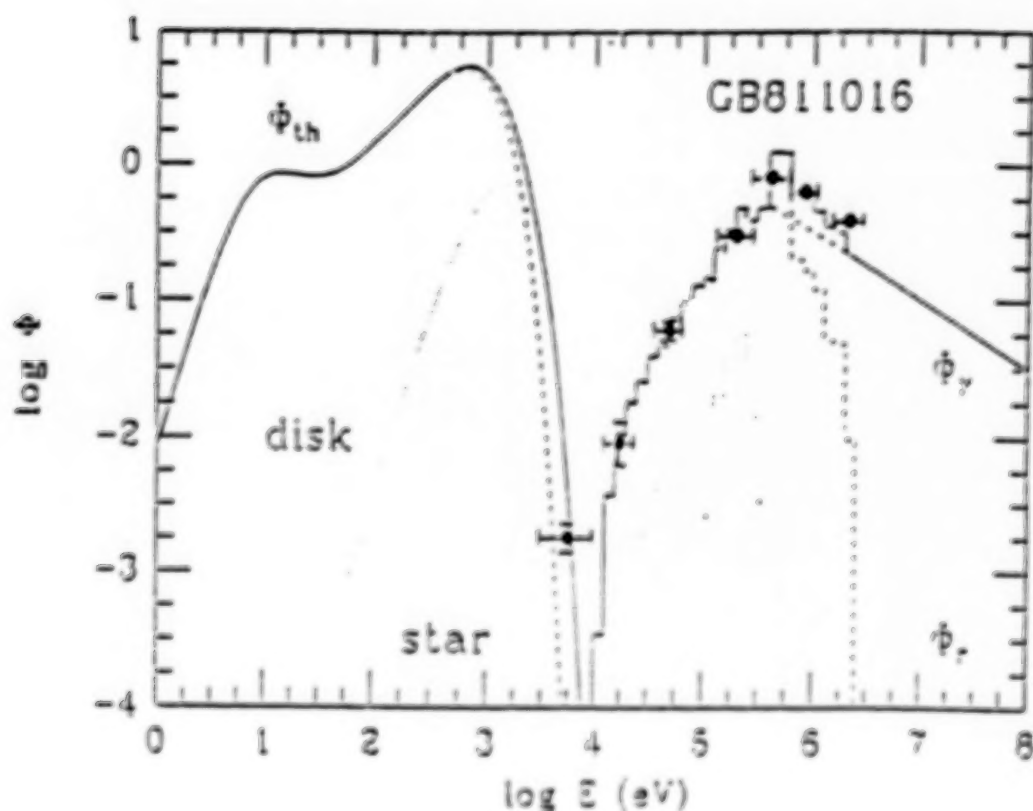
Fig. 4. This figure shows the composite spectrum resulting from the irradiation of a neutron star and an accretion disk by an incident power law gamma ray spectrum. The full spectrum is indicated by a solid line. The components are the thermal contributions from the disk and the star, the reflection of gamma rays at the reprocessing boundary, and the incident power law flux. The data points are simultaneous measurements by PVO (circles) and Hakucho (squares).

## IV. HIGH ENERGY SOLAR FLARES

Gamma rays from energetic solar flares provide information on the acceleration mechanisms of protons in solar flares whereas the X-rays provide information on the acceleration of the electrons. The time delay between the electron and proton acceleration varies greatly depending on the type of the flare. Figure 5 shows examples of two flares. In the impulsive flare of Feb 8, 1982, the protons (10-25 MeV gamma rays) were accelerated within 2 seconds of the electrons (40-120 keV X- rays) Whereas, in the gradual flare of April 27, 1981, the protons were accelerated nearly 48 seconds after the electrons. Clearly the details of the time histories associated with these two flares are different. Simultaneous measurements of the X-ray and high energy gamma ray data are needed to gain a better understanding of the flare mechanisms in the different flare types.

IMPULSIVE                                    GRADUAL



p acceleration delay time
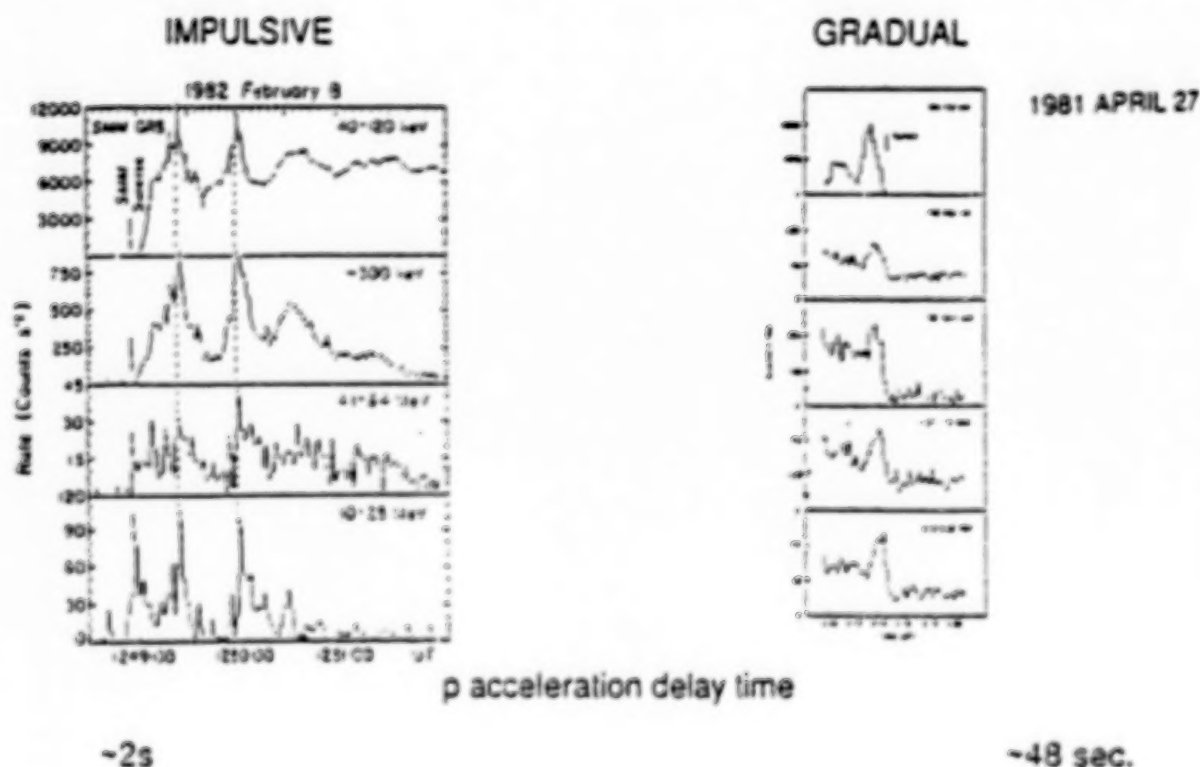
~2s                                          ~48 sec.


Fig. 5. This figure contains two examples of the time histories of solar
flares. The February, 1982 is an impulsive flare and the April, 1981
is a gradual flare. The gamma rays indicating proton acceleration
are delayed by different amounts relative to the x-rays.


The protons can also produce secondary reactions that can be observed by gamma
ray line emissions unique the reactions. Two prominent lines are the 2.22 and the 4.44 MeV
lines associated with capture of secondary neutrons and the de-excitation carbon nuclei
respectively. Yoshimori, 1989, showed that using a knowledge of the reaction cross sections
as a function of proton energy,and assuming a spectral model for the proton spectrum,
predictions of the ratio of the 4.44/2.22 MeV gamma rays can be made as a function of the
value of the model parameters. From these predictions and the observed ratio of the
4.44/2.22 MeV lines,the proton spectrum at the flare site can be derived. Figure 6 shows the
calculated ratios of the 4.44 MeV fluence to the 2.22 MeV fluence for a power law model, a
exponential rigidity model, and a Bessel function model as a function of the value of the
model parameters. The shaded area in the figure is the ratio observed for the flare of April 1,
1981. The deduced value of the parameters to be used with this flare falls within the overlap
of the data and the predictions. Yoshimori found that the proton spectra derived from the
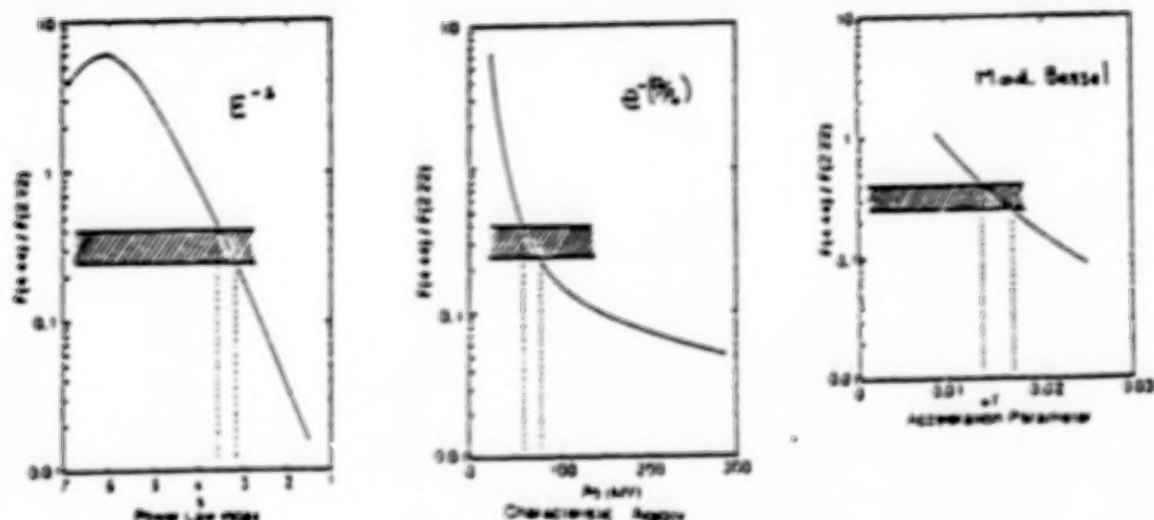gamma ray data did not vary too much from flare to flare.

239

Fig. 6. The calculated ration of the 4.44 MeV/2.22 MeV fluences are shown as a function of parameters value for a power low, exponential rigidity, and a Bessel function for the proton spectrum. The shaded area in the ratio observed for the April 1, 1981 flare.
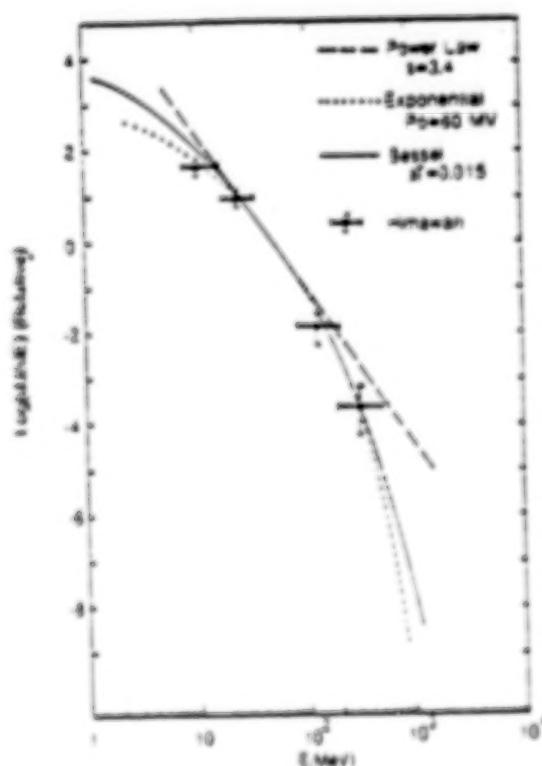


Fig. 7. Proton data obtained by HIMAWARI for the April 1, 1981 flare are compared to the normalized proton spectra derived from the fluence ratios.

Yoshimori studied the correlation between the flare associated gamma ray lines and the interplanetary protons. This correlation attempts to establish the relationship between trapping and escaping of accelerated protons. The HIMAWARI satellite located between the Sun and the earth has a silicon detector that measures the protons with energies of 1.2 to 500 MeV. For the April 1, 1981 flare, three proton spectra can be deduced from the previous analysis. These spectra are normalized at 60 MeV and compared to the proton data obtained by the HIMAWARI satellite (see Figure 7). The observed proton spectrum is in agreement with exponential spectrum derived from the gamma ray line emissions within error. However, this correlation between the gamma ray derived spectrum and the measured proton data near earth does not always hold up because the protons escaping the Sun are subject to complex propagation effects in the corona and interplanetary space. Therefore the gamma ray line measurements give the best estimate of the spectrum of the protons accelerated in a solar flare.

## V. CONCLUSIONS

The high energy spectroscopy measurements of the EGRET instrument on the GRO can provide important information on GRB's and energetic solar flares. The observation of GRB high energy gamma rays showing either a definite cut-off or no cut-off can help establish the upper limits of the magnetic fields in the GRB region of the magnetized neutron star. Likewise, the observation of the reaction lines and the total gamma ray spectrum can be used to derive the spectra of the accelerated protons. Interpretation of the proton spectrum can lead to a understanding of the flare acceleration mechanisms. The launch of the GRO should enhance the data base from which we can extract a better understanding of these high energy events.

## REFERENCES

Blaes, O., Blandford, R., Goldreich, P., and Madau, P., 1989, Ap.J., 343, 839.

Fenimore, E.E., Connor, J.P., Epstein, R.I., Klebesadel, R.W., Laros, J.G., Yoshida, A., Fujii, M., Hayashida, K., Itoh, M., Murakami T., Nishimura, J., Yamagani. T., Kondo, I., and Kawai, N., 1988, Ap.J. (Letters), 335, L71.

Hartmann, D., Woosley, S.E., and Arons, J., 1988, Ap.J., 332, 777.

Matz, S.M., Forrest, D.J., Vestrand, W.T., Chupp, E.L., Share, G.H., and Rieger, E., 1985, Ap.J. (Letters), 288, L37.

Melia, F., 1988a, Ap.J. (Letters), 334, L9.

Melia, F., 1988b, Ap.J. , 335, 965.

Meszaros, P., Bagely, Z., and Riffert, H., 1989, Ap.J. (Letters), 337, L23.

Yoshimori, M., 1989, Space Sci. Rev., 51, 85.

## DISCUSSION

*Chuck Dermer:*

The SMM analysis shows that strong magnetic fields are inconsistent with beaming of the high energy emission for small-angle polar cap geometries. If a large fraction of the neutron star radiates during a burst, this constraint is weakened. How large does this angle have to be for consistency?

*Ed Schneid:*

For fields greater than $B=2x10^{12}$ G, only the surface within 15 degrees of the poles will allow radiation of high energy gamma rays to get out because gamma rays from the surfaces at large angles would be crossing more field lines and therefore, would be attenuated. The field would have to be reduced in order for a larger fraction of the neutron stars to contribute.

*Daryl Leiter:*

What is the directional sensitivity of TASC in the 0.6 - 5 MeV region to Gamma Ray Transients as compared to COMPTEL & OSSE on the GRO?

*Ed Schneid:*

The calculation of effective area as a function of angle and energy due to spacecraft/TASC geometry is not completed. However, the TASC spectra does not have any field of view constraints due to experiment logic so it is ommidirectional and only modified by attenuation due to material and projected area of the TASC.

*Alice Harding:*

Peter Meszaros and his colleagues have shown that the SMM upper limit to the magnetic field strength in gamma-ray bursts may be misleading. They showed that a distribution of fields with some fraction of bursts having very high fields, is also consistent with the SMM data. Thus, some bursts may have beamed high energy emission.

*Ed Schneid:*

Yes, that is very possible with the statistics of the data so far.

*Chris Winkler:*

Could EGRET detect polarization of a strong GRB at high energies (e.g. GRB840805, see Share et al. (1986) Adv. Space Res. 6, No. 4, p. 15) assuming 100% polarization?

*Ed Schneid:*

No. An earlier presentation by John Mattox, showed that it would take a large number of photons, with spark chamber pictures for EGRET to measure polarization. Our Burst mode would have very few at most sparkchamber pictures.

# Normal Galaxies

# LOCAL NORMAL GALAXIES

Carl E. Fichtel
NASA/Goddard Space Flight Center
Greenbelt, MD 20771

## ABSTRACT

In the near future, high energy (E > 20 MeV) gamma ray astronomy offers the promise of a new means of examining the closest galaxies. Two and possibly three local galaxies, the Small and Large Magellanic Clouds and M31, should be visible to the high energy gamma ray telescope on the Gamma Ray Observatory, and the first two should be seen by GAMMA-1. With the assumptions of adequate cosmic ray production and reasonable magnetic field strengths, both of which should likely be satisfied, specific predictions of the gamma ray emission can be made separating the concepts of the galactic and universal nature of cosmic rays. A study of the synchrotron radiation from the Large Magellanic Cloud (LMC) suggests that the cosmic ray density is similar to that in the local region of our galaxy, but not uniform. It is hoped the measurements will be able to verify this independent of assumptions about the magnetic fields in the LMC.

## I.  INTRODUCTION

With this paper, the focus of this science symposium changes from our own galaxy and its contents to phenomena outside of it. The subject of this paper is normal galaxies, and specifically local normal galaxies since these are the only ones that would be expected to be detectable in the foreseeable future in the frequency range of high energy gamma rays. The local galaxies have been extensively studied at other wavelengths; some of the information from these observations, especially in the radio wavelength range are of considerable importance in the study to be described here. Gamma rays have not as yet been seen from any local normal galaxy beyond our own. The SAS-2 and COS-B gamma ray satellites which were launched in the early and mid 1970's were able to provide only upper limits to the gamma radiation from the closest galaxies. Calculations (Fichtel and Trombka, 1981, Houston et al., 1983, and Ozel and Berkhuijsen, 1987; Ozel and Fichtel, 1988), as well as those here, show that, on the basis of estimated density levels of the cosmic rays only upper limits would have been expected. Even with the next generation of high energy gamma-ray space instruments, only three appear to be detectable and, one just barely. The Large and Small Magellanic Clouds should be detectable at a level where several significant studies may be made.

There is an advantage to studying the other galaxies than our own in addition to the obvious merits of having more than a sample of one. Although they are further away and hence weaker and much less well resolved, there is not the complication of being buried inside in the middle of the plane as is the Sun. Hence, one does not have to attempt to understand variations over a large column throughout the plane

There are several facets associated with the scientific importance of studying galaxies in the frequency range of the high energy gamma rays. They include the fact that this is a quite direct means of measuring the

distribution of the nucleonic component of the cosmic rays, and hence the energy distribution of the cosmic rays since this component of the cosmic rays is by far the energy dominant one. Only the relevant matter distribution is needed to interpret the gamma ray m .surements and this is reasonably well known. These data are free of the uncertainties associated with the synchrotron data, which also will be discussed here because they are quite important, but do require assumptions regarding the magnetic field and are related to the cosmic ray electron component which carries only about 1 percent of the total energy. The level and density distribution of the cosmic rays is needed to understand the dynamic balance existing in a galaxy and the scale of coupling of the cosmic rays to the matter. It will be seen that it also may be possible to improve the knowledge of the normalization parameter for molecular hydrogen or at least set a limit.

In this paper, the relevant information on local galaxies will be reviewed first, including the data related to atomic and molecular hydrogen and synchrotron radiation. Next the approach to calculating estimated gamma ray intensities will be outlined and the intensities to be expected from some local galaxies will be given. This section will be followed by a discussion of synchrotron radiation and its interpretation. Particular attention then will be given to the Large Magellanic Cloud. The subject matter to be described here will draw heavily on the paper of Ozel and Fichtel (1988) and the work in progress of Fichtel, Ozel, and Stone (1990), to be submitted for publication soon.

## II. RELEVANT INFORMATION ON LOCAL GALAXIES

Whether one assumes the cosmic ray density in other normal galaxies is similar to our own or correlated with the matter, straightforward calculations of the type to be described in the next section suggest that only three are likely to be seen or close to being detectable by the next generation of high energy gamma ray telescopes. These are the Andromeda Galaxy, M31, and the Large and Small Magellanic Clouds. M31 is much further away, but is also larger. M31 would appear to be an especially attractive object for study because its structure and size are similar to our own. The Large Magellanic Cloud is only about 7 kpc in diameter and has much less mass than our own. The Small Magellancic Cloud has even less mass, but as will be discussed below, it has a possible bright region from the consideration of potential gamma ray emission. This paper, therefore, will be restricted to these three galaxies.

The three galaxies just mentioned will be discussed individually in regard to their hydrogen column densities. The angles between the normal to the plane of each galaxy and the line of sight are: 74° to 77° for M31, 30° to 33° for the LMC, and 60° to 73° for the SMC (Berkhuijsen, 1977; Ichikawa et al., 1985; de Vaucouleurs and Freeman, 1973; Luiseau et al., 1987).

The matter of interest for the discussion here is that with which cosmic rays interact to produce gamma rays. The basic observations needed are, therefore, those giving information on the diffuse atomic and molecular hydrogen. For atomic hydrogen, the interpretation, of the 21 cm data is, of course, straightforward, but, for molecular hydrogen, the CO measurements are not. The ratio $N_{H_2}/W_{CO}$, called $X_G$, is determined in a number of ways, including the gamma ray measurements in our own galaxy, and for our galaxy has

recently been estimated to be $2.8 \times 10^{20}$ cm$^{-2}$ K km s$^{-1}$ (Bloemen et al., 1984), although values in the range from (1 to 3) $\times 10^{20}$ cm$^{-2}$ K km s$^{-1}$ have been proposed. This range of values is not, however, universally true, as will be noted later.

For the atomic hydrogen column density of the Andromeda Galaxy (M31), the results of Davies and Gottesman (1970) are used. The galaxy has an oblong shape with two principal gas density maxima. The southern parts of M31 have been studied in enough detail to indicate that the CO distribution is similar on a course scale to that of the HI gas. The molecular hydrogen appears to form in cloudlike structures similar in size and shape to the galactic ones. Available overall CO studies of M31 indicate that the total molecular hydrogen mass is about an order of magnitude less than that of the atomic hydrogen (Stark, 1979) and, therefore, is of much less importance for the production of gamma rays than in our galaxy.

For the atomic hydrogen column density, the 21 cm map given by Mathewson and Ford (1984) for the SMC and LMC is used. Their diagram differs in its HI contours from those of Rohlf et al. (1984) by about a factor of two, but agrees well with the estimated total gas content of the SMC and LMC. The diffuse matter content of the Magellanic Clouds is known to differ from that of our galaxy in significant respects (Elmergreen et al., 1980). It is estimated that these smaller galaxies still contain 10 percent to 30 percent of their total mass in diffuse form, compared to a few percent for our galaxy and M31. The large size of the clouds and the weak emission require long integration times at a large number of positions for a full CO study. Cohen et al. (1988) have just recently completed a full survey of the central 6° x 6° of the LMC with an angular resolution of 8'.8 for the 1→0 line at 2.6 mm of CO. The emission is dominated by an extremely large complex of molecular clouds extending south from 30 Doradus in the general region of the maximum 21 cm emission. Cohen et al. found that the correlation of CO luminosisty with linewidth is similar to that for Galactic clouds, but, for a given linewidth, the LMC clouds are a factor 6 fainter in CO, comparable to the factor of 4 lower metallicity in the LMC. Assuming $N_{H_2}/W_{CO}$ is 6 times larger in the LMC than in the Galaxy, or about 1.7 x $10^{21}$ cm$^{-2}$ K km s$^{-1}$, the total molecular mass of the LMC is 1.5 x $10^8$ M$_0$., and the ratio of molecular to atomic mass is about 0.4 for the region of the CO survey.

For the SMC, the atomic hydrogen content is reasonably well known also, and the map of Mathewson and Ford (1984) and that of Loiseau (1984) were used, as noted. In the SMC, the CO emission is even significantly weaker than the LMC. Primarily for this reason, a full coverage has not yet been achieved, with only selected points having been examined (Israel, 1984). On the basis of the low level of the emission, and also the dust density being observed to be smaller, it is generally assumed that the molecular content of the SMC is relatively small, with the ratio of molecular to atomic hydrogen by mass being no more than about 0.1 (Rubio et al., 1984). The total mass of the gas is then estimated to be 4.8 x $10^8$ M$_0$. It should be noted that, whereas the observed atomic hydrogen column density is larger at its maximum for the SMC than the LMC in a limited region, the angle of the line of sight to the normal to the galaxy is larger for the SMC. The column density perpendicular to the plane of the SMC galaxy is estimated to be a factor of 2 1/2 or 3 smaller than the observed column density because of the large secant of the angle. The column densities perpendicular to the plane are then on the average smaller

for the SMC than the LMC. This feature is important in the discussion of the expected cosmic ray density to come later.

Synchrotron radiation also is detectable from local galaxies. Its interpretation is somewhat complex and involves some assumptions. Therefore, the calculation of expected high energy gamma radiation based on the matter distribution will be discussed first in the following section, with a description of the synchrotron radiation coming in the subsequent section to that.

### III. CALCULATION OF ESTIMATED GAMMA RAY INTENSITIES BASED ON THE MATTER DISTRIBUTIONS

As cosmic rays, which consist of electrons, protons, and other bare nuclei, traverse space, they interact with the diffuse matter and photons to create gamma rays. They also interact with the magnetic fields, but for interstellar space this interaction is negligible for the production of gamma rays compared to the other two. The cosmic ray nucleon interactions with interstellar matter give rise to gamma rays primarily through the production of neutral pions, with other channels producing lesser numbers of gamma rays. The resulting gamma ray spectrum has a maximum at about 70 MeV and is approximately symmetric on a logarithmic energy scale. Cosmic ray electron interactions with interstellar matter lead to a monotonically decreasing spectrum. For the relative numbers of electrons and nuclei that exist in our galaxy, the combined spectrum is one which decreases with energy, but has a bulge in the region of the neutral pion peak. Electrons also interact with the interstellar photons, optical, infrared, and blackbody, to produce gamma rays through the Compton process. The Compton gamma radiation thus produced is also a monotonically decreasing function with energy, but, for the case of our galaxy, is much less intense than the bremsstrahlung radiation. A general discussion of these processes together with intensity estimates and references to the original papers is given by Fichtel and Trombka (1981). The principal justification for this explanation of the galactic diffuse radiation is that the resulting intensity distribution and energy spectrum for the diffuse gamma radiation in our galaxy match the observations well. See, for example, figures 5-5 and 5-6 in Fichtel and Trombka.

For the calculations performed here it was assumed that the approach just described is valid and that the correction for elements heavier than hydrogen is the same in the other galaxies as it is in our own. Therefore, as in the calculation in our own galaxy, an estimate of the hydrogen density is made and then multiplied by the appropriate factor. The source functions used are those in the work described above slightly modified to take into account refinements made in recent work, particularly in the nuclei-nuclei interaction part (Stephens and Badhwar, 1981, Morris, 1984, Dermer, 1986, Stecker, 1988). The source function used for the number of gamma rays procured for energies above 100 MeV was $2.0 \times 10^{-25}$ $n_H$ $r_c$ gamma rays $cm^{-3} s^{-1}$, where $n_H$ is the number of hydrogen nuclei, atomic and molecular, $cm^{-3}$, and $r_c$ is the ratio of the cosmic ray density to that in the vicinity of the Earth.

In considering the galaxies closest to our own, the interstellar hydrogen can be estimated from the measurements of the 21 cm line, and, as in the case of our galaxy, the molecular hydrogen can be estimated from the CO radio data and other considerations, as will be discussed for each individual case

below.  The cosmic ray spectrum and composition in the other galaxies is, of course, not known.  The best initial assumption appears to be that the processes which produce the cosmic rays in our galaxy are the same elsewhere, and, unless the pathlength and lifetime are dramatically different in the other galaxy, the spectrum should be similar.  When gamma ray results exist, this assumption may be checked by comparing the observed spectral shape to the predicted one.  Since the observable photon density in the nearby galaxies is similar to our own, and the blackbody radiation is presumably the same, the Compton contribution to the gamma radiation should be relatively small.

The density distribution of the cosmic rays in the galaxy is, in fact, what it is hoped that the gamma ray measurements will reveal.  However, for the purpose of the work here, certain hypotheses will be made so that the predicted gamma ray intensity can be calculated.  These results will serve two purposes.  One is to provide an indication of the level of the gamma radiation

that might be expected, and the other is to provide a basis for testing the theoretical assumptions.

The simplest assumption is that the cosmic rays are uniform throughout the Galaxy; however, this is likely to be true only if the cosmic rays are universal rather than galactic.  The greatest theoretical problem with the cosmic rays being universal is the large amount of energy required.  It is too large to be supplied by galactic leakage, unless one assumes the average galaxy is quite different than our own.  The cosmic rays would, therefore, have to be primordial.  There are also other concerns, such as the energy spectrum.  Further, most authors (Bignami and Fichtel, 1974; Paul et al., 1974; Schlickeiser and Thielheim, 1974; Bignami et al., 1975; Fichtel et al., 1975; Stecker et al., 1975; Puget et al., 1976; Paul et al., 1976; Hartman et al., 1979; Bhat et al., 1985; Bloemen et al.,1986; Strong et al., 1987) who have examined the question for our own galaxy conclude that the cosmic ray density is not uniform there.  Although the various authors differ on details, they generally conclude that the cosmic ray density appears, at least on a course scale, to be enhanced where the matter density is greater.  However, the limited existing data does not permit an absolute statement on this matter at present.

There are fundamental theoretical considerations also which lead to the conclusion that the cosmic ray density is correlated with the matter density, at least on the scale of arms and large clouds (Bignami and Fichtel, 1974).  Briefly, under the presently generally accepted assumption that the cosmic rays and magnetic fields are primarily galactic and not universal, these fields and cosmic rays can only be constrained to the galactic disk by the gravitational attraction of the matter (Biermann and Davis, 1960; Parker, 1966, 1969, and 1977).  Together the total expansive pressure of these three effects is estimated to be approximately equal to the maximum that the gravitational attraction can hold in equilibrium.  Assuming the solar system is not at an unusual position in the galaxy, these features suggest that the cosmic ray density throughout the galaxy may generally be as large as could be contained under near equilibrium condition.

Perpendicular to the plane of the galaxy, since the scale height for the matter is small compared to that of the cosmic rays, the cosmic ray density may be taken as constant, i.e., independent of the distance perpendicular to

the plane, for the region relevant for the majority of the cosmic ray matter interactions.

Since the other galaxies being considered are being observed from the outside at other than a very small angle with respect to the plane, there is not the need to be concerned about variations of the cosmic ray density along the line of sight because the variations are believed to be on the scale of arms, or at least very large clouds. Then, the cosmic ray density may be removed from the integral and simply multiplied by the column density. Hence, for any direction the gamma ray flux above 100 MeV will be given by the expression:

$$j_\gamma = 2.0 \times 10^{25} \times \frac{1}{4\pi} \left( \int n_H dl + \int n_M dl \right) r_c$$

$$\text{photons (E>100 MeV) cm}^{-2}\text{s}^{-1} \tag{1}$$

Here, $r_c$ is the ratio of the cosmic ray density to that in the local region of our galaxy. There is a correction in the form of an addition for the Compton radiation, but it is almost certainly less than 10 percent for directions which are not within a small angle of the plane of a galaxy.

For the constant cosmic ray density case, $r_c = 1$. If the cosmic ray density is related to the matter on a course scale, then

$$r_c = \frac{\overline{\left( \int n_H dl + \int n_M dl \right)}}{N_1 \times 10^{20} \cos (i)}. \tag{2}$$

where the average is taken over the region in question as long as its dimensions are of the order of a kiloparsecs or greater. $N_1$ will be taken as 8 corresponding to an average hydrogen nucleus density of just over one for the local arm of our galaxy in the plane and the local scale height.

The Magellanic clouds are about 60 kpc away and hence 1° corresponds to about 1 kpc. Both have dimensions somewhat larger than an arm segment in our galaxy. If the cosmic rays are local to the galaxy, and there have been enough sources to fill them to their energy containment limit, the cosmic ray density might be larger in the central region of the LMC than in the local region of our galaxy due to the larger average column density. A gradient in $r_c$ would be expended. For the Small Magellanic Cloud, when the column density is corrected for the large inclination angle, it is smaller than for the LMC, $r_c$ would be smaller, or perhaps about one or less.

M31 is much further away; 1° in its case corresponds to about 12 kpc. The discernible structure seems limited. The column densities are rather lower, and the cosmic ray density over the region would, therefore, under similar assumptions, be similar to the local cosmic ray density, possibly enhanced a bit near the two highest density regions, but lower on the edges. Hence, no significant cosmic ray enhancement averaged over a square degree is expected; over most of the remaining region, it would be less.

The expected intensities integrated over the whole galaxy are shown in Figure 1 for the case of $r_c = 1.0$. According to the discussion above, all of the $r_c$ values might be expected to be near one. Gradients would be expected.
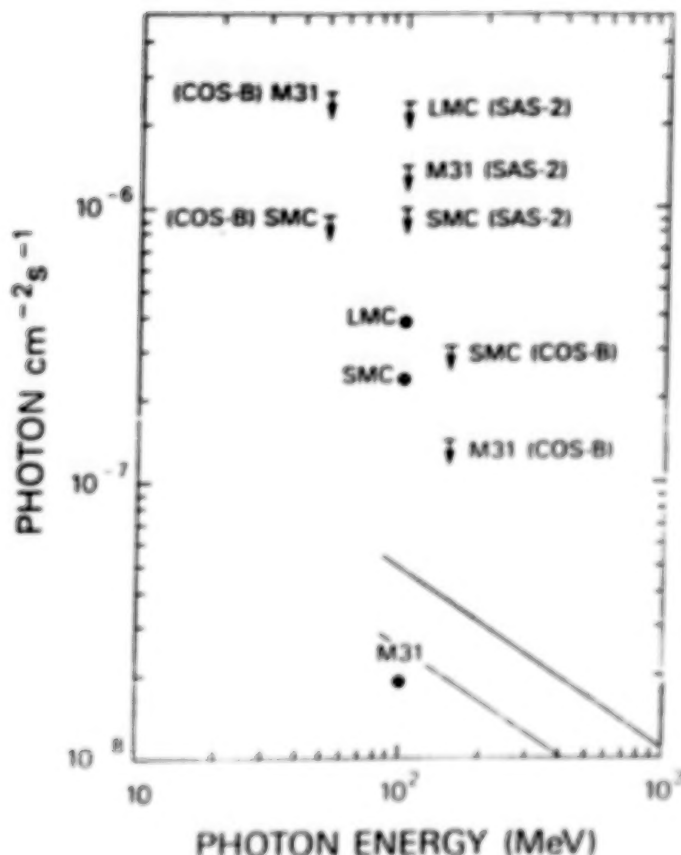
Fig. 1--Existing upper limits to the integral flux of gamma rays from the SMC, LMC, and M31 for the energy shown together with the fluxes calculated by Ozel and Fichtel (1988) shown as closed circles for the case where the average cosmic ray density is the same as in the local region of our galaxy. The SAS-2 limits are those of Fichtel et al. (1975), and the COS-B limits are those of Pollock et al. (1981). Also shown is the estimated GRO EGRET sensitivity limit for 2- and 4-week exposures; the GAMMA-1 limit is expected to be about a factor three higher. The exact sensitivity level depends also on the angle of the source with respect to the telescope axis as well as other factors.

## IV. SYNCHROTRON RADIATION

If the electrons have a spectrum of the form

$$N(E)dE = KE^{-\gamma}dE \tag{3}$$

where N(E) is the number of electrons ergs$^{-1}$ cm$^{-3}$, and where the electrons are homogenous and isotropic, then Ginzburg and Syrovatskii (1964) have shown that the intensity of the radiation is given by

$$I_\nu = 1.35 \times 10^{-22} a(\gamma) LKH^{(\gamma+1)/2} \left(\frac{6.26 \times 10^{18}}{\nu}\right)^{(\gamma-1)/2}$$
$$\text{ergs cm}^{-2} \text{ s}^{-1} \text{ ster}^{-1} \text{Hz}^{-1} \tag{4}$$

in the presence of random magnetic fields. In this expression, a is a slowly varying function of $\gamma$ with a value near 0.1 for the range of interest here, L is the length over which the electrons and magnetic fields are present, and H is the magnetic field strength. From equation (4), it is seen that, if the synchrotron spectrum is known, giving I as a function of $\nu$ over a reasonable frequency range, and L can be estimated, then K may be determined if H is known.

It is also important to know the relationship between the maximum in the synchrotron radiation and a given electron energy, which is

$$E_M = 4.7 \times 10^2 \left(\frac{\nu}{H_\perp}\right)^{1/2} \text{ eV} \tag{5}$$

If there is a spectrum of electrons of the type observed experimentally, rather than a monoenergetic distribution, then Webber has shown that the appropriate relationship is

$$E_{eff} = 2.5 \times 10^2 \left(\frac{\nu}{H_\perp}\right)^{1/2} \text{ eV} \tag{6}$$

The frequency range of interest in the LMC study here is from about 20 to 1400 MHz., corresponding then to electrons in the energy range from approximately 0.50 to 4.2 GeV for a 5 μG field, or in fact a somewhat broader range when the distribution functions are considered, and 0.30 to 2.5 GeV for a 14 μG field. The relevance of the magnetic field value range will be seen in the next paragraph.

It should be mentioned at this point, that historically there had been a concern regarding the synchrotron radiation observed in our galaxy. This was that the level appeared to be higher than would have been expected on the basis of the deduced electron spectrum and the magnetic field thought to exist. Recently, however, Fichtel, Özel, and Stone (1990) have shown that with the interstellar cosmic ray electron spectrum now believed to exist based in part on the SAS-2 and COS-B gamma ray data at high latitudes, and the range of values for the total magnetic field including the random part now estimated from several sources, agreement can be obtained. These authors deduce a random magnetic field of about 11 μG for the local region, consistent with the currently estimated range of 5 to 14 μG, deduced in other ways.

## V. THE LARGE MAGELLANIC CLOUD

Fichtel, Özel, and Stone further show that within the uncertainties of existing data the nonthermal radiation from the LMC and our galaxy have the same spectral shape. They then assume that the magnetic field pressure density in the LMC has the same relationship to the cosmic ray pressure as that in our galaxy as well as the relationship between the cosmic ray energy density and the electron spectrum being the same in the LMC as in our galaxy. Since the ratios of the cosmic ray electron intensity to the cosmic ray nucleon density and that to the magnetic field are assumed to be the same as in in our galaxy, there is a fixed relation between K and H in Equation (4). Specifically, since the magnetic field pressure is proportional to $H^2$, if $K_0$ and $H_0$ are the local values of K and H in our galaxy and $w(x_i)K_0$ is a value in a local region of the LMC, then the corresponding H value in the LMC is $[w(x_i)]^{1/2}H_0$, to maintain the relationship between the cosmic-ray and magnetic fields described earlier.

If L is known, $w(x_i)$ may be determined from the knowledge of the synchrotron radiation. Following Klein et al. (1989), Fichtel, Özel, and Stone used an effective disc thickness for L of 1 kpc, the same as in our galaxy (Remember L for the LMC is the full thickness, not the half thickness as in our galaxy where the Sun is in the middle of the plane.). They then proceed to calculate w as a function of position for the LMC. They studied three frequencies 45 MHz, 408 MHz, and 1.4 GHz. There are different considerations at each

frequency and for each measurement including the degree of the thermal resolution, the beam size, and uncertainties.

For purposes of illustration, the results of their study at 1.4 GHz based on the measurements of Klein et al. (1989) are shown in Figure 2. It is seen that the cosmic ray density level on the average is similar to our own on the average although a bit lower if the assumptions stated at the beginning of this section are valid. Notice also that a nonuniform cosmic ray level is predicted.
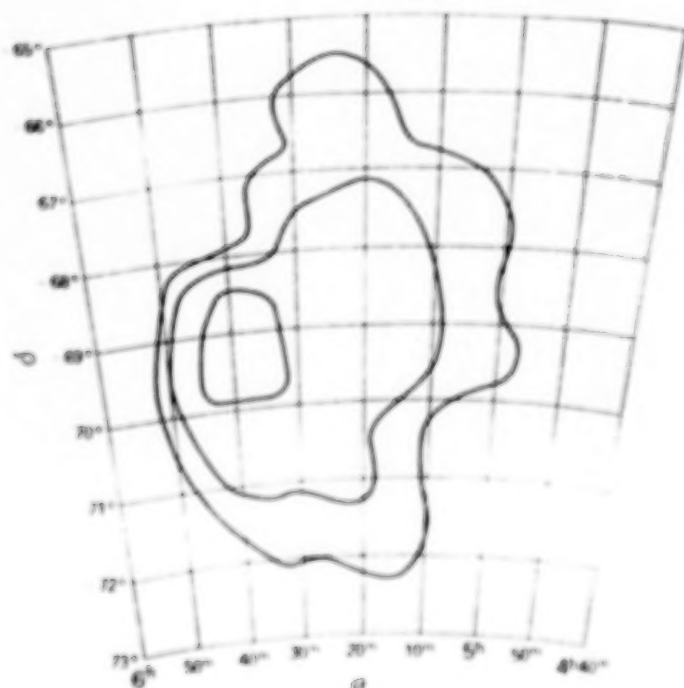


Fig. 2--The contour levels for the predicted cosmic ray energy density levels relative to those in our galaxy based on the 1400 MHz data of Haynes et al. (1986). The contour levels shown correspond to w equal to 0.59, 0.78, and 1.01. The contents of the figure are from Fichtel, Ozel, and Stone (1990).

In Section III, it was noted that, if the cosmic rays are galactic and not universal and if other assumptions hold, then a prediction can be made for the cosmic ray density level. Before th's step can be taken, however, the scale of coupling must be known. On the basis of the scale height perpendicular to the plane and other considerations it has been estimated that the scale height might be of the order of 1 kpc or somewhat greater. Consider the matter column densities shown in Figure 3 and remember that $1°$ corresponds approximately to 1 kiloparsec for the LMC. When corrected for the cosecant of the angle between the line of sight and the perpendicular to the plane of the LMC a level of $1.0 \times 10^{21}$ atoms $cm^{-2}$ is approximately equal to the local thickness of our galaxy. If one considers the coupling effect for the cosmic rays having a scale of 1 kpc or greater, one would predict the cosmic ray density profiles to be much flatter and not have nearly as sharp a peak. It is at least reasonable that such a process would lead to contours similar to those of Figure 2; however, it would appear that the magnitude would be somewhat different, perhaps by a factor of 1 1/2. This difference is within the known uncertainties. See Fichtel, Ozel, and Stone (1990) for a more detailed quantitive discussion.

As noted in Section II, future high energy gamma ray measurements should be able to provide information, which, although lacking the degree of angular

resolution that would be desired, will bear on this question and give a quantitative measure of the average cosmic ray density and hopefully some indication of their distribution. There are two benefits to the independent high energy gamma ray measurements in addition to their being a second
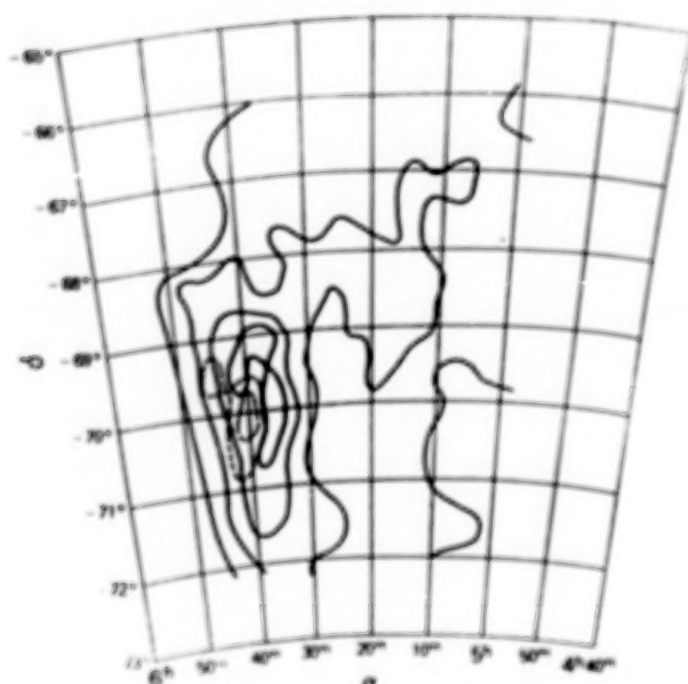


Fig. 3--The matter column density levels for the LMC. The solid contour lines refer to atomic hydrogen and correspond to column densities of (0.5, 1.0, 2.0, and 3.0) x $10^{21}$ atoms $cm^{-2}$. The dashed contour lines refer to molecular hydrogen and correspond to column densities of (0.5 and 1.0) x $10^{21}$ atoms $cm^{-2}$. For the atomic and molecular hydrogen column densities, the data of Mathewson and Ford (1984) and Cohen et al. (1988) respectively were used. The contents of the figure are from Fichtel, Ozel, and Stone (1990).

observation, one is that they are directly related to the dominant energy component of the cosmic rays, and the other is that their interpretation does not involve any assumptions about the magnetic fields.

## VI. SUMMARY

The study of the matter density distribution and the synchrotron radiation in the case of the LMC suggest that the SMC and the LMC should be detectable in high energy gamma rays with EGRET and GAMMA, and M31 might be detectable. It also seems that for all three of these galaxies the cosmic ray density is expected to be of the order of that in our own galaxy, but varying slowly with position if the cosmic rays are galactic in nature. The study of the LMC synchrotron radiation indeed supports the nonuniformity of the cosmic ray density there.

A study of the synchrotron radiation and the matter column density in the LMC seems to indicate that it is possible to construct a consistent picture of the LMC based on the dynamic balance between the cosmic rays, the magnetic fields, and the kinetic motion of matter on the one side and gravitational attraction on the other and the additional feature that the magnetic field must be strong enough to contain the cosmic rays. Further a comparison of the contours related to the matter density and those related to the cosmic ray density predicted by the synchrotron radiation suggests that the scale of the coupling between the cosmic rays and the matter is probably of the order of a kiloparsec or larger since there is a smoothing required relative to the matter density contours to make the cosmic ray contours more consistent with

those of the synchrotron radiation. This scale of coupling is quite
reasonable based on considerations of our own galaxy.

## REFERENCES

Berkhuijsen, M., 1977, Astron. Astrophys., 57, 9.
Bhat, C. L., Issa, M. R., Houston, B. P., Mayer, C. J., Wolfendale, A. W.,
    1985, Nature, 314, 511.
Biermann, L. and Davis, S., Jr., 1960, Zs, F. Ap., 51, 19.
Bignami, G. F. and Fichtel, C. E., 1974, Ap. J. (Letters), 109, L65.
Bignami, G. F., Fichtel, C. E., Kniffen, D. A., and Thompson, D. J., 1975, Ap.
    J., 199, 54.
Bloemen, J., et al., 1984, Atron. Astrophys., 139, 37.
Bloemen, J. B. G. M., et al., 1986, Astron. Astrophys. 154, 25.
Cohen, R. S., Dame, T. M., Garay, G., Montani, J., Rubio, M., and Thaddeus,
    P., 1988, Ap. J. (Letters).
Davies, R. D. and Gottesman, S. T., 1970, Mon. Nat. of Roy. Astron. Soc., 149,
    237.
de Vaucouleurs, G., Freeman, K. C., 1973, Vistas in Astron., 14, 163.
Dermer, C. D., 1986, Ap. J., 307, 47
Elmergreen, B. G., Elmegreen, D. M., Morris, M., 1980, Ap. J., 252, 461.
Fichtel, C. E., Hartman, R. C., Kniffen, D. A., Thompson, D. J., Bignami, G.
    F., Ogelman, H. B., Ozel, M. E., Tumer, T., 1975, Astrophys. J., 198, 163.
Fichtel, C. E. and J I. Trombka, 1981, Gamma Ray Astrophysics, New Insight
    into the Universe, NASA SP 453.
Fichtel, C. E., 1988, Proceedings of the Workshop on High Resolution Gamma Ray
    Cosmology, UCLA, November 2-5.
Fichtel, C. E., Ozel, M. E., and Stone, R., 1990, "Cosmic Rays and the Dynamic
    Balance in the Large Magellanic Cloud", submitted for publication.
Ginzburg, V. L. and Syrovatskii, S. I., 1964, The Origin of Cosmic Rays, New
    York, Macmillan.
Hartman, R. C., Kniffen, D. A., Thompson, D. J., Fichtel, C. E., Ogelman, H.
    B., Tumer, T., and Ozel, M. E., 1979, Ap. J., 230, 597.
Houston, B. P., Riley, P. A. Wolfendale, A. W., 1983, 18th International
    Cosmic Ray Conf., Bangalore, I. 89.
Ichikawa, T., et al., 1985, Pub. Astron., Soc., Japan, 37, 439.
Israel, F. P., 1984, "Structure and Evolution of Magellanic Clouds", ed. S.
    van den Berg and K. S. de Boer, p. 319.
Klein, U., Wielebinski, R., Haynes, R. F., Malin, D. F., 1989, Astron.
    Astrophys., 211, 280.
Loiseau, N., 1984, Ph.D. Thesis, University of LaPlata, Argentina.
Loiseau, N., Klein, U., Greybe, A., Wielebinski, R., Haynes, R. F., 1987,
    Astron. Astrophys., 178, 62.
Mathewson, D. S. and Ford, V. L., 1984, "Structure and Evolution of Magellanic
    Clouds", ed. S. van den Berg and K. S. de Boer, p. 125.
Morris, D. J., 1984, J. Geophys. Res., 89, 10685.
Ozel, M. E. and Berkhuijsen, E. M., 1987, Astron. Astrophys., 172, 378.
Ozel, M. E. and Fichtel, C. E., 1988, Ap. J., 335, 135.
Parker, E. N., 1966, Ap. J., 145, 811.
Parker, E. N., 1969, Space Sci. Rev., 9, 654.
Parker, E. N., 1977, Cosmic Ray Propagation and Containment, in "The Structure
    and Content of the Galaxy and Galactic Gamma Rays", NASA CP-002, 283-300.
Paul, J., Casse, M., and Cesarsky, C. J., 1974, in "The Context and Status of

Gamma Ray Astronomy", ed. B. G. Taylor (ESRO SP. 106), 246.

Paul, J., Casse, M., and Cesarsky, C. J., 1976, Ap. J., 207, 62.

Puget, J. L., Ryter, C., Serra, G., and Bignami, G., 1976, Astron. and Astrophys. 50, 247.

Rohlf, K., Kreitschmann, J., Siegman, B. C., Feitzinger, J. V., 1984, Astron. Astrophys., 137, 343.

Rubio, M., Cohen, R., Montani, J., 1984, "Structure and Evolution of Magellanic Clouds", 1984, ed. S. van den Berg and K. S. de Boer, Reidel pub., 399.

Schlickeiser, R. and Thielheim, K. O., 1974, Astron. Astrophys., 34, 109.

Stark, A. A., 1979, Ph.D. Thesis, Princeton University.

Stecker, F. W., Solomon, P. M., Scoville, N. Z., and Ryter, C. E., 1975, Ap. J., 201, 90.

Stecker, F. W., 1988, to be published in the Proceedings of the NATO Advance Study Institute on Cosmic Gamma-Rays and Cosmic Neutrinos.

Stephens, S. A. and Badhwar, G. D., 1981, Astrophysics and Space Science, 216, 213.

Strong, A. W., Bloemen, J. B. G. M., Dame, T. M., Grenier, I. A., Hermsen, W., Lebrun, F., Nyman, L. A., Pollock, A. M. T., and Thaddeus, P., 1987, Proc. of 20th International Cosmic Ray Conf., Moscow, OG 2.2-6.

# DISCUSSION

*Stan Hunter:*

When you use the magnetic field and cosmic ray abundance observed in our galaxy to predict the gamma-ray flux from the LMC, how do you account for spiral vs. irregular structural difference?

*Carl Fichtel:*

It is only assumed that the cosmic ray energy density and the magnetic field energy density have the same ratio. This implies that the cosmic ray sources are adequate. The latter seems justified on the basis of the relative level of the two. There seems no reason to suspect a difference between the two galaxies, particularly, since the irregular field appears to significantly exceed the uniform component in our galaxy.

# Active Galaxies

# GAMMA RAYS FROM ACTIVE GALACTIC NUCLEI

**Demosthenes Kazanas**

Laboratory for High Energy Astrophysics
NASA/Goddard Space Flight Center
Greenbelt, MD 20771

## ABSTRACT

The general properties of Active Galactic Nuclei (AGN) and quasars are reviewed with emphasis on their continuum spectral emission. Two general classes of models for the continuum emission are outlined and critically reviewed in view of the impending GRO launch and observations. The importance of GRO in distinguishing between these models and in general in furthering our understanding of AGN is discussed.

## I. INTRODUCTION

In this talk I will review in very broad terms the status of our current understanding of AGN. The subject of AGN is a vast one and occupies a large number of theorists and observers working on such diverse energy bands as radio and $\gamma$-rays. The short space allocated for this review is by no means sufficient to even touch upon these very diverse subjects in a comprehensive manner. Due to the very general and broad character of this review I apologize to the many authors whose work I am unable to quote and give proper credit.

There have been over twenty five years since the discovery of quasars and despite much observational and theoretical effort we lack a fundamental understanding of the physics of these objects. The few facts that have become generally accepted after much observational effort and debate is that quasars indeed represent extremes of galactic nuclear activity. In that sense are very similar to the Seyfert I galaxies that had been known for some time, except for their much greater luminosities. In fact, as it will be soon discussed, this similarity does not pertain only to their morphology but also to the spectral distribution of their radiation. Another fact for which consensus has been reached is that quasars and Seyfert galaxies along with an additional number of classes of objects (e.g. Seyfert IIs, BL Lacs, OVVs, LINERs etc.), collectively known as Active Galactic Nuclei, derive their
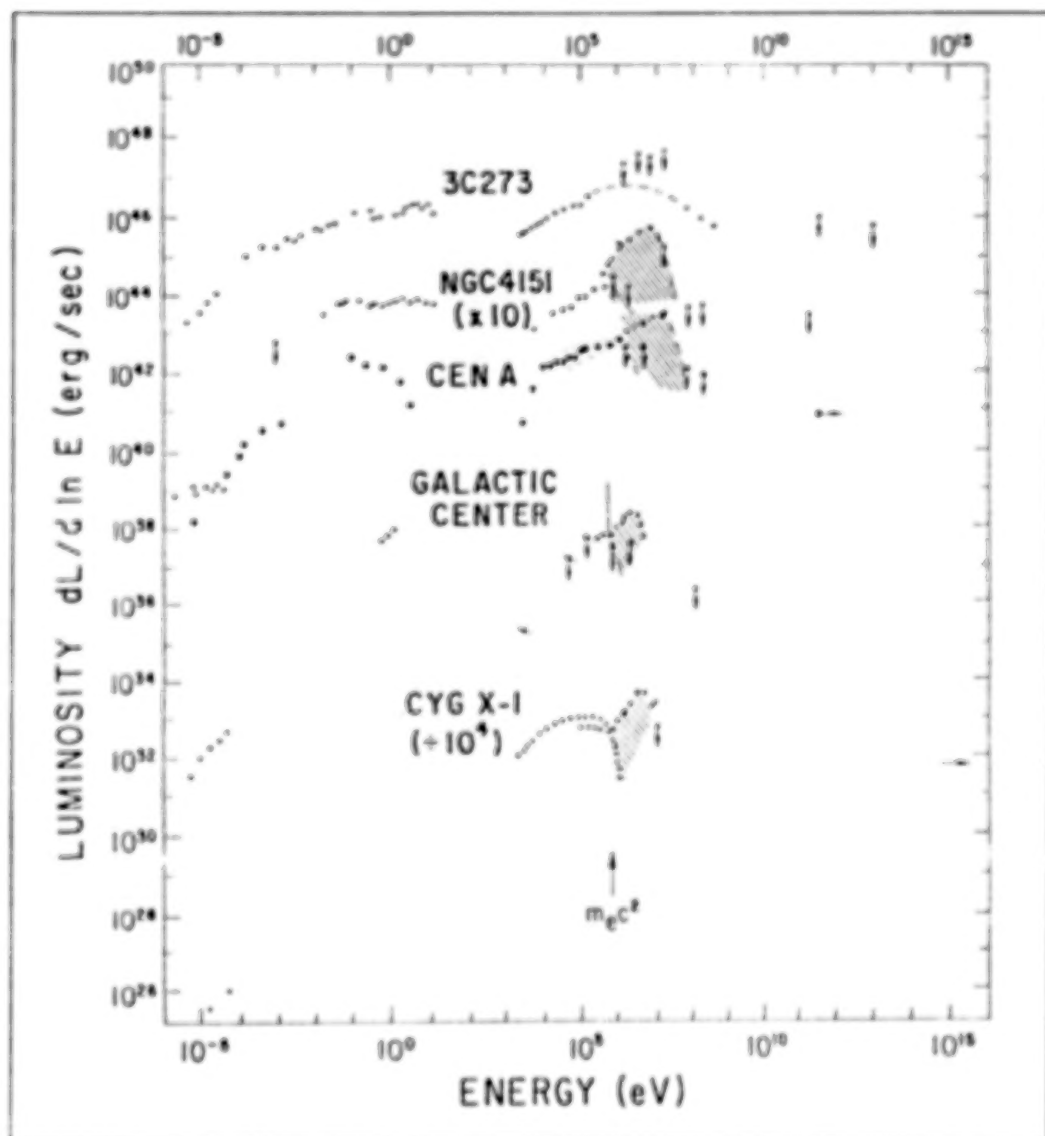
*Figure 1.* The broad band spectra of five accreting compact sources plotted in energy per decade versus frequency over the whole electromagnetic spectrum.The top three belong to AGN: A quasar (3C 273), a Seyfert I galaxy (NGC 4151) and a radio galaxy (Cen A). The other two spectra correspond to galactic objects (from Lingenfelter 1987).

power from accretion of matter onto a compact object, most likely a massive black hole (Rees 1984). This conclusion has been reached mainly on the basis of the observed rapid variability and arguments concerning their efficiency of radiation emission.

This is however where the consensus ends. Beyond this point opinions tend to diverge as to the many aspects of the problem; there is very little agreement even on the source of the matter that presumably powers by its accretion these objects. The fact that every energy band (from radio to γ-rays) seems to contain a sizable fraction of the total bolometric luminosity (see e.g. figure 1) gives confidence to the respective observers that they are looking at some important feature of the puzzle of the mechanism that powers these

objects. In addition, having agreed that accretion is the ultimate energy source of these · objects, the physical conditions near the black hole (where most of the energy is generated) are coupled to the physical conditions at much larger radii, where quite likely the source of accretion material resides. In addition to this dynamical coupling there is coupling of these regions through radiation transfer (e.g. by reprocessing part of the continuum radiation) which in general also changes the frequency of the transfered photons; this effect could in turn affect the local physical conditions thus changing the dynamics of accretion and so on. We are hence faced with the possibility of quite a complex system that (possibly but not necessarily) interrelates the dynamics and the radiation transfer and which spans 6-12 decades in frequency and over 4 decades in radius, and which might not even be in thermodynamic equilibrium. It should not therefore be surprising that not much progress has been achieved towards the "understanding" of these objects.

At this point one should reflect for a moment as to what is meant by "understanding", since this will determine not only when this goal has been achieved, but also strategies necessary for its achievement. It is my view that an "understanding" of these objects will have been attained when, through the dynamics of accretion, one is possible to account for their *major* spectral features and at the same time address their *major* morphological characteristics, along with the general aspects of their evolution, without the use of an inordinate number of free parameters (I personally would not allow for more than two). It is instructive to consider a class of astrophysical objects for which such an "understanding" has indeed been achieved, namely that of stars; as it is well known the general features of the spectral types of the main sequence and the general aspects of stellar evolution can be "understood" rather simply in terms of hydrostatic equilibrium, energy generation by nuclear reactions and *one* free parameter, namely their mass. Interestingly, for the stars it was their energy generation mechanism that was least understood, thus completely obscuring all the aspects of their evolution; once nuclear reactions were incorporated into the problem the right ages and the general evolutionary features of stars became apparent. In AGN, on the contrary, we think we understand the ultimate energy source (accretion), but we apparently do not understand the mechanism by which accretion energy is converted to radiation; therefore it becomes impossible to predict or understand the frequency distribution of emitted radiation. This lack of understanding of the central engine then percludes the further understanding of the other aspects of the problem (i.e. morphology and evolution).

The large number of decades in frequency over which the radiation is observed and the potentially large number of radii which could contribute to the radiation emission at a particular frequency, suggest that the problem under examination is inherently complicated and there may not necessarily exit a simple (i.e. of one or two parameters) solution to it. One can in fact easily think of a number of parameters that could in principle be relevant to the dynamics and/or radiation emission from these objects (such as the mass, the accretion rate, the specific angular momentum, the magnetic field, the angle to the line of sight). Bearing in mind the variety of features in the one parameter class of astrophysical objects we "understand", namely that of stars, one would in principle expect a much larger variation in the properties of the central engine alone. Actually, considering the above arguments, the spectra of AGN appear to be surprisingly similar in their general

outline. This is exemplified in figure 1 taken from Lingenfelter (1987), where the spectra of three morphologically different classes of AGN are presented, spanning roughly four orders of magnitude in luminosity. The apparent similarity in the spectral distribution of emitted radiation suggests that there ought to be an underlying (as yet unknown) mechanism which enforces it. It is true the that the detailed spectra do vary from object to object and trends have been suggested among classes of objects (Wilkes and Elvis 1987). However, some of this diversity must be attributable to the individual character of a particular object (or class of objects) and therefore not considered as "fundamental" when detailed modeling is attempted. Given however the roughly equal energy per decade observed and the possibility of interaction of the various energy bands through reprocessing of the radiation, as discussed above, it becomes very much a "judgement call" as to what constitutes a fundamental or an incidental feature. Nonetheless such a "choice" of the important features is quite necessary, or it is very difficult to produce any models which would provide a useful (i.e. with a small number of parameters) representation of reality.

In the following (section II) I will present two very different and general classes of models based on two different notions as to what are the "fundamental" features that should serve as the basis on which our models of these objects should be based and I will discuss the pros and cons of each class. In section III I will discuss the impact of GRO observations in distinguishing between these two classes of models. Finally, in section IV I will give an example of how a model could with a rather small number of parameters describe potentially a large number of classes of AGN and the implications of such a model on $\gamma$-ray observations.

## II. THE MODELS

### a. Accretion Disk - Blue Bump Models

The very fact that AGN are powered by the release of accretion energy allows some simple, straightforward estimates of the radiation characteristics (i.e. spectrum and efficiency) of this process. The mathematically and physically simplest model one can construct is that of spherical accretion and the free-free emission of radiation by the matter which is compressionally heated as it accretes on the black hole; unfortunately the efficiency of this process is very small ($\simeq 10^{-6}$), mainly because the free-free cooling time scale is much longer than the free-fall one. Thus, in the absence of a solid surface on which the radiation is released, most of the accretion energy is carried into the black hole (Shapiro 1973).

The obvious way to remedy the situation is to consider non-spherical accretion; this is not an unreasonble assumption, as even small amounts of net angular momentum could turn an almost spherically symmetric flow at large distances to a predominately azimouthal one near the horizon of the black hole; the dynamics in this case are therefore not governed by the free-fall and the efficiency of accretion can be much higher than in the spherical accretion case. In fact, since the dynamics in this case are governed by the dissipation of the azimouthal kinetic energy and its conversion into radiation, the mere assumption that the fate of accreting matter is its eventual fall into the black hole, requires that the efficiency of this process be high and for that reason it has served as a working hypothesis for most models of AGN. However, this additional modification of the dynamics adds
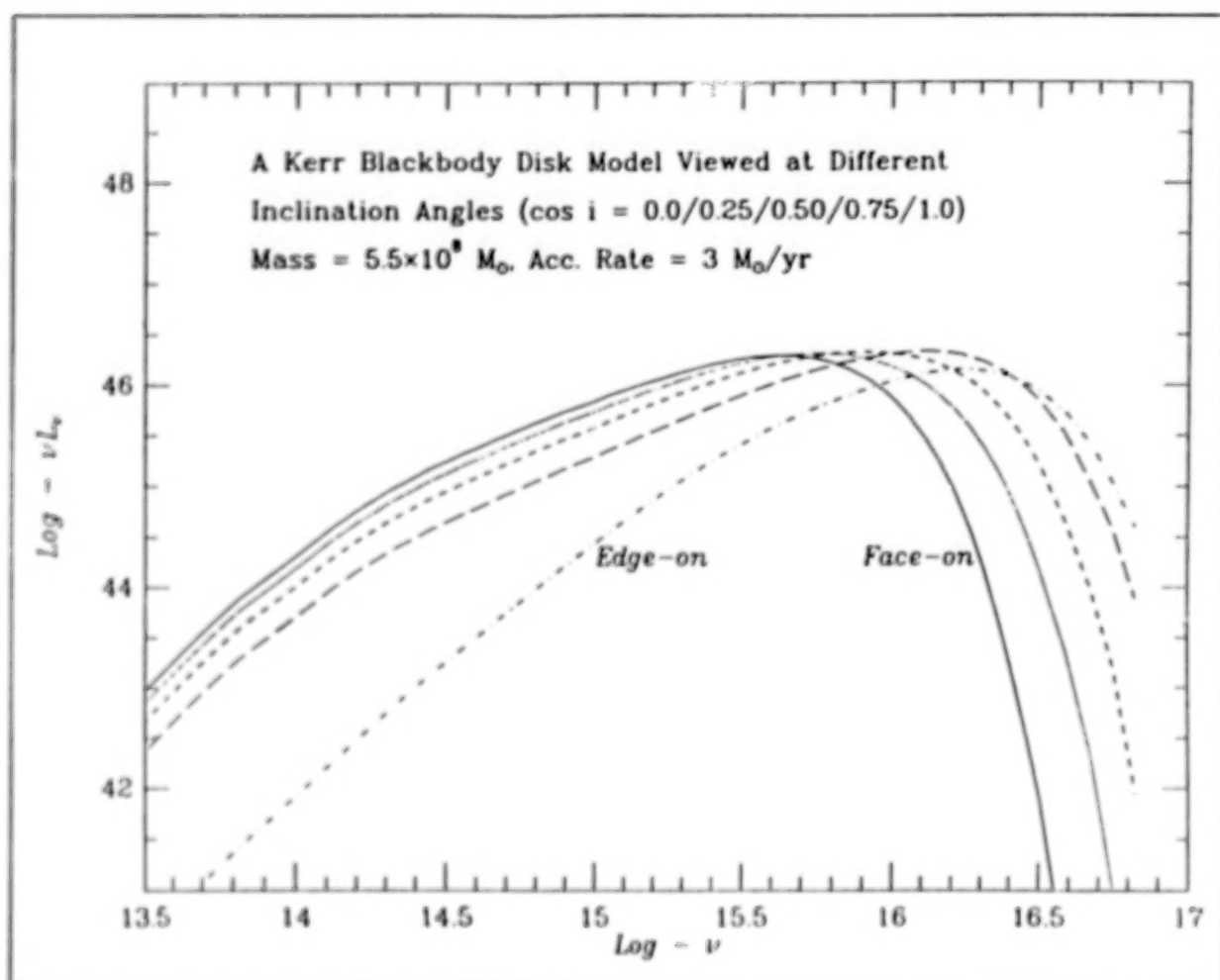
*Figure 2.* The spectrum of an accretion disk around an extreme Kerr black hole of mass $5.5 \times 10^8$ $M_\odot$ and accretion rate of 3 $M_\odot$ per year for various values of the cosine of the inclination angle (from Sun and Malkan 1989).

considerable complication and uncertainty in the models, since the mechanism responsible for the dissipation and the eventual infall into the black hole is unknown. The general spectral characteristics of the emitted radiation can nonetheless be estimated by assuming a particular emission mechanism. The assumption of black body emission then yields the following estimate of the characteristic temperature

$$T \simeq 3 \times 10^7 F^{1/4} \left( \frac{M}{M_\odot} \right)^{-1/4} x^{-1/2} \tag{1}$$

where $F$ is the fraction of the Eddington luminosity at which the source emits, $M$ is the mass of the black hole, and $x$ is the size of the inner parts of the disk measured in Schwarzschild radii (typically $x \simeq 3$ - 10).

For a black hole of the order of a solar mass, eq. (1) predicts emission in the few keV range, which has in fact been observed in the galactic black hole candidates. On the other hand for a luminous quasar ($L \simeq 10^{46}$ erg s$^{-1}$) which is expected to emit close to

the Eddington limit ($F \simeq 1 - 0.1$ implying a mass $M \simeq 10^8 - 10^9 \, M_\odot$), the resulting temperature is $T \sim 10^5 \, K$, and should thus manifest itself as a rather broad quasi-thermal component in the UV part of the spectrum; moreover, this component should contain, in principle, all of the available emitted power (if one ignores the possibility of reprocessing of radiation). The existence of such a component was suggested in the late 70's by Shields (1978); however detailed fits to observed spectra were not performed until five years later. Malkan and Sargent (1983) decomposed the IR to UV quasar spectra as a power law $F_\nu \propto \nu^{-1}$ and a black body of temperature $T \sim 30,000$ K, while Malkan (1983) in a similar decomposition, fitted the broad quasi-thermal component with a superposition of black bodies appropriate to an accretion disk. The identification of this component with black body emission from an accretion disk allowed then (through modeling and data fitting) the determination of the parameters of the accretion disk (i.e. the mass of the black hole $M$ and the accretion rate $\dot{M}$).

This quasi-thermal broad component that extends from the optical to the UV part of the spectrum of a large number of quasars became known as the "Blue Bump". The great advantage of the above interpretation of this feature is the direct way in which it associates the spectral emission in a given band to the dynamics of accretion. In addition, it suggests that, under these assumptions, this feature should be ubiquitous in AGN and should contain most of the available power. At its simplest version, this model seems to ignore the emission in the other energy bands and also the fact that the remainder constitutes a large fraction of the total power available. The emission at longer wavelengths could be accomodated by reprocessing of the UV radiation, however this model would have problems in accounting for the X-ray emission from these objects (though soft, $\sim 1$ keV emission could also be accomodated).

## b. Non-Thermal Models

The model discussed above has as its focal point the dynamics of accretion in conjunction with the assumption of black body emission. The latter assumption, however, imposes severe constraints the particular dynamics that must take place in these objects, in order that the resulting spectrum be similar to a black body. In addition, the spectral distribution of the emitted radiation is much broader than even the most optmistic accretion disk models would imply (figure 1). An alternative approach to "understanding" AGN is by considering their spectral power distribution as their fundamental feature. Indeed, as pointed out in the introduction, this is quite different from that of normal galaxies, whose emission spanning a couple of decades in energy can be accounted of as the superposition of the emission from the constituent stars. It is of particular interest that the "Blue Bump" notwithstanding, the overall distribution of power is roughly uniform from IR to X-, and whenever present, $\gamma$-rays. It appears that the dynamics somehow provide for such a non-thermal distribution of the emitted radiation.

Unfortunately, it is difficult to construct realistic non-thermal models without building in some sense the answer into the model; the reason is that the non-thermal emission depends absolutely on the emission mechanism employed (it is easy to see that the dominant such mechanism, for the relativistic electrons responsible for the radiation, should be inverse Compton or synchrotron losses) and the non-thermal electron distribution assumed (by contrast thermal models like that outlined above are largely indepedent of the emission

mechanism provided that large optical depths are involved). Moreover, the life time of relativistic electrons, thought responsible for the non-termal emission, is much shorter than the light crossing time accross the source, a fact that in view of their steady-state emission, demands a mechanism for continuous acceleration or injection of relativistic electrons. So any non-thermal model should at its very basis address the problem of acceleration of the radiating electrons. However, the spectral distribution of energy in AGN is such an imposing feature, that non-thermal models were nontheless introduced without addressing this question (Jones O'Dell and Stein 1974; Rees 1967).

Our understanding of particle acceleration underwent a major breakthrough in the late 70's (Bell 1978; Blandford and Ostriker 1978). It was shown that upstream diffusion of particles in shocks can indeed lead to acceleration of a number of them to very high energies; in particular it was shown that this mechanism produces a power law distribution of particles, which for strong shocks (it is not difficult to imagine that shocks could be strong in AGN) results in differential particle spectra $\propto E^{-2}$ i.e. spectra with equal energy per decade, as incidentally is the power distribution of AGN. Appealing as this fact may be at first sight it is not necessarily compelling, because, on one hand the energy distribution in particles need not be the same as that of the emitted photons, and on the other hand the shock acceleration mechanism as originally proposed is operative only for protons (mainly because of their much larger gyroradii for a given upstream velocity), thus making it an unlikely mechanism to use in AGN. Protheroe and Kazanas (1983), however suggested that the radiating relativistic electrons could be secondaries resulting from the decay of $\pi^+, \pi^-$ produced in nuclear collisions, by shock accelerated protons; thus it was made possible to relate the origin of relativistic electrons to a concrete model of the accelration mechanism. In addition, one can then easily show that if the relativistic proton spectrum is that predicted by shock acceleration (i.e. a power law $\propto E^{-2}$), the the photon spectrum resulting from the secondary electrons is also a power law, $F_\nu \propto \nu^{-1}$, i.e. of equal energy per decade. Besides the spectral characteristics which can be attributed to the presence of relativistic protons, these particles can also have significant dynamical influence on the dynamics of the accretion flow, because their energy loss time scale is in general longer that the local free-fall time scale, thus suggesting a coupling between the dynamics and the radiation emission mechanism. These notions, coupled with the dynamics of free-fall accretion can actually lead to a model that depends on only *one* free parameter, namely $\dot m/M$ or $\dot m/\dot m_E$, where $M$ is the mass of the black hole and $\dot m_E$ is the Eddington accretion rate (Kazanas and Ellison 1985).

Despite the fact that strong shocks can indeed produce non-thermal distributions which could in principle account for the overall (i.e. $F_\nu \propto \nu^{-1}$) spectral distribution of AGN as outlined above, a single power law fit appears to be in disagreement with observations, most notably those of "hard" (> 2 keV) X-rays, whose spectra were shown to be power laws, $F_\nu \propto \nu^{-\alpha}$, $\alpha \simeq 0.75$ with a small dispersion in the values of the power law index (Rothschild et al. 1983), indicating an energy per decade spectrum which is rising with frequency ($\nu F_\nu \propto \nu^{0.25}$). Since the X-rays are affected very little by obscuration, and because their variability is the most prominent among all of the spectral bands of AGN, they are thought to provide information about the dynamics of their innermost regions. The apparent disagreement of the observed X-ray spectra with those expected from the

simplest particle acceleration models and their "universality" suggested that something was fundamentally different in the "central engine" of AGN than so far considered.

This reasoning lead to the search for an alternative scale in the problem and to the consideration of the effects of $e^+e^-$-pair production due to photon-photon absorption within the source (Kazanas 1984, Zdziarski and Lightman 1985). The effects of this process ($\gamma\gamma \to e^+e^-$) is to remove all high energy photons and replace them with electron positron pairs which in turn are re-injected into the pool of radiating electrons to produce more high energy photons etc. Thus a cascade ensues which it was shown that, under certain conditions (viz. that most of the available energy is injected at energies well above the rest mass of the electron $m_e c^2$), "washes-out" all information about the original injection and produces an electron distribution $\propto E^{-3}$ down to the energy at which the opacity of the source to the above process becomes less than one. Below this energy the electron distribution is $\propto E^{-2}$ and could thus by inverse Compton produce a spectrum similar to that observed in the X-rays. This process then introduced a new scale namely the energy at which the $\gamma\gamma \to e^+e^-$ opacity is equal to one. Given that the cross section for the above process is roughly the Thomson cross section, $\sigma_T$, the ($\gamma$-ray) photon opacity to $e^+e^-$-pair production $\tau_{\gamma\gamma}$ at energy $\simeq m_e c^2$ is given by

$$\tau_{\gamma\gamma}(E_\gamma) \simeq \frac{L\sigma_T R}{4\pi R^2 c m_e c^2} \tag{2}$$

where $L$ is the luminosity of the source and $R$ its size. As it is apparent from eq. (2), the optical depth $\tau_{\gamma\gamma}(E_\gamma)$ depends only of the combination $L/R$ of the physical parameters (called the compactness) of a source; eq. (2) then defines the natural unit of compactness $l = m_e c^3/\sigma_T \simeq 3.4 \times 10^{28}$ erg cm s$^{-1}$. For $\gamma$-rays of energy $E_\gamma \gg m_e c^2$ the optical depth to photon-photon depends on the spectrum of the X-rays that fulfill the threshold condition for pair production. If the $L_s$ is the X-ray luminosity with spectral index $\alpha$ , the optical depth of a $\gamma$-ray of energy $E_\gamma$ is given by

$$\tau_{\gamma\gamma}(E_\gamma) \simeq 1 \left( \frac{L/R}{10^{29}\ C.G.S.} \right) \left( \frac{E_\gamma}{m_e c^2} \right)^\alpha \tag{3}$$

The energy $E_\gamma$ at which $\tau_{\gamma\gamma}(E_\gamma) \simeq 1$ constitutes the additional scale sought to account for the X-ray spectra. It should be noted that if L is measured in units of the Eddington luminosity and R in units of Schwarzschild radii the compactness is independent of the mass of the black hole, a situation similar to that encountered considering the effects of relativistic protons on the dynamics of accretion.

The process of pair cascades appeared to be very appealing since it would present us with a spectrum largely independent of the initial conditions of injection, whose origin could then be sought separetely. In addition, the final spectrum was dependent of only one source related parameter namely its compactness, whose value is also largely independent of the mass of the accreting black hole, thus suggesting this mechanism to be relevant and applicable to objects of largely different masses such as quasars and galactic black holes in binary systems (White et al. 1984; Kazanas 1986). Unfortunately, more detailed calculations have indicated that the correct values of X-ray slopes are obtained only for
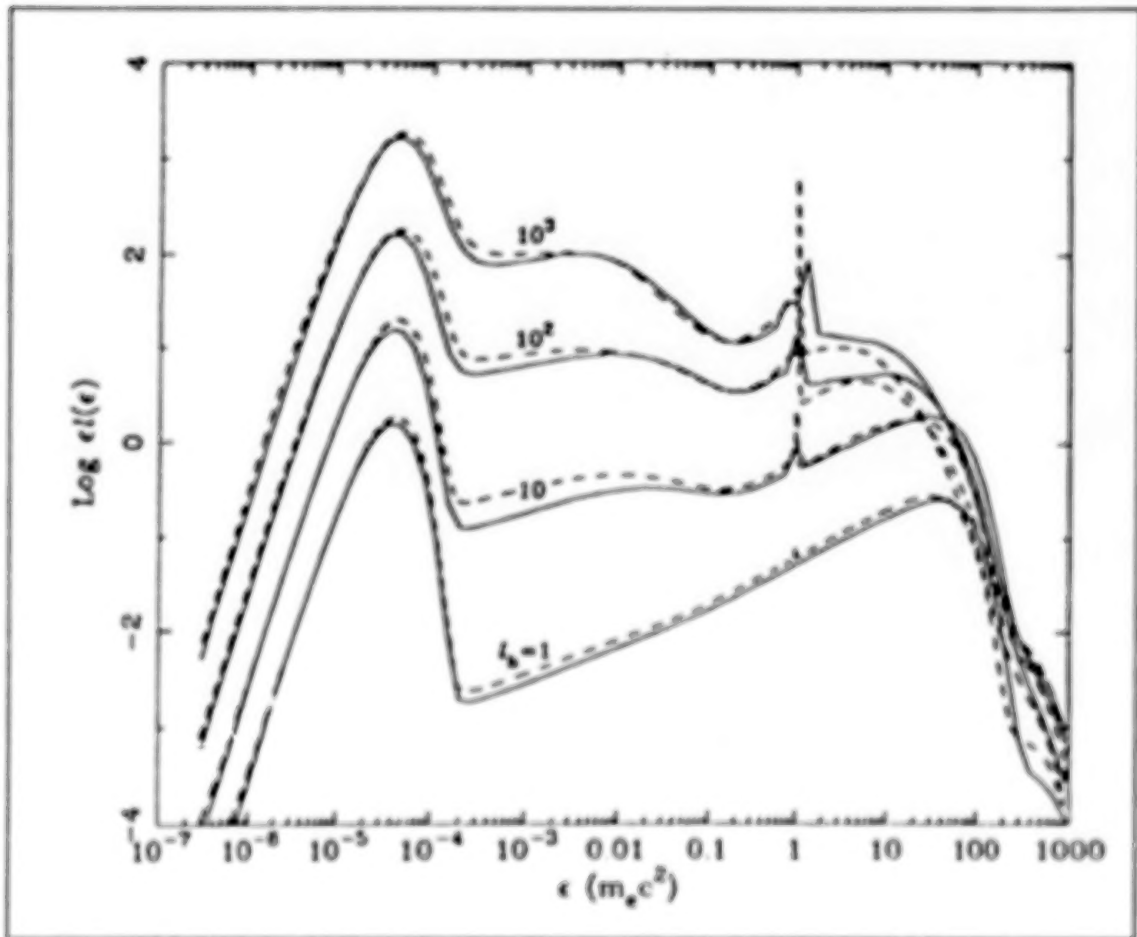
*Figure 3.* The pair cascade spectra for monoenergetic electron injection, for a source with compactness $l_h$, a black body distribution of soft photons of compactness $l_s$, for various values of the parameter $l_h$. Solid lines from Done and Fabian (1989), dashed lines from Lightman and Zdziarski (1987).

a narrow range of values of the compactness which is much too small compared with the observations (Lightman and Zdziarski 1987; Fabian et al 1987; Done and Fabian 1989). For values of the compactness appropriate to X-ray variability observations, the cascade converts most of the available power into $e^+e^-$-pairs which render the source thick to Thomson scattering and thus modify the escaping spectrum; these detailed calculations have indicated that the down-Comptonization of the emerging radiation would introduce a break at 10-50 keV which is apparently not observed. In addition, the very large optical depth to photon-photon absorption $\tau_{\gamma\gamma}$ guarantees the virtual absence of any $\gamma$-rays of energies $E \gtrsim m_e c^2$, though a large $e^+e^-$ annihilation feature is indeed expected at energies roughly that of the electron rest mass. Lower values of the compactness parameter could in fact lead to spectra in rough agreement with the observed ones, but the allowed range of L/R would have to be very small in order not to cause discrepancy with the AGN contribution to the extragalactic $\gamma$-ray background.

In conclusion, the introduction of pair cascades, though it can achieve what it has been invented for, it still requires AGN to lie in quite a restricted region of the available

parameter space, thus obviating the need of their introduction.

## III. THE CONTRIBUTION OF GRO

Having outlined the motivation and the main features of the two most prominent recent (i.e. introduced in the 80's) ideas on the nature of AGN and their spectra, I would like to discuss their pros and cons in view of the impending GRO observations.

One of them (black body emitting, geometrically thin accretion disks), motivated by the dynamics of accretion, it can account for a particular feature, namely the "blue bump". Moreover, by detailed modeling and fitting of the data associated with this feature, this model can provide the best so far estimates of the mass and accretion rates of these objects. Unfortunately there exists within the model an *a priori* additional physical parameter which can also be adjusted to either improve the fits or introduce a degeneracy in the values of the mass, $M$, and accretion rate, $\dot{m}$, which are obtained from the fits to the data; this is the inclination of the disk (which is assumed to be geometrically thin) to the line of sight of the observer. I find this redundancy of free parameters rather disturbing. In addition there have been reports of several objects which do not show any evidence of the "blue bump" - accretion disk emission (McDowell et al 1989). Since this feature is of such a central importance for the dynamics and the energy generation in AGN, its absence even in a small number of objects becomes a major problem.

The "blue-bump" - accretion disk models do not attempt to address the overall distribution of radiation in AGN. Given the large amount of optical-UV-soft X-ray emission that can potentially be produced in the "blue-bump" feature, one could argue that the lower frequency (near to far infrared) radiation could be the result of reprocessing in the AGN environment, mainly by dust (Sanders at al. 1989). There remains however the question of radio ($10^9 - 10^{10}$ Hz) emission. In the majority of AGN (radio quiet), the emission in this band is but a very small fraction ($\sim 10^{-6}$) of the total luminosity, and could argueably be ignored. However, in the radio loud AGN it constitutes a substantially larger fraction ($\sim 10^{-2}$), and in certain cases the extended radio emission (which is apparently energized from the nucleus by jets) seems to be comparable to or even outshine that of the nucleus. Yet, in these two classes of objects the emission in the far IR to X-rays is quite similar, though as argued by Wilkes and Elvis (1987) the X-ray spectra of radio loud AGN are in general "flatter" than those of the radio quiet. It is generally accepted that the radio loud AGN contain large amounts of non-thermal particles, which are thought responsible for the radio emission; should one then assume that the radio quiet objects are devoid of such particles though the look quite similar (with perhaps the exception of blazars) in their IR - X-ray spectra? Should one already concede at this fundamental level two very different classes of objects despite the apparent similarities, or may the observed differences be the result of the particular environments in which these different classes reside? Such are the questions model builders are called to decide *a priori* and hopefully answer by testing their models against the observations.

However, in my view, the major problem with this class of models is its inability to deal with the emission of hard ($> 2$ keV) X-rays, or for that matter any radiation that is harder than that. One might argue that because of the dominance of the "blue bump" emission in a number of objects (quasars) over the (non-thermal?) harder than 2 keV

X-ray emission, that we indeed have captured the *major* features that determine the most important part of the dynamics and that the remaining constitutes but a small fraction of it. It should be born in mind that this argument may be very misleading; it suffices to remember that the energy per decade seems to be rising with frequency in the X-ray band. How far does this rise continues? It appears that extrapolating this emission to roughly 1 MeV could produce a feature whose luminosity would, in most objects, rival that of the "blue bump". It thus becomes apparent the invaluable contribution of GRO in deciding this most important question, namely the frequency band in which most luminosity is emitted. The answer to this question, along with the fastest observed variability would then set the tone for the more comprehensive models that will follow these observations. The > 2 keV radiation could be accomodated by arguing that besides the black body emitting part of the disk, there exists a hot inner region with optically thin emission and harder radiation. My feeling is that such a model would be difficult to make consistent with observations, since the present disk models have to already consider maximally rotating Kerr holes and emission from the innermost stable orbits in order to be able to account for the observed UV - soft X-ray emission.

Hybrid models of the the standard accretion disk along with an additional arbitrary non-thermal component (a corona?) could in principle account for the harder X-ray and possible $\gamma$-ray emission. I personally find models of this kind rather uninteresting since they have no way of determining the mechanism by which the availble power is apportioned between these two independent components. This argument does not by itself mean that such models are wrong; they just have much less predictive power. On the other hand it is possible that these models may indeed be the correct ones; in this case it may never be possible to improve any further our understanding of the nature of AGN, but since at present we are not aware of that, we have to keep trying (maybe in vain!). A *non-linear* combination of these components would be indeed very interesting and instructive, since it not contain any additional free parameters, but I am not aware of either models or observations suggesting such a relation.

The other general class of models (non-thermal), does in fact address the broad band energy distribution in AGN, but only at the expense of the details of the dynamics that become murkier, as one has to deal with situations (shocks, turbulence etc.) not amenable to such clean modeling as the assumption of a nice, smooth, optically thick, geometrically thin disk (of, albeit, unspecified viscosity). The non-thermal models do, of course, account for the broad band emission of AGN (once an acceleration mechanism has been assumed); however these models are at difficulty in accounting for the "blue bump", unless they resort to additional components similar to those of the previous class. Finally, they can account for the observed "hard" (> 2 keV) X-ray emission, but its detailed slope can be obtained only for a small range of the available physical parameters.

The non-thermal models, in contrast to the "blue bump" ones, do predict the emission of a significant amount of $\gamma$-rays with fluxes detectable by GRO. EGRET in particular would be instrumental in providing clues as to the highest energy particles present in these objects and therefore severely constrain the parameter freedom of available models. Thus, positive detection of a number of AGN in the EGRET energy band would strongly argue in favor of non-thermal emission as a major component in the radiative processes

of AGN. The non-thermal models also predict that for large values of the compactness parameter a large fraction of the available luminosity should be emitted at $E \sim m_e c^2$ (due to the cascade caused by the $e^+ e^- \to \gamma\gamma$ process) while suppressing the emission at the EGRET energy range. Fortunately, the other instruments aboard GRO, (i.e. OSSE and COMPTEL) will provide the necessary coverage in this energy range. The $> 100$ MeV $\gamma$-rays observed in 3C 273 do suggest that emission in this energy band is indeed possible (see the contribution of C. von Montigny, these proceedings). The question is whether such an emission is typical of AGN or particular to 3C 273. The positive observation of $\gamma$-rays, especially in radio quiet objects, in which the existence of relativistic particles may not be deemed necessary, would be a significant fact in determining whether these high energy particles are indeed present in the "central engine" of AGN, irrespectively of the presence or not of radio emission. The presence of $\gamma$-rays in both radio loud and radio quiet objects would suggest the possibility that the the "central engine" is quite similar among all classes objects with the observed class diversity attributed to the particular "environmental conditions" prevailing in the vicinity of the compact object, or even to a particular range of the physical parameters at which these different operate. If the latter argument were to be proven true, it would provide a unifying point around which more detailed models could be built which would account for the particular observed characteristics, in accordance with the notions of "understanding" outlined in the introduction.

## IV. A MODEL

Before concluding, I would like to present a model which, in my opinion, conveys a flavor of what I have termed in the introduction "an understanding" of AGN. This model, originally conceived in order to account for the radio emission in radio loud objects, can at the same time address another major issue, namely the dichotomy of AGN in radio quiet and radio loud. The model is by no means complete and since it is mainly concerned with non-thermal emission it fails to address at all the issue of the "blue bump", as the latter is considered to be a thermal feature.

This model (developed in collaboration with P. Giovanoni of the University of Maryland) is a direct consequence of the models involving strongly interacting particles as a means of producing the radiating relativistic electrons in AGN (Protheroe and Kazanas 1983; Kazanas and Ellison 1985). One of the main channels of these reactions is that of charge exchange, which converts one of the protons to a neutron; in addition, neutrons can be the final product of photopion production reactions (Sikora et al. 1987), in which a high energy photon can produce a pion in a collision with a photon

$$pp \to nX \; , \quad p\gamma \to n\pi^+ \tag{4}$$

The neutrons resulting from these interactions can be relativistic and, not constrained by the ambient magnetic field, they escape and can transport away from the continuum source roughly half the available luminosity, which they can subsequently deposit upon their decay in the form of relativistic protons at distances $r \simeq 3 \times 10^{13} \gamma_n$ cm, where $\gamma_n$ is the neutron Lorentz factor.

Relativistic neutrons thus present a mechanism for energy transport in AGN whose efffects have been previously largely ignored (see however Kazanas and Ellison 1985b for

discussion of the effects of relativistic neutrons in galactic high energy sources; see also Sikora et al. 1989). The smooth continuous way they relate the dynamics and radiation emission in the vicinity of the compact object with that at much larger radii, makes them ideal candidates for the continuum emission in radio loud AGN, which is also smooth and continuous from $10^9$ to $10^{16}$ Hz (Landau et al. 1986). In particular, the spectra of the unresolved core (where the "central engine" resides) in radio galaxies and radio loud QSOs are "flat" i.e. $F_\nu \propto \nu^\alpha$, $\alpha \simeq 0$ from $10^9 - 10^{13}$ Hz (see e.g. Landau at al. 1986). Because synchrotron radiation (the main emission mechanism in these frequencies) from a region of size a few Schwarzschild radii would be self-absorbed at $\nu \simeq 10^{12.5} - 10^{13}$ Hz, the observed radio emission cannot be optically thin; on the other hand optically thick synchrotron emission has a much different spectral index $F_\nu \propto \nu^{2.5}$. It was then suggested that the radio flat spectra were the result of the superposition of synchrotron self-absorption edges from invreasingly larger radii extending out to $\simeq 1$ pc (Marscher 1977). This suggestion allowed the the modeling of the "flat" spectra by arbitrarily prescribing the magnetic field and the electron distribution as a function of radius and energy, i.e. $B(r) \propto B_o r^{-m}, N_e(\gamma_e) \propto r^{-n}\gamma^{-p}$ over the whole emission region (of size $\simeq 1$ pc). A suitable choice of the indices $m, n, p$ can then set the slope of the envelope of the self-absorbed components to any value and in particular to zero as observed. The fact that the physical conditions in AGN conspire to produce a combination of $m, n, p$ that yields a flat spectrum in the entire class of radio loud objects, when any other value is as likely, came to be known as "Cosmic Conspiracy" (Phinney 1985).

In addition to the free parameters $m, n, p$ such models do not address at all the origin of the relativistic electrons at the large distances ($\sim 1$ pc) from the "central engine" required to fit the spectra. This is a formidable problem considering the very short life times of these electrons. On the other hand, energy transport by neutrons does resolve the origin of relativistic electrons in a direct straightforward way, which is based on well defined physical process. Moreover, the neutron transport does not allow the arbitrary choice of the electron distribution function independently of the dynamics of the "central engine". In fact, energy transport by neutrons leads to an electron distribution function of the form $N_e(\gamma_e) \propto r^{-2}\gamma^{-2}$, in a largely model independent way (Giovanoni and Kazanas 1990). By then choosing in addition the radial dependence of the magnetic field to be $B \propto B_o r^{-1}$ (an assumption justified either on basis of equipartition with the photons or considering the magnetic field to be carried by an outflowing wind), one can obtain "flat" spectra in the $10^9 - 10^{13}$ Hz range, which then steepen to roughly $F_\nu \propto \nu^{-1}$ in very good agreement with the observations (figure 4).

The question which is immediately raised then is the following: Since the production of neutrons is inevitable once the presence of relativistic protons is considered, and given that neutrons can lead to emission at large distances from the continuum source, thereby accounting for the spectra of radio loud objects as proposed above, why are not all objects radio loud? (in fact the majority of them are radio quiet). One can simply conjecture that radio quiet objects are those in which relativistic protons are absent in their "central engine". Such an explanation however does not really improve our "understanding"; it simply reduces it to the addition of another free parameter, which quite likely we will never be able to determine. Is it possible then to account, within this model for the
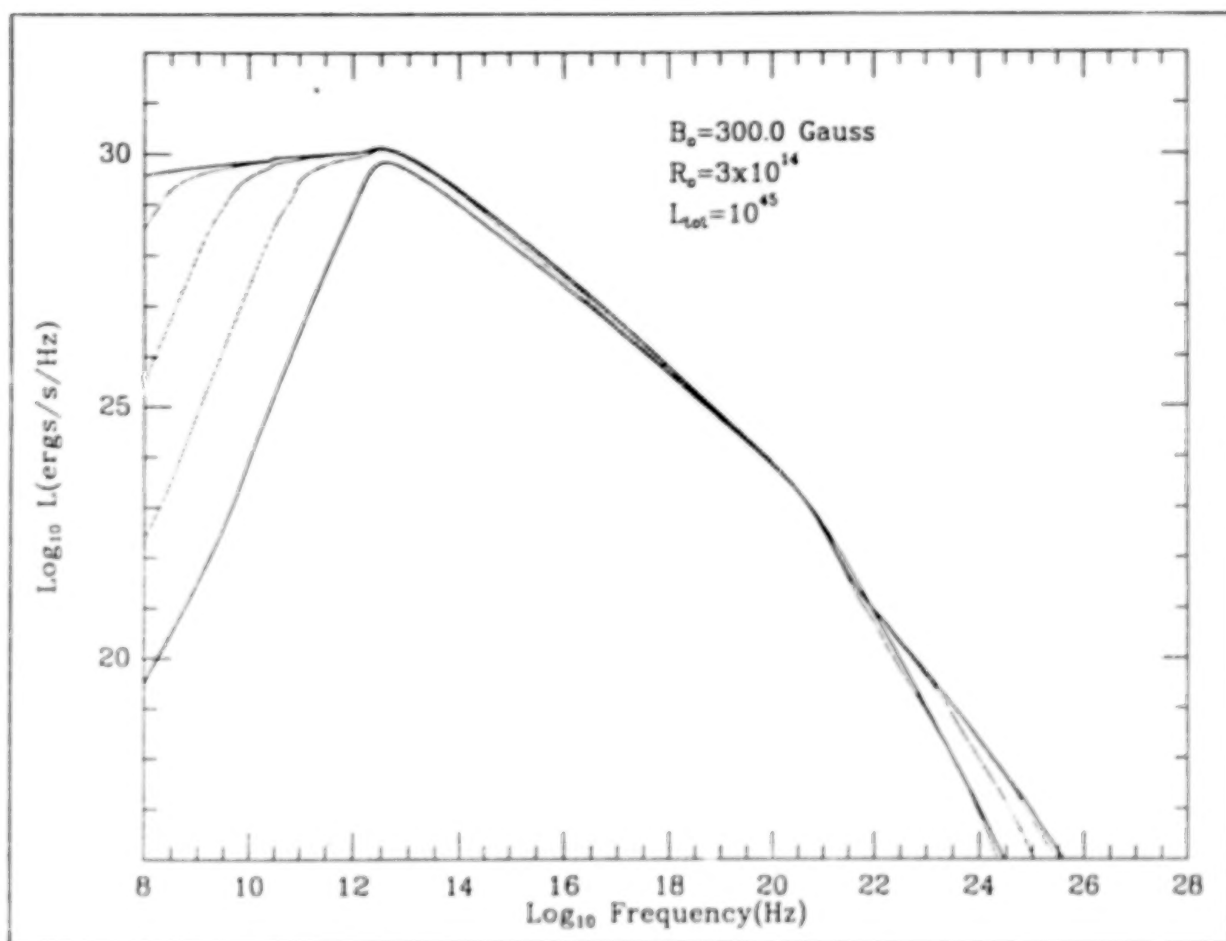
*Figure 4.* $L_\nu$ vs $\nu$ for a source with luminosity in neutrons (at $r = R_o$) $L_{tot}$, magnetic field at $r \leq R_o$, $B_o$ and central source size $R_o$, as indicated in the figure. The lower solid line is the spectrum of the central source, while the upper one is spectrum as observed at infinity. The dotted lines indicate the spectrum at $r = 10R_o$, $10^2 R_o$, $10^3 R_o$ respectively.

class of radio quiet objects without the introduction of an *arbitrary* free parameter? The answer is "yes". If one can simply prevent the neutrons from escaping the central source one would simply deplete emission from the larger radii, thereby leading to the absence of radio emission at frequencies $\lesssim 10^{12.5}$ Hz. Such an object would indeed qualify as a radio quiet object. The neutrons could be stopped by reactions similar to those that produce them i.e. $np \to pp\pi^-$ and $n\gamma \to p\pi^-$. Both these reactions tend to suppress preferentially the highest energy neutrons: the first one because the cross section increases (albeit logaritmically, but that is sufficient) with the neutron energy, while the second because there are more target photons at the reaction threshold for the higher energy neutrons. These processes are of roughly comparable importance for neutron Lorentz factors $\sim 10^5$, but their most important feature is that they both depend on other physical parameters of the source. For a free-fall accretion the first one depends on $\dot{m}/\dot{m}_E$, while the second depends on the compactness $L/R$; given however that in a dynamical model $L/R$ itself quite likely depends on $\dot{m}/\dot{m}_E$, the classification of AGN as radio loud and radio quiet could then be understood only in terms of a *single* parameter.

272

This is the best example of the notion of "understanding" as given in the introduction that I was able to come up with. Fortunately, it appears that it may be testable. As figure 4 indicates the $\gamma$-ray spectra of the central source (lower thick line; that should be similar to that of a radio quiet object) and that observed at infinity (upper thick curve; that is the emerging spectrum from a radio loud object) are different in the EGRET energy range, at least for the parameters used in this specific model. This of cource is no accident: in radio loud object, as presented in this talk, there exist high energy particles at large distances from the "central engine" whose $\gamma$-ray radiation is not absorbed by the $\gamma\gamma \to e^+e^-$ process. Radio loud ojects should then be systematically also $\gamma$-ray loud, or at least more so than the radio quiet ones. $\gamma$-rays of $E \gtrsim 100$ MeV should also be present in radio quiet objects but at lower levels, which one should in principle be able to determine from models like those of figure 3. For that however we first need to obtain the data. If I have to be consistent with my own prejudices, which I outlined in the last four sections, I would have to predict lots of positive observations and lots of excitement in this field in the next few years.

## REFERENCES

Bell, A. R., 1978, *M. N. R. A. S.* **182**, 147.

Blandford, R. D. and Ostriker, J. P., 1978, *Astrophys. J. Lett.* **221**, L29.

Done, C. and Fabian, A. C., 1989, *M.N.R.A.S.*, **240**, 81.

Fabian et al., 1986, it M.N.R.A.S., **221**, 931.

Giovanoni, P. and Kazanas, D. 1990, submitted.

Jones.m, T. W. O'Dell, S. L, and Stein, W. A. 1974, *Ap. J.*, **204**, 187.

Kazanas, D., 1984, *Ap. J.* **287**, 112.

Kazanas, D. 1986, *Astron. Ap. (Lett.)*, **166**, L19.

Kazanas, D. and Ellison, D. C., 1986a *Ap. J.*, **304** 178.

Kazanas and Ellison, 1986b *Nature*, **319**, 380.

Landau. R. et al. 1986, *Ap. J.*, **308**, 78.

Lightman, A. P. and Zdziarski, A. A., 1987, *Ap. J.*, **319**, 643.

Lingenfelter, R. E. 1987, *Int. Cosmic Ray Conf.*, **8**, 7, (Moscow).

Malkan, M. and Sargent, W. L. W., 1982, *Ap. J.*, **245**, 22.

Malkan, M. A., 1983, *Ap. J.*, **268**, 582.

Marscher, A. P., 1977, *Ap. J.*, **216**, 244.

McDowell, J. C. et al. 1989, *Ap. J. Lett.*, **345**, L13.

Phinney, E. S. 1985 *in Astrophysics of Active Galaxies and Quasi-Stellar Objects* 453-496. Univ. Science Books, J. S. Miller, Editor.

Protheroe, R. J. and Kazanas, D. 1983, *Ap. J.*, **265**, 620.

Rees, M. J. 1967, *M.N.R.A.S.*, **137**, 429.

Rees, M. J. 1984, *Ann. Rev. Astron. Ap.*, **22**, 471.

Rothschild, R. E. et al. 1983, *Ap. J.*, **269** 423.

Sanders, D. B. et al. 1989, *Ap. J.*, **347**, 29.

Shapiro, S. L. 1973, *Ap. J.*, **180**, 531.

Shields, G. A. 1978, *Nature*, **272**, 706.

Sikora. M. et al. 1989, *Ap. J. Lett.*, **341**, L33.

Sun, W.-H. and Malkan, M. A. 1989, *Ap. J.*, **346**, 68.
Wilkes, B. J. and Elvis, M. 1987, *Ap. J.*, **323**, 243.
Zdziarski, A. A. and Lightman, A. P. 1985, *Ap. J. Lett.*, **294**, L79.

## DISCUSSION

*Darryl Leiter:*

Can a cool disk be compatible with a hot corona for UV & gamma production in AGN?

*Demos Kazanas:*

Maybe, but such a model introduces unknowable (at present) parameters at a very basic level which I do not feel are very useful, at this stage, though it may be proven correct eventually.

*Richard Mushotzky:*

Since the break at gamma-ray energies is related to (L/R), with R determined by gamma-ray variability, shouldn't there be a relation between the X-ray variability times scale, d $t_x$, and the (gamma-ray/X-ray) ratio and the gamma-ray spectrum?

*Demos Kazanas:*

Yes, there should be such a relation. However, one should bear in mind that d $t_x$ is in general proportional to the mass of the black hole M while L/R may be quite insensitive to M (if L is a given fraction of the Eddington luminosity and R a few Schwarzchild radii). So though d $t_x$ may vary by many order of magnitude, L/R and hence all aspects associated with it, may vary very little.

*Dick Lamb:*

I would like to ask if the possible break in the 3C273 spectrum around 3 MeV is compatible with the high energy gammas being absorbed by X-rays creating $e^{\pm}$ pairs?

*Demos Kazanas:*

Yes! Look at Protheroe & Kazanas Ap. J. 1983 also Kazanas & Protheroe, Nature 1983 where similar arguments have been put forward to account for the diffuse gamma-ray background.

*Andy Strong:*

Presumably the effect of gamma-gamma pair production will be changed by the subsequent gamma-electron cascade.

*Demos Kazanas:*

Yes, if the intrinsic $vF_v$ emission increases with energy, i.e. most of the intrinsic luminosity is produced at the highest energies. For the example given here that $vF_v \propto v^o$ = constant, this feedback is not important.

# SPECTRAL EVOLUTION OF ACTIVE GALACTIC NUCLEI PENROSE COMPTON SCATTERING PROCESSES AND GAMMA RAY EMISSION FROM SEYFERT GALAXIES

Darryl Leiter[*] & Elihu Boldt
NASA Goddard Space Flight Center
Greenbelt, MD.

## ABSTRACT

In black hole spectral evolution models for active galactic nuclei (AGN), present epoch Seyfert galaxies evolve from an earlier precursor active galaxy (PAG) stage at redshift $z \sim 7$ where they acted as the thermal sources responsible for the residual cosmic X-ray background (RCXB). The Seyfert galaxies which emerge in this context emit Penrose Compton Scattering (PCS) gamma ray transients on the order of hours with a kinematic cutoff in the spectrum $\leq 3$ MeV. The EGRET/OSSE/COMPTEL/BATSE instruments on the Gamma Ray Observatory (GRO) are appropriate instruments to carry out further tests of this model by studying: 1) PCS gamma ray transient emission from individual galaxies and, 2) the possibility that present epoch PCS gamma ray emitting Seyfert galaxies contribute observable temporal variability to the excess diffuse gamma ray background component $\leq 3$ MeV.

## I. PRECURSOR ACTIVE GALAXIES (PAG) AND THE COSMIC X-RAY BACKGROUND

Black hole accretion disk dynamo processes are generally regarded as the central power source for AGN (Rees 1984). If such AGN begin their activity with Jeans mass $\gtrsim 10^6$ M$\odot$ black holes of pre-galactic origin then the X-ray radiation emitted during their lifetime will undergo the phenomenon of "spectral evolution" (Leiter & Boldt 1982; Boldt & Leiter 1986, 1987). When accretion disks are first formed at the onset of galaxy formation the accretion rate occurs at a high value of the luminosity/size compactness parameter $L/R > 10^{30}$ erg/cm-sec. Such high values of $L/R$ generate dynamic constraints (Cavaliere & Morrison 1980; Guilbert, Fabian, & Rees 1983), which suppress nonthermal black hole accretion disk dynamo processes in favor of thermal processes. This causes the spectrum of X-ray radiation emitted by early AGN to be predominantly thermal.

Since the hard X-ray radiation from thermal processes in the PAG accretion disk comes from a region of ~10 gravitational radii, L/R can be written in terms of $L/L_{Edd}$ as

(1)

$$L/R \hat{=} (L/L_{Edd}) \; 10^{32} \quad erg/cm\text{-}sec$$

where

(2)

$$L_{Edd} = 4\pi GMm_p c/\sigma_T$$

is the Eddington luminosity. In the Eddington limited precursor active galaxy (PAG) state, $L/L_{Edd} \hat{=} 1$ implies that the compactness parameter L/R is greater than $10^{30}$ erg/cm-sec and X-ray radiation is emitted in form of a thermal, flatt-ned Comptonized spectrum similar to that of the residual cosmic X-ray background (RCXB) (Zdziarski 1988).

At the end of the PAG lifetime the Eddington ratio falls to $L/L_{Edd} \hat{=} 0.01$ (i.e. $L/R \leq 10^{30}$ erg/cm-sec) and nonthermal black hole accretion disk dynamo processes (Rees, Begelman, Blandford, & Phinney 1982) become important, generating a broad band of non-thermal radiation including X-rays and gamma rays. Under these conditions the PAG spectrally evolve into Seyfert galaxies.

Spectral evolution of PAG into Seyfert galaxies is a consequence of the decrease with age of the compactness parameter associated with the central black hole accretion disk dynamo power source. Taking such spectral evolution into account leads to the possibility that the residual cosmic X-ray background (RCXB) is made up of a superposition of discrete PAG sources at high redshift, where the co-moving number density of PAG required is comparable to that of present epoch Seyfert galaxies.

## II. THERMAL COMPTONIZATION IN BLACK HOLE ACCRETION DISK SOURCES

If Precursor Active Galaxies (PAG) are the source of the residual cosmic X-ray background (Leiter & Boldt 1982) then observational constraints (Boldt & Leiter 1987) require that they:

a) originate at a redshift $z \sim 7$ with a luminosity in X-rays $\sim 10^{45}$ erg/sec,

b) have a constant comoving density $\hat{=} 4 \times 10^{-4}$ $MPC^{-3}$,

c) have a lifetime $\hat{=} 5 \times 10^8$ years during which they emit a thermal comptonized spectrum like that of the RCXB.

d) satisfy the observational constraint that the sky surface density of discrete RCXB sources is $\geq 5000$ sources/$deg^2$.

Taking electron-positron pair production effects into account, Zdziarski (1988) showed that the energy source of such PAG could be described in terms of comptonization of thermal cyclo-sychrotron photons in equipartion magnetic fields around a spherically accreting $\gtrsim 10^6$ solar mass black hole.

In general it is physically more realistic to expect the accreting plasma around a black hole in a PAG to possess enough angular momentum to form a disk. However, when the proton thermal energy is comparable to the proton gravitational energy in the hot optically thin inner region of an accretion disk, the plasma inflow resembles dissipative spherical accretion Meszaros (1975) in terms of dynamic quantitites averaged over spherical shells. In this context spherical accretion can be used as an approximation in describing the hot optically thin inner region of an accretion disk where the accreting plasma forms into a quasi-spherical torus.

From this point of view the spherical accretion calculation of Zdziarski (1988) can be used as a first order approximation to describe the quasi-spherical accretion flow in the hot inner region of the accretion disk as long as there are no internal or external sources of soft photons present stronger than that produced by thermal cyclo-synchrotron radiation generated in equipartition magnetic fields.

The PAG internal soft photon constraint required for the validity of this calculation can be addressed by noting that Dermer (1988) has shown that for the case of a two-temperature hot inner region of an accretion disk additional internal soft photons, generated by synchrotron emission from the positrons emitted by pion decay, will be negligible compared to thermal cyclo-sychrotron photons as long as the proton temperature is is constrained to remain $kT_p \lesssim 20$ MeV. Since the proton cooling rate is increased as a result of more frequent Coulomb interactions associated with the copious production of electron-positron pairs though photon-photon absoption, this constraint will most likely be satisfied for dimensionless PAG accretion rates $\dot{m} \gtrsim 1$ , above those values which allow a stable optically thick annulus to form inside of the hot inner region, Begelman, Sikora, & Rees (1986).

The external soft photon constraint required in this context can be addressed by calculating the ratio $(I_s/I_x)$ of the externally generated soft photon flux $I_s$, from the optically thick regions of the accretion disk to that of the X-ray flux $I_x$ emitted by the hot inner region of the accretion disk.

The Zdziarski (1988) PAG calculation is insensitive to the presence of external sources of soft photons of energy $E_s$ other than that generated by thermal cyclo-synchrotron processes if

$$I_s/I_x \quad < \quad (I_s/I_x)_{max} = (E_s/E_x)^{1-\alpha} = 1.3 \times 10^{-5} \qquad (3)$$

where $E_x \wedge 100$ KeV, $E_s \wedge 0.01$ KeV, and $\alpha \wedge 0.3$ is the low energy spectral index of the comptonized PAG spectrum (Zdziarski, A. A. (1989) private communication).

For an optically thick accretion disk with a hot, optically thin, quasi-spherical two-temperature inner region, Novikov & Thorne (1972), White & Lightman (1988), we find that

$$I_s/I_x \sim (r_x/r_s)^3 \qquad (4\text{-}a)$$

where

$$r_x \sim 10 \ r_G, \quad r_s \sim 5 \times 10^3 \ (\dot{M}_\Theta / M_\Theta)^{2/3} \ r_G, \ r_G = GM/c_2 \qquad (4\text{-}b)$$

with $\dot{M}_\Theta$ in units of solar masses per year.

Then since

$$\dot{M}_\Theta / M_\Theta = (1.3/6\epsilon) \ [\ L/L_{Edd}\ ], \qquad \epsilon < 1 \qquad (5)$$

equations (3), (4-a,b) and (5) imply that

$$L/L_{Edd} > 10^{-1} \ \epsilon \qquad (6)$$

which is automatically satisfied by the Eddington limited PAG which make up the residual cosmic X-ray background.

In this context the source of PAG is due to thermal comptonization processes in the hot ($kT_e$ 100 KeV) optically thin, quasi-spherical inner region of an accretion disk around a centrally rotating black hole, and the Zdziarski (1988) can be used to calculate the comptonized spectrum from the hot, spatially thick, inner region of the PAG accretion disk.

III. SEYFERT GALAXIES WHICH SPECTRALLY EVOLVE FROM PAG EMIT PENROSE COMPTON SCATTERING (PCS) GAMMA RAY TRANSIENTS ; MEV

At the end of the PAG lifetime, a reduction in the compactness Luminosity/Size parameter dynamically causes the PAG to spectrally evolve into active galactic nuclei (AGN), which have the canonical nonthermal x-ray spectrum associated with Seyfert galaxies and an average Seyfert black hole mass $M_s = 2 \times 10^7 \ M_\odot$.

Since the total accreted black hole mass divided by the inital PAG black hole mass is greater than 1.5 for these Seyfert galaxies, their central black holes are spun-up into a canonical Kerr state with angular momentum density $a/M = 0.998$ (Thorne 1974). This allows the turbulent, hot, optically thin inner region of the accretion disk to penetrate the ergosphere. Hence for Seyfert galaxies which spectrally evolve from the PAG the extraction of black hole rotational energy in terms of Penrose Compton Scattering (Piran & Shaham 1977; Leiter 1980) can occur.

The ergosphere around a Kerr black hole has the fundamental property that inertial frames are dragged around by the rotation of the black hole with respect to an inertial frame at infinity. With respect to a "local non-rotating inertial frame" in the ergosphere, electrons within a blob of hot plasma in the Penrose target zone bounded by the marginally bound $r_{mb}$ and marginally stable $r_{ms}$ orbit will undergo Compton Scattering with blueshifted photons entering the ergosphere. The blueshifted photon energy in the target zone is 10 to 30 time higher than the energy of the photons emitted from the hot, optically thin inner region of the accretion disk. For $\sim$ 100 KeV photons injected into the target region, blueshifting will cause electrons in a local nonrotating inertial frame in the target region to Compton scatter with photons $\gtrsim$ MeV. The average proper time that the plasma blob spends orbiting within the target region between the radii $r_{ms}$ and $r_{mb}$ in the ergosphere, when redshifted to an observer at infinity, is the observed PCS transient gamma ray emission time. It can be shown to be

(7)

$$\Delta T_{PCS} \approx 10 \text{ hours } ( M_5/(10^8 M_\odot) )$$

For Compton scattering in the ergosphere to be a Penrose Process the recoil electron has to be injected into the canonical Kerr black hole in a negative energy retrograde orbit opposing the black hole's rotational motion. The kinematic requirement for this to occur is that the retrograde recoil electron must be given a velocity boost of at least half the speed of light. This requires the blueshifted photon to have an energy $\gtrsim$ 1/2 MeV on the order the the rest energy of the recoil electron. When this occurs the $\gtrsim$ MeV Penrose Compton Scattered (PCS) photon is ejected from the ergosphere without being re-redshifted since it picks up energy from the rotational energy from the Kerr black hole).

Seyfert galaxies operator at $\sim$ 1% of their Eddington luminosity and the steady state MeV gamma ray luminosity from them is an order of magnitude less than this. Hence the optical depth to photon-photon absorption (Heterich 1974, Svenson & Zdziarski 1989) in an ergospherical region $R \sim 3$ gravitational radii is less than unity since
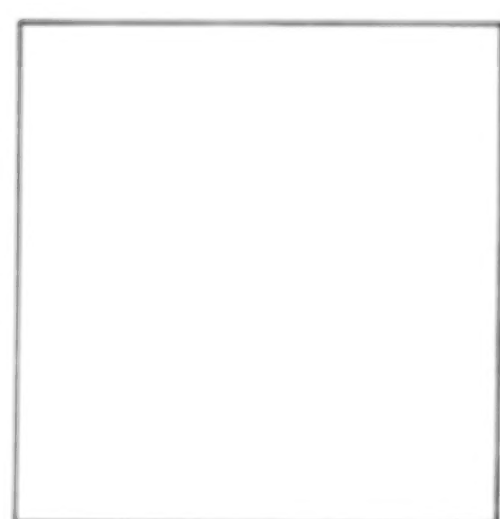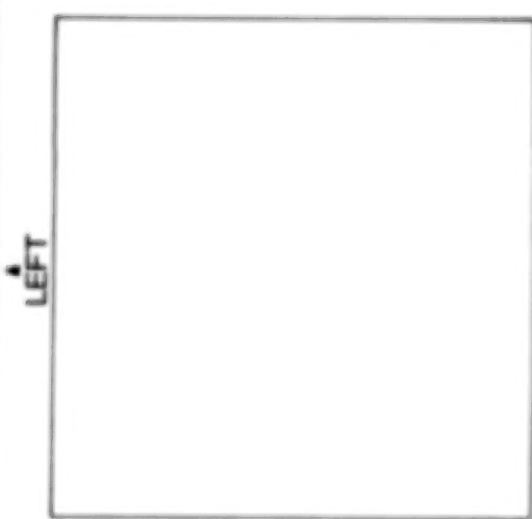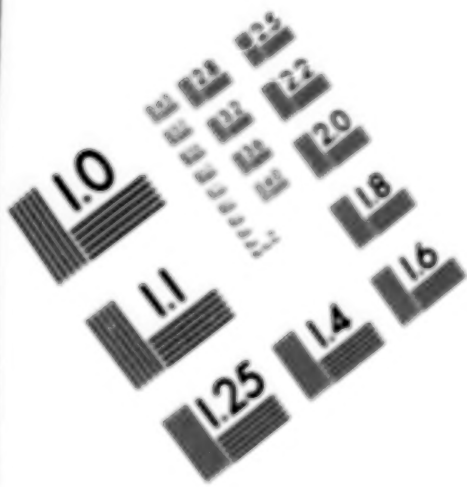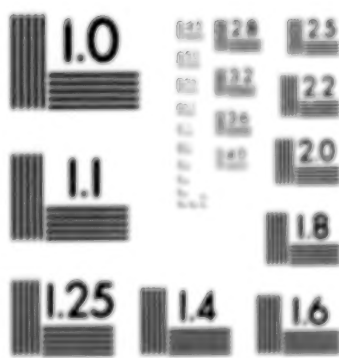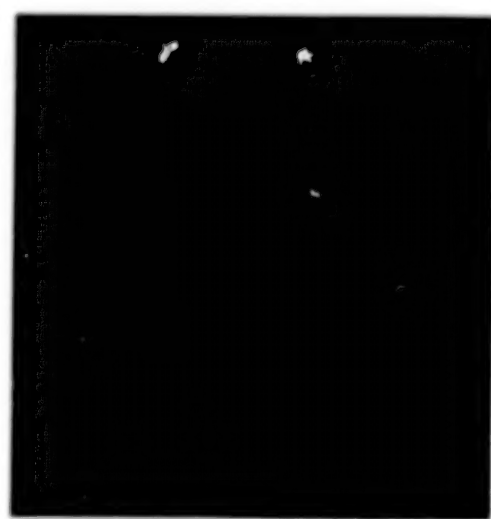
$$\tau_{\gamma\gamma} \approx (2.5)\ L(MeV)_{45}/R_{15} \tag{8}$$

$$\approx 0.25\ L_{45}/R_{15} \tag{9-a}$$

$$\approx 0.0025\ L_{Edd_{45}}/R_{15} \ <\ 1 \tag{10-b}$$

and the stochastically emitted PCS gamma ray transients escape from the ergosphere.

PCS gamma ray transient emission processes from Seyfert Galaxies have the following observational signatures (Leiter 1980; Piran, Shaham, 1977):

(a) PCS gamma ray spectra are flat over the energy range 300 KeV $\leq$ E $<$ 3 MeV with an upper cutoff energy $\leq$ 3 MeV strongly controlled by the Penrose Compton injected electron rest mass,

(b) PCS gamma ray emission transients occur stochastically with emission times $\sim$ 10 $M_s/(10^8\ M\odot)$ hours,

(c) PCS gamma ray emission occurs within a solid angle bounded above and below the equator of the Kerr black hole accretion disk by a $\sim$40 degree angle (see figure 1).

### IV. TEMPORAL VARIABILITY IN THE $\leq$ 3 MEV DIFFUSE GAMMA RAY BACKGROUND DUE TO PENROSE COMPTON SCATTERING (PCS)

For observations of the diffuse gamma ray background flux restricted to small pixels of the sky, let "N" be the total number of contributing Seyfert galaxies and "S" be the average gamma ray flux of their normal steady state spectrum. Of these N galaxies a subset "n" will emit, in addition to their normal steady state spectrum, a transient $\leq$ 3 MeV component of PCS gamma radiation with an average flux "s", where the dynamics of the PCS gamma ray transient process (Leiter 1980) imply that

$$n = \epsilon N \quad \text{where} \quad \epsilon \sim 0.01$$
$$s = \eta S \quad \text{where} \quad \eta \sim 10 \tag{10}$$

Then the total Seyfert galaxy contribution to the diffuse gamma ray flux observed within this restricted field of view given by

$$\Sigma = (NS + ns) = (NS + \sigma) \tag{11}$$

will contain a temporal variability due to PCS gamma ray transients $\leq$ 3 MeV occurring in $\sigma$ = ns. Taking into account the 5/2 power law associated with making a Euclidian assumption on
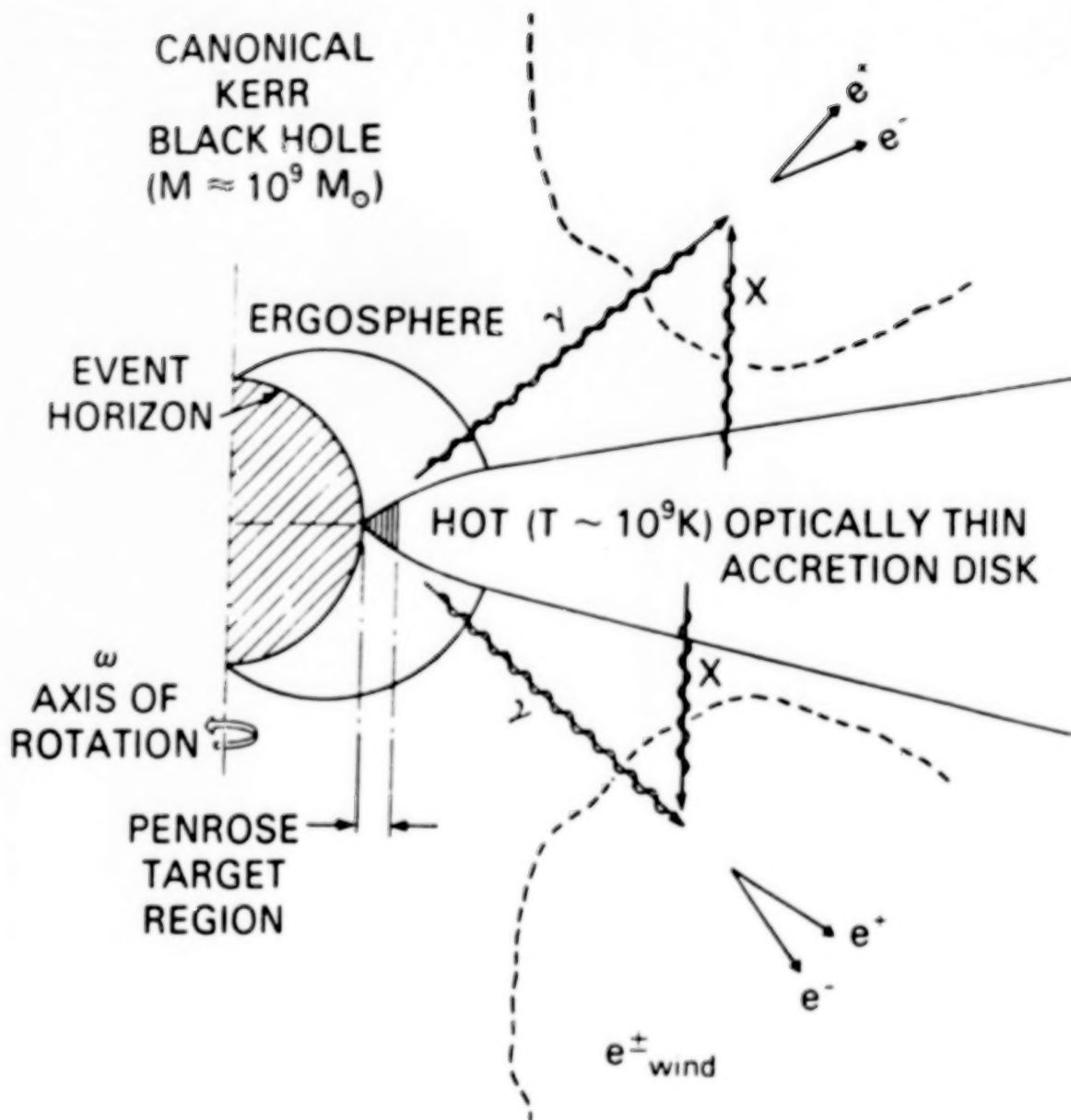
Fig. 1. An optically thin accretion disk with a hot, turbulent inner region, surrounds a massive Kerr black hole, $M_9 \gtrsim 1$, $a \approx m \lesssim 0.998$. Hot plasma blobs and blue shifted photons are injected sporadically into the Penrose target region $(r_{ph} < r < r_{ms})$ and cause PCS to occur. The resultant γ-ray bursts are focused into an angle of $\theta_{PCS} \gtrsim 40$ above and below the equator, and range over ~300 keV to ~2.7 MeV.

the log N - log S relationship, we find the fractional PCS
photon counting fluctuation associated with (10) and (11) as

(12)

$$\delta(\textstyle\sum)/\textstyle\sum = \delta(\sigma)/(NS + \sigma) = [1/3^{1/2} \ (N/N')^{1/6}] \ [\epsilon^{1/2}\eta/(1 + \epsilon\eta)]) \ / \ N^{1/2}$$

where N is the total number of contributing Seyfert sources, and
N' is the number of resolved Seyfert MeV gamma ray sources.

If N' is taken to be on the order of the number of Seyfert MeV
gamma ray sources expected to be resolved with the Gamma Ray
Observatory (Bignami (1989), and N is taken to be on the order
of the number of AGN resolved in the Einstein Observatory high
sensitivity survey, the ratio N'/N is

(13)

$$N'/N \ \approx \ 10^{-4}$$

Using (13) to evaluate (12) gives

(14)

$$\delta(\textstyle\sum)/\textstyle\sum \approx 3/N^{1/2}$$

A practical experiment using the Gamma Ray Observatory (GRO) to
detect PCS induced temporal variability in the $\leq$ 3 MeV diffuse
gamma ray background is one where flux measurements observed
within a solid angle $\Omega$ deg$^2$, and separated by time
intervals $\geq$ days, are compared for data accumulated over time
intervals $\geq$ hours.

Assuming an excess component of $\leq$ 3 MeV gamma ray photon flux
greater than $10^{-2}$ cm$^{-2}$sec$^{-1}$sr$^{-1}$ Webber, Lockwood, Simpson
(1981), the number C of photon counts in this excess component
is greater than 0.01 cm$^{-2}$-deg$^{-2}$-hr$^{-1}$. For an effective 1 MeV
detector area of 50 cm$^2$ typical of GRO/COMPTEL/OSSE, the
statistical photon counting error in a 3 hour measurement is

(15)

$$\delta C/C = (0.3 \cdot 50 \cdot \Omega)^{-1/2} = 0.8 \ \Omega^{-1/2}$$

In this context PCS induced temporal fluctuations in the < 3 MeV
diffuse gamma ray background are observable if

(16)

$$\delta(\textstyle\sum)/\textstyle\sum > \delta(C)/C$$

Using (14), (15) in (16) we find that GRO/COMPTEL/OSSE will be
able to observe PCS-induced temporal variability in the $\leq$ 3 MeV
diffuse gamma ray background if the total number of contributing
Seyfert galaxies per square degree is

(17)

$$(N/\Omega) < 14 \ deg^{-2}$$

This is a physically reasonable constraint for Seyfert AGN since: (a) the High Sensitivity Survey (HSS) for X-ray emitting AGN performed by the Einstein Observatory has shown that as few as~10 sources per square degree can account for~20% of the RCXB at 3 KeV, (b) further measurements with HEAO 1 imply that these AGN sources may also be able to account for as much as 100% of the CXB for energies greater than 100 KeV. Hence it is quite probable that galaxies satisfy the criteria (17) required for GRO/COMPTEL to be able to observe the PCS-induced temporal variability in the $\leq$ 3 MeV diffuse gamma ray background

## V. CONCLUSIONS

We have discussed a black hole spectral evolution model for AGN in which the majority of present epoch Seyfert galaxies have spectrally evolved from an earlier epoch of Precursor Active Galaxies (PAG) at redshift $z \sim 7$, a superposition of which acted as the source of the residual cosmic X-ray background (RCXB). As a by-product the process of Spectral Evolution the Seyfert galaxies which evolve from PAG contain canonical rotating Kerr black hole accretion disk dynamo systems which, in addition to emitting a broad band of nonthermal radiation typical of Seyfert galaxies, stochastically emit Penrose Compton Scattering (PCS) gamma ray transients from the ergosphere of the Kerr black hole.

These PCS gamma ray transients occur stochastically and:
(a) are observed over time intervals ~10 hours $M_8$

(b) have a flat spectrum over 300 KeV $\leq$ E $\leq$ 3 MeV with a universal cutoff $\leq$ 3 MeV,

(c) are focused into a "Penrose focusing angle" ~ 40 degrees above and below the plane of the Kerr black hole accretion disk system.

Since Seyfert galaxies tend to operate at ~ 1% of their Eddington luminosity, the photon-photon absorption optical depth for PCS gamma rays is less than one and they escape to infinity where they can be observed.

OSSE and COMPTEL on the Gamma Ray Observatory are appropriate instruments to carry out further tests by studying:

(a) PCS gamma ray transients from individual Seyfert galaxies whose orientation allows the Gamma Ray Observatory to fall within their respective Penrose focusing angles and,

(b) the possibility that present epoch PCS emitting Seyfert galaxies contribute observable temporal variability to the excess diffuse gamma ray background $\leq$ 3 MeV.

# REFERENCES

Begelman, M., Sikora, M., Rees, M. (1987), AP. J., 313, 689.
Bignami, G., in "Proc. GRO Science Workshop April, 1989"
Boldt, E., Leiter, D. 1986, Structure & Evolution of AGN
                    (Reidel 1986), 383.
Boldt, E., Leiter, D, 1987, Ap. J., 322, 689,
                        1984, Ap. J., 276, 427.
Cavaliere, A., Morrison, P., 1980, Ap. J., 238, L63.
Dermer, C., (1988), Ap. J.,335, L5.
Guilbert, P.W., Fabian, A.C., Rees, M.J., 1983, M.N.R.A.S.,
205, 593.
Heterich, K., 1974, NATURE, 250, 311.
Leiter, D., 1980, Astr. Ap., 89, 370; see also Kafatos, M,

Leiter, D., 1979, Ap. J., 229, 46.
Leiter, D., Boldt, E., 1982, Ap. J., 260, 1.
Meszaros, P. 1975, Astr. Ap. 49, 59.
Novikov, I., Thorne, K., ("Black Hole Astrophysics", pp. 393)
Piran, T., Shaham, J., 1977, Phys. Rev., 16-D, 1615;
                        (Black Holes, Gordon & Breach 1973)
                        1977, Ap, J., 214, 268.
Rees, M.J., 1984, Ann. Rev. Astr. & Ap., 22, 471.
Rees, M.J., Begelman, M.C., Blandford, R.D., & Phinney, E.S.,
            1982, NATURE, 295, 17.
Svenson, R., Zdziarski, A. A., (1989), AN INTRODUCTION TO

PAIR PLASMAS IN ASTROPHYSICS, pp. 1-23 ( in Proc. ST-Sci-GSFC
Workshop on Ultra-hot Plasmas & Electron-Positron Pairs in
Astrophysics, AUG. 1989)
Webber, W., Lockwood, J., & Simpson, G., 1981, Proc. 17th ICRC,
Vol. I, 247.
White, T. H., Lightman, A. F., (1988), CAP Preprint 2709.
Zdziarski, A.A., 1988, M.N.R.A.S., 233, 739.

(*) Now at Science Division, FSTC, Charlottesville, Virginia

# DISCUSSION

*Jim Kurfess:*

Why does the Pemrose Compton Scattering (PCS) model for AGN's require transient accretion of material, and not also operate in a steady-state mode?

*Darryl Leiter:*

Plasma containing electrons must have a tangential velocity in the Penrose Target region, between the marginally bound and marginally stable orbits in the ergosphere, for PCS to occur. This can only occur through transient, accretion via instabilities in the inner disk region.

*Alice Harding:*

What is the timescale for spin up of the black hole and does it depend on the angular momentum of the accreting material?

*Darryl Leiter:*

The a/M = 0.998 spin-up limit occurs when black hole mass doubles due to disk accretion. For efficiencies greater than 10%, this corresponds to $t > 10^8$ years if accretion occurs at less than the Eddington limit.

*Chuck Dermer:*

Does your model apply to solar-mass black-hole sources such as cygnus X-1. Also, what correlations do you predict between the X-ray and gamma-ray luminosities during a gamma-ray outburst?

*Darryl Leiter:*

Since A/m = 0.998 will take $> 10^8$ years for an efficiency of 10% and sub-Eddington luminosity, massive AGN galactic black hole are more likely to be spun-up than solar mass objects like CYG-X1. Only if X-ray flaring in the inner disk region is tied to disk instabilities will a correllation occur between PCS gamma-rays and X-ray flares.

# The High Energy Source 3C 273

Corinna von Montigny

Max-Planck-Institut für Physik u. Astrophysik

Institut für Extraterrestrische Physik

D-8046 Garching, F.R.G

## Abstract

In this paper I review the properties of 3C 273 and attempt to find an answer to the question why 3C 273 is the only extragalactic source so far, which has been detected at energies $\geq$ 50 MeV.

## Introduction

3C 273 ($(\alpha, \delta)$=1226-02, $z = 0.158$) is a very bright optical quasar with a one-sided, faint optical jet. Its apparent magnitude is $m_v = 12.5$ mag and its optical luminosity at 2500 Å is $L_{opt} = 2.3 \cdot 10^{31}$ erg/sec (Wilkes & Elvis, 1987).

In 1962 it was detected to be a very bright radio double source with an intensity at 20 cm of 46 Jy ($=46 \cdot 10^{-26} W/m^2 Hz$) (fig.1).
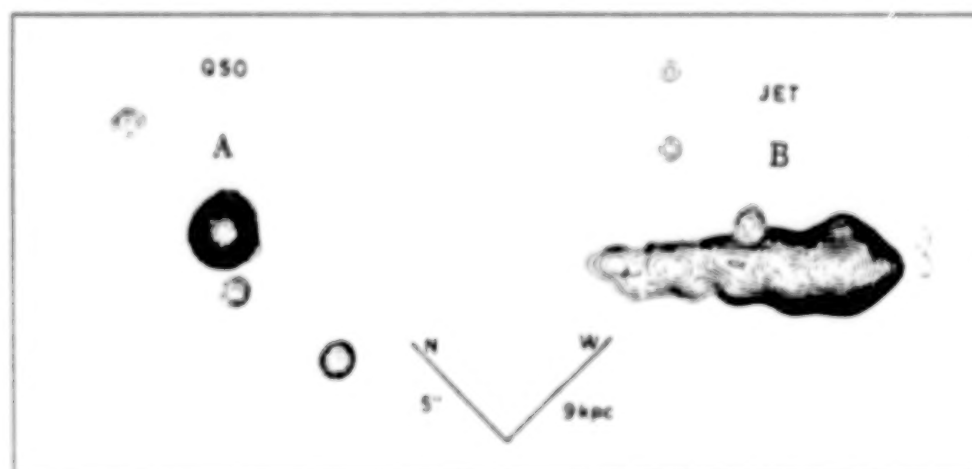


Figure 1: 408 MHz radio contour map of 3C 273 (adapted from Conway 1982).

Component A of the double source was identified with the optical quasar and has a very flat but complex radio spectrum with a spectral index between 2.7 GHz

and 5 GHz of $\alpha_r = 0.01 \pm 0.07$ (Kühr *et al.*, 1981). Component B is associated with the optical jet and its radio spectral index is $\alpha_r \approx 0.7$.

3C 273 was detected in X-rays in 1970. Its luminosity in the 2 - 10 keV band is $\sim 10^{46}$ erg/sec and the X-ray spectral index lies in the range $0.35 \leq \alpha_x \leq 0.5$. Two positive detections of a high energy source in the Virgo region have been reported with the COS-B satellite in 1976 and 1978. This source has been identified with 3C 273 because of the positional coincidence (Swanenburg *et al.*, 1978) and has been confirmed by Bignami *et al.*, 1981. So far the radio-loud quasar 3C 273 is the only extragalactic source which has been detected at energies $\geq 50$ MeV. Since it shows all the characteristics which are typical for high luminosity quasars: an optical and radio jet, superluminal motion and an UV excess, it seems to be the source which is best suited for detailed studies in order to learn more about the physical processes taking place in quasars.

## Observations

Recent simultaneous multifrequency observations from radio to X-rays (Courvoisier *et al.*, 1987) have once again confirmed that 3C 273 is variable in all wavebands. The source was observed at several epochs between December '83 and March '86. The temporal behavior of 3C 273 in the far infrared (FIR) and near infrared (NIR) regions is shown in fig. 2a. The fluxes were normalized to the flux of the first observation. To avoid confusion the flux variations in the three NIR bands have been averaged after the normalization. This seemed to be appropriate, because the temporal behavior in these three bands was the same.

As fig. 2a clearly shows there is no direct correlation between the FIR and the NIR. After a sharp rise shortly after the beginning of the observations, the FIR decreased rather steadily while the NIR stayed nearly constant, except for a possible dip in May '85. From this behavior can be followed that there have to be two well separated components which do not overlap. This implies a sharp cut-off of the FIR component between 10 and 5 $\mu$m, the beginning of the NIR (Courvoisier *et al.*, 1987).

The latest theories attempt to explain the generation of X-rays by inverse Compton scattering on infrared synchrotron photons. Therefore the temporal
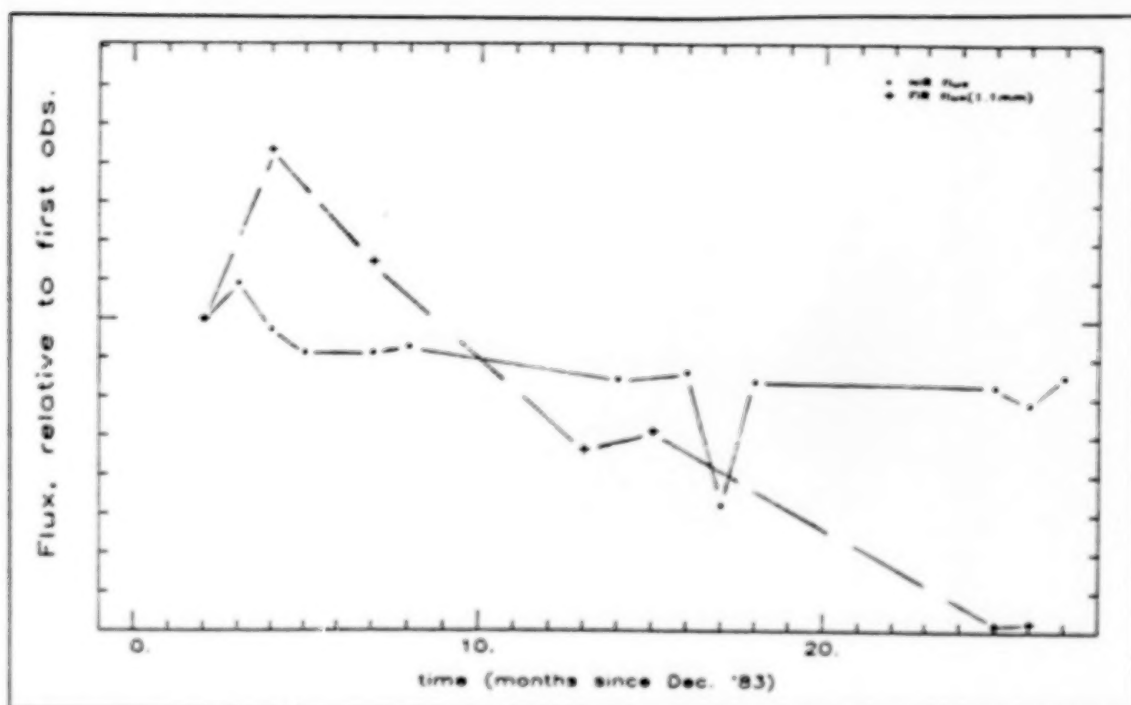
Figure 2a: Temporal behavior of 3C 273 in the FIR and NIR domain. Data from Courvoisier *et al.*, 1987)

behavior in these IR bands is of great interest to the X-ray observations (fig. 2b). After an irregular decrease of the soft and hard X-rays, the flux increased again slowly while the FIR flux decreases further and the NIR is nearly constant.

In the sub-mm band there was a totally different behaviour: During '84 the flux was constant and decreased in '85 and '86 (fig.2c).

From this behaviour and the absence of direct correlations it is concluded that the same electron population cannot be responsible for the FIR synchrotron emission and the self-Comptonization process generating the X-ray emission. Therefore, simple homogeneous SSC models can be excluded.

However, one has to be aware of the fact that the observations still did not have a complete temporal coverage and the span of ~ 2.3 years was rather short. Very subtle correlations might therefore have been missed.

The overall energy distribution of 3C 273 at different observation periods is shown in fig.3. In all three spectra one can see that the FIR varied not only in flux but also in spectral slope whereas the NIR slope was almost constant. This
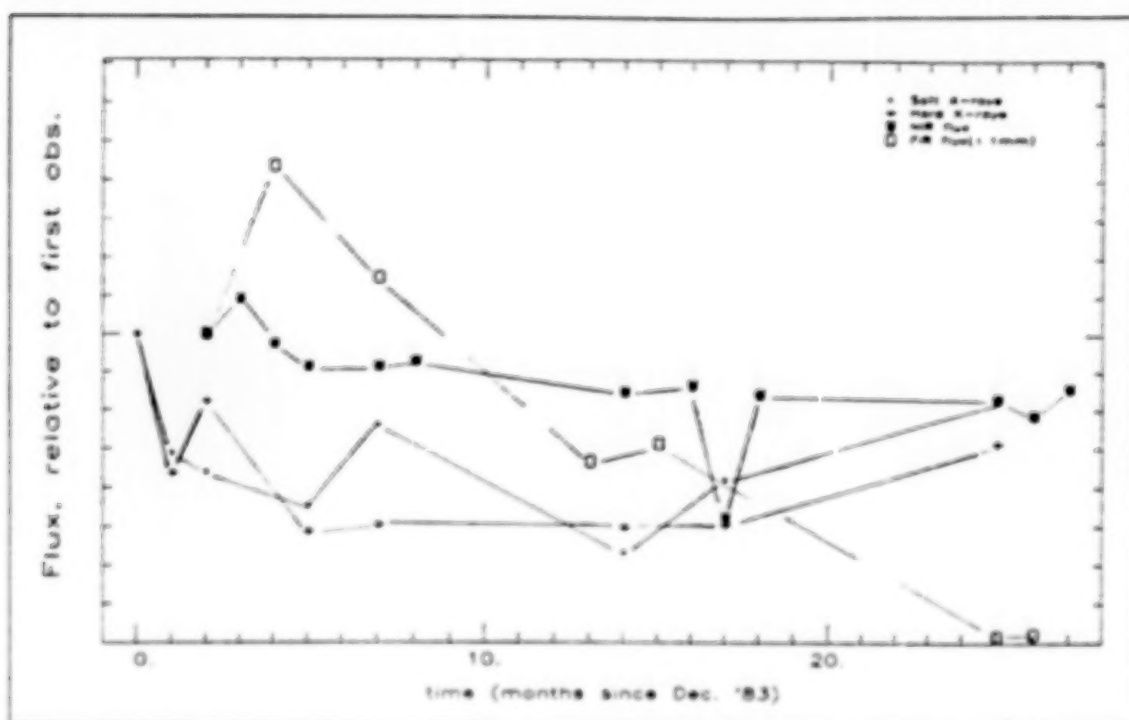
291

Figure 2b: Temporal behavior of 3C 273 in the FIR and NIR domain compared to the variations of the soft and hard X-ray fluxes. Data from Courvoisier *et al.*, 1987)

leads to the presence of a break at ~ 10$\mu$m which can be seen in all three spectra and is illustrated by the lines. A spectral fit by two powerlaws is not convincing from the spectral data alone but together with the different temporal behavior it is justified. From these arguments follows that the "cut-off" of the FIR is really a true feature.

The spectra of 3C 273 have therefore been fitted by three powerlaws and two blackbody distributions (Courvoisier *et al.*,1987). Fig.4 shows the spectral energy distribution from Feb. 84 to which the IUE data were added. Best fit values for the spectral slopes are $\alpha_{FIR} = 0.58$ for the far infrared region, $\alpha_{NIR} = 1.76$ for the near infrared and for the X-rays between 2 - 10 keV $\alpha_x = 0.45$. The optical and UV data have been fitted with two black body components with temperatures of $(16.2 \pm 0.3) \cdot 10^3 K$ and $(122 \pm 56) \cdot 10^3 K$. The fit in the UV domain (second black body distribution) is of course not very well constrained because of the lack of observational data.

Although 3C 273 is variable in all wavebands the shape of its spectrum does not change dramatically. The spectral slopes in the NIR band vary from 1.5 to
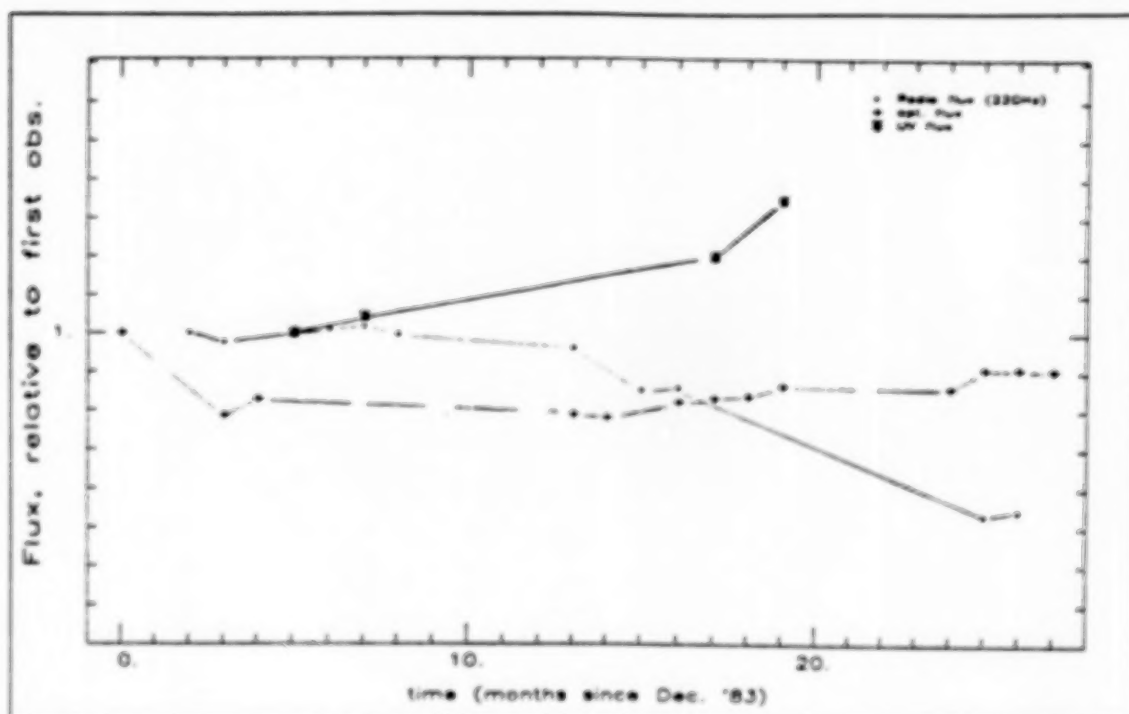
Figure 2c: Temporal behavior of 3C 273 in the Radio, optical and UV domain. Data from Courvoisier *et al.*, 1987)

1.75, in the FIR band from 0.6 - 0.9 and in the 2 - 10 keV X-ray range from 0.35 - 0.5. All in all it is a very usual spectrum.

## Comparison with other QSR's and AGN's

Since the Einstein IPC database is now available many investigations of large samples of quasars and AGN's (here Seyfert I) have been done. One of those investigations was performed by Wilkes & Elvis, 1987. They found that radio-loud (RL) quasars have a flatter X-ray spectrum than radio-quiet (RQ) quasars (see fig. 5). 3C 273, a member of their sample, is encircled by a dashed line. This correlation between radio-loudness and steepness of the X-ray spectrum has been very well confirmed by Brunner *et al.*, 1989.

In the beginning of 1989 Canizares & White published investigations of high redshift quasars. They had a more detailed look into the properties of RL quasars. They found that if they divide them into two classes, one class with flat radio spectra (FRS; $\alpha_r \leq 0.35$) and one class with steep radio spectra (SRS; $\alpha_r \geq 0.35$), the average steepness of the X-ray spectra is different (fig. 6). Unfortunately,
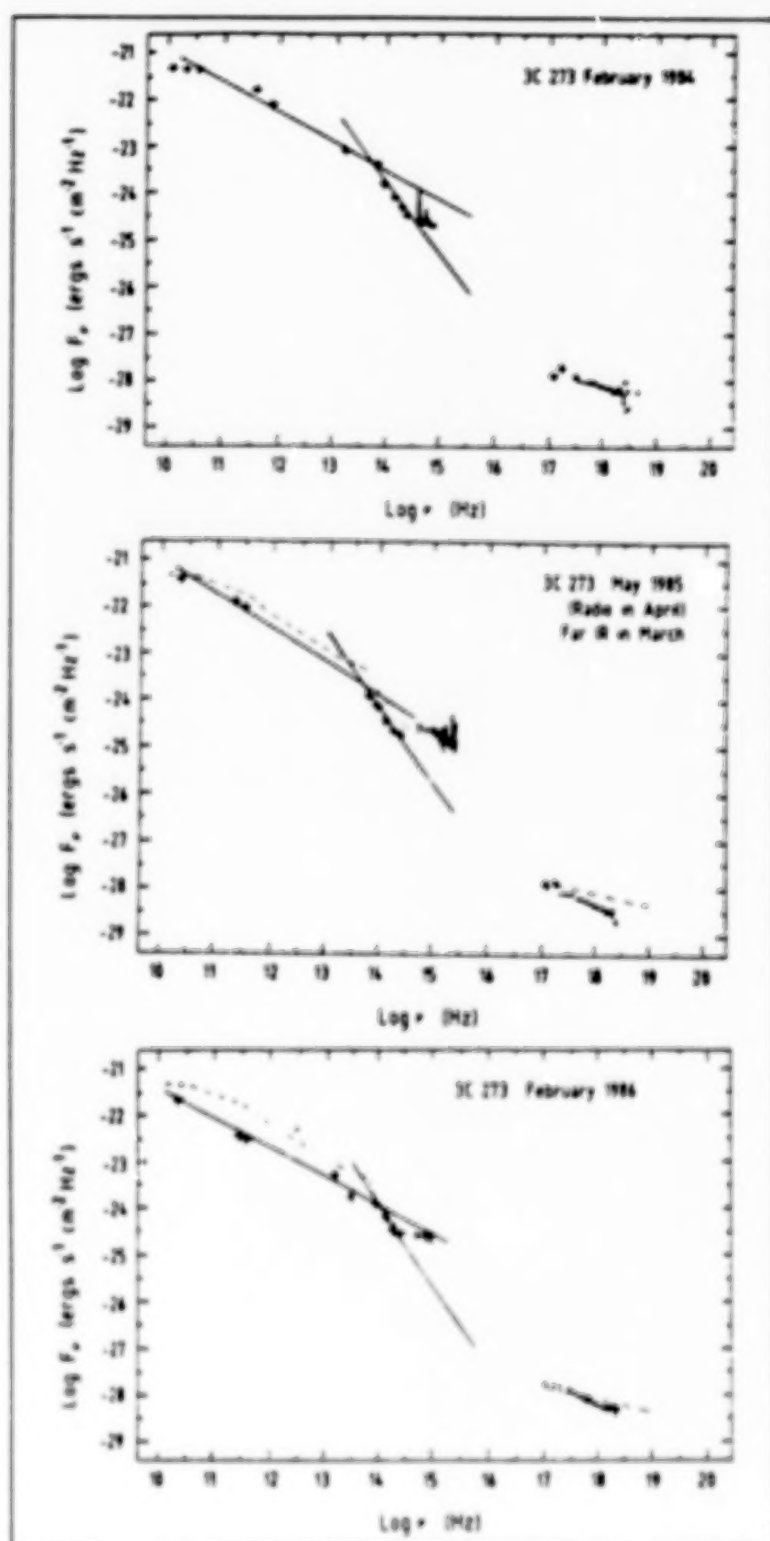
Figure 3: Overall energy distributions of 3C 273 from different observations where the spectral coverage was most complete (adapted from Courvoisier et al., 1987).
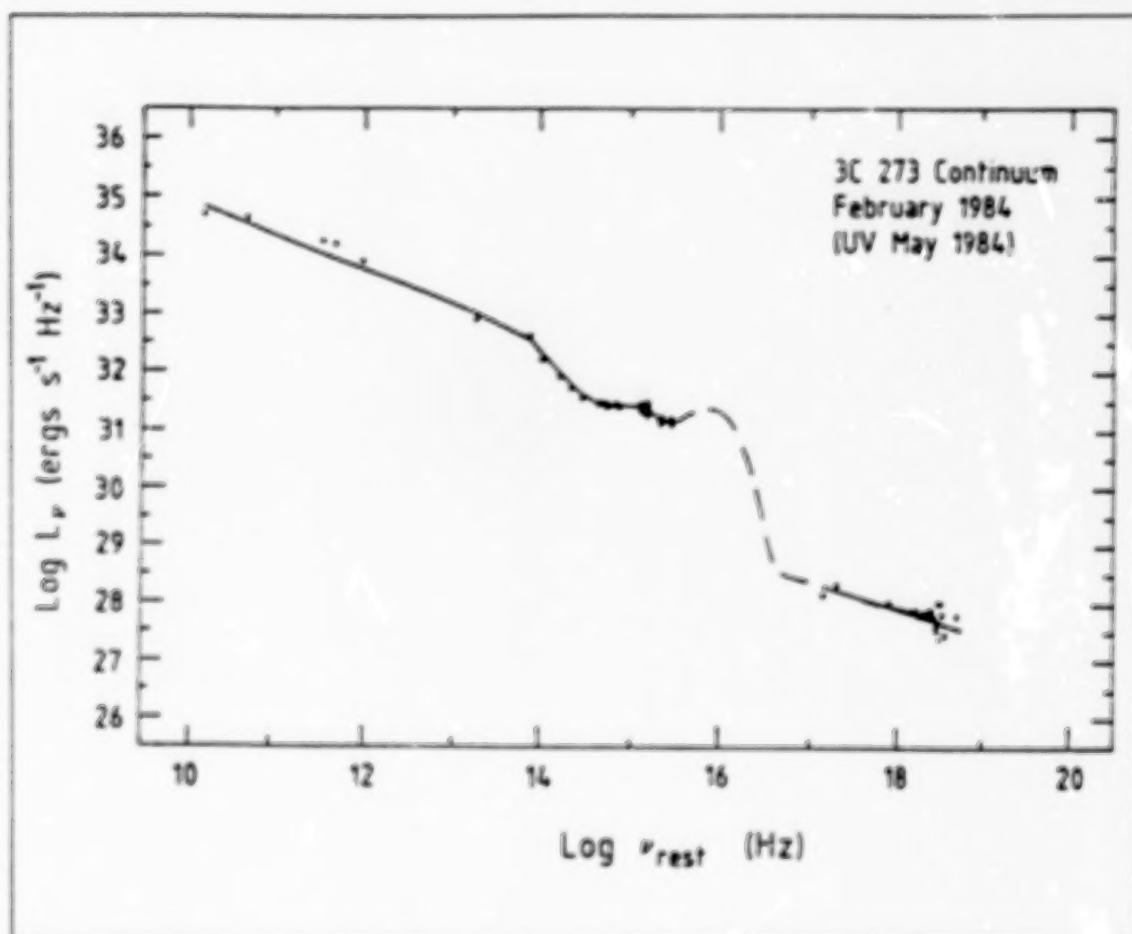
Figure 4: Fitted continuum spectrum of 3C 273. Data are shown as crosses and the best fit is given by the continous line (from Courvoisier *et al.*, 1987).

3C 273 was not a member of their sample. But it fits in very well if one localizes its position (asterisk) in figure 6.

Another investigation of a large sample of QSR's and AGN's has been published by Mushotzky & Wandel, 1989. They investigated the IR-UV continuum to X-ray ratio of about 120 objects. Since 3C 273 was also a member of their sample it could be identified in their results (fig. 7a-d).

In fig.7a the correlation of the X-ray luminosity and the "blue" luminosity at 4200 Å is illustrated. The position of 3C 273 is marked by the arrow. Fig.7b demonstrates the very good correlation between the X-ray luminosity and the "red" luminosity at 7500 Å for AGN's. This behavior of a large sample (see also: Malkan, 1984) is in contrast to the behavior of 3C 273 in the detailed
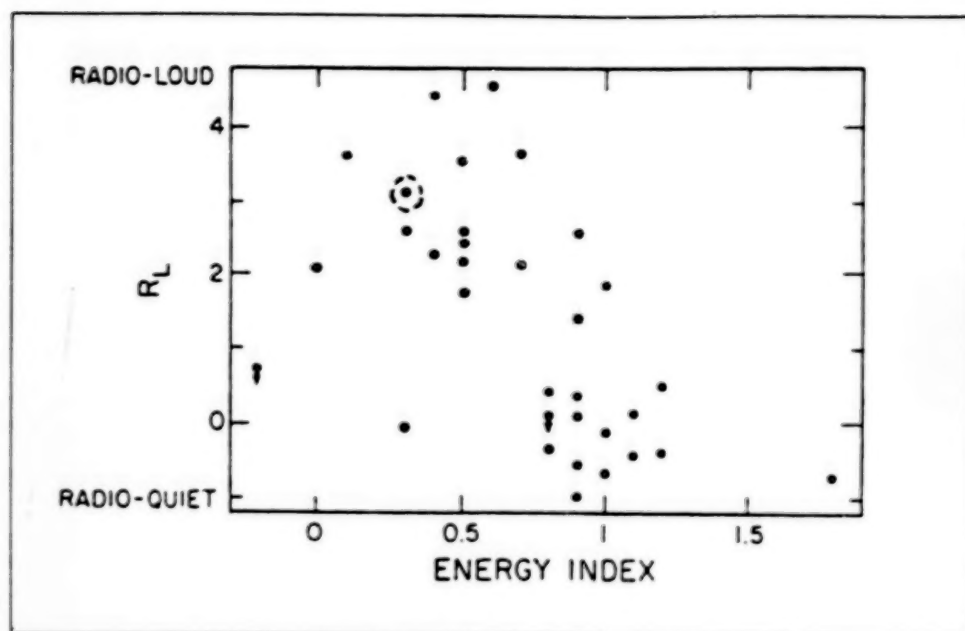
Figure 5: Radio loudness of quasars versus X-ray slope $\alpha_E$ (from Wilkes & Elvis, 1987).
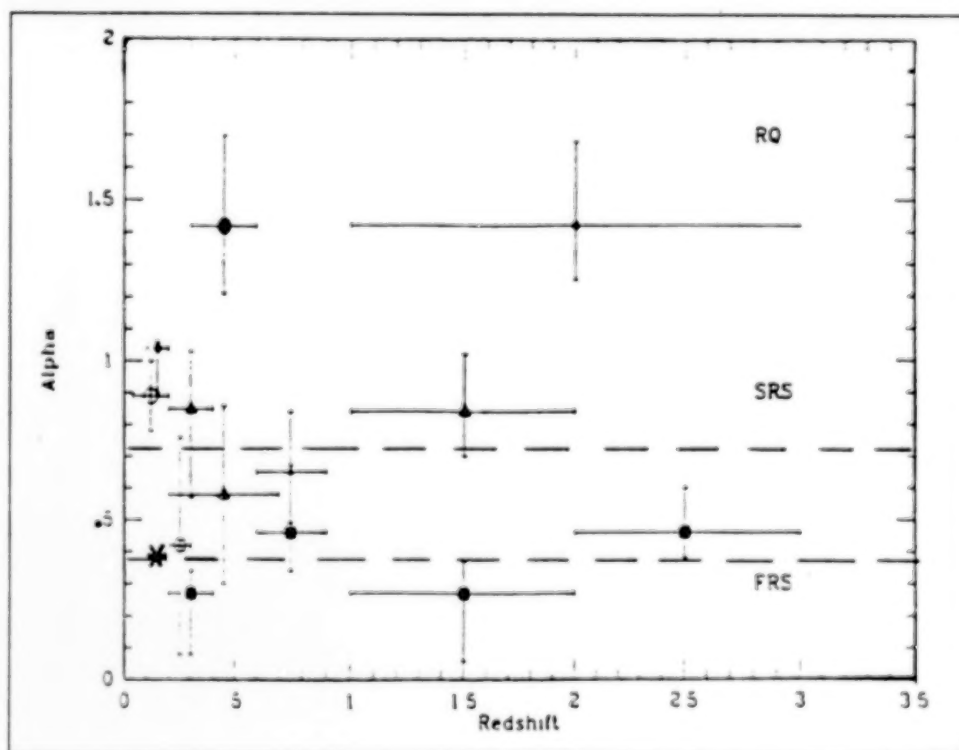


Figure 6: X-ray power-law index $\alpha$ versus redshift for FRS, SRS and radio quiet (RQ) quasars.

observations by Courvoisier *et al.* 1987, where a correlation between the infrared and X-ray emission could not be found. Therefore, there must exist some kind
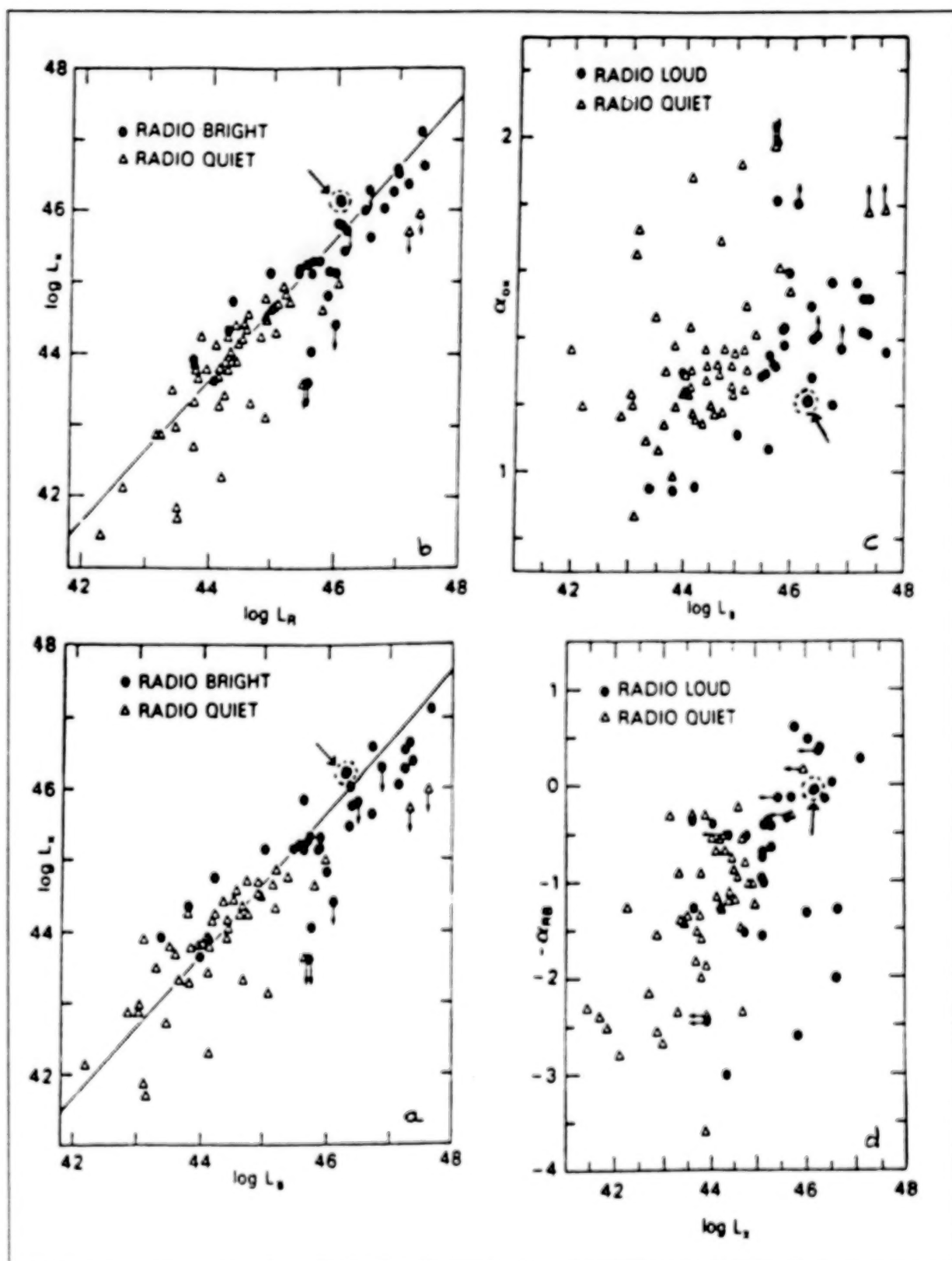
Fig.7a-d: relations between the "blue" and "red" luminosity and the X-ray luminosity and the spectral slopes $\alpha_{ox}$ and $\alpha_{rx}$.

of time averaging mechanism which correlates the infrared to the X-ray emission. But this does not change the fact that even here 3C 273 behaves very normal.

Figures 7c and 7d show the relation between the "blue" luminosity of AGN's (quasars and Seyfert I's) and their spectral slopes between the optical and the X-ray region ($\alpha_{ox}$) and between the "red" and the X-ray region ($\alpha_{rx}$), respectively. Although there is no correlation between these parameters these figures demonstrate that 3C 273 fits in here, too.

The only difference which could be found is demonstrated in figure 8 where the 2 - 10 keV X-ray luminosities of the Mushotzky & Wandel sample are plotted versus redshift. Here, 3C 273 clearly stands out against the general trend which might be due to some kind of evolution effect.

## Conclusion

3C 273 is not at all a particularly special source. This follows from the comparisons with other active galactic nuclei. It shows no extraordinary spectral features, neither in its radio to X-ray ratio nor in its IR-UV continuum to X-ray ratio. The only peculiarity is its extreme luminosity in all wavebands together with a relatively small distance ($z = 0.158$). It is therefore very probable that the $\gamma$-ray emission is not a special feature of 3C 273 but is common for all quasars and Seyfert I galaxies. Under this assumption and the requirement that the $\gamma$-ray luminosity is at least as high as the X-ray luminosity (as it is the case for 3C 273 and possibly for all radio loud quasars) EGRET should be able to detect some more AGN's in the $\gamma$-ray domain.

This prediction is illustrated by figure 9 which shows once again the 2-10 keV X-ray luminosity of quasars and AGN's versus redshift relation. Since 3C 273 was the only source detected by COS-B it is taken as reference point. The solid line then indicates the detection limit for sources to be detectable by COS-B.

A corresponding limit is shown for EGRET (broken line). Here a sensitivity for EGRET is assumed which is at least a factor of ten better than that of COS-B. As can be seen then from figure 9, EGRET should be able to detect new sources especially at low redshifts. Since the radio loud sources are expected to be more luminous in the $\gamma$-ray region than the radio quiet AGN's (Kazanas, 1989)
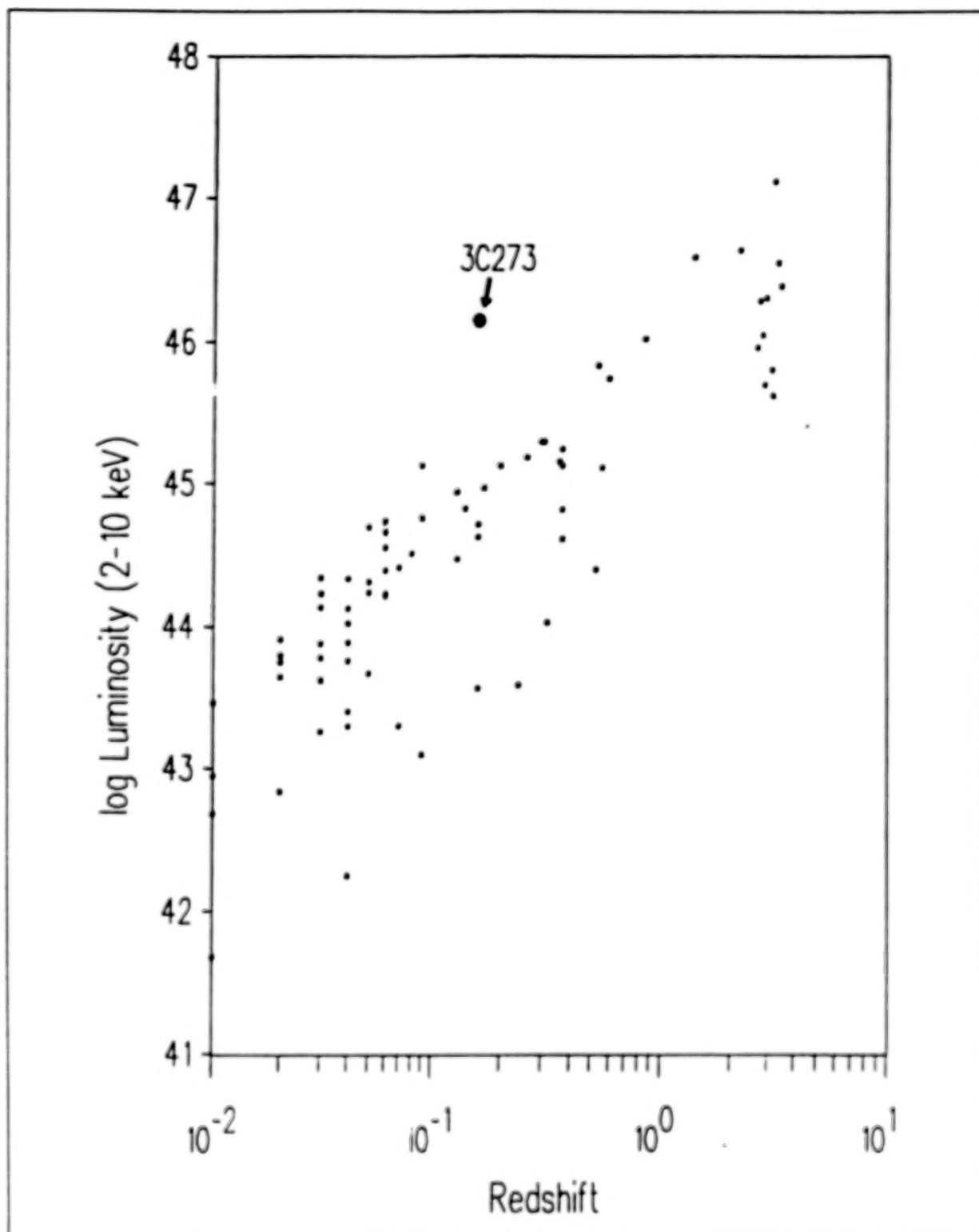
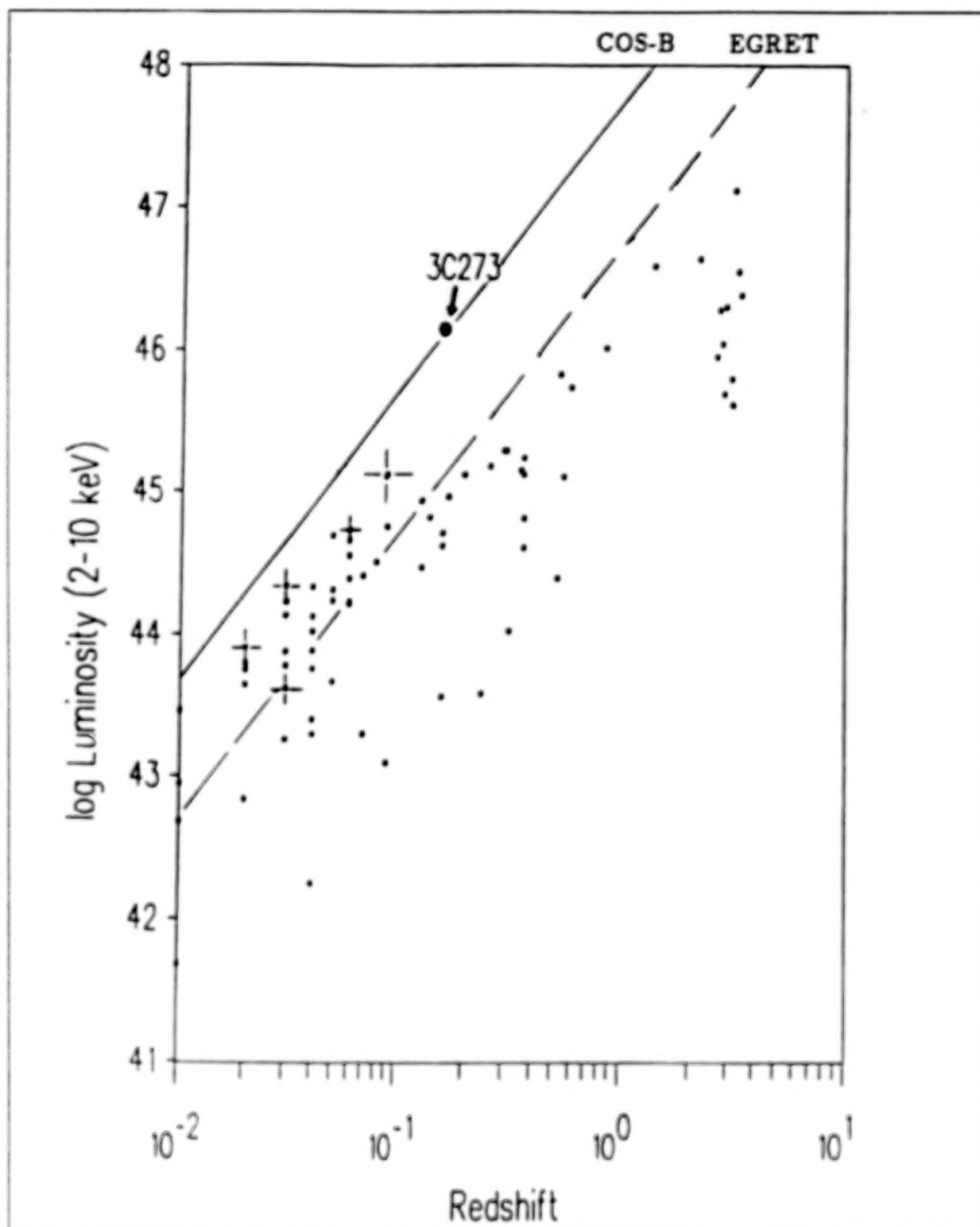Fig.8: 2-10 keV X-ray luminosity of quasars and AGN's versus redshift (Data from Mushotzky & Wandel, 1989).

Fig.9: 2-10 keV X-ray luminosity of quasars and AGN's versus redshift. The solid line indicates the "detection limit" of COS-B, the broken line that of EGRET. The crosses mark the radio loud quasars and AGN's.

the probability of detecting RL quasars (marked by crosses) is of course higher. These radio loud objects are: MCG 8-11-11, 3C 120, 3C 390.3, III Zw 2 and Mkn 618. These sources should therefore be good candidates for an observation with EGRET.

## References

Bignami, G.F., *et al.* 1981, *Astron. Astrophys.*, **93**, 71.

Brunner, H., Worrall, D.M., Wilkes, B.J. and Elvis, M. 1989, in press

Canizares, C.R. and White, J.L. 1989, *Ap. J.*, **339**, 27.

Conway *et al.* 1982, *IAU Symp. 97: Extragalactic Radio Sources*, Dordrecht, p. 167.

Courvoisier, T.J.-L., *et al.* 1987, *Astron. Astrophys.*, **176**, 197.

Kazanas, D. 1989, priv. communication.

Kühr, H. *et al.* 1981, *Astron. Astrophys. Supp.*, **45**, 367.

Malkan, M.A. 1984, *Proc. X-Ray and UV Emission from AGN's*, MPE report 1984, eds. W. Brinkmann, J. Trümper, p. 121.

Mushotzky, R.F. and Wandel, A. 1989, *Ap. J.*, **339**, 674.

Swanenburg, B.N., *et al.* 1978, *Nature*, **275**, 298.

Wilkes, B.J. and Elvis, M., 1987, *Ap. J.*, **323**, 243.

## DISCUSSION

*Richard Mushotzky:*

The diagram shown is conservative in its prediction of the number of AGN that EGRET will detect because the x-ray data are not a complete sample over the relevant flux range. The ROSAT complete sample should provide several times the numbers of candidate objects as shown in the figure.

*Corinna Von Montigny:*

Yes, that's true.

# COMPTEL OBSERVATIONS OF ACTIVE GALACTIC NUCLEI

## V. SCHONFELDER
### MAX-PLANCK-INSTITUT FÜR EXTRATERRESTRISCHE PHYSIK
### 8046 GARCHING, FRG

## ABSTRACT

The number of AGN's that might be observed by COMPTEL around 1 MeV is of the order of two dozens or less. The estimate is based on the HEAO-1 measurements between 2 keV and 100 keV and on the assumption that the power law spectra of AGN's at X-ray energies extend to at most 3 MeV before they break off.

## I. INTRODUCTION

Active Galactic Nuclei belong - among others - to the most interesting objects in the sky. The engine in the center that powers these galaxies is not yet really known. Most people tend to believe that a massive black hole is somehow involved.

At least some of the AGN's do have their absolute maximum of luminosity at MeV gamma ray energies. Therefore, it is reasonable to speculate that the key for an understanding of the central energy source may be found at MeV gamma ray energies. In this short talk I want to address the capabilities of COMPTEL to observe AGN's. The two most outstanding features of AGN's at gamma ray energies are their "time variability" and their "power law energy spectra" over a broad spectral range with a break or even cut off at MeV-energies or somewhere below. Both these features are illustrated in figures 1 and 2.

Figure 1 shows the time variability of the soft and hard X-ray emission of the radio galaxy Cen A. Here the 3 to 12 keV and the 100 keV flux is plotted over a time interval of more than 10 years. Clearly, the luminosity of Cen A has changed by more than a factor of 4 within - say 1 year. If therefore, comparisons between observations of one and the same object with different intruments in different spectral ranges are made, it is essential that these observations are performed simultaneously. The shortest time variabilities that have been observed from AGN's constrain the size of the central energy source to less than about $10^{15}$ cm.
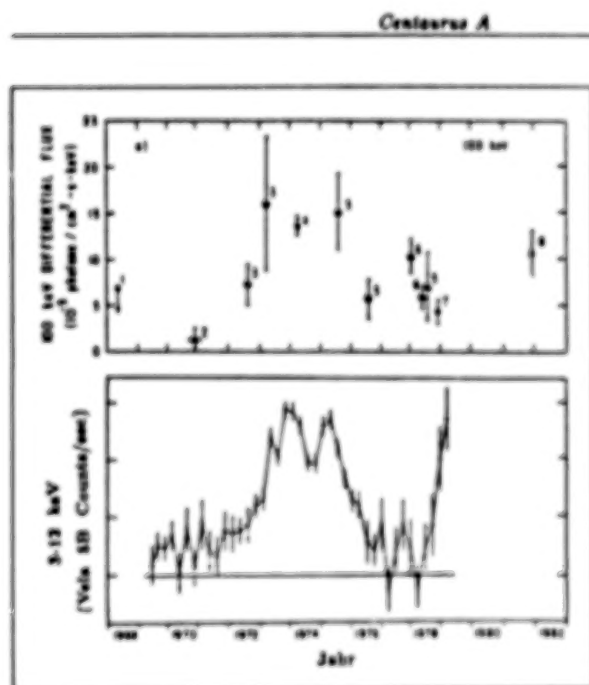


Figure 1. Time variation of the Centaurus X-ray flux at 100 keV (top) and between 3 to 12 keV (bottom). Compilation of measurements adopted from v. Ballmoos (1985).

The power law shape of the energy spectra of AGN's over wide spectral ranges is illustrated on figure 2, which shows the spectrum of the quasar 3C 273 from radio to gamma ray energies. The spectrum is an eye fit to the existing measurements. The fit is based on 4 power law components and two blackbody components in the visible and in the UV. In a crude sense the energy spectra of other AGN's like Seyferts, radio galaxies and BL Lac's look similar, though there are of course certain differences.

If the energy spectrum of figure 2 is converted into a luminosity spectrum, then it becomes evident that the maximum of luminosity is located near $10^{20}$ Hz, corresponding to a photon energy of a few MeV. The bending of the power law energy spectrum, which leads to this maximum, must exist for the majority of AGN's either around 3 MeV or at somewhat lower energies in order not to be in conflict with the observations of the gamma ray background (e.g. Rothschild et al., 1983).
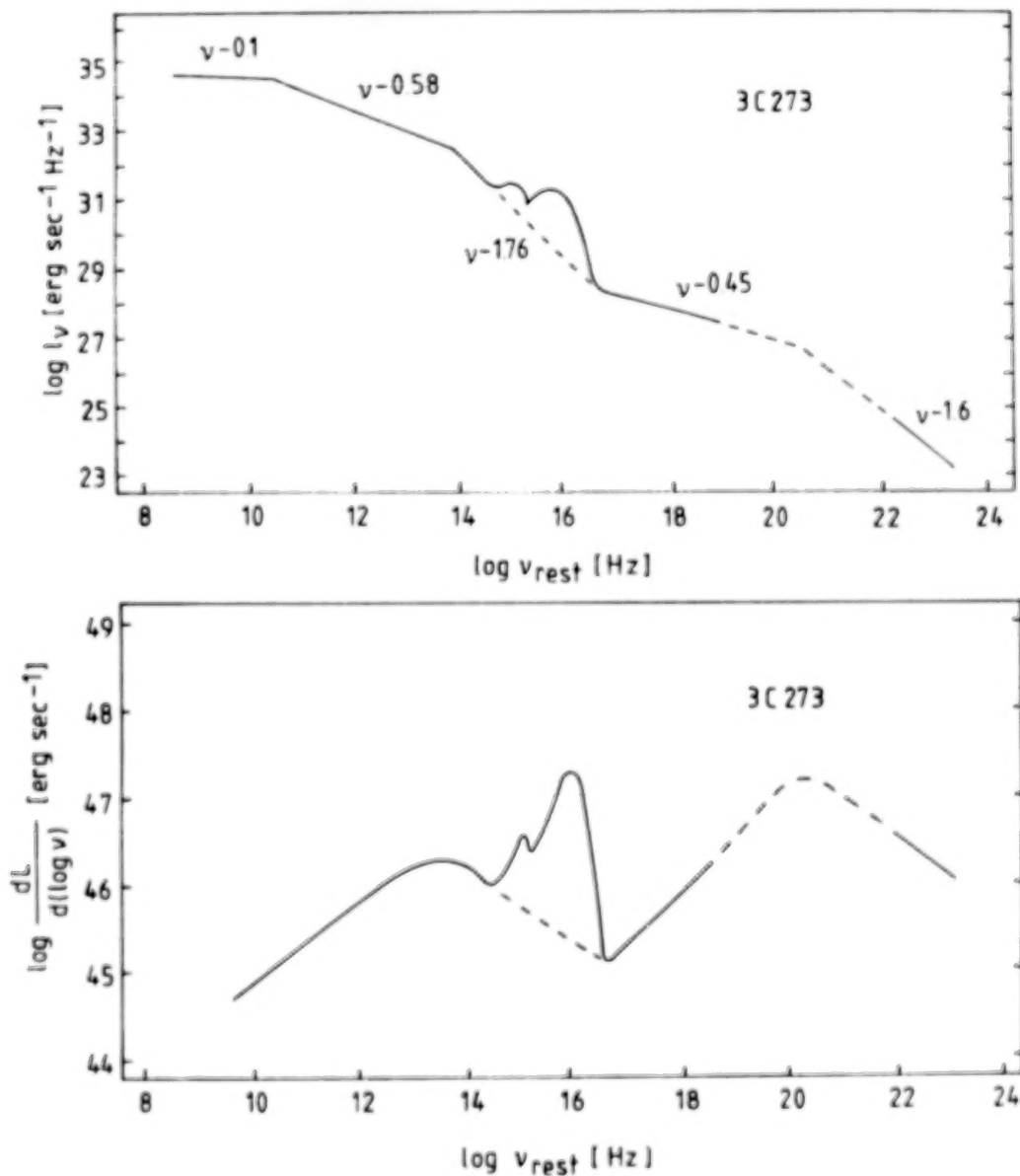


Figure 2. Eye fit to measurements of the quasar 3C 273 from radio to gamma ray energies (adopted from Courvoisier et al., 1987).

Various possibilities exist to explain the bending. The break may simply reflect thermal emission with kT-values of the order 1 MeV, or in case of non-thermal emission (as in case of 3C 273) it may be caused by a cut off of the relativistic electron spectra (due to energy losses), or due to photon - photon absorption in the high photon density field as a necessary consequence of the compactness of the source, or due to the Penrose Compton process.

So far observations of gamma ray emission have been reported from only 5 different objects. These are the Seyfert galaxies NGC 4151 and MCG 8-11-11, the radio galaxy Cen A, the quasar 3C 273, and NGC 1275, the radio galaxy within the core of the Perseus cluster.

NGC 4151 seems to be highly variable at MeV-energies. Only 2 positive detections have been reported above 1 MeV by the MISO-group. Some of the upper limits of other observations (at other times ) to the MeV-flux were about 10-times lower than the reported MISO-fluxes (see Bazzano et al., 1989). MCG 8-11-11 is known to be a highly variable Seyfert I galaxy at low X-ray energies. A positive detection of this object at MeV energies by the same MISO instrument showed a flux and a spectral shape similar to those found for NGC 4151 (Bazzano et al., 1989). Cen A is a very strong X-ray source with a power law energy spectum which well extends into the MeV-range. The gamma ray spectrum must steepen at about 10 MeV (or somewhat below) in order not to be in conflict with upper flux limits set by SAS-2 and COS-B above 35 MeV or 50 MeV, respectively (see v. Ballmoos et al., 1987). 3C 273 at present is the only extragalactic object observed at high gamma ray energies. Interpolation between existing X-ray and $\gamma$-ray measurements suggest that 3C 273 has its maximum of luminosity at 2 to 3 MeV (see figure 2 and Hermsen et al., 1981, and Bezler et al., 1984). Strong and Bignami (1983) report a possible detection of gamma ray emission by COS-B from NGC 1275. The excess of gamma ray counts at the position of the galaxy is only marginal.

## II. COMPTEL OBSERVATIONS OF AGN'S

COMPTEL's nominal energy range is 1 to 30 MeV. The actual energy threshold will be at 550 keV. COMPTEL has a large field-of-view of about 1 steradian and an angular resolution of (2 to 5) degree FWHM within that field-of-view. The sensitivity of COMPTEL to observe gamma ray emission from AGN's in a two week observation period is illustrated in figure 3. Here the 3 $\sigma$ - sensitivity limits are compared with several reference spectra (Cen A, 3C 273, and 12 AGN's observed by HEAO-1(A4) between 10 keV and 100 keV). The 12 AGN's (mostly Seyferts) observed by HEAO-1 were not the result of a survey, but were the brightest high latitude sources identified with AGN'S before the launch of HEAO-1 (Rothschild et al., 1983). They are listed in Table 1.

### TABLE I
#### 12 AGN'S OBSERVED BY HEAO-1 (A4)

| | |
|---|---|
| NGC 4151 | Seyfert I |
| NGC 1275 | Seyfert I in Perseus |
| MCG 5-23-16 | Seyfert II |
| MKN 509 | Seyfert I |
| NGC 5548 | Seyfert I |
| NGC 6814 | Seyfert I |
| NGC 3783 | Seyfert I |
| 3C 390.3 | Seyfert I |
| 3C 120 | Seyfert I |
| ESO 141-G55 | Seyfert I |
| MKN 279 | Seyfert I |
| MKN 335 | Seyfert I |

All 12 AGN's can be fitted by power law spectra with a photon number spectral index of -1.62 between 2 and 165 keV. The galaxy to galaxy variation of the spectral index was found to be less than 0.15. The detectability of these 12 AGN's by COMPTEL will depend on how the spectra continue towards higher energies. If they have spectra similar to 3C 273 or Cen A, then COMPTEL may be able to observe all of them.

The total number of AGN's that might be detected by COMPTEL during the GRO survey in the first year of the mission can be estimated in the following way: above the HEAO-1 (A2) sensitivity limit of $3.1 \times 10^{-11}$ erg/cm$^2$ sec, the complete sky survey of this instrument in the 2 to 10 keV range contained 30 objects with latitudes $|b| > 20°$ (corresponding to 8.2 ster): 25 of them were Seyferts, 4 were BL Lac's and 1 a quasar. The log N - log S relationship of these 30 objects was consistent with an Euclidian one (Picinotti et al., 1982):
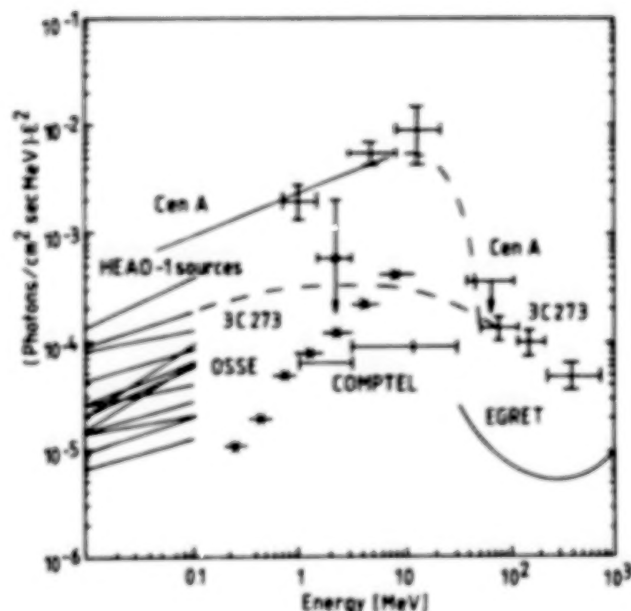


Figure 3. 3 $\sigma$ sensitivity ($5 \cdot 10^5$ sec observation time) of COMPTEL for observation of AGN's.

$$N(>S) = a \, S^{-1.5} \text{ ster}^{-1}$$

For $N(> 3.1 \cdot 10^{-11} \text{ erg/cm}^2 \text{ sec}) = 30$ per 8.2 ster we obtain $a = 0.63 \cdot 10^{-15}$.

Under the optimistic assumption that all 30 objects have power law spectra up to 3 MeV with the same spectral photon number index of -1.62 as that found by HEAO-1 (A4) for the 12 AGN's the following estimate can be made:

The derived log N - log S realtionship for the 600 keV to 3 MeV range is

$$N(>S) = 0.63 \cdot 10^{-15} \cdot 300^{+0.38} \, S^{-1.5} \text{ ster}^{-1}$$

Since COMPTEL's (0.6 to 3) MeV sensitivity limit for a two week observation period ($5 \cdot 10^5$ sec) is $1.8 \cdot 10^{-10}$ erg/cm$^2$ sec, one obtains

$$N(> S_{min}) = \begin{cases} 30 \text{ objects over } 4\pi\text{-sky} \\ 20 \text{ objects for } |b| > 20° \end{cases}$$

We therefore can expect that COMPTEL will observe about 2 dozens of AGN's, if they all have power law spectra up to at least 3 MeV. If some spectra break off earlier, the number will be smaller.

In case of a positive detection of a larger number of AGN's, it will be possible to derive their luminosity function at gamma ray energies. The lunimosity function together with the measured properties of individual galaxies may lead to a better understanding of the central source of AGN's. The knowledge of the luminosity function will allow a realistic estimate of the contribution of unresolved AGN's to the cosmic gamma ray background.

Table 2 contains a list of AGN's which we consider to be the 16 most promising ones to be studied by COMPTEL.

<div align="center">

## TABLE II
### AGN-CANDIDATES FOR COMPTEL OBSERVATIONS

</div>

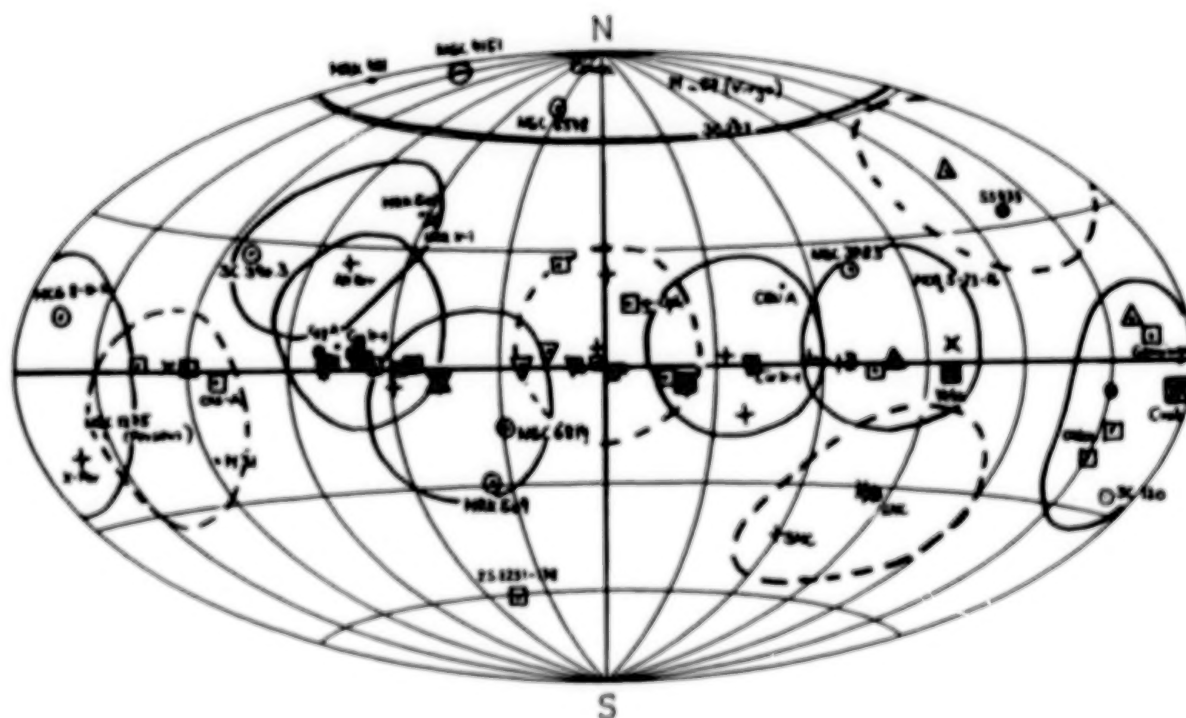| | |
|---|---|
| Seyfert I galaxies: | 3C 120, MCG 8-11-11, NGC 3783, NGC 4151, NGC 5548, 3C390.3, NGC 6814, MRK 509 |
| Seyfert II galaxies: | MCG 5-23-16 |
| Quasars: | 3C 273 |
| Bl-Lac objects: | MRK 421, MRK 501 |
| Radio galaxies: | NGC 1275, M 87, Cen A, Cyg A |



Figure 4. Suggested pointing directions during the second year of the GRO mission to perform an indepth observation of the most promising galactic and extragalactic objects (including of 16 objects of Table 2) which are covered by the 8 pointings marked by full circles (Steinle, 1989).

In order to improve the sensitivity of the AGN-observations it might be worthwhile to look longer towards them during the second year of the mission (e.g. for 28 days per target). If the pointing directions are selected carefully, a set of 8 pointings would be sufficient to include the 16 AGN's of Table 2.

The 16 objects and 8 possible pointing directions of the GRO spacecraft are shown in figure 4. A circle of 25° radius is drawn around each pointing direction indicating the field-of-view of COMPTEL during each observation. Since most of the pointing directions happen to be concentrated around the galactic plane, many galactic objects can be studied at the same time to quite same extent (like radio pulsars, X-ray binaries and other galactic objects). Indeed, by adding 4 more pointings (as indicated in figure 4) an indepth study of the most promising galactic and extragalactic objects can be accomplished in the second year of the mission.

I think that such a viewing strategy during the second year of the mission might also be of interest to EGRET; and if the exact locations of the viewing directions are selected carefully, it might allow OSSE to select proper secondary targets in addition.

For the understanding of AGN's it will be very important to make correlated observations at different wavelengths. As stated before, such observations have to be made simultaneously because of the time variability of the objects. I hope that we shall obtain quite a number of proposals for correlated observations during the GRO survey year in response to the NASA-Research Announcement.

## REFERENCES

v. Ballmoos, P., Diehl, R., and Schönfelder, V., 1987,
    Ap. J., 312, 134
v. Ballmoos, P., 1985, Ap. J., 269, 423
Bazzano, A. et al., 1989, Proc. of the Gamma Ray Observatory
    Science Workshop, GSFC, page 4-22
Bezler, M. et al., 1984, Astron. & Astrophys., 136, 351
Courvoisier, T.J.-L. et al., 1987, Astron. & Astrophys., 176, 197
Hermsen, W. et al., 1981, Proc. of 17th ICRC, Vol. 1, 230
Picinotti, G. et al., 1982, Ap. J., 253, 485
Rothschild, M.E., Mushotzky, R.F., Baity, W.A., Gruber, D.E.,
    Matteson, J.L., and Peterson, L.E., 1983, Ap. J., 269, 423
Steinle, H., 1989, special report, MPI
Strong, A.W. and Bignami, G.F., 1983, Ap. J., 274, 549

## DISCUSSION

*Carl Fichtel:*

The material presented in the last two talks shows that the sensitivity of the GRO instruments should very likely allow a reasonably definitive answer to the question whether active galactic nuclei can explain the majority of the diffuse gamma radiation from both intensity and spectral viewpoints.

*Volker Schonfelder:*

Yes, I agree with you. This is a very important issue. If there really is a contribution of unresolved active galactic nuclei to the cosmic bodyground, then we can subtract this component from the measurements, and we shall see whether a really diffuse component is left over, and what spectral shape it has.

*Darryl Leiter:*

Could COMPTEL detect temporal (1 hour) variability in the diffuse gamma-ray background at E ~ 1-3 MeV, possibly due to Seyfert galaxies.

*Volker Schonfelder:*

The detectability will depend on the level of variability. The determination of the diffuse cosmic gamma ray background is probably the most difficult one of all GRO measurements. It will only be possible in the late part of the mission, after we have studied variations of the instrumental background and after we have learned how to extract cosmic gamma ray sources (point like and extended) from our data. If the variations in the diffuse cosmic background which you are expecting are of the order of a few percent or higher, we might be able to see them.

# OSSE OBSERVATIONS OF
# ACTIVE GALACTIC NUCLEI

W. Neil Johnson
Naval Research Laboratory
Washington DC

## ABSTRACT

The Oriented Scintillation Spectrometer Experiment (OSSE) has been designed to address a broad range of scientific objectives through gamma ray observations in the 0.05 - 10 MeV energy range. A significant number of these observations shall be directed to the study of Active Galactic Nuclei (AGN). The characteristics of the OSSE instrument and the current observation plans are discussed. Examples of the scientific issues which OSSE expects to address are provided.

## INTRODUCTION

The Oriented Scintillation Spectrometer Experiment (OSSE), one of four experiments on NASA's Gamma Ray Observatory Satellite, has been designed to undertake comprehensive gamma-ray observations in the 0.05 to 10 MeV energy range. The instrument incorporates four actively-shielded NaI(Tl)-CsI(Na) phoswich detectors which have $3.8^\circ$ x $11.4^\circ$ fields of view defined by tungsten collimators. The characteristics of OSSE are summarized in Table 1; a more complete description of the instrument and its capabilities can be found in Johnson *et al.* (1989).

OSSE's relatively small field of view dictates the approach to AGN observations which will consist of long exposures to specific AGN targets. The AGN targets shall be selected from an OSSE catalog of interesting AGNs which has been developed primarily from AGN observations by HEAO-1, HEAO-2, and EXOSAT in the X-ray band. The nominal exposure will be two weeks on a given source. OSSE uses offset pointing for background measurements to reduce systematic errors associated with orbital background effects. The OSSE target AGN will generally be in the fields of view of the other GRO instruments permitting coordinated observations over six decades in gamma ray energy. However, OSSE's orientation control system permits observations outside the fields of view of COMPTEL and EGRET; this capability will be used on orbital time scales to observe a second target (perhaps an AGN) while the co-aligned instrument viewing direction is occulted by the Earth. Consequently, OSSE will usually study two target sources per two-week interval, or approximately 52 targets per year. Thus, over the expected lifetime of GRO (possibly greater than 5 years), OSSE will have observed as many as 100 AGNs. Examples of the expected scientific results of such observations are presented below.

## Table 1.
## OSSE SUMMARY

Detectors

| | |
|---|---|
| Aperture Area (total): | 2620 cm$^2$ |
| Effective Area: | 1920 cm$^2$ at 0.511 MeV |
| Field-of-View: | 3.8° x 11.4° FWHM |
| Energy Resolution: | 8.2% at 0.661 MeV |
| | 3.8% at 6.13 MeV |
| Time Resolution: | 4 sec in normal mode |
| | 0.125 msec in pulsar mode |
| | 4 msec in burst mode |

Experiment Sensitivities ($10^6$ sec)

| | |
|---|---|
| 0.1 - 10 MeV Line $\gamma$s | $\sim 2 - 5 \times 10^{-5}$ $\gamma$ cm$^{-2}$s$^{-1}$ |
| 0.1 - 1 MeV Continuum | 0.005 x Crab |
| 1 - 10 MeV Continuum | 0.05 x Crab |
| Gamma Ray Bursts | $1 \times 10^{-7}$ erg cm$^{-2}$ |
| Solar Flare Line $\gamma$s ($10^3$ sec flare) | $1 \times 10^{-3}$ $\gamma$ cm$^{-2}$s$^{-1}$ |
| Solar Flare Neutrons (>10 MeV) | $5 \times 10^{-3}$ n cm$^{-2}$s$^{-1}$ |

## AGNS AND THE COSMIC DIFFUSE BACKGROUND

Surveys of AGN in the X-ray band show that they emit a significant fraction of their power in X rays and above. Consequently, the contribution of the summed emission from unresolved AGNs to the X-ray diffuse background has been a topic of interest since Setti and Woltjer (1973) first suggested that quasars would contribute much of the X-ray background if the X-ray to optical flux ratio observed for 3C273 was typical for quasars in general. The HEAO-1 and HEAO-2 missions have provided X-ray surveys which indicate that in the 2 - 10 keV range AGNs contribute ~20% of the observed cosmic diffuse background (Piccinotti *et al.* 1982).

At higher energies, the HEAO-1 mission observed the spectra of 12 AGN out to an energy of ~100 keV (Rothschild *et al.* 1983). These Seyfert galaxies had similar spectra which were well represented by power law model with photon index of ~1.6. Rothschild *et al.* (1983) use the AGN luminosity function from the 2 - 10 keV range (Piccinotti *et al.* 1982) with their average AGN high energy spectrum to estimate the AGN contribution to the cosmic diffuse background above 10 keV. Their result is shown in Figure 1 which displays the observed diffuse background and two estimates of the integrated AGN contribution with differing assumptions on the lower bound of the luminosity function used in the integral.

As can be seen in the figure, the hardness of the observed AGN spectra causes the AGN contribution to the diffuse background to grow with energy until it reaches and/or exceeds the observed diffuse background somewhere in

the 100 keV to 4 MeV range. A softening or break in the spectra of AGN likely occurs in this energy range to prevent the integrated AGN flux from exceeding the gamma ray diffuse background. Above ~500 keV only four AGNs have been observed mainly by balloon experiments (see Bassani and Dean 1983). However, OSSE should be able to measure the spectra of ~ 30 - 100 AGNs in this energy range and thereby observe any softening in the spectra which would provide information on the AGN contribution to the $\gamma$ ray diffuse background and perhaps provide insight into the fundamental energy source in AGNs. The OSSE observations of this number of AGNs might also provide a greater understanding of the differences in Type I and II Seyferts. If the main difference in these types is dust opacity, at $\gamma$-ray energies the dust may become optically thin so that both types have similar $\gamma$-ray characteristics. Figure 2 displays the OSSE sensitivity for $10^6$ sec observations along with some of the AGNs measured by HEAO-1 and two high energy $\gamma$-ray measurements.
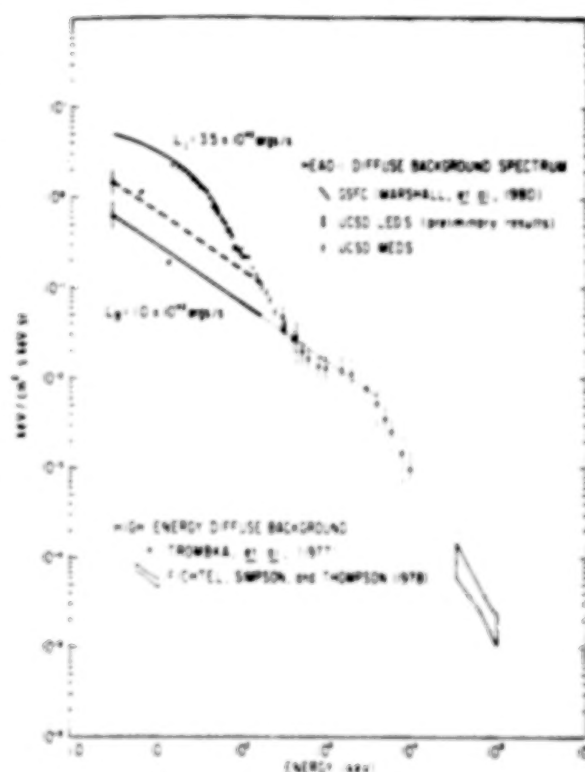


Figure 1. AGN Contribution to Diffuse Background (from Rothschild et al. 1983). Two estimates for the integrated power law contribution from unresolved Seyferts are displayed.

## AGN TEMPORAL VARIABILITY

Active galactic nuclei have demonstrated temporal variability in X rays on time scales of days to months. Intensity variations by factors of 2 - 100 have been reported. At gamma-ray energies there are many fewer observations and, consequently, only variations of NGC 4151 have been reported (Perotti *et al.* 1981). The time scales of the variations are generally taken as evidence for association of the emission with the central power source of the AGN. The model of accretion onto a massive black hole provides some interesting predictions which OSSE can address in its observations of AGN. One example of the variability is in the form of Penrose Compton Scattering (PCS) transients as proposed by Leiter and Boldt (1989).

Penrose Compton Scattering (Figure 3) occurs in the ergosphere around a Kerr black hole when blue shifted photons from the accretion disk scatter off of infalling electrons and escape with increased energy as high as 2.7 MeV. The emission is beamed relative to the accretion disk and the spectrum of the emitted gamma rays is essentially flat from 300 keV to ~ 3 MeV with a kinematic cut-off controlled by the electron rest mass. Leiter and Boldt (1989)
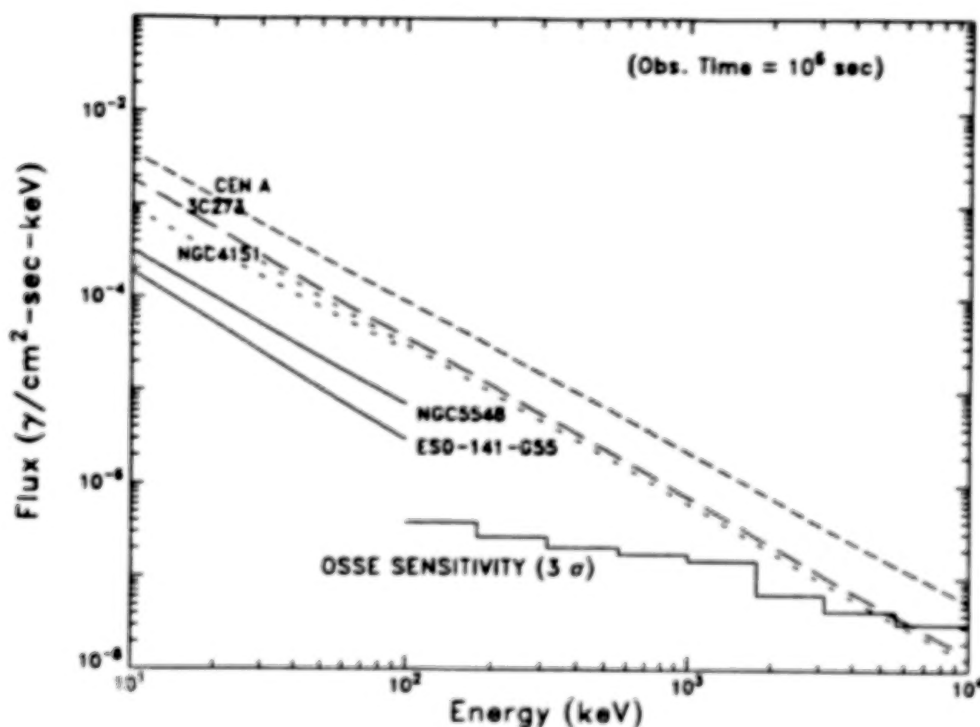
Figure 2. OSSE continuum sensitivity and X-ray and gamma-ray measurements of several AGN.

have suggested this mechanism as an alternate explanation for the "bump" in the diffuse background spectrum at a few MeV (see Figure 1). The duration of a PCS gamma-ray transient is associated with the time required for a plasma blob in the accretion disk to cross the Penrose target region and is on the order of hours.

Leiter (1980) predicts that for NGC 4151 PCS transients of 2.2 hour duration with few percent duty cycle should be observed. These individual outbursts from NGC 4151 in the 300 keV - 3 MeV range should be detectable by OSSE. Detection of these events from several AGN displaying the same cutoff energy would not only confirm the Penrose Compton Scattering theory but also address the possibility of the PCS explanation for the MeV "bump" in the diffuse background spectrum.
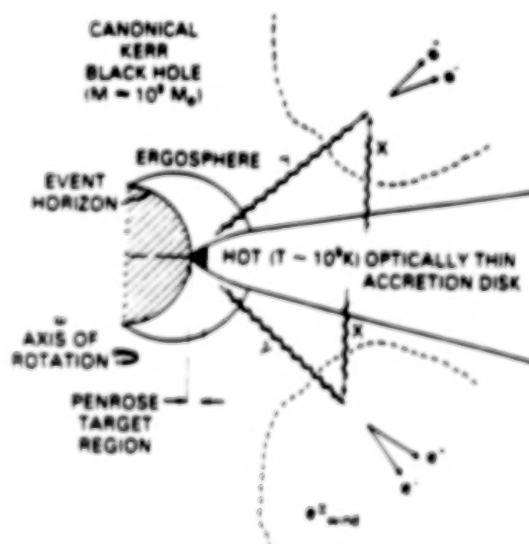


Figure 3. Penrose Compton Scattering of gamma rays from accretion disk around a Kerr black hole. From Leiter and Boldt (1989).

# OBSERVATION PLAN

The observing plan for GRO is determined well in advance with scientific priorities identified by the GRO science teams, the GRO Users Group, and the user community via the GRO Guest Investigator Program. The primary objective of the initial 15 months of the GRO mission is to provide a full sky survey with the EGRET and COMPTEL broad field of view instruments. This shall consist of ~30 two-week observations designed to give uniform sky coverage. For each observation period, OSSE will select two targets from its catalogs for study. The desire for uniform sky coverage provides ample opportunity for OSSE observations of AGN. Table 2 summarizes the OSSE AGN targets which are currently planned for the first 15 months of the mission. The final observing plan for GRO depends on the actual launch date so that this list of AGNs will likely undergo minor changes until the launch date of GRO is fixed. The final plan is expected to be available two months before launch. OSSE expects to make significant contributions to the understanding of AGNs from the observations of these 20 sources as well as from many other sources in the subsequent years of the GRO mission.

## TABLE 2.
### OSSE AGN Targets
### (1st 15 months of GRO Mission)

| Target | Class[1] | Target | Class[1] |
|--------|----------|--------|----------|
| M82 | 2 | PKS 2155-304 | 3 |
| CEN A | 1 | MRK 590 | 1 |
| 3C 273 | 4 | 3C 390.3 | 1 |
| M87 | 1 | 3C 120 | 1 |
| NGC 5548 | 1 | MCG 8-11-11 | 1 |
| NGC 4151 | 1 | PKS 0521-365 | 3 |
| 3C 317 | 1 | MRK 279 | 1 |
| NGC 1275 | 1 | MRK 421 | 3 |
| III ZW2 | 1 | NGC 5506 | 2 |
| MRK 335 | 1 | ESO-141-G55 | 1 |

[1]Classes:  1) Type 1 Seyferts, Radio Gal;  2) Type 2 Seyferts, Starburst, NELG;  3) BL Lacs;  4) Quasars

# REFERENCES

Bassani, L., A.J. Dean 1983, *Space Sci. Rev.*, **35**, 367.

Johnson, W.N., *et al.* 1989, *Proceedings of the Gamma Ray Observatory Science Workshop*, NASA/GSFC, 2-22.

Leiter, D. 1980, *Astron. Astrophys.*, **89**, 370.

Leiter, D., E. Boldt 1989, *Proceedings of the Gamma Ray Observatory Science Workshop*, NASA/GSFC, 4-14.

Perotti, A., *et al.* 1981, *Ap. J. (Letters)*, **247**, L63.

Piccinotti, G., R.F. Mushotzky, E.A. Boldt, S.S. Holt, F.E. Marshall, P.J. Serlemitsos, R.A. Shafer 1982, *Ap. J.*, **253**, 485.

Rothschild, R.E., R.F. Mushotzky, W.A. Baity, D.E. Gruber, J.L. Matteson, L.E. Peterson 1983, *Ap. J.*, **269**, 423.

# DISCUSSION

*Chuck Dermer:*

Please comment on a recent reanalysis of SAS-2 data by Young and Yu (Ap.J. 330, L5, 1988), in which they claim detections of 129 quasars and 7 seyfert galaxies.

*Carl Fichtel:*

There seems to be no solid justification for these claims in the SAS-2 data. You may wish to refer to the SAS-2 catalog. Added comment by David Thompson - the statistics of the SAS-2 catalog are too small to support such detections, in many cases involving only a few photons.

# Extragalactic Diffuse Radiation

# GAMMA RAY COSMOLOGY: THE EXTRA GALACTIC GAMMA SPECTRUM AND METHODS TO DETECT THE UNDERLYING SOURCE*

## DAVID B. CLINE

Departments of Physics & Astronomy, University of California at Los Angeles
405 Hilgard Avenue, Los Angeles, California 90024

## ABSTRACT

We discuss the possible sources of extragalactic gamma rays and methods to distinguish the different sources. The sources considered are 1) Early Universe decays and annihilation of Particles, 2) ANG Sources and 3) Baryon-Antibaryon Annihilation in a Baryon Symmetric Cosmology. We describe the energy spectrum and possible angular fluctuations due to these sources.

## I. INTRODUCTION – COSMOLOGICAL RADIATION

The study of the early universe proceeds largely by observing relics of an earlier period. The relics discovered or interpreted in this way, so far, are:

 i)  Baryon Excess – GUT Era to SU(2)XU(1) Era
 ii) Relic Neutrinos (undetected) – 1 sec
 iii) Primordial Nucleosynthesis – $\sim$ first 60 sec
 iv) 2.7° Microwave Radiation – $\sim$ 300,000 years

Clearly detection of more relics of the early universe is urgently needed, if they exist, to gain a better understanding of the evolution and properties of the early universe.

Windows on the early universe are mostly obscured by dust or gas in the universe. There are two windows in the electromagnetic spectrum in which to obtain cosmological information ($Z > 10$ for example) before galaxy formation: 1) the microwave region and 2) the MeV Gamma Ray region. As discussed most recently by Spergel (1989) and previously by Stecker (1973), the universe is relatively transparent to a few MeV to GeV radiation (see Figure 1).

What cosmological information could we learn from this region of the spectrum? In the first place they could be unstable particles and the annihilation of relatively long lived particles such as cold dark matter particles. One example of a decay process is the decay of a few GeV gravitino (Olive and Silk; Stecker and Tylka, 1989)

$$\dot{G} \rightarrow \gamma + \tilde{\gamma}$$

at $\sim 10^7$ sec. Figure 2 shows the type of structure that could be detected from such a process. Heavy long lived neutrinos could give similar effects (for example a 4th Family

neutrino with a mass of $\sim 100$ GeV and a lifetime of $\sim 10^7 \to 10^{10}$ sec)(D. Cline, Y.T. Gao, 1990).
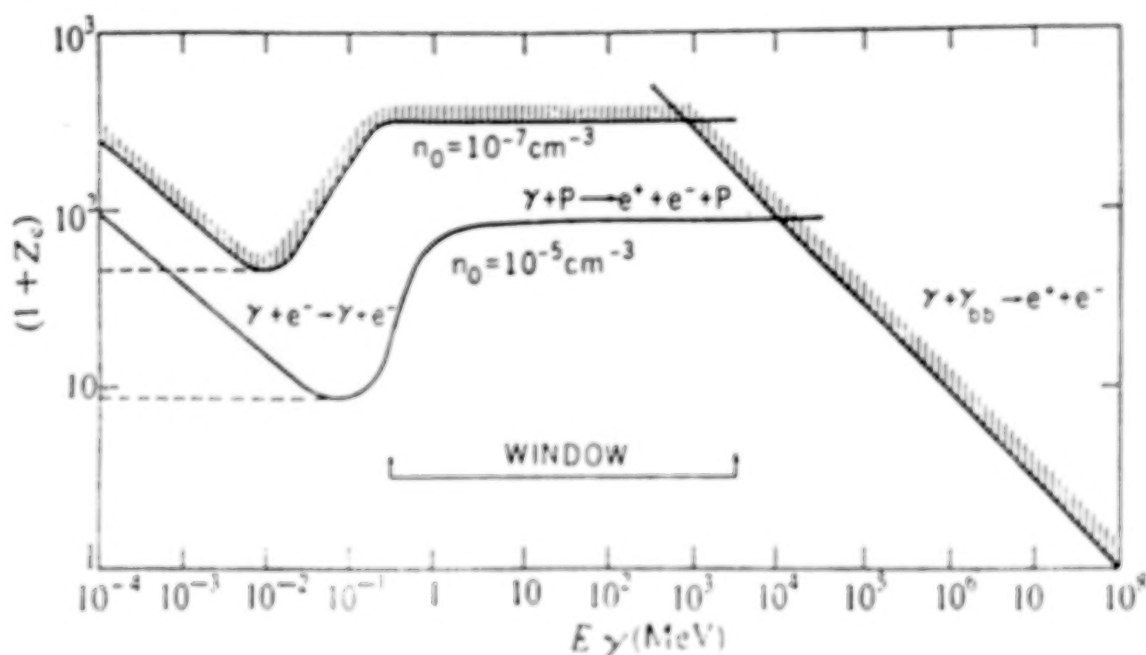


Figure 1.  Redshift at which the universe becomes opaque to photons as a function of observed energy. $n_o$ is the mean atomic density of the cosmic medium.

Another cosmological effect could be the detection of significant gamma ray flux from

$$\bar{p}p \to \pi^o + X$$
$$\hookrightarrow \gamma$$

This could establish a significant component of antimatter in the universe (see, for example, Stecker 1973).

The most pressing question is how to extract signals for the cosmological effect. It is essential that first a diffuse, extragalactic component of the gamma ray spectrum be established. This has only been done for the energy range of 1 MeV – 20 MeV, so far. The rapidly falling spectrum and the poor gamma ray telescopes used, so far, have combined to make this a very difficult problem. GRO and EGRET will be of great significance in this regard.

Once a diffuse extragalactic signal is established, the search for cosmological components can be started. there are two techniques proposed so far

i) Observation of structure in the energy spectrum that is related to the cosmological effect

ii) Study of the angular distribution fluctuations compared to observe the underlying source (D. Cline and Y.T. Gao, 1989).

At present the activity is one of modeling the various extra galactic processes and cosmological processes to see if the magnitude of the expected effects are comparable to the

observed properties of the gamma ray spectrum. We call these effects Gamma Ray Cosmology. A related issue is the required characteristics of telescopes (Energy and angular resolution and viewing area) that can be used to observe these cosmological effects.
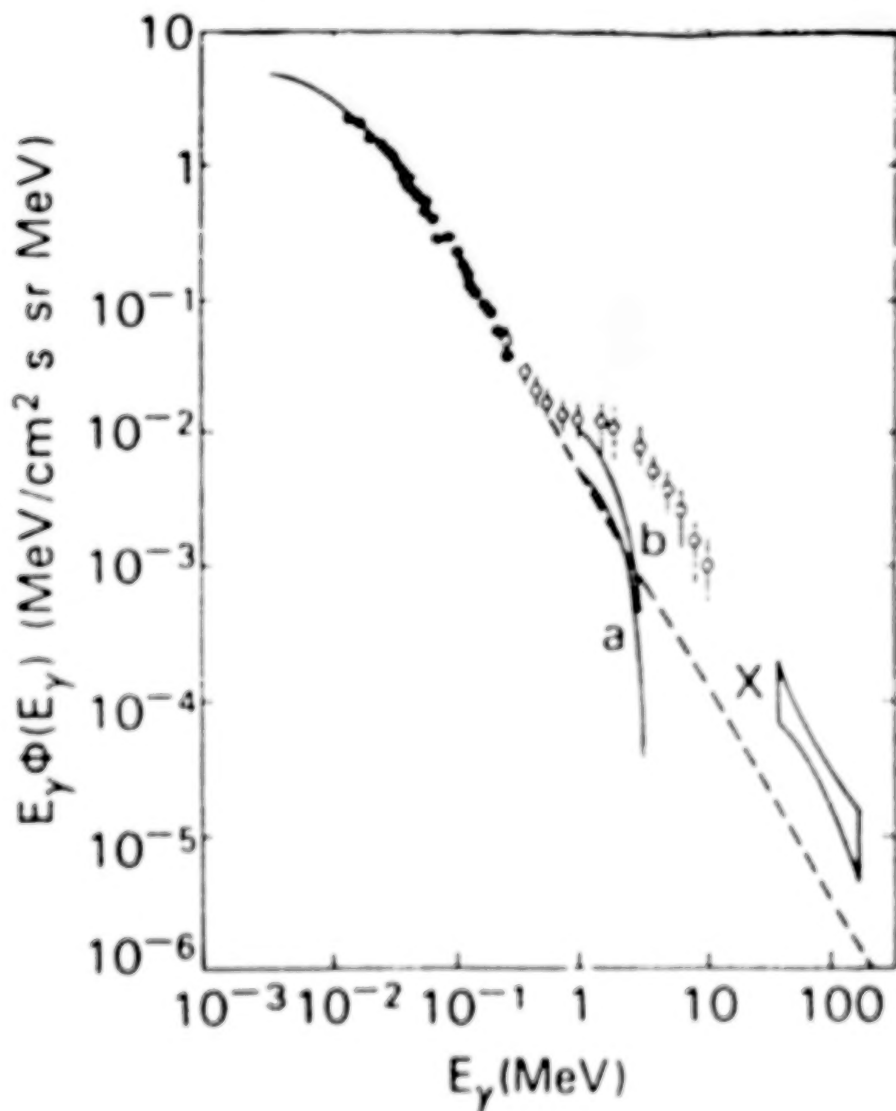


Figure 2. The Observed CGB energy spectrum together with the critical spectra from: a) Stecker (1988) and b) Olive and Silk (1985).

In this report we describe a program that has been initiated at UCLA to identify the possible signals of $\gamma$ Cosmology.

## II. FINE SCALE ANISOTROPY TO IDENTIFY THE UNDERLYING SOURCE

Y. T. Gao and I have been studying the type of angular fluctuation that could come from various models of the diffuse, extra galactic gamma radiation (D. Cline and Y.T. Gao, 1989 and Gao, Cline and Stecker, 1990).

There are currently two attractive theories predicting a diffuse background which are the active galactic nuclei (AGN) model and the baryon-symmetric big-bang (BSBB) model.
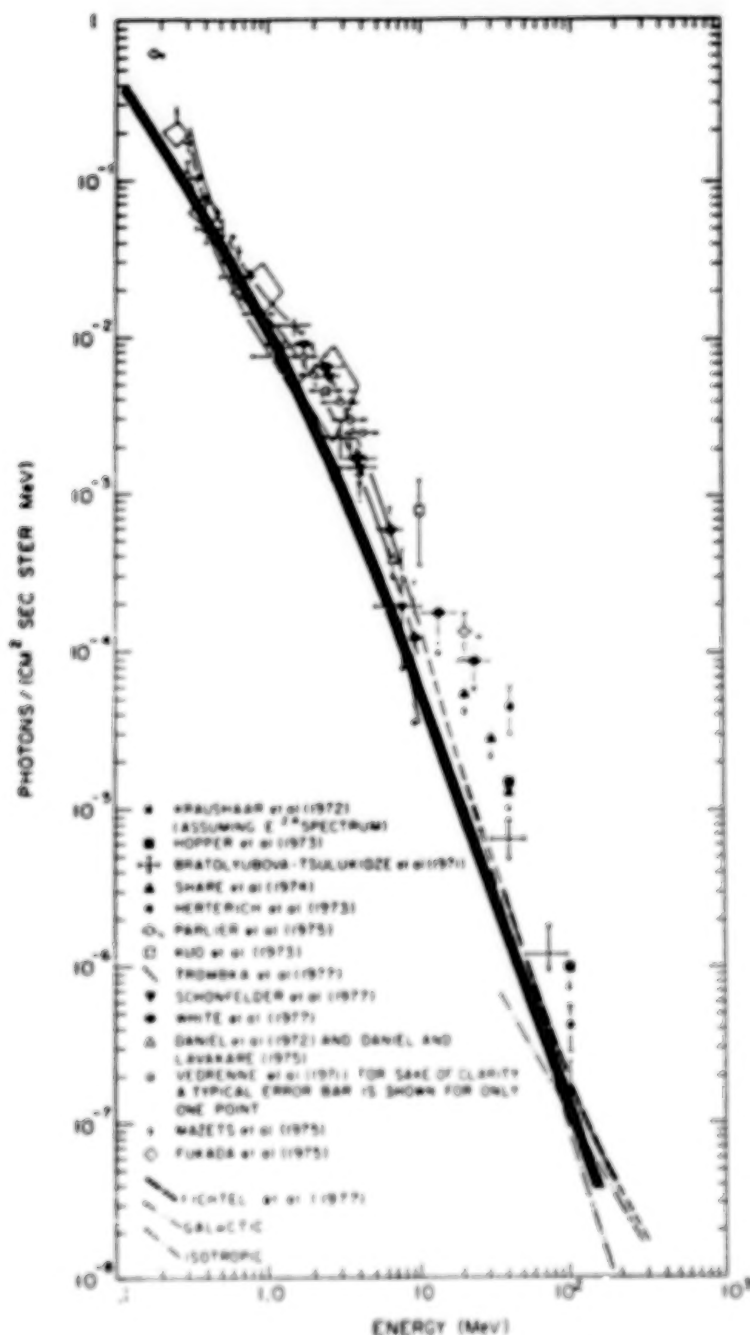
Figure 3. Energy spectrum of cosmic ray background (heavy line)
calculated by Cline and Gao (1989)[for reference to the data see
this paper as well].

We notice that the AGN and BSBB models give rise to different intensity fluctuation
patterns and we need to investigate how the new-generation high-resolution telescopes can
pinpoint the generation mechanisms.

Bignami, Fichtel, Hartman & Thompson (1979) have shown that both quasars and
Seyfert galaxies could make a large contribution to the diffuse flux but there is still a great
deal of uncertainty because of the very limited sample of active galaxies from which γ rays
have been detected and because of the possibility of the evolutionary effects in these
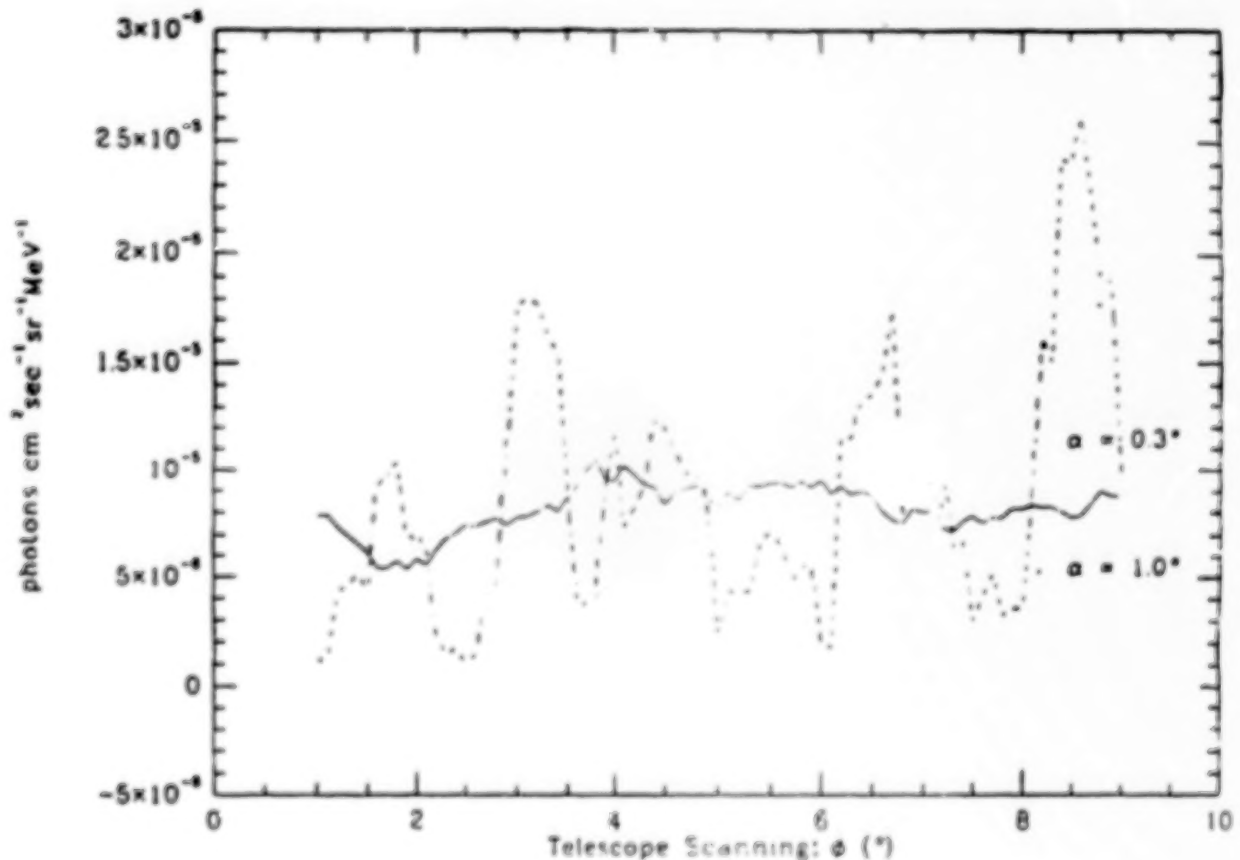
Figure 4.

galaxies at very large redshifts. Based on the pioneers' work, differential intensity of the background radiation is given as follows,

$$j(E_o, t_o) = \frac{dJ}{dE} = \frac{c}{4\pi H_o} \sum_i \int_{z_{min}}^{z_{max}} \frac{Q_i(E_o(1=z), z)n_i(z)}{(1+z)(1+2q_o z)^{1/2}} dz$$

$$\text{(photons } cm^{-2} sec^{-1} sr^{-1} KeV^{-1})$$

(1)

where $q_o$ is the cosmological deceleration parameter; $n_i(z)$ is the comoving density of galaxies of type $i$; $Q_i(E, z)$ is the average source strength or emissivity (photons per time interval and energy interval). That expression is valid for the standard universe in the matter dominated era and the absorption has been reasonably assumed negligible.

Assuming active galaxies (mainly quasars and Seyfert galaxies) dominated the $\gamma$ ray background, we perform the Monte Carlo simulation with the AGN model we predict, with the new generation $\gamma$ ray telescopes, the following effects might be observable:

1. As expected, the extragalactic $\gamma$ ray background is largely reproducible with the contribution from AGN's only. However, simulation can not reproduce the observed MeV bump very well (Figure 3). This poor reproduction quality of the bump strengthens the conjecture that there is more than one generation process involved, such as BSBB and/or the gravitino decay

2. Fig. 4 shows that the fractional deviation increases monotonically with the observed energy, as predicted. This is a cosmological effect and the reason is that there are

323

more AGNs at higher redshifts and the contributions from those far away AGNs are redshifted down to the lower energy regions. As Fichtel (private communication) points out, in high energy regions the background might be observed anisotropic with the GRO satellite, another new generation telescope which may go up in the next year or so.
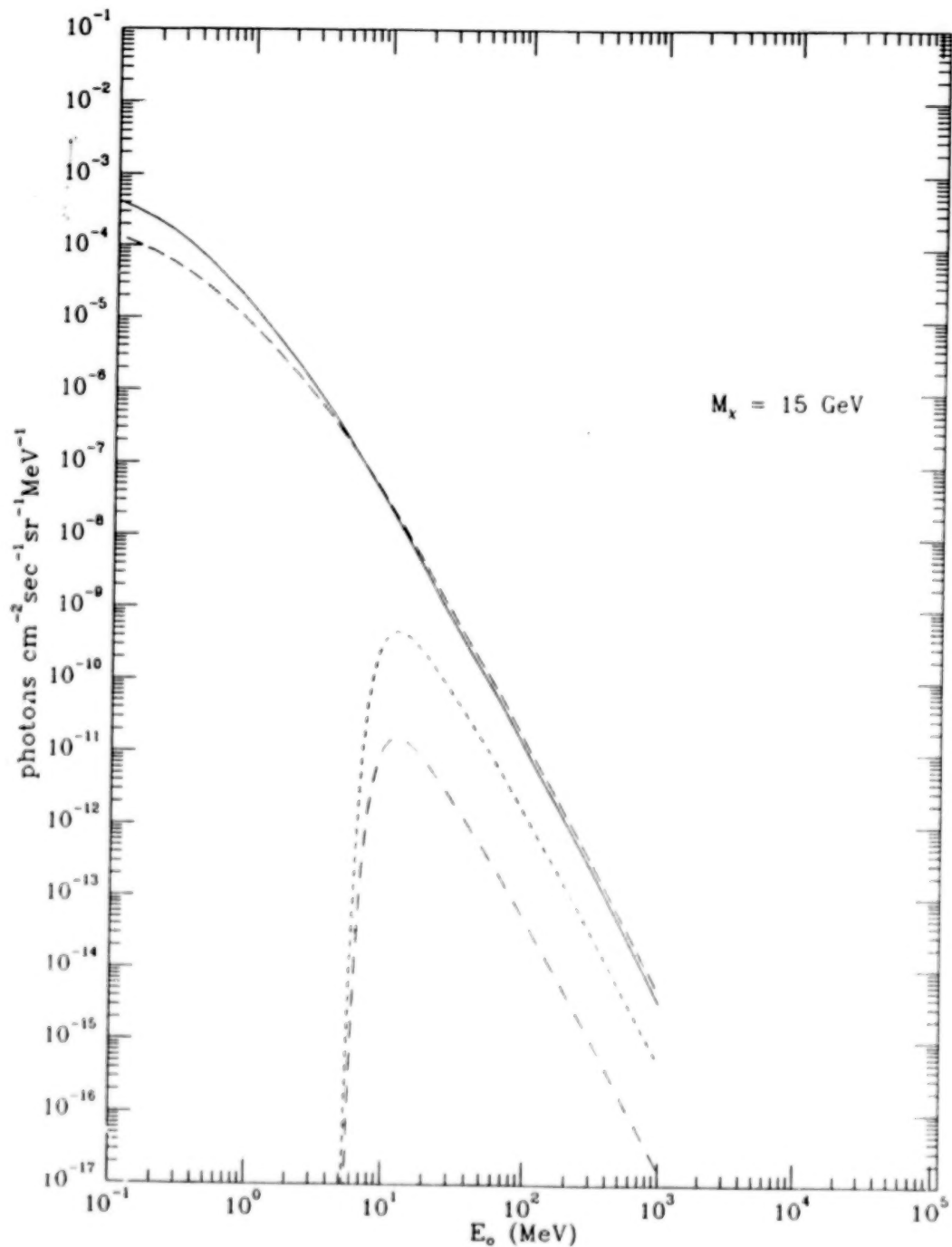


Figure 5.

## III. THE ANNIHILATION OF SUSY PARTICLES IN THE EARLY UNIVERSE

Part of the diffuse extragalactic spectrum could arise from the annihilation of exotic particles in the early universe. The remaining particles could form the Cold Dark Matter present in the Universe. We have carried out some simple calculation for photon lines and report some preliminary results here (see also, Stecker and Tylka 1989).

It would be of cosmological and particle physics importance if a characteristic feature of the low energy diffuse cosmic $\gamma$ ray spectrum could arise from the annihilation of supersymmetric particles in the early universe. for example, for the annihilation occurring at $z \sim 10^3$, the energy of the present photons would be redshifted down to

$$E_{\gamma,o} \sim (z+1)^{-1} E_\chi \sim \text{MeV} \tag{2}$$

provided that $E_\chi \sim$ GeV.

The essential feature of supersymmetric theories which makes them amenable to cosmological study is that, in many models, one of the superpartners are gauge fermions (gluinos, photinos, winos, etc.), Higgs fermions (higgsinos), scalar quarks and leptons (squarks and sleptons), and the gravitinos. In the very early universe, all these particles would be present in thermal equilibrium. As the temperature falls, the heavier ones decay into lighter ones. Eventually only the lightest supersymmetric particles (LSP) will be left. They can disappear only by pair annihilation.

By far the best candidates for the LSP are neutral gauge/Higgs fermions, which are in general mixed and the mass eigenstates "neutrolinos" contain both fermion and Higgs components. It is most probable that the LSP is either almost a pure higgsino $\tilde{H}$ or a pure photino $\tilde{\gamma}$.

We take $H_o = 65 \text{ kms}^{-1}\text{Mpc}^{-1}$, and use the simplification that $\chi$, our specified type of LSP, is formed with either pure photinos or pure higgsinos. We also assume that the universe is $\chi$-dominated, with $\Omega_{tot} = 1$. This assumption gives $\Omega_\chi \simeq 1$, implying that

$$n_\chi R^3 \simeq \text{const} \simeq n_{\chi,o} R_o^3 \quad \text{or} \quad n_\chi(z) \simeq \frac{\Omega_{\chi,o}\rho_{crit.,o}}{M_\chi}(1+z)^3 \tag{3}$$

where $n_\chi(z)$ is the cosmological number density of $\chi$. In fact, the pair annihilation should be efficient enough to reduce the present day number density of the LSP to an acceptable level. Our assumption is nothing but an ideal case. Detailed discussions about $n_\chi(z)$ are in the literature.

CDM, including $\tilde{\gamma}$ and $\tilde{H}$, are non-relativistic at decoupling, i.e., $E_\chi \simeq M_\chi c^2$. The annihilation cross section is approximated by

$$< \sigma V >_{ann} = a + b \cdot \frac{kT}{E_\chi} \tag{4}$$

where a and b are specific for particular models. Since $T \sim (1+z)$, we can, no loss of generality, consider two extreme cases, namely,

$$< \sigma V >_{ann} = < \sigma V >^o_{ann} \cdot (1+z)^J \tag{5}$$

325

where $J = 0, 1$. The annihilation cross section today $< \sigma V >^\circ_{ann}$ are taken as follows:

- $\chi\chi \to \gamma\gamma$:

$$- \chi = \tilde{\gamma} : \sim 8 \times 10^{-31} cm^3/sec \text{ for } M_{\tilde{\gamma}} = 5\,GeV \text{ and}$$
$$\sim 6 \times 10^{-30} cm^3/sec \text{ for } M_{\tilde{\gamma}} = 15\,GeV \text{ (Rudaz 1989)};$$
$$- \chi = \tilde{H} : \sim 2.5 \times 10^{-33} cm^3/sec \text{ for } M_{\tilde{H}} = 5\,GeV \text{ and}$$
$$\sim 2 \times 10^{-31} cm^3/sec \text{ for } M_{\tilde{H}} = 15\,GeV \text{ (Rudaz 1989)};$$

- $\chi\chi \to$ hadronic jets $\to \gamma$ rays:

$$- \chi = \tilde{\gamma} : \text{ The value } \sim 2.2 \times 10^{-27} cm^3/sec, \text{ the}$$
$$\text{maximum corresponding to the lower limit on the}$$
$$\text{squark mass } (\sim 80 \text{ GeV})$$

Figure 5 show the results of these calculations. The expected flux is far too small to be separated from the observed diffuse spectrum.

## IV. ANGULAR EFFECTS DUE TO A BARYON-ANTIBARYON SYMMETRIC COSMOLOGY

We have been carrying out calculations of the expected angular fluctuations in the diffuse gamma spectrum due to $\bar{B}B$ annihilation. Preliminary results (reported to the meeting) show that measurable and quite specific patterns of fluctuations may appear. This work is still in progress and will be reported elsewhere.

## V. DETECTOR RESOLUTION AND VIEWING AREA REQUIRED TO DETECT THE UNDERLYING PROCESS

We held a workshop at UCLA in 1988 to determine the processes in the development of high resolution gamma ray telescopes (D. Cline and E. Fenyves, 1989). We believe that angular resolution on the milliradiation level and energy resolution of the less than 1% level are possible to achieve with new telescopes provided a strong R & D program is undertaken. Recently the UCLA/UT-D group has developed a scintillating fiber prototype that gives several m-rad resolution in the MeV energy range.

In order to detect the effects described here the viewing areas of the telescope need to be in the $m^2$ range and the time duration of years is likely required.

## VI. SUMMARY

We have described work in progress at UCLA to estimate the magnitude of possible cosmological effects in the diffuse gamma ray spectrum and experimental techniques to observe these effects. The EGRET / GRO observations will be a key ingredient in the understanding of this possibility, hopefully leading to another generation of $\gamma$ ray telescopes that are optimized for the search.

# VII. ACKNOWLEDGEMENTS

## REFERENCES

[1]   Bignami,G., Fichtel,C., Hartman,R. and Thompson,D. 1979, Aps.J. 232, 649.

[2]   Cline,D., Gao,Y.T. 1989, Ap.J. 348, in press.

[3]   Cline,D., Gao,Y.T. 1990, Work in progress on the Effects of the Decay of Massive 4th Family Neutrinos in the Early Universe.

[3]   Cline,D., Fenyves,E. 1989, in Proceedings of the Workshop on High Resolution Gamma Ray Cosmology, Nucl.Phys.B Supl, edited by Cline,D. and Fenyves,E.

[4]   Gao,Y.T., Cline,D., Stecker,F. 1990, The Cosmological Evolution Models of Active Galaxies and the Extra Galactic γ Ray Background, UCLA preprint #APH0026-UCLA-1/90 and submitted to Ap.J.Letts.

[5]   Rudaz,S. 1989, preprint UMN-TH-716/89.

[6]   Sperge,C. 1989, in Proceedings of the Workshop on High Resolution Gamma Ray Cosmology, Nucl.Phys.B Supl, edited by Cline,D. and Fenyves,E.

[7]   Stecker,F. 1973, Nature, Vol. 241, pp.74-77.

[8]   Stecher,F., Tylka,J. 1989, Ap.J. 343, 169.

## DISCUSSION

*R.J. Slobdrian:*

In this picture of baryon-antibaryon symmetry by what mechanism would one arrive at separated regions of baryonic and antibaryonic matter?

*Floyd Stecker:*

Such a universe could arise from a grand unified theory with spontaneous CP symmetry breaking. (see Stecker, F.W., 1985, Nucl. Phys. B252, 25, and references therein.)

# DIPOLE ANALYSIS ON EGRET DATA OF EXTRAGALACTIC GAMMA RAY BACKGROUND RADIATION

YING-CHI LIN

High Energy Physics Laboratory, Stanford University, Stanford, CA 94305

## I. INTRODUCTION

A dipole analysis on the EGRET data seems to be one of the numerous subjects that we can investigate for the extragalactic gamma ray background radiation. By the end of the first one and half years after launch, the all-sky survey program of GRO will be completed. The EGRET detector will cover the full sky area fairly well by that time. We will then have at our disposal a set of gamma ray data suitable for dipole moment calculations. Furthermore, there now exist in the literature several dipole anisotropy results calculated for optical and infrared observations on the distribution of galaxies in the full sky. We can compare the results of dipole moment analysis from gamma ray observations with those at other wavebands, and hopefully we can gain some deeper understanding on the large scale structure of the Universe in the end.

## II. CALCULATION OF DIPOLE MOMENT FOR EGRET DATA

The dipole moment of the gamma ray data from EGRET observations can be defined, in principle at least, in a straightforward way. For a sample of $N$ gamma ray events distributed over the full sky, let $\hat{r}_i$ be a unit vector in the inverse direction of arrival of the $i^{th}$ gamma ray, i.e., $\hat{r}_i$ is pointing at the source of the incoming photon. Then the dipole moment of the distribution of the $N$ events can be defined as

$$\mathbf{D} = \frac{\sum_{i=1}^{N} \omega_i \hat{r}_i}{\sum_{i=1}^{N} \omega_i}, \tag{1}$$

where $\omega_i$ is a weighting factor for the $i^{th}$ event, to normalize observations under different instrumental conditions, and to deal with uneven coverage of different parts of the sky. A nonzero value of $\mathbf{D}$ represents the direction and the magnitude of the dipole anisotropy of the $N$ gamma ray events. On the other hand, a value of $\mathbf{D}$ consistent with zero means the gamma ray events are isotropic within the experimental errors.

In practice, however, obtaining a meaningful value for the dipole moment in a sample of EGRET observations may not be very simple. The variations of the instrumental conditions can probably be handled with fair amount of confidence. The EGRET detector has been studied in all aspects at great length over the years. We believe we can treat things like the variation of EGRET detection efficiency over long periods of observation quite well. Likewise the treatment of uneven coverage of the sky at different detector orientations and different observation times can be handled in a routine manner, although the rpocedure can be quite time-comsuming. What constitutes the most serious obstacle in the way of

obtaining a meaningful value for **D** according to *Eq.*(1) is probably the contamination of the galactic component in the full set of the diffuse background radiation data. From SAS-2 observations (Fictel, Simpson and Thompson 1978; Thompson and Fichtel 1982), which provide the only existing information on the extragalactic diffuse background radiation at energies comparable to the dynamic range of EGRET, we can see that at low galactic latitudes, the galactic component completely dominates the observations. Even at high galactic latitudes, the diffuse background is still heavily tinted with the galactic component. In fact the galactic component extends all the way to the galactic poles. Then to what extent can we expect to see the global effect of the extragalactic component alone is not immediately clear. For this we will no doubt need extensive studies on different aspects of these two components once we have the actual data.

In addition to the galactic part of the diffuse radiation, the EGRET detector itself will also generate a gamma ray background once in orbit. The cosmic ray protons may interact with EGRET window material at a grazing angle such that the protons will not intercept the anticoincidence scintillator dome to set off a trigger veto. The produced gamma rays will then be accepted by EGRET as valid incident photons. But preliminary studies on the results of the proton beam calibration at Brookhaven National Laboratory indicate that this locally generated gamma ray background will be very small. This background component will be isotropic on the average anyway, and will not contribute significantly to the value of **D** as calculated according to *Eq.*(1). But still we should keep in mind this possible source of uncertainty in **D**. Furthermore, the known celestial gamma ray sources in the field of view of EGRET detector should be subtracted from the full data set.

We can make an order of magnitude estimate for **D** in this way. The GRO all-sky survey program calls for about 30 detector orientations, each with an observation time of two weeks. Ten of these sightings will be centered around the galactic plane, and thus will not be useful for extraglactic diffuse background studies. The other 20 or so sightings will have a combined total observation time of 40 weeks. Let us use a duty factor of 0.5, meaning that the EGRET detector will be actively taking data in about half of this time. From SAS-2 observations (Fichtel, Simpson and Thompson 1978), the extragalactic diffuse background radiation has been found to be $\sim 5 \times 10^{-5} cm^{-2} sr^{-1} s^{-1}$ for gamma ray energies greater than 35 $MeV$. If we take the average combined EGRET effective area and solid angle to be $\sim 500\ cm^2 sr$ above 35 $MeV$, then in 40 seeks we should be able to collect

$$5 \times 10^{-5} \times 500 \times 40 \times 7 \times 86400 \times 0.5 \approx 3 \times 10^5$$

extragalactic diffuse background gamma rays. If we also demand good energy measurement, this number will probably be cut in half. In any case, based on statistical uncertainties alone, if the dipole anisotropy has the magnitude of $>\sim 1.0\%$, we should be able to see it. If we can find a robust value for **D**, we can go one step further. We can try to determine the energy dispersion in it, or maybe some other properties too that we can conceive.

## III. DIPOLE ANISOTROPIES AT OPTICAL AND INFRARED FREQUENCIES

Ever since the all-sky galaxy surveys became available in optical and in infrared ob-

servations, efforts have been made to determine the dipole anisotropy in the distribution of galaxies in the full sky (Yahil, Sandage and Tamman 1980; Davis and Huchra 1982; Yahil, Walker and Rowan-Robinson 1986; Meiksin and Davis 1986; Villumsen and Strauss 1987; Lahav 1987; Harmon, Lahav and Meurs 1987; Rowan-Robinson 1988; Lahav, Rowan-Robinson and Lynden-Bell 1988; Kaiser and Lahav 1989). This dipole anisotropy is then compared with the dipole moment of the cosmic microwave background radiation (MBR). Based on the proximity of these two dipole directions, a case can be made that the surface brightness dipole moment is a measure of the peculiar acceleration of the Local Group. Then a linear theory, as the one developed by P. J. E. Peebles (Peebles 1980) which tie the peculiar velocity, the peculiar acceleration and the cosmological density parameter together, can be used to determine the cosmological density parameter with a proper choice of the peculiar velocity. In the paper by Kaiser and Lahav (Kaiser and Lahav 1989), the dipole anisotropy in the distribution of galaxies is also interpreted as a manifestation of some Gaussian isentropic density fluctuations at some very early time in the cold dark matter model, a viewpoint not shared by the authors of the other dipole moment papers.

## TABLE I
### DIPOLE ANISOTROPIES IN OPTICAL AND INFRARED SURVEYS

| Authors | Survey Catalog | Dipole Anisotropy Direction (deg) | | Angle with MBR Dipole (deg) | $\Omega_0$ |
|---|---|---|---|---|---|
| | | l | b | | |
| Yahil, Sandage and Tammann 1980 | RSA | Centered on Virgo cluster | | | $\ll 0.5$ |
| Davis and Huchra 1982 | CfA | Toward Virgo cluster | | | $0.4 - 0.5$ |
| Yahil, Walker and Rowan-Robinson 1986 | IRAS | $248 \pm 9$ | $40 \pm 8$ | $26 \pm 10$ | $0.85 \pm 0.16$ |
| Meiksin and Davis 1986 | IRAS | 235 | 45 | $< 30$ | $\approx 0.5$ |
| Villumsen and Strauss 1987 | IRAS | 239 | 36 | 28 | $1.2 \pm 0.36$ |
| Lahav 1987 | UGC,ESO | $227 \pm 23$ | $42 \pm 8$ | $\approx 37$ | $\approx 0.3$ |
| Harmon, Lahav and Meurs 1987 | IRAS | 274.6 | 31.3 | 7.2 | —— |
| Rowan-Robinson 1988 | IRAS | $248.2 \pm 9.6$ | $39.5 \pm 9.5$ | 20.7 | $\approx 1$ |
| Lahav, Rowan-Robinson and Lynden-Bell 1988 | UGC,ESO | 261 | 29 | $< 7$ | $0.16 \pm 0.07$ |
| | IRAS | 250 | 38 | —— | |
| Kaiser and Lahav 1989 | UGC,ESO | 261 | 27 | —— | 0.3 |
| | IRAS | 259 | 34 | —— | 0.5 |

In Table 1, we summarize the typical results of these investigations. The directions of these calculated dipole moments all agree quite well with each other and with the cosmic microwave background radiation. But the magnitudes of these dipole moments can be

quite different in different papers, although most of them are in the $10-20\%$ range. Then, compounded with different choices of value for the peculiar velocity of the Local Group, the inferred cosmological density parameter $\Omega_0$ exhibits a wide range of variation. It is difficult to see what one can make out of these $\Omega_0$ values.

## IV. DISCUSSIONS

At present the most promising explanation for the origin of the extragalactic gamma ray background radiation is the idea that these gamma rays are produced by active galaxies too far away or too weak to be resolved by the detecting instrument (Bignami, Fichtel, Hartman and Thompson 1979). Although there is only one active galaxy, the qusar 3C273, that has been identified with the only gamma ray source at high galactic latitude in the COS-B catalog, this situation will certainly change with the launch of GRO. We expect to see several more active galaxies as point gamma ray sources with the EGRET detector. Then the question as how the active galaxies combine to produce the extragalactic gamma ray background radiation will become more clear. Suppose that the idea of active galaxies as origin of extragalactic diffuse background radiation will be further strengthened under EGRET observation, which we have good reasons to believe will be the case. Then the study of the extragalactic gamma ray background radiation will be a study of the large scale distribution of active galaxies. We will then certainly take a critical look at the dipole anisotropy results in optical and infrared observations and compare with the gamma ray results. Hopefully we will gain some deeper understanding on the large scale structure of the Universe at that time.

## REFERENCES

Bignami, G. F., Fichtel, C. E., Hartman, R. C., and Thompson, D. J. 1979, *Ap.J.*, **232**, 649.

Davis, M., and Huchra, J. 1982, *Ap.J.*, **254**, 437.

Fichtel, C. E., Simpson, G. A., and Thompson, D. J. 1978, *Ap.J.*, **222**, 883.

Harmon, R. T., and Lahav, O. 1987, *M.N.R.A.S.*, **228**, 5p.

Kaiser, N., and Lahav, O. 1989, *M.N.R.A.S.*, **237**, 129.

Lahav, O. 1987, *M.N.R.A.S.*, **225**, 213.

Lahav, O., Rowan-Robinson, M., and Lynden-Bell, D. 1988, *M.N.R.A.S.*, **234**, 667.

Meiksin, A., and Davis, M. 1986, *A.J.*, **91**, 191.

Peebles, P. J. E. 1980, *The Large Scale Structure of the Universe*, Princeton University Press, Princeton.

Rowan-Robinson, M. 1988, In: *Comets to Cosmology: 3rd IRAS Conference*, ed. Lawrence, A., Springer-Verlag.

Thompson, D. J., and Fichtel, C. E. 1982, *Astron.Astrophys.* **109**, 352.

Villumsen, J. V., and Strauss, M. A. 1987, *Ap.J.*, **322**, 37.

Yahil, A., Sandage, A., and Tammann, G. A. 1980, *Ap.J.*, **242**, 118.

Yahil, A., Walker, D., and Rowan-Robinson, M. 1986, *Ap.J.(Letters)*, **301**, L1.

# FEASIBILITY FOR EGRET DETECTION

## OF ANTIMATTER CONCENTRATIONS IN THE UNIVERSE

R. C. Hartman
NASA/Goddard Space Flight Center
Greenbelt, MD 20771

## INTRODUCTION

Although the Grand Unified Theories of elementary particle dynamics have to some extent reduced the aesthetic attraction of matter-antimatter symmetry in the Universe, the idea is still not ruled out. Although first introduced by Alfven(1965), most of the theoretical development related to gamma-ray astronomy has been carried out by Stecker, who has proposed (Stecker, Morgan and Bredekamp, 1971) matter-antimatter annihilation extending back to large redshifts as a possible explanation of the apparently extragalactic diffuse gamma radiation. Other candidate explanations have also been proposed, such as superposition of extragalactic discrete sources.

Clearly, the existence of significant amounts of antimatter in the universe would be of great cosmological importance; its detection, however, is not simple. Since the photon is its own antiparticle, it carries no signature identifying whether it originated in a matter or an antimatter process; even aggregates of photons (spectra) are expected to be identical from matter and antimatter processes. The only likely indicator of the presence of concentrations of antimatter is evidence of its annihilation with normal matter, assuming there is some region of contact or overlap.

The EGRET telescope on the Gamma Ray Observatory, with a substantial increase in sensitivity compared with earlier high energy gamma-ray telescopes, may be able to address this issue. This paper is a preliminary consideration of the feasibility of using EGRET in such a search for antimatter annihilation in the Universe.

## ANNIHILATION PROCESSES AND THEIR DETECTION

Two processes are available for study; annihilation between electrons and positrons, with an energy release of about 1 MeV per pair, and annihilation between nucleons and antinucleons, with an energy release of nearly 2 GeV per nucleon/antinucleon pair. Although the electron-positron annihilation should produce the well-known 511 keV line, there are observational problems which reduce the likelihood of success in its use for cosmological observations. First, the half-MeV line forms its own unavoidable background in any instrument which can observe

it. In addition, positron annihilation is likely to be present in a wide range of astrophysical settings, including stellar flares, supernovae ejecta and active galactic nuclei, even if antimatter does not form a significant portion of the Universe.

Nucleon/antinucleon annihilation is more complicated than that of electrons and positrons. Even annihilation of a nucleon-antinucleon pair at rest produces several particles; most of these are pions, including both charged and neutral. The only significant production of photons in this process is via the decay of the neutral pions. Although the $\pi^\circ$ decay is two-body, the decaying pions have energies comparable to their rest mass, so the photon line is smeared out into a broad hump peaked at 68 MeV, as shown in Figure 1.

Gamma-ray detectors in this energy range are largely free of internal background, so it is necessary to contend only with astronomical sources of background, which are discussed later.
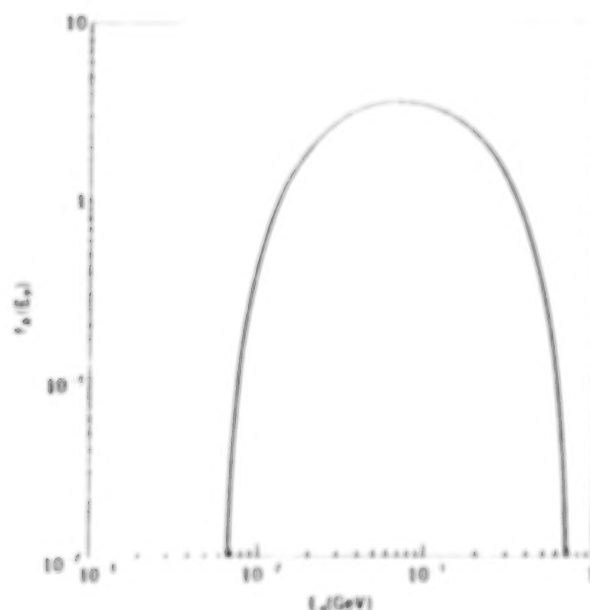


Figure 1 - The normalized gamma-ray spectrum from proton-antiproton annihilation.

## WHERE COULD ANTIMATTER BE CONCENTRATED?

There is strong evidence that no significant amount of antimatter exists within our own galaxy, nor anywhere within the Local Group of galaxies. Such a concentration would be clearly visible in high energy gamma radiation, but has not been identified by the SAS-2 or COS-B instruments. Bel and Martin (1975) have shown that it is not possible for individual

galaxies to be randomly divided into matter galaxies and antimatter galaxies, since the annihilation radiation resulting from galaxy collisions throughout the universe would produce a gamma-ray background two to three orders of magnitude greater than that seen by SAS-2. Similarly, Harwitt (1989) has shown that the IRAS ultraluminous galaxies cannot all be due to collisions between matter and antimatter galaxies. Thus we are forced to consider structures as large as galaxy clusters or even superclusters as possible domains of matter and antimatter. It is assumed here that such domains must be separated by voids in the distribution of luminous matter; this seems reasonable, since the energy released in annihilation at the domain boundaries should be quite adequate to prevent the formation of matter condensations.

Figure 2 (on the last page of these proceedings) shows the northern sky distribution of galaxy clusters, sorted into superclusters, out to a redshift z of 0.1. The definition of a supercluster is rather loose; the groupings depend upon somewhat arbitrary assumptions regarding the minimum physical separation assumed between associated clusters. The 48 superclusters shown in Figure 2 were identified recently by West (1989) using a minimum distance between associated clusters of 25 Mpc. About half of the superclusters shown contain from 3 to 13 galaxy clusters; the other half each contain only a pair of clusters. Some of these pairs are quite closely spaced and almost certainly associated, but others would not be linked were a slightly smaller distance requirement used. In the sample used by West, which includes all 286 clusters in the northern Abell catalog for which redshifts of less than 0.1 have been measured, only about 65% of the galaxy clusters were found to lie within superclusters according to his criteria. Other authors (e.g. Bahcall and Soneira, 1986) have used different selection criteria, with correspondingly different (but not inconsistent) results.

Figure 3 (on the last page of these proceedings) shows the resulting sky distribution if the non-associated clusters are included. The added 99 clusters are not within 25 Mpc of any other cluster in the sample. Note that many of the apparently empty regions seen in Figure 2 are now filled in.

Figures 2 and 3 do not give any information about the distances of the clusters; Figure 4 (last page of these proceedings) shows the same clusters, separated into three equal redshift-intervals, to indicate crudely the distance to each cluster. As would be expected, there are few superclusters in the closest distance interval, and those have very substantial angular size (up to 25 degrees).

It is important to note that, even when all of the clusters are considered, there are regions of the sky which appear empty. These might be considered as potential boundaries between matter/antimatter domains, and therefore as possible sites of

annihilation. However, several cautions must be stated in this connection. First, redshift measurements are not available for all galaxy clusters out to z=0.1, so there may actually be clusters in some of the regions which appear empty here. Second, and probably more important for the topic studied here, the fraction of luminous mass in the Universe which falls within clusters has been estimated by various authors (e.g., Bahcall and Soneira, 1984) to be within the range 10-25%. The remainder is in the isolated galaxies referred to as field galaxies. Thus the absence of clusters and superclusters in a region does not necessarily imply the absence of all luminous matter.

Another very striking way of looking at the large-scale distribution of matter in the Universe is that of Kirshner et al.(1981) and deLapparent et al.(1986). Figure 5(a) hows the positions of all galaxies brighter than $m_B$ = 15.5 out to a redshift of about 0.05, for a 6 degree slice in declination, 9 hours wide in right ascension. The important feature here is obvious: much of the area of the plot is essentially empty of observable galaxies. Included in this diagram is the Coma cluster, which turns out to be merely the densest portion of a network of apparent filaments. Examination of the three-dimensional structure near this slice indicates that, rather than a true filamentary connection, the galaxy distribution forms a series of nearly empty bubbles. Note that in Figure 5 there is no obvious separation of the galaxy shells into structures which might be matter and antimatter. However, this slice covers only a small fraction of the sphere extending out to z=0.1.

## HOW MUCH ANNIHILATION RADIATION SHOULD THERE BE?

We examine an idealized geometry, shown in Figure 6, with semi-infinite regions of matter and antimatter separated by an overlap region in which annihilation occurs. As an illustration, several parameters are defined with minimal justification.

For gas density, a value of $4 \times 10^{-8}$ $cm^{-3}$ (pure hydrogen or antihydrogen) is used; this is only about 1% of the closure density for $H_0$ = 60 km s$^{-1}$ Mpc$^{-1}$. In the boundary layer, this density is equally divided between matter and antimatter.

There is no clear guideline to a choice of temperature; it is a crucial parameter, however, because the annihilation rate is temperature dependent. In particular, Stecker (1971) has shown that, at a temperature of a few thousand degrees (where hydrogen becomes largely ionized), the annihilation rate drops precipitously, by about three orders of magnitude. Initially, a temperature of $10^5$ degrees is utilized here, but the effect of other choices will be examined later.
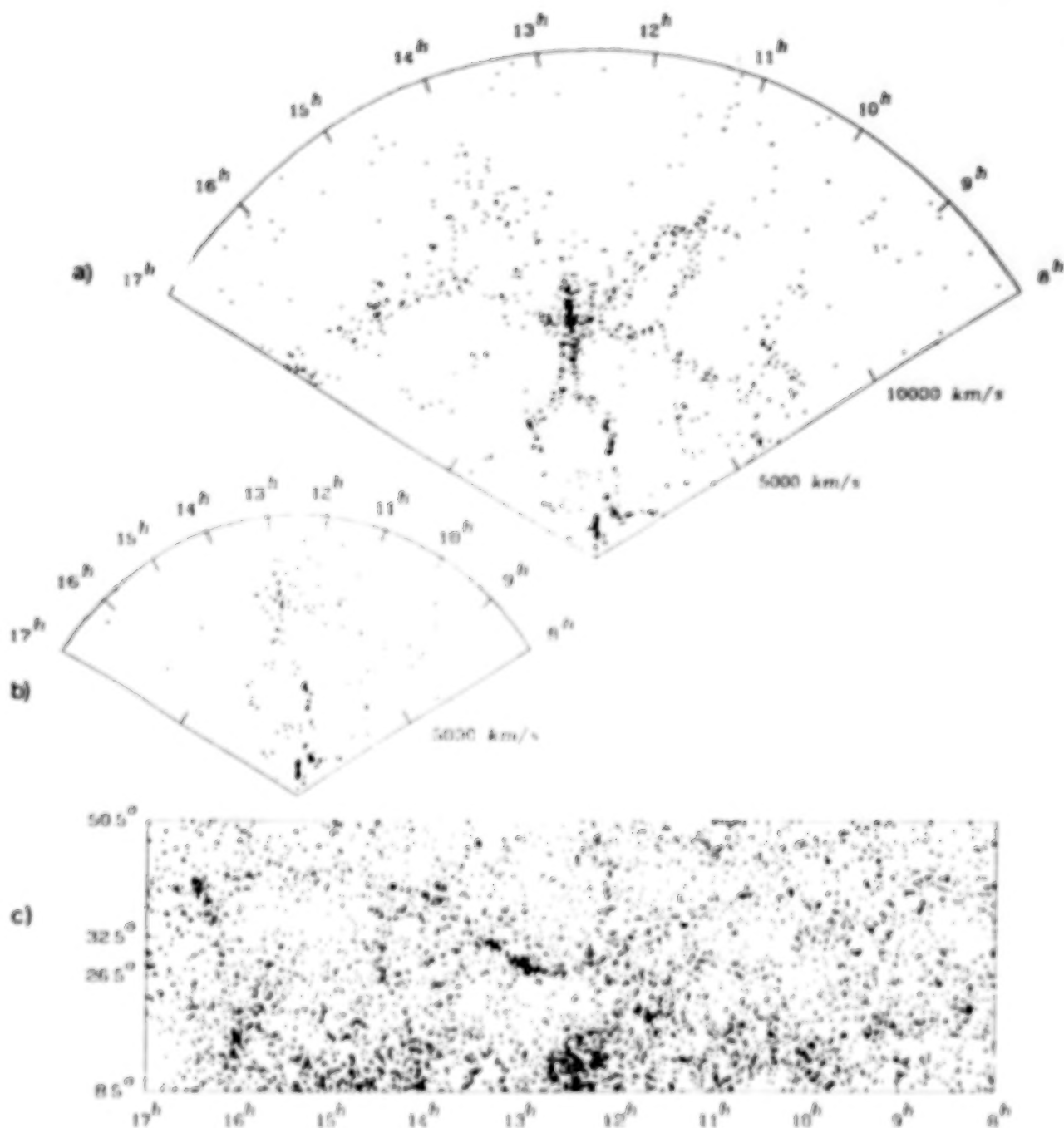
Figure 5 (from de Lapparent et al., 1986) - (a) Map of observed velocity plotted vs. right ascension in the declination wedge 26.5°-32.5°, for 1061 objects with $m_B \leq 15.5$ and velocity $\leq 15,000$ km s$^{-1}$. (b) same as (a), but for 182 galaxies with $m_B \leq 14.5$ and velocity $\leq 10,000$ km s$^{-1}$. (c) Projected map of 7031 objects with $m_B \leq 15.5$.

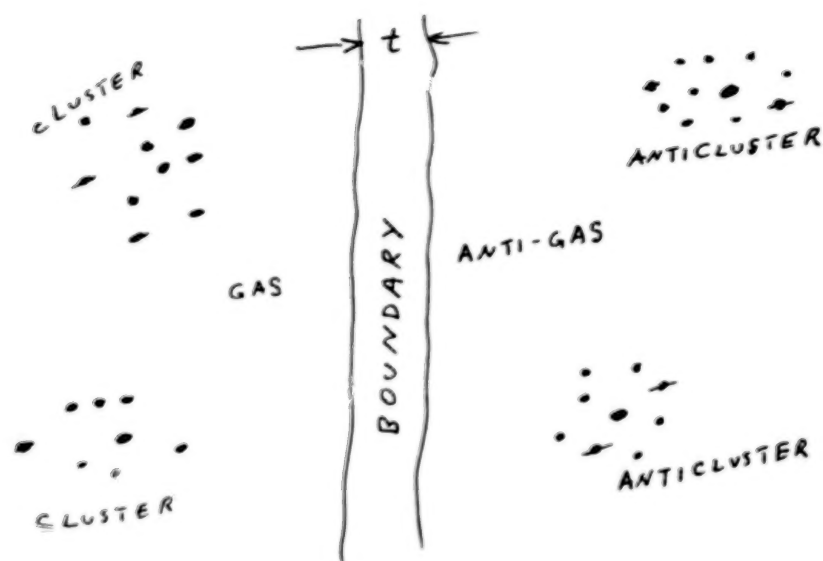Figure 6 - Idealization of the boundary between a matter domain and an antimatter domain.

If the matter and antimatter are permitted to intermix freely at the boundary, its thickness t depends upon the mean free path for annihilation, which is given by (Stecker and Puget, 1972) $t = 2.8/(n\sigma)$. Using the parameters mentioned above, this leads to a boundary layer thickness of 450 Mpc, which is more than an order of magnitude greater than the typical distance between superclusters. Reducing the temperature to $10^4$ K and increasing the gas density by an order of magnitude (about the maximum allowable) reduces the boundary layer thickness to 3 Mpc, which seems reasonable.

The annihilation gamma-ray intensity is given by:

$$I = \frac{1}{4\pi} \int n_p \, n_{ap} \, \langle v\sigma \rangle \, dl$$

$$= 10^{-14} \, n_p \, n_{ap} \, L \, T_6^{-0.5} \, cm^{-2} \, s^{-1} \, sr^{-1} \qquad (1)$$

where $n_p$ and $n_{ap}$ are the number densities of the two components, $T_6$ is the temperature in millions of degrees, and L is the line of sight distance through the boundary layer. $\langle v\sigma \rangle$ is the annihilation gamma-ray production rate for unit densities and for the specific temperature selected, derived from Stecker(1971), which scales with temperature as $T^{-0.5}$ over the range $10^4$ K to $10^{11}$ K.

Inserting into Equation 1 the temperatures and densities discussed above leads to gamma-ray intensities of 0.02 to $0.07/(cm^2 \, s \, sr)$. Emission this bright would have been easily visible in the SAS-2 and COS-B instruments, but was not seen;

this forces us to conclude that, if antimatter does exist within domains in the universe, matter and antimatter cannot be freely mixing at the domain boundaries.

One possibility for inhibiting the mixing would be turbulent pressure stimulated by the annihilation itself. In addition to the neutral pions produced in nucleon-antinucleon annihilation, charged pions are also produced. These decay quickly, resulting in relativistic electrons and positrons in addition to neutrinos. The electrons and positrons streaming away from the boundary may, in the presence of a magnetic field, be able to generate sufficient turbulent pressure to inhibit the flow of gas toward the interface, leading to substantially lower gas densities in the annihilation region. A complex computation would be required to determine how effective such a process might be.

A rough estimate of what density is permitted by the observations can be made by assuming that an intensity of $10^{-4}$ $cm^{-2}$ $s^{-1}$ $sr^{-1}$ (> 100 MeV) would have been detectable by SAS-2 away from the galactic plane. For a temperature of $10^6$ K and a boundary layer thickness of 1 Mpc, a density of about $6 \times 10^{-8}$ $cm^{-3}$ (equally divided between matter and antimatter) would be permitted. If $10^4$ K and 10 Mpc are chosen instead, the density in the boundary region can be only about $6 \times 10^{-9}$ $cm^{-3}$.

OBSERVING EXTRAGALACTIC DIFFUSE HIGH ENERGY GAMMA RAYS

The first problem in making detailed observations of extragalactic gamma radiation is development of an accurate model of the high-latitude emission from our own galaxy. This emission arises from interactions between galactic cosmic rays, both electrons and nuclei, and several components of the interstellar medium. Some of these components, such as atomic hydrogen, are reasonably well defined. Densities of cosmic ray electrons and nuclei, however, are known with confidence only in the solar neighborhood. Gamma-ray observations from SAS-2 and COS-B have shown that there are cosmic rays throughout the Galaxy; however, the details of their distribution in the Galaxy are not well determined.

As in other wavelength bands, extragalactic gamma-ray observations must be made through one to several half-thicknesses of the disk of the Galaxy. Indeed, the SAS-2 discovery of the apparently extragalactic gamma radiation around 100 MeV was made by comparing gamma-ray fluxes at high galactic latitudes with line-of-sight integrals of various components of the interstellar medium. As illustrated in Figure 7, the extragalactic gamma-ray component is the flux obtained by extrapolating to zero the line-of-sight integral of another component. Even at high galactic latitudes, the galactic contribution to the observed gamma-ray intensity is in general quite substantial.
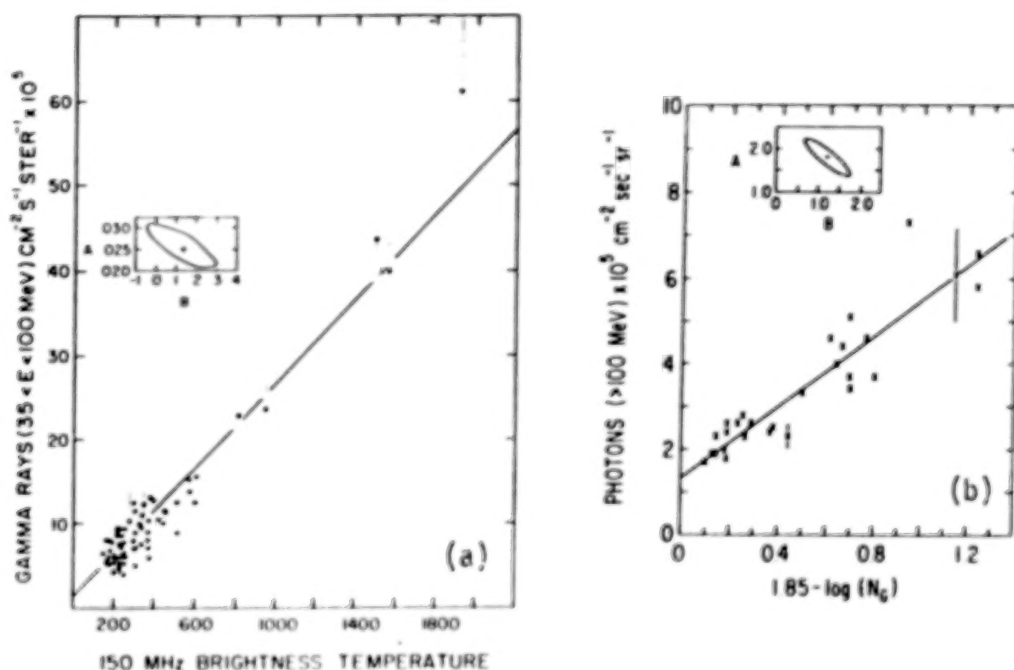
Figure 7 - (a) (from Fichtel, Simpson and Thompson 1978) Gamma-ray intensity (35 - 100 MeV) vs. 150 MHz brightness temperature. (b) (from Thompson and Fichtel 1982) Gamma-ray intensity (E>100 MeV) vs. the function 1.85-log(galaxy counts per square degree) for galactic latitudes |b|>10°.

In the SAS-2 discovery of the extragalactic high energy gamma radiation, the relatively poor statistical weight of the gamma-ray observations was a severe limitation. The EGRET telescope, with a factor of 15 better sensitivity and in principal a much longer lifetime for such observations, should greatly reduce those statistical limitations. Furthermore, complete high-latitude observations of atomic hydrogen are now available (Heiles and Habing 1974; Colomb, Poppel and Heiles 1980), and observations of CO, the tracer for molecular hydrogen, are underway at high galactic latitudes (Stacy 1989). It seems likely that, unless the cosmic ray distribution at high latitudes is more "clumpy" than expected, a relatively accurate subtraction of the galactic high energy gamma-ray background will be possible. It is less certain that it will be possible to obtain useful spectra, in sky regions as small as a few square degrees, for the extragalactic radiation remaining after subtraction of the galactic component.

## WHAT SHOULD WE LOOK FOR?

From the considerations given above, it is clear that matter-antimatter boundaries *might* be detectable with reasonable values for their width and density. Since there appears to be no way to put useful lower limits on those parameters, it is not true that domain boundaries *must* be observable. A search must therefore be carried out, but negative results probably would not rule out the existence of antimatter domains in the Universe.

It appears that a likely approach would be to search for correlation between the angular density of luminous matter (galaxies and clusters) and the observed gamma-ray intensity after subtraction of galactic background. A *negative* correlation would indicate that the optically empty regions are producing more gamma rays than the luminous matter, and would therefore support the idea of a domain structure of matter and antimatter in the Universe. Additional very strong support would come from a demonstration that the spectrum of the gamma radiation from the apparently empty regions is similar to that shown in Figure 1, very different from the spectrum of gamma rays generated within our own galaxy or that observed from active galactic nuclei. As mentioned above, however, it is not certain that the spectrum obtained after galactic background subtraction would be sufficiently accurate to make such a determination.

**REFERENCES**

Alfven, H. 1965, *Rev. Mod. Phys.*, **37**, 652.

Bahcall, N. A., and Soneira, R. M. 1984, *Ap. J.*, **277**, 27.

Bel, N., and Martin, P. 1975, *Astr. Ap.*, **46**, 455.

Colomb, F. R., Poppel, W. G. L., and Heiles, C. 1980, *Astr. Ap. Suppl.*, **40**, 47.

Fichtel, C. E., Simpson, G. A., and Thompson, D. J. 1978, *Ap. J.*, **222**, 833.

Harwitt, M. 1989, *Ap. J.*, **347**, 688.

Kirshner, R. P., Oemler, A., Schecter, P. L., and Shectman 1981, *Ap. J. (Letters)*, **248**, L57.

de Lapparent, V., Geller, M. J., and Huchra, J. P. 1986, *Ap. J. (Letters)*, **302**, L1.

Stacy, J. G. 1989, private communication.

Stecker, F. W., Morgan, D. L., and Bredekamp, J. 1971, *Phys. Rev.*, **27**, 1469.

Stecker, F. W. 1971, *Cosmic Gamma Rays* (NASA SP-249).

Stecker, F. W., and Puget, J. L. 1972, *Ap. J.*, **178**, 57.

Thompson, D. J., and Fichtel, C. E. 1982, *Astr. Ap.*, **109**, 352.

West, M. J. 1989, *Ap. J.*, **347**, 610.

# DISCUSSION

*R.J. Slobdrian:*

There is also speculation on the existence of strings of very high density matter, then, of course, one may have similar strings of antimatter, and upon collision they would produce very strong sources of radiation.
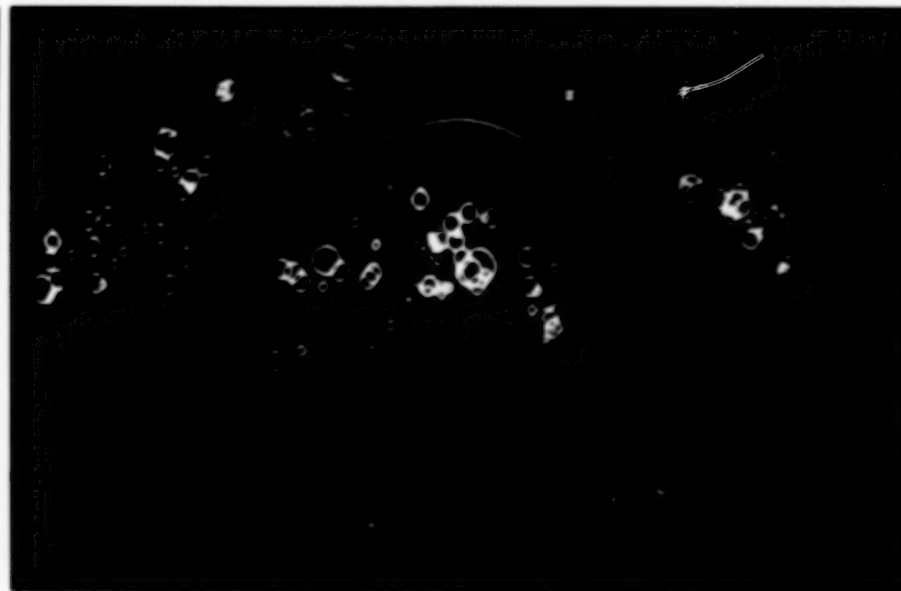
*Bob Hartman:*

Clearly, we will be alert to unexpected features in the diffuse radiation. Unfortunately, there is no indication of where such features should occur, or even what their angular scale might be. If they are to be separable from point sources, they would probably have to be several degrees in size.
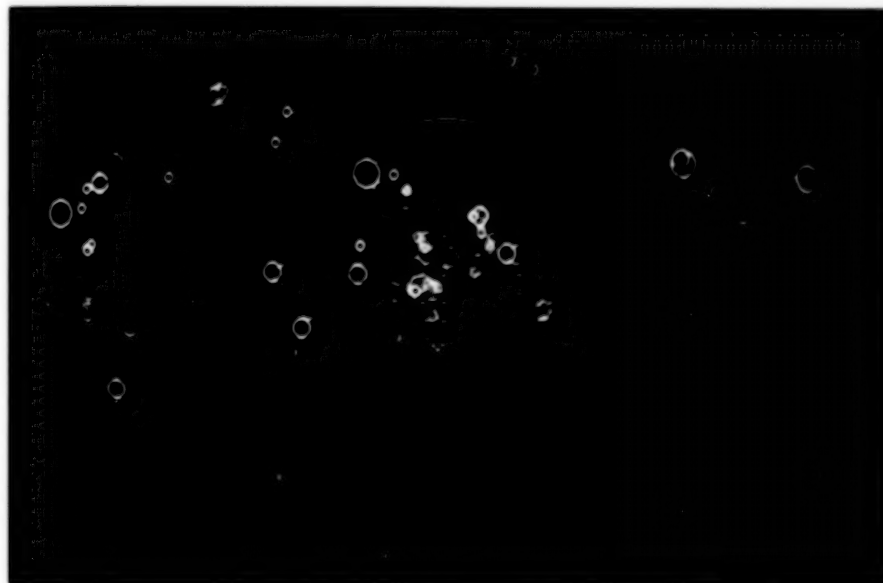
344
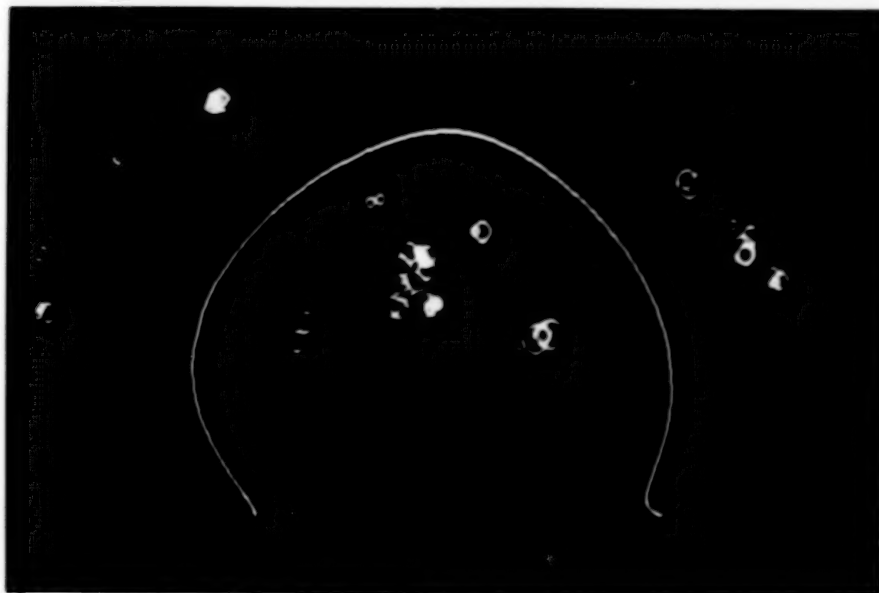
**(4)**



Figure 2. Aitoff plot in celestial coordinates of Abell clusters (z < 0.1) assigned to superclusters by West(1989). The circle sizes indicate Abell richness class (0 - 5). Member clusters in a supercluster are shown in the same color; however, each color is used to represent several well-separated superclusters.

Figure 3. Same as Figure 2, but showing in white the Abell clusters which are not within a supercluster (more than 25 Mpc from all other clusters).

Figure 4. Abell clusters with z < 0.1, color coded into three redshift intervals: yellow, 0.000 - 0.033; orange, 0.033 - 0.067; red, 0.067 - 1.000.

# NASA

National Aeronautics and
Space Administration

# Report Documentation Page

| 1. Report No. | 2. Government Accession No. | 3. Recipient's Catalog No. |
|---|---|---|
| NASA CP-3071 | | |

| 4. Title and Subtitle | 5. Report Date |
|---|---|
| The Energetic Gamma-Ray Experiment Telescope (EGRET) Science Symposium | May 1990 |
| | 6. Performing Organization Code |
| | 660 |

| 7. Author(s) | 8. Performing Organization Report No. |
|---|---|
| Carl Fichtel, Stanley Hunter, Parameswaran Sreekumar, and Floyd Stecker, Editors | 90B00088 |
| | 10. Work Unit No. |

| 9. Performing Organization Name and Address | 11. Contract or Grant No. |
|---|---|
| NASA/Goddard Space Flight Center Greenbelt, MD 20771 | |
| | 13. Type of Report and Period Covered |

| 12. Sponsoring Agency Name and Address | Conference Publication Nov 15-16, 1989 |
|---|---|
| National Aeronautics and Space Administration Washington, DC 20546-0001 | 14. Sponsoring Agency Code |

### 15. Supplementary Notes

C. E. Fichtel, Goddard Space Flight Center, Greenbelt, MD
S. Hunter, Goddard Space Flight Center, Greenbelt, MD
P. Sreekumar, Universities Space Research Association, Goddard Space Flight Center
F. Stecker, Goddard Space Flight Center, Greenbelt, MD

### 16. Abstract

The EGRET Science Symposium was held at the Goddard Space Flight Center on November 15 and 16, 1989. The principal purpose of the symposium was to provide the EGRET scientists and those with whom they have been working an opportunity to study and improve their understanding on high energy gamma ray astronomy. With this goal in mind, the participation of each of the EGRET scientists was encouraged and most presented talks which are included in the proceedings. Each of the groups with whom the EGRET team is collaborating and with whom they have been working over the last several years were invited to present talks and did so, as did each of the groups associated with the other instruments on the Gamma Ray Observatory (GRO). Several theorists were asked to complete the program by presenting related talks. The Symposium began with the galactic diffusion radiation both because of its importance in studying galactic cosmic rays, galactic structure and dynamic balance, and because an understanding of its characteristics is important in the study of galactic sources. The galactic objects to be reviewed included pulsars, bursts, solar flares, and other galactic sources of several types. The symposium papers then proceeded outward from our galaxy to normal galaxies, active galaxies, and the extragalactic diffuse radiation.

| 17. Key Words (Suggested by Author(s)) | 18. Distribution Statement |
|---|---|
| Gamma Rays, High Energy Astrophysics, EGRET (The Energetic Gamma-Ray Experiment Telescope), GRO (The Gamma Ray Observatory) | Unlimited Unclassified STAR Category 90 |

| 19. Security Classif. (of this report) | 20. Security Classif. (of this page) | 21. No. of pages | 22. Price |
|---|---|---|---|
| Unclassified | Unclassified | 350 | A16 |

National Aeronautics and
Space Administration
Code NTT-4

Washington, D.C.
20546-0001

# NASA